

The Separation of Detergent Range Alkanes and Alcohol Isomers with Supercritical Carbon Dioxide

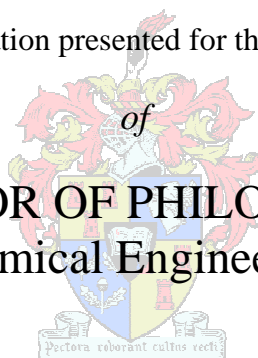
by

Michelle Zamudio

Dissertation presented for the Degree

of

DOCTOR OF PHILOSOPHY
(Chemical Engineering)



in the Faculty of Engineering
at Stellenbosch University

Prof. J.H. Knoetze

Dr. C.E. Schwarz

April 2014

DECLARATION

By submitting this dissertation electronically, I declare that the entirety of the work contained therein is my own, original work, that I am the sole author thereof (save to the extent explicitly otherwise stated), that reproduction and publication thereof by Stellenbosch University will not infringe any third party rights and that I have not previously in its entirety or in part submitted it for obtaining any qualification.

Michelle Zamudio

.....

Signature

February 2014

.....

Date

Copyright © 2014 Stellenbosch University

All rights reserved

ABSTRACT

Data on the process performance at different operating conditions are required to determine the feasibility of a separation process. Such data can be experimentally measured, but due to the time and costs associated with pilot plant scale experiments, the use of predictive process models are often preferred. The main aim of this project is to establish a working process model in Aspen Plus[®] that can be used to predict the separation performance of a supercritical fluid fractionation process aimed at the separation of mixtures of detergent range alkanes and alcohol isomers where similar boiling points or low relative volatilities can occur.

Currently, an azeotropic distillation process is employed for the separation of detergent range alkanes and alcohols. Although this process shows good separation performance, some concerns regarding the operating conditions are raised: the preferred entrainer, diethylene glycol, is toxic to humans; very low operating pressures of 0.016 – 0.031 MPa and high temperatures of 473 K are required; additional processing units and materials are required to remove the entrainer from the product streams. An alternative process, supercritical fluid fractionation, is proposed in this work after previous studies have reported that this process have potential for the separation of alkanes and alcohols. The supercritical fluid fractionation process addresses the concerns of the azeotropic distillation process in the following ways: a non-toxic solvent, CO₂, is used as the separating agent; mild temperatures of 344 K is proposed, but at the cost of the low operating pressures of the azeotropic process; and a single process unit and no additional material is required to separate the solvent from the product streams.

A process model was developed in Aspen Plus[®] to evaluate the separation performance of the newly proposed supercritical fluid fractionation process and compare it to the current azeotropic distillation process. The development of the process model included the development of an accurate thermodynamic model in Aspen Plus[®]. After thorough evaluation of a number of cubic equations of state, the RK-ASPEN model was found to be superior in its representation and prediction of phase transition pressures for multi-component mixtures of detergent range alkanes and alcohols in the temperature range 318 – 348 K. Phase transition pressures could be predicted with an error of less than 6 % with the inclusion of regressed polar parameters and binary solute-solvent interaction parameters for two multi-component mixtures: CO₂ + (20 % *n*-dodecane + 70 % *l*-decanol + 10 %

3,7-dimethyl-1-octanol) and CO₂ + (25 % *n*-decane + 25 % 1-decanol + 25 % 3,7-dimethyl-1-octanol + 25 % 2,6-dimethyl-2-octanol).

Polar parameters were regressed from pure component vapour pressure data predicted with correlations available in Aspen Plus®. Binary interaction parameters were regressed from experimental bubble and dew point data. Binary bubble and dew point data were measured for a number of systems containing ethane or CO₂ and a C₁₀-alkane or C₁₀-alcohol isomer at temperatures between 308 K and 353 K, and compositions ranging between 0.01 and 0.7 mass fraction solute. A comparison between the phase equilibrium data measured for these systems revealed that the structure of the molecule, and not only the molecular weight, influences its solubility in the supercritical solvent. The phase transition pressures of *n*-decane, 2-methylnonane, 3-methylnonane and 4-methylnonane did not differ significantly in CO₂ or ethane, and these compounds will in all likelihood not be separated in a supercritical fluid fractionation process. The phase transition pressures measured for the C₁₀-alcohol isomers decreased in both CO₂ and ethane in the following order: 1-decanol, 3,7-dimethyl-1-octanol, 2-decanol, 2,6-dimethyl-2-octanol and 3,7-dimethyl-3-octanol. The position of the hydroxyl group and the number, length and position of the side branches, all influence the solubility behaviour and phase transition pressures of the isomeric alcohols in the supercritical solvent. Since the use of ethane did not show any significant benefits with regard to selectivity, the use of the less harmful and less expensive solvent, CO₂, in further investigations was justified.

The RK-ASPEN thermodynamic model, with the inclusion of the regressed polar and binary solute-solvent interaction parameters, was implemented in the process model and the separation performance of the process was simulated at different operating conditions for the CO₂ + (25 % *n*-decane + 25 % 1-decanol + 25 % 3,7-dimethyl-1-octanol + 25 % 2,6-dimethyl-2-octanol) mixture. A comparison to experimental pilot plant data revealed that the model cannot be used to predict the separation performance at low fractionation temperatures (316 K) due to shortcomings in the thermodynamic model. However, the performance of the process at high fractionation temperatures (344 K) could be predicted well, with an error of 10 – 36 %. Simulations for the CO₂ + (25 % *n*-decane + 25 % 1-decanol + 25 % 3,7-dimethyl-1-octanol + 25 % 2,6-dimethyl-2-octanol) and CO₂ + (20 % *n*-dodecane + 70 % 1-decanol + 10 % 3,7-dimethyl-1-octanol) mixtures showed that the composition of the feed mixture have a significant effect on the location and size of the operating window and optimum operating conditions. The optimum operating conditions were defined as the conditions where an acceptable selectivity ratio and alcohol recovery occurred simultaneously. Since

the selectivity ratio and alcohol recovery have opposing optimization approaches, a number of possible optimum operating conditions exist, based on the product specifications. When an alcohol and an alkane with similar phase behaviour exist in a mixture, a distinct minimum selectivity ratio will occur at a point within the extract-to-feed ratio limits of the process. When the alkanes and alcohols present in a mixture do not have similar or overlapping phase transition pressures, the minimum selectivity ratio will typically cover a small range of extract-to-feed ratios at the high end limit of the extract-to-feed ratio range.

To summarize: a process model was established in Aspen Plus[®] that can be used to determine the feasibility and separation performance of a supercritical fractionation process for a feed mixture of detergent range alkane and alcohol isomers. The model was used to prove that an SFF process is a feasible alternative process to consider for the removal of alkanes from mixtures of detergent range alcohol isomers, even where overlapping boiling points or low relative volatilities occur. During the development of the process model, the following significant novel contributions were made:

- New phase equilibrium data were measured for C₁₀-alkane and C₁₀-alcohol isomers in supercritical ethane, as published in *The Journal of Supercritical Fluids* 58 (2011) 330 – 342.
- New phase equilibrium data were measured for C₁₀-alkane and C₁₀-alcohol isomers in supercritical CO₂, as published in *The Journal of Supercritical Fluids* 59 (2011) 14 – 26.
- A thermodynamic model was developed in Aspen Plus[®] that can accurately predict the phase transition pressures of binary, ternary and multi-component mixtures of detergent range alkanes and alcohols in supercritical CO₂, as published in *The Journal of Supercritical Fluids* 84 (2013) 132 – 145.
- A process model was developed in Aspen Plus[®] that can be used to predict the separation performance of a supercritical fluid fractionation process for the separation of mixtures of detergent range alkanes and alcohols.
- Experimental and simulated results indicated that a supercritical fluid fractionation process can be implemented successfully to separate an alkane from a mixture of alcohol isomers, as was shown for two mixtures: CO₂ + (25 % *n*-decane + 25 % *l*-decanol + 25 % 3,7-dimethyl-*l*-octanol + 25 % 2,6-dimethyl-2-octanol) and CO₂ + (20 % *n*-dodecane + 70 % *l*-decanol + 10 % 3,7-dimethyl-*l*-octanol).

OPSOMMING

Data oor die omvang van skeiding by verskillende bedryfstoeistande word benodig om die lewensvatbaarheid van 'n skeidingsproses te bepaal. Sulke data kan eksperimenteel gemeet word, maar as gevolg van die tyd en kostes geassosieer met eksperimente op loodsaanlegskaal, word die gebruik van prosesmodelle verkies. Die hoofdoel van hierdie projek is om 'n werkende prosesmodel, wat daarop gemik is om $C_8 - C_{20}$ alkane en alkohol isomere te skei, in Aspen Plus[®] tot stand te bring om die omvang van die skeiding van 'n superkritiese fraksioneringsproses te meet.

Tans word azeotropiese distillasie gebruik vir die skeiding van $C_8 - C_{20}$ alkane en alkohol-isomere. Alhoewel goeie skeiding met hierdie proses bewerkstellig word, is daar sekere eienskappe van die proses wat aandag vereis: die voorgestelde skeidingsagent, dietileen glikol, is giftig vir mense; baie lae bedryfsdrukke van 0.016 – 0.031 MPa en hoë temperature van 473 K word benodig; addisionele prosesseenhede en materiaal is nodig om die skeidingsagent van die produkte te verwyder. Die gebruik van 'n alternatiewe proses - superkritiese fraksionering - word in hierdie werk voorgestel nadat vorige studies getoon het dat hierdie proses die potensiaal het om alkane en alkohole te skei. Die superkritiese fraksioneringsproses spreek al die kommerwekkende eienskappe van azeotropiese distillasie aan soos volg: 'n veilige oplosmiddel, CO_2 , word as die skeidingsagent gebruik; gemiddelde temperature van 344 K word voorgestel, maar ten koste van lae bedryfsdrukke; 'n enkele proseseenheid en geen addisionele materiaal word benodig om die oplosmiddel van die produkte te skei nie.

'n Prosesmodel is in Aspen Plus[®] ontwikkel om die omvang van die skeiding wat deur die voorgestelde superkritiese fraksioneringsproses teweeggebring is, te evalueer en te vergelyk met die azeotropiese distillasieproses wat tans in gebruik is. Die ontwikkeling van die prosesmodel sluit die ontwikkeling van 'n akkurate termodinamiese model in Aspen Plus[®] in. Na deeglike evaluasie van 'n aantal kubiese toestandsvergelykings is gevind dat die RK-ASPEN-model die faseoorgangsdrukke van multi-komponentmengsels van $C_8 - C_{20}$ alkane en alkohole die beste voorspel binne die temperatuurbereik van 318 – 348 K. Faseoorgangsdrukke kon voorspel word met 'n fout van minder as 6 % met die insluiting van voorafbepaalde polêre parameters en binêre interaksie-parameters vir twee multi-komponentmengsels: $CO_2 + (20 \% n\text{-dodekaan} + 70 \% I\text{-dekanol} +$

10 % 3,7-dimetiesel-1-oktanol) and CO_2 + (25 % *n*-dekaan + 25 % 1-dekanol + 25 % 3,7-dimetiesel-1-oktanol + 25 % 2,6-dimetiesel-2-oktanol).

Polêre parameters is bepaal met dampdruk data, wat voorspel is met korrelasies in Aspen Plus[®]. Binêre interaksieparameters is van eksperimentele faseoorgangsdata bepaal. Binêre faseoorgangsdata is vir 'n aantal sisteme wat uit etaan of CO_2 en 'n C_{10} -alkaan- of C_{10} -alkohol-isomeer bestaan, gemeet by temperature tussen 308 K en 353 K en samestellings van tussen 0.01 en 0.7 massafraksie van die opgeloste stof. 'n Vergelyking tussen die gemete fase-ewewigsdata het onthul dat die struktuur van die molekule, en nie net die molekulêre massa nie, die oplosbaarheid van die stof in die superkritiese oplosmiddel beïnvloed. Die faseoorgangsdrukke van *n*-dekaan, 2-metieselnonaan, 3-metieselnonaan en 4-metieselnonaan het geen skynbare verskille getoon in etaan of CO_2 nie en dus sal hierdie stowwe in alle waarskynlikheid nie met 'n superkritiese fraksioneringsproses geskei kan word nie. Die faseoorgangsdrukke wat vir die C_{10} -alkohol gemeet is, het in beide etaan en CO_2 afgeneem in die volgende volgorde: 1-dekanol, 3,7-dimetiesel-1-oktanol, 2-dekanol, 2,6-dimetiesel-2-oktanol en 3,7-dimetiesel-3-oktanol. Die posisie van die hidroksielgroep en die aantal, lengte en posisie van die sytakke beïnvloed die oplosbaarheidsgedrag van die alkohol-isomere in die superkritiese oplosmiddel. Aangesien die gebruik van etaan nie enige voordele ten opsigte van selektiwiteit inhou nie, is die gebruik van die minder skadelike en goedkoper oplosmiddel, CO_2 , vir verdere ondersoek geregtig.

Die ontwikkelde termodinamiese model, met die insluiting van die polêre parameters en binêre interaksieparameters, is in die prosesmodel ingesluit en die omvang van die skeiding van die proses is gesimuleer by verskillende bedryfstoeë vir die CO_2 + (25 % *n*-dekaan + 25 % 1-dekanol + 25 % 3,7-dimetiesel-1-oktanol + 25 % 2,6-dimetiesel-2-oktanol) mengsel. 'n Vergelyking tussen die gesimuleerde data en die eksperimentele loodsaanlegdata het onthul dat die model nie die omvang van die skeiding kan voorspel by lae fraksioneringstemperature (316 K) nie as gevolg van die tekortkominge in die termodinamiese model. Die omvang van die skeiding by hoë temperature (344 K) kon egter goed voorspel word met 'n fout van 10 – 36 %. Simulasies van die CO_2 + (25 % *n*-dekaan + 25 % 1-dekanol + 25 % 3,7-dimetiesel-1-oktanol + 25 % 2,6-dimetiesel-2-oktanol) en CO_2 + (20 % *n*-dodekaan + 70 % 1-dekanol + 10 % 3,7-dimetiesel-1-oktanol) mengsels het getoon dat die samestelling van die voermengsel 'n beduidende effek op die grootte van die bedryfsvenster en optimum bedryfstoeë het. Die optimum bedryfstoeë word gedefinieer as die toë waar 'n aanvaarbare selektiwiteitsverhouding en alkoholherwinning terselfdertyd voorkom. Aangesien die selektiwiteitsverhouding en alkoholherwinning teenstrydige optimeringsbenaderings het, bestaan daar

'n aantal optimum bedryfstoestande gebaseer op die produkspesifikasies. Wanneer 'n alkohol en 'n alkaan met ooreenstemmende fasegedrag saam in 'n mengsel voorkom, bestaan daar 'n duidelike minimum selektiwiteitsverhouding by 'n punt binne die ekstrak-tot-voer-verhoudingslimiete van die proses. Wanneer die alkane en alkohole in 'n mengsel nie ooreenstemmende fasegedrag toon nie, sal die minimum selektiwiteitsverhouding oor 'n reeks ekstrak-tot-voer-verhoudings voorkom, tipies by die hoë limiet van die ekstrak-tot-voer-verhoudingsreeks.

Om op te som: 'n prosesmodel is in Aspen Plus[®] tot stand gebring wat die lewensvatbaarheid en omvang van die moontlike skeiding van 'n superkritiese fraksioneringsproses vir voermengsels van C₈ – C₂₀ alkane en alkohol-isomere kan voorspel. Die model is gebruik om te bewys dat 'n superkritiese proses 'n lewensvatbare alternatiewe proses is om te oorweeg vir die verwydering van alkane uit mengsels van alkohol-isomere, self waar ooreenstemmende kookpunte of lae relatiewe vlugtigheid tussen komponente voorkom. Tydens die ontwikkeling van die prosesmodel is die volgende beduidende nuwe bydraes gemaak:

- Nuwe fase-ewewigsdata is gemeet vir C₁₀-alkaan- en C₁₀-alkohol-isomere in superkritiese etaan, soos gepubliseer in *The Journal of Supercritical Fluids* 58 (2011) 330 – 342.
- Nuwe fase-ewewigsdata is gemeet vir C₁₀-alkaan and C₁₀-alkohol isomere in superkritiese CO₂, soos gepubliseer in *The Journal of Supercritical Fluids* 59 (2011) 14 – 26.
- 'n Termodinamiese model is ontwikkel in Aspen Plus[®] wat die faseoorgangsdrukke van binêre, ternêre en multi-komponent mengsels van C₈ – C₂₀ alkane en alkohol-isomere in superkritiese CO₂ akkuraat kan voorspel, soos gepubliseer in *The Journal of Supercritical Fluids* 84 (2013) 132 – 145.
- 'n Prosesmodel is ontwikkel in Aspen Plus[®] wat die omvang van die moontlike skeiding van 'n superkritiese fraksioneringsproses, gemik op die skeiding van mengsels van C₈ – C₂₀ alkane en alkohol-isomere, kan voorspel.
- Eksperimentele en gesimuleerde resultate toon aan dat 'n superkritiese fraksioneringsproses suksesvol geïmplementeer kan word vir die skeiding van 'n alkaan vanuit 'n mengsel van alkohol-isomere, soos bewys vir twee mengsels: CO₂ + (25 % *n*-dekaan + 25 % *I*-dekanol + 25 % 3,7-dimetiel-*I*-oktanol + 25 % 2,6-dimetiel-2-oktanol) en CO₂ + (20 % *n*-dodekaan + 70 % *I*-dekanol + 10 % 3,7-dimetiel-*I*-oktanol).

LIST OF CONTRIBUTIONS

- **M. Zamudio, C.E. Schwarz, J.H. Knoetze**, Phase equilibria of branched isomers of C₁₀-alcohols and C₁₀-alkanes in supercritical ethane, *The Journal of Supercritical Fluids* 58 (2011) 330 – 342.
- **M. Zamudio, C.E. Schwarz, J.H. Knoetze**, Phase equilibria of branched isomers of C₁₀-alcohols and C₁₀-alkanes in supercritical carbon dioxide, *The Journal of Supercritical Fluids* 59 (2011) 14 – 26.
- **M. Zamudio, C.E. Schwarz, J.H. Knoetze**, The effect of branched alcohol isomers on the separation of alkanes and alcohols with supercritical CO₂, 13th European Meeting on Supercritical Fluids, 2011, The Hague, Netherlands (Poster presentation).
- **M. Zamudio, C.E. Schwarz, J.H. Knoetze**, Using Aspen Plus[®] to determine the viability of a supercritical fluid fractionation process for the separation of detergent range alkane and alcohol isomers, 6th International Symposium on High Pressure Process Technology, 2013, Belgrade, Serbia (Oral presentation).
- **M. Zamudio, C.E. Schwarz, J.H. Knoetze**, Experimental measurement and modelling with Aspen Plus[®] of the phase behaviour of supercritical CO₂ + (*n*-dodecane + *I*-decanol + 3,7 dimethyl *I*-octanol), *The Journal of Supercritical Fluids* 84 (2013) 132 – 145.

ACKNOWLEDGEMENTS

This work is based on the research supported in part by the National Research Foundation of South Africa (Grant specific unique reference number (UID) 83966) and Sasol Technology (Pty) Ltd. The authors acknowledge that opinions, findings and conclusions or recommendations expressed in any publication generated by the supported research are that of the authors, and that the sponsors accepts no liability whatsoever in this regard.

Aspen Plus[®] is a registered trademark of Aspen Technology Inc.

A special word of gratitude is conveyed to the following people:

- My supervisors, Dr. C. E. Schwarz and Prof. J. H. Knoetze, for sharing their invaluable knowledge and insight.
- My parents and sister, for their unconditional love and words of encouragement.
- My husband, Jacques, for his continuous love, support, encouragement and patience.

TABLE OF CONTENTS

1. INTRODUCTION.....	1
2. DETERGENT RANGE ALCOHOLS	11
3. SUPERCRITICAL FLUID PROCESSING	27
4. PHASE BEHAVIOUR OF MIXTURES AT HIGH PRESSURES.....	59
5. EXPERIMENTAL BUBBLE AND DEW POINT DATA	95
6. THERMODYNAMIC MODELLING OF MIXTURES AT HIGH PRESSURE USING ASPEN PLUS®	167
7. ESTABLISHING A SUPERCRITICAL FLUID FRACTIONATION PROCESS MODEL.....	233
8. CONCLUSIONS AND RECOMMENDATIONS.....	293
BIBLIOGRAPHY	309
APPENDICES.....	321

1. INTRODUCTION

1.1 PROJECT RELEVANCE	2
1.1.1 Current Separation Process: Azeotropic Distillation.....	2
1.1.2 Proposed Separation Process: Supercritical Fluid Fractionation.....	3
1.2 AIMS AND OBJECTIVES.....	5
1.3 PROJECT SCOPE.....	6
1.3.1 Chemical Components.....	6
1.3.2 Thermodynamic Region	7
1.3.3 Thermodynamic Data and Models	7
1.3.4 Process Data and Models.....	7
1.4 MANUSCRIPT LAYOUT.....	8
1.5 SIGNIFICANT CONTRIBUTIONS	9
1.6 NOMENCLATURE.....	10
1.7 REFERENCES	10

Development and advancement in process technology led to the establishment of a need for more information in a shorter time. Fortunately, the development of computers and computing ability aided in this requirement. Today, many companies in the chemical processing industry make use of mathematical models and simulation software to predict the performance of processes before pivotal decisions concerning process feasibility, operating window, production capacity, product purity, etc.,

are made. The use of process models instead of experimental runs to generate important data, has led to a significant decrease in the amount of time it takes to gather essential information. This project contributes a novel idea in the form a process model, generated in a commercial software program (Aspen Plus[®]), which can predict the performance of a supercritical fractionation process aimed at separating detergent range alkanes from mixtures of detergent range alcohol isomers, where close-boiling compounds can occur. Further contributions will be made by showing for the first time that it is possible to remove detergent range alkanes from mixtures of detergent range alcohol isomers, utilizing a supercritical fluid fractionation process.

1.1 Project Relevance

In the detergent, surfactant and plasticizer industries alcohol isomers with carbon numbers ranging from 8 to 20 are commonly used. One of the more widely used process routes for the production of these alcohols, is the Oxo process [1]. The Oxo process requires an olefin feedstock which is firstly hydroformylated, and then hydrogenated to produce alcohol isomers within a specific carbon number range. Since alcohol production generally occur as a downstream process in the petroleum industry, the feedstock to the Oxo process is often routed directly from synthetic fuel manufacturing plants. These streams contain mainly olefins, but alkanes and small amounts of oxygenates are also present. The alkanes, often present in significant amounts, do not take part in the alcohol production process and exit in the product stream. The alcohol product stream thus contains unconverted alkanes that must be removed from it to improve the purity thereof. The detergent range alkanes and alcohol isomers have boiling point ranges that overlap, therefore the use of conventional distillation processes to separate these compounds are not feasible. One process that has been found to produce a satisfying degree of separation is azeotropic distillation [2].

1.1.1 Current Separation Process: Azeotropic Distillation

Azeotropic distillation refers to the use of an entrainer to form an azeotrope with one or more of the compounds in a feed mixture to increase the relative volatility of the key components for enhanced separation through distillation. This is the only process applied in the separation of detergent range alkane-alcohol mixtures currently discussed in the open literature.

The azeotropic distillation process is discussed by Crause [2] with respect to specifically the separation of $C_{11} - C_{14}$ alkanes from $C_{12} - C_{15}$ alcohols. In this range *n*-tetradecane and *l*-dodecanol

are the compounds that are the most difficult to separate, possibly due to their low relative volatility or the formation of an azeotrope [2]. The proposed process for the effective separation of these close-boiling detergent range alkanes and alcohols, are azeotropic distillation at 0.016 – 0.031 MPa (which limits the bottoms temperature to 473 K), with diethylene glycol (DEG) as the entrainer in an entrainer-to-feed ratio of 1:1.8. A more detailed discussion on this process is provided in Chapter 2.

The azeotropic distillation process currently employed for the separation of close-boiling detergent range alkanes and alcohols has some characteristics that raises concern:

1. There is a need for an additional chemical compound, the entrainer, in significant amounts.
2. Some of the entrainers best suited for this specific application, e.g. DEG, are toxic to humans. This not only poses a health risk for plant operators, but also limits the use of the alkane or alcohol product generated by this process to products not intended for human consumption.
3. The azeotropic distillation column requires extreme operating conditions of low vacuum pressures and high temperatures. The high operating temperatures can lead to the degradation of the products that are being processed.
4. Both the overheads and bottoms streams produced in the azeotropic distillation column require additional processing to remove the entrainer from the alkane and alcohol product, respectively.

The weaknesses of the azeotropic distillation process were considered and a different separation process, supercritical fluid fractionation, was proposed to eradicate some of the concerns. In this study the technical feasibility of the proposed process will be investigated.

1.1.2 Proposed Separation Process: Supercritical Fluid Fractionation

Supercritical fluid fractionation (SFF) has previously been investigated [3,4] as a potential process for the separation of close-boiling detergent range alkanes and alcohols – specifically *n*-tetradecane and *l*-dodecanol. According to the investigations SFF is a feasible process to consider since it is based on the separation of compounds that exhibit different phase behaviour in a supercritical solvent – a characteristic often displayed by compounds of different nature, e.g. alkanes and alcohols.

It was decided to investigate the SFF process for the separation of detergent range alkanes and alcohol isomers more closely, to determine if the separation performance thereof is acceptable and comparable to that of the azeotropic distillation process currently employed. If the investigation reveals that the separation performance of SFF is similar to that of azeotropic distillation, it would be recommended that SFF be employed for this application, since it addresses some of the concerns that surround the azeotropic distillation process in the following way:

1. Although an additional chemical compound, known as the solvent, is still required, the proposed solvent (CO_2) is abundantly available at a low cost. CO_2 can often be obtained from the flue gas of another process, which makes it easier to acquire compared to the specific entrainers required for use in azeotropic distillation.
2. The proposed supercritical solvent, CO_2 , is non-flammable, non-toxic and inert, and poses a much lower health risk to plant operators. At atmospheric conditions the solubility of CO_2 in the alkane and alcohol products are insignificant and potential health risks to consumers of such products are not of concern.
3. The SFF process requires operation at extreme pressures, but the operating temperatures are usually kept low, which allows heat sensitive compounds to be processed. The fractionation process occurs at conditions slightly above the critical point of the selected solvent – in this case CO_2 is selected and thus the operation will occur at pressures and temperatures slightly higher than 7.38 MPa and 304.1 K.
4. Only the overheads product stream requires additional processing to remove the solvent. The bottoms product stream exits the fractionation column at conditions that does not allow solvent solubility. No additional materials are required to remove the solvent from the products.

The abovementioned points highlight some of the advantages of the use of SFF instead of azeotropic distillation, but the feasibility and performance of a process is the main consideration when evaluating the choice of separation process. This investigation is aimed at producing a model for the proposed SFF process that will allow the prediction of the separation performance of such a process where it is employed to separate close-boiling detergent range alkanes and alcohol isomers. Once such a model has been established, information regarding the feasibility and separation performance of the SFF process can be generated and evaluated.

1.2 Aims and Objectives

The main aim of this study is to establish a process model utilizing a commercial process simulation program, which can predict the separation performance of an SFF process intended for the separation of detergent range alkanes and alcohol isomers. One of the requirements for an accurate process model is the use of a thermodynamic model that can accurately predict the phase behaviour of the mixtures involved. It was thus required to experimentally investigate the phase behaviour of the mixtures considered and use the insight gained to establish an accurate thermodynamic model. After developing both the models, first the thermodynamic model and then the process model, the accuracy of the proposed models were verified by comparing the model predictions to experimentally measured data.

In order to achieve the aims of this project, the following objectives were formulated:

1. Conduct a literature review to determine the source, production and application of alkane-alcohol mixtures that occur in the detergent and surfactant industries, and the current separation technologies employed to separate such mixtures.
2. Report on the use of SFF for the purpose of separating detergent range alkane-alcohol mixtures, as well as on the modelling of SFF processes, as published in the literature.
3. Conduct a literature review to determine the expected phase behaviour of the mixtures to be used in this study, and report on previous attempts to model the phase behaviour of such mixtures.
4. Investigate the phase behaviour of isomers of detergent range alkanes and alcohols in supercritical solvents by experimentally measuring and comparing bubble and dew point data. These results will also be used to investigate solute-solvent interactions for the different compounds.
5. Investigate the effect of solute-solute interactions in mixtures by experimentally measuring the bubble and dew point data of ternary and multi-component mixtures and comparing it to the phase behaviour of that reported for the binary mixtures.
6. Develop a thermodynamic model in Aspen Plus[®] that can accurately predict the phase behaviour of the multi-component mixtures used in this investigation. The accuracy of

the model will be verified by comparing it to experimentally measured bubble and dew point data.

7. Develop a process model in Aspen Plus[®] that can accurately predict the process performance of an SFF process intended for the separation of close-boiling detergent range alkanes and alcohol isomers. The accuracy of the model will be verified by comparing it to experimentally measured pilot plant data.
8. Determine the feasibility of an SFF process for the separation of detergent range alkanes from mixtures of detergent range alcohol isomers, by evaluating the predicted separation performance for different feed mixtures.

1.3 Project Scope

1.3.1 Chemical Components

The components selected for this investigation were certain C₁₀-alkane isomers, C₁₀-alcohol isomers and *n*-dodecane. The component selection was based on the commercial availability of close-boiling isomeric compounds that fall within the detergent range (C₈ – C₂₀). The C₁₀-alkane isomers and C₁₀-alcohol isomers were used to investigate the effect of branching on the phase behaviour of compounds (Objective 4 and 5). The *n*-dodecane and selected C₁₀-alcohol isomers were used to investigate the ability of SFF to separate close-boiling compounds (Objective 5, 6 and 7).

In Table 1-1 the compounds and their respective boiling points, as found in the Aspen Plus[®] database [5], are given.

Table 1-1 Compounds and their respective boiling points [5], selected for use in this study

C ₁₀ -alkanes		C ₁₂ -alkanes		C ₁₀ -alcohols	
Compound	<i>T_b</i> (K)	Compound	<i>T_b</i> (K)	Compound	<i>T_b</i> (K)
<i>n</i> -decane	447.3	<i>n</i> -dodecane	489.5	1-decanol	503.0
2-methylnonane	440.2			2-decanol	491.7
3-methylnonane	441.0			3,7-dimethyl-1-octanol	497.3
4-methylnonane	438.9			2,6-dimethyl-2-octanol	471.0
				3,7-dimethyl-3-octanol	468.2

The supercritical solvents investigated in this work are limited to ethane and CO₂. Bubble and dew point data were measured for all the components listed in Table 1-1 with both ethane and CO₂. Based on the results generated, one solvent will be selected to be used for further investigation.

1.3.2 Thermodynamic Region

The thermodynamic region investigated in this study was bound by the temperature and pressure limits of the experimental equipment.

Bubble and dew point data were measured at temperatures between 308 and 348 K, and pressures between 3.0 and 27.5 MPa. This operating window was also applied to the pilot plant experiments and model development.

The composition range covered for the phase equilibrium measurements in this study was 0.01 – 0.7 mass fraction of the solute, where the solute can refer to a pure compound or a constant composition mixture of compounds.

1.3.3 Thermodynamic Data and Models

The experimental equipment that was made available for this study only allowed for bubble and dew point measurements to be taken. Bubble and dew points were measured for a number of binary, ternary and multi-component mixtures, within the operating range as discussed in paragraph 1.3.2. For modelling purposes vapour-liquid equilibrium (VLE) data was required, and thus the measured bubble and dew point data of the binary mixtures were manually converted to VLE data. This conversion procedure could not be applied to the ternary and multi-component mixtures, and a different modelling strategy was implemented for these data sets (discussed in detail in Chapter 6).

In this study only cubic equations of state (EoS) were considered in an attempt to model the phase behaviour of multi-component mixtures. In Chapter 6 a detailed discussion is given on the reason for selecting the cubic EoS. The reasons are mainly based on the simplicity and robustness of the cubic EoS, a characteristic that make them attractive for industrial applications.

1.3.4 Process Data and Models

The main aim of this project is to establish a working process model for an SFF process in Aspen Plus[®]. A commercial process simulation program was selected as the computational tool in

this study to highlight the potential industrial application of the developed methodology. Most companies in the chemical processing industry will resort to acquiring a commercial simulation program for process screening purposes, rather than developing an advanced in-house simulation program. The potential process models that could be used to model the SFF process are limited to those built into the Aspen Plus[®] software package.

SFF pilot plant data was measured with the sole intent of serving as verification data for the process model developed in Aspen Plus[®]. Since the pilot plant data was only intended for verification purposes, a small amount of data points was deemed sufficient. This approach highlights the purpose of the process model, i.e. to gather separation performance data with the use of minimal experimental data.

1.4 Manuscript Layout

Table 1-2 Manuscript layout and content

Chapter	Objective	Content
1 Introduction		Project is defined in terms of the relevance, aims, scope and contributions.
2 Detergent Range Alcohols	1	Literature review to determine the compositions and applications of commonly encountered mixtures of detergent range alcohols. This information contributes to the motivation of the relevance of this project.
3 Supercritical Fluid Processing	2	Literature review on the supercritical fluid fractionation process. Information is provided on previous studies where SFF was investigated for similar applications. Previous attempts to model the SFF process in Aspen Plus [®] are also discussed. This information is intended to guide the selection of operating region and process model.
4 Phase Behaviour of Mixtures at High Pressure	3	Literature review on the phase behaviour exhibited by mixtures at pressures that exceed the critical pressure of one component. Information is provided on the expected phase behaviour of the mixtures investigated in this work. The thermodynamic models often applied to high pressure mixtures are discussed, and motivation for the choice of cubic EoS for further investigation is provided.
5 Experimental Bubble and Dew Point Data for Mixtures	4 & 5	The experimental method employed in this work to measure bubble and dew point data for the components mentioned in Table 1-1 with supercritical ethane and CO ₂ , are discussed. The experimental results are compared and the effect of side branching, functional group position and solvent on the phase behaviour of the binary mixtures are revealed. Measured ternary and multi-component bubble and dew point data are also given and the effect of solute-solute interaction is investigated.

Table 1-2 (continued) Manuscript layout and content

Chapter	Objective	Content
6 Thermodynamic Modelling of Mixtures at High Pressure using Aspen Plus®	6	Measured binary bubble and dew point data are converted to VLE data and binary solvent-solute interaction parameters are determined with regression for four thermodynamic models in Aspen Plus®. The most appropriate thermodynamic model is selected based on its ability to represent the binary mixtures and predict multi-component data. The effect of the inclusion of binary interaction parameters on the predictive capabilities of the model is investigated. Ternary bubble and dew point data are used to determine solute-solute interaction parameters, and the effect of the inclusion of such parameters on the predictive ability of the model is investigated.
7 Establishing a Supercritical Fluid Fractionation Process Model	7 & 8	A discussion is given on the development of the SFF process model in Aspen Plus®. Validation data in the form of pilot plant data was provided. The experimental method employed in the measuring of the pilot plant data is also discussed in detail. After validation the developed process model is used to predict the separation performance of the SFF process under different operating conditions, and with different feed mixtures. Optimum operating windows are suggested depending on the specifications of the product streams.
8 Conclusions and Recommendations		A summary of the most important findings of this project is given, along with suggestions for future work that can aid in improving the developed process model.

1.5 Significant Contributions

This project was structured in such a way that it produced the following significant novel contributions:

1. High pressure phase equilibrium data for C₁₀-alkane and C₁₀-alcohols isomers in supercritical ethane.
2. High pressure phase equilibrium data for C₁₀-alkane and C₁₀-alcohols isomers in supercritical CO₂.
3. A thermodynamic model that has the ability to accurately predict the phase behaviour of mixtures of close-boiling detergent range alkanes and alcohol isomers in supercritical CO₂.

4. A process model that has the ability to accurately predict the separation performance of an SFF process intended for the separation of detergent range alkanes from alcohol isomers.
5. Experimental and simulated results were produced to prove that the SFF process is a feasible process to consider when attempting to remove detergent range alkanes from mixtures of detergent range alcohol isomers, even where the compounds have overlapping boiling points or low relative volatilities.

1.6 Nomenclature

Symbol/ Acronym	Description
DEG	Diethylene glycol
EoS	Equation of State
SFF	Supercritical Fluid Fractionation
VLE	Vapour-Liquid Equilibrium

1.7 References

- [1] H. Bahrmann, H. Bach, Oxo Synthesis, Ullmann's Encyclopaedia of Industrial Chemistry. (2012).
- [2] J.C. Crause, Production of detergent range alcohols, US 7652173 B2, 2010.
- [3] G.J.K. Bonthuys, C.E. Schwarz, A.J. Burger, J.H. Knoetze, Separation of alkanes and alcohols with supercritical fluids. Part I: Phase equilibria and viability study, The Journal of Supercritical Fluids. 57 (2011) 101 – 111.
- [4] C.E. Schwarz, G.J.K. Bonthuys, R.F. van Schalkwyk, D.L. Laubscher, A.J. Burger, J.H. Knoetze, Separation of alkanes and alcohols with supercritical fluids. Part II. Influence of process parameters and size of operating window, The Journal of Supercritical Fluids. 58 (2011) 352 – 359.
- [5] Aspen Plus[®], AspenTech, 2000.

2. DETERGENT RANGE ALCOHOLS

2.1 SOURCES OF DETERGENT RANGE ALCOHOL ISOMERS.....	12
2.1.1 Natural Sources	12
2.1.2 The Fischer-Tropsch Process	12
2.1.3 The Oxo Alcohol Production Process	14
2.2 SEPARATION OF ALKANE-ALCOHOL MIXTURES.....	17
2.2.1 Azeotropic Distillation	17
2.2.2 Supercritical Fluid Fractionation.....	18
2.3 APPLICATIONS OF DETERGENT RANGE ALCOHOL ISOMERS.....	20
2.3.1 Isomeric Alcohol Mixtures.....	20
2.3.2 Alcohol Mixtures with a Range of Carbon Numbers.....	21
2.4 OUTCOMES OF THIS CHAPTER	22
2.5 NOMENCLATURE.....	23
2.6 REFERENCES.....	24

Alcohols with carbon numbers between 8 and 20 are commonly referred to as detergent range alcohols. This classification is mainly attributed to the application of these alcohols in the manufacturing of detergents. The detergent industry ranges from the manufacturing of personal and household cleaning aids to industrial detergents and surfactants.

The aim of this chapter is to provide the relevant background information to identify the industrial niche of this project. The specific sources, manufacturing routes and applications of detergent range alcohols are discussed in this chapter.

2.1 Sources of Detergent Range Alcohol Isomers

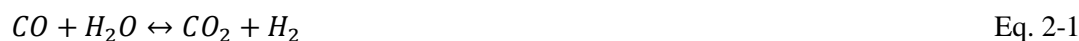
2.1.1 Natural Sources

Detergent range alcohol isomers are not present in any significant quantities in natural sources. C₈ – C₂₀ alcohols can, however, be derived from natural sources e.g. coconut oil, palm kernel oil and tallow oil [1]. In natural fats and oils certain carboxylic acid esters are isolated, transesterified to methyl-esters and reduced by sodium (Bouveault-Blanc reduction) or catalytic hydrogenation to yield alcohols [1,2]. Alcohols derived in this manner are considered to be of natural origin.

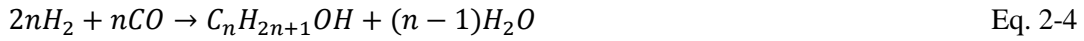
2.1.2 The Fischer-Tropsch Process

The Fischer-Tropsch synthesis process is a set of chemical reactions that convert carbon monoxide and hydrogen into liquid hydrocarbons – thus creating a synthetic fuel.

In the first step of this process natural gas, coal, and/or biomass, is converted to a mixture of carbon monoxide and hydrogen (commonly known as synthesis gas) through partial oxidation and/or steam reforming. The mechanism of this reaction is shown in Equation 2-1 [3].



The purified synthesis gas is then passed over a Group VIII metal catalyst to produce a range of hydrocarbons, alcohols, aldehydes, ketones and acids. The reaction mechanisms of the main chemical reactions for the formation of alkanes (Equation 2-2), olefins (Equation 2-3) and alcohols (Equation 2-4) are given below [3].



The range of products generated by the Fischer-Tropsch process consist of a complex multi-component mixture of linear and branched hydrocarbons and oxygenated compounds of which the ratios can be controlled by slightly adjusting the catalyst and/or operating conditions.

The Low Temperature Fischer-Tropsch (LTFT) reaction takes place at approximately 450 – 550 K and at pressures of 1.0 – 5.0 MPa and favours the production of less oxygenated compounds [4]. The High Temperature Fischer-Tropsch (HTFT) reaction usually takes place at 560 – 630 K and at 2.0 – 5.0 MPa and generally leads to a product stream with more unsaturated compounds and oxygenates [4]. This trend is also evident from Table 2-1 where the typical C₅ – C₁₈ component distributions for the products streams of the LTFT and HTFT processes are given.

Table 2-1 C₅ – C₁₈ component distribution in LTFT and HTFT product streams (with iron catalyst) [3]

Component (%)	LTFT				HTFT	
	Tubular Fixed-Bed Reactor		Slurry Bed Reactor		C ₅ – C ₁₀	C ₁₁ – C ₁₄
	C ₅ – C ₁₂	C ₁₃ – C ₁₈	C ₅ – C ₁₂	C ₁₃ – C ₁₈		
Alkanes	53	65	29	44	13	15
<i>n-Alkanes</i>	95	99	96	95	55	60
<i>Other Alkanes</i>	5	1	4	5	45	40
Olefins	40	28	64	50	70	60
Aromatics	0	0	0	0	5	15
Oxygenates	7	7	7	6	12	10

The aliphatic compounds synthesized in the Fischer-Tropsch reactor are usually separated into fractions according to carbon number. In Table 2-2 the typical carbon number ranges of the fractionated product streams are shown.

Table 2-2 Carbon number distribution in LTFT and HTFT product streams [3]

Product	LTFT		HTFT	
	Min (wt %)	Max (wt %)	Min (wt %)	Max (wt %)
CH ₄	2.0	5.0	10.0	11.0
C ₂ H ₄	0.1	0.2	4.0	7.5
C ₂ H ₆	1.8	2.4	4.0	7.5
C ₃ H ₆	2.0	2.7	12.0	13.0
C ₃ H ₈	1.7	2.8	2.0	13.0
C ₄ H ₈	2.8	3.0	9.0	11.0
C ₄ H ₁₀	1.7	2.2	2.0	11.0
C ₅ -C ₁₁ (gasoline and naphtha)	18.0	22.5	37.0	40.0
C ₁₂ -C ₁₈ (diesel and kerosene)	14.0	15.0	7.0	11.0
C ₁₉ -C ₂₃ (soft waxes)	6.0	7.0	3.5	4.0
C ₂₄ -C ₃₅ (medium wax)	17.0	20.0	3.5	4.0
>C ₃₅ (hard wax)	18.0	25.0	not available	not available
Nonacid chemicals	3.0	3.5	5.0	6.0
Acids	0.2	0.4	not available	not available

The main aim of the Fischer-Tropsch process is to create olefins and alkanes. Alcohol formation is a side reaction of the Fischer-Tropsch process. The product streams, containing mainly olefins and alkanes, are routed to downstream processing areas where they are converted to alcohols according to certain reactions. Detergent range alkanes and alcohols are mostly present in the gasoline, naphtha, kerosene and diesel fractions.

2.1.3 The Oxo Alcohol Production Process

The majority of detergent range alcohols used in industrial processes is synthetically produced via a variety of different alcohol manufacturing processes. The most common detergent range alcohol production processes are the Oxo and the Ziegler processes [1]. These processes, as well as other alcohol production processes, are discussed in detail by Falbe et al. [1] and Lundeen [5]. Most of these processes occur as part of a larger manufacturing process in the surfactant and detergent industries.

The Oxo process is generally used to synthesize alcohols with carbon numbers ranging from 3 to 20. In the Oxo process α -olefins are hydroformylated by allowing them to react with synthesis gas in the presence of cobalt or rhodium based catalysts to form a mixture of aldehydes. The aldehydes

generated contain one more carbon atom than the olefin used as the feedstock. The aldehydes are then hydrogenated to form an alcohol with the corresponding number of carbon atoms. In one version of the Oxo process, known as the Shell process, the two-step reaction take place in a single reactor due to the presence of a Rh-catalyst with very strong hydrogenating activity [1]. An additional advantage of the Shell process is the isomerization of ω -olefins in the feedstock to α -olefins that can also take part in the reaction and consequently form up to 80% linear alcohols [1]. The reaction mechanism of the Oxo reaction is illustrated in Figure 2-1. Depending on the process conditions, structural isomers of the aldehyde can be generated which can lead to the formation of branched alcohols.

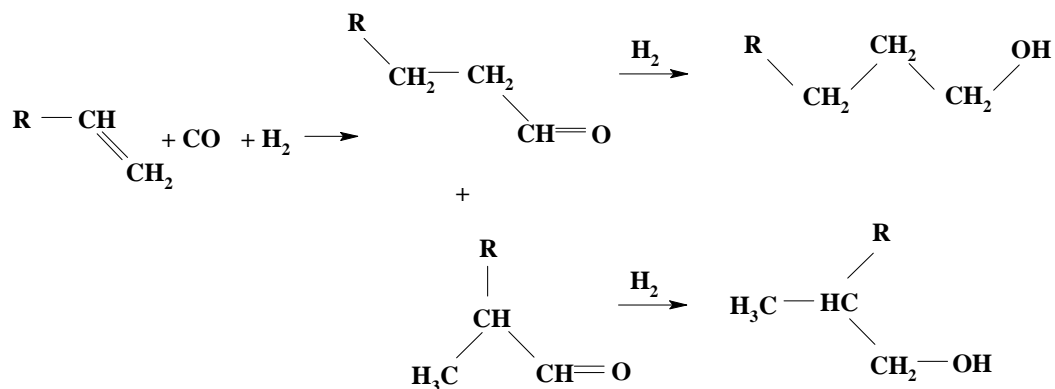


Figure 2-1 Reaction mechanism of the Oxo process (redrawn from [6])

Since the Oxo process is generally applied in a petroleum manufacturing environment, process streams that contain the required feedstock compounds (i.e. olefins) are often routed directly to the Oxo process. Streams containing mostly $\text{C}_{10} - \text{C}_{18}$ olefins and alkanes, are recovered from the Fischer-Tropsch reaction through distillation and fractionated into streams with a narrower carbon number distribution. To reduce the acid content of these streams oxygenates are removed by using liquid-liquid extraction, dehydration or hydrogenation [4]. However, significant amounts of alkanes can still be present in the process streams when it reaches the alcohol production plant. The product stream of the Oxo process thus mainly consists of a mixture of linear and methyl-branched primary alcohols and possibly some unconverted olefins, aldehydes and alkanes. In Table 2-3 the effect of the process conditions on the alcohol product of different versions of the Oxo process is shown.

Table 2-3 Comparison of product distributions of different Oxo processes [7]

Catalyst	[RhH(CO)(PR ₃) ₃]		[RhH(CO) ₄]	[CoH(CO) ₃ PR ₃]	[CoH(CO) ₄]
	R=C ₆ H ₅	R=3-C ₆ H ₄ SO ₃ Na			
Hydroformylation Conditions					
Pressure (MPa)	1.5 – 2.0	1.0 – 10.0	20.0 – 30.0	5.0 – 10.0	20.0 – 35.0
Temperature (K)	358 – 388	323 – 403	373 – 413	433 – 473	383 – 453
Results					
Aldehyde selectivity	High	High	High	Low	Medium
n/i Ratio	92:8	95:5	50:50	88:12	80:20
Hydrogenation	Low	Low	Low	High	Medium

To ensure that the production of detergent range alcohols from Fisher-Tropsch olefins is economically viable the ratio of olefins to alkanes in the feedstock need to be high enough. This is usually achieved in the HTFT reaction utilizing a Fe-based catalyst [4] (see Table 2-1). However, irrespective of the type of Fischer-Tropsch reaction employed, the condensate products will contain a certain amount of alkanes along with the main olefin product. The alkanes are not converted to alcohols during hydroformylation and thus the alcohol/aldehyde product generated during hydroformylation need to be separated from the unconverted alkanes. Crause [8] discuss a particular example where a feedstock containing C₁₁ – C₁₄ olefins and alkanes are sent to the hydroformylation reactor to form a mixture of C₁₂ – C₁₅ aldehydes and the corresponding alcohols. The exit stream typically contains a mixture of unconverted C₁₁ – C₁₄ alkanes and the C₁₂ – C₁₅ isomeric alcohol product. In this carbon number range the two compounds most difficult to separate are the n-tetradecane and 1-dodecanol. Even though their boiling points differ by 10 K (see Table 2-4), conventional distillation does not allow for the separation of these two compounds. This phenomenon can possibly be attributed to a low relative volatility or the formation of an azeotrope [8]. It has been found that azeotropic distillation provides sufficient separation of these compounds. However, extreme operating conditions of low vacuum pressure (0.016 – 0.031 MPa abs) and high temperature (> 473 K), as well as specific entrainers (DEG), are required [8].

Table 2-4 Boiling points of alkanes and alcohols within the range C₁₁-C₁₅ [9]

Carbon Number	Alkane	Alcohol
	T _b (K)	T _b (K)
C ₁₁	469	-
C ₁₂	490	537
C ₁₃	509	554
C ₁₄	527	569
C ₁₅	-	583

2.2 Separation of Alkane-Alcohol Mixtures

2.2.1 Azeotropic Distillation

Azeotropic distillation requires the addition of a compound, known as an entrainer, to allow the formation of an azeotrope with one or more of the feed components and thereby enhancing the relative volatility towards the desired separation. A schematic representation of the azeotropic distillation process currently used for the separation of detergent range alkanes and alcohols are shown in Figure 2-2. The important details of the current separation process are mentioned below, while a detailed discussion can be found elsewhere [4,8].

The hydrocarbon feed (consisting of alkanes and alcohols within a certain carbon number range) is introduced in the middle of the azeotropic distillation column, and the entrainer at the top. For effective separation the azeotropic distillation column must operate at 0.016 – 0.031 MPa abs. By operating the column under vacuum, the bottoms temperature is limited to 473 K. The optimum number of theoretical stages in the azeotropic distillation column is 30 – 35.

Crause [8] found that using a mid-boiling entrainer is more effective than a high- or low-boiling entrainer for the separation of C₁₁ – C₁₄ alkanes from C₁₂ – C₁₅ alcohols. For this specific application diethylene glycol (DEG) is the preferred entrainer. The addition of DEG leads to the formation of azeotropes with both *l*-dodecanol and *n*-tetradecane (the two components with the closest boiling points in the range investigated) thereby increasing the relative volatility of the azeotropes compared to the relative volatility of the pure compounds. The preferred entrainer-to-feed ratio lie within the range 1:1.05 – 1:1.3, with the optimum at 1:1.8 [8].

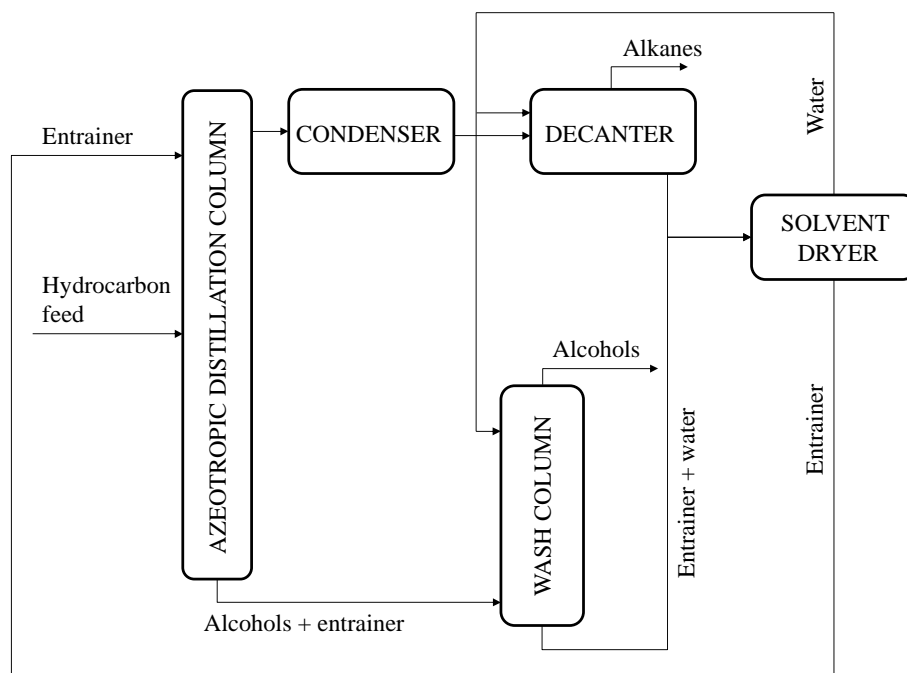


Figure 2-2 Schematic of the currently employed azeotropic distillation process [8]

There are some attributes of this process that raises concern (discussed in Chapter 1), but according to Crause [8] the separation performance is adequate. The investigation into an alternative separation process is thus not motivated by the poor performance of established methods, but rather by the progression of technology and the possibility of more economic operating conditions, larger yield, safer plant environment, and greater product purity.

2.2.2 Supercritical Fluid Fractionation

Supercritical fluid fractionation (SFF) is the process where a fractionation column is operated at conditions that exceed the critical state of a solvent to allow the solvent to preferentially dissolve selected components from a mixture. The SFF process was proposed as an alternative process for the separation of close-boiling detergent range alkanes and alcohols, based on the results obtained in previous studies [10,11] where it was shown that it is possible to use an SFF process to separate a linear alkane (*n*-tetradecane) from a primary linear alcohol (*1*-dodecanol).

In reality, alcohol isomers are also present in the hydrocarbon feed stream to the separation process. A part of this study is dedicated towards determining what the effect of the presence of

alcohol isomers in the hydrocarbon feed stream will be on the separation performance of the SFF process.

A schematic representation of the proposed SFF process is given in Figure 2-3. Details concerning the proposed operating region of the SFF process will be discussed in Chapter 7 of the manuscript.

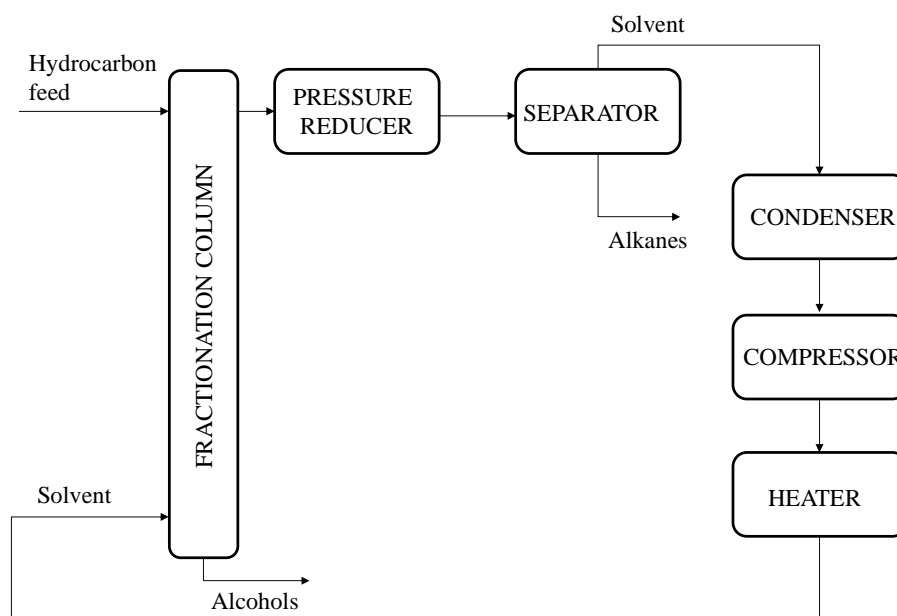


Figure 2-3 Schematic of the proposed SFF process

The main aim of the post-production separation process is to remove the unreacted alkanes from the alcohol isomers. After purification the alcohol product is sold to numerous industries where it is used in the manufacturing of countless household and industrial products. The intended application of the alcohol product will dictate the purity specifications thereof. The need for pure primary linear alcohols are limited and often not directed at alcohols manufactured via the Oxo process. In most cases a mixture of branched and linear alcohols, or a mixture of alcohols covering a certain carbon number range are produced.

2.3 Applications of Detergent Range Alcohol Isomers

There are numerous applications for detergent range alcohol isomer mixtures, of which most are discussed in detail by a number of authors [1,2,12].

For industrial purposes isomeric mixtures of alcohols and mixtures of alcohols with a range of carbon numbers are often preferred, since they are less expensive compared to pure alcohols, and in many cases they are advantageous in their specific applications [1].

2.3.1 Isomeric Alcohol Mixtures

Pure linear alcohols are hard to come by since they almost always exist as a mixture of isomeric compounds. The isomeric mixtures encountered most frequently in industry were compiled into Table 2-5.

Table 2-5 Applications of detergent range isomeric alcohol mixtures [1]

Carbon number	Major derivatives	Important isomers	Applications
C ₈	Esters, ethers, acetates, ethoxides, sulfuric acid esters, organophosphorous compounds	3,4-dimethyl-1-hexanol 3,5-dimethyl-1-hexanol 4,5-dimethyl-1-hexanol 3-methyl-1-heptanol 5-methyl-1-heptanol and others	Solvent for organic compounds Baking enamel Foam suppressant Extracting agent for metal salts Emulsifier and stabilizer in oil Modifier for PVC pastes Polishing agent for polymers Bath additive in galvanization Intermediate for plasticizer manufacturing (DIOP)
C ₉	Phthalates, esters, sulfates, phosphates	3,5,5-trimethyl-1-hexanol dimethyl-1-heptanols trimethyl-1-hexanols and others	Intermediate for plasticizer manufacturing (DINP)
C ₁₀	Phthalates, esters, detergent derivatives	Complex multi-branched mixture of primary alcohols	Intermediate for plasticizer manufacturing (DIDP)

The main use of $C_8 - C_{10}$ isomeric alcohol mixtures is in the production of phthalates used in the plasticizer, lubricant and surfactant industries. Phthalates are produced by the chemical reaction between an alcohol and phthalic anhydride. Phthalates are clear, colourless and odourless liquids of which approximately 90 % are used to make PVC (polyvinyl chloride) soft and flexible for the construction, automotive, wire and cable industries [13]. Phthalates are also present in common household and personal equipment used by people on a daily basis, e.g. PVC raincoats, plastic toys, shower curtains, medical tubing, etc.

The most commonly used phthalates are di-isononyl phthalate (DINP), dipropylheptyl phthalate (DPHP), di-isodecyl phthalate (DIDP), di-oundecyl phthalate (DIUP), and di-tridecyl phthalate (DTDP). These phthalates represent more than 85 % of the phthalates produced in Europe in 2010 [13]. The alcohols used to manufacture these phthalates are produced by the Oxo process, thus branched alcohols are also present in the alcohol feedstock. The phthalates produced thus also contain branches and are subsequently termed “iso”-phthalates. Phthalates that are the product of straight chain alcohols or at least a mixture of straight chain alcohols and primary 2-methyl branched alcohols, give rise to plasticizers that have much better characteristics than phthalates produced from a highly branched alcohol feedstock [14].

2.3.2 Alcohol Mixtures with a Range of Carbon Numbers

An extremely large amount of commercial alcohol mixtures with different carbon number ranges are available in industry. In Table 2-6 the main applications of the most common linear and isomeric mixtures of detergent range alcohols are shown.

It is clear from the information provided in Table 2-5 and Table 2-6 that detergent range alcohols are widely used in the manufacturing of many compounds. It is thus important that an effective separation process be employed after the Oxo process to ensure that the product specifications of detergent range alcohols is adhered to.

Table 2-6 Applications of linear and isomeric alcohol mixtures with carbon number ranges [1]

Mixture	Sources	Applications
Linear C₁₂ - C₁₈ mixtures	Natural Ziegler Oxo (Shell)	Intermediates in manufacturing of detergents Wetting agent Emulsifying agent Viscosity index improvers of lubricating oils Foaming agent
Isomeric C₁₃ - C₁₈ mixtures	Oxo	Preparation of plasticizers Manufacturing of surfactants Antifrothing agent Solvent Flotation and extraction agent Intermediates for detergents, wetting agents, etc. Manufacture of synthetic lubricants and hydraulic fluids Cosmetics

2.4 Outcomes of this Chapter

This chapter expanded on the life cycle of detergent range alcohols - from source, through manufacturing, to application. Information was provided that enabled the reader to identify the industrial niche of the separation process proposed in this work. Objective 1, as mentioned in Chapter 1, was thus achieved. Supercritical fluid processing and the proposed SFF process will be discussed in more detail in the next chapter.

The key findings of this chapter are:

- The ratio of alkanes to olefins in the Fischer-Tropsch process depends on the operating conditions employed during the Fischer-Tropsch synthesis reaction. Since the Oxo process is fed directly from the Fischer-Tropsch product streams, the alkane/olefin ratio will impact the composition of the alcohol product formed in the Oxo process.
- The degree of alcohol formation, as well as degree of isomerization in the Oxo process is dependent on the operating conditions selected for the Oxo process.

- The alcohol product stream thus contains linear and branched alcohols (ratio determined by the Oxo process operating conditions) and unreacted alkanes (amount determined by the Fischer-Tropsch operating conditions). Applications of the alcohol product require the unreacted alkanes to be removed from the isomeric alcohol mixture.
- Overlapping boiling points, low relative volatility and possible formation of azeotropes [8] does not allow the use of conventional distillation techniques for the separation of the alkanes from the isomeric alcohol mixture.
- Azeotropic distillation at 0.016 – 0.031 MPa (> 473 K) with DEG as an entrainer, has been identified as an effective separation process to remove the unreacted alkanes from the isomeric alcohol mixture.
- Due to certain concerns regarding the currently employed azeotropic distillation process as mentioned in Chapter 1, an alternative separation process, SFF, was proposed. The proposal was based on the successful outcome of previous studies [10,11] on the use of SFF for the separation of close-boiling detergent range alkanes and alcohols.

2.5 Nomenclature

Symbol/Acronym	Description
DEG	Diethylene glycol
DINP	Di-isononyl phthalate
DPHP	Dipropylheptyl phthalate
DIDP	Di-isodecyl phthalate
DIUP	Di-isoundecyl phthalate
DTDP	Di-tridecyl phthalate
HTFT	High Temperature Fischer-Tropsch
LTFT	Low Temperature Fischer-Tropsch
PVC	Polyvinyl chloride
- R	Alkyl group
SFF	Supercritical Fluid Fractionation

Symbol/Acronym	Description
<i>T</i>	Temperature

Sub/Superscripts	Description
<i>b</i>	Boiling

2.6 References

- [1] J. Falbe, W. Lipps, D. Mayer, Alcohols, Aliphatic, Ullmann's Encyclopaedia of Industrial Chemistry. (2012).
- [2] Longman Group Ltd, J.H. de Bussy, Natural organic materials and related synthetic products, Materials and Technology. V (1972).
- [3] T. Kaneko, F. Derbyshire, E. Makino, D. Gray, M. Tamura, K. Li, Coal liquefaction, Ullmann's Encyclopaedia of Industrial Chemistry. (2012).
- [4] I.P. Greager, J.C. Crause, Production of detergent range alcohols, US2009/0203804A1, 2009.
- [5] A.J. Lundeen, Alcohols, Chemical and Process Technology Encyclopaedia. (1974).
- [6] C.E. Schwarz, The processing of wax and wax additives with supercritical fluids, PhD Dissertation, Stellenbosch University, 2005.
- [7] H. Bahrmann, H. Bach, Oxo Synthesis, Ullmann's Encyclopaedia of Industrial Chemistry. (2012).
- [8] J.C. Crause, Production of detergent range alcohols, US 7652173 B2, 2010.
- [9] C.L. Yaws, Yaws' Thermophysical Properties of Chemicals and Hydrocarbons (Electronic Edition), Knovel, 2010.
- [10] G.J.K. Bonthuys, C.E. Schwarz, A.J. Burger, J.H. Knoetze, Separation of alkanes and alcohols with supercritical fluids. Part I: Phase equilibria and viability study, The Journal of Supercritical Fluids. 57 (2011) 101 – 111.

- [11] C.E. Schwarz, G.J.K. Bonthuys, R.F. van Schalkwyk, D.L. Laubscher, A.J. Burger, J.H. Knoetze, Separation of alkanes and alcohols with supercritical fluids. Part II. Influence of process parameters and size of operating window, *The Journal of Supercritical Fluids*. 58 (2011) 352 – 359.
- [12] H.A. Mills, Alcohols, Fatty (via Hydrogenation), *Chemical and Process Technology Encyclopaedia*. (1974).
- [13] European Council for Plasticisers and Intermediates (ECP), Plasticisers, Plasticisers and Flexible PVC Information Centre. (2010).
- [14] S.J. Fusco, R.C. Maggart, W.F. Overberger, Linear Oxo Phthalate Plasticizers, in: *Plasticizer and Plasticizer Processes*, n.d.

3. SUPERCRITICAL FLUID PROCESSING

3.1 GLOBAL PHASE BEHAVIOUR OF A SUPERCRITICAL FLUID	28
3.2 PROPERTIES OF SUPERCRITICAL FLUIDS	31
3.2.1 Density.....	31
3.2.2 Diffusivity and Viscosity.....	33
3.3 SUPERCRITICAL FLUID FRACTIONATION	33
3.3.1 Definition of Terms Used.....	34
3.3.2 Modes of Operation.....	34
3.3.3 Evaluation of SFF Process Performance	36
3.3.4 Advantages and Disadvantages	39
3.4 SELECTING A SUPERCRITICAL SOLVENT.....	40
3.5 SFF PILOT PLANT DATA FOR SIMILAR SYSTEMS	41
3.5.1 Separation of <i>n</i> -Alkanes	42
3.5.2 Separation of <i>n</i> -Alkanes and <i>I</i> -Alcohols (Part I)	43
3.5.3 Separation of <i>n</i> -Alkanes and <i>I</i> -Alcohols (Part II).....	44
3.6 SFF PROCESS MODELLING	45
3.6.1 Equilibrium-stage Modelling Concept	47
3.6.2 Equilibrium-stage Modelling in Aspen Plus®	48
3.6.3 Aspen Plus® Equilibrium-stage Modelling for Other Fluid-Fluid Systems	50
3.6.3.1 Deterpenation of Lemon Essential Oil.....	50
3.6.3.2 Palm Oil Refining	51

3.7 OUTCOMES OF THIS CHAPTER	53
3.8 NOMENCLATURE.....	54
3.9 REFERENCES.....	55

This chapter contains information on supercritical fluids, their characteristic properties and their application in fractionation processes. The aim of the chapter is to provide the necessary background information on the SFF process proposed for the separation of detergent range alkanes and alcohol isomers. Important information on previous attempts to separate similar mixtures than those considered in this study, will be conveyed.

The end goal of this project is to establish a working model of the SFF process in Aspen Plus[®] and thus previous attempts to model SFF processes in Aspen Plus[®] will also be reported in this chapter. The information provided in Chapter 3 is aimed at reaching Objective 2, as discussed in Chapter 1.

3.1 Global Phase Behaviour of a Supercritical Fluid

The phase behaviour of every pure substance can be graphically depicted on a P - v - T phase diagram. The phase diagram shows what combinations of pressure, temperature and molar volume a chemical species can simultaneously attain. A chemical substance above its critical temperature, T_c , and critical pressure, P_c , is referred to as a supercritical fluid. Figure 3-1 and Figure 3-2 (a) and (b) shows the critical point of a pure component on its phase diagram projections. Any combination of pressure, temperature and molar volume that lies beyond the critical point lies in the supercritical region.

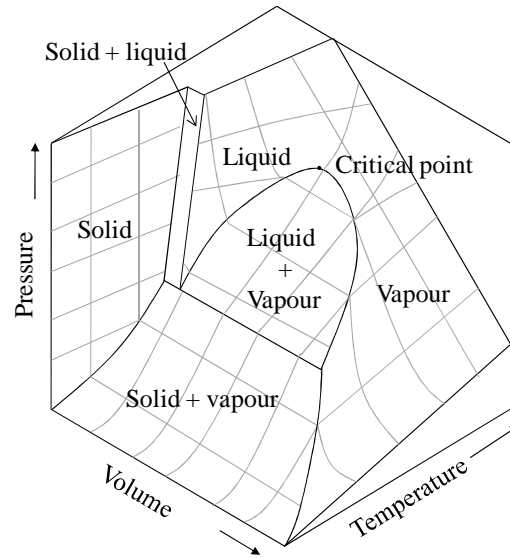


Figure 3-1 P-v-T behaviour of a pure substance (redrawn from [5])

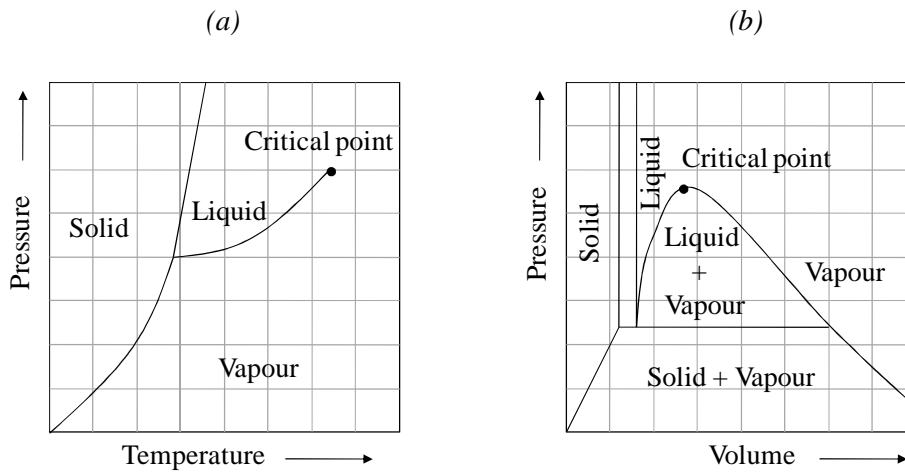


Figure 3-2 (a) Typical P-T projection of the phase behaviour of a pure substance and (b) Typical P-v projection of the phase behaviour of a pure substance (redrawn from [5])

In Figure 3-3 the change in phase behaviour of a substance at temperatures below, at and above the critical temperature, is illustrated on a P-v diagram. At temperatures very far away from the critical point ($T \gg T_c$) the pressure-volume curve only appears at high molar volumes and approaches the shape of a curve describing an ideal gas, i.e. P is proportional to $1/v$. As the temperature is lowered ($T > T_c$) the isotherm starts to show a slight indication of an inflection point. At the critical

temperature ($T = T_c$) the slope of the inflection is equal to zero, indicating the critical point. The mathematical definition of the critical point for a pure substance is given in Equation 3-1 and Equation 3-2 [6].

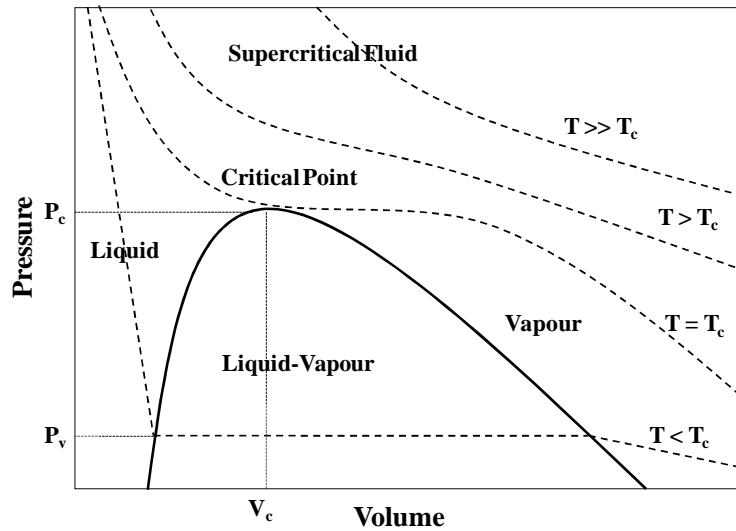


Figure 3-3 Isothermal P - v behaviour of a pure substance at temperatures below, equal to, and above the critical temperature

$$\left(\frac{\partial P}{\partial v}\right)_T = 0 \quad \text{Eq. 3-1}$$

$$\left(\frac{\partial^2 P}{\partial v^2}\right)_T = 0 \quad \text{Eq. 3-2}$$

At temperatures lower than the critical temperature ($T < T_c$) the phase behaviour is divided into three areas: in the liquid phase the pressure changes dramatically with small changes in molar volume, while changes in pressure due to changes in molar volume are more subtle in the vapour phase. Between the liquid and vapour phase regions, a liquid-vapour mixture co-exists.

3.2 Properties of Supercritical Fluids

3.2.1 Density

The characteristic features of the critical state of pure fluids are: (a) the disappearance of the difference between vapour and liquid states; (b) the divergence of the compressibility, and (c) the phenomenon of critical opalescence [6]. All of the abovementioned features are consequences of the unique density behaviour exhibited by substances near their critical point.

At subcritical temperatures the densities of the co-existing liquid and vapour phases differ significantly, giving rise to the formation of a distinct meniscus separating the liquid and vapour phases. As the temperature approaches the critical temperature of the substance, the density of the liquid phase decrease due to thermal expansion and the density of the vapour phase increase due to the rise in pressure [7]. The densities of the two co-existing phases thus approach one another and the meniscus separating them become less distinct. At the critical temperature the meniscus disappear, giving rise to the formation of a single homogenous phase – the supercritical phase. A substance in its supercritical phase display properties intermediate between those of liquids and gasses (see Table 3-1).

Table 3-1 Comparison between properties of gases, supercritical fluids and liquids [8]

Physical property	Gases	Supercritical fluids	Liquids
Density (kg/m ³)	1	200-1000	600-1600
Diffusivity (m ² /s)	10 ⁻⁵	10 ⁻⁷	10 ⁻⁹
Viscosity (kg/m.s)	10 ⁻⁵	10 ⁻⁴	10 ⁻³

Most supercritical processes are conducted at $1 < T_r < 1.15$ and $1 < P_r < 2$, and thus it is necessary that the behaviour of the fluid at this point is well understood [9]. Near the critical point of a substance, the density changes radically with a small change in temperature or pressure. The ability to tune the density and consequently the solubility of a solute is a characteristic of supercritical fluids that make them ideal solvents. The density is firstly adjusted to dissolve as much as possible of the desired solute, and once removed from the matrix of compounds, the density is adjusted again by changing the pressure or temperature to allow the solute to precipitate from the solvent. From Figure 3-4 it is clear that at a constant pressure the solubility of a low-volatility substance will increase with

temperature in a subcritical solvent until it reaches the critical temperature. Above the critical temperature the solubility will decrease if operating at a “low” pressure, and increase further if operating at a “high” pressure. For most systems “medium” pressure refers to 10 MPa [10].

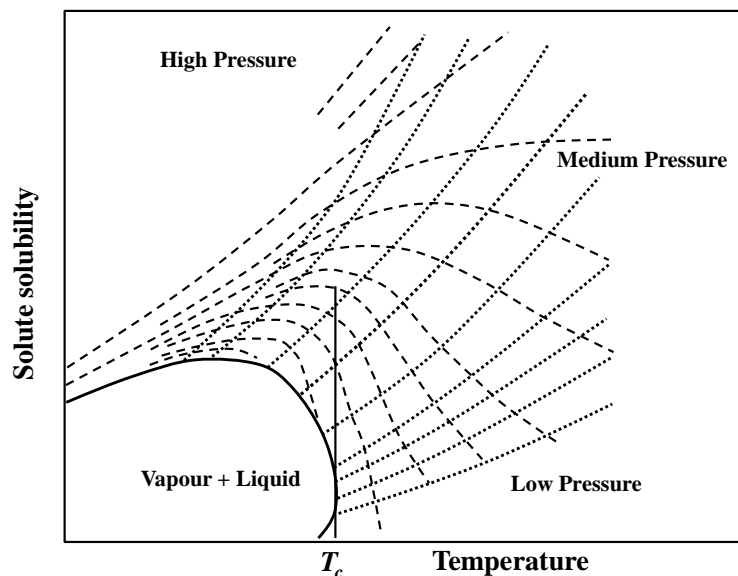


Figure 3-4 Variations in solubility of a low-volatility substance in a subcritical ($T < T_c$) or supercritical ($T > T_c$) solvent as a function of process temperature, process pressure (-----) and solvent density (·····) (redrawn from [10])

At “low” pressures, the decrease in solubility of a low-volatility substance is caused by the rapid decrease in solvent density and consequently solvent power [10]. At “high” pressures, however, the density change with temperature is more moderate and the increase in vapour pressure of the solute will dominate the behaviour [10].

The large density fluctuations close to the critical point of a substance also give rise to a phenomenon known as critical opalescence. Critical opalescence is the scattering of visible light. The occurrence of critical opalescence indicates that the density fluctuations have a range comparable with the wavelength of visible light, which exceeds molecular dimensions up to the order of 10^3 [6]. Visually, critical opalescence appears milky white in reflected light and dark in transmitted light.

3.2.2 Diffusivity and Viscosity

The most important transport properties concerning supercritical fluids and their applications are diffusivity and viscosity. These two properties, together with the density, govern the mass and energy transfer rates in supercritical fluids.

Diffusivity refers to the transport of mixture components along a concentration gradient. In supercritical fluids diffusion is generally faster than in liquids. The self-diffusivity of supercritical CO₂ (which is approximately the same as the diffusivity of a similarly sized solute molecule in supercritical CO₂) is 1 to 2 orders of magnitude higher than the diffusivity of solutes in liquids [11]. Similar to the trends observed for density, the diffusivity of a supercritical solvent changes rapidly in the critical region. Diffusivities of supercritical fluids are usually measured with specialized equipment and non-intrusive techniques e.g. solid dissolution, capillary peak broadening, photon resolution spectroscopy and nuclear magnetic resonance spectroscopy, and consequently such data is scarce [12].

Viscosity is the measure of resistance of a fluid that is being transformed by either shear or tensile stress. The viscosities of supercritical fluids are much lower than those of liquids which lead to more favourable hydrodynamic behaviour when it is pumped or flowing through a packed bed.

3.3 Supercritical Fluid Fractionation

Supercritical separation processes are most favourable for the extraction of small quantities of non-volatile solutes from solid matrices (supercritical fluid extraction) or liquid mixtures (supercritical fluid fractionation) where conventional methods do not attain the required separation. Many studies and investigations have been conducted on SFF processes as an alternative for distillation, enhanced distillation, and liquid-liquid extraction, but it has been found that where these other techniques are feasible, a high pressure process usually cannot compete economically [13]. However, when conventional separation methods do not achieve the required separation, or requires extreme operating temperatures which can lead to product degradation, SFF can be considered.

SFF capitalizes on both the difference in mixture component volatilities (the driving force of distillation) and the difference in interaction between mixture components and solvent (the driving force of liquid-liquid extraction), to separate a binary or multi-component mixture [11].

3.3.1 Definition of Terms Used

Throughout the manuscript, the following definitions apply:

- desired component: the chemical species that is targeted for removal from the feed matrix and required to report to the overheads product
- undesired component: the chemical species not to be dissolved by the supercritical solvent, and required to stay part of the feed matrix during fractionation/extraction and consequently report to the bottoms product
- overheads product (also referred to as the loaded solvent): the solvent that exits the top of the fractionation/extraction column that contains the desired components removed from the feed mixture
- bottoms product (used interchangeably with the term, raffinate): the product stream that exits at the bottom of the fractionation/extraction column and that contains all the residual compounds not removed by the supercritical solvent from the feed matrix
- extract: the liquid/solid product that exits the bottom of the separator and that represents one of the products of the separation process

3.3.2 Modes of Operation

There are two main modes of operation used in SFF processes: the single-stage or batch mode (Figure 3-5), and the counter-current multi-stage mode (Figure 3-6) [10].

Both the single-stage and multi-stage modes of operation consist of two distinct steps: extraction and separation. The extraction chamber is a high pressure vessel to which two streams are fed: the feed stream containing the mixture from which a specific compound or group of compounds are to be removed, and the solvent stream containing the solvent in its supercritical state. The supercritical solvent flows through the extraction chamber and selectively absorbs a certain compound or group of compounds from the feed mixture. The specific compounds and their respective concentrations in the loaded solvent are determined by the underlying thermodynamic phase behaviour of the system, which can be controlled to a certain extent by controlling the temperature and pressure conditions in the extraction vessel. The loaded solvent stream flows to a separator vessel where the conditions differ from that in the extraction vessel. The temperature and pressure

3 | Supercritical Fluid Processing

conditions in the separator vessel are usually selected to decrease the solubility of the extracted compounds in the solvent. The extracted compounds are freed from the solvent and recovered from the separator. The clean solvent is recompressed and recycled to the extraction chamber.

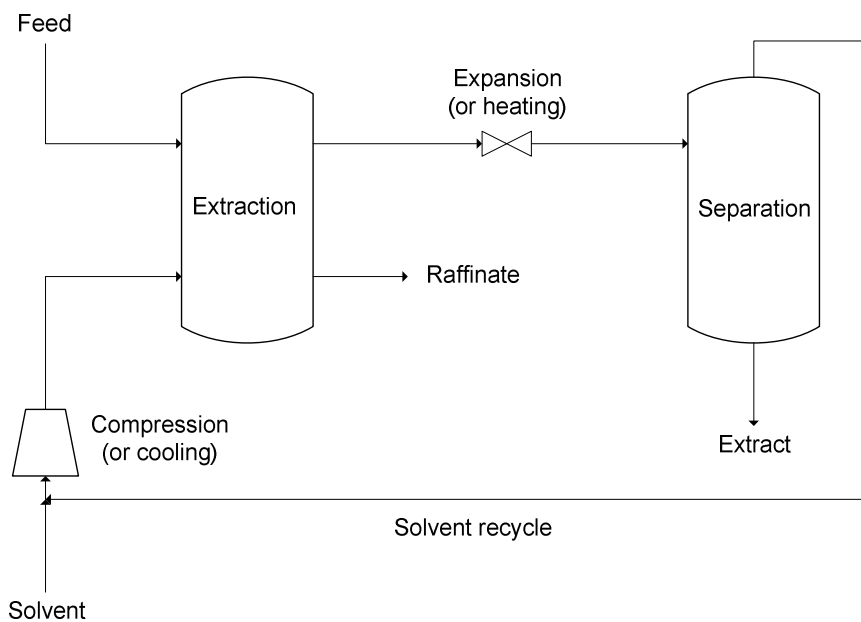


Figure 3-5 Schematic diagram of a single-stage supercritical fluid extraction process

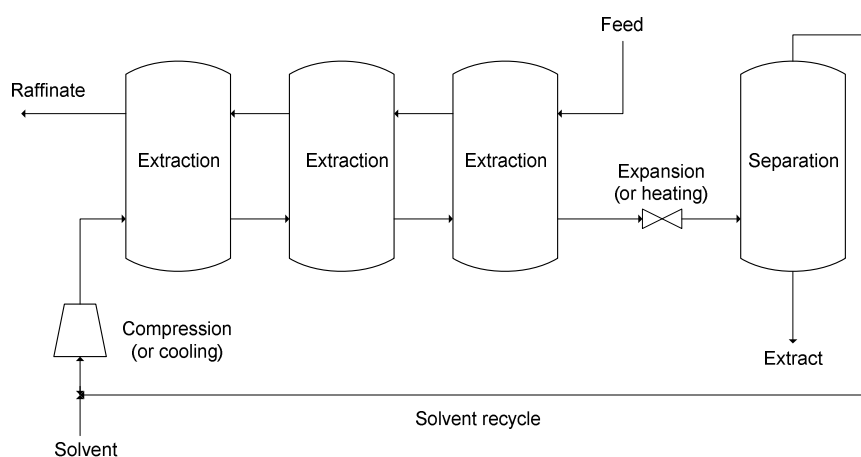


Figure 3-6 Schematic diagram of a counter-current multi-stage supercritical extraction process

In most cases where extraction from solids is concerned, the single-stage or batch mode of operation is employed, since solids are difficult to handle continuously in pressurized vessels [10]. For feed mixtures in the liquid state, the extraction/fractionation process is usually carried out in a counter-current multistage mode, since this is the most effective way to address their generally low separation factors [10].

In the counter-current multi-stage mode, each stage of extraction/fractionation can be operated at different temperature and pressure conditions to ensure the maximum removal of the desired compound by the solvent. When the counter-current multi-stage extraction/fractionation process is conducted in a continuous manner, the stages are attained by a column fitted with random or structured packing. In such cases the stage temperatures are usually kept constant and the stage pressures varied according to the pressure drop in the column.

The continuous counter-current extraction/fractionation processes works well to separate two compounds from a mixture where the compounds differ in their solubility in the supercritical solvent. It can, however, also be used to split multi-component mixtures. The process must then be designed to allow the key components that need to be separated to attain their maximum concentrations at the two column ends, while the accompanying compounds will distribute themselves along the column height. Such a process is typically referred to as a supercritical fluid fractionation process, since each product stream will contain a different fraction of all the components present in the feed stream.

3.3.3 Evaluation of SFF Process Performance

There are many ways to evaluate the performance of a SFF process, but in this work the main parameters considered are: the extract-to-feed ratio, the solvent-to-feed ratio, the component selectivity, the selectivity ratio and the recovery. These parameters provide insight into both the economic and technical feasibility of the process.

The extract-to-feed ratio (Equation 3-3) is an indication of the product yield and can be used to evaluate the limits of the operating window. Theoretically operation is possible at extract-to-feed ratio values of 0 to 1.

$$\frac{E}{F} = \frac{\dot{m}_{extract}}{\dot{m}_{feed}} \quad \text{Eq. 3-3}$$

The solvent-to-feed ratio (Equation 3-4) is an important economic factor, since it indicates the amount of solvent required, as well as the capacity of the process vessels.

$$\frac{S}{F} = \frac{\dot{m}_{\text{solvent}}}{\dot{m}_{\text{feed}}} \quad \text{Eq. 3-4}$$

The third important parameter to consider is the component selectivity (Equation 3-5). The component selectivity is important when evaluating the technical feasibility of the process. It is expressed, for each component, as the ratio of the mass fraction of that component in the extract product stream to the mass fraction of the same component in the bottoms product stream.

$$S_i = \frac{Y_{i,\text{extract}}}{X_{i,\text{bottoms}}} \quad \text{Eq. 3-5}$$

The component selectivity indicates the degree of separation that occurs for each component. A component selectivity value of 1 indicates that a component will exist in similar concentrations in both product streams – this is usually not desirable. A value much larger than 1 will indicate that a component will attain a large concentration in the extract product stream, while a value of less than 1 will indicate a larger concentration of the component in the bottoms product stream.

The selectivity ratio is a parameter that takes into account the aim of the separation process and expresses the separation performance of the process with regard to the defined separation task. The selectivity ratio (Equation 3-6) can be calculated for both the extract and/or the bottoms product stream, but it finds its main application in the optimization of process conditions when calculated for the main product stream.

$$SR = \frac{\sum S_{i,\text{desired}}}{\sum S_{i,\text{undesired}}} \quad \text{Eq. 3-6}$$

In defining the separation task, the main product stream and the main component(s) required in that stream, must be identified. The selectivity ratio can then be calculated for the main product stream, by giving the ratio of the sum of the component selectivity of the desired components, to the sum of the component selectivity of the undesired components. The selectivity ratio is not intended to be evaluated as a standalone value, but rather as a tool for comparing the separation performance of a process at different operating conditions. If the extract product stream is the main product stream, larger values for the selectivity ratio will indicate better separation performance. If the main product stream is the bottoms product stream, a smaller value for the selectivity ratio will indicate better separation performance.

The recovery refers to the percentage of the desired components fed to the column, which reports to the main product stream.

$$\% R_{product\ stream} = \frac{(\sum \dot{m}_{i,desired})_{product\ stream}}{(\sum \dot{m}_{i,desired})_{feed}} \times 100 \quad \text{Eq. 3-7}$$

The proper use of the evaluative parameters can be explained at the hand of the following simple example:

A feed stream contains component A, component B and component C, and is required to be separated by pure solvent S. The separation task is to remove component A from the feed mixture. Component A is the main component required in this separation process, and will report the extract product stream. Component B and C will report to the bottoms product stream and are not the main products required from this separation process. The separation performance can now be evaluated by determining the performance parameters as indicated:

$$\frac{E}{F} = \frac{\dot{m}_{(A+B+C),extract}}{\dot{m}_{(A+B+C),feed}}$$

$$\frac{S}{F} = \frac{\dot{m}_S}{\dot{m}_{(A+B+C),feed}}$$

$$S_A = \frac{Y_{A,extract}}{X_{A,bottoms}}$$

$$S_B = \frac{Y_{B,extract}}{X_{B,bottoms}}$$

$$S_C = \frac{Y_{C,extract}}{X_{C,bottoms}}$$

$$SR_{extract} = \frac{s_A}{(s_B + s_C)}$$

$$\% R_{extract} = \frac{(\dot{m}_A)_{extract}}{(\dot{m}_A)_{feed}} \times 100$$

3.3.4 Advantages and Disadvantages

The advantages of using SFF processes are as follows:

- The density, and therefore the solvent strength of the supercritical fluid, can be adjusted by changing the operating conditions, to control the selectivity and yield of the process.
- Supercritical fluids generally have improved transport properties compared to liquids, that allow for easier pumping and flow through packing material, which leads to faster processing times and improved mass transfer.
- The solvent can be easily recovered and recycled.
- For high molecular mass products there is minimal solvent residue in the product, due to the fact that most supercritical fluids are gasses at ambient conditions.
- For the processing of high molecular mass products the operating temperatures are just above the critical temperature of the solvent and well below the boiling temperature of the low-volatility solute, allowing the processing of heat sensitive products.
- When using CO₂ as the supercritical solvent, the fluid is inert, non-toxic, non-flammable, inexpensive, easily acquired and usable at mild temperatures.

The main disadvantages of SFF processes are:

- High operating pressures are required, which require the use of more expensive equipment.
- Complicated phase behaviour occurs for supercritical mixtures, which cannot be easily predicted by conventional or modified equations of state.

3.4 Selecting a Supercritical Solvent

During the past few decades many compounds have been investigated as possible supercritical solvents. The most common solvents used in high pressure binary systems are given in Table 3-2 along with their critical properties.

Table 3-2 Critical properties of compounds commonly used as supercritical solvents [11]

Solvent	Critical Temperature (K)	Critical Pressure (MPa)
CO ₂	304.3	7.38
Ethane	305.4	4.88
Ethylene	282.5	5.04
Propane	369.9	4.25
Propylene	365.1	4.62
Cyclohexane	553.5	4.07
Isopropanol	508.4	4.76
Benzene	562.2	4.89
Toluene	591.8	4.11
<i>p</i> -Xylene	616.3	3.52
Chlorotrifluoromethane	302.1	3.92
Trichlorofluoromethane	471.3	4.41
Ammonia	405.7	11.28
Water	647.4	22.05

The choice of supercritical solvent is governed by many factors: the availability, the safety concerns, the solubility of the compounds, the compound selectivity, etc.

Irrespective of its complex phase behaviour CO₂ is still the most widely used supercritical solvent. This is due to its low critical temperature and the fact that it is non-toxic, non-flammable, easy to acquire and inexpensive. According to Schwarz [7] CO₂ works well as a solvent for fluorinated compounds, but due to its polar nature it does not solvate high molecular mass hydrocarbons and polymers very well. The detergent range alkanes and alcohols that were used in this investigation have a relatively low molecular mass compared to other hydrocarbons for which binary phase equilibrium data with CO₂ have been successfully measured. Published data on CO₂ + *i*-alcohol [14,15] and CO₂ + *n*-alkane [15,16] systems within the C₈ – C₂₀ carbon number range, revealed that reasonably low (< 30 MPa) total solubility pressures can be expected for the

compounds investigated. It would thus be advisable to consider CO₂ as a possible supercritical solvent for the desired separation, as this would be the solvent of choice in large scale industrial applications.

Ethane and ethylene are also considered as attractive supercritical solvents, due to their relatively low critical temperatures – similar to that of CO₂. These two compounds also have the added advantage of low critical pressures. Due to the similarity in the molecular structures, it is expected that ethane and ethylene will work well with high molecular mass hydrocarbons and polymers.

The project scope and the accompanying limitations allowed for the investigation of one additional solvent, and thus ethane was selected as the other supercritical solvent to consider for the desired separation. Data found in the literature for ethane + *l*-alcohol [17] and ethane + *n*-alkane [18] systems, within the detergent range, revealed that the total solubility pressures are slightly lower (< 20 MPa) than that of the same compounds in supercritical CO₂. For similar separation performance, the solvent that allows for operation at lower pressures holds a distinct advantage. However, ethane is flammable and much more expensive than CO₂ – a factor that will have to be considered in the economic evaluation of the proposed SFF process.

In Chapter 5 the solubility and phase behaviour of the compounds selected for investigation in this work, will be compared in both supercritical CO₂ and ethane. Such a comparison will reveal if any one of these solvents are superior in component selectivity – one of the most important factors to consider in determining the technical feasibility of the proposed SFF process.

3.5 SFF Pilot Plant Data for Similar Systems

An in-depth literature review revealed that very little supercritical pilot plant tests have been done on alkane and/or alcohol systems. SFF is mainly used in industrial applications where the extraction of compounds from natural products like seed oils, has proven to be feasible. The compounds most often extracted from natural oils and plant materials are carotenoids, lipid materials, flavour and fragrance compounds, triterpenes and sterols, alkaloids, mycotoxins and others [19]. Literature sources that provide data on the SFF of systems closely related to those investigated in this study are discussed in this section. These studies provide good insight into the possible ranges of the

operating parameters and also on how certain operating parameters influence the selectivity and capacity of the solvent.

3.5.1 Separation of *n*-Alkanes

Crause [20] investigated the feasibility of an SFF process for the fractionation of a feed stream containing $C_{11} - C_{30}$ *n*-alkanes. Supercritical CO_2 and ethane was investigated as possible solvents. The operating conditions of the SFF pilot plant experiments conducted by Crause [20] are given in Table 3-3.

Table 3-3 Pilot plant specifications and operating conditions used by Crause [20]

Column diameter (m)	0.028	
Packed height (m)	2 x 2.16	
Type of packing	Sulzer DX structured packing	
Feed stream	<i>n</i> - $C_{11} - n$ - C_{30} alkanes	
Solvent	CO_2	Ethane
Feed flow rate ($kg/(s.m^2)$)	0.07 – 0.19	0.13 – 0.30
Solvent flow rate ($kg/(s.m^2)$)	1.80 – 6.32	1.80 – 4.51
Solvent/Feed Ratio	15 - 65	6 - 29
Operating pressures (MPa)	10.0 – 14.5 ($P_r = 1.36 - 1.96$)	6.6 – 8.8 ($P_r = 1.35 - 1.80$)
Operating temperatures (K)	328 – 338 ($T_r = 1.08 - 1.11$)	333 ($T_r = 1.09$)
Reflux Ratio	0 and 1.4 – 13.7	0 and 2.5 – 7.2

The results of this study were evaluated according to how well the feed mixture could be fractionated into product streams with smaller ranges of carbon numbers. Crause [20] found that the separation efficiency was poor, with both the overheads and bottoms product having a large range of alkanes with different hydrocarbon backbone lengths. With the introduction of reflux, however, the separation performance was increased dramatically, with significantly more light hydrocarbons and less heavy hydrocarbons reporting to the overheads product.

From the work done by Crause [20] it was thus concluded that an SFF process can effectively split a feed stream containing *n*-alkanes with a range of carbon numbers, into two product streams

with carbon number distributions that differ from that of the feed stream, i.e. *n*-alkanes can be separated according to their molecular weight. Crause [20] also contributed by showing that the use of reflux provide sharper cuts in the product streams.

3.5.2 Separation of *n*-Alkanes and *I*-Alcohols (Part I)

Bonthuys et al. [1] conducted SFF experiments on a mixture of *I*-dodecanol (C₁₂H₂₄O) and *n*-tetradecane (C₁₄H₂₈). These two compounds have proved most difficult to separate with a conventional distillation process, due to their low relative volatility. It thus seemed most appropriate to consider these components in determining if an SFF process is a feasible alternative technique to separate these components. Supercritical CO₂ and ethane were used as solvents, after propane was found to be inappropriate due to its poor component selectivity. Fourteen experimental runs were conducted at different operating conditions (see Table 3-4).

Table 3-4 Pilot plant specifications and operating conditions used by Bonthuys et al. [1]

Column diameter (m)	0.028	
Packed height (m)	2 x 2.16m	
Type of packing	Sulzer DX structured packing	
Feed stream	50/50 mixture of <i>I</i> -dodecanol and <i>n</i> -tetradecane	
Solvent	CO ₂	Ethane
Feed flow rate (kg/(s.m ²))	0.12 – 0.28	0.14 – 0.27
Solvent flow rate (kg/(s.m ²))	6.32 – 8.12	4.20 – 4.78
Solvent/Feed Ratio	23 - 67	18 - 30
Operating pressures (MPa)	9.2 – 13.3 (<i>P_r</i> = 1.25 – 1.80)	5.7 – 8.9 (<i>P_r</i> = 1.17 – 1.82)
Operating temperatures (K)	313 – 353 (<i>T_r</i> = 1.03 – 1.16)	314 - 345 (<i>T_r</i> = 1.03 – 1.13)
Reflux Ratio	0, 3.5 and 6.2	0 and 3.4

From the study by Bonthuys et al. [1] it was found that SFF is a viable technique to consider for the separation of a primary linear alcohol and a linear alkane, where the compounds have similar boiling points (or low relative volatility).

3.5.3 Separation of *n*-Alkanes and *l*-Alcohols (Part II)

The study by Bonthuys et al. [1] was continued by Schwarz et al. [2] and in the second part of the investigation the influence of the process parameters was directly addressed and the controllability of the system investigated by determining the size of the operating window. More experiments were conducted for the same system (*l*-dodecanol and *n*-tetradecane) with both supercritical CO₂ and ethane as the respective solvents. The ranges of the parameters investigated are set out in Table 3-5.

Table 3-5 Pilot plant specifications and operating conditions used by Schwarz et al. [2]

Column diameter (m)	0.028	
Packed height (m)	2 x 2.16m	
Type of packing	Sulzer DX structured packing	
Feed stream	50/50 mixture of <i>l</i> -dodecanol and <i>n</i> -tetradecane	
Solvent	CO ₂	Ethane
Feed flow rate (kg/(s.m ²))	0.08 – 0.22	0.11 – 0.26
Solvent flow rate (kg/(s.m ²))	3.61 – 8.12	4.29 – 4.69
Solvent/Feed Ratio	27 - 106	17 - 38
Operating pressures (MPa)	8.2 – 15.0 ($P_r = 1.11 - 2.03$)	6.2 – 9.2 ($P_r = 1.27 - 1.89$)
Operating temperatures (K)	312 – 354 ($T_r = 1.03 - 1.16$)	315 - 354 ($T_r = 1.03 - 1.16$)
Reflux Ratio	0, 6.6 and 8.8	0, 4.5 and 9.2

One of the aims of the study by Schwarz et al.[2] was to determine the operating window of the process. A larger operating window allows for easier process controllability. It was found that at lower temperatures the selectivity of the system is very good, while at higher temperatures the controllability is very good.

When using CO₂ as the solvent, the process is much more sensitive to variations in the temperature compared to when ethane is used as the supercritical solvent. Generally, the controllability of the process was much better when utilizing supercritical ethane as the solvent. With supercritical CO₂ as the solvent, reflux is necessary to ensure good selectivity, but with supercritical ethane as the solvent, reflux is not necessary.

An investigation into the operating window regarding the solvent-to-feed ratio revealed that it is a less important parameter to consider than temperature and pressure when considering the controllability of the process. Small changes in the solvent-to-feed ratio and solvent flow rate should not influence the product qualities. According to Schwarz et al. [2] the hydrodynamics and energy principles should rather be considered when determining the optimum solvent-to-feed ratio and solvent flow rate.

3.6 SFF Process Modelling

The use of an accurate process model allows the prediction of the behaviour of a system at certain conditions. Process modelling involves the simultaneous solution of a large number of equations, and thus it only became popular when computerized calculations became possible. Computer-aided design, simulation and optimization in the chemical processing industry have grown dramatically during the past decades. Along with this, the development of improved thermodynamic models and prediction methods for physicochemical properties also occurred. The use of improved thermodynamic and predictive property models in combination with rigorous mathematical modelling of unit operations, opens the way to the application of computer modelling and optimization of supercritical processes – which is of great interest, considering the cost of high pressure pilot plant facilities and industrial scale experimentation [21].

The modelling of counter-current fluid-fluid processes (e.g. SFF) are mainly approached in two ways: the equilibrium-stage approach and the mass-transfer-rate-based approach. Both these models have been successfully applied to SFF processes as discussed in the examples given by Diaz and Brignole [21]. In this study the equilibrium-stage approach will be followed. It is often perceived to be the less complex approach since it requires fewer input parameters and fewer equations to solve simultaneously (see Table 3-6).

A process model can only produce accurate results when the input parameters are as close as possible to the real values. Many of the physical properties required in these models are not available in literature since they can only be measured by expensive equipment and/or complex techniques for high pressure systems. Often the physical parameters of high pressure systems are estimated by a semi-empirical model, which opens the door to erroneous values being used in the process model. Since the mass-transfer-rate-based model requires significantly more input parameters it can be

viewed as the approach with more possibilities for error, if the input parameters are estimated rather than measured. The mass-transfer-rate-based approach requires information that are much scarcer for high pressure systems, like the mass and energy transfer coefficients, and hydrodynamic properties (see Table 3-6).

Table 3-6 Comparison between the input requirements of the two separation process modelling approaches[22]

	Equilibrium-stage	Mass-transfer-rate-based
Physical Property Requirements	Activity coefficients Vapour Pressure Fugacity coefficients Density Enthalpy	Activity coefficients Vapour Pressure Fugacity coefficients Density Enthalpy Diffusivities Viscosities Surface tension Thermal conductivity Mass-transfer coefficients Heat-transfer coefficients Interfacial areas
Model Requirements: Equations	Mass balances Energy balances Equilibrium equations Summation equations	Phase mass balances Phase energy balances Equilibrium equations Summation equations Mass transfer in vapour phase Mass transfer in liquid phase Energy transfer

Both the approaches require an accurate thermodynamic model to describe the phase behaviour of the system involved. This is another opportunity for error to be introduced into the process model. The development and improvement of equations of state (EoS) that can accurately describe the phase behaviour of systems at high pressure have been a main focus area of research in the supercritical field. This topic will be discussed in detail in the following chapter, but it is important to note that an accurate thermodynamic model is essential for the development of an accurate process model. The shortcomings of a thermodynamic model will be much more prominent in the equilibrium-stage approach, while it may be masked by errors in the physical properties used in the mass-transfer-rate-

based approach. By using the equilibrium-stage method as a first attempt to model the SFF of the detergent range alkane/alcohol system used in this investigation, the detection of possible problem areas in the basic requirements for process models will be easier. Once the problem areas in the basic requirements, which is similar for both the equilibrium-stage and the mass-transfer-rate-based model, have been dealt with, the more complex process modelling approach can be attempted.

3.6.1 Equilibrium-stage Modelling Concept

The equilibrium-stage model is developed for a continuous, steady-state vapour-liquid or liquid-liquid separator consisting of a number of stages arranged in a counter-current cascade [13]. In Figure 3-7 a schematic representation of an equilibrium stage is shown. The following assumptions apply [13]:

- phase equilibrium is achieved at each stage,
- no chemical reactions occur,
- entrainment of liquid drops in vapour and occlusion of vapour bubbles in liquid are negligible.

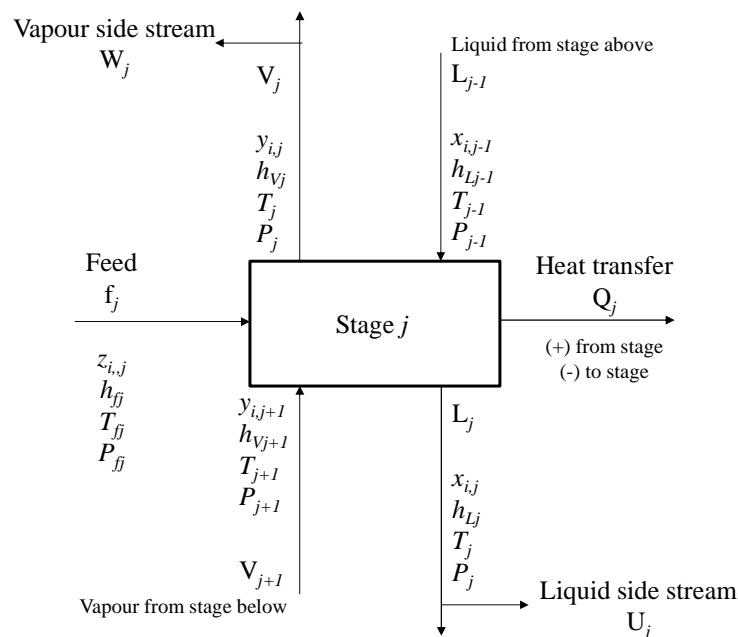


Figure 3-7 Counter-current equilibrium stage (redrawn from [13])

Each stage in a counter-current cascade is modelled by four sets of equations: component material balances (Equation 3-8), equilibrium relations (Equation 3-9), summation equations (Equation 3-10 and 3-11), and component energy balances (Equation 3-12).

$$M_{i,j} = L_{j-1}x_{i,j-1} + V_{j+1}y_{i,j+1} + F_jz_{i,j} - (L_j + U_j)x_{i,j} - (V_j + W_j)y_{i,j} = 0 \quad \text{Eq. 3-8}$$

$$E_{i,j} = y_{i,j} - K_{i,j}x_{i,j} = 0 \quad \text{Eq. 3-9}$$

$$(S_y)_j = \sum_{i=1}^C y_{i,j} - 1.0 = 0 \quad \text{Eq. 3-10}$$

$$(S_x)_j = \sum_{i=1}^C x_{i,j} - 1.0 = 0 \quad \text{Eq. 3-11}$$

$$H_j = L_{j-1}h_{L,j-1} + V_{j+1}h_{V,j+1} + F_jh_{F_j} - (L_j + U_j)h_{L,j} - (V_j + W_j)h_{V,j} - Q_j = 0 \quad \text{Eq. 3-12}$$

In general, the phase equilibrium ratio ($K_{i,j}$) and vapour and liquid phase enthalpy ($h_{V,j}$ and $h_{L,j}$) are functions of stage temperature (T_j) and pressure (P_j), as well as the component mole fractions of the streams leaving the stage. If Equations 3-8 to 3-12 are set up for C components and N stages, a large number of nonlinear equations are derived, that can only be solved by iterative techniques. Since the development of the equilibrium-stage model many algorithms and iterative solution strategies have been developed for the simultaneous solution of the set of nonlinear equations that evolve around such a counter-current cascade. In general, the solution procedure entails equation partitioning in conjunction with equation tearing and/or linearization by Newton-Raphson techniques [13]. Nowadays, these procedures are readily programmed into commercial process simulators, and converge rapidly without excessive use of computer storage space. Seader and Henley [13] give an in-depth discussion on the algorithms employed in techniques like the bubble-point method for distillation (for compounds with a narrow range of volatility), the sum-rates method for absorption and stripping (for compounds with a wide range of volatility), and the isothermal sum-rates method for liquid-liquid extraction.

3.6.2 Equilibrium-stage Modelling in Aspen Plus®

In this investigation the commercial process simulation package, Aspen Plus®, will be used during the thermodynamic and process modelling stages. Commercial simulation software finds its

main use in the early stages of determining the process feasibility, while highly specialized in-house developed simulation programs are more suitable to use in later stages of process optimization. Since in-house developed simulation programs are expensive to set up, the feasibility of a process must be confirmed either through pilot plant tests or commercial simulation software, before resources are allocated to the development of highly specialized simulators.

In this section the methodology and input requirements for the modelling of an SFF process in Aspen Plus[®] are discussed. The steps to set up a process model are as follows:

1. Build a process flow diagram consisting of process units and connecting process streams.
2. Characterize the feed mixture and specify the chemical components that will be present throughout the process. If compounds are not listed in the Aspen Plus[®] database, an entry must be created for such a compound. Relevant properties of such compounds must be entered by the user or estimated with built-in functions.
3. Specify a thermodynamic model to be used during the process simulation. If necessary, adjust the parameters of the thermodynamic model to improve its accuracy.
4. Specify the operating conditions for each process unit and all input process streams.
5. Select appropriate convergence algorithms and relevant parameters, if the default selections are not preferred.

The units required to build a process flowsheet can easily be found in the Aspen Plus[®] model library. It is worth mentioning that there are a number of columns available in the Aspen Plus[®] model library, with none specifically developed for SFF. The columns available in Aspen Plus[®] include shortcut distillation columns (*DSTWU*, *Distl* and *SCFrac*), rigorous fractionation columns (*RadFrac* and *MultiFrac*), a petroleum refining column (*PetroFrac*) and a liquid-liquid extraction column (*Extract*).

From the choice of columns given in the Aspen Plus[®] model library the liquid-liquid extraction column closely resemble an SFF column. The fractionation columns only allow for the introduction of additional co-current feed streams, but the liquid-liquid extraction column allows for the addition of a solvent stream that flows in a counter-current manner to the feed stream. Use of the liquid-liquid extraction column model in Aspen Plus[®] is however limited to scenarios where the feed stream is

introduced at the top stage, i.e. scenarios where the column acts as a stripping section. Also, no provision was made for a reflux stream in the model, and thus if reflux is required it must be handled manually as an additional feed stream to the column.

3.6.3 Aspen Plus[®] Equilibrium-stage Modelling for Other Fluid-Fluid Systems

Diaz and Brignole [21] mentions a number of studies where liquid fed SFF plants were modelled. The majority of the simulations were conducted with a combination of in-house developed simulation programs and commercial algorithm solvers. The use of a commercial simulation program, like Aspen Plus[®], requires fewer resources compared to specialized in-house developed simulators and is very useful in the early stages of process design. Two examples of the application of Aspen Plus[®] in SFF process modelling are discussed below.

3.6.3.1 Deterpenation of Lemon Essential Oil

Benvenuti et al. [3] investigated the removal of terpenes from lemon essential oil (a mixture of mainly terpenes, oxygenates and sesquiterpenes). Experimental data were gathered and a model was developed in Aspen Plus[®] to simulate a single-stage semi-continuous extraction process utilizing supercritical CO₂. Good agreement was found between the simulated and experimental data, which served as verification for the selected thermodynamic model.

The thermodynamic characterization of the system was extended by simulating the more complex multi-stage continuous process in Aspen Plus[®]. In Table 3-7 the steps that were taken by Benvenuti et al. [3] to set up the multi-stage process in Aspen Plus[®] are given:

Table 3-7 Aspen Plus® model development by Benvenuti et al. [3]

Process flow sheet setup	
<i>Extraction</i>	Counter-current eight-stage column made up of consecutive flash drums operating at the same constant temperature and pressure.
<i>Separation</i>	Single-stage flash separator.
<i>Additional info</i>	Solvent recycle.
Component specification	
<i>Feed</i>	Feed oil was simulated as a mixture of five components: limonene, γ -terpinene, linalool, geranial and β -caryophyllene.
<i>Solvent</i>	CO ₂
Thermodynamic model	
<i>Model selected</i>	Peng-Robinson with Van der Waals mixing rules.
<i>Component constants</i>	Determined with group contribution methods.
<i>Adjustments to model</i>	Two binary interaction parameters for each solvent-solute pair were included (determined from experimental solubility data).
Process operating conditions	
<i>Extraction</i>	T = 316 K, P = 8.5 MPa, Feed flow rate = 6 kg/h, Solvent flow rate = effect investigated between 176 and 440 kg/h
<i>Separation</i>	T = 316 K P = effect investigated between 1.0 and 6.0 MPa
Convergence algorithms	
<i>Algorithm selected</i>	No information (assume default).

The results of the multi-stage Aspen Plus® process model developed by Benvenuti et al. [3] was not verified with experimental data. The Aspen Plus® model was only used to indicate that it is possible to upgrade the process from a single-stage semi-continuous process to a multi-stage continuous process, which is of greater practical interest.

3.6.3.2 Palm Oil Refining

In the study by Manan et al. [4] the use of supercritical CO₂ to simultaneously refine and recover valuable minor components in palm oil, were investigated. The development of the Aspen Plus® model used this investigation is shown in Table 3-8.

Table 3-8 Aspen Plus® model development by Manan et al.[4]

Process flow sheet setup	
<i>Extraction</i>	Counter-current twelve-stage column made up of consecutive flash drums operating at a fixed temperature and pressure
<i>Separation</i>	Single-stage flash separator
<i>Additional info</i>	Solvent recycle. Extract reflux.
Component specification	
<i>Feed</i>	Feed oil was simulated as a mixture of five components: tripalmitin, triolein, oleic acid, β -carotene and α -tocopherol.
<i>Solvent</i>	CO ₂
Thermodynamic model	
<i>Model selected</i>	Redlich-Kwong-Aspen with Van der Waals mixing rules.
<i>Component constants</i>	Determined with built-in property constant estimation methods.
<i>Adjustments to model</i>	Two temperature-dependant binary interaction parameters for each solvent-solute pair were included (determined from experimental solubility data). Temperature-dependant polar parameters for each pure component in the feed mixture were included (determined from experimental binary solubility data and/or extrapolated vapour pressure data).
Process operating conditions	
<i>Extraction</i>	T = effect investigated between 353 and 373 K, P = effect investigated between 20 and 30 MPa, S/F ratio = effect investigated
<i>Separation</i>	Unknown
Convergence algorithms	
<i>Algorithm selected</i>	No information (assume default)

The development of the thermodynamic model used in the study by Manan et al. [4] is discussed in more detail by Lim et al. [23]. Regression was performed on experimental solubility data to determine the polar and binary interaction parameters for the five components in the feed mixture. If reliable vapour pressure data for the components in the required temperature ranges could be found in literature, it was used, instead of the phase equilibrium data, to determine the polar parameters for the pure components. The maximum percentage average absolute deviation (%AAD) encountered during regression was 2.78% and 0.76% for the light and heavy phases respectively.

The predictive ability of the thermodynamic model for the multi-component mixture was verified by comparing the simulated data to experimental data. The maximum %AAD was calculated to be 5.06% and 0.275% for the light and heavy phases respectively.

The results generated by the process model are also compared to experimental pilot plant data and good agreement between the measured and calculated results was found.

3.7 Outcomes of this Chapter

The aim of this chapter is to provide the necessary background information on SFF processes to allow the reader to understand the workings of the process proposed in this work for the separation of detergent range alkanes and alcohols – thereby achieving Objective 2, as discussed in Chapter 1.

The key findings of this chapter are:

- The unique density behaviour of the supercritical fluid phase led to the development of supercritical separation processes. In a mixture the solubility of a solute(s) is directly affected by the density of the supercritical fluid. The characteristic continuous density-temperature and density-pressure relationship of the supercritical fluid phase, provides a means of control over the solubility of low-volatility solutes.
- There are two main modes of operation for supercritical separation processes – single-stage and multi-stage. Single-stage operation is usually applied to extraction processes where the feed is in the solid state, while multi-stage operation is more popular with liquid fed processes.
- By operating a multi-stage SFF process in a continuous manner, the contact stages can be represented by stages in a packed column.
- The solvent selection depends on a number of factors with the most important being the phase behaviour, i.e. the solubility and selectivity, of the components intended for separation.
- Previous pilot plant work [20] on the separation of a mixture of C_{11} – C_{30} *n*-alkanes showed that the *n*-alkanes distribute themselves along the column length according to carbon chain length (or molecular weight), with the light *n*-alkanes exiting in the extract product stream and the heavy *n*-alkanes exiting in the bottoms product stream.

- Previous pilot plant work [1] on the separation of an alkane-alcohol mixture, where the two compounds (*1*-dodecanol and *n*-tetradecane) have a low relative volatility, showed that the *n*-alkane can be separated from the *1*-alcohol with SFF.
- The size of the operating window of the SFF process determines the controllability thereof. Processes utilizing supercritical CO₂ as the solvent generally exhibits less controllability compared to processes utilizing supercritical ethane as the solvent [2].
- Previous studies [3,4,23] on the modelling of SFF processes in Aspen Plus® showed that it can be done successfully. It also indicated that the development of the thermodynamic is very important and must be verified before employed in the SFF process model.

From the information provided in this chapter it can be concluded that SFF is a potential process to consider for the separation of close-boiling detergent range *n*-alkanes from mixtures of alcohol isomers. However, the feasibility of the process for any application is dependent on the thermodynamic behaviour of the compounds involved. In the next chapter the phase behaviour of mixtures at high pressures will be discussed by looking at generalized phase diagrams and thermodynamic model predictions. Later, in Chapter 5, the phase behaviour of the specific compounds used in this investigation will be discussed in more detail.

3.8 Nomenclature

Symbol/ Acronym	Description
AAD	Average absolute deviation
C	Number of components
E	Extract
F	Feed
f	Feed molar flow rate
<i>h</i>	Molar enthalpy
L	Liquid molar flow rate
m	Mass flow rate
N	Number of stages

Symbol/ Acronym	Description
<i>P</i>	Pressure
<i>Q</i>	Heat transfer rate
SFF	Supercritical Fluid Fractionation
<i>T</i>	Temperature
<i>V</i>	Vapour molar flow rate
<i>v</i>	Volume
S	Solvent
<i>s</i>	Selectivity
SR	Selectivity ratio
<i>U</i>	Liquid side stream molar flow rate
W	Vapour side stream molar flow rate
X	Mass fraction in heavy phase
<i>x</i>	Mole fraction in heavy phase
Y	Mass fraction in light phase
<i>y</i>	Mole fraction in light phase
z	Total mole fraction

Sub/Superscripts	Description
<i>c</i>	Critical
<i>i</i>	Component <i>i</i>
<i>j</i>	Stage <i>j</i>
<i>L</i>	Liquid/heavy phase
<i>r</i>	Reduced
<i>V</i>	Vapour/light phase

3.9 References

- [1] G.J.K. Bonthuys, C.E. Schwarz, A.J. Burger, J.H. Knoetze, Separation of alkanes and alcohols with supercritical fluids. Part I: Phase equilibria and viability study, *The Journal of Supercritical Fluids*. 57 (2011) 101 – 111.

-
- [2] C.E. Schwarz, G.J.K. Bonthuys, R.F. van Schalkwyk, D.L. Laubscher, A.J. Burger, J.H. Knoetze, Separation of alkanes and alcohols with supercritical fluids. Part II. Influence of process parameters and size of operating window, *The Journal of Supercritical Fluids*. 58 (2011) 352 – 359.
- [3] F. Benvenuti, F. Gironi, L. Lamberti, Supercritical deterpenation of lemon essential oil, experimental data and simulation of the semi-continuous extraction process, *The Journal of Supercritical Fluids*. 20 (2001) 29 – 44.
- [4] Z.A Manan, C.S. Lim, A.N. Mustapa, Development of a new process for palm oil refining based on supercritical fluid extraction technology, *Industrial & Engineering Chemistry Research*. 48 (2009) 5420 – 5426.
- [5] B. Hu, The universality of critical phenomena in chemical reactions in a binary liquid mixture, PhD Dissertation, The University of Alabama, 2009.
- [6] J.M.H. Levelt Sengers, Critical behaviour of fluids: concepts and applications, in: *Supercritical Fluids: Fundamentals for Application*, Kluwer Academic Publishers, The Netherlands, 1994.
- [7] C.E. Schwarz, Phase equilibrium of alkanes and supercritical fluids, Masters Thesis, Stellenbosch University, 2001.
- [8] D.J. Dixon, K.P. Johnston, *Supercritical Fluids*, Encyclopaedia of Separation Technology. (1997).
- [9] C. A. Eckert, B. L. Knutson, P. G. Debenedetti, Supercritical fluids as solvents for chemical and materials processing, *Nature*. 383 (1996) 313 – 318.
- [10] G. Brunner, Supercritical fluids: technology and application to food processing, *Journal of Food Engineering*. 67 (2005) 21 – 33.
- [11] M.A. McHugh, V.J. Krukoni, *Supercritical Fluid Extraction: Principles and Practice*, 2nd ed., Butterworth-Heinemann, Massachusettes, 1994.
- [12] K. K. Liong, P. A. Wells, N. R. Foster, Diffusion in supercritical fluids, *The Journal of Supercritical Fluids*. 4 (1991) 91 – 108.
- [13] J.D. Seader, E.J. Henley, *Separation Process Principles*, 2nd ed., John Wiley & Sons, Inc., New Jersey, 2006.

- [14] F.C.v.N. Fourie, C.E. Schwarz, J.H. Knoetze, Phase equilibria of alcohols in supercritical fluids: Part I. The effect of the position of the hydroxyl group for linear C₈ alcohols in supercritical carbon dioxide, *The Journal of Supercritical Fluids*. 47 (2008) 161 – 167.
- [15] A. Kordikowski, G. M. Schneider, Fluid phase equilibria of binary and ternary mixtures of supercritical carbon dioxide with low-volatility organic substances up to 100 MPa and 393 K: cosolvency effects and miscibility windows, *Fluid Phase Equilibria*. 90 (1993) 149 – 162.
- [16] I. Nieuwoudt, M. du Rand, Measurement of phase equilibria of supercritical carbon dioxide and paraffins, *The Journal of Supercritical Fluids*. 22 (2002) 185 – 199.
- [17] C.E. Schwarz, A.J. de Villiers, C.B. McClune, G.J.K. Bonthuys, A.J. Burger, J.H. Knoetze, High pressure phase equilibrium measurements of long chain alcohols in supercritical ethane, *The Journal of Supercritical Fluids*. 55 (2010) 554 – 565.
- [18] C.E. Schwarz, I. Nieuwoudt, J.H. Knoetze, Phase equilibria of long chain *n*-alkanes in supercritical ethane: Review, measurements and prediction, *The Journal of Supercritical Fluids*. 46 (2008) 226 – 232.
- [19] Q. Lang, C. M. Wai, Supercritical fluid extraction in herbal and natural product studies — a practical review, *Talanta*. 53 (2001) 771 – 782.
- [20] J.C. Crause, *Supercritical Fluid Extraction of Paraffin Wax*, PhD Dissertation, Stellenbosch University, 2001.
- [21] M.S. Diaz, E.A. Brignole, Modelling and optimization of supercritical fluid processes, *Journal of Supercritical Fluids*. 47 (2009) 611 – 618.
- [22] R. Taylor, R. Krishna, H. Kooijman, Real-world modelling of distillation, *CEP*. (2003) 28 – 39.
- [23] C.S. Lim, Z.A Manan, M.R. Sarmidi, Simulation modelling of the phase behaviour of palm oil-supercritical carbon dioxide, *Journal of the American Oil Chemists' Society*. 80 (2003) 1147 – 1156.

4. PHASE BEHAVIOUR OF MIXTURES AT HIGH PRESSURE

4.1 CLASSIFICATION OF BINARY PHASE BEHAVIOUR	60
4.1.1 Phase Diagrams of Types of Binary Mixtures	62
4.1.2 Trends Observed for Homologous Series.....	63
4.1.3 Extension to Multi-component Mixtures.....	64
4.2 METHODS OF MEASURING HIGH PRESSURE PHASE EQUILIBRIUM DATA	65
4.3 HIGH PRESSURE PHASE EQUILIBRIUM DATA FOR SIMILAR SYSTEMS	67
4.3.1 Binary Systems of C ₈ – C ₁₂ Alkanes with Supercritical Ethane or CO ₂	67
4.3.2 Binary Systems of C ₈ – C ₁₂ Alcohols with Supercritical Ethane or CO ₂	72
4.4 THERMODYNAMIC MODELLING OF HIGH PRESSURE PHASE EQUILIBRIUM DATA	78
4.4.1 Model Selection.....	78
4.4.2 Cubic Equations of State	79
4.4.2.1 <i>Pure Component Parameter Estimation</i>	81
4.4.2.2 <i>Binary Interaction Parameter Estimation</i>	82
4.4.2.3 <i>Advantages and Shortcomings of Cubic Equations of State</i>	83
4.5 OUTCOMES OF THIS CHAPTER	84
4.6 NOMENCLATURE.....	86
4.7 REFERENCES	87

The aim of this chapter is to provide insight into the general phase behaviour exhibited by mixtures when they exist at conditions above the critical point of one component. In the previous chapter it was mentioned that supercritical fluid fractionation (SFF) processes operate at conditions slightly above the critical point of the selected solvent ($1 < T_r < 1.15$ and $1 < P_r < 2$). The supercritical phase exhibits complex phase phenomena and it is of the utmost importance that the thermodynamics of mixtures at high pressures be fully understood before it can be successfully translated into process development. In this chapter the characterization of phase behaviour, methods of acquiring phase behaviour data and thermodynamic modelling of complex phase behaviour, will be discussed. Literature data on the phase behaviour of systems similar in nature to those investigated in this work are given to allow the reader to build an expectation of the phase behaviour that will be encountered for the systems investigated in this work.

4.1 Classification of Binary Phase Behaviour

A classification system was derived by van Konynenburg and Scott [1] that allows the classification of binary mixtures into six classes. As more systems were researched, the shortcomings of this method of classification were realised when certain binary systems, e.g. water + *l*-butanol and water + 2-butanol [2], did not fit into any of the classes proposed by van Konynenburg and Scott [1]. Later Bolz [3] developed a new classification system and accompanying nomenclature that allowed the classification of all systems. Although this new classification system is superior to that of van Konynenburg and Scott [1], most of the earlier research was presented according to the older classification system and translation between the systems can become tedious.

The classification system of van Konynburg and Scott [1] is still used today for systems that can be included therein, while the Bolz [3] classification system is not yet readily applied in research papers. In this work the phase behaviour of mixtures will be discussed according the classification system of van Konynenburg and Scott [1] (see Figure 4-1).

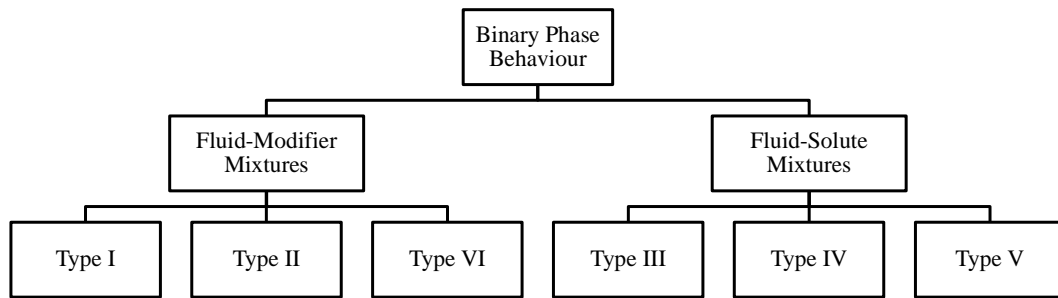


Figure 4-1 Van Konynenburg and Scott classification system of binary phase behaviour

The fluid-modifier class contains all the types of phase behaviour exhibited by symmetric systems and systems containing a solute with a molecular mass and critical temperature slightly higher than that of the solvent. A solute is usually added to slightly modify the solvation characteristics of the solvent. The main characteristics of the solvent that are affected by the addition of modifiers are: polarity, aromaticity, chirality and ability to solvate complex metal-organic compounds [4].

The fluid-solute class contains all the types of phase behaviour exhibited by systems containing a solute with a much higher molecular mass and critical temperature than that of the solvent. In this case the solvent is used to dissolve the solute, a characteristic of supercritical separation processes.

Although accurate experimental solubility and vapour-liquid equilibrium (VLE) data are required to determine the operating region of a supercritical separation process, knowledge of the type of phase behaviour can aid in determining the feasibility of such a process prior to conducting copious amounts of experimental work. If a binary mixture can be classified as a certain type based on limited amounts of solubility data, expected phase behaviour at other conditions can be anticipated.

The main difference between the types of phase behaviour within one class is the phase behaviour at temperatures below and slightly above the critical point of the solvent. For certain types of phase behaviour vapour-liquid-liquid equilibrium (VLLE) regions occur at conditions near the solvent critical point. Very few SFF processes are conducted at conditions near the critical point of the solvent, due to the difficulty associated with the controllability of the process at such conditions. Consequently, the phase behaviour of systems near the critical point of the solvent are often excluded from investigations. VLLE regions are thus not often observed which make it difficult to classify certain systems into one of the types proposed by van Konynenburg and Scott [1]. If, however, VLLE

regions are identified at conditions far away from the critical point of the solvent, operation of SFF processes at such conditions must also be avoided.

4.1.1 Phase Diagrams of Types of Binary Mixtures

The six types of phase behaviour as classified by van Konynenburg and Scott [1] are discussed briefly in this section, with more detailed discussions available elsewhere [2,5].

Pereda et al. [6] introduces a simple method of quick classification into one of the six types of phase behaviour (see Figure 4-2). For Type I phase behaviour complete miscibility is observed at all temperatures. If partial liquid miscibility occurs at subcritical temperatures, the system exhibits Type II phase behaviour. Type I phase behaviour is usually encountered in mixtures of components with similar molecular size and chemical nature, i.e. systems that do not deviate much from ideal behaviour. Type II phase behaviour is typically exhibited by non-ideal mixtures of components with similar sized molecules. When the liquid non-ideality persists at higher pressures and temperatures, the system is of Type III. When the difference in molecular size becomes significant in almost ideal systems, liquid-liquid immiscibility is observed near the critical temperature of the more volatile component. If, however, complete miscibility is recovered at low temperatures, the system can be classified as Type V. Type IV systems show discontinued liquid-liquid immiscibility, with immiscibility at low and high temperatures, but not at intermediate temperatures. Certain homologous series exhibit Type IV phase behaviour as a transition between Type V and Type III, e.g. $\text{CO}_2 + n$ -alkanes.

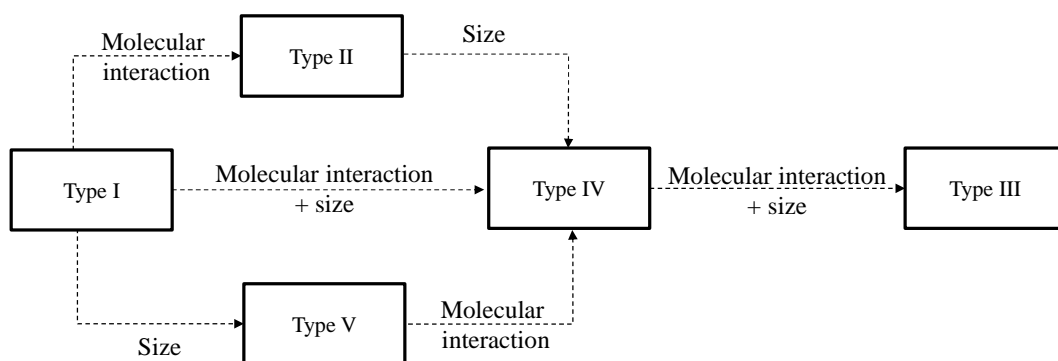


Figure 4-2 Main characteristics of a mixture that determines the type of phase behaviour (redrawn from [6])

4.1.2 Trends Observed for Homologous Series

Peters and Gauter [7] adopted three-phase experimental data from other authors to generate plots that show the transition of phase behaviour from Type II to Type IV to Type III for the homologous series $\text{CO}_2 + n$ -alkanes and $\text{CO}_2 + I$ -alcohols. These trends are depicted in Figure 4-3. At the high and low end of the carbon number range the three-phase region can be masked by the formation of a solute (S_B) or solvent (S_A) solid phase.

Similar plots were established with data from Peters [8] for the ethane + n -alkane and ethane + I -alcohol homologous series (see Figure 4-4). The classification of the type of phase behaviour was done with information provided by other sources [6,9].

The trends indicated in Figure 4-3 and Figure 4-4 can aid in determining whether a three phase region occur for mixtures of certain n -alkanes and I -alcohols with either CO_2 or ethane. The plots do not, however, indicate at what composition of the binary mixture the three phase region exists.

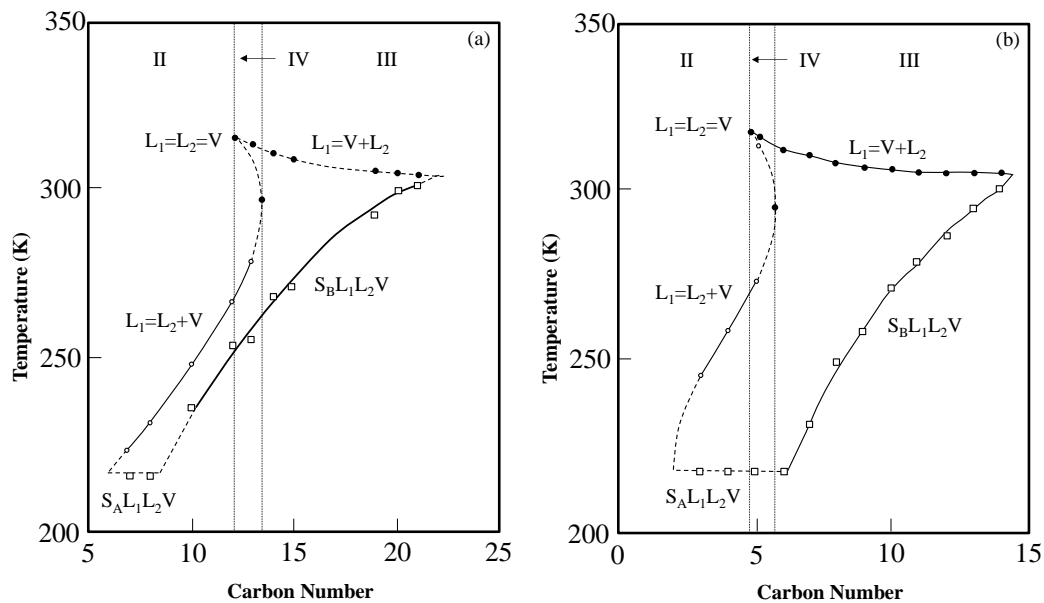


Figure 4-3 Trends observed for the phase behaviour of (a) $\text{CO}_2 + n$ -alkanes and (b) $\text{CO}_2 + I$ -alcohols (redrawn from [7])

4 | Phase Behaviour of Mixtures at High Pressure

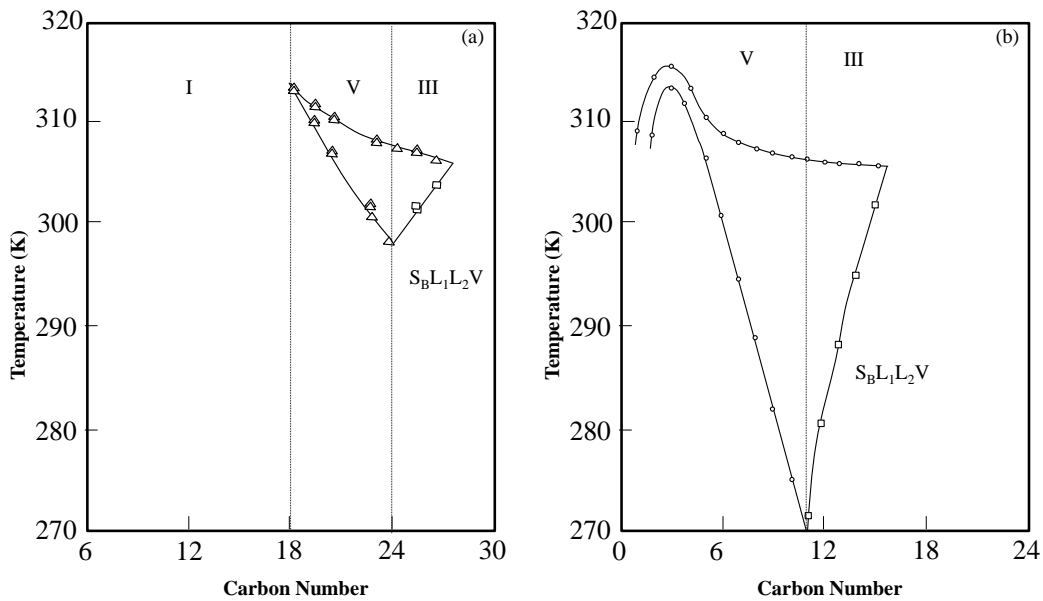


Figure 4-4 Trends observed for the phase behaviour of (a) ethane + n-alkanes and (b) ethane + 1-alcohols (redrawn from [8])

4.1.3 Extension to Multi-component Mixtures

In contrast to the systematic characterization of binary mixtures, investigations into ternary and multi-component mixtures have been fragmented and incomplete. This is mainly due to the fact that the characterization of multi-component mixtures is a time and resource consuming task. The full characterization of pure component and binary mixture phase behaviour requires the generation of points and lines, respectively, but the full characterization of critical ternary phase behaviour requires the generation of a composition-dependant surface [10]. The scarcity of ternary and multi-component data is further propagated by the more complex equipment required to measure VLE data for ternary and multi-component systems, compared to that required for binary systems.

The phase behaviour of some ternary mixtures are likely to be a simple extension of phenomena exhibited by the constituent binary mixtures, especially if the binary mixtures are of Type I or Type II [6]. If the constituent binary mixtures are of Type III, IV, V or VI, the resulting ternary mixture is likely to generate a diverse range of phenomena not traceable to the phenomena observed for the comprising binary mixtures.

4 | Phase Behaviour of Mixtures at High Pressure

Certain solute mixtures (specifically *n*-alkane + *I*-alcohol mixtures) with near critical CO₂, exhibit co-solvency effects and formation of holes in the three-phase surface [7]. Also, in a very narrow solute-solute composition range the type of phase behaviour may change a number of times. This complex phase behaviour can lead to difficulties in SFF processes. From the study by Peters and Gauter [7] it is apparent that knowledge of the type of phase behaviour exhibited by the contributing binary mixtures is necessary but not sufficient to determine the type of phase behaviour that will occur in ternary or multi-component mixtures.

4.2 Methods of Measuring High Pressure Phase Equilibrium Data

Fonseca et al. [11] reviewed all the experimental techniques that have been used for the measurement of high pressure phase equilibrium data. The popularity of the techniques for the period 2000 – 2004 and 2005 – 2008 are shown in Table 4-1. It clearly shows that the use of synthetic methods has increased in recent years.

Table 4-1 Popularity of experimental methods for the measurement of high pressure phase equilibrium data [11]

Method	Symbol	2000 – 2004	2005 - 2008
Analytical Methods		46.7%	37.6%
<i>With sampling</i>			
Isothermal	AnT	27.6%	19.7%
Isobaric	AnP	0.0%	0.0%
Isothermal-isobaric	AnPT	15.4%	11.2%
<i>Without sampling</i>			
Spectroscopic	AnSpec	1.5%	1.1%
Gravimetric	AnGrav	1.1%	5.0%
Other	AnOth	1.1%	0.6%
Synthetic		53.3%	62.4%
<i>With phase transition</i>			
Visual	SynVis	36.4%	36.0%
Non-visual	SynNon	8.4%	13.4%
<i>Without phase transition</i>			
Isothermal	SynT	6.1%	11.8%
Isobaric	SynP	0.2%	0.5%
Other	SynOth	2.2%	0.7%

4 | Phase Behaviour of Mixtures at High Pressure

Analytical methods involve the analytical determination of the composition of co-existing phases at certain pressure and temperature conditions. The composition of the mixture is not known at the start of the experiment. It is required that the temperature and pressure conditions be adjusted to allow the mixture to separate into two or more phases of which the composition is then determined. The composition of the phases can be determined by extracting a sample or by leaving it in the equilibrium cell and analysing with physico-chemical methods.

Synthetic methods require the generation of a mixture of known composition at the start of the experiment. The mixture is then observed in an equilibrium cell and properties like temperature and pressure is measured at equilibrium conditions. In synthetic methods with phase transition, the temperature, pressure or composition is gradually changed until the transition from a homogenous phase to a heterogeneous phase is observed. The composition of the first bulk phase is set at the overall composition of the mixture, while the composition of the second phase is not known. Often data generated in this manner are referred to as bubble point, dew point or solubility data. For a binary mixture the synthetic method with phase transition yields information regarding the phase compositions (VLE data), but for ternary and multi-component mixtures no information regarding the phase compositions of co-existing phases are generated.

In synthetic methods without phase transition, properties like temperature, pressure, phase volumes and phase densities are measured and the phase compositions are then calculated with material balances.

All of the abovementioned techniques have their advantages and disadvantages, and the selection of a specific experimental technique is determined by the available resources, the system investigated, the phases investigated and the type of data required. The scope of this investigation includes the measurement of phase equilibrium data for a number of binary, ternary and multi-component systems. The main use of the measured phase equilibrium data is in determining the feasibility of the proposed SFF process and therefore it is recommended that a measurement technique requiring equipment that is readily available or easily constructed, be used. The synthetic visual (SynVis) was selected as the method to be used in this investigation for the measurement of bubble and dew point data for selected binary, ternary and multi-component systems.

4.3 High Pressure Phase Equilibrium Data for Similar Systems

This study focuses on the phase behaviour of C₁₀-alkane isomers and C₁₀-alcohol isomers in both supercritical CO₂ and ethane. It was decided to investigate the phase behaviour published for similar systems, to create an expectation of the type of phase phenomena that occur. A literature review on high pressure bubble and dew point, VLE, and solubility data for C₈ – C₁₂ alkane and C₈ - C₁₂ alcohol systems in supercritical ethane or CO₂, brought forth very little phase behaviour data for isomeric compounds within this range. Only phase equilibrium data for isomers of C₈-alkanes and C₈-alcohols in supercritical CO₂ was found. This data, along with published data for the ethane + *n*-decane, CO₂ + *n*-decane, ethane + *l*-decanol and CO₂ + *l*-decanol systems are given in Table 4-2 to Table 4-7. The literature sources used to construct Table 4-2 to Table 4-7 are those sources that are readily available in reputable journals. Additional sources, not covered in this investigation, may be available for the specific systems considered.

4.3.1 Binary Systems of C₈ – C₁₂ Alkanes with Supercritical Ethane or CO₂

Table 4-2 contain summaries of the conditions at which phase equilibrium data was published for systems containing C₈-alkane isomers in supercritical CO₂.

Table 4-2 Phase equilibrium data for C₈- alkane isomers in supercritical CO₂

Carbon number	Solute	<i>T</i> and <i>P</i> range	Type of Data	Source
8	<i>n</i> -Octane	<u>Temp:</u> 313.2 – 348.2 K <u>Pres:</u> Up to 11.5 MPa	VLE	Weng and Lee [17]
		<u>Temp:</u> 313.1 – 368.1 K <u>Pres:</u> Up to 13.5 MPa	VLE	Choi and Yeo [18]
	2,3-Dimethylhexane	<u>Temp:</u> 318.2 – 328.2 K <u>Pres:</u> Up to 24.0 MPa	Solubility	Lee et al. [19]
	2,5-Dimethylhexane	<u>Temp:</u> 278.2 – 413.2 K <u>Pres:</u> Up to 12.5 MPa	Vap. Comp.	Mutelet et al. [20]
	2,2,4-Trimethylpentane	<u>Temp:</u> 278.2 – 393.2 K <u>Pres:</u> Up to 11.0 MPa	Vap. Comp.	Mutelet et al. [20]

4 | Phase Behaviour of Mixtures at High Pressure

In the range of alkanes investigated only phase equilibrium data for isomers of C₈-alkanes in supercritical CO₂ could be found in the open literature. These isomers were: *n*-octane, 2,3-dimethylhexane, 2,5-dimethylhexane and 2,2,4-trimethylpentane. In Figure 4-5 the phase behaviour of three of the C₈-alkane isomers in supercritical CO₂ are compared at 328 K and 348 K. The data provided by Lee et al. [19] for the CO₂ + 2,3-dimethylhexane system only contained solubility data at solute mass fractions of less than 0.02 and pressures below 2.4 MPa, and thus fell outside the range of interest.

From Figure 4-5 it is clear that the phase behaviour of the branched C₈-alkane isomers differ from that of linear *n*-octane. The lower bubble point pressures indicate that the branched alkane isomers are slightly more soluble in the supercritical CO₂. Although the compounds are all of similar nature and all have the same molecular mass, the phase behaviour still differs due to the structural shape of the molecules. The increased solubility of the branched isomers can be attributed to the shorter length of the hydrocarbon backbone. Slight differences in the phase behaviour of the branched and linear C₁₀-alkanes investigated in this study, can thus also be expected.

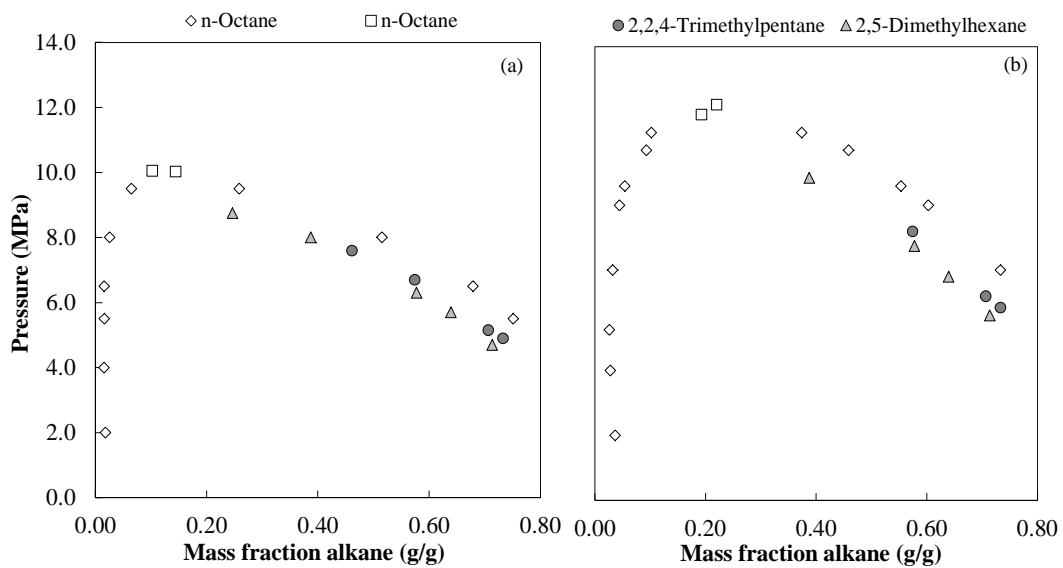


Figure 4-5 Phase behaviour of CO₂ + C₈-alkane isomers (\diamond[17], \square[18], \bullet , \blacktriangle[20]) at (a) 328 K and (b) 348 K

4 | Phase Behaviour of Mixtures at High Pressure

Literature data for the CO₂ + *n*-decane systems were readily available in the open literature. The data that fall within the same composition, temperature and pressure ranges used in this investigation are presented in Table 4-3.

Table 4-3 Phase equilibrium data for *n*-decane in supercritical CO₂

Carbon number	Solute	<i>T</i> and <i>P</i> range	Type of Data	Source
10	<i>n</i> -Decane	<u>Temp:</u> 277.6 – 510.9 K <u>Pres:</u> Up to 18.8 MPa	VLE Densities	Reamer and Sage [21]
		<u>Temp:</u> 217.0 – 248.8 K <u>Pres:</u> Up to 1.6 MPa	LLV SLV	Kukarni et al. [22]
		<u>Temp:</u> 283.2 – 313.5 K <u>Pres:</u> 0.1 MPa partial	Solubility	Wilcock et al. [23]
		<u>Temp:</u> 362.6 – 583.7 K <u>Pres:</u> Up to 5.0 MPa	VLE	Sebastian et al. [24]
		<u>Temp:</u> 342.9 – 594.2 K <u>Pres:</u> Up to 18.0 MPa	VLE	Inomata et al. [25]
		<u>Temp:</u> 344.3 - 377.6 K <u>Pres:</u> Up to 16.5 MPa	VLE Densities	Nagarajan and Robinson [26]
		<u>Temp:</u> 344.3 - 377.6 K <u>Pres:</u> Up to 15.5 MPa	VLE	Chou et al. [27]
		<u>Temp:</u> 311.0 K <u>Pres:</u> 8.0 MPa	Solubility Density	Han et al. [28]
		<u>Temp:</u> 344.3 – 444.3 K <u>Pres:</u> Up to 16.5 MPa	Vap. Comp.	Chen et al. [29]
		<u>Temp:</u> 311.0 - 344.3 K <u>Pres:</u> Up to 12.0 MPa	VLE	Iwai et al. [30]
		<u>Temp:</u> 344.3 K <u>Pres:</u> Up to 12.0 Mpa	VLE	Jennings and Schucker [31]
		<u>Temp:</u> 304.3 – 617.9 K <u>Pres:</u> Up to 18.5 MPa	Critical loci	Chester and Haynes [32]
		<u>Temp:</u> 313 K <u>Pres:</u> Up to 8.0 MPa	Solubility	Chylinski and Gregorowicz [33]
		<u>Temp:</u> 344.3 K <u>Pres:</u> Up to 13.0 MPa	VLE Densities	Shaver et al. [34]

4 | Phase Behaviour of Mixtures at High Pressure

Table 4-3(continued) Phase equilibrium data for *n*-decane in supercritical CO₂

Carbon number	Solute	<i>T</i> and <i>P</i> range	Type of Data	Source
10	<i>n</i> -Decane	<u>Temp:</u> 344.2 K <u>Pres:</u> Up to 13.0 MPa	Solubility	Eustaquio-Rincón and Trejo [35]
		<u>Temp:</u> 344.3 K <u>Pres:</u> Up to 12.0 MPa	Liq. Comp. Liq. Dens.	Tsuji et al. [36]
		<u>Temp:</u> 319.1 – 372.9 K <u>Pres:</u> Up to 16.0 MPa	VLE	Jiménez-Gallegos et al. [37]

The CO₂ + *n*-decane system (Figure 4-6) is well-researched and agreeable data are found in the literature for this system. In the next chapter the CO₂ + *n*-decane system will be used to verify the accuracy of the experimental method employed in this investigation for the measurement of C₁₀-alkane isomers and C₁₀-alcohol isomers.

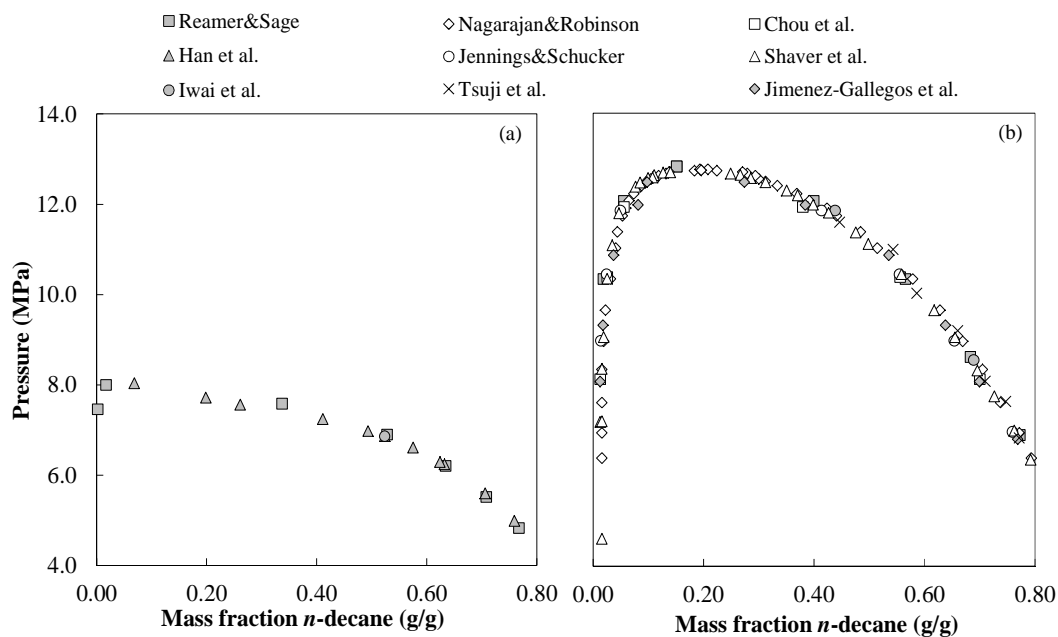


Figure 4-6 Phase equilibrium data of the CO₂ + *n*-decane system (■....[21], ◇....[26], □....[27], ▲....[28], ○....[31], △....[34], ●....[30], ×....[36], ◆....[37]) at (a) 311 K and (b) 344 K

4 | Phase Behaviour of Mixtures at High Pressure

Table 4-4 contain the operating ranges and sources of published phase equilibrium data for the ethane + *n*-decane system. The data that fall within the same temperature, pressure and composition ranges are plotted in Figure 4-7.

Table 4-4 Phase equilibrium data for *n*-decane in supercritical ethane

Carbon number	Solute	<i>T</i> and <i>P</i> range	Type of Data	Source
10	<i>n</i> -Decane	<u>Temp:</u> 277.6 – 510.9 K <u>Pres:</u> Up to 11.8 MPa	VLE	Reamer and Sage [12]
		<u>Temp:</u> 277.6 – 410.9 K <u>Pres:</u> Up to 8.2 MPa	VLE	Bufkin et al. [13]
		<u>Temp:</u> 309.4 – 324.8 K <u>Pres:</u> Up to 6.6 MPa	Critical loci	Singh et al. [14]
		<u>Temp:</u> 411.0 – 444.3 K <u>Pres:</u> Up to 9.2 MPa	VLE	Gardeler et al. [15]
		<u>Temp:</u> 310.0 – 360.0 K <u>Pres:</u> Up to 9.3 MPa	VLE	Schwarz et al. [16]

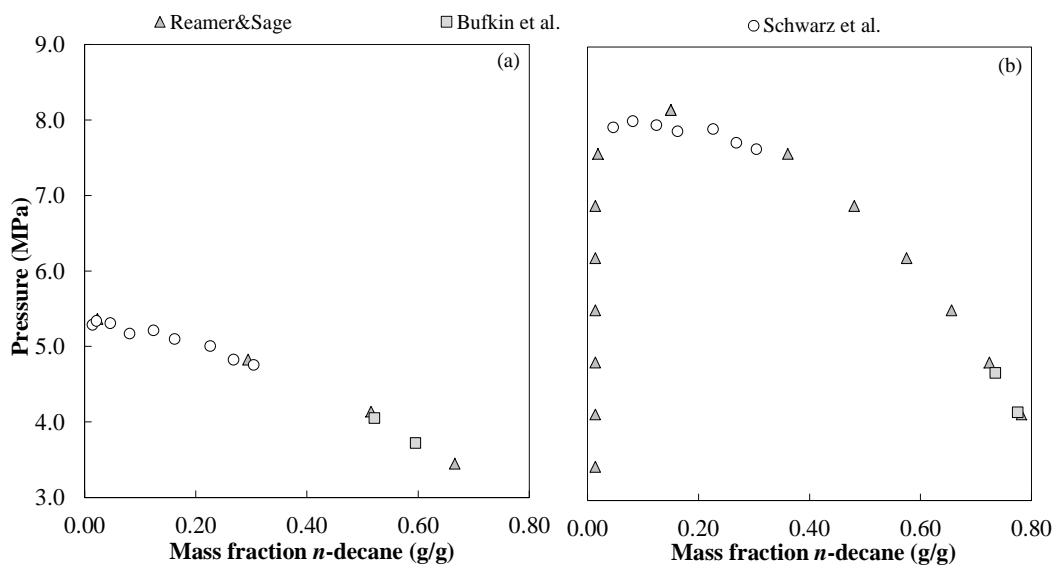


Figure 4-7 Phase behaviour of the ethane + *n*-decane system (\blacktriangle[12], \blacksquare[13], \circ[16]) at (a) 311 K and (b) 344 K

What to expect:

The behaviour of the C₈-alkane isomers in CO₂ (Figure 4-7) indicate that increased solubility can be expected for branched alkanes compared to linear alkanes. From Figure 4-7 and Figure 4-6 the following conclusions can therefore be drawn: the total solubility pressure of the C₁₀-alkanes in ethane is expected to be less than 5.4 MPa at 311 K and less than 8.2 MPa at 344 K, and in supercritical CO₂ less than 8.0 MPa at 311 K and less than 12.8 MPa at 344 K.

4.3.2 Binary Systems of C₈ – C₁₂ Alcohols with Supercritical Ethane or CO₂

Table 4-5 contain information regarding published phase equilibrium data for C₈-alcohol isomers in supercritical CO₂.

Table 4-5 Phase equilibrium data for C₈- alcohol isomers in supercritical CO₂

Carbon number	Solute	T and P range	Type of Data	Source
8	1-Octanol	<u>Temp:</u> 250.3 – 309.1 K <u>Pres:</u> Up to 8.0 MPa	LLV	Lam et al. [41]
		<u>Temp:</u> 313.2 – 348.2 K <u>Pres:</u> Up to 19.0 MPa	VLE	Weng and Lee [42]
		<u>Temp:</u> 348.2 – 453.2 K <u>Pres:</u> Up to 5.0 MPa	VLE	Lee and Chen [43]
		<u>Temp:</u> 403.2 – 453.2 K <u>Pres:</u> Up to 19.0 MPa	VLE	Weng et al. [44]
		<u>Temp:</u> 313.2 K <u>Pres:</u> Up to 15.0 MPa	VLE	Chrisochoou et al. [45]
		<u>Temp:</u> 308.2 – 328.2 K <u>Pres:</u> Up to 15.0 MPa	VLE Densities	Chang et al. [46]
		<u>Temp:</u> 328.2 K <u>Pres:</u> Up to 13.4 MPa	VLE	Feng et al. [47]
		<u>Temp:</u> 328.2 K <u>Pres:</u> Up to 13.3 MPa	VLE	Hwu et al. [48]
		<u>Temp:</u> 308.2 – 348.2 K <u>Pres:</u> Up to 18.0 MPa	VLE	Fourie et al. [49]

4 | Phase Behaviour of Mixtures at High Pressure

Table 4-5 (continued) Phase equilibrium data for C₈-alcohol isomers in supercritical CO₂

Carbon number	Solute	T and P range	Type of Data	Source
8	2-Octanol	<u>Temp:</u> 303.2 – 323.2 K <u>Pres:</u> Up to 9.1 MPa	VLE	Gamse and Marr [50]
		<u>Temp:</u> 308.2 – 348.2 K <u>Pres:</u> Up to 15.0 MPa	VLE	Fourie et al. [49]
	3-Octanol	<u>Temp:</u> 308.2 – 348.2 K <u>Pres:</u> Up to 14.5 MPa	VLE	Fourie et al. [49]
	4-Octanol	<u>Temp:</u> 308.2 – 348.2 K <u>Pres:</u> Up to 14.3 MPa	VLE	Fourie et al. [49]
	2,2,4-Trimethyl- <i>I</i> -pentanol	<u>Temp:</u> 308.2 – 348.2 K <u>Pres:</u> Up to 14.2 MPa	VLE	Schwarz et al. [51]
	2,4,4-Trimethyl- <i>I</i> -pentanol	<u>Temp:</u> 308.2 – 348.2 K <u>Pres:</u> Up to 14.6 MPa	VLE	Schwarz et al. [51]
	4-Methyl-3-heptanol	<u>Temp:</u> 308.2 – 348.2 K <u>Pres:</u> Up to 13.8 MPa	VLE	Schwarz et al. [51]
	6-Methyl-2-heptanol	<u>Temp:</u> 308.2 – 348.2 K <u>Pres:</u> Up to 14.4 MPa	VLE	Schwarz et al. [51]
	2-Propyl- <i>I</i> -pentanol	<u>Temp:</u> 308.2 – 348.2 K <u>Pres:</u> Up to 16.0 MPa	VLE	Schwarz et al. [51]
2-Ethyl- <i>I</i> -hexanol	<u>Temp:</u> 313.0 – 323.0 K <u>Pres:</u> Up to 18.0 MPa	Solubility	Ghaziaskar et al. [52]	
	<u>Temp:</u> 308.2 – 348.2 K <u>Pres:</u> Up to 16.0 MPa	VLE	Schwarz et al. [51]	

The phase equilibrium data for the CO₂ + C₈-alcohol isomer systems that fall within the same composition, temperature and pressure range used in this investigation are depicted in Figure 4-8 and Figure 4-9. In Figure 4-8 the phase behaviour of linear isomers of *I*-octanol are compared to one another at 308 K and 348 K. At 308 K very little difference in the phase behaviour of 2-octanol, 3-octanol and 4-octanol is observed. At 348 K, however, the total solubility pressures of these compounds start to differ marginally. The solubility of the linear C₈-alcohol isomers decrease in the following order: *I*-octanol, 2-octanol, 3-octanol and 4-octanol.

4 | Phase Behaviour of Mixtures at High Pressure

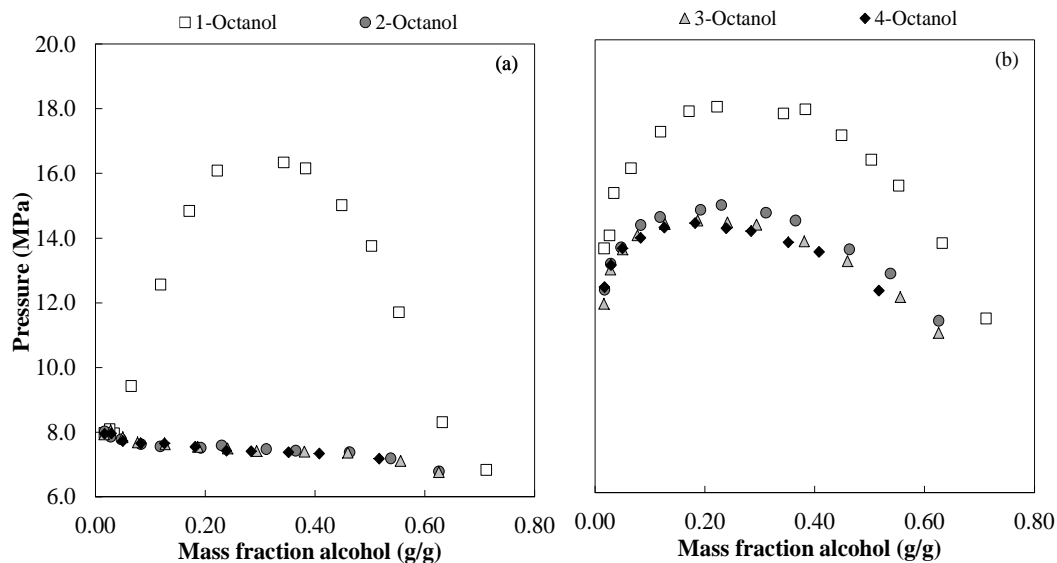


Figure 4-8 Phase behaviour of CO₂ + linear C₈- alcohol isomers (□, ●, ▲, ◆....[49]) at (a) 308 K and (b) 348 K

As the hydroxyl-group moves away from the terminal end of the hydrocarbon backbone, the compounds become more soluble in supercritical CO₂. Fourie et al. [49] ascribes this phenomenon to the shielding of the polar hydroxyl-group by the hydrocarbon backbone. When the polar hydroxyl group is exposed on the terminal end of the hydrocarbon backbone (like in *1*-octanol), stronger intermolecular interactions between the solutes as well as between the solvent and solute molecules can occur. When the polar hydroxyl group is located further away from the terminal end of the hydrocarbon backbone, the intermolecular interactions are less fierce and consequently the solubility of the compounds increases.

At 308 K and compositions ranging between 0.05 and 0.7 mass fraction solute, *1*-octanol displays significantly higher phase transition pressures compared to its linear isomers. The unique behaviour of *1*-octanol at low temperatures is due to the presence of a temperature inversion. At lower temperatures the phase transition pressures of *1*-octanol decreases with increasing temperature, a phenomena that contradicts the common behaviour of increasing phase transition pressures with increasing temperature, generally expected for these compounds [49]. Temperature inversions has also been observed for CO₂ + *1*-dodecanol [54] and CO₂ + *1*-hexadecanol [55].

4 | Phase Behaviour of Mixtures at High Pressure

What to expect:

For the compounds investigated in this study, it would thus be expected that the $\text{CO}_2 + 2$ -decanol system display lower phase transition pressures than the $\text{CO}_2 + 1$ -decanol system, with the difference in phase behaviour being more noticeable at higher temperatures. In all likelihood, a temperature inversion would thus also be observed for the $\text{CO}_2 + 1$ -decanol system investigated in this work.

In Figure 4-9 the phase behaviour of a number of branched C_8 -alcohol isomers are shown alongside that of 1 -octanol in supercritical CO_2 .

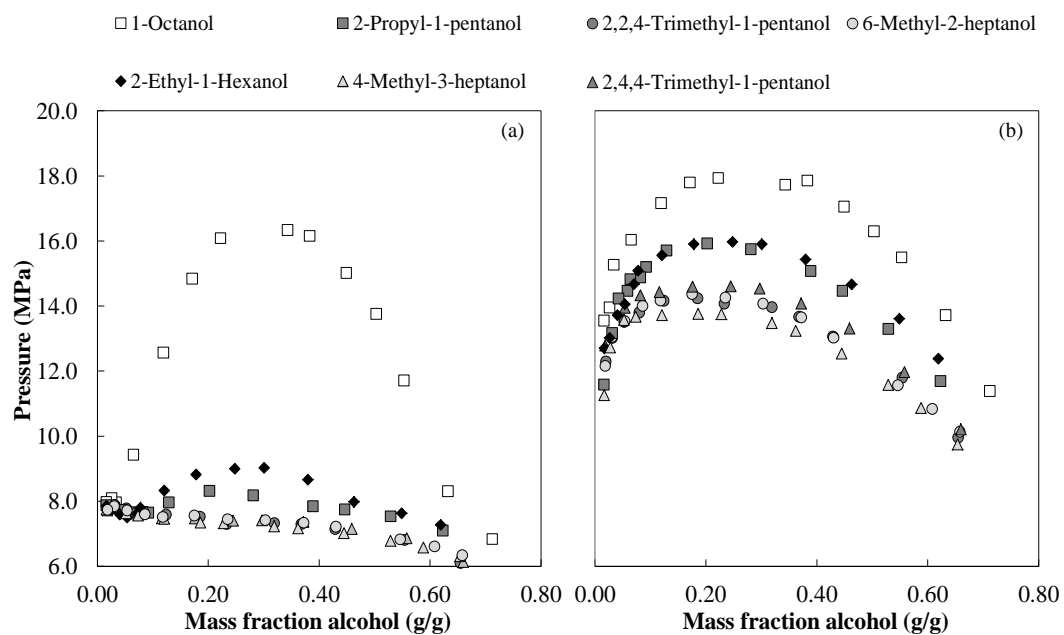


Figure 4-9 Phase behaviour of $\text{CO}_2 +$ branched C_8 - alcohol isomers (\square , \blacksquare , \bullet , \circ , \blacklozenge , \blacktriangle , \triangle[51]) at (a) 308 K and (b) 348 K

Schwarz et al. [51] ascribes the difference in phase behaviour to the shielding of the polar group by the side branches. The length, number and position of the side branches clearly influence the phase behaviour of the isomers. The order of decreasing solubility are as follows: 4-methyl-3-heptanol, 2,2,4-trimethyl-1-pentanol, 6-methyl-2-heptanol, 2,4,4-trimethyl-1-pentanol,

4 | Phase Behaviour of Mixtures at High Pressure

2-propyl-1-pentanol, 2-ethyl-1-hexanol, 1-octanol. The greater the degree of shielding provided by the side branches to the hydroxyl group, the less polar the nature of the molecule. When the molecule has a reduced polarity, the mixture becomes less asymmetric and consequently the solubility of the solute in supercritical CO₂ increases [51].

What to expect:

The C₁₀-alcohol isomers will thus in all likelihood also have phase transition pressures that are lower than that of 1-decanol. It can thus be expected that the phase behaviour of the C₁₀-alcohol isomers investigated in this study, will differ according to the length, number and position of the side branches.

In Table 4-6 and Table 4-7 the literature sources that published phase equilibrium data for the CO₂ + 1-decanol and ethane + 1-decanol systems are provided.

Table 4-6 Phase equilibrium data for 1-decanol in supercritical CO₂

Carbon number	Solute	T and P range	Type of Data	Source
10	1-Decanol	<u>Temp</u> : 284.0 – 313.5 K <u>Pres</u> : 0.1 MPa partial	Solubility	Wilcock et al. [23]
		<u>Temp</u> : 270.5 – 307.2 K <u>Pres</u> : Up to 7.8 MPa	LLV	Lam et al. [41]
		<u>Temp</u> : 348.2 – 453.2 K <u>Pres</u> : Up to 5.0 MPa	VLE	Lee and Chen [43]
		<u>Temp</u> : 348.2 – 453.2 K <u>Pres</u> : Up to 19.0 MPa	VLE	Weng et al. [44]
		<u>Temp</u> : 271.1 – 279.6 K <u>Pres</u> : Up to 3.2 MPa	Liq. Comp.	Patton and Luks [40]
		<u>Temp</u> : 308.1 – 328.2 K <u>Pres</u> : Up to 15.0 MPa	VLE Densities	Chang et al. [46]
		<u>Temp</u> : 318 K <u>Pres</u> : Up to 12.4 MPa	VLE	Gardeler and Gmehling [53]

4 | Phase Behaviour of Mixtures at High Pressure

Table 4-7 Phase equilibrium data for 1-decanol in supercritical ethane

Carbon number	Solute	T and P range	Type of Data	Source
10	1-Decanol	Temp: 275.3 – 306.8 K Pres: Up to 5.0 MPa	LLV	Lam et al. [38]
		Temp: 308.0 – 350.0 K Pres: Up to 14.8 MPa	VLE	Schwarz et al. [39]
		Temp: 263.0 – 279.6 K Pres: Up to 1.8 MPa	Liq. Comp.	Patton and Luks [40]
		Temp: 411.0 – 444.3 K Pres: Up to 11.5 MPa	VLE	Gardeler et al. [15]

In Figure 4-10 the phase equilibrium data that correspond to the composition, temperature and pressure ranges used in this investigation, are plotted for the ethane + 1-decanol and CO₂ + 1-decanol systems.

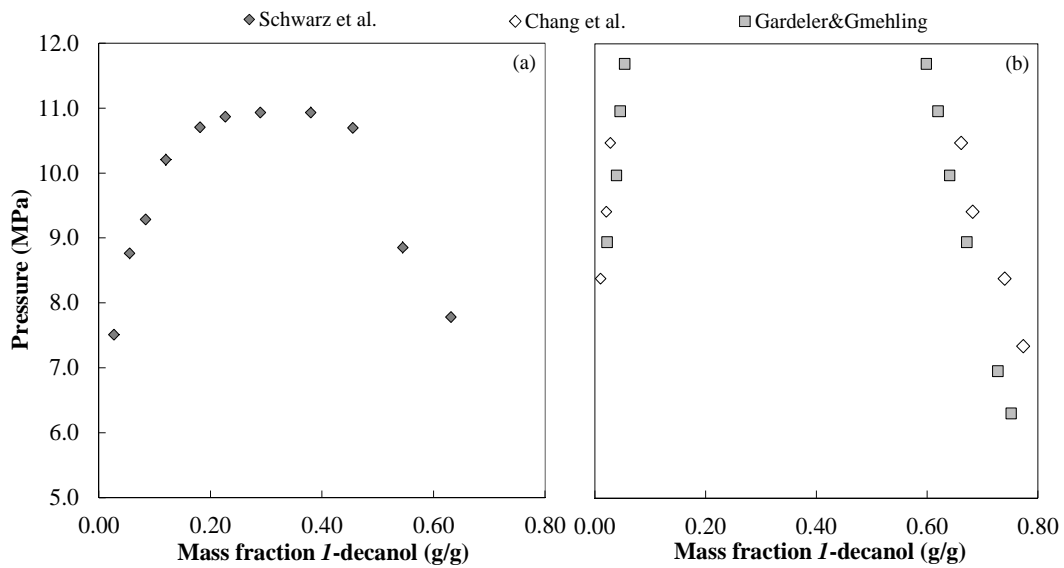


Figure 4-10 Phase behaviour at 318 K for (a) ethane + 1-decanol (♦....[39]) and (b) CO₂ + 1-decanol (◇....[46], ■....[53])

Both the ethane + *l*-decanol and CO₂ + *l*-decanol systems are poorly researched in the region surrounding the mixture critical point, and the data measured in this investigation for these two systems will contribute significantly to the high pressure phase equilibrium database.

What to expect:

The phase transition pressures of the branched C₁₀-alcohols in ethane will be below 11.0 MPa at 318 K. None of the sources for the CO₂ + *l*-decanol system reported in Table 4-5 include phase equilibrium data that extends to the mixture critical point at temperatures between 308 K and 348 K. This study will strive to include the mixture critical point of the CO₂ + *l*-decanol system in the measured bubble and dew point data, if it occurs within the pressures limits of the experimental equipment at temperatures between 308 K and 348 K.

4.4 Thermodynamic Modelling of High Pressure Phase Equilibrium Data

A number of thermodynamic models have been developed over the years – none of which are applicable to all systems at all conditions. The available thermodynamic models include equations of state (EoS), activity coefficient models, statistical models, empirical models, fundamental models, and more. The well-known basic thermodynamic models are constantly being adapted to improve the prediction of specific thermodynamic properties for a certain group of compounds or limited phase region.

4.4.1 Model Selection

A literature survey was conducted to determine which thermodynamic models have previously been used to accurately predict high pressure phase equilibrium data for systems consisting of supercritical CO₂ or ethane, and detergent range (C₈ – C₂₀) alkanes and alcohols. Numerous thermodynamic models have been applied in the literature to model mixtures at high pressures, some of which were more successful than others. Many forms of adaptations to common thermodynamic models have also been developed by researchers to increase the accuracy of the models for a specific thermodynamic property. Examples of such variations include: the use of Peng-Robinson (PR) EoS

with a group contribution estimation method for a temperature dependent interaction parameter [56,57], the use of perturbed chain statistical associating fluid theory model (PC-SAFT) with regressed binary interaction parameters [58], and a semi-predictive global phase diagram approach (GPDA) [59]. The number of approaches and variations that has been applied by researchers over the years to model high pressure systems is overwhelming.

In the petroleum industry simple cubic equations of state like Peng-Robinson and Soave-Redlich-Kwong (SRK) are very reliable high pressure VLE models, and no incentive has been found for the use of more complex non-cubic EoS [60]. This claim is supported by reports [61,62] that show that the use of a highly sophisticated models (e.g PC-SAFT or SAFT) did not bring about significant improvements in the accuracy of the VLE predictions, compared to simple cubic EoS (e.g. PR), of certain high pressure systems.

Cubic EoS are robust and easy to use for a first time approach at modelling a complex mixture, and thus they were selected as the thermodynamic models of choice for further investigation in this work. From the literature survey conducted, it seems that many researchers are in favour of cubic EoS to be used to generate VLE data with an acceptable level of accuracy. Other researchers claim that generating exact VLE data is of the utmost importance, irrespective of the computational load it requires, and thus prefer the use of more complex models. However, research on the topic of thermodynamic model development is at a stage where a more “complex” model often just refers to a model with a large amount of parameters that are fitted to experimental data. The use of a large number of fitted parameters hides the theoretical shortcomings of the model and inhibits the fundamental development thereof.

4.4.2 Cubic Equations of State

Kontogeorgis and Folas [63] and Valderrama [64] both identify EoS, especially the cubic EoS, as the thermodynamic models best suited for the prediction of high pressure phase behaviour. The SRK and PR EoS are simple models that are typically employed in the petroleum and chemical industries. Valderrama [64] also mentions that the SRK EoS (Equation 4-1) [65] and PR EoS (Equation 4-2) [66] have yielded some of the best results in attempts to model systems that contain supercritical fluids.

4 | Phase Behaviour of Mixtures at High Pressure

$$P = \frac{RT}{v-b} - \frac{a(T)}{v(v+b)} \quad \text{Eq. 4-1}$$

$$P = \frac{RT}{v-b} - \frac{a(T)}{v(v+b)+b(v-b)} \quad \text{Eq. 4-2}$$

The SRK and PR equations of state are two-parameter models, i.e. it contains an energy parameter, a , and a co-volume parameter, b . These parameters are determined from pure component properties like critical temperature (T_c), critical pressure (P_c) and acentric factor (ω). Equations 4-1.1 to 4-1.4 are applicable to the SRK EoS [65] and Equations 4-2.1 to 4-2.4 are applicable to the PR EoS [66].

$$a_c = 0.42747 \frac{(RT_c)^2}{P_c} \quad \text{Eq. 4-1.1}$$

$$b = 0.08664 \frac{RT_c}{P_c} \quad \text{Eq. 4-1.2}$$

$$a(T) = a_c [1 + m(1 - \sqrt{T_r})]^2 \quad \text{Eq. 4-1.3}$$

$$m = 0.48 + 1.574\omega - 0.176\omega^2 \quad \text{Eq. 4-1.4}$$

$$a_c = 0.45724 \frac{(RT_c)^2}{P_c} \quad \text{Eq. 4-2.1}$$

$$b = 0.07780 \frac{RT_c}{P_c} \quad \text{Eq. 4-2.2}$$

$$a(T) = a_c [1 + m(1 - \sqrt{T_r})]^2 \quad \text{Eq. 4-2.3}$$

$$m = 0.37464 + 1.54226\omega - 0.26992\omega^2 \quad \text{Eq. 4-2.4}$$

When dealing with mixtures, mixing rules are required for the energy and co-volume parameters. There are a multitude of mixing rules available, with the most well-known being the van der Waals (vdW) mixing rules. The vdW mixing rules includes a quadratic composition dependency

4 | Phase Behaviour of Mixtures at High Pressure

for both parameters (see Equations 4-3.1 and 4-3.2) with the geometric mean rule for the cross energy parameter (Equation 4-4.1) and the arithmetic mean rule for the cross co-volume parameter (Equation 4-4.2).

$$a = \sum_{i=1}^n \sum_{j=1}^n x_i x_j a_{ij} \quad \text{Eq. 4-3.1}$$

$$b = \sum_{i=1}^n \sum_{j=1}^n x_i x_j b_{ij} \quad \text{Eq. 4-3.2}$$

$$a_{ij} = \sqrt{a_i a_j} (1 - k_{ij}) \quad \text{Eq. 4-4.1}$$

$$b_{ij} = \frac{b_i + b_j}{2} (1 - l_{ij}) \quad \text{Eq. 4-4.2}$$

The great success of the cubic equations of state together with the vdW mixing rules lies in the ability for fast calculations (the roots can be determined analytically) and accurate representation of low and high pressure VLE for mixtures of hydrocarbons with gases (CH₄, CO₂, N₂, H₂S, etc.) – i.e. mixtures which are especially important in the petroleum industry [63].

4.4.2.1 Pure Component Parameter Estimation

Equations 4-1.1 to 4-1.4 and 4-2.1 to 4-2.4 require values for pure component properties like critical temperature, critical pressure and acentric factor. The values of these properties are not always available for all pure compounds, due to the scarcity of the compound or the difficulty in measuring the property experimentally. There are a number of estimation techniques available in literature, the majority of which is discussed in detail by Poling et al. [67]. Most of the estimation techniques discussed by Poling et al. [67] are of the group, bond, or atom contribution type, which means that the property value is established from contributions from its elements. Well-known estimation techniques that are often used, include the method of Joback [68,69], the method of Constantinou and Gani [70], the method of Wilson and Jasperson [71] and the method of Marrero and Pardillo [72]. These methods are often incorporated into process simulation software.

Alternative estimation techniques include factor analysis, where weighted contributions from measurable properties like molecular weight and normal boiling point, are added [67]. Additionally quantitative structure-property relationships based on contributions from molecular properties such as electron charge or molecular surface area can also be used [67]. These methods, although promising in accuracy and reliability, require extensive computational power, and have not yet been implemented in process simulation software.

For certain mixtures the thermodynamic model predictions of VLE data in the high pressure region are very sensitive to the pure component properties, and great care must be taken to ensure that the values used in the equations of state are as close as possible to the real values [73]. The availability of pure component properties for the components used in this study must first be investigated and if found to be limited, one of the mentioned estimation techniques can be employed. This topic will be discussed further in Chapter 6.

4.4.2.2 Binary Interaction Parameter Estimation

The interaction parameters shown in Equations 4-4.1 and 4-4.2 are usually determined by fitting the thermodynamic model data to experimental data. The k_{ij} -interaction parameter is considered the more important parameter [63], but both parameters are required for polar or complex mixtures. For non-polar mixtures the values of the interaction parameters are low, while for polar and hydrogen-bonding fluids, the values can become very high.

Estimation techniques for interaction parameters are available, but are rarely used. Many generalized correlations have been developed, applicable to specific EoS. These correlations allow the estimation of interaction parameters based on the characteristics of the mixture components, e.g. acentric factors. [63]. Stamataki and Tassios [73] showed that such generalized correlations have a very limited application and often yield inaccurate interaction parameters, especially when the mixture becomes highly asymmetric.

If the use of both interaction parameters does not improve the model VLE predictions, alternative mixing and combining rules can be considered. According to Valderrama [64] the use of Gibbs free energy models in the EoS parameters and non-quadratic mixing rules with interaction parameters in the volume constants of the EoS give the best results for mixtures containing a supercritical component. However, the familiarity and practicality of the vdW mixing rules allows it to dominate in practical and industrial applications [63].

4.4.2.3 Advantages and Shortcomings of Cubic Equations of State

Cubic EoS have the following characteristics that make them attractive for use in industry [63]:

- They are simple models of which the roots can be determined analytically.
- They are applicable over a wide range of pressures and temperatures.
- They are capable of describing properties of compounds in both liquid and vapour phases.
- There is no need, in most cases, for more than one interaction parameter for gas-hydrocarbon mixtures.
- Often good multi-component VLE prediction is achieved for mixtures containing hydrocarbons, gasses and other non-polar compounds (using interaction parameters from binary data).
- Many existing databases and correlations are available for k_{ij} .
- Well-established vdW and classical combining rules work well for simple systems and also for correlating VLE of many polar mixtures.

Cubic EoS do however, have the following shortcomings [63]:

- In most cases, predictions (i.e. setting all the interaction parameters to zero) are not possible for binary systems.
- Often poor correlation of complex VLE of polar mixtures is obtained.
- When two interaction parameters are used (i.e both k_{ij} and l_{ij}), the models often become highly flexible and represent complex VLE accurately, but unfortunately these two interaction parameters cannot easily be generalized as a function of some characteristic of the molecules involved.
- LLE of highly immiscible systems is not correlated satisfactorily.
- Results are poor for complex, multi-component VLE and LLE, especially in the presence of associating compounds and water.

- Cubic EoS cannot easily be extended to more complex molecules like electrolytes and biomolecules.

4.5 Outcomes of this Chapter

Objective 3, as mentioned in Chapter 1, is addressed in this chapter by providing the reader with the essential information necessary to generate an expectation of the phase behaviour to be exhibited by the type of binary systems investigated in this work. A literature survey on published phase equilibrium data for binary systems similar in nature to those investigated, suggests that no complex phase behaviour is present for such systems, and consequently the simple cubic EoS were selected as the thermodynamic models for these binary mixtures.

The key findings of Chapter 4 are:

- There are six types of phase behaviour that can occur for binary mixtures according to van Konynenburg and Scott [1]. The main differences between the types of phase behaviour lie in the occurrence and location of three phase regions, which generally appears at temperatures near and below the critical point of the more volatile component. The study of this region falls beyond the scope of this work, and thus classification of the phase behaviour for the mixtures investigated in this work might not be possible for all the systems.
- Type II phase behaviour can be expected to occur for the $\text{CO}_2 + n$ -decane system, with a three phase region and solid formation occurring at temperatures well below the critical temperature of the solvent (from Figure 4-3).
- Type III phase behaviour can be expected to occur for the $\text{CO}_2 + 1$ -decanol system, with a three phase region occurring near and below the critical point of the solvent, and solid formation occurring at temperatures well below the critical temperature of the solvent (from Figure 4-3).
- Type I phase behaviour can be expected to occur for the ethane + n -decane system, with complete miscibility over the entire temperature range (from Figure 4-4).

4 | Phase Behaviour of Mixtures at High Pressure

- Type V phase behaviour can be expected to occur for the ethane + *l*-decanol system, with a three phase region occurring near and below the critical point of the solvent (from Figure 4-4).
- The synthetic visual method will be used in this investigation to measure bubble and dew point data for selected binary, ternary and multi-component mixtures. Since this project is concerned with the early stages of process development, with the focus on determining the feasibility, the selection of the experimental method was based on the fact that the required equipment is readily available and easily operated.
- Published phase equilibrium data for CO₂ + C₈-alkane isomer systems and CO₂ + C₈-alcohol isomer systems revealed that the phase behaviour of the branched molecules are dependent on the size, length and number of side branches. Generally, the phase transition pressures of the branched molecules in the supercritical solvents are lower compared to that of the linear molecules.
- Published data for the ethane + *n*-decane, ethane + *l*-decanol, CO₂ + *n*-decane and CO₂ + *l*-decanol systems gave an indication of the location of the phase transition curves at temperatures of interest. This information will aid in the experimental measurement of the bubble and dew point data of these systems, reported in the next chapter.
- No overly complex phase behaviour is expected to occur for the systems consisting of C₁₀-alkane isomers and C₁₀-alcohol isomers with supercritical CO₂ or ethane, and thus the simple, robust cubic EoS were selected as appropriate models to represent these systems. Previous studies [61,62] showed that the results generated by more complex models, e.g. SAFT, are not superior to that generated with cubic EoS for certain systems.

In the next two chapters the application of the information provided in this chapter is revealed. In Chapter 5 the high pressure bubble and dew point data measured for the systems relevant to this study are discussed, while Chapter 6 will report on the thermodynamic modelling of these mixtures.

4.6 Nomenclature

Symbol/ Acronym	Description
<i>a</i>	Energy parameter
<i>b</i>	Co-volume parameter
EoS	Equation of State
GPDA	Global Phase Diagram Approach
<i>k</i>	Interaction parameter
L	Liquid phase
LCEP	Lower critical End Point
LLE	Liquid-liquid Equilibrium
<i>l</i>	Interaction parameter
<i>m</i>	Parameter defined by Eq. 4-1.4 and Eq. 4-2.4
<i>P</i>	Pressure
PC-SAFT	Perturbed Chain Statistical Associating Fluid Theory
PR	Peng-Robinson
<i>R</i>	Universal gas constant
S	Solid phase
SAFT	Statistical Associating Fluid Theory
SFF	Supercritical Fluid Fractionation
SRK	Sove-Redlich-Kwong
<i>T</i>	Temperature
UCEP	Upper Critical End Point
V	Vapour/Gas phase
<i>V</i>	Volume
VdW	Van der Waals
VLE	Vapour-Liquid Equilibrium
VLLE	Vapour-liquid-liquid Equilibrium
<i>v</i>	Molar volume
<i>ω</i>	Acentric Factor
<i>x</i>	Mole fraction

Sub/Superscripts	Description
A	Solute
B	Solvent
<i>c</i>	Critical
<i>r</i>	Reduced
<i>i</i>	Component <i>i</i> in a mixture
<i>j</i>	Component <i>j</i> in a mixture

4.7 References

- [1] P.H. van Konynenburg, R.L. Scott, Critical lines and phase equilibria in binary van der Waals Mixtures, *Philosophical Transactions of the Royal Society of London*. A 298 (1980) 495 – 540.
- [2] T. de Loos, Understanding phase diagrams, in: *Supercritical Fluids: Fundamentals for Application*, Kluwer Academic Publishers, The Netherlands, 1994.
- [3] A. Bolz, U. K. Deiters, C. J. Peters, T. W. de Loos, Nomenclature for phase diagrams with particular reference to vapour-liquid and liquid-liquid equilibria, *Pure & Applied Chemistry*. 70 (1998) 2233 – 2257.
- [4] T. Clifford, *Fundamentals of Supercritical Fluids*, Oxford University Press, Inc., New York, 1999.
- [5] M.A. McHugh, V.J. Krukonis, *Supercritical Fluid Extraction: Principles and Practice*, 2nd ed., Butterworth-Heinemann, Massachusettes, 1994.
- [6] S. Pereda, S. B. Bottini, E. A. Brignole, *Fundamentals of Supercritical Fluid Technology*, (n.d.).
- [7] C. J. Peters, K. Gauter, Occurance of holes in ternary fluid multiphase systems of near-critical carbon dioxide and certain solutes, *Chemical Reviews*. 99 (1999) 419 – 431.
- [8] C. J. Peters, Multiphase equilibria in near-critical solvents, in: *Supercritical Fluids: Fundamentals for Application*, Kluwer Academic Publishers, The Netherlands, 1994.
- [9] K. D. Luks, The occurrence and measurement of multiphase equilibria behaviour, *Fluid Phase Equilibria*. 29 (1986) 209 – 224.

- [10] Y. S. Wei, R. J. Sadus, Phase behaviour of ternary mixtures: a theoretical investigation of the critical properties of mixtures with equal size components, *Physical Chemistry Chemical Physics*. (1999) 4329 – 4336.
- [11] M.S. Fonseca, R. Dohrn, S. Peper, High-pressure fluid-phase equilibria: Experimental methods and systems investigated (2005-2008), *Fluid Phase Equilibria*. 300 (2011) 1 – 69.
- [12] H. H. Reamer, B. H. Sage, Phase equilibria in hydrocarbon systems. Volumetric and phase behaviour of the ethane-*n*-decane system, *Journal of Chemical & Engineering Data*. 7 (1962) 161 – 168.
- [13] B. A. Bufkin, R. L. Robinson, S. S. Estrera, K. D. Luks, Solubility of ethane in *n*-decane at pressures up to 8.2 MPa and temperatures from 278 to 411 K, *Journal of Chemical & Engineering Data*. 31 (1986) 421 – 423.
- [14] H. Singh, F. P. Lucien, N. R. Foster, Critical properties for binary mixtures of ethane containing low concentrations of *n*-alkane, *Journal of Chemical & Engineering Data*. 45 (2000) 131 – 135.
- [15] H. Gardeler, K. Fischer, J. Gmehling, Experimental determination of vapour–liquid equilibrium data for asymmetric systems, *Industrial & Engineering Chemistry Research*. 41 (2002) 1051 – 1056.
- [16] C.E. Schwarz, I. Nieuwoudt, J.H. Knoetze, Phase equilibria of long chain *n*-alkanes in supercritical ethane: Review, measurements and prediction, *The Journal of Supercritical Fluids*. 46 (2008) 226 – 232.
- [17] W. L. Weng, M. J. Lee, Vapour-liquid equilibrium of the octane/carbon dioxide, octane/ethane, and octane/ethylene systems, *Journal of Chemical & Engineering Data*. 37 (1992) 213 – 215.
- [18] E-J. Choi, S-D. Yeo, Critical properties for carbon dioxide + *n*-alkane mixtures using a variable-volume view cell, *Journal of Chemical & Engineering Data*. 43 (1998) 714 – 716.
- [19] L-S. Lee, J-F. Huang, O-X. Zhu, Solubilities of solid benzoic acid, phenanthrene, and 2,3-dimethylhexane in supercritical carbon dioxide, *Journal of Chemical & Engineering Data*. 46 (2001) 1156 – 1159.

- [20] F. Mutelet, S. Vitu, R. Privat, J-N. Jaubert, Solubility of CO₂ in branched alkanes in order to extend the PPR78 model (predictive 1978, Peng-Robinson EOS with temperature-dependent k_{ij} calculated through a group contribution method) to such systems, *Fluid Phase Equilibria*. 238 (2005) 157 – 168.
- [21] H. H. Reamer, B. H. Sage, Phase equilibria in hydrocarbon systems. Volumetric and phase behavior of the *n*-decane-CO₂ System., *Journal of Chemical & Engineering Data*. 8 (1963) 508 – 513.
- [22] A. A. Kukarni, B. Y. Zarah, K. D. Luks, J. P. Kohn, Phase-equilibrium behaviour of system carbon dioxide-*n*-decane at low temperatures, *Journal of Chemical & Engineering Data*. 19 (1974) 92 – 94.
- [23] R. J. Wilcock, R. Battino, W. F. Danforth, E. Wilhelm, Solubilities of gases in liquids II. The solubilities of He, Ne, Ar, Kr, O₂, N₂, CO, CO₂, CH₄, CF₄, and SF₆ in *n*-octane *l*-octanol, *n*-decane, and *l*-decanol, *The Journal of Chemical Thermodynamics*. 10 (1978) 817 – 822.
- [24] H. M. Sebastian, J. J. Simnick, H-M. Lin, K-C. Chao, Vapour-liquid equilibrium in binary mixtures of carbon dioxide + *n*-decane and carbon dioxide + *n*-hexadecane, *Journal of Chemical & Engineering Data*. 25 (1980) 138 – 140.
- [25] H. Inomata, K. Arai, S. Saito, Measurement of vapour-liquid equilibria at elevated temperatures and pressures using a flow type apparatus, *Fluid Phase Equilibria*. 29 (1986) 225 – 232.
- [26] N. Nagarajan, R. L. Robinson, Equilibrium phase compositions, phase densities, and interfacial tensions for carbon dioxide + hydrocarbon systems. 2. Carbon dioxide + *n*-decane, *Journal of Chemical & Engineering Data*. 31 (1986) 168 – 171.
- [27] G. F. Chou, R. R. Forbert, J. M. Prausnitz, High-pressure vapour-liquid equilibria for carbon dioxide/*n*-decane, carbon dioxide/tetralin, and carbon dioxide/*n*-decane/tetralin at 71.1 and 104.4 degree C, *Journal of Chemical & Engineering Data*. 35 (1990) 26 – 29.
- [28] B. Han, D-Y. Peng, C-T. Fu, G. Vilcsak, An apparatus for phase equilibrium studies of carbon dioxide+heavy hydrocarbon systems, *Canadian Journal of Chemical Engineering* 70 (1992) 1164 – 1171.
- [29] S. J. Chen, R. E. Randelman, R. L. Seldomridge, M. Radosz, Mass spectrometer composition probe for batch cell studies of supercritical fluid phase equilibria, *Journal of Chemical & Engineering Data*. 38 (1993) 211 – 216.
-

- [30] Y. Iwai, N. Hosotani, T. Morotomi, Y. Koga, Y. Arai, High-pressure vapour-liquid equilibria for carbon dioxide + linalool, *Journal of Chemical & Engineering Data*. 39 (1994) 900 – 902.
- [31] D. W. Jennings, R. C. Schucker, Comparison of high-pressure vapour-liquid equilibria of mixtures of CO₂ or propane with nonane and C₉ alkylbenzenes, *Journal of Chemical & Engineering Data*. 41 (1996) 831 – 838.
- [32] T. L. Chester, B. S. Haynes, Estimation of pressure-temperature critical loci of CO₂ binary mixtures with methyl-tert-butyl ether, ethyl acetate, methyl-ethyl ketone, dioxane and decane, *The Journal of Supercritical Fluids*. 11 (1997) 15 – 20.
- [33] K. Chylinski, J. Gregorowicz, Solubilities of *l*-propanol and *l*,2-propanediol in supercritical carbon dioxide. New analytical procedure and measurements, *Fluid Phase Equilibria*. 143 (1998) 163 – 172.
- [34] R. D. Shaver, R. L. Robinson, K. A. M. Gasem, An automated apparatus for equilibrium phase compositions, densities, and interfacial tensions: data for carbon dioxide + decane, *Fluid Phase Equilibria*. 179 (2001) 43 – 66.
- [35] R. Eustaquio-Rincon, A. Trejo, Solubility of *n*-octadecane in supercritical carbon dioxide at 310, 313, 333, and 353 K, in the range 10-20 MPa, *Fluid Phase Equilibria*. 185 (2001) 231 – 239.
- [36] T. Tsuji, S. Tanaka, T. Hiaki, R. Saito, Measurements of bubble point pressure for CO₂ + decane and CO₂ + lubricating oil, *Fluid Phase Equilibria*. 219 (2004) 87 – 92.
- [37] R. Jiménez-Gallegos, L. A. Galicia-Luna, O. Elizalde-Solis, Experimental vapour-liquid equilibria for the carbon dioxide + octane and carbon dioxide + decane systems, *Journal of Chemical & Engineering Data*. 51 (2006) 1624 – 1628.
- [38] D. H. Lam, A. Jangkamolkulchai, K. D. Luks, Liquid-liquid-vapour phase equilibrium behavior of certain binary ethane + *n*-alkanol mixtures, *Fluid Phase Equilibria*. 59 (1990) 263 – 277.
- [39] C.E. Schwarz, A.J. de Villiers, C.B. McClune, G.J.K. Bonthuys, A.J. Burger, J.H. Knoetze, High pressure phase equilibrium measurements of long chain alcohols in supercritical ethane, *The Journal of Supercritical Fluids*. 55 (2010) 554 – 565.
- [40] C. L. Patton, K. D. Luks, Multiphase equilibria of the binary mixture xenon + *l*-decanol, *Fluid Phase Equilibria*. 98 (1994) 201 – 211.

- [41] D. H. Lam, A. Jangkamolkulchai, K. D. Luks, Liquid-liquid-vapour phase equilibrium behaviour of certain binary carbon dioxide + *n*-alkanol mixtures, *Fluid Phase Equilibria*. 60 (1990) 131 – 141.
- [42] W. L. Weng, M. J. Lee, Phase equilibrium measurements for the binary mixtures of *l*-octanol plus CO₂, C₂H₆ and C₂H₄, *Fluid Phase Equilibria*. 73 (1992) 117 – 127.
- [43] M-J. Lee, J-T. Chen, Vapour-liquid equilibrium for carbon dioxide/alcohol systems, *Fluid Phase Equilibria*. 92 (1994) 215 – 231.
- [44] W-L. Weng, J-T. Chen, M-J. Lee, High-pressure vapour-liquid equilibria for mixtures containing a supercritical fluid, *Industrial & Engineering Chemistry Research*. 33 (1994) 1955 – 1961.
- [45] A. A. Chrisochoou, K. Schaber, K. Stephan, Phase equilibria with supercritical carbon dioxide for the enzymatic production of an enantiopure pyrethroid component. Part 1. Binary systems, *Journal of Chemical & Engineering Data*. 42 (1997) 551 – 557.
- [46] C. J. Chang, K-L. Chiu, C-Y. Day, A new apparatus for the determination of *P*-*x*-*y* diagrams and Henry's constants in high pressure alcohols with critical carbon dioxide, *The Journal of Supercritical Fluids*. 12 (1998) 223 – 237.
- [47] L-C. Feng, K-W. Cheng, M. Tang, Y-P. Chen, Vapour-liquid equilibria of carbon dioxide with ethyl benzoate, diethyl succinate and isoamyl acetate binary mixtures at elevated pressures, *The Journal of Supercritical Fluids*. 21 (2001) 111 – 121.
- [48] W-H. Hwu, J-S. Cheng, K-W. Cheng, Y-P. Chen, Vapour-liquid equilibrium of carbon dioxide with ethyl caproate, ethyl caprylate and ethyl caprate at elevated pressures, *The Journal of Supercritical Fluids*. 28 (2004) 1 – 9.
- [49] F.C.v.N. Fourie, C.E. Schwarz, J.H. Knoetze, Phase equilibria of alcohols in supercritical fluids: Part I. The effect of the position of the hydroxyl group for linear C₈ alcohols in supercritical carbon dioxide, *The Journal of Supercritical Fluids*. 47 (2008) 161 – 167.
- [50] T. Gamse, R. Marr, Phase equilibrium properties of the *l*-phenylethanol-carbon dioxide and 2-octanol-carbon dioxide binary systems at 303.15 K, 313.15 K and 323.15 K, *Journal of Chemical & Engineering Data*. 46 (2001) 117 – 119.

- [51] C.E. Schwarz, F.C.v.N. Fourie, J.H. Knoetze, Phase equilibria of alcohols in supercritical fluids Part II. The effect of side branching on C₈ alcohols in supercritical carbon dioxide, *The Journal of Supercritical Fluids*. 51 (2009) 128 – 135.
- [52] H. S. Ghaziaskar, H. Eskandari, A. Daneshfar, Solubility of 2-ethyl-1-hexanol, 2-ethylhexanoic acid, and their mixtures in supercritical carbon dioxide, *Journal of Chemical & Engineering Data*. 48 (2003) 236 – 240.
- [53] H. Gardeler, J. Gmehling, Experimental determination of phase equilibria and comprehensive examination of the predictive capabilities of group contribution equations of state with a view to the synthesis of supercritical extraction processes, in: *Supercritical Fluids as Solvents and Reaction Media*, Elsevier B.V., Amsterdam, 2004.
- [54] G.J.K. Bonthuys, C.E. Schwarz, A.J. Burger, J.H. Knoetze, Separation of alkanes and alcohols with supercritical fluids. Part I: Phase equilibria and viability study, *The Journal of Supercritical Fluids*. 57 (2011) 101 – 111.
- [55] A. Kramer, G. Thodos, Solubility of 1-hexadecanol and palmitic acid in supercritical carbon dioxide, *Journal of Chemical & Engineering Data*. 33 (1988) 230 – 234.
- [56] S. Vitu, R. Privat, J-N. Jaubert, F. Mutelet, Predicting the phase equilibria of CO₂+hydrocarbon systems with the PPR78 model (PR EOS and k_{ij} calculated through a group contribution method), *Journal of Supercritical Fluids*. 45 (2008) 1 – 26.
- [57] J-N. Jaubert, F. Mutelet, VLE predictions with the Peng-Robinson equation of state and temperature dependant k_{ij} calculated through a group contribution method, *Fluid Phase Equilibria*. 224 (2004) 285 – 304.
- [58] D. Fu, L. Liang, X-S. Li, S. Yan, T. Liao, Investigation of vapour-liquid equilibria for supercritical carbon dioxide and hydrocarbon mixtures by perturbed-chain statistical associating fluid theory, *Industrial & Engineering Chemistry Research*. 45 (2006) 4364 – 4370.
- [59] I. Polishuk, J. Wisniak, H. Seguro, Simultaneous prediction of the critical and sub-critical phase behaviour in mixtures using equations of state II. Carbon dioxide-heavy *n*-alkanes, *Chemical Engineering Science*. 58 (2003) 2529 – 2550.
- [60] C. Tsonopoulos, J. L. Heidman, High pressure vapour-liquid equilibria with cubic equations of state, *Fluid Phase Equilibria*. 29 (1986) 391 – 414.

- [61] C.E. Schwarz, M.L. Hahn, A.J. de Villiers, J.H. Knoetze, Phase behaviour of high molecular mass methyl esters in supercritical ethane, *Fluid Phase Equilibria*. 311 (2011) 36 – 44.
- [62] E.C. Voutsas, G.D. Pappa, K. Magoulas, D.P. Tassios, Vapour-liquid equilibrium modelling of alkane systems with Equations of State: “Simplicity versus complexity,” *Fluid Phase Equilibria*. 240 (2006) 127 – 139.
- [63] G. M. Kontogeorgis, G. K. Folas, *Thermodynamic Models for Industrial Applications: From Classical and Advanced Mixing rules to Association Theories*, 1st ed., John Wiley & Sons Ltd, United Kingdom, 2010.
- [64] J. O. Valderrama, The state of the cubic equations of state, *Industrial & Engineering Chemistry Research*. 42 (2003) 1603 – 1618.
- [65] G. Soave, Equilibrium constants from a modified Redlich-Kwong equation of state, *Chemical Engineering Science*. 27 (1972) 1197 – 1203.
- [66] D.Y. Peng, D.B. Robinson, A new two-constant equation of state, *Industrial and Engineering Chemistry Fundamentals*. 15 (1976) 59 – 64.
- [67] B. E. Poling, J. M. Prausnitz, J. P. O’Connell, *The Properties of Gases and Liquids*, 5th ed., McGraw-Hill Companies, Inc., United States of America, 2001.
- [68] K. G. Joback, A unified approach to physical property estimation using multivariate statistical techniques, S. M. Thesis, Massachusetts Institute of Technology, 1984.
- [69] K. G. Joback, R. C. Reid, Estimation of pure-component properties from group-contributions, *Chemical Engineering Communications*. 57 (1987) 233 – 243.
- [70] L. Constantinou, R. Gani, New group contribution method for estimating properties of pure compounds, *AIChE Journal*. 40 (1994) 1697 – 1710.
- [71] G. M. Wilson, L. V. Jasperson, Critical constants T_c , P_c , estimation based on zero first and second order methods, in: New Orleans, LA, 1996.
- [72] J. Marerro-Morejon, E. Pardillo-Fontdevila, Estimation of pure compound properties using group-interaction contributions, *AIChE Journal*. 45 (1999) 615 – 621.

4 | Phase Behaviour of Mixtures at High Pressure

[73] S. Stamatakis, D. Tassios, Performance of cubic EoS at high pressures, *Oil & Gas Science and Technology*. 53 (1998) 367 – 377.

5. EXPERIMENTAL BUBBLE AND DEW POINT DATA

5.1 EXPERIMENTAL METHOD	98
5.1.1 Chemicals Used	98
5.1.2 Experimental Setup	98
5.1.3 Factors that Require Special Attention.....	101
5.1.3 Generation of Isothermal Data	103
5.1.4 Accuracy and Reproducibility of the Data	104
5.1.5 Verification of the Accuracy of the Experimental Method.....	106
5.2 MEASURED DATA FOR BINARY ETHANE + ALKANE MIXTURES.....	107
5.2.1 Contradicting Solubility Results for the Ethane + <i>n</i> -decane System	110
5.2.2 Classification of the Ethane + Alkane Systems.....	113
5.3 MEASURED DATA FOR BINARY ETHANE + ALCOHOL MIXTURES	113
5.3.1 Comparison to Literature Data	118
5.3.2 Classification of the Systems.....	118
5.4 MEASURED DATA FOR BINARY CO₂ + ALKANE MIXTURES	119
5.4.1 Classification of the Systems.....	122
5.5 MEASURED DATA FOR BINARY CO₂ + ALCOHOL MIXTURES.....	122
5.5.1 Unique Phase Behaviour of the CO ₂ + <i>I</i> -decanol System.....	127
5.5.2 Comparison to Literature Data	129

5 | Experimental Bubble and Dew Point Data

5.5.3 Classification of the Systems.....	130
5.6 DISCUSSION ON THE PHASE BEHAVIOUR OF THE BINARY MIXTURES INVESTIGATED ..	130
5.6.1 Effect of Temperature.....	131
5.6.2 Effect of Composition	133
5.6.3 Effect of Solvent.....	134
5.6.4 Effect of Functional End Group	135
5.6.5 Effect of the Hydroxyl Group Position	136
5.6.6 Effect of Number, Length and Position of the Side Branches	138
5.7 MEASURED DATA FOR TERNARY MIXTURES	140
5.7.1 Rationale for Further Investigation	140
5.7.2 Measured Data for CO ₂ + Mixture A	142
5.7.3 Measured Data for CO ₂ + Mixture B	143
5.7.4 Measured Data for CO ₂ + Mixture C	145
5.8 DISCUSSION ON THE PHASE BEHAVIOUR OF THE TERNARY MIXTURES INVESTIGATED	147
5.9 MEASURED DATA FOR MULTI-COMPONENT MIXTURES.....	152
5.9.1 Rationale for Further Investigation	152
5.9.2 Measured Data for CO ₂ + Mixture 1	152
5.9.3 Measured Data for CO ₂ + Mixture 2	154
5.10 DISCUSSION ON THE PHASE BEHAVIOUR OF THE MULTI-COMPONENT MIXTURES INVESTIGATED.....	155
5.11 OUTCOMES OF THIS CHAPTER	158

5.12 SIGNIFICANT CONTRIBUTIONS	161
5.13 NOMENCLATURE.....	162
5.14 REFERENCES	162

From the information provided in the previous two chapters it is clear that data on the phase behaviour of a mixture is required in order to make an accurate evaluation on the feasibility of a supercritical fluid fractionation (SFF) process for the separation of that mixture. In this chapter phase behaviour data is not only reported for the multi-component mixtures of interest, but also for comprising binary and ternary mixtures and mixtures with similar components to allow a full investigation to be conducted on the interactions that occur between the specific components. This chapter reports on experimentally measured bubble and dew point data for binary, ternary and multi-component mixtures consisting of supercritical CO₂ or ethane, and: *n*-dodecane, *n*-decane, 2-methylnonane, 3-methylnonane, 4-methylnonane, 1-decanol, 2-decanol, 3,7-dimethyl-1-octanol, 2,6-dimethyl-2-octanol, and/or 3,7-dimethyl-3-octanol. The data measured and reported in this chapter was published as two novel contributions in The Journal of Supercritical Fluids 58 (2011) 330 – 342 and The Journal of Supercritical Fluids 59 (2011) 14 – 26.

The measured phase equilibrium data of the binary mixtures are evaluated with the purpose of determining the influence of structural isomerism of detergent range alkanes and alcohols on their phase behaviour in supercritical CO₂ or ethane. This data will provide information regarding the specific solute-solvent interaction that take place between the specific components and the solvents, and will be used in Chapter 6 to establish an accurate thermodynamic model for these systems.

The data measured for the ternary and multi-component mixtures will be used to investigate the degree and influence of *n*-alkane + 1-alcohol, *n*-alkane + branched alcohol and 1- alcohol + branched alcohol interactions. If these interactions are found to be significant, they can also aid in the development of an accurate thermodynamic model in Chapter 6.

The main aim of this chapter is to provide information on the phase behaviour of mixtures that can aid in determining the feasibility of the proposed SFF process for the separation of detergent range alkanes from a mixture of alcohol isomers.

5.1 Experimental Method

5.1.1 Chemicals Used

Table 5-1 lists the compounds used as solutes in this investigation, along with the suppliers, catalogue number, CAS number and the respective purities. The solvents used in this investigation were CO₂ and ethane, both obtained from Afrox at a purity of 99.9%.

Table 5-1 Chemicals used for high pressure bubble and dew point measurements

Solute	Supplier	CAS number	Catalogue no.	Purity (mass%)
<i>1-Decanol</i>	Aldrich	112-30-1	239763	≥ 99
<i>2-Decanol</i>	Aldrich	1120-06-5	118311	98
<i>3,7-Dimethyl-1-octanol</i>	Aldrich	106-21-8	305774	99
<i>3,7-Dimethyl-1-octanol</i>	SAFC	106-21-8	W23,910-0-K	≥ 98
<i>2,6-Dimethyl-2-octanol</i>	SAFC	18479-57-7	W51,650-3	95
<i>3,7-Dimethyl-3-octanol</i>	Aldrich	78-69-3	309915	98
<i>n-Decane</i>	Sigma	124-18-5	457116	≥ 99
<i>2-Methylnonane</i>	Fluka	871-83-0	68070	≥ 99
<i>3-Methylnonane</i>	Fluka	5911-04-6	68080	≥ 99
<i>4-Methylnonane</i>	Fluka	17301-94-9	68090	≥ 98
<i>n-Dodecane</i>	Fluka	112-40-3	44010	≥ 99

5.1.2 Experimental Setup

In this investigation two variable volume view cells were used simultaneously, due to the large amount of data that had to be measured. The two cells work on exactly the same principle and differ mainly in size. The one view cell has an internal volume of $8 \times 10^{-5} \text{ m}^3$ and the other $4 \times 10^{-5} \text{ m}^3$.

5 | Experimental Bubble and Dew Point Data

Details on the design of the small variable volume cell are given by Schwarz [1]. Figure 5-1 is a schematic representation of the experimental equipment utilized in this investigation.

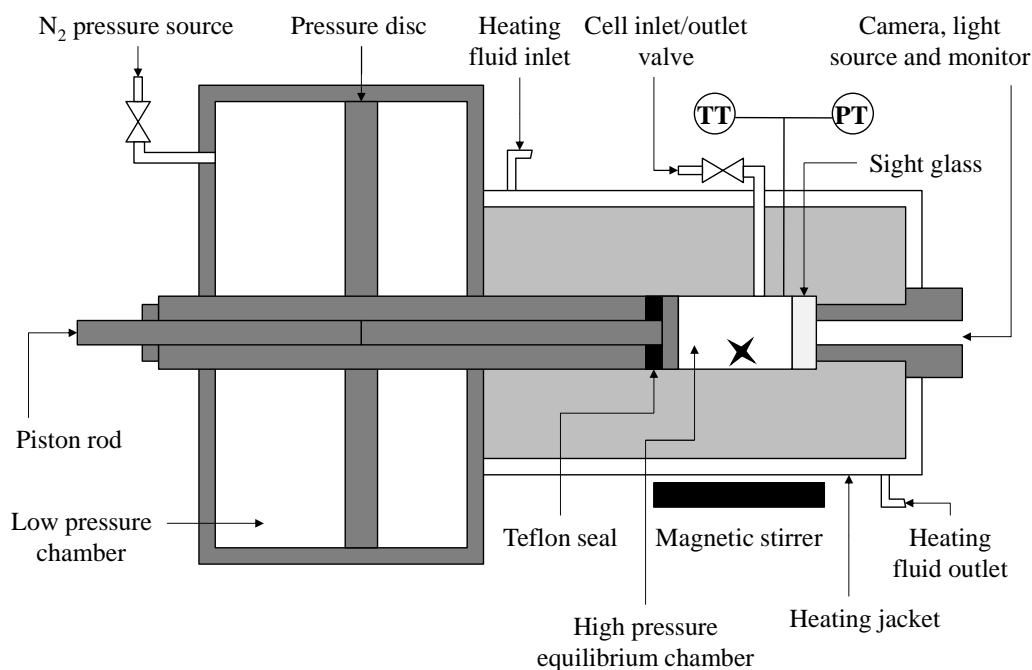


Figure 5-1 Schematic diagram of experimental equipment

The large cell was used to measure the low solute concentration phase transition points. For the low solute concentration data points very small amounts of solute are required. By using the large cell a larger mass of the solute can be used compared to the small cell, to make up a mixture of the same concentration – thus increasing the accuracy of the mass solute weighed.

The small cell was generally used to measure the phase transition points at high solute concentrations. By using the small cell for the high concentration data points the amount of solute required is minimized – which proved to be economically favourable due to the limited availability of some of the solutes.

The equilibrium cell is a piston-cylinder type apparatus manufactured from stainless steel. The piston moves inside the equilibrium cell to change the volume and consequently the pressure inside the cell. The addition of nitrogen to the low pressure chamber causes the piston to move inwards,

5 | Experimental Bubble and Dew Point Data

leading to an increase in the pressure inside the cell. The low pressure chamber is designed to handle a maximum pressure of 1.5 MPa and the high pressure chamber up to 50.0 MPa. Working pressure inside the high pressure cell is however restricted to 27.5 MPa, since hydrostatic calibration and safety testing of the unit is limited to 29 MPa within the temperature range 308 – 348 K.

The high pressure nature of the experiments requires excellent sealing mechanisms. In Figure 5-2 the main sealing mechanisms are indicated.

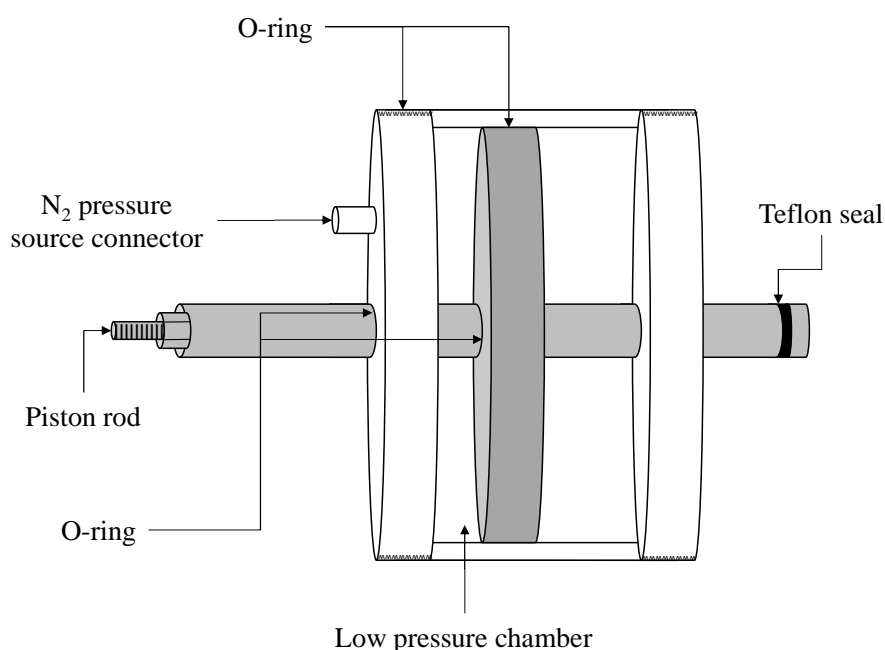


Figure 5-2 Schematic diagram of the low pressure chamber to indicate important sealing mechanisms

Proper sealing of the high pressure chamber is established with a Teflon seal on the piston rod end (indicated in Figure 5-1 and Figure 5-2). As the piston rod is tightened with the nut, the Teflon seal compresses and expands in the radial direction, which accomplishes sealing.

In the low pressure chamber sealing is required to prevent the loss of nitrogen to the atmosphere. If nitrogen leaks from the low pressure chamber the required pressure in the high pressure chamber will not be attained. O-rings were used in four locations to completely seal off the low pressure chamber. The positions of the O-rings are indicated in Figure 5-2.

5 | Experimental Bubble and Dew Point Data

At the one end of the equilibrium cell a sight glass is fitted to allow visual observation of the contents of the cell. The sight glass has an operating temperature limit of 473 K and an operating pressure limit of 50.0 MPa. An endoscope attached to a light source is placed in front of the sight glass (as indicated in Figure 5-1) and the images are then projected on a monitor. This setup enables very accurate visual observation of the appearance of a second phase.

The temperature of the cell contents is controlled by the flow of heating fluid in the heating jacket. For the large cell water was used as the heating fluid and for the small cell, oil. The temperature in the cell is monitored with an accuracy of better than 0.1 K with a 4-wire PT-100 probe which is inserted into a well in the equilibrium cell wall.

Direct pressure measurement was found to be much more accurate than indirect pressure measurement with the nitrogen regulator [1] and therefore a pressure sensor was positioned in the cell wall of the high pressure chamber. The pressure sensor is accurate to 0.02 MPa (details are provided in section 5.1.4).

A magnetic stirrer is placed in the cell to ensure that the contents form a homogenous mixture. The stirring action is controlled by the magnetic plate that is placed underneath the equilibrium cell during operation.

5.1.3 Factors that Require Special Attention

The operating procedure for the variable volume equilibrium cells are given in Appendix D.

High pressure phase equilibrium experiments are of such a nature that very small and seemingly insignificant factors can have a large influence on the accuracy of the data. In most cases the experience of the operator contribute more to the accuracy of the data than following the written procedures in an operating manual [2]. Fonseca et al. [2] and Raal and Mühlbauer [3] discussed some features of high pressure phase equilibrium experiments that require special attention. The relevant points were considered in either the design of the experimental equipment or during the experimental procedure.

- To avoid any contamination of the mixture in the cell, the equipment must be thoroughly cleaned before an experimental run can commence. Any stubborn solutes from previous experimental runs must be dissolved and washed out of the cell. A good

5 | Experimental Bubble and Dew Point Data

equilibrium cell design minimizes, or ideally avoids, any nooks and corners where material can accumulate.

- The mass of solute and solvent transferred to the equilibrium cell must be weighed very accurately. Very small masses are generally used and thus the possible error in the measurement is very large. In this investigation a balance with a precision of 0.01 g was used to weigh the solvent container (mass varied between 30 g and 4 g), and a balance with a precision of 0.0001 g was used to weigh the solute container (mass varied between 15 g and 0.1 g).
- Thorough mixing of the equilibrium cell contents is required to ensure true equilibrium is reached. In this study mixing was achieved by a magnetic stirrer bar. The stirrer bar is large enough compared to the cell volume to ensure that all the phases are included in the mixture.
- The question as to whether the phenomena observed in the equilibrium cell is the true phase separation point, is a very subjective topic. It is this question that causes most discrepancies between data obtained with the same experimental equipment, but different operators. Some of the phase changes can be easily observed visually, but especially in the mixture critical region, the exact point of phase transition is very much dependant on the operator's judgement. To ensure that the phase transition point was observed correctly, the data measured in this study was compared to data measured by other reputable research groups for the same systems. If the measured data and published data corresponded, it was then taken as proof of correct phase transition observation.
- It is important that isothermal equilibrium conditions exist during data capturing. The mixture must be left a sufficient length of time after the temperature has been adjusted to obtain isothermal conditions (typically 30 min for a 15 K increase in the water bath, and 50 min for a 15 K increase in the oil bath). The design and setup of the equilibrium cell must also eliminate the possibility of thermal gradients, hot spots and dead volume.
- It is very important that the temperature and pressure inside the cell is measured accurately. The temperature sensors used in this investigation was calibrated by a South African National Accreditation Service (SANAS) outlet. Both the

thermocouples used had an accuracy of 0.1 K in the operating range used. The calibration of the pressure sensor was done every six months with a dead weight tester, and covered the entire operating range.

5.1.3 Generation of Isothermal Data

Binary phase equilibrium data are often presented as isothermal pressure-composition diagrams. All the data points measured in this investigation could not be measured at the exact same temperatures, due to fluctuations in the ambient conditions on the days when the experimental method was employed. Typically temperatures varied between 1 K and 2 K from the intended temperature in the cell.

To present the data as isothermal data, correlations were fitted to the experimentally measured P - T data at each composition, to enable interpolation between temperatures. This interpolation method has been successfully applied by numerous researchers for similar systems [4–10].

For the majority of data points a linear correlation was sufficient to describe the data over the small temperature range covered in this investigation (308 – 348 K). In the low solute concentration region, second order polynomial correlations were found to fit the data better. In the mixture critical region of especially mixtures containing primary alcohols, the P - T trend was non-linear and second order, or in some cases third order, polynomials were fitted to the data. In Figure 5-3 the P - T relationship at three different compositions of the CO_2 + 3,7-dimethyl-1-octanol mixture is shown to demonstrate the data fitting procedure.

5 | Experimental Bubble and Dew Point Data

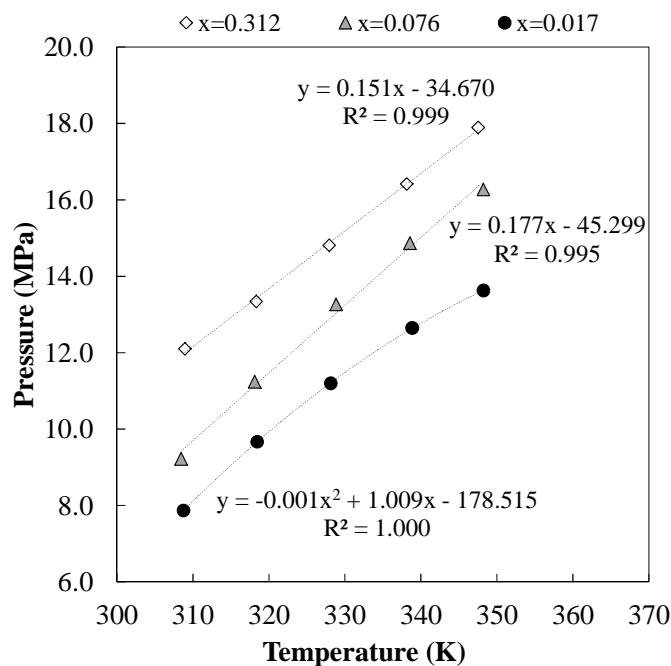


Figure 5-3 P-T relationship at different compositions of the CO₂+3,7-dimethyl-1-octanol system

Generally, where a linear fit gave an R² value of less than 0.98 or where the non-linear trend was visually apparent, a higher order polynomial was employed. It is recommended that the P-T correlations that were determined, only be used for interpolation and very limited extrapolation (up to 10 K).

5.1.4 Accuracy and Reproducibility of the Data

The accuracy of the temperature and pressure sensors and the accuracy of the mass solvent and solute loaded into the equilibrium cell, contribute to the overall accuracy of the data measured. Since the same two equilibrium cells designed by Fourie et al. [11] and Schwarz and Nieuwoudt [4] respectively, were used, the same accuracies apply to the data measured in this investigation. The experiments were conducted with the following accuracy:

- The mass of solute loaded into the cell was weighed on a calibrated analytical balance with a precision of 0.0001g. The gas sample cylinder used to convey the solvent was weighed on a calibrated analytical balance with a precision of 0.01g. Taking into account the error in the mass of solute and solvent introduced by the transfer process

5 | Experimental Bubble and Dew Point Data

into the equilibrium cell, as well as the error introduced by the flushing procedure, the mass of solute and solvent was determined with an accuracy of less than 1 % of the mass fraction value.

- The temperature sensor was calibrated by a SANAS accredited company and was reported to have an accuracy of better than 0.1 K. Calibration data is included in Appendix A.
- The pressure sensor was calibrated biannually to an accuracy of 0.02 MPa with a dead weight tester. Calibration data is included in Appendix A. The error involved in the visual observation of the phase transition point was added to the pressure sensor accuracy, and thus the total accuracy of the observed phase transition pressure was determined as 0.06 MPa.

It is very important that the data measured in this investigation can be reproduced at any time by any competent researcher with similar equipment. To prove the reproducibility of the data, two data points of very similar composition of the same system were measured at different times in different equilibrium cells and with different loadings and pressure calibration data.

In Figure 5-4 two data points at compositions of 0.0323 and 0.0344 mass fraction 3,7-dimethyl-1-octanol are compared. The measured pressures for the two points compare very well to one another and can serve as proof of reproducibility of the data measured in this investigation. Errors in pressure and composition were smaller than the markers used to represent the data points.

The reliability of the data measured in this study is further supported by the data presented in Figure 5-8 (details are discussed in section 5.2.1). The same data point was measured by another competent operator and similar phase transition pressures were observed for the ethane + *n*-decane system.

5 | Experimental Bubble and Dew Point Data

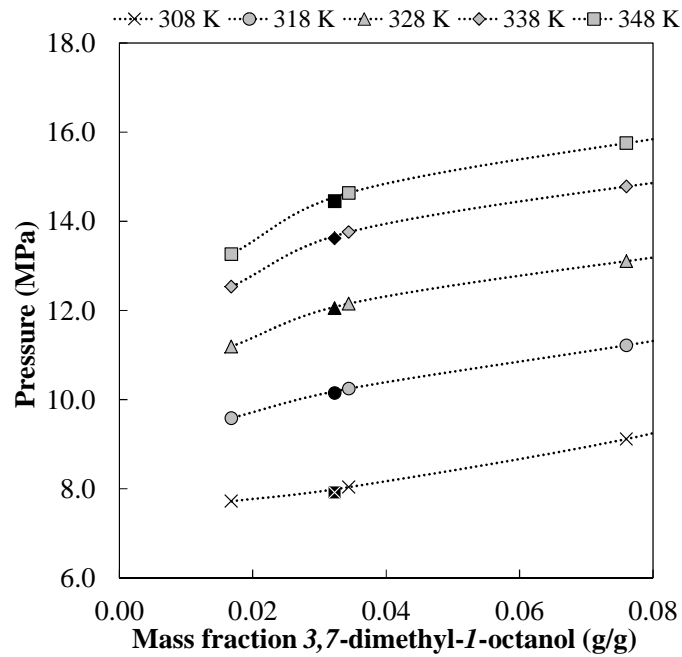


Figure 5-4 P-x plot for the CO_2 +3,7-dimethyl-1-octanol system to show the reproducibility of the data

5.1.5 Verification of the Accuracy of the Experimental Method

The accuracy of the experimental method employed in this investigation was verified by comparing the measured data to reliable published data for the CO_2 +*n*-decane system. The comparison between the data sets is shown in Figure 5-5.

5 | Experimental Bubble and Dew Point Data

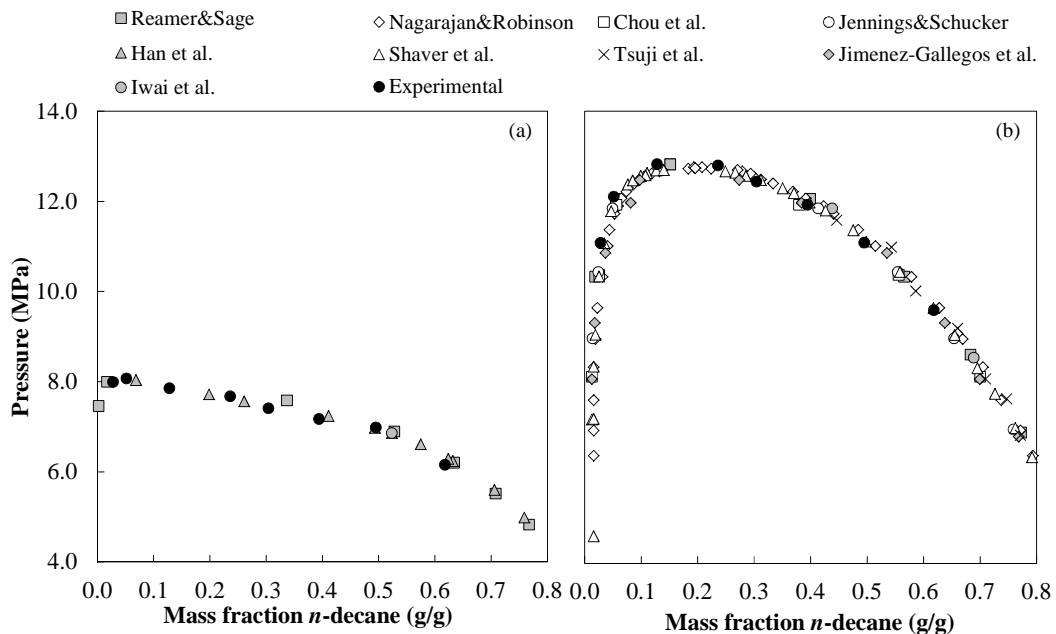


Figure 5-5 Comparison between the measured phase equilibrium data (●....this work) and published phase equilibrium data (■....[12], ◇....[13], □....[14], ○....[15], ▲....[16], △....[17], ×....[18], ◆....[19], ●....[20],) for the $\text{CO}_2 + n\text{-decane}$ system at (a) 311 K and (b) 344 K

Figure 5-5 indicates that the $\text{CO}_2 + n\text{-decane}$ system is a well-researched system, and consequently the data presented by the authors are considered to be accurate. The data generated in this investigation agrees with the data found in literature at both 311 K and 344 K. Agreement between the measured and published data for the $\text{CO}_2 + n\text{-decane}$ system thus serves as verification of the accuracy of the experimental method employed in this study. All other data presented in this work can thus be considered accurate.

5.2 Measured Data for Binary Ethane + Alkane Mixtures

Table 5-2 to Table 5-5 contain the isothermal data that were generated for the systems: ethane + $n\text{-decane}$, ethane + 2-methylnonane, ethane + 3-methylnonane and ethane + 4-methylnonane. The tables also contain the parameters that were used to generate the isothermal data. These parameters can be used to generate isothermal data at any temperature within the temperature range 308 – 348 K. The experimentally measured data is supplied in Appendix B.

5 | Experimental Bubble and Dew Point Data

Table 5-2 Isothermal data for the ethane+n-decane system

Mass fraction solute (g/g)	Parameters for temperature correction					Temperature (K)				
	$P = A \cdot T^3 + B \cdot T^2 + C \cdot T + D$					308	318	328	338	348
	A	B	C	D	R ²	Pressure (MPa)				
0.662	0	0	0.062082	-15.924	1.000	3.20	3.82	4.44	5.06	5.68
0.559	0	0	0.073547	-18.946	1.000	3.71	4.44	5.18	5.91	6.65
0.462	0	0	0.083016	-21.531	1.000	4.04	4.87	5.70	6.53	7.36
0.370	0	0	0.088092	-22.853	0.999	4.28	5.16	6.04	6.92	7.80
0.303	0	0	0.091443	-23.706	0.998	4.46	5.37	6.29	7.20	8.12
0.224	0	0	0.090628	-23.205	0.999	4.71	5.61	6.52	7.43	8.33
0.180	0	0	0.087216	-22.053	0.998	4.81	5.68	6.55	7.43	8.30
0.120	0	0	0.081058	-20.059	0.998	4.91	5.72	6.53	7.34	8.15
0.0753	0	0	0.073201	-17.608	0.994	4.94	5.67	6.40	7.13	7.87
0.0483	0	0	0.063573	-14.616	0.986	4.96	5.60	6.24	6.87	7.51
0.0278	0	-0.00085645	0.60989	-101.726	0.999	4.87	5.61	6.18	6.57	6.79

Table 5-3 Isothermal data for the ethane+2-methylnonane system

Mass fraction solute (g/g)	Parameters for temperature correction					Temperature (K)				
	$P = A \cdot T^3 + B \cdot T^2 + C \cdot T + D$					308	318	328	338	348
	A	B	C	D	R ²	Pressure (MPa)				
0.658	0	0	0.062427	-16.081	0.997	3.15	3.77	4.39	5.02	5.64
0.529	0	0	0.074262	-19.100	0.999	3.77	4.51	5.26	6.00	6.74
0.459	0	0	0.080706	-20.873	0.999	3.98	4.79	5.60	6.41	7.21
0.363	0	0	0.087223	-22.527	1.000	4.34	5.21	6.08	6.95	7.83
0.288	0	0	0.089061	-22.899	1.000	4.53	5.42	6.31	7.20	8.09
0.211	0	0	0.087568	-22.253	0.998	4.72	5.59	6.47	7.34	8.22
0.142	0	0	0.084067	-20.986	0.999	4.91	5.75	6.59	7.43	8.27
0.0741	0	-0.00049561	0.39853	-70.696	1.000	5.03	5.92	6.70	7.38	7.97

5 | Experimental Bubble and Dew Point Data

Table 5-4 Isothermal data for the ethane+3-methylnonane system

Mass fraction solute (g/g)	Parameters for temperature correction					Temperature (K)				
	$P = A*T^3 + B*T^2 + C*T + D$					308	318	328	338	348
	A	B	C	D	R ²	Pressure (MPa)				
0.596	0	0	0.070380	-18.074	0.999	3.60	4.31	5.01	5.71	6.42
0.517	0	0	0.078038	-20.136	0.999	3.90	4.68	5.46	6.24	7.02
0.408	0	0	0.086359	-22.334	0.999	4.26	5.13	5.99	6.86	7.72
0.273	0	0	0.090344	-23.189	0.999	4.64	5.54	6.44	7.35	8.25
0.152	0	0	0.084711	-21.176	0.997	4.91	5.76	6.61	7.46	8.30
0.111	0	0	0.078452	-19.123	0.995	5.04	5.82	6.61	7.39	8.18
0.0444	0	-0.00086317	0.62601	-105.838	1.000	5.09	5.95	6.63	7.14	7.48

Table 5-5 Isothermal data for the ethane+4-methylnonane system

Mass fraction solute (g/g)	Parameters for temperature correction					Temperature (K)				
	$P = A*T^3 + B*T^2 + C*T + D$					308	318	328	338	348
	A	B	C	D	R ²	Pressure (MPa)				
0.587	0	0	0.071226	-18.416	0.998	3.52	4.23	4.95	5.66	6.37
0.467	0	0	0.080363	-20.723	0.999	4.03	4.83	5.64	6.44	7.24
0.355	0	0	0.087200	-22.497	1.000	4.36	5.23	6.10	6.98	7.85
0.230	0	0	0.088723	-22.661	0.999	4.67	5.55	6.44	7.33	8.21
0.181	0	0	0.084861	-21.326	0.998	4.81	5.66	6.51	7.36	8.21
0.116	0	0	0.078171	-19.111	0.996	4.97	5.75	6.53	7.31	8.09
0.0653	0	-0.00049591	0.39648	-70.121	1.000	4.95	5.81	6.57	7.23	7.80
0.0362	0	-0.00077110	0.56694	-96.401	0.997	5.07	5.91	6.60	7.13	7.51

In Figure 5-6 the phase behaviour of all five C₁₀-alkane isomers in supercritical ethane are plotted at 308 K and 348 K. From this figure it is clear that methyl-branched isomers of *n*-decane have phase behaviour very similar to that of the linear alkane.

5 | Experimental Bubble and Dew Point Data

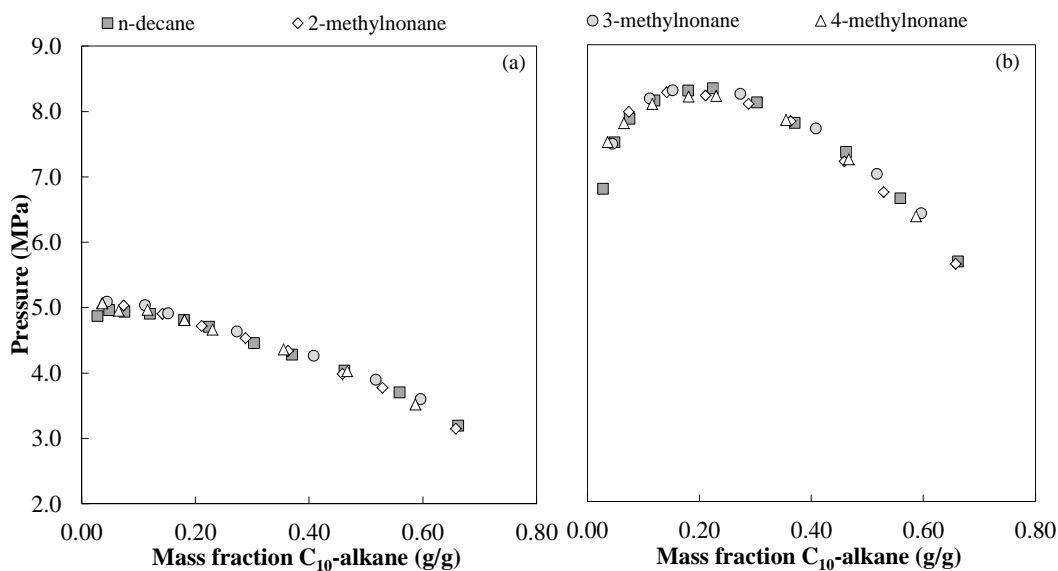


Figure 5-6 Phase behaviour of C_{10} -alkanes with supercritical ethane at (a) 308 K and (b) 348 K

5.2.1 Contradicting Solubility Results for the Ethane + n -decane System

Reported phase equilibrium data for the ethane + n -decane system from three reputable sources were compared to the data measured in this work. The location of the observed bubble points corresponded well, but the location of the dew points measured in this study deviated from that published by two other authors (see Figure 5-7 and Figure 5-8).

5 | Experimental Bubble and Dew Point Data

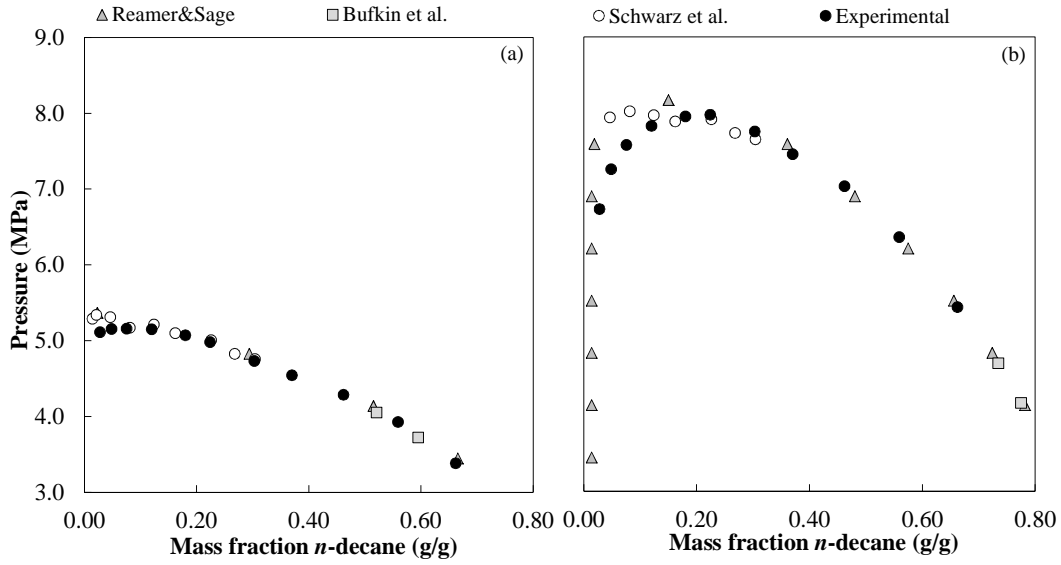


Figure 5-7 Comparison between the measured phase equilibrium data (●....this work) and published phase equilibrium data (▲....[21], ■....[22], ○....[8]) of the ethane+n-decane system at (a) 311 K and (b) 344 K

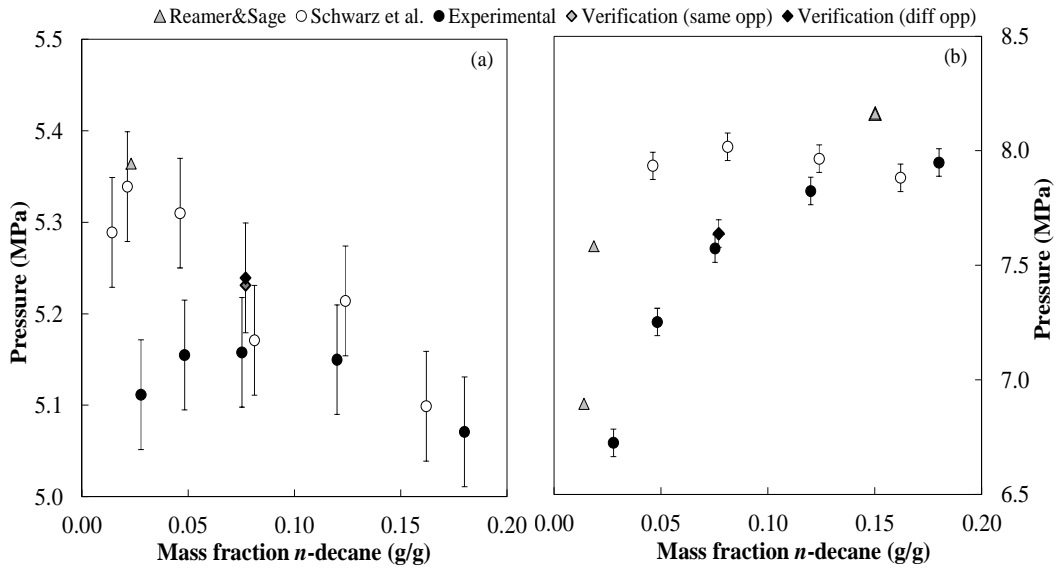


Figure 5-8 Comparison between the measured phase equilibrium data (●, ◆, ◆....this work) and published phase equilibrium data (▲....[21], ○....[8]) of the low solute concentration region of the ethane+n-decane system at (a) 311 K and (b) 344 K

The largest difference between the measured dew point pressures and the published dew point pressures is approximately 0.1 MPa (at 344 K). This value is higher than the uncertainty of the

5 | Experimental Bubble and Dew Point Data

pressure measurements (0.06 MPa). The errors in pressure measurement are indicated by error bars on the magnified phase diagrams given in Figure 5-8. The errors in composition measurements were less than the width of the markers.

Verification of the experimental method (as reported in section 5.1.5) assured that the data measured in this investigation was accurate. Although these results were presented with confidence, an investigation into the possible causes of deviation was undertaken.

The accuracy of the data was tested again by re-measuring one composition data point, firstly by the same operator that measured the entire data set, and then secondly by an independent researcher with considerable experience in the field. By bringing in a second operator, possible error due to faulty phase transition observation was eliminated. In the magnified phase diagrams (Figure 5-8) the two independently measured data points correlate well to one another as well as to the rest of the experimentally measured data. It was assumed that the measured data was correct and thus other possible reasons for the discrepancies were investigated.

Schwarz et al. [8] measured the low concentration data points using the exact same experimental method and equipment used in this investigation. The only difference is that the low *n*-decane concentration phase transition points were measured using the small equilibrium cell. The dew points of the ethane + *n*-decane system were especially hard to observe due to the onset of murkiness in the mixture before a small droplet manifests itself on the sight glass. For a smaller mass of material in the equilibrium cell, as used by Schwarz et al. [8], the possibility of error in the observation of the dew points is therefore much larger. The reason for the deviation of the data measured in this investigation from the data published by Schwarz et al. [8] can be ascribed to the fact that Schwarz et al. [8] used a much smaller mass of *n*-decane and thus possibly observed the onset of the murkiness of the mixture as the phase transition point, because the droplets were too small to observe.

The difference between the measured data and the data published by Reamer and Sage [21] can be found in the experimental methods used. Reamer and Sage [21] used an isolated cell containing a known amount of ethane and *n*-decane and under isothermal conditions determined the molal volume at different pressures for the mixture. The volumetric measurements were plotted and the bubble points were established from the discontinuous change in the isothermal derivative of volume with respect to pressure at constant composition. The composition of the dew point gas was determined by withdrawing a sample under isobaric, isothermal conditions and then applying a partial condensation

procedure. The use of the volume-pressure gradient to determine the phase transition point is fairly accurate for compositions far away from the mixture critical point where the densities of the co-existing phases differ significantly from one another. However, close to the mixture critical point the densities of the co-existing phases approach one another and the exact point where the gradient of the volume-pressure relationship changes, becomes hard to pinpoint. Also, at low concentrations of *n*-decane the contribution of the liquid phase to the overall density becomes negligible, and the identification of the point of phase transition becomes problematic [1]. It is thus these difficulties in the method used by Reamer and Sage [21] that may explain the discrepancies between the data measured by them and the data measured in this work.

After considering the good agreement between the data measured in this work and data published by reputable sources for the CO₂ + *n*-decane (see section 5.1.5) and ethane + 1-decanol (see section 5.3.1) systems, the data measured in this investigation for the ethane + *n*-decane system was assumed to be accurate within the error margins indicated in Figure 5-8. This does not invalidate the published data, but rather highlights the discrepancies that can creep in when using different experimental methods and equipment.

5.2.2 Classification of the Ethane + Alkane Systems

Peters et al. [23] reported the occurrence of total miscibility for mixtures of ethane, and *n*-alkanes with carbon numbers up to 17 (discussed in detail in Chapter 4, section 4.1.2). Due to the similar nature of the components, it is suggested that the ethane + *n*-decane system be classified as Type I phase behaviour [24,25]. The ethane + C₁₀-alkane isomer systems have phase behaviour very similar to that of ethane + *n*-decane and can tentatively be assumed to also exhibit Type I phase behaviour, but more information on the phase behaviour in the low temperature region is required to confirm this.

5.3 Measured Data for Binary Ethane + Alcohol Mixtures

Table 5-6 to Table 5-10 contain the isothermal data that were generated for the systems: ethane + 1-decanol, ethane + 2-decanol, ethane + 3,7-dimethyl-1-octanol, ethane + 2,-dimethyl-2-octanol and ethane + 3,7-dimethyl-3-octanol.

5 | Experimental Bubble and Dew Point Data

Table 5-6 Isothermal data for the ethane+1-decanol system

Mass fraction solute (g/g)	Parameters for temperature correction					Temperature (K)				
	$P = A \cdot T^3 + B \cdot T^2 + C \cdot T + D$					308	318	328	338	348
	A	B	C	D	R ²	Pressure (MPa)				
0.656	0	0	0.14227	-38.078	0.993	5.74	7.17	8.59	10.01	11.43
0.568	0	0	0.13742	-34.492	0.999	7.83	9.21	10.58	11.95	13.33
0.442	0	0	0.12883	-30.239	0.987	9.44	10.73	12.02	13.31	14.59
0.380	0	0	0.12634	-29.173	0.987	9.74	11.00	12.27	13.53	14.79
0.290	0	0	0.12451	-28.575	0.987	9.77	11.02	12.26	13.51	14.75
0.226	0	0	0.12322	-28.260	0.987	9.69	10.92	12.16	13.39	14.62
0.186	0	0	0.12020	-27.566	0.985	9.46	10.66	11.86	13.06	14.26
0.122	0	0	0.11298	-25.750	0.983	9.05	10.18	11.31	12.44	13.57
0.0798	0	-0.0012726	0.95303	-164.931	1.000	7.87	9.44	10.75	11.80	12.60
0.0507	0	-0.0013746	1.0127	-174.566	1.000	6.96	8.48	9.73	10.70	11.40
0.0284	0	-0.0011721	0.87877	-153.730	1.000	5.74	7.19	8.41	9.39	10.13
0.0182	0	-0.0013356	0.97821	-169.175	1.000	5.41	6.83	7.99	8.87	9.49

Table 5-7 Isothermal data for the ethane+3,7-dimethyl-1-octanol system

Mass fraction solute (g/g)	Parameters for temperature correction					Temperature (K)				
	$P = A \cdot T^3 + B \cdot T^2 + C \cdot T + D$					308	318	328	338	348
	A	B	C	D	R ²	Pressure (MPa)				
0.644	0	0	0.13023	-35.207	0.999	4.90	6.21	7.51	8.81	10.11
0.550	0	0	0.14636	-39.216	0.993	5.86	7.32	8.79	10.25	11.72
0.454	0	0	0.14381	-37.601	0.987	6.69	8.13	9.57	11.01	12.44
0.378	0	0	0.14045	-36.220	0.990	7.04	8.44	9.85	11.25	12.66
0.295	0	0	0.13699	-35.175	0.992	7.02	8.39	9.76	11.13	12.50
0.224	0	0	0.13815	-35.538	0.988	7.01	8.39	9.77	11.16	12.54
0.176	0	0	0.13317	-34.172	0.987	6.84	8.17	9.51	10.84	12.17
0.115	0	-0.0013374	1.0112	-178.398	1.000	6.19	7.93	9.40	10.61	11.54
0.0745	0	-0.0012826	0.96283	-169.109	1.000	5.77	7.37	8.71	9.80	10.63
0.0499	0	-0.0014332	1.0518	-182.628	1.000	5.36	6.91	8.17	9.14	9.83
0.0267	0	-0.0010362	0.78329	-137.740	0.998	5.22	6.56	7.70	8.63	9.36
0.0202	0	-0.0011019	0.82002	-142.991	1.000	5.04	6.35	7.43	8.29	8.93

5 | Experimental Bubble and Dew Point Data

Table 5-8 Isothermal data for the ethane+2-decanol system

Mass fraction solute (g/g)	Parameters for temperature correction					Temperature (K)				
	$P = A \cdot T^3 + B \cdot T^2 + C \cdot T + D$					308	318	328	338	348
	A	B	C	D	R ²	Pressure (MPa)				
0.648	0	0	0.11220	-29.890	0.999	4.67	5.79	6.91	8.03	9.16
0.546	0	0	0.13417	-35.815	0.993	5.51	6.85	8.19	9.54	10.88
0.468	0	0	0.13287	-34.677	0.990	6.25	7.58	8.90	10.23	11.56
0.384	0	0	0.13069	-33.679	0.991	6.58	7.88	9.19	10.50	11.80
0.302	0	0	0.12863	-32.935	0.989	6.68	7.97	9.26	10.54	11.83
0.228	0	0	0.12627	-32.285	0.989	6.61	7.87	9.13	10.39	11.66
0.172	0	0	0.12607	-32.467	0.987	6.36	7.62	8.89	10.15	11.41
0.119	0	0	0.12020	-30.908	0.986	6.11	7.31	8.52	9.72	10.92
0.0822	0	0	0.11477	-29.564	0.985	5.79	6.93	8.08	9.23	10.38
0.0519	0	0	0.10668	-27.355	0.982	5.50	6.57	7.63	8.70	9.77
0.0298	0	-0.0011668	0.86957	-152.110	0.999	5.03	6.43	7.58	8.51	9.20
0.0120	0	-0.00098943	0.72987	-125.782	1.000	5.16	6.26	7.17	7.88	8.39

Table 5-9 Isothermal data for the ethane+2,6-dimethyl-2-octanol system

Mass fraction solute (g/g)	Parameters for temperature correction					Temperature (K)				
	$P = A \cdot T^3 + B \cdot T^2 + C \cdot T + D$					308	318	328	338	348
	A	B	C	D	R ²	Pressure (MPa)				
0.642	0	0	0.089091	-22.713	0.999	4.73	5.62	6.51	7.40	8.29
0.529	0	0	0.10631	-27.708	1.000	5.04	6.10	7.16	8.22	9.29
0.445	0	0	0.11531	-30.425	0.999	5.09	6.24	7.40	8.55	9.70
0.387	0	0	0.11489	-30.159	0.999	5.23	6.38	7.53	8.67	9.82
0.298	0	0	0.11904	-31.437	0.997	5.23	6.42	7.61	8.80	9.99
0.237	0	0	0.11671	-30.661	0.996	5.29	6.45	7.62	8.79	9.95
0.174	0	0	0.11558	-30.370	0.995	5.23	6.38	7.54	8.70	9.85
0.122	0	0	0.10800	-27.949	0.994	5.31	6.39	7.47	8.55	9.63
0.0800	0	0	0.095807	-24.148	0.990	5.36	6.32	7.28	8.24	9.19
0.0535	0	0	0.085124	-20.810	0.985	5.41	6.26	7.11	7.96	8.81
0.0285	0	-0.00085577	0.63480	-109.061	1.000	5.28	6.27	7.09	7.74	8.21
0.0150	0	-0.0010478	0.74860	-125.863	1.000	5.30	6.23	6.95	7.46	7.75

5 | Experimental Bubble and Dew Point Data

Table 5-10 Isothermal data for the ethane+3,7-dimethyl-3-octanol system

Mass fraction solute (g/g)	Parameters for temperature correction					Temperature (K)				
	$P = A \cdot T^3 + B \cdot T^2 + C \cdot T + D$					308	318	328	338	348
	A	B	C	D	R ²	Pressure (MPa)				
0.651	0	0	0.080207	-20.064	0.999	4.64	5.44	6.24	7.05	7.85
0.595	0	0	0.089668	-22.782	0.999	4.84	5.73	6.63	7.53	8.42
0.459	0	0	0.10561	-27.521	1.000	5.01	6.06	7.12	8.17	9.23
0.389	0	0	0.10973	-28.715	0.999	5.08	6.18	7.28	8.37	9.47
0.302	0	0	0.11240	-29.475	0.999	5.15	6.27	7.39	8.52	9.64
0.232	0	0	0.11182	-29.330	0.999	5.11	6.23	7.35	8.47	9.58
0.203	0	0	0.11020	-28.793	0.999	5.15	6.25	7.35	8.46	9.56
0.124	0	0	0.10202	-26.238	0.998	5.18	6.20	7.22	8.24	9.26
0.0808	0	0	0.09573	-24.253	0.998	5.23	6.19	7.15	8.10	9.06
0.0513	0	0	0.08128	-19.678	0.992	5.36	6.17	6.98	7.80	8.61
0.0314	0	-0.00073039	0.54940	-94.727	1.000	5.20	6.12	6.90	7.53	8.01
0.0202	0	-0.00088649	0.64285	-108.662	1.000	5.24	6.12	6.82	7.35	7.69

In Figure 5-9 the phase behaviour of the five C₁₀-alcohol isomers in supercritical ethane are compared at 308 K and 348 K. The phase transition pressures of the alcohol isomers in supercritical ethane decrease in the following order: 1-decanol, 3,7-dimethyl-1-octanol, 2-decanol, 2,6-dimethyl-2-octanol and 3,7-dimethyl-3-octanol.

The region of importance for SFF processes is the low solute mass fraction region (typically less than 10 mass % solute). If the compounds show significant difference in solubility in this region, successful separation with SFF is likely. From Figure 5-9 and Figure 5-10 it is clear that at 308 K all the branched isomers have similar phase behaviour in the low solute mass fraction region, while their phase behaviour at 348 K is more distinguishable. This phenomenon can possibly lead to better separation occurring between C₁₀-alcohol isomers at higher operation temperatures. The pairs, 2-decanol and 3,7-dimethyl-1-octanol, and 2,6-dimethyl-2-octanol and 3,7-dimethyl-3-octanol show similar phase transition pressures in the low solute concentration region. Consequently, the likelihood of SFF separation for these pairs with supercritical ethane is low.

5 | Experimental Bubble and Dew Point Data

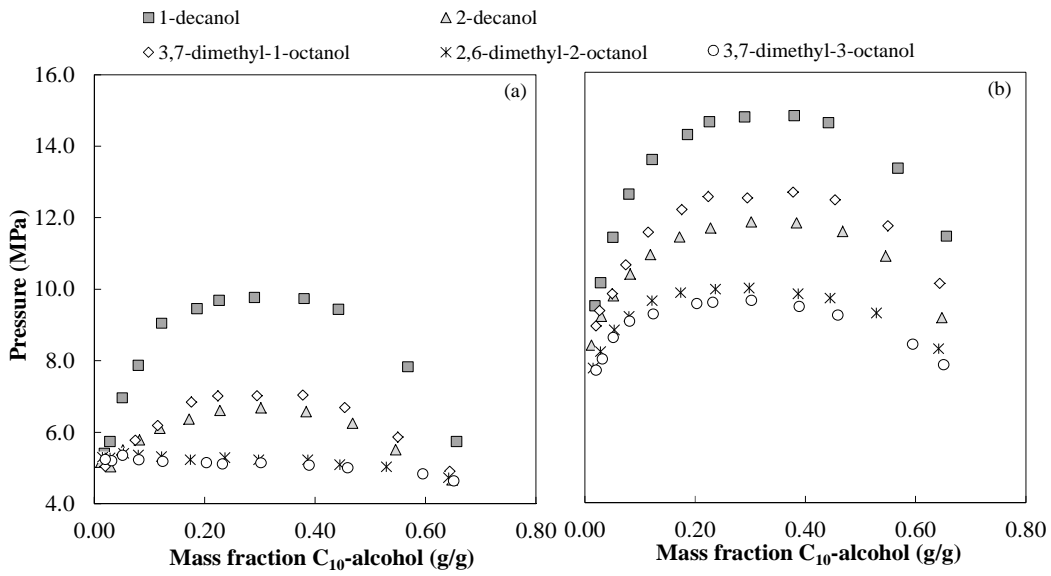


Figure 5-9 Phase behaviour of C_{10} -alcohol isomers in supercritical ethane at (a) 308 K and (b) 348 K

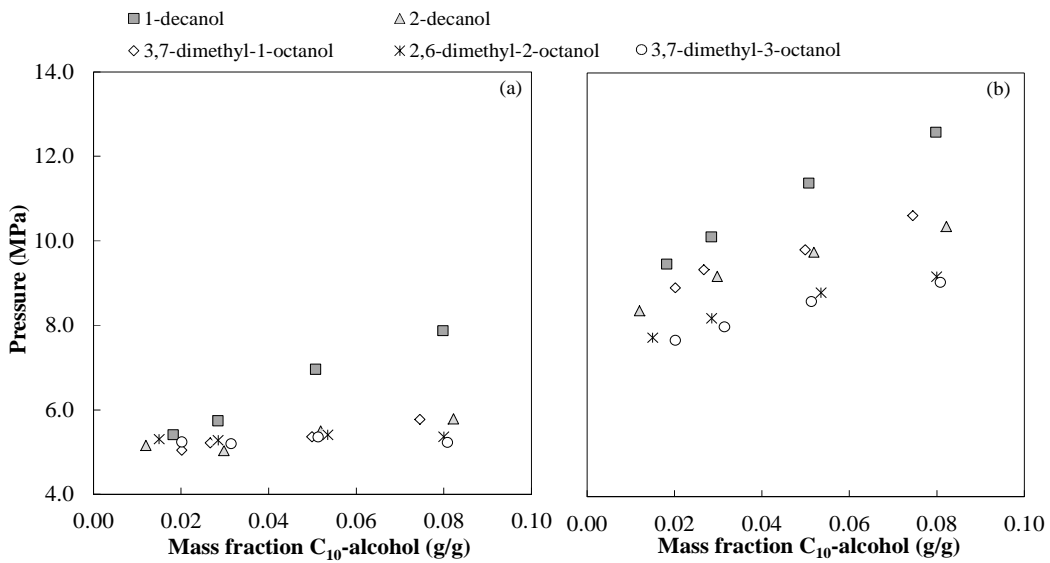


Figure 5-10 Phase behaviour of C_{10} -alcohol isomers in supercritical ethane in the low solute concentration region at (a) 308 K and (b) 348 K

5.3.1 Comparison to Literature Data

Schwarz et al. [7] reported phase equilibrium data within similar temperature, pressure and composition ranges as those used in this study for the system ethane + *I*-decanol. From Figure 5-11 it is clear that the data measured in this study correspond well to that published by Schwarz et al. [7].

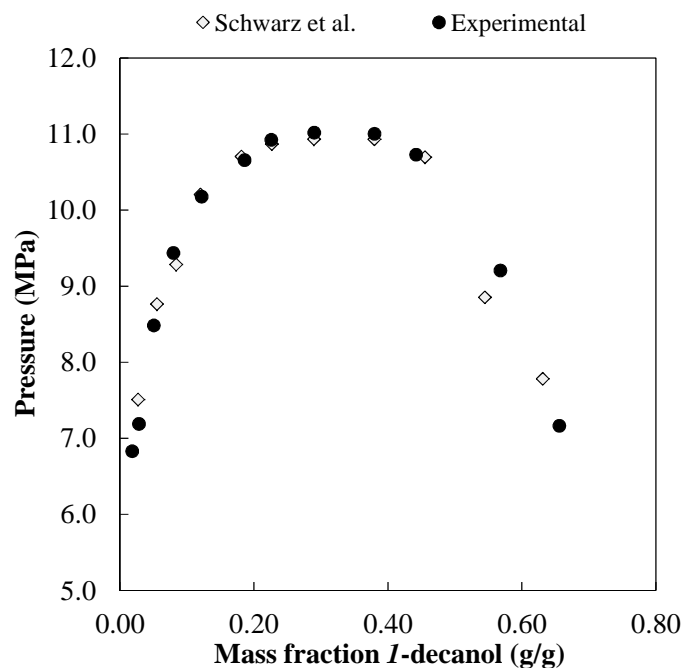


Figure 5-11 Comparison between the measured phase equilibrium data (●....this work) and published phase equilibrium data (◇....[7]) of the ethane+*I*-decanol system at 318 K

5.3.2 Classification of the Systems

According to Gardeler and Gmehling [24] the system ethane + *I*-decanol can either belong to Type III, IV or V. The temperature-carbon number plot provided in Chapter 4 section 4.1.2, indicates that it is likely that Type V phase behaviour occurs for the ethane + *I*-decanol system.

From the experimental data provided for ethane + 2-decanol (Table 5-8), ethane + 2,6-dimethyl-2-octanol (Table 5-9) and ethane + 3,7-dimethyl-3-octanol (Table 5-10), it can be suggested that a three phase region might be present at very low concentrations of the respective

5 | Experimental Bubble and Dew Point Data

solutes at temperatures near the critical point of ethane. The phase equilibrium data measured for these systems at 308 K, show an increase in phase equilibrium pressure at the lowest measured concentration. More experimental data in the low solute concentration region of these systems are required to confirm the presence of a three phase region and to accurately classify the ethane + C₁₀-alcohol isomer systems.

5.4 Measured Data for Binary CO₂ + Alkane Mixtures

Table 5-12 to Table 5-15 contain the isothermal data for the CO₂ + *n*-dodecane, CO₂ + *n*-decane, CO₂ + 2-methylnonane, CO₂ + 3-methylnonane and CO₂ + 4-methylnonane systems.

Table 5-11 Isothermal data for the CO₂+*n*-dodecane system

Mass fraction solute (g/g)	Parameters for temperature correction					Temperature (K)				
	P = A*T ³ + B*T ² + C*T + D					308	318	328	338	348
	A	B	C	D	R ²	Pressure (MPa)				
0.631	0	0	0.11320	-28.427	1.000	6.44	7.57	8.70	9.83	10.97
0.568	0	0	0.13236	-33.912	1.000	6.85	8.18	9.50	10.83	12.15
0.453	0	0	0.16200	-42.638	1.000	7.26	8.88	10.50	12.12	13.74
0.393	0	0	0.17518	-46.668	0.999	7.29	9.04	10.79	12.54	14.29
0.304	0	0	0.18705	-50.130	0.999	7.48	9.35	11.22	13.09	14.96
0.220	0	0	0.19203	-51.669	0.999	7.47	9.39	11.31	13.24	15.16
0.174	0	0	0.19281	-51.942	0.999	7.44	9.37	11.30	13.23	15.15
0.122	0	0	0.19149	-51.487	0.999	7.49	9.41	11.32	13.24	15.15
0.081	0	-0.00039788	0.44466	-91.774	0.999	7.44	9.39	11.27	13.06	14.78
0.050	0	-0.0010302	0.84001	-153.507	0.998	7.49	9.44	11.18	12.72	14.06

5 | Experimental Bubble and Dew Point Data

Table 5-12 Isothermal data for the CO₂+n-decane system

Mass fraction solute (g/g)	Parameters for temperature correction					Temperature (K)				
	$P = A*T^3 + B*T^2 + C*T + D$					308	318	328	338	348
	A	B	C	D	R ²	Pressure (MPa)				
0.618	0	0	0.10439	-26.307	1.000	5.84	6.89	7.93	8.98	10.02
0.495	0	0	0.12464	-31.781	1.000	6.61	7.86	9.10	10.35	11.60
0.394	0	0	0.14420	-37.675	1.000	6.74	8.18	9.62	11.07	12.51
0.304	0	0	0.15257	-40.042	1.000	6.95	8.48	10.00	11.53	13.05
0.236	0	0	0.15538	-40.648	1.000	7.21	8.76	10.32	11.87	13.42
0.128	0	0	0.15073	-39.023	0.999	7.40	8.91	10.42	11.92	13.43
0.0513	0	-0.00086242	0.68737	-122.287	1.000	7.61	9.09	10.39	11.52	12.48
0.0278	0	-0.0010418	0.77620	-132.638	0.999	7.60	8.84	9.87	10.69	11.31

Table 5-13 Isothermal data for the CO₂+2-methylnonane system

Mass fraction solute (g/g)	Parameters for temperature correction					Temperature (K)				
	$P = A*T^3 + B*T^2 + C*T + D$					308	318	328	338	348
	A	B	C	D	R ²	Pressure (MPa)				
0.642	0	0	0.090948	-22.400	1.000	5.61	6.52	7.43	8.34	9.25
0.534	0	0	0.11323	-28.599	1.000	6.28	7.41	8.54	9.67	10.81
0.454	0	0	0.12801	-32.842	1.000	6.59	7.87	9.15	10.43	11.71
0.361	0	0	0.14099	-36.617	1.000	6.81	8.22	9.63	11.04	12.45
0.332	0	0	0.14394	-37.434	1.000	6.90	8.34	9.78	11.22	12.66
0.251	0	0	0.15063	-39.315	1.000	7.08	8.59	10.09	11.60	13.10
0.176	0	0	0.15092	-39.190	0.999	7.29	8.80	10.31	11.82	13.33
0.0748	0	0	0.13492	-33.906	0.996	7.65	9.00	10.35	11.70	13.05
0.0343	0	-0.0013967	1.0105	-171.049	0.999	7.71	9.07	10.15	10.96	11.48

5 | Experimental Bubble and Dew Point Data

Table 5-14 Isothermal data for the CO₂+3-methylnonane system

Mass fraction solute (g/g)	Parameters for temperature correction					Temperature (K)				
	$P = A \cdot T^3 + B \cdot T^2 + C \cdot T + D$					308	318	328	338	348
	A	B	C	D	R ²	Pressure (MPa)				
0.664	0	0	0.084250	-20.575	1.000	5.37	6.22	7.06	7.90	8.74
0.520	0	0	0.11773	-29.827	1.000	6.43	7.61	8.79	9.96	11.14
0.450	0	0	0.13181	-33.933	1.000	6.66	7.98	9.30	10.62	11.94
0.307	0	0	0.14976	-39.101	1.000	7.02	8.52	10.02	11.52	13.01
0.234	0	0	0.15227	-39.684	1.000	7.21	8.74	10.26	11.78	13.30
0.144	0	0	0.14854	-38.292	0.999	7.46	8.94	10.43	11.91	13.40
0.0902	0	0	0.13891	-35.088	0.998	7.70	9.09	10.47	11.86	13.25
0.0514	0	0	0.11943	-28.863	0.995	7.92	9.12	10.31	11.50	12.70

Table 5-15 Isothermal data for the CO₂+4-methylnonane system

Mass fraction solute (g/g)	Parameters for temperature correction					Temperature (K)				
	$P = A \cdot T^3 + B \cdot T^2 + C \cdot T + D$					308	318	328	338	348
	A	B	C	D	R ²	Pressure (MPa)				
0.609	0	0	0.10195	-25.572	1.000	5.83	6.85	7.87	8.89	9.91
0.526	0	0	0.11578	-29.375	1.000	6.28	7.44	8.60	9.76	10.92
0.469	0	0	0.12554	-32.175	1.000	6.49	7.75	9.00	10.26	11.51
0.375	0	0	0.13910	-36.023	1.000	6.82	8.21	9.60	10.99	12.38
0.313	0	0	0.14521	-37.789	1.000	6.94	8.39	9.84	11.29	12.74
0.228	0	0	0.15082	-39.291	1.000	7.16	8.67	10.18	11.68	13.19
0.180	0	0	0.14916	-38.643	0.999	7.30	8.79	10.28	11.77	13.26
0.130	0	0	0.14473	-37.157	0.999	7.42	8.87	10.31	11.76	13.21
0.0882	0	0	0.13706	-34.628	0.998	7.59	8.96	10.33	11.70	13.07
0.0441	0	-0.00089263	0.70370	-124.438	0.997	7.62	9.07	10.34	11.43	12.35

The CO₂ + *n*-decane system was used as the verification data set for the experimental method employed (see section 5.1.5). Very good agreement was found between published data and the bubble and dew point data measured in this work.

In Figure 5-12 the phase behaviour of the C₁₀-alkane isomers in supercritical CO₂ are compared at 308 K and 348 K. The phase transition pressures of the four isomers are very similar at high and

low temperatures. The use of SFF for the separation of compounds that exhibit such similar phase behaviour will in all likelihood prove unsuccessful.

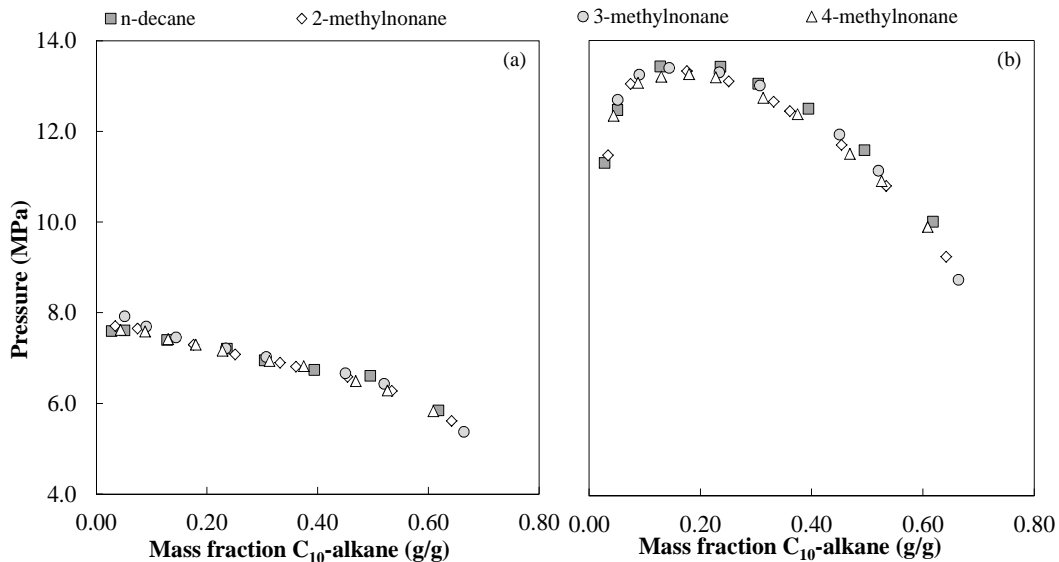


Figure 5-12 Phase behaviour of C_{10} -alkanes in supercritical CO_2 at (a) 308 K and (b) 348 K

5.4.1 Classification of the Systems

It is widely known that the $CO_2 + n$ -decane system exhibits Type II phase behaviour [26]. Since the $CO_2 + C_{10}$ -alkane isomer systems investigated have phase behaviour very similar to that of the $CO_2 + n$ -decane system, it is expected that they will also exhibit Type II behaviour, but more information on the phase behaviour at subcritical conditions is required to be certain.

5.5 Measured Data for Binary $CO_2 +$ Alcohol Mixtures

Table 5-16 to Table 5-20 contain the isothermal phase equilibrium data for the following systems: $CO_2 + 1$ -decanol, $CO_2 + 2$ -decanol, $CO_2 + 3,7$ -dimethyl- 1 -octanol, $CO_2 + 2,6$ -dimethyl- 2 -octanol and $CO_2 + 3,7$ -dimethyl- 3 -octanol.

5 | Experimental Bubble and Dew Point Data

Table 5-16 Isothermal data for the CO₂ + 1-decanol system

Mass fraction solute (g/g)	Parameters for temperature correction					Temperature (K)				
	$P = A \cdot T^3 + B \cdot T^2 + C \cdot T + D$					308	318	328	338	348
	A	B	C	D	R ²	Pressure (MPa)				
0.697	0	0	0.12583	-31.138	0.996	7.6	8.9	10.1	11.4	12.7
0.667	0	0	0.11923	-27.930	0.996	8.79	9.99	11.18	12.37	13.56
0.639	0	0.0020001	-1.2329	201.305	0.985	11.30	11.49	12.08	13.07	14.46
0.605	-0.00013739	0.13944	-47.061	5296.195	0.997	14.98	13.43	13.56	14.53	15.53
0.509	-0.00034643	0.35207	-119.19	13461.214	0.998	25.88	19.62	17.67	17.96	18.41
0.398	-0.00035416	0.36186	-123.20	13996.396	0.998	31.09	23.37	20.45	20.20	20.51
0.303	-0.00039904	0.40734	-138.56	15726.336	0.998	32.83	24.29	21.08	20.80	21.07
0.242	-0.00038266	0.39100	-133.12	15123.868	0.998	32.54	24.18	21.00	20.72	21.04
0.182	-0.00030121	0.30825	-105.10	11959.422	0.999	29.71	23.02	20.51	20.37	20.80
0.126	-0.00024716	0.25217	-85.686	9716.649	0.996	25.39	20.62	19.12	19.42	20.02
0.0808	-0.00012160	0.12340	-41.627	4685.021	0.998	17.34	16.14	16.42	17.45	18.49
0.0521	0	0	0.11602	-23.606	0.991	12.13	13.29	14.45	15.61	16.77
0.0275	0	0	0.16454	-41.831	0.993	8.85	10.49	12.14	13.78	15.43
0.0180	0	0	0.15445	-39.192	1.000	8.38	9.92	11.47	13.01	14.56

Table 5-17 Isothermal data for the CO₂+3,7-dimethyl-1-octanol system

Mass fraction solute (g/g)	Parameters for temperature correction					Temperature (K)				
	$P = A \cdot T^3 + B \cdot T^2 + C \cdot T + D$					308	318	328	338	348
	A	B	C	D	R ²	Pressure (MPa)				
0.624	0	0	0.13345	-33.637	0.999	7.47	8.80	10.14	11.47	12.81
0.522	0	0	0.15558	-38.894	0.998	9.03	10.58	12.14	13.69	15.25
0.460	0	0	0.15437	-37.378	1.000	10.17	11.71	13.25	14.80	16.34
0.402	0	0	0.14613	-33.652	0.999	11.36	12.82	14.28	15.74	17.20
0.312	0	0	0.15107	-34.670	0.999	11.86	13.37	14.88	16.39	17.90
0.188	0	0	0.14645	-33.341	0.999	11.76	13.23	14.69	16.16	17.62
0.117	0	0	0.16262	-39.522	0.997	10.56	12.19	13.82	15.44	17.07
0.0760	0	-0.0010708	0.88053	-160.501	1.000	9.12	11.22	13.11	14.78	16.24
0.0344	0	-0.0015109	1.1668	-207.989	1.000	8.04	10.25	12.15	13.76	15.06
0.0168	0	-0.0013143	1.0095	-178.515	1.000	7.72	9.59	11.19	12.53	13.61

5 | Experimental Bubble and Dew Point Data

Table 5-18 Isothermal data for the CO₂+2-decanol system

Mass fraction solute (g/g)	Parameters for temperature correction					Temperature (K)				
	$P = A \cdot T^3 + B \cdot T^2 + C \cdot T + D$					308	318	328	338	348
	A	B	C	D	R ²	Pressure (MPa)				
0.607	0	0	0.13120	-32.710	0.998	7.70	9.01	10.32	11.64	12.95
0.531	0	0	0.13810	-33.910	0.998	8.62	10.01	11.39	12.77	14.15
0.434	0	0.0011200	-0.61393	93.714	0.999	10.87	11.74	12.84	14.16	15.70
0.368	0	0.0015550	-0.90553	143.152	0.995	11.77	12.44	13.44	14.74	16.35
0.288	0	0.0014827	-0.85385	134.237	0.996	11.91	12.65	13.69	15.03	16.66
0.225	0	0.0012009	-0.65799	100.285	0.997	11.55	12.48	13.66	15.08	16.74
0.173	0	0.0007872	-0.37658	52.323	0.998	11.01	12.18	13.50	14.97	16.61
0.125	0	0.0000000	0.15650	-38.190	0.999	10.01	11.58	13.14	14.71	16.27
0.0758	0	-0.0011149	0.90819	-165.466	1.000	8.49	10.59	12.47	14.13	15.56
0.0485	0	-0.0014607	1.1370	-203.950	1.000	7.68	9.90	11.84	13.48	14.83
0.0271	0	-0.0012101	0.94996	-170.156	1.000	7.64	9.56	11.24	12.68	13.88
0.0193	0	-0.0012662	0.96913	-170.618	0.999	7.76	9.52	11.03	12.29	13.30
0.0153	0	-0.0013661	1.0262	-178.592	1.000	7.89	9.60	11.04	12.20	13.09

Table 5-19 Isothermal data for the CO₂+2,6-dimethyl-2-octanol system

Mass fraction solute (g/g)	Parameters for temperature correction					Temperature (K)				
	$P = A \cdot T^3 + B \cdot T^2 + C \cdot T + D$					308	318	328	338	348
	A	B	C	D	R ²	Pressure (MPa)				
0.636	0	0	0.10408	-25.640	1.000	6.42	7.46	8.50	9.54	10.58
0.537	0	0	0.13063	-33.422	1.000	6.81	8.12	9.42	10.73	12.04
0.434	0	0	0.15216	-39.734	1.000	7.13	8.65	10.17	11.70	13.22
0.380	0	0	0.16220	-42.823	1.000	7.13	8.76	10.38	12.00	13.62
0.300	0	0	0.17116	-45.462	1.000	7.26	8.97	10.68	12.39	14.10
0.232	0	0	0.17586	-46.896	0.999	7.27	9.03	10.79	12.54	14.30
0.158	0	0	0.17349	-46.042	0.999	7.39	9.13	10.86	12.60	14.33
0.119	0	0	0.16967	-44.783	0.999	7.48	9.17	10.87	12.57	14.26
0.0818	0	0	0.16106	-42.035	0.999	7.57	9.18	10.79	12.40	14.01
0.0523	0	0	0.14563	-37.118	0.996	7.74	9.19	10.65	12.11	13.56
0.0285	0	0	0.12478	-30.601	0.991	7.83	9.08	10.33	11.57	12.82
0.0183	0	-0.0012481	0.92095	-157.475	0.999	7.78	9.17	10.32	11.22	11.87

5 | Experimental Bubble and Dew Point Data

Table 5-20 Isothermal data for the CO₂+3,7-dimethyl-3-octanol system

Mass fraction solute (g/g)	Parameters for temperature correction					Temperature (K)				
	$P = A \cdot T^3 + B \cdot T^2 + C \cdot T + D$					308	318	328	338	348
	A	B	C	D	R ²	Pressure (MPa)				
0.629	0	0	0.10470	-25.977	0.999	6.27	7.32	8.36	9.41	10.46
0.529	0	0	0.12977	-33.267	1.000	6.70	8.00	9.30	10.59	11.89
0.440	0	0	0.14804	-38.606	1.000	6.99	8.47	9.95	11.43	12.91
0.362	0	0	0.16176	-42.732	1.000	7.09	8.71	10.32	11.94	13.56
0.306	0	0	0.16769	-44.476	1.000	7.17	8.85	10.53	12.21	13.88
0.248	0	0	0.17034	-45.205	1.000	7.26	8.96	10.67	12.37	14.07
0.183	0	0	0.17194	-45.643	1.000	7.31	9.03	10.75	12.47	14.19
0.121	0	0	0.16617	-43.791	0.999	7.39	9.05	10.71	12.38	14.04
0.0819	0	0	0.15792	-41.112	0.999	7.53	9.10	10.68	12.26	13.84
0.0590	0	0	0.15040	-38.715	0.997	7.61	9.11	10.62	12.12	13.63
0.0290	0	0	0.12095	-29.355	0.991	7.90	9.11	10.32	11.52	12.73
0.0181	0	-0.0011640	0.86643	-148.741	0.999	7.70	9.08	10.22	11.13	11.81

In Figure 5-13 and Figure 5-14 the phase behaviour of the C₁₀-alcohol isomers in supercritical CO₂ are shown at two temperatures. At 308 K the phase behaviour of 2-decanol and 3,7-dimethyl-1-octanol are very similar, but at 348 K the phase behaviour of these two isomers start to differ with 2-decanol exhibiting lower phase transition pressures. At both 308 K and 348 K the phase behaviour of 2,6-dimethyl-2-octanol and 3,7-dimethyl-3-octanol are hardly distinguishable from one another. When comparing the numerical values in Table 5-19 and Table 5-20, it is clear that 3,7-dimethyl-3-octanol have slightly lower phase transition pressures in the mixture critical region. The order of decreasing phase transition pressure in supercritical CO₂ are as follows: 1-decanol, 3,7-dimethyl-1-octanol, 2-decanol, 2,6-dimethyl-2-octanol and 3,7-dimethyl-3-octanol. The order of decreasing phase transition pressures for the C₁₀-alcohol isomers are therefore the same in both supercritical CO₂ and ethane.

5 | Experimental Bubble and Dew Point Data

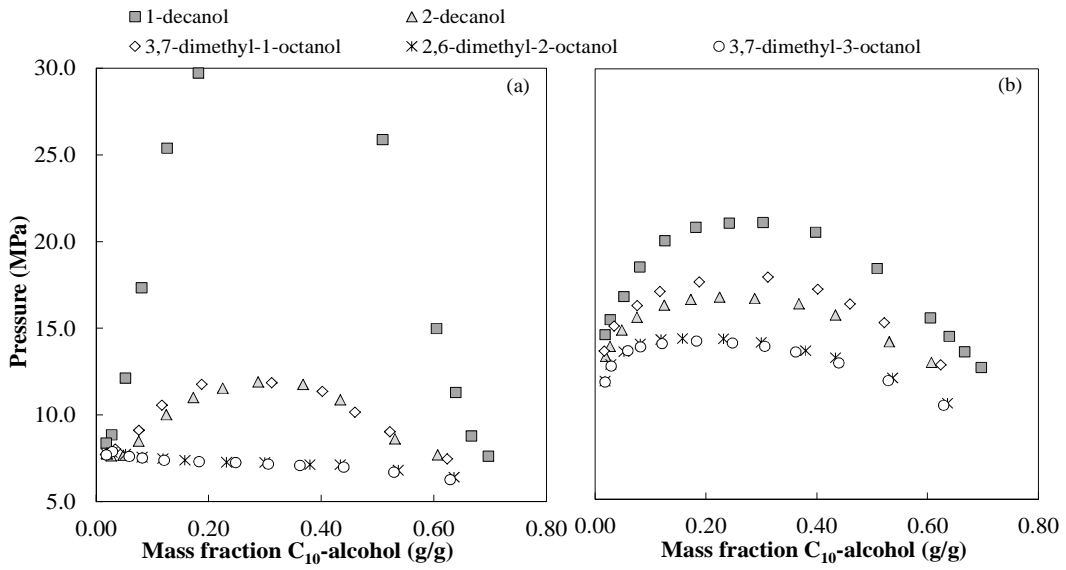


Figure 5-13 Phase behaviour of C_{10} -alcohol isomers in supercritical CO_2 at (a) 308 K and (b) 348 K

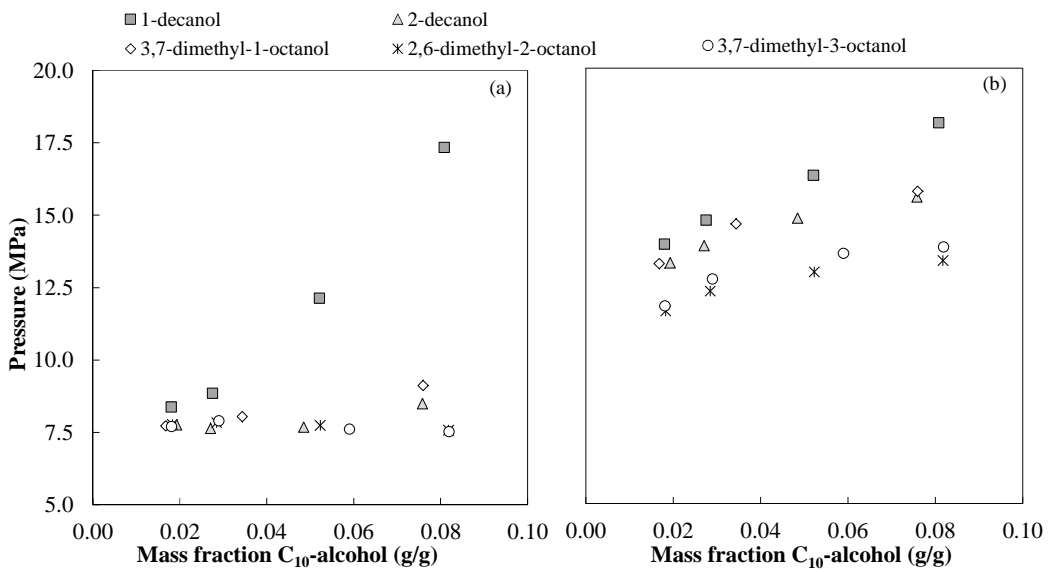


Figure 5-14 Phase behaviour of C_{10} -alcohol isomers in supercritical CO_2 in the low solute concentration region at (a) 308 K and (b) 348 K

The trends shown in Figure 5-14 indicate that 2-decanol and 3,7-dimethyl-1-octanol, and 2,6-dimethyl-2-octanol and 3,7-dimethyl-3-octanol, will in all likelihood stay paired when SFF is

employed to separate the C_{10} -alcohol isomers investigated. Only those compounds that show significant differences in phase transition pressures (or solubility) can possibly be separated by SFF.

5.5.1 Unique Phase Behaviour of the $CO_2 + 1$ -decanol System

Unlike any of the other binary systems measured in this study, the phase transition pressures of the $CO_2 + 1$ -decanol system at 308 K is much higher than the phase transition pressures at 348 K (see Figure 5-15). Such behaviour is often referred to as a temperature inversion and occurs at compositions between approximately 0.07 and 0.64 mass fraction 1 -decanol in CO_2 . In Figure 5-16 the P - T relationship of the $CO_2 + 1$ -decanol system is plotted at compositions close to 0.07 and 0.64, to indicate the occurrence of the temperature inversion.

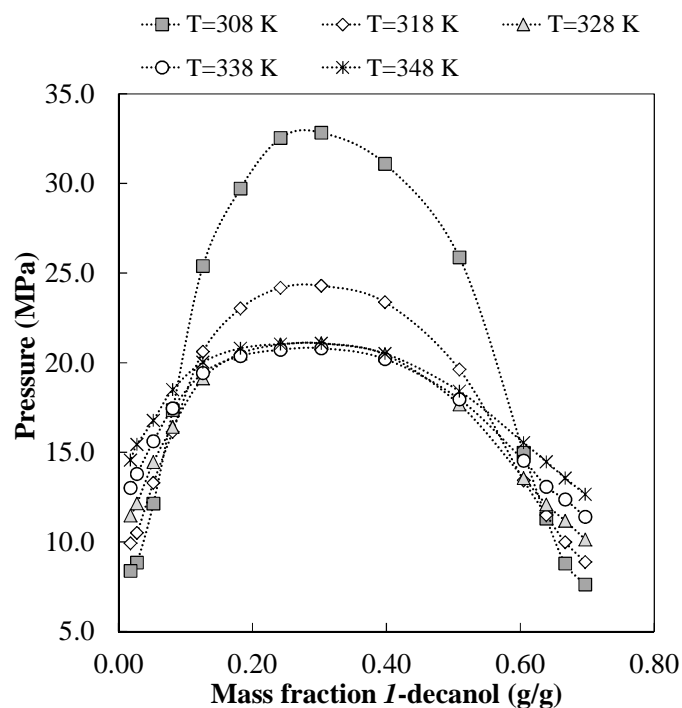


Figure 5-15 Phase behaviour of the $CO_2 + 1$ -decanol system between 308 K and 348 K

5 | Experimental Bubble and Dew Point Data

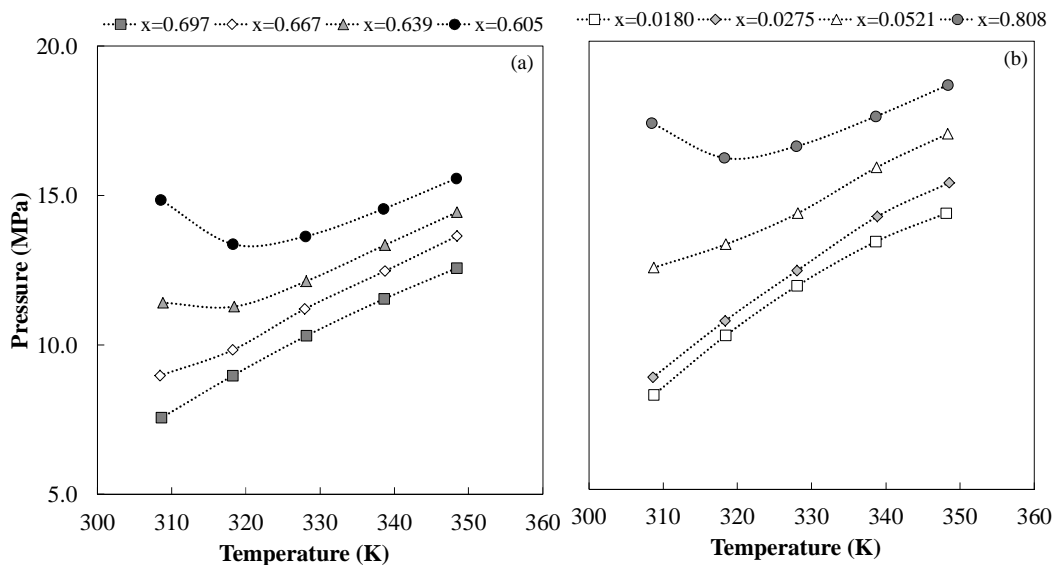


Figure 5-16 P-T relationship of the $\text{CO}_2 + 1\text{-decanol}$ system indicating the temperature inversion

For most solvent/solute systems the solubility of a compound decreases as the temperature increases, which leads to a higher phase transition pressure being observed at higher temperatures. For the $\text{CO}_2 + 1\text{-decanol}$ system the phase transition pressures decrease between 308 K and 338 K, after which the normal trend resumes and it increases again as the temperature is increased to 348 K. As mentioned in the previous chapter, temperature inversions have also been observed for the $\text{CO}_2 + 1\text{-octanol}$ [11], $\text{CO}_2 + 1\text{-dodecanol}$ [27] and $\text{CO}_2 + 1\text{-hexadecanol}$ [28] systems, and is thus a common occurrence for a certain range of the $\text{CO}_2 + 1\text{-alcohol}$ homologous series.

A possible explanation of the unique phase behaviour exhibited by a certain group of $\text{CO}_2 + 1\text{-alcohol}$ systems is the strong solvent-solute and solute-solute interactions that occur. The exposed hydroxyl group in primary linear alcohols form multimer hydrogen bonds that lead to a very compact alcohol structure [29]. At low temperatures the kinetic energy of the alcohol molecules are too low to overcome the multimer bonds and consequently a very high pressure is required to force enough CO_2 molecules in between the solute molecules to allow it to dissolve into a single phase. As the temperature increases the kinetic energy of the solutes increase, making it easier for the solvent molecules to disrupt the multimer hydrogen bonds and exist at the required density around the solute molecules to make the solute soluble. At a certain point the kinetic energy of the molecules are too high to maintain a large amount of multimers and lower pressures are sufficient for total solubility.

5 | Experimental Bubble and Dew Point Data

Once outside the temperature range in which the occurrence of multimers dominates, normal phase behaviour trends resume.

At *I*-decanol mass fractions lower than 0.07 and higher than 0.64, the general trend of increasing phase transition pressure with increasing operating temperature is observed. In very dilute mixtures the *I*-decanol molecules will exist as monomers irrespective of the temperature. There are simply not enough *I*-decanol molecules to form multimers and still be evenly distributed throughout the solvent. At very high concentrations of *I*-decanol in supercritical CO₂, multimers will form irrespective of the temperature, and thus no temperature inversion is observed.

5.5.2 Comparison to Literature Data

Figure 5-17 shows a comparison at 318 K between the data measured in this investigation for the CO₂ + *I*-decanol system, and data published by reputable sources.

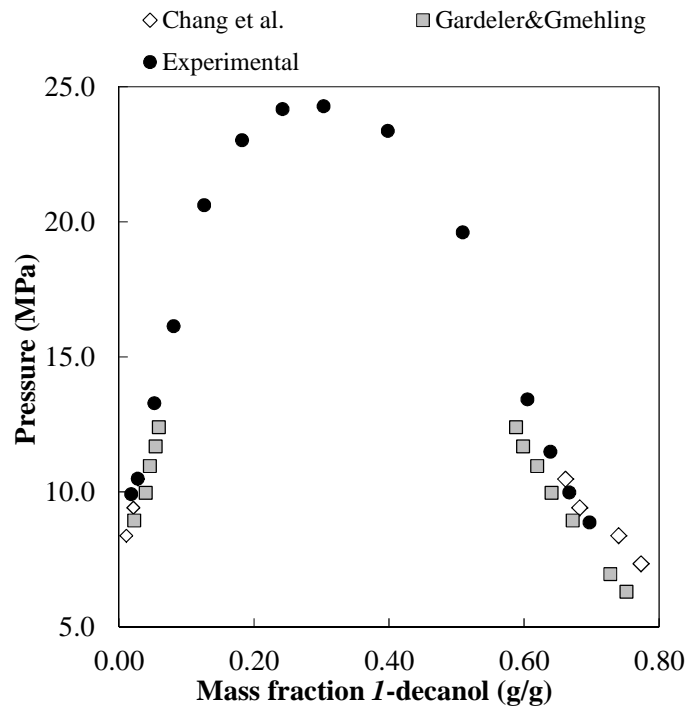


Figure 5-17 Comparison between measured phase equilibrium data (●....this work) and published phase equilibrium data (◇....[30], ■....[24]) for the CO₂+*I*-decanol system at 318 K

The data published by Chang et al. [30] and Gardeler and Gmehling [24] show some slight disagreement which can possibly be attributed to the use of different experimental methods. Chang et al. [30] measured the densities of the co-existing phases with densitometers (devices used to measure density by measuring the degree of darkness of a semi-transparent sample or reflecting surface) and converted it to compositions by combining it with a set of density data based on overall mass balances and the phase rule. Gardeler and Gmehling [24] used a static view cell with on-line samplers to determine the composition of the co-existing phases. A number of difficulties accompany the use of an experimental technique that requires sampling to determine the phase compositions of mixtures at high pressures. Such complications are discussed in detail by Peper and Dohrn [31] who mentions that small differences in sampling location, sampling technique, sample preparation and sample analysis can lead to errors in the data generated. The data measured in this investigation corresponds more closely to the data published by Chang et al. [30] especially in the high solute concentration region.

5.5.3 Classification of the Systems

It has been reported that the binary system $\text{CO}_2 + 1$ -decanol exhibits Type III phase behaviour [32,33]. Since none of the other $\text{CO}_2 + \text{C}_{10}$ -alcohol isomer systems have similar phase behaviour, more information over larger temperature, pressure and composition ranges is required to assign a type to these systems.

The slight increase in phase transition pressure at low solute concentrations of the $\text{CO}_2 + 2$ -decanol system (see Table 5-18) can possibly indicate the existence of a three phase region near the critical temperature of CO_2 . However, more phase equilibrium data at subcritical temperatures is required to confirm the type of phase behaviour.

5.6 Discussion on the Phase Behaviour of the Binary Mixtures Investigated

In this section the bubble and dew point data reported in previous sections will be discussed with the emphasis on the main factors that influence the phase behaviour of the C_{10} -alkane and C_{10} -alcohol isomers in supercritical CO_2 and ethane.

5.6.1 Effect of Temperature

The phase behaviour results presented in this chapter show an increased phase transition pressure at increased operating temperatures, with the exception of the CO₂ + *I*-decanol system. The low solute concentration region is important when determining the feasibility of an SFF process. The separation task considered in this investigation is the removal of *n*-alkanes from mixtures of alcohol isomers - specifically the removal of *n*-decane from a mixture of C₁₀-alcohol isomers. In Figure 5-18 and Figure 5-19 the low solute concentration region are shown to indicate the relative difference in phase transition pressure at 308 K and 348 K between *n*-decane and *I*-decanol in supercritical CO₂ and ethane, respectively.

From these figures it is clear that a significant difference in the phase transition pressures of *n*-decane and *I*-decanol occur in both supercritical CO₂ and ethane, and thus successful separation with SFF with either solvent is possible. It is however interesting to note that the difference in phase transition pressures at 5 mass % solute between *n*-decane and *I*-decanol in ethane increases from 2 MPa to 3.9 MPa as the temperature increases from 308 K to 348 K (see Figure 5-18). The difference in phase transition pressure between *n*-decane and *I*-decanol in supercritical CO₂ stay approximately the same at 4.5 MPa at 308 K and 4.2 MPa at 348 K. The temperature inversion that occurs for the CO₂ + *I*-decanol mixture will, however, lead to much larger differences in phase transition pressures as the solute concentration increases at lower temperatures. The overall composition of the mixture will thus dictate whether operation at high or low temperature will bring about better separation with SFF.

5 | Experimental Bubble and Dew Point Data

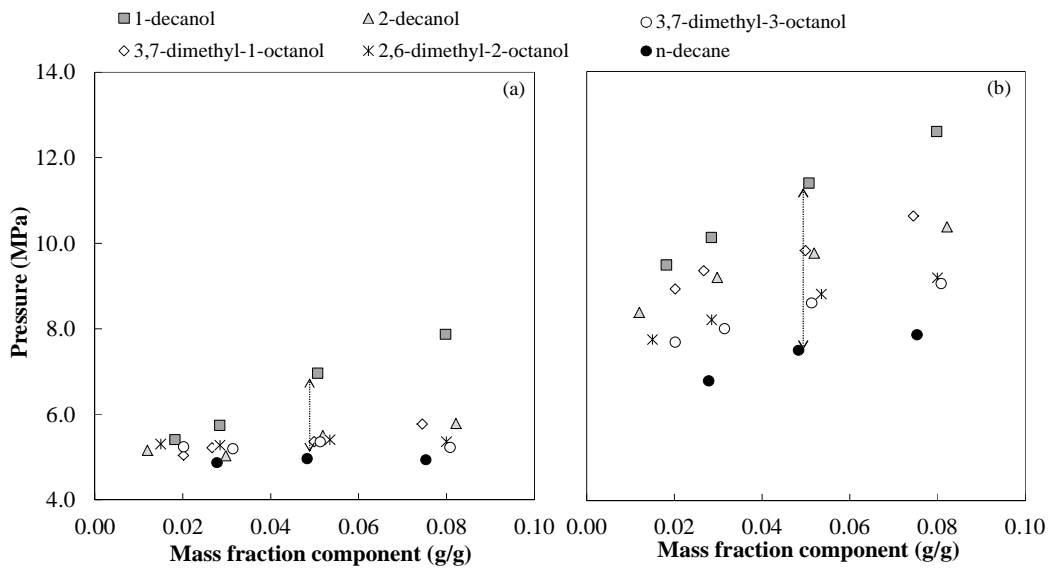


Figure 5-18 Phase behaviour of *n*-decane and C_{10} -alcohol isomers in supercritical ethane at (a) 308 K and (b) 348 K

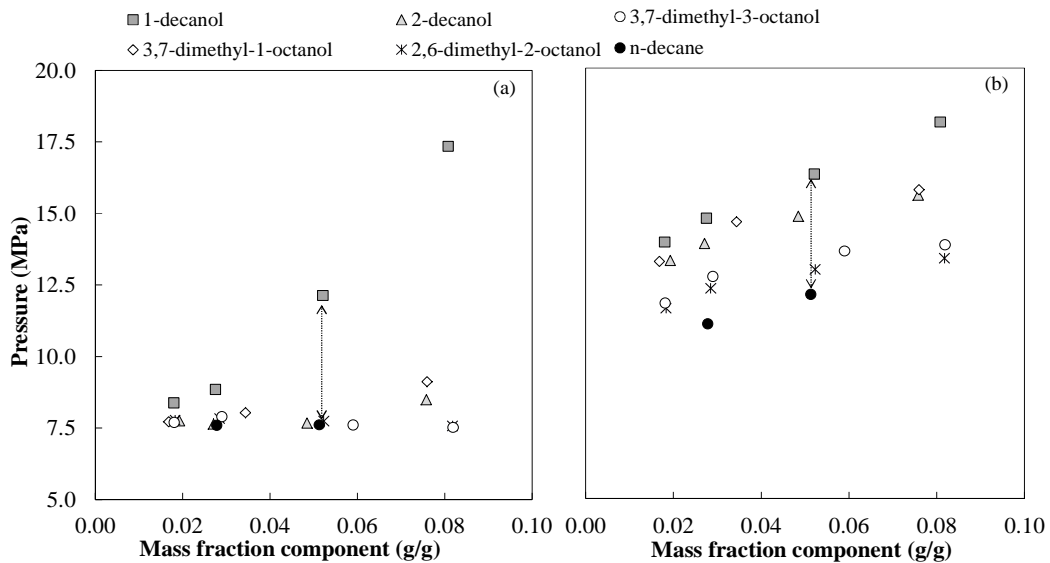


Figure 5-19 Phase behaviour of *n*-decane and C_{10} -alcohol isomers in supercritical CO_2 at (a) 308 K and (b) 348 K

At 308 K the C_{10} -alcohol isomers have phase transition pressures much closer to one another, compared to that at 348 K, in both supercritical solvents. If the aim of the SFF process is to create

5 | Experimental Bubble and Dew Point Data

more defined cuts between the C₁₀-alcohol isomers, higher operating temperatures seem to be more feasible.

As the temperature increases the mixture critical point shifts to higher solute concentrations and a more defined dew point region develops. This is especially prominent in the phase behaviour of the *n*-alkanes, and is illustrated in Figure 5-20 for the CO₂ + *n*-decane system.

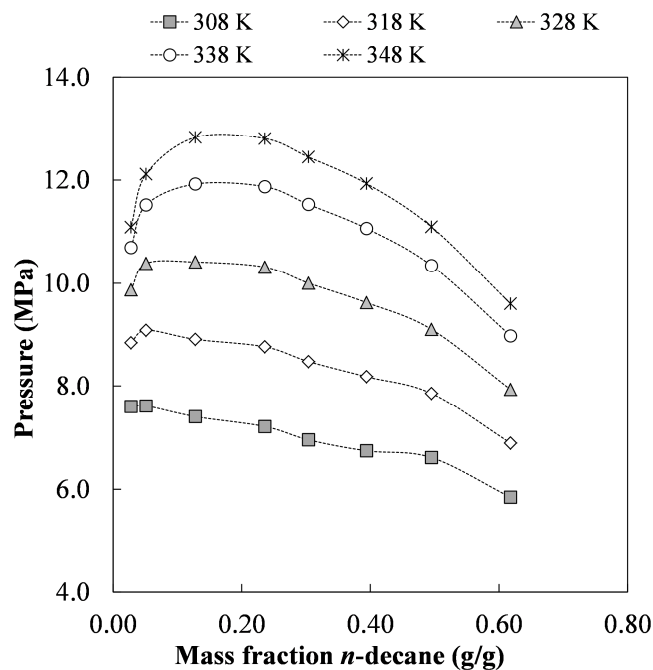


Figure 5-20 Isothermal phase behaviour of the CO₂+*n*-decane system to illustrate the movement of the mixture critical point

5.6.2 Effect of Composition

The overall composition of a binary mixture consisting of a solute and a supercritical solvent will determine what phase transition phenomenon will be observed. Generally bubble points are observed at high solute concentrations as the mixture transitions from a homogenous to a heterogeneous phase. At low concentrations of the solute, dew points are commonly observed as the phase transition from a homogenous to heterogeneous phase occurs. In a certain intermediate composition range the mixture critical point will be observed. The mixture critical point is generally

considered the point where the bubble point and dew point regions meet. At the mixture critical point the mixture can exhibit many different visual effects depending on the compounds present. In most cases the mixture critical point will present itself as the onset of an opalescent cloudiness or dark murkiness.

If the mixture under consideration belongs to any type of phase behaviour, other than Type I, additional phase regions may be present at supercritical conditions. For the compounds investigated in this study the existence of a three phase region at low solute concentrations and temperatures close to the critical temperature of the solvent, is possible. If such a region is present an additional, and likely smaller, bubble point region, mixture critical point and dew point region will establish itself at certain low solute concentration compositions.

Most SFF processes are conducted with feed mixtures consisting of compositions within the dew point region, i.e. low concentrations of the solutes. If a three phase region is present for a binary mixture at low solute concentrations, operation within such a region must be avoided, since sufficient separation might not occur.

5.6.3 Effect of Solvent

The critical point of CO₂ is at 304.3 K and 7.38 MPa, while that of ethane is at 305.4 K and 4.88 MPa. Even though the critical temperatures of the two solvents are very similar, their critical pressures differ by 2.5 MPa, with $P_c(\text{CO}_2) = 1.5 \times P_c(\text{Ethane})$. Generally, the phase transition pressures of the binary systems containing ethane will be lower than that of the same solute with CO₂.

It may seem beneficial to select the solvent that requires lower operating conditions, but for SFF processes the most important factor to consider is the selectivity of the solvent. The selectivity can be defined as the ratio of the concentration of a solute in the vapour phase to the concentration of that solute in the liquid phase (see Equation 3-4 in Chapter 3). A solvent will thus be considered a good solvent if it can selectively remove a certain component or group of components from a feed mixture, without allowing too much of the undesired components to come along, i.e. show a high selectivity for the desired compounds and a low selectivity for the undesired compounds.

Figure 5-18 and Figure 5-19 illustrate the phase behaviour of *n*-decane and selected C₁₀-alcohol isomers in supercritical CO₂ and ethane. The main difference in the phase behaviour exhibited by the solutes in the two solvents is the temperature inversion that occurs for the CO₂ + 1-decanol mixture,

but not for the ethane + *l*-decanol mixture. Neither of the solvents seems to be superior in solute selectivity for the components involved. The binary mixtures containing CO₂ show a slightly larger difference in phase transition pressures in the low solute concentration region between *n*-decane and *l*-decanol, compared to ethane. Since *n*-decane and *l*-decanol are the main components to be separated, a larger difference in phase transition pressures (or solubility) might aid in the separation performance of the proposed SFF process.

CO₂ is less expensive and more readily available than ethane, and where large quantities are required the use thereof instead of ethane, is more economical. CO₂ was selected as the supercritical solvent to use in further investigation of the proposed SFF process, which includes pilot plant runs and process modelling.

5.6.4 Effect of Functional End Group

In this study two groups of compounds were considered: alkanes and alcohols, all containing 10 carbon atoms. In both supercritical CO₂ and ethane the binary systems containing the alcohol isomers had higher phase transition pressures compared to the binary systems containing the alkane isomers (see Figure 5-21), which can in all likelihood be attributed to the larger molecular mass and/or increased polarity of the alcohols. This observation is in agreement with the findings of Schwarz et al. [34] who investigated the effect of functional end groups on the phase behaviour of alkanes, alcohols, acids, ethyl esters and methyl esters.

According to Schwarz et al. [34] the polarity of the functional end group is responsible for the decreased solubility of the alcohols compared to the alkanes. As mentioned earlier, the presence of polar hydroxyl groups lead to the formation of hydrogen bonded multimers, which makes the alcohol structure very hard to penetrate. The non-polar alkanes will not form multimers and consequently it is easier for the solvent to get access to the alkane molecules, and thus the alkanes are generally more soluble in supercritical CO₂ and ethane.

5 | Experimental Bubble and Dew Point Data

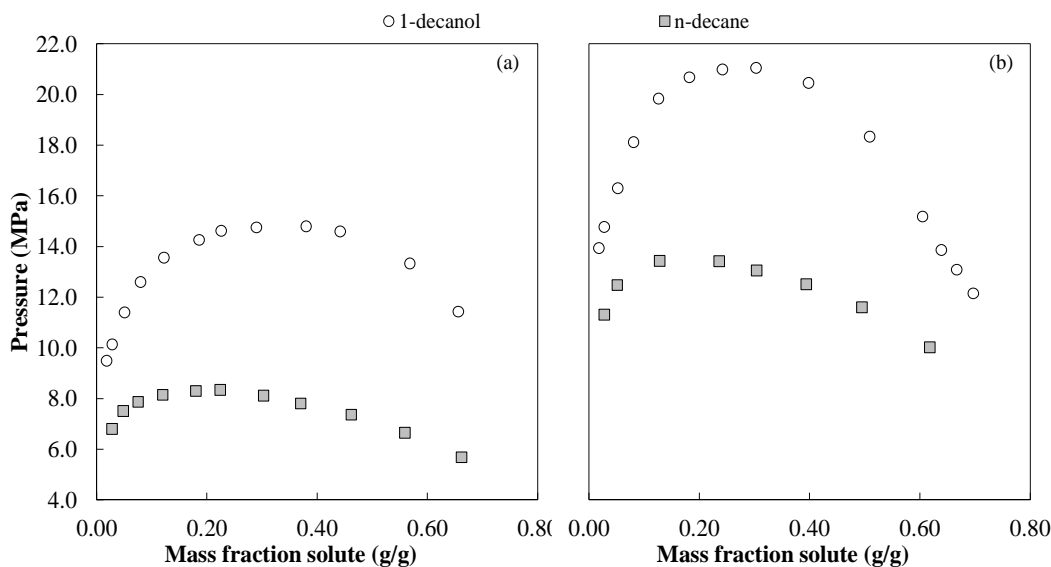


Figure 5-21 Comparison between the phase behaviour of *n*-decane and *1*-decanol at 348 K in (a) supercritical ethane and (b) supercritical CO₂

In an SFF process the more soluble compound will exit in the overheads product stream, while the less soluble compounds will exit in the bottoms product stream. In this investigation, an attempt to separate the alkanes from the alcohols, will lead to an overheads product rich *n*-decane and a bottoms product rich in *1*-decanol. Since the alcohol isomers have phase transition pressures that vary between that of the alkanes and primary linear alcohol, they will distribute between the two product streams.

5.6.5 Effect of the Hydroxyl Group Position

Figure 5-22 illustrates the influence of the hydroxyl group position on the phase behaviour of alcohols by comparing the phase behaviour of *1*-decanol and *2*-decanol in supercritical ethane and CO₂ respectively. It is clear that the phase transition pressures of *1*-decanol are higher than that of *2*-decanol in both solvents. Taking into account that these two compounds have exactly the same molecular weight, the difference in phase transition pressure can only be ascribed to the difference in the hydroxyl group position. As the hydroxyl group moves away from the terminal end, the compound becomes more soluble in the supercritical solvent, and consequently the phase transition pressure is lower. This trend is in agreement with the findings of Fourie et al. [11] for CO₂ + *1*-octanol and CO₂ + *2*-octanol (discussed in Chapter 4, section 4.3.2).

5 | Experimental Bubble and Dew Point Data

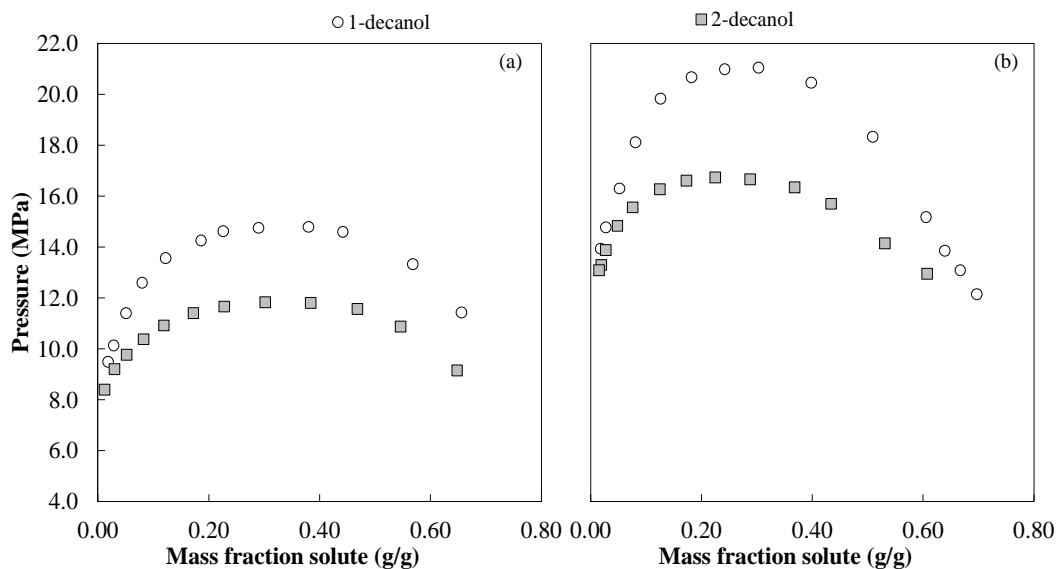


Figure 5-22 Comparison between the phase behaviour of 1-decanol and 2-decanol at 348 K in (a) supercritical ethane and (b) supercritical CO₂

The location of the polar hydroxyl group affects the nature of the solute-solute interaction that can take place. When the hydroxyl group is located at the terminal end of the alcohol molecule, it is quite exposed which allows it to interact and bond easily with other alcohol molecules. This leads to the formation of multimers which inhibit the solvent from surrounding the alcohol molecules with sufficient density for solubility to occur. When the hydroxyl group is located further away from the terminal end of the molecule, it is shielded by the hydrocarbon backbone and therefore the molecules can now interact only partially with surrounding alcohol molecules. Due to the limited interaction between the solute molecules the solvent can now gain access to the solute molecules.

In Figure 5-23 the phase behaviour of 3,7-dimethyl-1-octanol and 3,7-dimethyl-3-octanol in supercritical ethane and CO₂ are compared. The only difference between these two compounds is the position of the hydroxyl group. The isomer with the hydroxyl group in the terminal position (3,7-dimethyl-1-octanol) exhibits higher phase transition pressures, and consequently lower solubility, in both solvents. The observation regarding the hydroxyl group - solubility relationship, can thus be extended to branched isomers of alcohols as well.

5 | Experimental Bubble and Dew Point Data

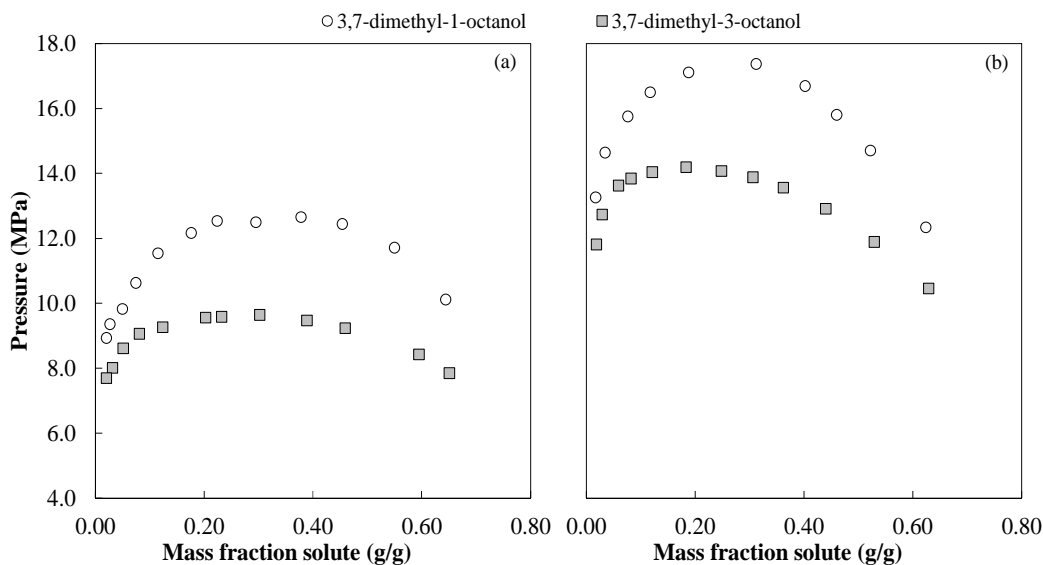


Figure 5-23 Comparison between the phase behaviour of 3,7-dimethyl-1-octanol and 3,7-dimethyl-3-octanol at 348 K in (a) supercritical ethane and (b) supercritical CO₂

5.6.6 Effect of Number, Length and Position of the Side Branches

The effect of methyl-branching of C₁₀-alcohols is presented in Figure 5-24 for two sets of binary systems. In both cases it is clear that the methyl-branched isomer is more soluble compared to the linear alcohol where the hydroxyl group is located in the same position. Although not presented in this figure, the same behaviour is observed for these solutes with supercritical ethane.

In Figure 5-24 (a) the phase behaviour of 1-decanol and 3,7-dimethyl-1-octanol in supercritical CO₂ are compared. These two compounds have the same molecular weight and hydroxyl group position, but 3,7-dimethyl-1-octanol exhibits lower phase transition pressures and can thus be considered to be more soluble in supercritical CO₂, compared to 1-decanol. This increase in solubility can be ascribed to two possible phenomena: the shorter length of the hydrocarbon backbone, and/or the increased shielding of the polar hydroxyl group by the methyl-branches. The same can be said for the two systems compared in Figure 5-24 (b).

5 | Experimental Bubble and Dew Point Data

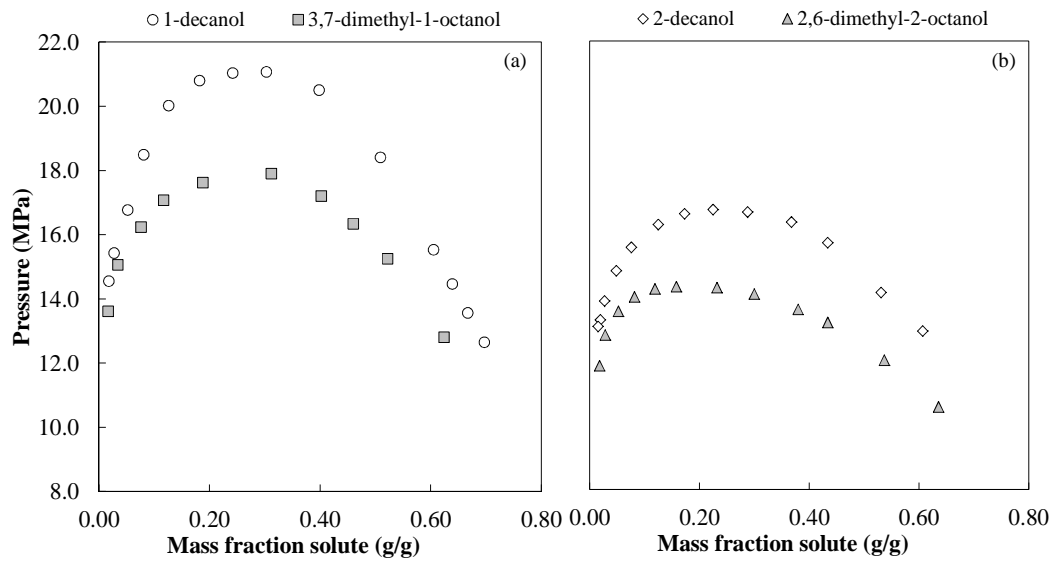


Figure 5-24 Comparison between the phase behaviour at 348 K of (a) CO_2 +1-decanol and CO_2 +3,7-dimethyl-1-octanol, and (b) CO_2 +2-decanol and CO_2 +2,6-dimethyl-2-octanol

In Figure 5-25 the phase transition pressures of 1-octanol and 2-octanol are added to the phase equilibrium data depicted in Figure 5-24. By comparing the phase behaviour of these compounds, the effect of the molecular weight and hydrocarbon backbone length can be investigated.

Figure 5-25 indicates that the phase behaviour of the CO_2 + 3,7-dimethyl-1-octanol system is much closer to that of CO_2 + 1-octanol than CO_2 + 1-decanol. Similarly, the phase behaviour of CO_2 + 2,6-dimethyl-2-octanol are closer to that of CO_2 + 2-octanol, than that of CO_2 + 2-decanol. The increase in phase transition pressures usually brought about by an increase in molecular weight is counteracted by the shorter hydrocarbon backbone length and shielding of the hydroxyl group position, for the branched alcohols investigated.

5 | Experimental Bubble and Dew Point Data

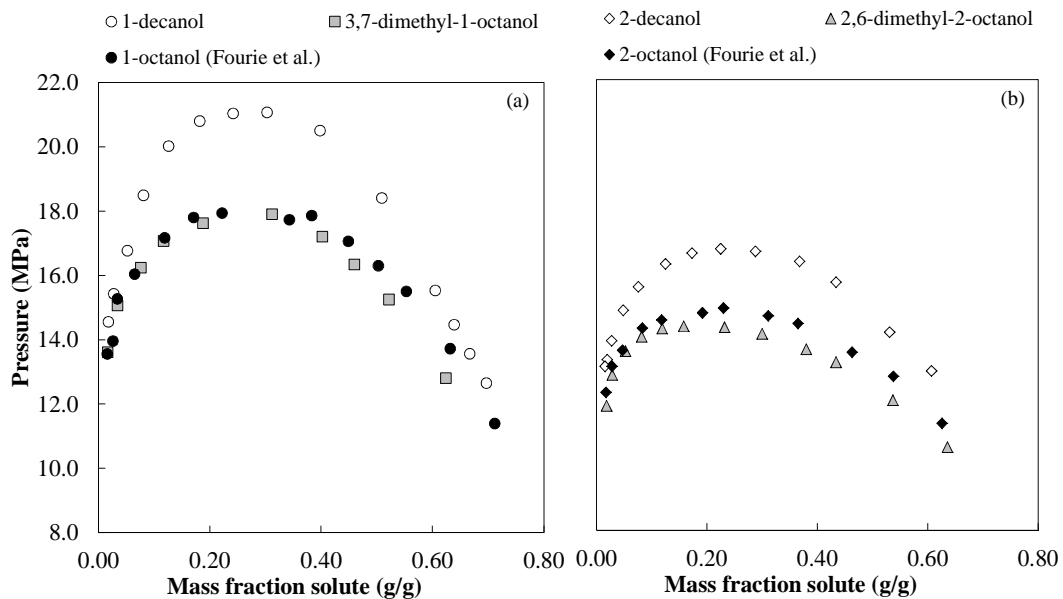


Figure 5-25 Comparison between the phase behaviour at 348 K of (a) CO_2 +1-decanol, CO_2 +3,7-dimethyl-1-octanol and CO_2 +1-octanol (●....[11]), and (b) CO_2 +2-decanol, CO_2 +2,6-dimethyl-2-octanol and CO_2 +2-octanol (◆....[11])

The length of the hydrocarbon backbone is not the only factor that influences the solubility of alcohol isomers in supercritical solvents. From the work done by Schwarz et al. [35] it is apparent that the number and more importantly, the length of the side branches play a significant role in the solubility of alcohol isomers. All the C_{10} -alcohol isomers investigated in this study, had the same number and length of side branches, and thus this phenomenon was not investigated in this study.

5.7 Measured Data for Ternary Mixtures

5.7.1 Rationale for Further Investigation

In the preceding sections binary bubble and dew point data for nineteen binary systems were measured and reported. The differences in phase behaviour of the binary systems that was caused by operating temperature, composition, solvent selection and structural isomerism were the main focus of the discussion. It was found that the methyl-branched C_{10} -alkane isomers and linear n -decane did not show any significant difference in phase transition pressures, and thus it can be concluded that similar

solvent-solute interactions exist for these compounds. The C₁₀-alcohol isomers investigated did however show significant differences in phase transition pressures. The solute-solvent interactions that are present in binary mixtures of these alcohols and CO₂ or ethane are thus influenced by the structure of the molecules, irrespective of their similar molecular mass.

Since real SFF processes generally deal with feed mixtures comprising of multiple components, it is important to investigate the possibility of interactions between solutes. Solute-solute interactions, if significant, might lead to unexpected phase behaviour in a supercritical solvent, compared to when these solutes exist as single components in a binary mixture with a solvent.

For the components used in this investigation three types of significant solute-solute interactions were identified: *n*-alkane + *I*-alcohol, *n*-alkane + branched alcohol and *I*-alcohol + branched alcohol. The following assumptions were thus inferred:

- The solute-solute interaction between the methyl-branched alkanes and alcohol isomers, are similar to that of the linear alkane with the alcohol isomers.
- The solute-solute interactions between all the alcohol isomers with two methyl branches and a linear alkane or primary linear alcohol, are similar.
- The solute-solute interactions between all the alcohol isomers with two methyl branches are zero.

To investigate solute-solute interactions and their influence on the phase behaviour of mixtures, three ternary mixtures were constructed and their bubble and dew point data measured. *I*-Decanol was selected to represent the primary linear alcohols, and 3,7-dimethyl-*I*-octanol was selected to represent the branched alcohols. During this part of the investigation the linear alkane was represented by *n*-dodecane instead of *n*-decane. This decision was based on the fact that the boiling point of *n*-dodecane is closer to that of the selected alcohols (see Chapter 1, Table 1-1), and will thus allow the investigation of the phase behaviour of mixtures of close-boiling compounds. The investigations in the previous sections were concerned with the effect of structural isomerism on the phase behaviour of mixtures, but from here on the investigations will focus more on the ability of SFF to separate close-boiling alkanes and alcohol isomers. The ternary mixtures selected to investigate the solute-solute interactions are as follows:

5 | Experimental Bubble and Dew Point Data

- Mixture A: 22.2 % *n*-dodecane + 77.8 % *l*-decanol
- Mixture B: 87.5 % *l*-decanol + 12.5 % 3,7-dimethyl-*l*-octanol
- Mixture C: 66.7 % *n*-dodecane + 33.3 % 3,7-dimethyl-*l*-octanol

The component ratios were selected based on information [36,37] regarding the typical product streams wherein these compounds exist as mixtures (refer to Chapter 2 for a detailed discussion).

5.7.2 Measured Data for CO₂ + Mixture A

In Table 5-21 the phase equilibrium data for CO₂ + (22.2 % *n*-dodecane + 77.8 % *l*-decanol) is supplied.

Table 5-21 Isothermal data for the CO₂ + (22.2 % *n*-dodecane + 77.8 % *l*-decanol) system

Mass fraction solute (g/g)	Parameters for temperature correction					Temperature (K)				
	P = A*T ³ + B*T ² + C*T + D					308	318	328	338	348
	A	B	C	D	R ²	Pressure (MPa)				
0.654	0	0	0.12055	-29.974	0.997	7.16	8.36	9.57	10.77	11.98
0.551	0	0	0.13324	-32.018	0.996	9.02	10.35	11.68	13.02	14.35
0.448	0	0.0029091	-1.8527	308.736	0.973	14.09	13.77	14.04	14.88	16.31
0.375	-0.00012464	0.12696	-42.985	4854.191	0.995	16.83	15.38	15.54	16.57	17.71
0.312	-0.00015625	0.15892	-53.762	6066.308	0.996	18.21	16.18	16.12	17.09	18.16
0.239	-0.00017884	0.18174	-61.447	6929.772	0.997	19.32	16.87	16.64	17.57	18.58
0.174	-0.00016906	0.17157	-57.927	6523.269	0.996	18.31	16.16	16.07	17.02	18.01
0.121	-0.00011508	0.11653	-39.208	4400.148	0.998	15.80	14.91	15.37	16.49	17.57
0.078	0	0	0.13509	-30.431	1.000	11.18	12.53	13.88	15.23	16.58
0.051	0	-0.00084055	0.71839	-132.438	1.000	9.09	11.01	12.76	14.35	15.77
0.0276	0	-0.0012735	0.99807	-178.844	0.999	7.75	9.76	11.52	13.02	14.26
0.0177	0	-0.0013820	1.0480	-184.118	1.000	7.56	9.39	10.94	12.22	13.22

Since the majority of Mixture A consists of *l*-decanol, it is suspected that the features of the CO₂ + *l*-decanol phase behaviour will dominate. Figure 5-26 shows that the most prominent feature of the CO₂ + *l*-decanol system, the temperature inversion, is also present for the CO₂ + (*n*-dodecane +

5 | Experimental Bubble and Dew Point Data

l-decanol) system. The temperature inversion does, however, cover a smaller composition and temperature range compared to that of the CO₂ + *l*-decanol system (see Figure 5-15).

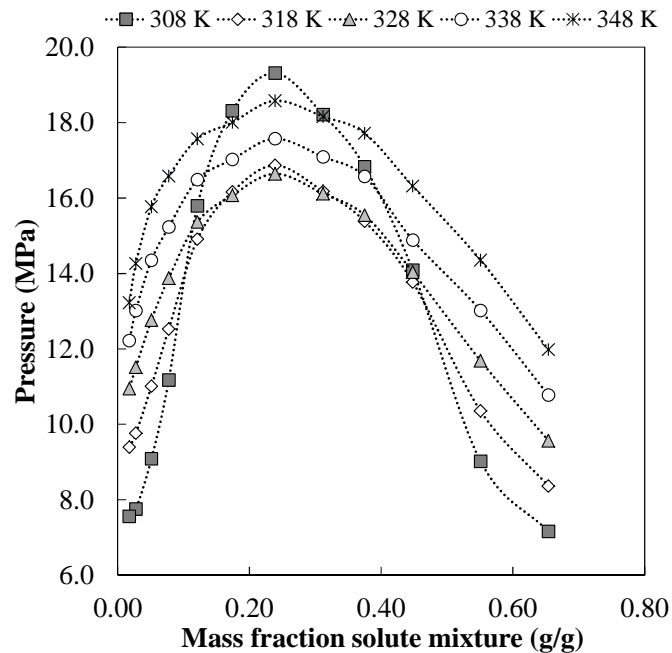


Figure 5-26 Phase behaviour of the CO₂ + (22.2 % n-dodecane + 77.8 % *l*-decanol) mixture at temperatures between 308 K and 348 K

5.7.3 Measured Data for CO₂ + Mixture B

Table 5-22 contains the phase equilibrium data for the CO₂ + (87.5 % *l*-decanol + 12.5 % 3,7-dimethyl-*l*-octanol) mixture. Like for Mixture A, the major component in Mixture B is *l*-decanol, and thus a temperature inversion can be identified for the CO₂ + (*l*-decanol + 3,7-dimethyl-*l*-octanol) mixture as well (see Figure 5-27). The temperature and composition ranges of the temperature inversion observed for Mixture B closely resembles that of the binary CO₂ + *l*-decanol mixture (see Figure 5-15).

5 | Experimental Bubble and Dew Point Data

Table 5-22 Isothermal data for the CO₂ + (87.5 % 1-decanol + 12.5 % 3,7-dimethyl-1-octanol) system

Mass fraction solute (g/g)	Parameters for temperature correction					Temperature (K)				
	P = A*T ³ + B*T ² + C*T + D					308	318	328	338	348
	A	B	C	D	R ²	Pressure (MPa)				
0.650	0	0	0.12576	-30.751	0.994	7.98	9.24	10.50	11.76	13.01
0.563	-0.00010992	0.11176	-37.763	4255.206	0.999	14.47	13.37	13.65	14.64	15.70
0.467	-0.00031934	0.32417	-109.61	12364.523	0.998	24.96	19.47	17.89	18.30	18.78
0.383	-0.00031378	0.32045	-109.02	12377.895	0.998	29.03	22.48	20.15	20.15	20.61
0.303	-0.00041763	0.42345	-143.04	16118.449	0.991	29.67	22.49	20.32	20.65	20.96
0.237	-0.00032661	0.33273	-112.92	12786.110	0.997	28.68	22.37	20.29	20.47	20.97
0.181	-0.00021458	0.21987	-75.027	8546.526	0.999	25.76	21.11	19.50	19.62	20.20
0.118	-0.00021270	0.21577	-72.862	8208.498	0.995	21.14	18.05	17.52	18.30	19.09
0.082	-0.000096619	0.097785	-32.865	3685.039	0.999	15.73	15.21	15.82	16.97	18.08
0.049	0	0	0.15262	-36.472	0.999	10.54	12.06	13.59	15.11	16.64
0.0272	0	-0.0016385	1.2453	-220.191	1.000	7.93	10.13	12.00	13.54	14.75
0.0179	0	-0.0016321	1.2187	-212.859	1.000	7.67	9.64	11.29	12.60	13.60

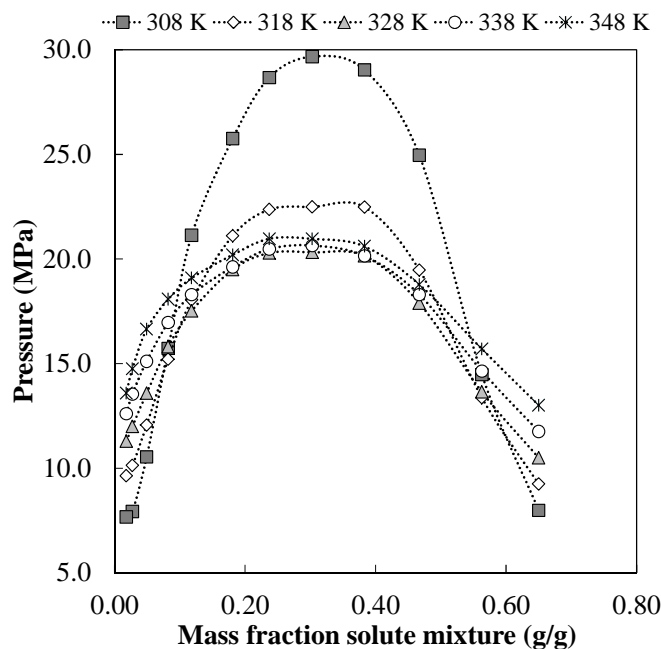


Figure 5-27 Phase behaviour of the CO₂ + (87.5 % 1-decanol + 12.5 % 3,7-dimethyl-1-octanol) mixture at temperatures between 308 K and 348 K

5.7.4 Measured Data for CO₂ + Mixture C

Due to difficulty in obtaining 3,7-dimethyl-*I*-octanol (305774) at a purity of 99 %, the CO₂ + (*n*-dodecane + 3,7-dimethyl-*I*-octanol) mixture was constructed with 3,7-dimethyl-*I*-octanol (W23,910-0-K) at a minimum purity of 98 %. However, GC-MS analysis of the 3,7-dimethyl-*I*-octanol sold at a minimum purity of 98 % did not detect any impurities within the limits of the detector, and it can thus be assumed to also be at least 99 % pure. The phase equilibrium data also showed no significant deviation (except for the experimental error) between the phase behaviour of 3,7-dimethyl-*I*-octanol (305774) and that of 3,7-dimethyl-*I*-octanol (W23,910-0-K) in supercritical CO₂ (see Figure 5-28).

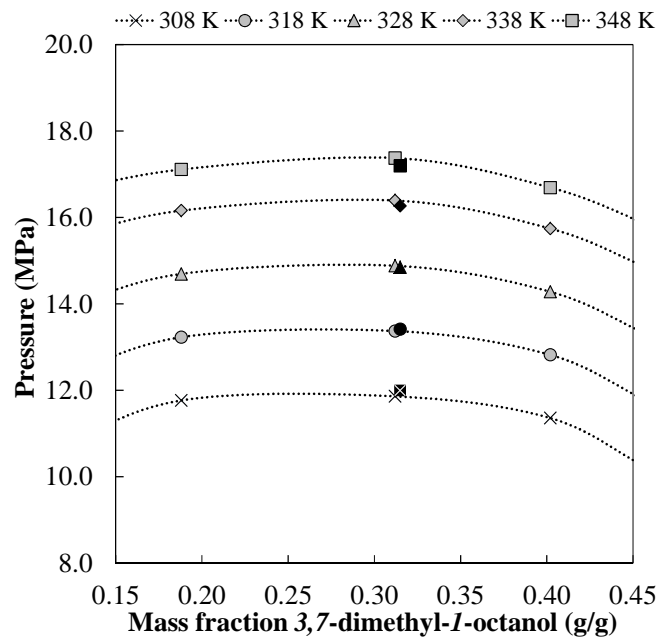


Figure 5-28 Comparison between the phase behaviour of 3,7-dimethyl-*I*-octanol: 305774 (grey markers) and 3,7-dimethyl-*I*-octanol: W23,910-0-K (black markers) in supercritical CO₂

The phase equilibrium data measured for the system CO₂ + (66.7 % *n*-dodecane + 33.3 % 3,7-dimethyl-*I*-octanol), is given in Table 5-23.

5 | Experimental Bubble and Dew Point Data

Table 5-23 Isothermal data for the CO₂ + (66.7 % *n*-dodecane + 33.3 % 3,7-dimethyl-1-octanol) system

Mass fraction solute (g/g)	Parameters for temperature correction					Temperature (K)				
	$P = A \cdot T^3 + B \cdot T^2 + C \cdot T + D$					308	318	328	338	348
	A	B	C	D	R ²	Pressure (MPa)				
0.640	0	0	0.10151	-24.960	1.000	6.30	7.32	8.33	9.35	10.36
0.563	0	0	0.12088	-30.562	1.000	6.67	7.88	9.09	10.30	11.51
0.462	0	0	0.14681	-38.157	1.000	7.06	8.53	10.00	11.47	12.93
0.377	0	0	0.16434	-43.421	1.000	7.19	8.84	10.48	12.12	13.77
0.298	0	0	0.17565	-46.819	1.000	7.28	9.04	10.79	12.55	14.31
0.233	0	0	0.18425	-49.426	1.000	7.32	9.17	11.01	12.85	14.69
0.184	0	0	0.18637	-50.111	0.999	7.29	9.16	11.02	12.88	14.75
0.118	0	0	0.17988	-48.063	0.999	7.34	9.14	10.94	12.74	14.53
0.080	0	-0.00051399	0.50867	-100.592	0.999	7.32	9.19	10.96	12.62	14.18
0.054	0	-0.00069010	0.61258	-115.783	0.999	7.43	9.23	10.90	12.43	13.82
0.0288	0	-0.00097947	0.77321	-137.690	0.997	7.54	9.14	10.55	11.76	12.77
0.0171	0	-0.0013247	0.97302	-166.369	0.998	7.66	9.10	10.27	11.18	11.82

In Figure 5-29 the phase behaviour of Mixture C in supercritical CO₂ is plotted at 308 K to 348 K. The data presented in Figure 5-29 and Table 5-23 at 308 K indicate the possibility of a three phase region occurring at low solute mixture concentrations (indicated by the slight increase in phase transition pressure). The phase equilibrium data measured for the CO₂ + *n*-dodecane system (see Table 5-11) also showed an indication of a three phase region at 308 K and low solute concentrations, and since *n*-dodecane make up the majority of Mixture C, such an occurrence is possible. However, more data at subcritical temperatures are required to confirm the existence of such a three phase region.

5 | Experimental Bubble and Dew Point Data

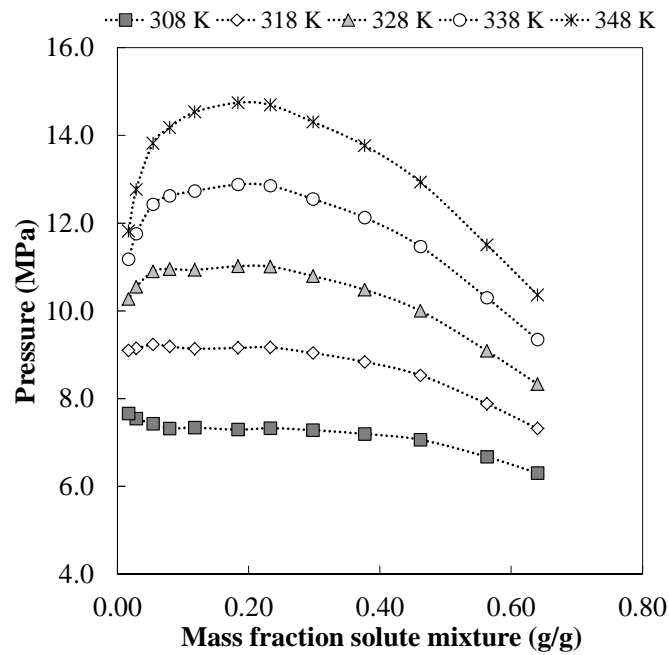


Figure 5-29 Phase behaviour of the CO_2 + (66.7 % n-dodecane + 33.3 % 3,7-dimethyl-1-octanol) mixture at temperatures between 308 K and 348 K

5.8 Discussion on the Phase Behaviour of the Ternary Mixtures Investigated

In Figure 5-30, Figure 5-31 and Figure 5-32 the phase behaviour of the ternary mixtures (defined as Mixture A, B and C) are plotted alongside that of their comprising binary mixtures.

5 | Experimental Bubble and Dew Point Data

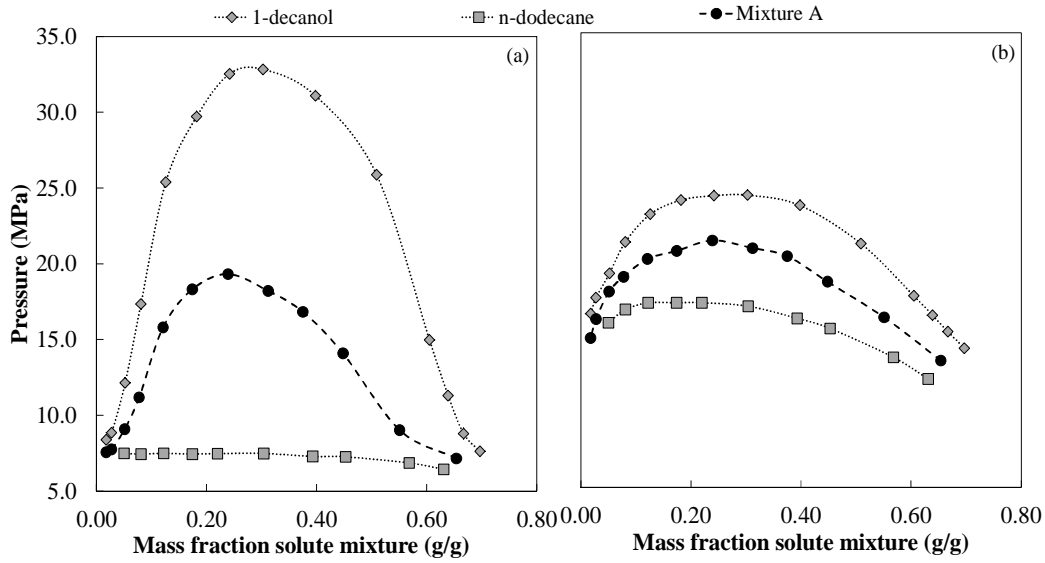


Figure 5-30 Comparison of the phase behaviour of the $CO_2 + (22.2\% \text{ n-dodecane} + 77.8\% \text{ 1-decanol})$ mixture with that of $CO_2 + \text{n-dodecane}$ and $CO_2 + \text{1-decanol}$ at (a) 308 K and (b) 348 K

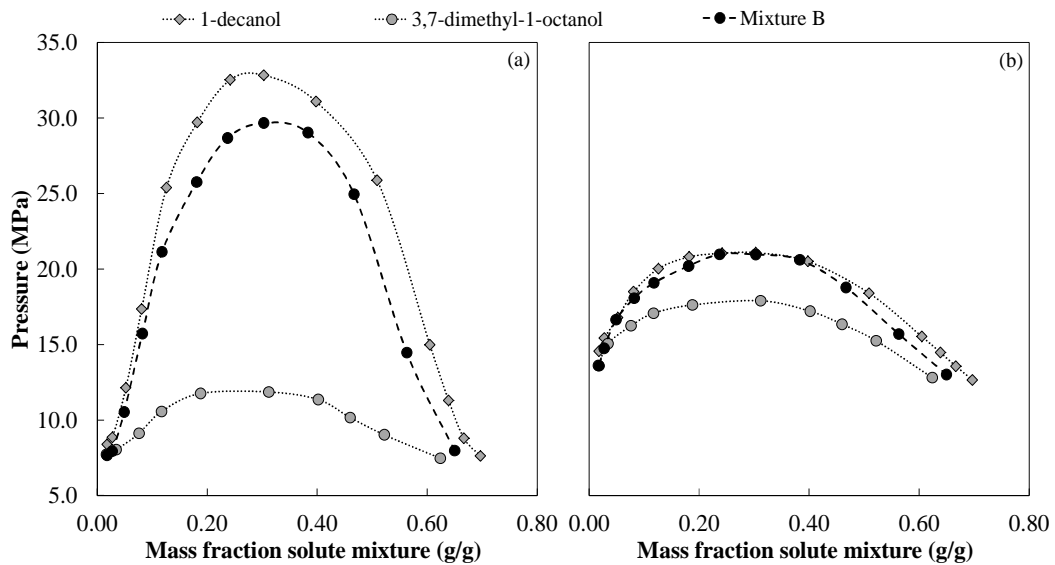


Figure 5-31 Comparison of the phase behaviour of the $CO_2 + (87.5\% \text{ 1-decanol} + 12.5\% \text{ 3,7-dimethyl-1-octanol})$ mixture with that of $CO_2 + \text{1-decanol}$ and $CO_2 + \text{3,7-dimethyl-1-octanol}$ at (a) 308 K and (b) 348 K

5 | Experimental Bubble and Dew Point Data

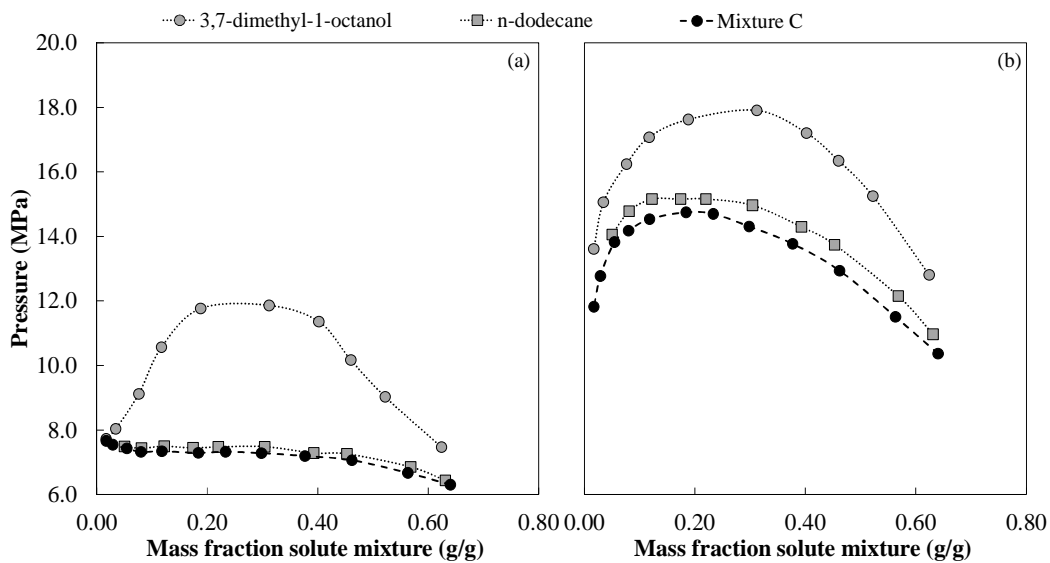


Figure 5-32 Comparison of the phase behaviour of the $\text{CO}_2 + (66.7\% \text{ n-dodecane} + 33.3\% \text{ 3,7-dimethyl-1-octanol})$ mixture with that of $\text{CO}_2 + \text{n-dodecane}$ and $\text{CO}_2 + \text{3,7-dimethyl-1-octanol}$ at (a) 308 K and (b) 348 K

Mixture A (Figure 5-30) consisted of 22.2% *n*-dodecane and 77.8% *l*-decanol, while Mixture B (Figure 5-31) consisted of 12.5% 3,7-dimethyl-*l*-octanol and 87.5% *l*-decanol. It is interesting to note that even though both these mixtures had a high concentration of *l*-decanol, only the $\text{CO}_2 + \text{Mixture B}$ system display phase transition pressures that are very similar to that of $\text{CO}_2 + \text{l-decanol}$. In Mixture A where *n*-dodecane is present in a small amount, the phase transition pressures of the $\text{CO}_2 + \text{Mixture A}$ system is significantly lower than that of the $\text{CO}_2 + \text{l-decanol}$ system. In Mixture A the usual formation of multimers by the alcohol molecules, are disrupted by the presence of non-polar *n*-dodecane. In Mixture B, the formation of multimers can still continue since both components in the mixture are polar alcohols with a hydroxyl group in a prominent position, and therefore both can contribute to the formation of multimers.

Very interesting phase behaviour was observed for Mixture C (Figure 5-32), which consisted of 66.7% *n*-dodecane and 33.3% 3,7-dimethyl-*l*-octanol. From the trends observed for Mixture A and B, it is expected that the phase transition curve of Mixture C would be located somewhere between the phase transition curves of the two comprising binary mixtures. However, Figure 5-32 clearly shows that the phase transition curve of Mixture C is located at pressures lower than that of both comprising binary mixtures, $\text{CO}_2 + \text{n-dodecane}$ and $\text{CO}_2 + \text{3,7-dimethyl-1-octanol}$. At this specific composition of 66.7 % *n*-dodecane and 33.3 % 3,7-dimethyl-1-octanol, the mixture show better

5 | Experimental Bubble and Dew Point Data

solubility in supercritical CO₂ than the individual components. This phenomenon has been investigated and observed by numerous researchers for CO₂ + alkane + alcohol ternary systems [38–43] and are commonly referred to as the co-solvency effect. The co-solvency effect is best described as the occurrence of a pressure minimum in the ternary critical curve, i.e. the phase transition pressure of the ternary mixture will be lower than that of the comprising binary systems.

The solute-solute interactions present in Mixtures A and B cause large deviation from the phase behaviour of the binary mixture of CO₂ and the majority component in especially the high solute mixture concentration region (bubble point region). In the dew point region of the CO₂ + Mixture A and CO₂ + Mixture B systems, the phase transition curves of the ternary mixtures pursue that of the binary mixture of CO₂ and the majority component. In the dew point region, the concentrations of the solutes are low enough to ensure that minimal solute-solute interactions occur. The phase behaviour thus resembles the combined phase behaviour of the contributing binary mixtures, i.e. the phase behaviour where only solute-solvent interactions occur. Since solute-solute interactions are minimal in the low solute mixture concentration region, the phase transition pressure of the ternary mixture can be predicted by the summation of the phase transition pressures of the comprising binary mixtures in the appropriate ratios (see the calculations that follow). As the overall mixture composition approaches the mixture critical composition and the bubble point curve, the solute-solute interactions become a more prominent factor and deviations from the summation of binary phase behaviour occur. At higher solute mixture concentrations, more solute molecules are present and consequently the extent of interaction among each other increase. This observation does not hold for Mixture C where co-solvency effects come into play. The observations mentioned above are illustrated in the calculations that follow for Mixture A. It is evident from the calculations that the presence of a temperature inversion for the CO₂ + *l*-decanol system at temperatures below 338 K, cause deviation from the simple summation principle.

At 348 K:

$$\begin{aligned} (P_{0.05}^{Mixture A})_{348K} &= (x^{1-decanol} \times P_{0.05}^{1-decanol})_{348K} + (x^{n-dodecane} \times P_{0.05}^{n-dodecane})_{348K} \\ &= (0.778 \times 16.66) + (0.222 \times 14.06) \\ &= 16.0 \approx 15.7 \text{ MPa} \end{aligned}$$

5 | Experimental Bubble and Dew Point Data

$$\begin{aligned}
 (P_{0.5}^{MixtureA})_{348K} &= (x^{1-decanol} \times P_{0.5}^{1-decanol})_{348K} + (x^{n-dodecane} \times P_{0.5}^{n-dodecane})_{348K} \\
 &= (0.778 \times 18.58) + (0.222 \times 13.09) \\
 &= 17.4 \neq 12.1 \text{ MPa}
 \end{aligned}$$

At 308 K:

$$\begin{aligned}
 (P_{0.5}^{MixtureA})_{308K} &= (x^{1-decanol} \times P_{0.5}^{1-decanol})_{308K} + (x^{n-dodecane} \times P_{0.5}^{n-dodecane})_{308K} \\
 &= (0.778 \times 11.85) + (0.222 \times 7.49) \\
 &= 10.9 \neq 9.0 \text{ MPa}
 \end{aligned}$$

$$\begin{aligned}
 (P_{0.5}^{MixtureA})_{308K} &= (x^{1-decanol} \times P_{0.5}^{1-decanol})_{308K} + (x^{n-dodecane} \times P_{0.5}^{n-dodecane})_{308K} \\
 &= (0.778 \times 26.30) + (0.222 \times 7.09) \\
 &= 22.0 \neq 9.9 \text{ MPa}
 \end{aligned}$$

It is evident from trends plotted in Figure 5-30 to Figure 5-32 that significant solute-solute interaction occur between *n*-alkanes, *l*-alcohols and branched alcohols, especially in the high solute mixture concentration region. In some instances the solute-solute interactions can be calculated by the summation of the interactions that occur in the comprising binary systems, but it is still important that the phase behaviour of true mixtures, and not only that of the comprising binary systems, be evaluated before the feasibility of an SFF process can be determined. Phenomena like co-solvency effects are caused by very specific solute-solute interactions that cannot be predicted by binary phase behaviour, and which can lead to the manifestation of complex phase behaviour in SFF processes.

5.9 Measured Data for Multi-component Mixtures

5.9.1 Rationale for Further Investigation

In the preceding section it was shown that solute-solute interactions play a significant role in the phase behaviour of multi-component mixtures, and consequently the presence of such interactions cannot be ignored. It was also revealed that although the type and qualitative effect of solute-solute interaction in a multi-component mixture can be anticipated, the extent thereof cannot be predicted from the phase behaviour of the comprising binary systems (especially at high solute concentrations). Since experimental measurement of the phase equilibrium data of binary, ternary and multi-component systems is a tedious and time consuming task, the use of a thermodynamic model to predict the phase behaviour of multi-component mixtures is proposed. If a database can be established of typical values for solute-solvent and solute-solute interaction parameters for use in a thermodynamic model, experimental measurement of the phase equilibrium data of mixtures can be drastically minimized.

In the next chapter the development of a thermodynamic model for the prediction of the phase equilibrium data of multi-component mixtures containing alkanes and alcohol isomers, will be discussed. To determine the accuracy of the developed thermodynamic model, the predicted data will be compared to experimentally measured data. It was decided to construct two different multi-component mixtures containing detergent range alkanes and alcohol isomers in different ratios, for this verification step.

The compositions of the mixtures are as follows:

- Mixture 1: 20 % *n*-dodecane + 10 % 3,7-dimethyl-*I*-octanol + 70 % *I*-decanol
- Mixture 2: 25 % *n*-decane + 25 % *I*-decanol + 25 % 3,7-dimethyl-*I*-octanol + 25 % 2,6-dimethyl-2-octanol

5.9.2 Measured Data for CO₂ + Mixture 1

In Figure 5-33 and Table 5-24 the isothermal phase equilibrium data of the CO₂ + (20 % *n*-dodecane + 10 % 3,7-dimethyl-*I*-octanol + 70 % *I*-decanol) system is given.

5 | Experimental Bubble and Dew Point Data

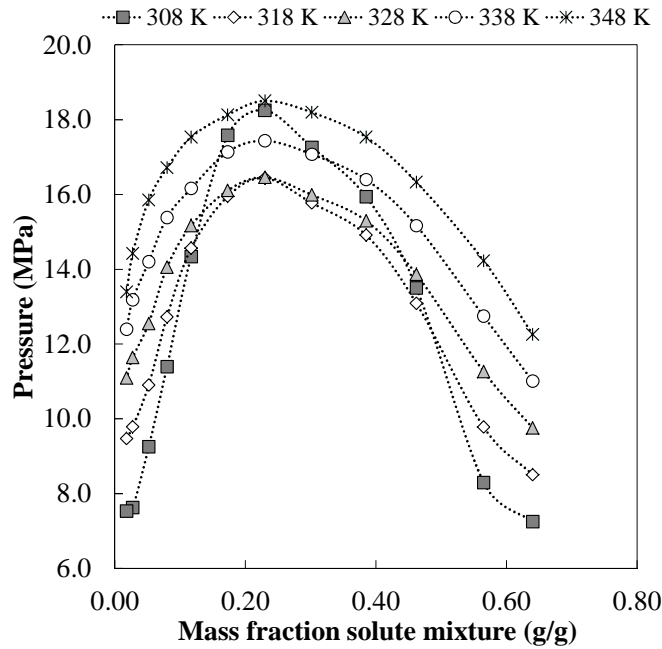


Figure 5-33 Phase behaviour of the CO₂ + (20 % n-dodecane + 10 % 3,7-dimethyl-1-octanol + 70 % 1-decanol) mixture at temperatures between 308 K and 348 K

Table 5-24 Isothermal data for the CO₂ + (20 % n-dodecane + 10 % 3,7-dimethyl-1-octanol + 70 % 1-decanol) system

Mass fraction solute (g/g)	Parameters for temperature correction					Temperature (K)				
	P = A*T ³ + B*T ² + C*T + D					308	318	328	338	348
	A	B	C	D	R ²	Pressure (MPa)				
0.637	0	0	0.095416	-23.085	1.000	6.30	7.26	8.21	9.17	10.12
0.559	0	0	0.12322	-31.071	0.999	6.88	8.11	9.34	10.58	11.81
0.467	0	0	0.15201	-39.637	1.000	7.18	8.70	10.22	11.74	13.26
0.388	0	0	0.17151	-45.412	0.999	7.41	9.13	10.84	12.56	14.27
0.291	0	0	0.18542	-49.486	0.999	7.62	9.48	11.33	13.19	15.04
0.226	0	0	0.17780	-46.589	0.999	8.17	9.95	11.73	13.51	15.29
0.177	0	0	0.17601	-45.703	0.999	8.51	10.27	12.03	13.79	15.55
0.115	0	0	0.17594	-45.667	0.998	8.52	10.28	12.04	13.80	15.56
0.076	0	-0.0012490	0.99898	-181.453	1.000	7.75	9.92	11.84	13.51	14.93
0.050	0	-0.0014981	1.1475	-203.612	0.999	7.71	9.81	11.61	13.11	14.31
0.0283	0	-0.0011955	0.93160	-165.829	1.000	7.70	9.53	11.12	12.48	13.59
0.0189	0	-0.0011461	0.88217	-155.164	1.000	7.82	9.47	10.89	12.08	13.04

Mixture 1 contains 70% 1-decanol and thus phase behaviour is dominated by the alcohol, which is evident from the observed temperature inversion.

5.9.3 Measured Data for CO₂ + Mixture 2

Mixture 2 consists of CO₂ + (25 % *n*-decane + 25 % 1-decanol + 25 % 3,7-dimethyl-1-octanol + 25 % 2,6-dimethyl-2-octanol). Phase equilibrium data for this system is presented in Figure 5-34 and Table 5-25.

Although Mixture 2 also contains 1-decanol, it does not exhibit a region of temperature inversion, as that exhibited by Mixture 1. This may be attributed to the smaller fraction of 1-decanol present, and the fact that it is not the majority component. The strong polar interactions associated with 1-decanol do however present itself as an oddly shaped hump on the phase transition curves at lower temperatures.

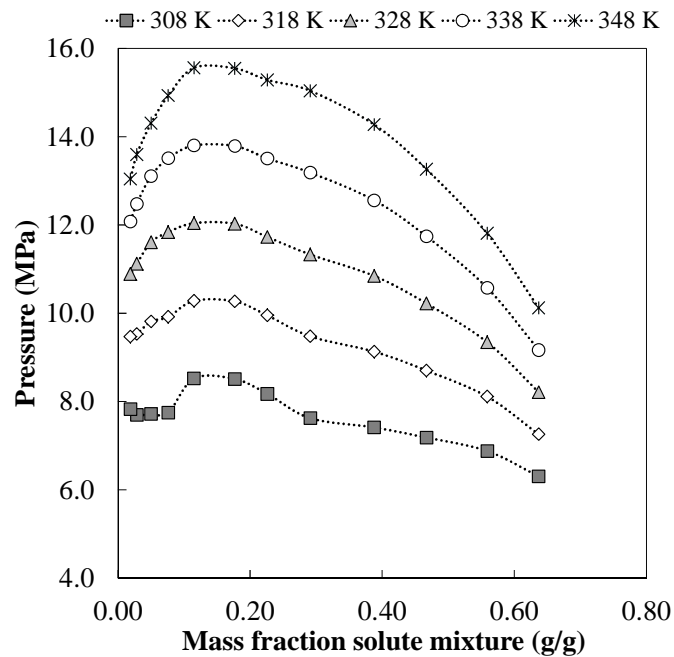


Figure 5-34 Phase behaviour of the CO₂ + (25 % *n*-decane + 25 % 1-decanol + 25 % 3,7-dimethyl-1-octanol + 25 % 2,6-dimethyl-2-octanol) mixture at temperatures between 308 K and 348 K

5 | Experimental Bubble and Dew Point Data

Table 5-25 Isothermal data for the CO₂ + (25 % *n*-decane + 25 % 1-decanol + 25 % 3,7-dimethyl-1-octanol + 25 % 2,6-dimethyl-2-octanol) system

Mass fraction solute (g/g)	Parameters for temperature correction					Temperature (K)				
	$P = A \cdot T^3 + B \cdot T^2 + C \cdot T + D$					308	318	328	338	348
	A	B	C	D	R ²	Pressure (MPa)				
0.640	0	0	0.12516	-31.296	0.998	7.25	8.51	9.76	11.01	12.26
0.565	0	0	0.14827	-37.368	0.999	8.30	9.78	11.26	12.75	14.23
0.462	-0.00011030	0.11116	-37.208	4151.030	0.999	13.50	13.09	13.86	15.16	16.33
0.385	-0.00011483	0.11659	-39.338	4426.671	0.997	15.94	14.91	15.29	16.40	17.53
0.302	-0.00013921	0.14133	-47.705	5370.349	0.998	17.26	15.77	15.99	17.07	18.19
0.230	-0.00014555	0.14802	-50.061	5647.911	0.997	18.25	16.44	16.45	17.43	18.50
0.173	-0.00015257	0.15451	-52.040	5846.460	0.996	17.58	15.95	16.10	17.14	18.13
0.117	0	0.0019137	-1.1755	194.864	0.992	14.34	14.56	15.17	16.16	17.53
0.080	0	0	0.13295	-29.555	0.998	11.39	12.72	14.05	15.38	16.71
0.052	0	0	0.16493	-41.545	0.997	9.25	10.90	12.55	14.20	15.85
0.0275	0	-0.0015396	1.1799	-209.720	1.000	7.62	9.78	11.64	13.18	14.42
0.0182	0	-0.0015729	1.1783	-206.160	1.000	7.53	9.47	11.09	12.40	13.39

5.10 Discussion on the Phase Behaviour of the Multi-component Mixtures Investigated

In Figure 5-35 the phase behaviour of CO₂ + Mixture 1 is compared to that of the comprising binary mixtures.

It is interesting to note that the phase transition pressures of the dew point curve of Mixture 1 occur at values that can be approximated from the phase transition pressures of the contributing binary mixtures. An example of such calculation is given below. Calculations like these are not applicable to the dew point region or temperatures below 338 K (the upper temperature limit for the temperature inversion observed for the CO₂ + 1-decanol system) for mixtures containing 1-decanol.

5 | Experimental Bubble and Dew Point Data

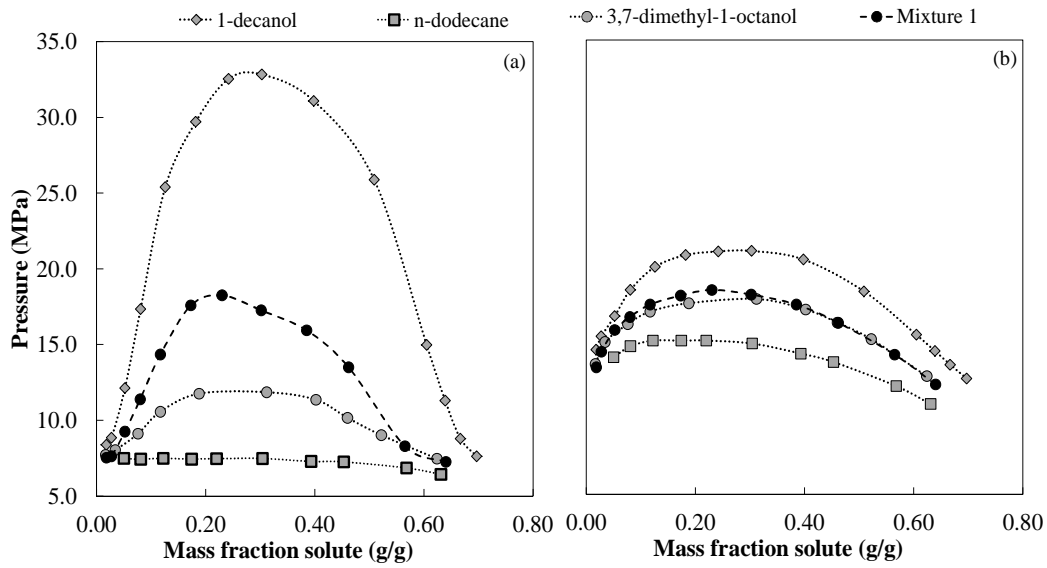


Figure 5-35 Comparison between the phase behaviour of the $\text{CO}_2 + (20\% \text{ n-dodecane} + 10\% \text{ 3,7-dimethyl-1-octanol} + 70\% \text{ 1-decanol})$ system and the comprising binary mixtures, $\text{CO}_2 + \text{n-dodecane}$, $\text{CO}_2 + \text{1-decanol}$ and $\text{CO}_2 + \text{3,7-dimethyl-1-octanol}$ at (a) 308 K and (b) 348 K

$$\begin{aligned}
 (P_{0.05}^{\text{Mixture1}})_{348\text{K}} &= (x^{\text{1-decanol}} \times P_{0.05}^{\text{1-decanol}})_{348\text{K}} + (x^{\text{3,7-dim-1-oct}} \times P_{0.05}^{\text{3,7-dim-1-oct}})_{348\text{K}} \\
 &+ (x^{\text{n-dodecane}} \times P_{0.05}^{\text{n-dodecane}})_{348\text{K}} \\
 &= (0.7 \times 16.66) + (0.1 \times 15.50) + (0.2 \times 14.06) \\
 &= 16.0 \approx 15.7 \text{ MPa}
 \end{aligned}$$

Like for Mixture 1, the phase behaviour of the comprising binary mixtures is compared to that of Mixture 2 in Figure 5-36.

5 | Experimental Bubble and Dew Point Data

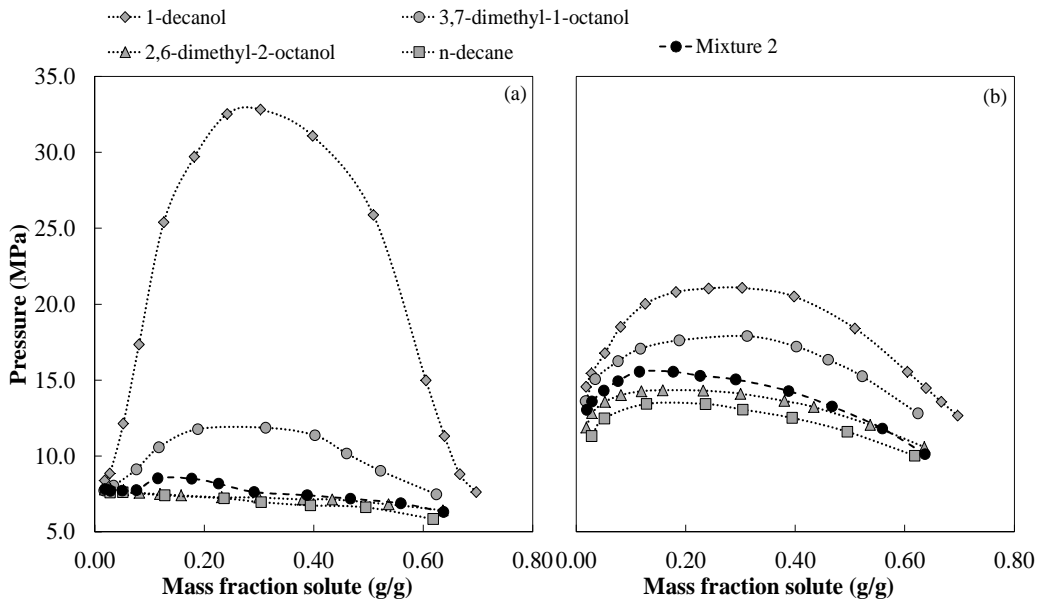


Figure 5-36 Comparison between the phase behaviour of the $CO_2 + (25\% \text{ n-decane} + 25\% \text{ 1-decanol} + 25\% \text{ 3,7-dimethyl-1-octanol} + 25\% \text{ 2,6-dimethyl-2-octanol})$ system and the comprising binary mixtures, $CO_2 + \text{n-decane}$, $CO_2 + \text{1-decanol}$, $CO_2 + \text{3,7-dimethyl-1-octanol}$ and $CO_2 + \text{2,6-dimethyl-2-octanol}$ at (a) 308 K and (b) 348 K

Once again it can be shown that the dew point pressures of the multi-component mixture can be approximated by the dew point pressures of the contributing binary mixtures. It is proposed that this estimation method for the dew point pressure of multi-component mixtures be used with care and only where quick evaluation, not accurate values, are required.

$$\begin{aligned}
 (P_{0.05}^{Mixture2})_{348K} &= (x^{1-decanol} \times P_{0.05}^{1-decanol})_{348K} + (x^{3,7-dim-1-oct} \times P_{0.05}^{3,7-dim-1-oct})_{348K} \\
 &+ (x^{2,6-dim-2-oct} \times P_{0.05}^{2,6-dim-2-oct})_{348K} + (x^{n-decane} \times P_{0.05}^{n-decane})_{348K} \\
 &= (0.25 \times 16.66) + (0.25 \times 15.50) + (0.25 \times 13.49) + (0.25 \times 12.41) \\
 &= 14.5 \approx 14.3 \text{ MPa}
 \end{aligned}$$

The bubble and dew point data reported in this section for the two multi-component mixtures in supercritical CO₂ will be used in the next chapter as verification data for the developed thermodynamic model. The binary, ternary and multi-component data measured up to this point indicate that both solute-solvent and solute-solute interactions make significant contributions to the phase behaviour of mixtures of alkanes and alcohol isomers. In Chapter 6, the aim will be to develop a thermodynamic model that can accurately represent the interactions in these systems.

5.11 Outcomes of this Chapter

Objective 4 and 5, as discussed in Chapter 1, was addressed in this chapter. The main aim of the chapter was to present experimental bubble and dew point data for binary, ternary and multi-component systems consisting of detergent range alkane and alcohol isomers. Binary bubble and dew point data was measured for nineteen systems containing supercritical ethane or CO₂ and one of the following solutes: *n*-dodecane, *n*-decane, 2-methylnonane, 3-methylnonane, 4-methylnonane, 1-decanol, 2-decanol, 3,7-dimethyl-1-octanol, 2,6-dimethyl-2-octanol and 3,7-dimethyl-3-octanol. The purpose of the measured binary data was to aid in determining whether structural isomerism of alkanes and alcohols influence their phase behaviour in supercritical solvents, and if so, to what extent. This allowed conclusions to be made about the solute-solvent interactions that occur for these compounds.

The ternary bubble and dew point data were measured with the intent to evaluate the significance of solute-solute interactions between the following pairs: *n*-alkane + 1-alcohol, *n*-alkane + branched alcohol and 1-alcohol + branched alcohol.

Lastly, multi-component bubble and dew point data were measured to generate a data set to be used in the verification process of the thermodynamic model to be developed in the next chapter. Although binary phase equilibrium data can be employed to a certain extent to anticipate the phase behaviour of multi-component mixtures, accurate predictions cannot be made utilizing such limited information. The multi-component mixtures investigated in this chapter have compositions typically encountered in product streams in the detergent and surfactant industries, and thus it is important that the thermodynamic model be able to predict the phase behaviour of such mixtures accurately.

The key observations made in this chapter are:

- No deviation from the expected phase behaviour of the CO₂ + *n*-decane, CO₂ + *l*-decanol, ethane + *n*-decane and ethane + *l*-decanol systems, as reported in Chapter 4, was observed.
- The ethane + *n*-decane system exhibit Type I phase behaviour and thus no liquid-liquid immiscibility will occur over the entire temperature range. The CO₂ + *n*-decane system exhibit Type II phase behaviour with a three phase region occurring at temperatures well below the critical temperature of CO₂. For the ethane + *l*-decanol and CO₂ + *l*-decanol systems a three phase region is expected to occur near and below the respective critical temperatures of the solvents, with ethane + *l*-decanol system exhibiting Type V phase behaviour and the CO₂ + *l*-decanol system exhibiting Type III phase behaviour. No three phase region was observed for either of these mixtures, but the possibility still exist that such a region can be present at slightly lower solute concentrations and/or temperatures than those measured in this work.
- The phase behaviour of the C₁₀-alkane isomers did not differ significantly from one another in either supercritical CO₂ or ethane. It was assumed that for alkane isomers that exhibit similar phase behaviour, one compound can be selected to represent the phase behaviour of the group of compounds. *n*-Decane was thus selected as the representative alkane isomer for the methyl-branched C₁₀-alkane isomers.
- Certain C₁₀-alcohol isomers showed significant differences in phase behaviour in both supercritical CO₂ and ethane. The phase behaviour of the alcohol isomers are influenced by the number, length and quantity of side branches, as well as the position of the hydroxyl group. Generally, 2,6-dimethyl-2-octanol and 3,7-dimethyl-3-octanol exhibited similar phase behaviour, and 2-decanol and 3,7-dimethyl-*l*-octanol as well.
- The operating temperature influences the phase behaviour of compounds. At certain operating temperatures the difference in phase transition pressures between compounds are more significant than at other temperatures. This holds especially true for the CO₂ + *l*-decanol mixture, which displays a temperature inversion below 338 K. Although such a phenomenon may increase the complexity of the phase behaviour, it may also prove beneficial when attempting to separate *l*-decanol from other components, where

the other components exhibit much lower phase transition pressures below 338 K. From the binary phase equilibrium measurements no definite conclusions could be drawn regarding the optimum operating temperatures for the separation of alkanes from alcohol isomers.

- Generally, similar phase behaviour trends were observed in supercritical CO₂ and in supercritical ethane for all the compounds investigated, except for *l*-decanol, which exhibited a temperature inversion when in a mixture with supercritical CO₂, but not with supercritical ethane. No distinct advantage could be found for the use of one solvent instead of the other. Supercritical CO₂ displayed slightly larger differences in phase transition pressures, and thus solubility, between *n*-decane and *l*-decanol (the two key components). This phenomenon, and the fact that CO₂ is safer, less expensive and more easily available, encouraged the selection of CO₂ as the solvent for all further investigations.
- Since the phase behaviour of the alcohol isomers differ from one another in both supercritical CO₂ and ethane, it can be concluded that different solute-solvent interactions are present. These solute-solvent interactions are significant and should be considered when developing a thermodynamic model to accurately represent binary mixtures containing detergent range alkane and alcohol isomers in supercritical CO₂ and ethane.
- Bubble and dew point measurements of ternary mixtures revealed that significant solute-solute interactions occur for mixtures of *n*-alkane + *l*-alcohol, *n*-alkane + branched alcohol, and *l*-alcohol + branched alcohol, in supercritical CO₂. These solute-solute interactions diminish at higher temperatures in the low solute mixture concentration region, and thus the phase transition pressures in this region can be estimated from binary phase equilibrium data for certain mixtures. At all other compositions, however, the solute-solute interactions contribute significantly to the phase behaviour and cannot be predicted from binary data.
- The ratio of components in a mixture determines the type of phase behaviour displayed. In many cases the phase behaviour of the mixture can be anticipated from that of the binary phase behaviour of the majority compound in the solvent. However, the

occurrence of complex effects in ternary mixtures, like co-solvency, cannot be predicted from binary phase behaviour.

In Chapter 6 a thermodynamic model will be established to accurately predict multi-component phase equilibrium data for mixtures of detergent range alkanes and alcohol isomers. With the aid of the measured binary and ternary bubble and dew point data, solute-solvent and solute-solute binary interactions can now be quantified and incorporated into a thermodynamic model as interaction parameters. The phase equilibrium data measured for the two multi-component mixtures in section 5.9, can be used to verify the accuracy of the model in its phase transition pressure predictions for multi-component mixtures.

5.12 Significant Contributions

This chapter contributes novel phase equilibrium data for C₁₀-alkane isomers and C₁₀-alcohol isomers in supercritical ethane and CO₂. The binary bubble and dew point data presented in this chapter were published in two papers:

- M. Zamudio, C.E. Schwarz, J.H. Knoetze, Phase equilibria of branched isomers of C₁₀-alcohols and C₁₀-alkanes in supercritical ethane, *The Journal of Supercritical Fluids*. 58 (2011) 330 – 342.
- M. Zamudio, C.E. Schwarz, J.H. Knoetze, Phase equilibria of branched isomers of C₁₀-alcohols and C₁₀-alkanes in supercritical carbon dioxide, *The Journal of Supercritical Fluids*. 59 (2011) 14 – 26.

New data were also measured for ternary and multi-component mixtures. The bubble and dew point data measured for the multi-component mixture, Mixture 1, is part of an investigation that involves the development of a thermodynamic model, and is presented as part of a publication mentioned in the significant contributions of Chapter 6.

5.13 Nomenclature

Symbol/ Acronym	Description
SFF	Supercritical Fluid Fractionation

5.14 References

- [1] C.E. Schwarz, Phase equilibrium of alkanes and supercritical fluids, Masters Thesis, Stellenbosch University, 2001.
- [2] M.S. Fonseca, R. Dohrn, S. Peper, High-pressure fluid-phase equilibria: Experimental methods and systems investigated (2005-2008), *Fluid Phase Equilibria*. 300 (2011) 1 – 69.
- [3] J.D. Raal, A.L. Mulbauer, *Phase Equilibria: Measurement and Computation*, Taylor & Francis, Washington D.C, 1998.
- [4] C. E. Schwarz, I. Nieuwoudt, Phase equilibrium of propane and alkanes: Part I. Experimental procedures, dotriacontane equilibrium and EOS modelling, *The Journal of Supercritical Fluids*. 27 (2003) 133 – 144.
- [5] C. J. Peters, J. L. de Roo, J. de Swaan Arons, Measurement and calculations of phase equilibria in binary mixtures of propane + tetratriacontane, *Fluid Phase Equilibria*. 72 (1992) 251 – 266.
- [6] C. J. Peters, J. L. de Roo, J. de Swaan Arons, Phase equilibria in binary mixtures of propane and hexacontane, *Fluid Phase Equilibria*. 85 (1993) 301 – 312.
- [7] C.E. Schwarz, A.J. de Villiers, C.B. McClune, G.J.K. Bonthuys, A.J. Burger, J.H. Knoetze, High pressure phase equilibrium measurements of long chain alcohols in supercritical ethane, *The Journal of Supercritical Fluids*. 55 (2010) 554 – 565.
- [8] C.E. Schwarz, I. Nieuwoudt, J.H. Knoetze, Phase equilibria of long chain *n*-alkanes in supercritical ethane: Review, measurements and prediction, *The Journal of Supercritical Fluids*. 46 (2008) 226 – 232.
- [9] I. Nieuwoudt, Vapour-liquid equilibria and densities for the system butane + hexacontane, *Journal of Chemical & Engineering Data*. 41 (1996) 1024 – 1027.

- [10] J. Gregorowicz, T. W. de Loos, J. de Swaan Arons, The system propane and eiconsane: P , T , and x measurements in the temperature range 288 - 358 K, *Journal of Chemical & Engineering Data*. 37 (1992) 356 – 358.
- [11] F.C.v.N. Fourie, C.E. Schwarz, J.H. Knoetze, Phase equilibria of alcohols in supercritical fluids: Part I. The effect of the position of the hydroxyl group for linear C_8 alcohols in supercritical carbon dioxide, *The Journal of Supercritical Fluids*. 47 (2008) 161 – 167.
- [12] H. H. Reamer, B. H. Sage, Phase equilibria in hydrocarbon systems. Volumetric and phase behavior of the n -decane- CO_2 System., *Journal of Chemical & Engineering Data*. 8 (1963) 508 – 513.
- [13] N. Nagarajan, R. L. Robinson, Equilibrium phase compositions, phase densities, and interfacial tensions for carbon dioxide + hydrocarbon systems. 2. Carbon dioxide + n -decane, *Journal of Chemical & Engineering Data*. 31 (1986) 168 – 171.
- [14] G. F. Chou, R. R. Forbert, J. M. Prausnitz, High-pressure vapour-liquid equilibria for carbon dioxide/ n -decane, carbon dioxide/tetralin, and carbon dioxide/ n -decane/tetralin at 71.1 and 104.4 °C, *Journal of Chemical & Engineering Data*. 35 (1990) 26 – 29.
- [15] D. W. Jennings, R. C. Schucker, Comparison of high-pressure vapour-liquid equilibria of mixtures of CO_2 or propane with nonane and C_9 alkylbenzenes, *Journal of Chemical & Engineering Data*. 41 (1996) 831 – 838.
- [16] B. Han, D-Y. Peng, C-T. Fu, G. Vilcsak, An apparatus for phase equilibrium studies of carbon dioxide+heavy hydrocarbon systems, *Canadian Journal of Chemical Engineering* 70 (1992) 1164 – 1171.
- [17] R. D. Shaver, R. L. Robinson, K. A. M. Gasem, An automated apparatus for equilibrium phase compositions, densities, and interfacial tensions: data for carbon dioxide + decane, *Fluid Phase Equilibria*. 179 (2001) 43 – 66.
- [18] T. Tsuji, S. Tanaka, T. Hiaki, R. Saito, Measurements of bubble point pressure for CO_2 + decane and CO_2 + lubricating oil, *Fluid Phase Equilibria*. 219 (2004) 87 – 92.
- [19] R. Jiménez-Gallegos, L. A. Galicia-Luna, O. Elizalde-Solis, Experimental vapour-liquid equilibria for the carbon dioxide + octane and carbon dioxide + decane systems, *Journal of Chemical & Engineering Data*. 51 (2006) 1624 – 1628.

- [20] Y. Iwai, N. Hosotani, T. Morotomi, Y. Koga, Y. Arai, High-pressure vapour-liquid equilibria for carbon dioxide + linalool, *Journal of Chemical & Engineering Data*. 39 (1994) 900 – 902.
- [21] H. H. Reamer, B. H. Sage, Phase equilibria in hydrocarbon systems. Volumetric and phase behaviour of the ethane-*n*-decane system, *Journal of Chemical & Engineering Data*. 7 (1962) 161 – 168.
- [22] B. A. Bufkin, R. L. Robinson, S. S. Estrera, K. D. Luks, Solubility of ethane in *n*-decane at pressures to 8.2 MPa and temperatures from 278 to 411 K, *Journal of Chemical & Engineering Data*. 31 (1986) 421 – 423.
- [23] C. J. Peters, R. N. Lichtenthaler, J. de Swaan Arons, Three phase equilibria in binary mixtures of ethane and higher *n*-alkanes, *Fluid Phase Equilibria*. 29 (1986) 495 – 504.
- [24] H. Gardeler, J. Gmehling, Experimental determination of phase equilibria and comprehensive examination of the predictive capabilities of group contribution equations of state with a view to the synthesis of supercritical extraction processes, in: *Supercritical Fluids as Solvents and Reaction Media*, Elsevier B.V., Amsterdam, 2004.
- [25] F. Llovel, L. F. Vega, Phase equilibria, critical behavior and derivative properties of selected *n*-alkane/*n*-alkane and *n*-alkane/*l*-alkanol mixtures by the crossover soft-SAFT equation of state, *The Journal of Supercritical Fluids*. 41 (2007) 204 – 216.
- [26] T. de Loos, Understanding phase diagrams, in: *Supercritical Fluids: Fundamentals for Application*, Kluwer Academic Publishers, The Netherlands, 1994.
- [27] G.J.K. Bonthuys, C.E. Schwarz, A.J. Burger, J.H. Knoetze, Separation of alkanes and alcohols with supercritical fluids. Part I: Phase equilibria and viability study, *The Journal of Supercritical Fluids*. 57 (2011) 101 – 111.
- [28] A. Kramer, G. Thodos, Solubility of *l*-hexadecanol and palmitic acid in supercritical carbon dioxide, *Journal of Chemical & Engineering Data*. 33 (1988) 230 – 234.
- [29] X. Gui, Z. Tang, W. Fei, Solubility of CO₂ in alcohols, glycols, ethers, and ketones at high pressures from (288.15 to 318.15) K, *Journal of Chemical & Engineering Data*. 56 (2011) 2420 – 2429.

- [30] C. J. Chang, K-L. Chiu, C-Y. Day, A new apparatus for the determination of P - x - y diagrams and Henry's constants in high pressure alcohols with critical carbon dioxide, *The Journal of Supercritical Fluids*. 12 (1998) 223 – 237.
- [31] S. Peper, R. Dohrn, Sampling from fluid mixtures under high pressure: review, case study and evaluation, *The Journal of Supercritical Fluids*. 66 (2012) 2 – 15.
- [32] D. H. Lam, A. Jangkamolkulchai, K. D. Luks, Liquid-liquid-vapour phase equilibrium behaviour of certain binary carbon dioxide + n -alkanol mixtures, *Fluid Phase Equilibria*. 60 (1990) 131 – 141.
- [33] C. J. Peters, L. J. Florusse, S. Hahre, J. de Swaan Arons, Fluid multiphase equilibria and critical phenomena in binary and ternary mixtures of carbon dioxide, certain n -alkanols and tetradecane, *Fluid Phase Equilibria*. 110 (1995) 157 – 173.
- [34] C.E. Schwarz, G.J.K. Bonthuys, J.H. Knoetze, A.J. Burger, The influence of functional end groups on the high-pressure phase equilibria of long chain molecules in supercritical propane, *The Journal of Supercritical Fluids*. 46 (2008) 233 – 237.
- [35] C.E. Schwarz, F.C.v.N. Fourie, J.H. Knoetze, Phase equilibria of alcohols in supercritical fluids Part II. The effect of side branching on C_8 alcohols in supercritical carbon dioxide, *The Journal of Supercritical Fluids*. 51 (2009) 128–135.
- [36] H.M. Weir, *The OXO Process For Alcohol Manufacture From Olefins*, 1945.
- [37] H. Bahrmann, H. Bach, Oxo synthesis, *Ullmann's Encyclopedia of Industrial Chemistry*. (2012).
- [38] A. L. Scheidgen, G. M. Schneider, Fluid phase equilibria of (carbon dioxide + a l -alkanol + an alkane) up to 100 MPa and $T=393$ K: cosolvency effect, miscibility windows, and holes in the critical surface, *Journal of Chemical Thermodynamics*. 32 (2000) 1183 – 1201.
- [39] A. L. Scheidgen, G. M. Schneider, New phase phenomena in ternary systems at high pressures - cosolvency and miscibility windows up to 100 MPa, *Physical Chemistry Chemical Physics*. 4 (2002) 963 – 967.

- [40] H. Pohler, A. L. Scheidgen, G. M. Schneider, Fluid phase equilibria of binary and ternary mixtures of supercritical carbon dioxide with a *I*-alkanol and an *n*-alkane up to 100 MPa and 393 K - cosolvency effect and miscibility windows (Part II), *Fluid Phase Equilibria*. 115 (1996) 165 – 177.
- [41] A. Kordikowski, G. M. Schneider, Fluid phase equilibria of binary and ternary mixtures of supercritical carbon dioxide with low-volatility organic substances up to 100 MPa and 393 K: cosolvency effects and miscibility windows, *Fluid Phase Equilibria*. 90 (1993) 149 – 162.
- [42] M. Spee, G. M. Schneider, Fluid phase equilibrium studies on binary and ternary mixtures of carbon dioxide with hexadecane, *I*-dodecanol, *I*,8-octanediol and dotriacontane at 393.2 K and at pressures up to 100 MPa, *Fluid Phase Equilibria*. 65 (1991) 263 – 274.
- [43] I. F. Holscher, M. Spee, G. M. Schneider, Fluid-phase equilibria of binary and ternary mixtures of CO₂ with hexadecane, *I*-dodecanol, *I*-hexadecanol and 2-ethoxy-ethanol at 333.2 and 393.2 K and at pressures up to 33 MPa, *Fluid Phase Equilibria*. 49 (1989) 103 – 113.

6. THERMODYNAMIC MODELLING OF MIXTURES AT HIGH PRESSURE USING ASPEN PLUS®

6.1 MODEL SELECTION	170
6.1.1 Models Suggested by Aspen Plus®	171
6.1.2 Predictive Capability	172
6.1.3 PR-BM.....	177
6.1.4 RKS-BM.....	178
6.1.5 RK-ASPEN.....	179
6.1.6 SR-POLAR.....	180
6.2 PURE COMPONENT PARAMETERS.....	182
6.2.1 Pure Component Critical Properties	182
6.2.2 Acentric Factors.....	183
6.2.3 Vapour Pressure Data	184
6.2.4 Polar Parameters	186
6.2.4.1 RK-ASPEN Polar Parameters	187
6.2.4.2 SR-POLAR Polar Parameters.....	188
6.3 BINARY SOLUTE-SOLVENT INTERACTION PARAMETERS	188
6.3.1. Factors that Require Special Attention.....	189
6.3.2 Determining Binary Solute-Solvent Interaction Parameters	190
6.3.2.1 PR-BM	190
6.3.2.2 RKS-BM.....	192
6.3.2.3 RK-ASPEN.....	193

6 | Thermodynamic Modelling of Mixtures at High Pressure using Aspen Plus®

6.3.2.4 <i>SR-POLAR</i>	195
6.3.3 Predictive Capability at Low Temperatures	196
6.3.3.1 <i>PR-BM</i>	196
6.3.3.2 <i>RKS-BM</i>	199
6.3.3.3 <i>RK-ASPEN</i>	201
6.3.3.4 <i>SR-POLAR</i>	203
6.3.4 Thermodynamic Model Comparison and Selection	205
6.4 PREDICTING MULTI-COMPONENT PHASE BEHAVIOUR.....	206
6.4.1 <i>RKS-BM</i>	206
6.4.2 <i>RK-ASPEN</i>	209
6.4.3 Thermodynamic Model Comparison and Selection	210
6.5 BINARY SOLUTE-SOLUTE INTERACTION PARAMETERS.....	213
6.5.1 Rationale for Further Investigation	213
6.5.2 Factors that Require Special Attention.....	215
6.5.3 Determining Binary Solute-Solute Interaction Parameters	215
6.5.4 Predicting Multi-component Phase Behaviour.....	222
6.6 OUTCOMES OF THIS CHAPTER	226
6.7 SIGNIFICANT CONTRIBUTIONS	228
6.8 NOMENCLATURE.....	229
6.9 REFERENCES	231

6 | Thermodynamic Modelling of Mixtures at High Pressure using Aspen Plus®

The aim of this chapter is to establish a thermodynamic model that can predict accurate phase equilibrium data for mixtures containing supercritical CO₂ as the solvent, and different compositions of detergent range alkanes and alcohol isomers – thus addressing Objective 6, as outlined in Chapter 1. In this work the “development” or “establishment” of a thermodynamic model, refers to the evaluation, selection and improvement of established thermodynamic models in Aspen Plus®. Thermodynamic models are evaluated and selected to represent CO₂ + alkane and CO₂ + alcohol systems according to the following criteria:

- Ability to accurately predict binary vapour-liquid (VLE) data for CO₂ + alkane and CO₂ + alcohol mixtures within the temperature range 308 K – 348 K.
- Ability to accurately represent binary VLE data for CO₂ + alkane and CO₂ + alcohol mixtures within the temperature range 338 K – 348 K, during the regression of binary solute-solvent interaction parameters.
- Ability to accurately predict binary VLE data for CO₂ + alkane and CO₂ + alcohol mixtures within the temperature range 318 K – 328 K with the inclusion of regressed binary solute-solvent interaction parameters.
- Ability to accurately predict multi-component phase transition pressure data for mixtures of CO₂ and different compositions of alkanes and alcohols, within the temperature range 318 K – 348 K with the inclusion of regressed binary solute-solvent interaction parameters.

Aspen Plus® was selected as the software package to be used in all the process simulations and solution calculations. A commercial process simulator is used instead of custom, in-house developed software, to demonstrate the ease of application of the methodology presented in this work. Commercial process simulators, like Aspen Plus® are readily available to any entity in the chemical industry and similar strategies to the one developed in this work can be implemented with ease for similar separation processes to determine its feasibility.

The binary bubble and dew point measurements reported in the previous chapter will be used to determine quantitative parameters that represent the specific solute-solvent interactions that take place between the respective alkanes and alcohol isomers, and CO₂. The solute-solute interactions, although believed to have a smaller effect on the overall phase behaviour of a mixture compared to

6 | Thermodynamic Modelling of Mixtures at High Pressure using Aspen Plus®

the solute-solvent interactions, can also be incorporated in the thermodynamic model. The measured bubble and dew point data for the ternary systems reported in Chapter 5, are used to determine values for parameters to quantify the *n*-alkane + *l*-alcohol, *n*-alkane + branched alcohol and *l*-alcohol + branched alcohol interactions. Once all the parameters have been determined and incorporated into the selected thermodynamic model, the accuracy of the thermodynamic model is verified by comparing its prediction of phase transition pressure data to experimentally measured bubble and dew point measurements for the two multi-component systems reported in Chapter 5.

6.1 Model Selection

A lot of thermodynamic models have been developed over the years, some more complex than others. In this work the focus will be on the more simple and robust cubic equations of state (EoS). A detailed discussion on the motivation behind the selection of cubic EoS for use in this work can be found in Chapter 4, section 4.4.1. For ease of reference the main reasons are briefly mentioned again:

- The methodology developed in this work is aimed at determining the feasibility of a new separation process. This work is thus part of an initial screening process and accurate trends must be predicted in a timely manner. Once at the process design stage the use of more complex thermodynamic models may prove beneficial.
- Previous studies [1,2] have shown that for similar systems complex thermodynamic models, like the statistical associating fluid theory (SAFT) and the perturbed chain statistical associating theory (PC-SAFT), did not lead to any significant increase in accuracy over simple cubic EoS, like Peng-Robinson (PR).
- The pure component properties of the compounds used in this investigation are not widely available. Complex thermodynamic models generally require pure component parameters that are more difficult to come by and verify, e.g. segment number, segment diameter and dispersion energy. The use of estimated values with large error margins for pure component properties, can lead to the generation of inaccurate VLE data.

6 | Thermodynamic Modelling of Mixtures at High Pressure using Aspen Plus®

6.1.1 Models Suggested by Aspen Plus®

The Aspen Plus® software guide suggested the use of certain models for high pressure and supercritical applications. According to the Aspen Plus® guide, the models mentioned can deal with high pressures and temperatures, mixtures close to their critical point, and liquid-liquid separation at high pressure. These models were listed under the following categories:

Equation-of-State Property Methods for High-Pressure Hydrocarbon Applications

- Benedict-Webb-Rubin-Lee-Starling (BWR-LS)
- Benedict-Webb-Rubin-Starling (BWRS)
- Lee-Kesler-Plöcker (LK-PLOCK)
- Peng-Robinson-Boston-Mathias (PR-BM)
- Redlich-Kwong-Soave-Boston-Mathias (RKS-BM)

Flexible and Predictive Equation-of-State Property Methods

- Peng-Robinson with modified Huron-Vidal mixing rules (PRMHV2)
- Peng-Robinson with Wong-Sandler mixing rules (PRWS)
- Redlich-Kwong-Soave with modified Huron-Vidal mixing rules (RKSMHV2)
- Redlich-Kwong-Soave with Wong-Sandler mixing rules (RKSWS)
- Redlich-Kwong-Soave with Holderbaum-Gmehling mixing rules (PSRK)
- Redlich-Kwong-Soave with Mathias mixing rules (RK-ASPEN)
- Redlich-Kwong-Soave with Schwarzenuber-Renon mixing rules (SR-POLAR)

As mentioned in Chapter 1, the scope of this project is limited to the application of cubic EoS and thus the thermodynamic models based on the virial EoS (BWR-LS, BWRS, LK-PLOCK) were

6 | Thermodynamic Modelling of Mixtures at High Pressure using Aspen Plus®

not considered. All the other thermodynamic models are based on either the Peng-Robinson [3] or Soave-Redlich-Kwong (SRK) [4] EoS.

The main differences between the proposed thermodynamic models are in the selection of alpha function and mixing rules. The thermodynamic models that incorporate the modified Huron-Vidal mixing rules (PRMHV2 and RKSMHV2), the Wong-Sandler mixing rules (PRWS and RKSWS) and the Holderbaum-Gmehling mixing rules (PSRK) require previously determined low pressure activity coefficient parameters for predictions at high pressures. The property methods that utilize these mixing rules are thus predictive in nature, and binary interaction parameters determined at high pressures cannot be incorporated. It is anticipated that the thermodynamic models that incorporate such mixing rules will not predict accurate data for the systems considered in this investigation due to the lack of low pressure activity coefficient parameters in the database for the isomeric components used in this study. The use of such low pressure activity coefficient parameters are limited and the determination thereof falls beyond the scope of this investigation.

The other thermodynamic models all incorporate the original Van der Waals (VdW) mixing rules or some slight adaptation thereof, and differ mainly in the selection of the alpha function. The PR-BM and RKS-BM thermodynamic models contain the Boston-Mathias alpha function which provides the option to include binary interaction parameters. The RK-ASPEN and SR-POLAR thermodynamic models contain modified versions of the Boston-Mathias alpha function and have the option to include binary interaction parameters as well as pure component polar parameters. The option to include additional parameters in the RK-ASPEN and SR-POLAR models will in all likelihood lead to better predictions of phase equilibrium data. It should however be noted that the addition of fitting parameters usually decreases the robustness and range of applicability of a property method.

6.1.2 Predictive Capability

The ability to generate accurate high pressure multi-component data will depend firstly on the thermodynamic model that is selected, and secondly on the interaction parameters incorporated. Certain models perform better at specific conditions, while other models work well for specific mixtures. The ability of the proposed thermodynamic models to predict accurate phase equilibrium data for mixtures of CO₂ and detergent range alkanes (see Figure 6-1 to Figure 6-3) and alcohols (see Figure 6-4 to Figure 6-6) in the temperature range 308 – 348 K was tested by using *n*-decane and

6 | Thermodynamic Modelling of Mixtures at High Pressure using Aspen Plus®

n-Decanol as representative compounds. By testing the models' predictive ability in the selected temperature range and for the selected compounds, an initial screening can be done to remove incompetent thermodynamic models from consideration. If a thermodynamic model approaches the experimentally observed phase behaviour trends, it will be selected for further investigation. If the specific model has the option of incorporating additional parameters, determined from experimental high pressure data, it will in all likelihood perform even better with the inclusion of such parameters, and therefore further investigation is warranted.

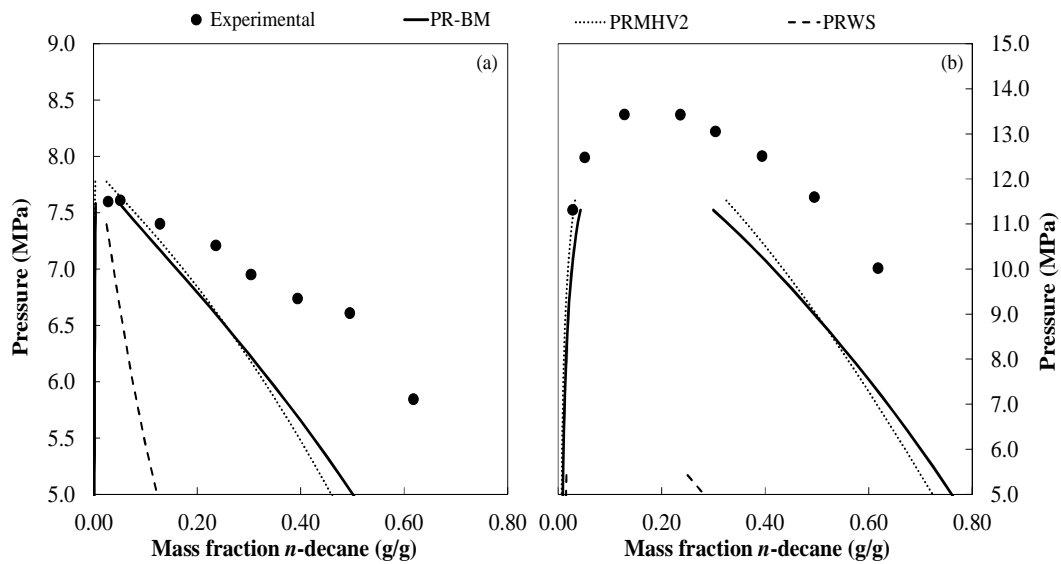


Figure 6-1 Comparison between experimental data and predicted data with the PR-BM, PRMHV2 and PR-WS models for $\text{CO}_2 + n$ -decane at (a) 308 K and (b) 348 K

6 | Thermodynamic Modelling of Mixtures at High Pressure
using Aspen Plus®

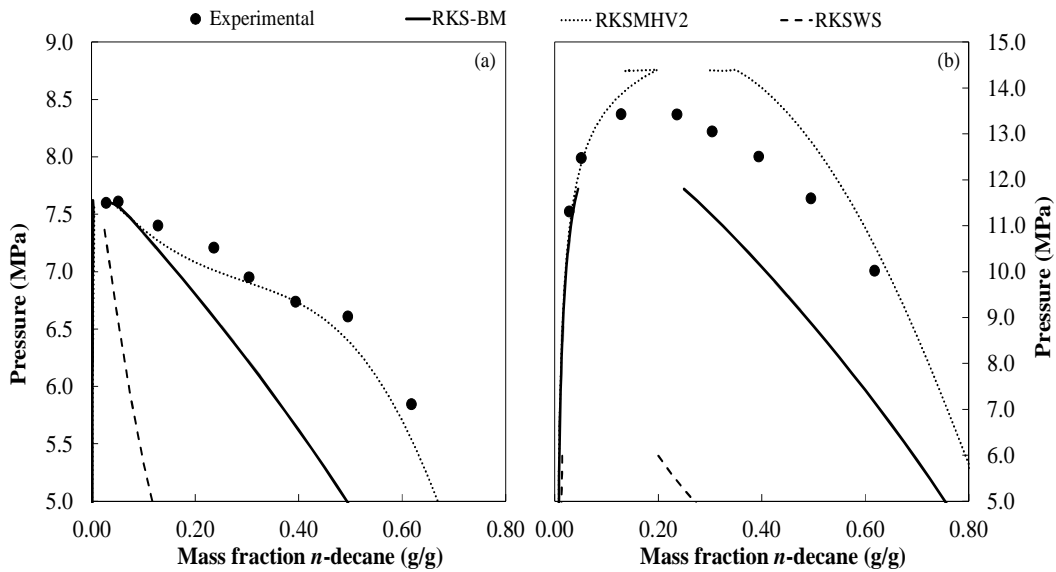


Figure 6-2 Comparison between experimental data and predicted data with the RKS-BM, RKSMHV2 and RKS-WS models for CO_2 + *n*-decane at (a) 308 K and (b) 348 K

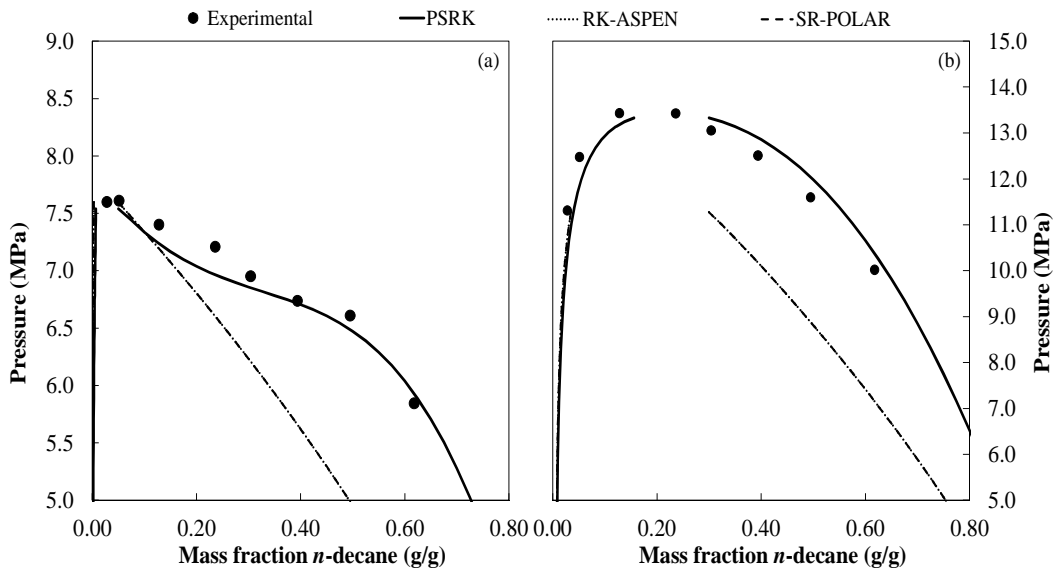


Figure 6-3 Comparison between experimental data and predicted data with the PSRK, RK-ASPEN and SR-POLAR models for CO_2 + *n*-decane at (a) 308 K and (b) 348 K

In Figure 6-1 to Figure 6-3 the predictive abilities of nine thermodynamic models are tested for mixtures of CO_2 and alkanes, by comparing it to experimentally measured data for the

6 | Thermodynamic Modelling of Mixtures at High Pressure using Aspen Plus®

CO₂ + *n*-decane system at 308 K and 348 K. Only two models approached the VLE trends at the low temperature of 308 K – the RKSMHV2 and PSRK models. Both these models also predicted VLE data at 348 K that approaches the experimental data, with the PSRK model giving slightly better results.

The RK-ASPEN and SR-POLAR models gave similar results that seem to assume the correct trend, but not the correct numerical values. Since both these models have the option of inclusion of additional experimentally determined parameters, their predictive abilities can be improved.

The nine thermodynamic models were also evaluated by comparing their predictive abilities for mixtures of CO₂ and alcohols, with the CO₂ + *l*-decanol mixture as the representative mixture. The results are shown in Figure 6-4 to Figure 6-6.

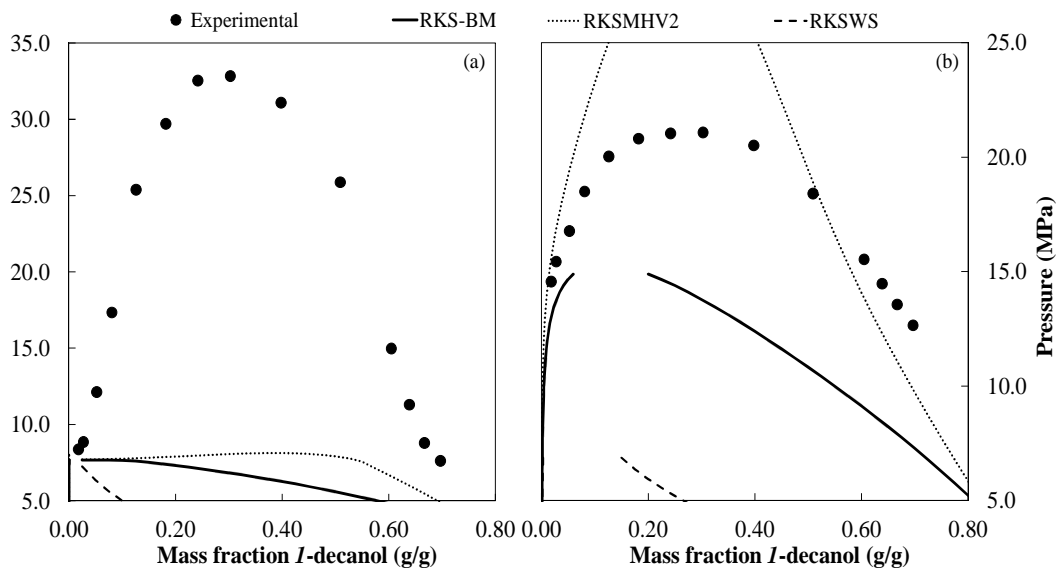


Figure 6-4 Comparison between experimental data and predicted data with the PR-BM, PRMHV2 and PR-WS models for CO₂ + *l*-decanol at (a) 308 K and (b) 348 K

6 | Thermodynamic Modelling of Mixtures at High Pressure
using Aspen Plus®

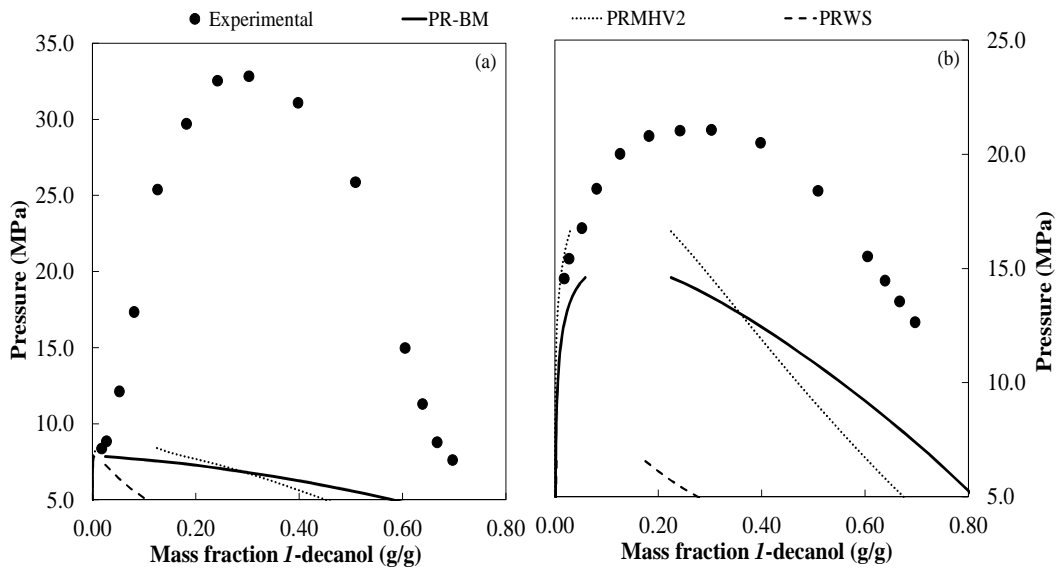


Figure 6-5 Comparison between experimental data and predicted data with the RKS-BM, RKSMHV2 and RKS-WS models for $\text{CO}_2 + 1\text{-decanol}$ at (a) 308 K and (b) 348 K

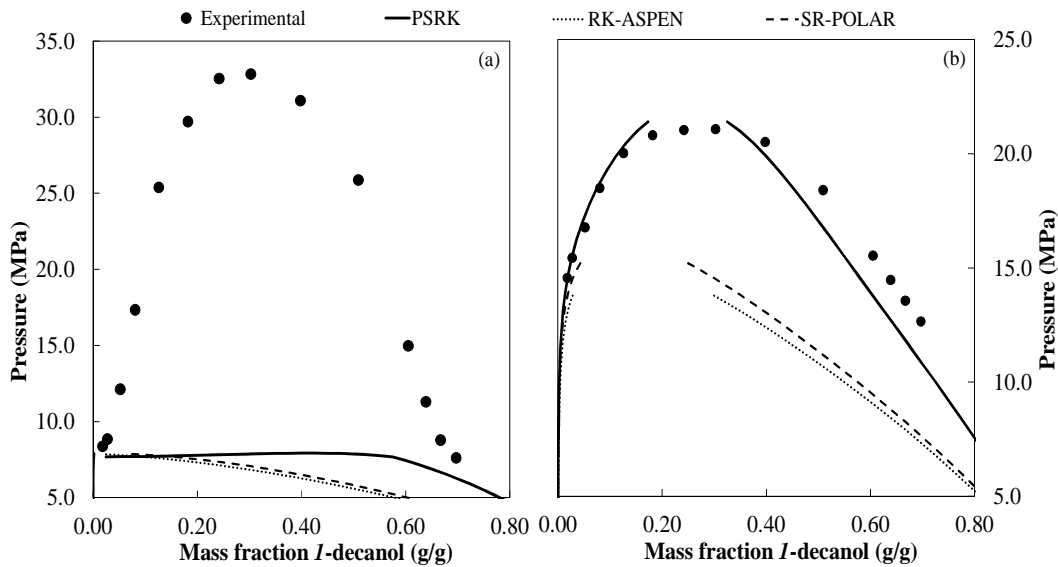


Figure 6-6 Comparison between experimental data and predicted data with the PSRK, RK-ASPEN and SR-POLAR models for $\text{CO}_2 + 1\text{-decanol}$ at (a) 308 K and (b) 348 K

6 | Thermodynamic Modelling of Mixtures at High Pressure using Aspen Plus®

The CO₂ + 1-decanol system displays a temperature inversion at temperatures below 338 K, which can clearly not be predicted by any of the thermodynamic models considered. However, very accurate VLE data were generated by the PSRK model at 348 K. The PR-BM, RKS-BM, RK-ASPEN and SR-POLAR models approached the experimental data in displaying similar trends, but did not reach the required phase transition pressure values. All four of these models have the option of incorporating interaction and/or pure component parameters that should in all likelihood lead to an increase in the accuracy of the predicted data.

The PSRK model cannot be employed further since the Aspen Plus® database does not contain any low-pressure UNIFAC parameters for the isomeric compounds used in this investigation. The model does however show a lot of promise and it is recommended that the UNIFAC parameters for these compounds be determined in future investigations. The PR-BM, RKS-BM, RK-ASPEN and SR-POLAR models will now be investigated further. In the remainder of this chapter the required additional parameters will be calculated and incorporated into the respective models. Their ability to represent binary VLE data and multi-component phase transition data with the inclusion of the calculated parameters will then be evaluated.

6.1.3 PR-BM

The PR-BM model (Table 6-1) is based on the standard Peng-Robinson EoS [3] and the Boston-Mathias extrapolation of the alpha function [5]. The alpha function involves the correlation of the pure component vapour pressure and was originally introduced by Soave in the Redlich-Kwong EoS [4]. Later it was also incorporated into the PR EoS. The Boston-Mathias extrapolation of the alpha function applies to those components that exist above their critical temperatures. For all components below their critical temperature the standard PR alpha function applies. Binary interaction parameters, k_{ij} and l_{ij} , can be included to increase the accuracy of the PR-BM property method [6]. For all the models investigated the interaction parameters can be made temperature dependant by including more parameters in the model.

6 | Thermodynamic Modelling of Mixtures at High Pressure
 using Aspen Plus®

Table 6-1 Equations used for the PR-BM property method

PR-BM	
$P = \frac{RT}{V_m - b} - \frac{a}{V_m(V_m + b) + b(V_m - b)}$	
Alpha Function	Mixing rules
$m_i = 0.37464 + 1.54226\omega_i - 0.26992\omega_i^2$ <p>For supercritical components:</p> $\alpha_i(T) = \left[\exp\left[c_i\left(1 - \frac{T}{T_{ri}}\right)\right] \right]^2$ $d_i = 1 + \frac{m_i}{2}$ $c_i = 1 - \frac{1}{d_i}$ <p>For subcritical components:</p> $\alpha_i(T) = \left[1 + m_i \left(1 - \frac{T}{T_{ri}} \right) \right]^2$	$a = \left[\sum_{i=1}^n \sum_{j=1}^n x_i x_j (a_i a_j)^{0.5} (1 - k_{ij}) \right] + \left[\sum_{i=1}^n x_i \left(\sum_{j=1}^n x_j ((a_i a_j)^{0.5} l_{ij})^{\frac{1}{3}} \right)^3 \right]$ $b = \sum_i x_i b_i$ $a_i = \alpha_i 0.45724 \frac{R^2 T_{ci}^2}{P_{ci}}$ $b_i = 0.07780 \frac{RT_{ci}}{P_{ci}}$ $k_{ij} = k_{ij}^{(1)} + k_{ij}^{(2)} T + \frac{k_{ij}^{(3)}}{T} \text{ with } k_{ij} = k_{ji}$ $l_{ij} = l_{ij}^{(1)} + l_{ij}^{(2)} T + \frac{l_{ij}^{(3)}}{T} \text{ with } l_{ij} \neq l_{ji}$
Input Parameters	
Pure Component	Mixture
ω, T_c, P_c	$k_{ij}^{(1)}, l_{ij}^{(1)}, k_{ij}^{(2)}, l_{ij}^{(2)}, k_{ij}^{(3)}, l_{ij}^{(3)}$

6.1.4 RKS-BM

The RKS-BM property method (Table 6-2) is based on the Redlich-Kwong EoS [7] with the alpha function introduced by Soave [4]. Similar to the PR-BM property method, the Boston-Mathias extrapolation of the alpha function is applied to those components that exist above their critical temperatures [5]. It is suggested that binary parameters, k_{ij} and l_{ij} , be included to increase the accuracy of the RKS-BM property method [6].

6 | Thermodynamic Modelling of Mixtures at High Pressure
 using Aspen Plus®

Table 6-2 Equations used for the RKS-BM property method

RKS-BM	
$P = \frac{RT}{V_m - b} - \frac{a}{V_m(V_m + b)}$	
Alpha Function	Mixing rules
$m_i = 0.48508 + 1.55171\omega_i - 0.15613\omega_i^2$ <p>For supercritical components:</p> $\alpha_i(T) = \left[\exp\left[c_i\left(1 - T_{ri}^{d_i}\right)\right] \right]^2$ $d_i = 1 + \frac{m_i}{2}$ $c_i = 1 - \frac{1}{d_i}$ <p>For subcritical components:</p> $\alpha_i(T) = \left[1 + m_i \left(1 - T_{ri}^{\frac{1}{2}} \right) \right]^2$	$a = \left[\sum_{i=1}^n \sum_{j=1}^n x_i x_j (a_i a_j)^{0.5} (1 - k_{ij}) \right] + \left[\sum_{i=1}^n x_i \left(\sum_{j=1}^n x_j ((a_i a_j)^{0.5} l_{ij})^{\frac{1}{3}} \right)^3 \right]$ $b = \sum_i x_i b_i$ $k_{ij} = k_{ij}^{(1)} + k_{ij}^{(2)}T + \frac{k_{ij}^{(3)}}{T} \text{ with } k_{ij} = k_{ji}$ $l_{ij} = l_{ij}^{(1)} + l_{ij}^{(2)}T + \frac{l_{ij}^{(3)}}{T} \text{ with } l_{ij} \neq l_{ji}$ $a_i = \alpha_i 0.42747 \frac{R^2 T_{ci}^2}{P_{ci}}$ $b_i = 0.08664 \frac{RT_{ci}}{P_{ci}}$
Input Parameters	
Pure Component	Mixture
ω, T_c, P_c	$k_{ij}^{(1)}, l_{ij}^{(1)}, k_{ij}^{(2)}, l_{ij}^{(2)}, k_{ij}^{(3)}, l_{ij}^{(3)}$

6.1.5 RK-ASPEN

The RK-ASPEN property method (Table 6-3) employs the Redlich-Kwong-Soave EoS [4,7] with the Mathias alpha function for subcritical components [8] and the Boston-Mathias extrapolation with a modified d_i parameter for the supercritical components [5]. The RK-ASPEN property method requires additional pure component polar parameters, η_i . The polar parameters can be regressed from pure component vapour pressure data. The inclusion of the polar parameters should significantly increase the accuracy of the RK-ASPEN model for polar compounds.

6 | Thermodynamic Modelling of Mixtures at High Pressure
 using Aspen Plus®

Table 6-3 Equations used for the RK-ASPEN property method

RK-ASPEN	
$P = \frac{RT}{V_m - b} - \frac{a}{V_m(V_m + b)}$	
Alpha Function	Mixing rules
$m_i = 0.48508 + 1.55171\omega_i - 0.15613\omega_i^2$ <p>For supercritical components:</p> $\alpha_i(T) = \left[\exp[c_i(1 - T_{ri}^{d_i})] \right]^2$ $d_i = 1 + \frac{m_i}{2} + 0.3\eta_i$ $c_i = 1 - \frac{1}{d_i}$ <p>For subcritical components:</p> $\alpha_i(T) = \left[1 + m_i \left(1 - T_{ri}^{\frac{1}{2}} \right) - \eta_i(1 - T_{ri})(0.7 - T_{ri}) \right]^2$	$a = \sum_{i=1}^n \sum_{j=1}^n x_i x_j (a_i a_j)^{0.5} (1 - k_{a,ij})$ $b = \sum_{i=1}^n \sum_{j=1}^n x_i x_j \frac{(b_i + b_j)}{2} (1 - k_{b,ij})$ $k_{a,ij} = k_{a,ij}^0 + k_{a,ij}^1 \frac{T}{1000}$ $k_{b,ij} = k_{b,ij}^0 + k_{b,ij}^1 \frac{T}{1000}$ $a_i = \alpha_i 0.42747 \frac{R^2 T_{ci}^2}{P_{ci}}$ $b_i = 0.08664 \frac{RT_{ci}}{P_{ci}}$
Input Parameters	
Pure Component	Mixture
ω, T_c, P_c, η	$k_{a,ij}^{(0)}, k_{b,ij}^{(0)}, k_{a,ij}^{(1)}, k_{b,ij}^{(1)}$

6.1.6 SR-POLAR

The SR-POLAR property method (Table 6-4) is an extension of the Redlich-Kwong-Soave EoS [4,7]. The extended Mathias alpha function is applied to subcritical components [9] and the Boston-Mathias extrapolation of the alpha function with a modified d_i parameter is applied to the supercritical components.

6 | Thermodynamic Modelling of Mixtures at High Pressure
 using Aspen Plus®

Table 6-4 Equations used for the SR-POLAR property method

SR-POLAR	
$P = \frac{RT}{V_m - b} - \frac{a}{V_m(V_m + b)}$	
Alpha Function	Mixing rules
$m_i = 0.48508 + 1.55171\omega_i - 0.15613\omega_i^2$ <p>For supercritical components:</p> $\alpha_i(T) = \left[\exp[c_i(1 - T_{ri}^d)] \right]^2$ $d_i = 1 + \frac{m_i}{2} - p_{1,i}(1 + p_{2,i} + p_{3,i})$ $c_i = 1 - \frac{1}{d_i}$ <p>For subcritical components:</p> $\alpha_i(T) = \left[1 + m_i \left(1 - T_{ri}^{\frac{1}{2}} \right) - p_{1,i}(1 - T_{ri})(1 + p_{2,i}T_{ri} + p_{3,i}T_{ri}^2) \right]^2$	$a = \sum_{i=1}^n \sum_{j=1}^n x_i x_j (a_i a_j)^{0.5} [1 - k_{a,ij} - l_{ij}(x_i - x_j)]$ $b = \sum_{i=1}^n \sum_{j=1}^n x_i x_j \frac{b_i + b_j}{2} (1 - k_{b,ij})$ $k_{a,ij} = k_{a,ij}^{(0)} + k_{a,ij}^{(1)}T + \frac{k_{a,ij}^{(2)}}{T} \text{ with } k_{a,ij} = k_{a,ji}$ $k_{b,ij} = k_{b,ij}^{(0)} + k_{b,ij}^{(1)}T + \frac{k_{b,ij}^{(2)}}{T} \text{ with } k_{b,ij} = k_{b,ji}$ $l_{ij} = l_{ij}^{(0)} + l_{ij}^{(1)}T + \frac{l_{ij}^{(2)}}{T} \text{ with } l_{ij} = -l_{ji}$ $a_i = \alpha_i 0.42747 \frac{R^2 T_{ci}^2}{P_{ci}}$ $b_i = 0.08664 \frac{RT_{ci}}{P_{ci}}$
Input Parameters	
Pure Component	Mixture
$\omega, T_c, P_c, p_1, p_2, p_3$	$k_{a,ij}^{(0)}, k_{b,ij}^{(0)}, k_{a,ij}^{(1)}, l_{ij}^{(0)}, l_{ij}^{(1)}, l_{ij}^{(2)}$ $k_{b,ij}^{(1)}, k_{a,ij}^{(2)}, k_{b,ij}^{(2)}$

The polar parameters required in the SR-POLAR model can be regressed from pure component vapour pressure data. The SR-POLAR property method has two more polar parameters than the RK-ASPEN property method. The additional parameters may increase the accuracy of the property method, but decreases its robustness. Binary interaction parameters, $k_{a,ij}^{(0)}$ and $l_{ij}^{(0)}$ are usually sufficient to represent VLE data [6]. If the binary interaction parameters are made temperature dependant, only two parameters are needed, but the general form of the interaction parameters allows a choice to be made in whether linear temperature dependence in T or $1/T$ is required. Generally, a linear dependence in T is sufficient for vapour-liquid equilibrium data [9].

6.2 Pure Component Parameters

Pure component critical properties, acentric factors and polar parameters are required to calculate VLE data with the thermodynamic models discussed in Table 6-1 to Table 6-4. The values of these properties are used in the calculation of the energy parameter, a , and the co-volume parameter, b .

The Aspen Plus® simulation software program includes a rather large database of pure component properties. If the property required is not available for the compound of interest, predictive functions (e.g. the built-in NIST Thermo Data Engine (TDE)) can be used to determine such properties. Numerous researchers have also developed estimation techniques for some of the pure component properties. The most popular estimation techniques for pure component critical properties, acentric factors and vapour pressures are reported by Poling et al. [10].

The pure component properties of certain components are very difficult to measure and consequently varying values for such properties are often published (see Table 6-5 and Table 6-6). The values of the pure component properties used in the thermodynamic model can have an effect on the accuracy of the data generated.

6.2.1 Pure Component Critical Properties

Values of the pure component critical properties can be found in databases or can be calculated with estimation techniques. For some of the compounds used in this investigation, especially for the lesser known C₁₀-alcohol isomers, very little data are available, and often the data published show some disagreement.

In Table 6-5 the values of the critical temperature and pressure are given for the compounds used in this investigation as obtained from three reliable databases [6,11,12].

6 | Thermodynamic Modelling of Mixtures at High Pressure using Aspen Plus®

Table 6-5 Comparison between the pure component critical properties as given by Aspen Plus® [6], Yaws [12] and DIPPR [11]

Component	T_c (K)			P_c (MPa)		
	Aspen Plus® [6]	Yaws [12]	DIPPR [11]	Aspen Plus® [6]	Yaws [12]	DIPPR [11]
<i>n</i> -decane	617.7	617.7	617.7	2.11	2.11	2.11
<i>n</i> -dodecane	658.0	658.0	658.0	1.82	1.82	1.82
<i>1</i> -decanol	688.0	687.3	688.0	2.31	2.32	2.31
<i>2</i> -decanol	668.5	673.2	-	2.31	2.36	-
<i>3,7</i> -dimethyl- <i>1</i> -octanol	667.0	638.5	-	2.34	2.33	-
<i>2,6</i> -dimethyl- <i>2</i> -octanol	645.0	644.4	-	2.33	2.36	-
<i>3,7</i> -dimethyl- <i>3</i> -octanol	657.0	623.3	-	2.42	2.36	-
CO ₂	304.2	304.2	304.2	7.38	7.38	7.38

There is no way to verify the values reported for the critical properties of these components, since each source claims that their values are accurate. It was decided to use the values obtained from the built-in Aspen Plus® database, since it agrees well with that published in the other databases.

6.2.2 Acentric Factors

Pure component acentric factors are much harder to come by compared to critical properties. In Table 6-6 the acentric factors are given for the compounds of interest, as obtained from the databases of Aspen Plus® [6] and Yaws [12], and reported by DIPPR [11].

As for the pure component critical constants discussed in section 6.2.1, large discrepancies are observed between the values of the acentric factor obtained by different sources. To allow for consistency throughout all the calculations, the values obtained from the Aspen Plus® database for the acentric factors were used in the calculations presented in this chapter. The values found in the Aspen Plus® database also agreed well with those found in the DIPPR database for limited components.

6 | Thermodynamic Modelling of Mixtures at High Pressure using Aspen Plus®

Table 6-6 Comparison between the pure component acentric factors as given by Aspen Plus® [6], Yaws [12] and DIPPR [11]

Component	ω		
	Yaws [12]	Aspen Plus® [6]	DIPPR [11]
<i>n</i> -decane	0.492	0.492	0.492
<i>n</i> -dodecane	0.576	0.576	0.576
1-decanol	0.622	0.607	0.607
2-decanol	0.575	0.643	-
3,7-dimethyl-1-octanol	0.852	0.732	-
2,6-dimethyl-2-octanol	0.788	0.591	-
3,7-dimethyl-3-octanol	0.788	0.468	-
CO ₂	0.228	0.224	0.224

6.2.3 Vapour Pressure Data

Pure component vapour pressure data are required to determine the pure component polar parameters. Since the mixtures considered in this work are at temperatures higher than the critical temperature of CO₂, no polar parameters, and consequently no vapour pressure data, are required. Vapour pressure data are often presented as a set of Antoine parameters applicable within a certain temperature range. Due to a lack of available data, it is often necessary to extrapolate vapour pressure data to temperatures outside of the recommended temperature range.

Vapour pressure data for the components used in this investigation was gathered from the Aspen Plus® database [6] and the NIST database [13]. Aspen Plus® has a number of calculation routes that it uses to determine pure component vapour pressures. If Antoine constants are available for a component, it utilizes the extended Antoine equation (see Equation 6-1) to calculate the vapour pressure [6]. For temperatures outside of the bounds set by C_{8i} and C_{9i} , extrapolation of P_i^* versus $1/T$ occurs.

$$\ln P_i^* = C_{1,i} + \frac{C_{2,i}}{T+C_{3,i}} + C_{4,i}T + C_{5,i} \ln T + C_{6,i}T^{C_{7,i}} \quad C_{8,i} \leq T \leq C_{9,i} \quad \text{Eq.6-1}$$

6 | Thermodynamic Modelling of Mixtures at High Pressure using Aspen Plus®

For components that have no documented Antoine constants, Aspen Plus® proposes the use of the Wagner 25 liquid vapour pressure equation (Equation 6-2) to estimate the vapour pressures [6]. Linear extrapolation of P_i^* versus T occurs outside the temperature limits.

$$\ln P_i^* = \ln P_{Ci} + \frac{(C_{1i}(1-T_{ri}) + C_{2i}(1-T_{ri})^{15} + C_{3i}(1-T_{ri})^{25} + C_{4i}(1-T_{ri})^5)}{T_{ri}} \quad C_{5i} \leq T \leq C_{6i} \quad \text{Eq.6-2}$$

Table 6-7 contain the values of the constants to be used in the extended Antoine equation (components indicated with ⁺) and Wagner 25 liquid vapour pressure equation to calculate the vapour pressures of the components used in this study. The constants were obtained from the Aspen Plus® database [6]. The vapour pressure is to be calculated in MPa and the temperatures are given in K.

Table 6-7 Constants obtained from Aspen Plus® [6] database for use in the extended Antoine equation and Wagner 25 liquid vapour pressure equation

Component	C_1	C_2	C_3	C_4	C_5	C_6	C_7	C_8	C_9
<i>n</i> -decane ⁺	98.91	-9749.60	0	0	-13.25	7.1e-6	2.00	243.51	617.70
<i>n</i> -dodecane ⁺	123.65	-11976.00	0	0	-16.70	8.1e-6	2.00	263.57	658.00
<i>l</i> -decanol ⁺	142.42	-15212.00	0	0	-18.42	8.5e-18	6.00	280.05	688.00
2-decanol	-8.29	0.14	-3.12	-12.24	270.80	668.50	-	-	-
3,7-dimethyl- <i>l</i> -octanol	-8.40	-1.39	-0.36	-10.92	210.00	667.00	-	-	-
2,6-dimethyl-2-octanol	-9.21	2.89	-5.37	-4.32	200.00	645.00	-	-	-
3,7-dimethyl-3-octanol	-8.47	2.35	-4.07	-3.85	200.00	657.00	-	-	-

In Table 6-8 the constants for use in the basic Antoine equation (Equation 6-3) as reported in the NIST database [13], are shown for the compounds of interest. The vapour pressure is to be calculated in bar and the temperatures are given in K.

$$\log_{10} P_i^* = C_{1,i} - \left(\frac{C_{2,i}}{T + C_{3,i}} \right) \quad C_{4i} \leq T \leq C_{5i} \quad \text{Eq.6-3}$$

6 | Thermodynamic Modelling of Mixtures at High Pressure using Aspen Plus®

The constants reported in the Aspen Plus® database for use in Equation 6-1 and 6-2 are all applicable in the temperature range 308 – 348 K. However, the constants published in the NIST database [13] for use in Equation 6-3 are not all applicable within the temperature range of interest. For the compounds reported in Table 6-8, not enough vapour pressure data could be generated within the temperature range of interest, and thus the data provided by the Aspen Plus® database [6] was used in the calculations presented in this chapter.

Table 6-8 Constants obtained from the NIST database [13] for use in the extended Antoine equation and NIST Wagner 25 liquid vapour pressure equation

Component	C_1	C_2	C_3	C_4	C_5
<i>n</i> -decane	0.21021	440.616	-156.896	243.39	310.59
	4.07857	1501.268	-78.67	367.63	448.27
<i>n</i> -dodecane	4.10549	1625.928	-92.839	399.53	490.49
<i>l</i> -decanol	4.53321	1742.392	-115.236	349.37	406.18
	3.85752	1373.019	-147.727	400.41	528.32
	3.51869	1180.306	-168.829	378.00	504.00
3,7-dimethyl- <i>l</i> -octanol	7.70489	3535.48	-7.093	341.00	366.70

6.2.4 Polar Parameters

The pure component polar parameters are not listed in the Aspen Plus® database, but can be regressed from pure component vapour pressure data. Pure component vapour pressure data was generated in Aspen Plus® (as discussed in section 6.2.3) and the built-in data regression function was used to determine the polar parameters required in the RK-ASPEN and SR-POLAR models, respectively.

The Britt-Luecke algorithm was implemented to perform a maximum-likelihood estimation of the minimization of the error between the generated and regressed data. This is the standard regression method employed in the Aspen Plus® data regression function. The quality of the regressed data was evaluated by using the average absolute deviation (AAD) between the measured and calculated values (Equation 6-4).

6 | Thermodynamic Modelling of Mixtures at High Pressure using Aspen Plus®

$$\%AAD = \frac{1}{K} \sum_{n=1}^K \left| \frac{Z_n - ZM_n}{ZM_n} \right| \times 100 \quad \text{Eq. 6-4}$$

6.2.4.1 RK-ASPEN Polar Parameters

RK-ASPEN polar parameters, as regressed from the pure component vapour pressures, are given in Table 6-9.

The %AAD reported in Table 6-9 show the fit of the regressed data to the vapour pressure data generated using the extended Antoine (Equation 6-1) and Wagner 25 liquid vapour pressure (Equation 6-2) equations, for the components of interest. Regression was done on generated vapour pressure data within the temperature range 300 – 360 K.

Table 6-9 RK-ASPEN polar parameters

Component	η_i	%AAD _T	%AAD _P
<i>n</i> -decane	0.0253	0.18	0.02
<i>n</i> -dodecane	0.0096	0.39	0.03
<i>1</i> -decanol	-0.4196	0.33	0.02
<i>2</i> -decanol	-0.0750	0.17	0.01
<i>3,7</i> -dimethyl- <i>1</i> -octanol	0.0924	0.63	0.04
<i>2,6</i> -dimethyl- <i>2</i> -octanol	0.0214	0.27	0.02
<i>3,7</i> -dimethyl- <i>3</i> -octanol	0.0145	0.25	0.02

All the polar parameters shown in Table 6-9 are of similar magnitude, except the *1*-decanol polar parameter. The large negative value of the polar parameter of *1*-decanol is not uncommon, as this trend was previously observed for higher alcohols [8].

It is expected that the value of the polar parameter will be zero for non-polar compounds, but Mathias [8] clearly states that the polar factor is a highly empirical parameter that cannot be correlated in terms of pure component properties like dipole moments. The value of the polar parameter is the lumped result of different effects, including the inadequacy of the RKS EoS.

6 | Thermodynamic Modelling of Mixtures at High Pressure using Aspen Plus®

6.2.4.2 SR-POLAR Polar Parameters

The polar parameters used in the SR-POLAR property method were also regressed from the vapour pressure data generated with the correlations used in Aspen Plus®. Only one polar parameter, $p_{1,i}$, was regressed to allow an equal comparison to the RK-ASPEN property method. The values of $p_{2,i}$ and $p_{3,i}$ were kept at zero. Values for the polar parameters and %AAD are given in Table 6-10 for the compounds of interest.

Table 6-10 SR-POLAR polar parameters

Component	$p_{1,i}$	%AAD _T	%AAD _P
<i>n</i> -decane	0.0043	0.04	0.01
<i>n</i> -dodecane	0.0021	0.34	0.02
1-decanol	-0.5340	0.41	0.02
2-decanol	-0.0154	0.64	0.04
3,7-dimethyl-1-octanol	0.0193	0.13	0.01
2,6-dimethyl-2-octanol	0.0042	0.14	0.01
3,7-dimethyl-3-octanol	0.0030	0.16	0.01

Although not explicitly stated by Schwartzenruber and Renon [9], it is assumed that the same characteristics as those mentioned for the polar parameter employed in the RK-ASPEN model, holds true for the polar parameters employed in the SR-POLAR model, i.e. it cannot be correlated to any pure component property, since it is a value that represents a number of combined effects.

6.3 Binary Solute-Solvent Interaction Parameters

The measured binary phase equilibrium data presented in Chapter 5 were used to determine binary interaction parameters between CO₂ and each of the solutes. The ability of the PR-BM, RKS-BM, RK-ASPEN and SR-POLAR models to fit the binary VLE data with the inclusion of regressed binary interaction parameters is evaluated in this section. The Aspen Plus® data regression function was utilized to fit the VLE data predicted by the respective thermodynamic models to the experimentally measured data. Once again the Britt-Luecke algorithm was implemented to perform a maximum-likelihood estimation of the minimization of the error between the experimental and

6 | Thermodynamic Modelling of Mixtures at High Pressure using Aspen Plus®

regressed data. The quality of the regressed data was evaluated by using the average absolute deviation (AAD) between the measured and calculated values (Equation 6-3) for different parameters.

6.3.1. Factors that Require Special Attention

A number of important factors were identified while attempting to fit the thermodynamic models to the experimental VLE data.

- Only vapour-liquid equilibrium data can be used as input data for a regression case in Aspen Plus®. The data measured in Chapter 5 were presented as bubble and dew point data. The conversion from bubble and dew point data to VLE data is relatively simple for binary mixtures. At a certain pressure the composition of the co-existing phases is required, i.e. the compositions of the dew point and the bubble point that occur at the same pressure on the phase transition curve. The VLE data were determined manually from the phase transition curves and are given in Appendix C.
- The method of converting bubble and dew point data to VLE data allowed an unlimited amount of data points to be generated from a line. The number of VLE data points entered for a regression case affects the closeness of fit of the thermodynamic model. If a larger number of data points are entered, a better fit of the thermodynamic model can be expected. However, if too many data points are entered the difference between subsequent temperature, pressure and/or composition values of the data points become smaller than the possible error introduced by the thermodynamic model. After some trial-and-error runs with the data regression function in Aspen Plus® it was decided to generate VLE data points in increments of 0.2 MPa for all binary mixtures (see Appendix C).
- The solution algorithm employed in the regression function, was unable to fit the thermodynamic model to a point where the liquid and vapour phases had the same composition. Data points that caused a problem with convergence in the parameter fitting procedure were removed from the experimental data sets. These were usually the data points at the highest pressures. No critical points were included in the parameter fitting procedure. Difficulties with regression in the mixture critical region is common and have been reported by other researchers [14,15].

6 | Thermodynamic Modelling of Mixtures at High Pressure using Aspen Plus®

- Some of the binary mixtures that were investigated displayed very flat solubility curves. It is very difficult to accurately convert bubble and dew point data to VLE data for very flat curves, and consequently very little data at limited temperatures (usually only at 338 K and 348 K) could be generated for these mixtures (e.g. CO₂ + 3,7-dimethyl-3-octanol and CO₂ + *n*-dodecane).
- Most thermodynamic models struggle to predict data close to the critical temperature of the solvent (i.e. 304.2 K), due to the complexity of the phase behaviour at such temperatures (see section 6.1.2). Other researchers have also reported difficulties in regression procedures for binary VLE data at temperatures close to the critical temperature of the solvent [15]. The low temperature region was thus excluded from the regression cases and only the temperature range 338 – 348 K was considered. Once the binary interaction parameters were determined, it was used to predict the VLE data at temperatures outside the range 338 – 348 K (see section 6.3.2).
- The four models considered in this section, the PR-BM, RKS-BM, RK-ASPEN and SR-POLAR models, all have the option to include temperature dependent interaction parameters to improve the fit of the model at different temperatures. However, the use of a single temperature independent interaction parameter is preferred since it allows the thermodynamic model to retain its predictive qualities, rather than just fitting the experimental data set [15]. In this work the thermodynamic models were fitted to the measured binary data using two temperature independent interaction parameters. Although this might not result in the best possible fit of the model to the data, the model will still retain its fundamental characteristics.

6.3.2 Determining Binary Solute-Solvent Interaction Parameters

6.3.2.1 PR-BM

High pressure binary VLE data at 338 K and 348 K for each of the solutes listed in Table 6-11 with supercritical CO₂ was used as input data for the regression case (see Appendix C). The %AAD calculated at each temperature was averaged and are also reported in Table 6-11.

6 | Thermodynamic Modelling of Mixtures at High Pressure
using Aspen Plus®

Table 6-11 Regressed binary interaction parameters for the PR-BM property method

Mixture CO ₂ + ...	k_{ij}	l_{ij}	%AAD _T	%AAD _P	%AAD _x	%AAD _y
<i>n</i> -decane	0.0008	-0.1334	1.54	0.83	0.23	9.06
<i>n</i> -dodecane	-0.0671	-0.2379	1.22	0.58	0.19	6.50
<i>1</i> -decanol	0.1042	0.0133	2.89	2.24	0.89	22.80
<i>2</i> -decanol	0.0833	0.0169	1.32	0.71	0.20	7.85
<i>3,7</i> -dimethyl- <i>1</i> -octanol	0.0807	0.0168	0.95	0.60	0.23	11.99
<i>2,6</i> -dimethyl- <i>2</i> -octanol	0.0306	-0.0436	1.19	0.80	0.16	13.21
<i>3,7</i> -dimethyl- <i>3</i> -octanol	-0.0166	-0.1219	1.34	0.92	0.17	12.34

In Figure 6-7 the experimental binary VLE data are shown alongside the VLE data generated with the PR-BM model employing two binary temperature independent interaction parameters, k_{ij} and l_{ij} .

From the %AAD values in Table 6-11 and the plots in Figure 6-7 it can be deduced that the PR-BM property method fit the binary VLE data well, with the exception of the CO₂ + *1*-decanol system. The shape of the phase transition curve of the CO₂ + *1*-decanol system is slightly misrepresented, especially as the mixture critical point is approached. Since the PR-BM model does not include a polar parameter, poor representation of mixtures containing polar compounds is expected.

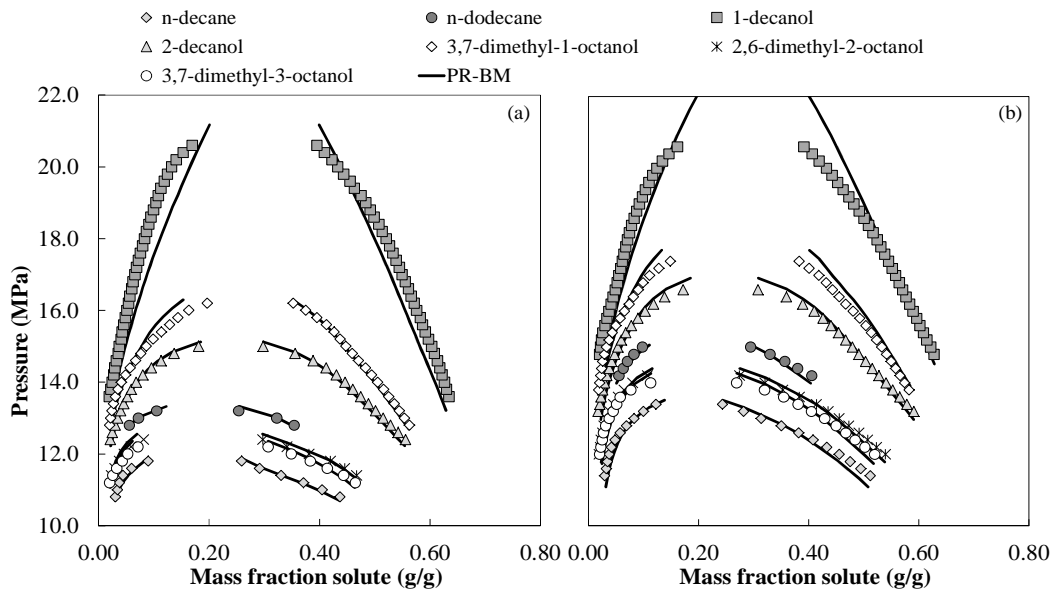
6 | Thermodynamic Modelling of Mixtures at High Pressure
 using Aspen Plus®


Figure 6-7 PR-BM property model fit to binary VLE data at (a) 338 K and (b) 348 K

6.3.2.2 RKS-BM

The RKS-BM model (Table 6-2) was employed in the regression case and values for the two interaction parameters, k_{ij} and l_{ij} , for each of the binary solvent-solute pairs were determined. These values along with the %AAD of the temperature, pressure and phase compositions are given in Table 6-12.

Table 6-12 Regressed binary interaction parameters for the RKS-BM property method

Mixture CO ₂ + ...	k_{ij}	l_{ij}	%AAD _T	%AAD _P	%AAD _x	%AAD _y
<i>n</i> -decane	0.0975	-0.0008	0.52	0.64	0.07	15.16
<i>n</i> -dodecane	0.1004	-0.0018	0.93	0.66	0.08	17.43
<i>l</i> -decanol	0.1106	-0.0038	2.08	1.75	0.69	12.05
<i>2</i> -decanol	0.0814	0.00002	1.49	0.74	0.27	8.87
<i>3,7</i> -dimethyl- <i>l</i> -octanol	0.0735	0.0022	1.08	0.56	0.24	5.26
<i>2,6</i> -dimethyl- <i>2</i> -octanol	0.0655	-0.0001	0.90	0.66	0.15	12.08
<i>3,7</i> -dimethyl- <i>3</i> -octanol	0.0672	-0.0004	0.69	0.64	0.11	16.56

6 | Thermodynamic Modelling of Mixtures at High Pressure using Aspen Plus®

In Figure 6-8 the fit of the RKS-BM model is depicted at 338 K and 348 K. It is clear that the largest deviations occurred for the mixtures containing the more polar compounds (1-decanol, 2-decanol and 3,7-dimethyl-1-octanol), especially near the mixture critical points.

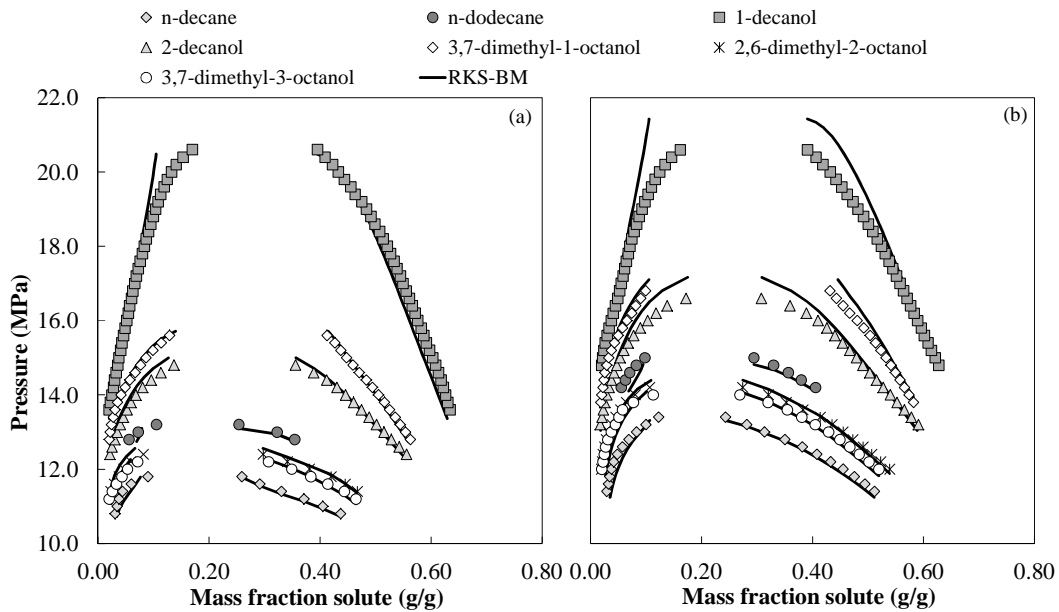


Figure 6-8 RKS-BM property model fit to binary VLE data at (a) 338 K and (b) 348 K

6.3.2.3 RK-ASPEN

The RK-ASPEN property method (Table 6-3) differs in one major aspect from the RKS-BM property method – it contains a corrective term for polar compounds. It is thus expected that the RK-ASPEN property method will fit the VLE data of the mixtures containing the polar compounds better. The polar parameters determined from the pure component vapour pressure data were fixed at their respective regressed values (given in Table 6-9), while the values of the two binary interaction parameters, $k_{a,ij}$ and $k_{b,ij}$, were determined. The binary interaction parameters determined for each binary pair are given in Table 6-13.

6 | Thermodynamic Modelling of Mixtures at High Pressure
using Aspen Plus®

Table 6-13 Regressed binary interaction parameters for the RK-ASPEN property method

Mixture CO ₂ + ...	$k_{a,ij}$	$k_{b,ij}$	%AAD _T	%AAD _P	%AAD _x	%AAD _y
<i>n</i> -decane	0.0957	0.0286	1.01	0.52	0.14	5.96
<i>n</i> -dodecane	0.0899	0.0487	0.80	0.34	0.13	6.10
1-decanol	0.0850	-0.0305	1.87	1.64	0.68	11.29
2-decanol	0.0628	-0.0128	0.96	0.48	0.17	6.55
3,7-dimethyl-1-octanol	0.0774	-0.0140	0.84	0.51	0.20	10.60
2,6-dimethyl-2-octanol	0.0655	-0.0034	0.83	0.60	0.14	12.59
3,7-dimethyl-3-octanol	0.0669	0.0223	0.89	0.70	0.14	12.26

The RK-ASPEN property method represents the shape of the phase transition curves for the mixtures containing polar compounds better, compared to the PR-BM and RKS-BM property methods (see Figure 6-9).

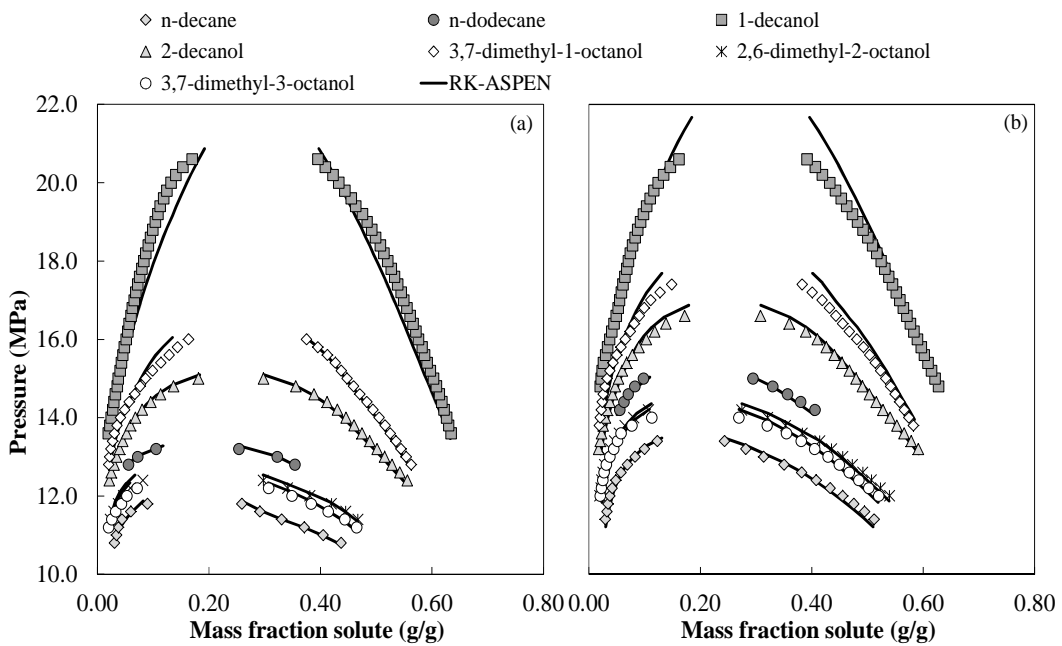


Figure 6-9 RK-ASPEN property model fit to binary VLE data at (a) 338 K and (b) 348 K

6 | Thermodynamic Modelling of Mixtures at High Pressure using Aspen Plus®

There is still some deviation around the mixture critical point between the measured VLE data and the RK-ASPEN model estimation, but the deviation is significantly smaller than those obtained with the PR-BM and RKS-BM property methods due to the inclusion of the polar parameters.

6.3.2.4 SR-POLAR

The SR-POLAR model (Table 6-4) is very similar to the RK-ASPEN model, since it also contains a regressed pure component polar parameter (given in Table 6-10). Binary interaction parameters, $k_{a,ij}^{(0)}$ and $k_{b,ij}^{(0)}$, were determined for each binary mixture, and are given in Table 6-14.

Table 6-14 Regressed binary interaction parameters for the SR-POLAR property method

Mixture CO ₂ + ...	$k_{a,ij}^{(0)}$	$k_{b,ij}^{(0)}$	%AAD _T	%AAD _P	%AAD _x	%AAD _y
<i>n</i> -decane	0.0958	0.0290	1.01	0.52	0.14	5.99
<i>n</i> -dodecane	0.0900	0.0489	0.81	0.34	0.13	6.11
<i>l</i> -decanol	0.0072	-0.0891	6.68	3.72	0.39	42.19
<i>2</i> -decanol	0.0757	-0.0261	0.99	0.49	0.18	6.64
<i>3,7</i> -dimethyl- <i>l</i> -octanol	0.0773	-0.0167	0.86	0.58	0.18	12.59
<i>2,6</i> -dimethyl- <i>2</i> -octanol	0.0656	-0.0030	0.83	0.60	0.14	14.01
<i>3,7</i> -dimethyl- <i>3</i> -octanol	0.0670	0.0226	0.90	0.70	0.14	12.26

The %AAD for the temperature, pressure and phase compositions are similar to those generated with the RK-ASPEN property method for all binary mixtures, except CO₂ + *l*-decanol. The SR-POLAR property method struggles to predict the dew curve compositions for the CO₂ + *l*-decanol mixture (see Figure 6-10). Although the SR-POLAR model was modified to account for polar compounds, it seems as if there are certain interactions between the highly polar *l*-decanol molecules that cannot be represented accurately.

6 | Thermodynamic Modelling of Mixtures at High Pressure using Aspen Plus®

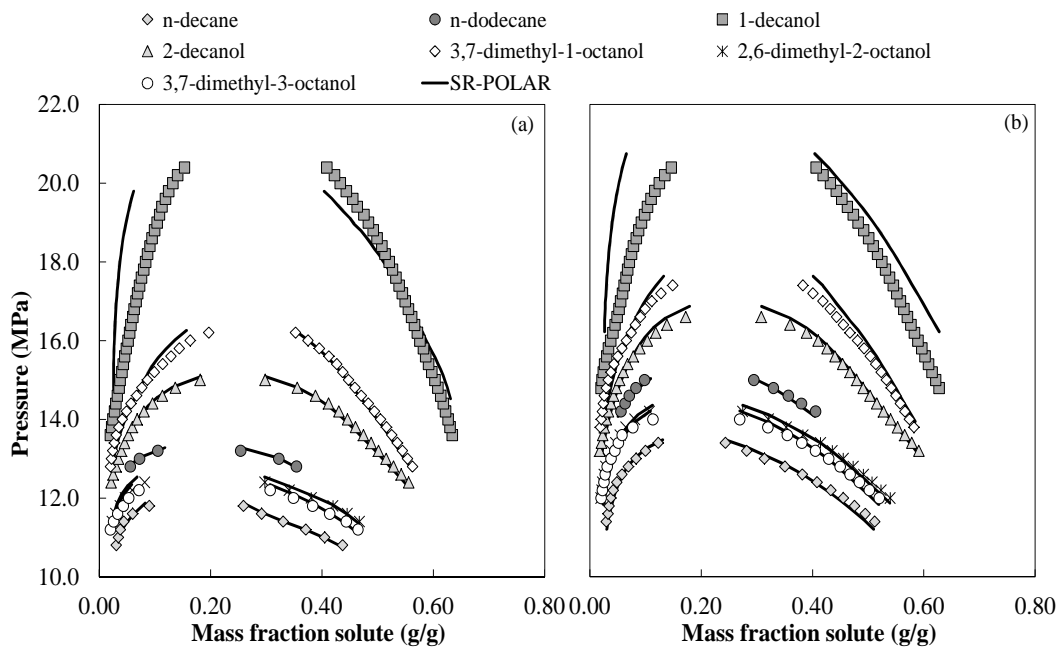


Figure 6-10 SR-POLAR property model fit to binary VLE data at (a) 338 K and (b) 348 K

6.3.3 Predictive Capability at Low Temperatures

During regression of the binary solute-solvent interaction parameters from experimentally measured data, some difficulties were experienced at temperatures that approach the critical temperature of the solvent. It was decided to exclude the low temperature region from the regression case, and only use data at 338 K and 348 K to determine the temperature independent binary interaction parameters for each solute-solvent pair. In this section the applicability of the calculated binary interaction parameters in lower temperature ranges (318 – 328 K) will be evaluated. A robust thermodynamic model should be able to predict good VLE data at temperatures that extend marginally outside the range in which the interaction parameters were determined.

6.3.3.1 PR-BM

In Figure 6-11 to Figure 6-13 the VLE data as predicted with the PR-BM model with the inclusion of the regressed interaction parameters (Table 6-11), are shown at 318 K and 328 K for the binary mixtures considered in this investigation. VLE trends and values of acceptable accuracy were

6 | Thermodynamic Modelling of Mixtures at High Pressure using Aspen Plus®

predicted for the $\text{CO}_2 + n\text{-decane}$ and $\text{CO}_2 + n\text{-dodecane}$ systems, as well as for $\text{CO}_2 + 2,6\text{-dimethyl-2-octanol}$ and $\text{CO}_2 + 3,7\text{-dimethyl-3-octanol}$ systems. However, the extrapolated VLE data for the $\text{CO}_2 + 1\text{-decanol}$, $\text{CO}_2 + 2\text{-decanol}$ and $\text{CO}_2 + 3,7\text{-dimethyl-1-octanol}$ systems were poor, especially at 318 K, due to the polarity of these solutes. The accuracy of the predicted data diminishes as the temperature decreases, due to the approach of the complex near-critical region of the solvent and the extrapolation from the validity range of the binary interaction parameters.

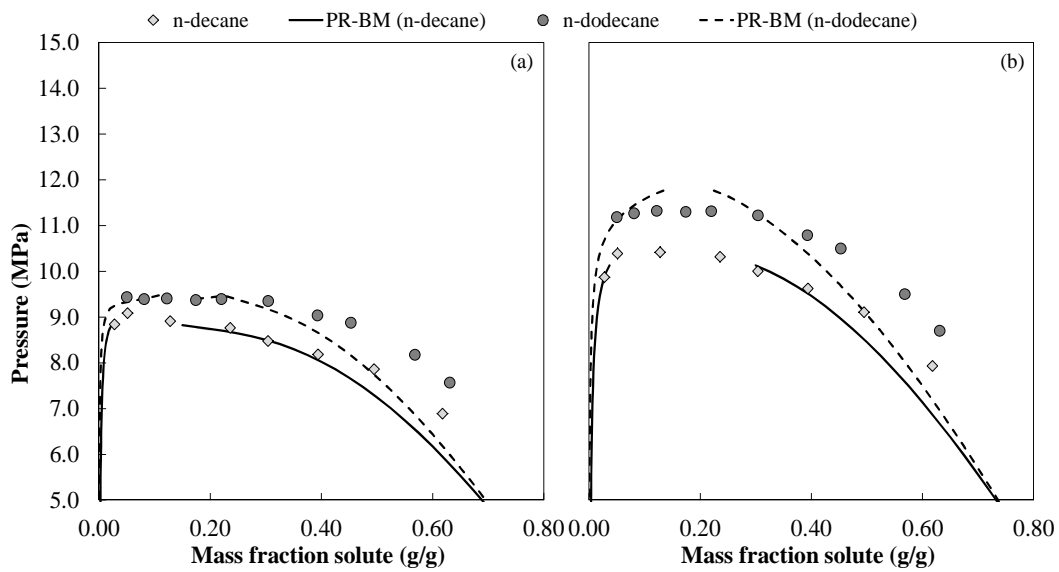


Figure 6-11 VLE prediction with PR-BM (including interaction parameters) for $\text{CO}_2 + n\text{-decane}$ and $\text{CO}_2 + n\text{-dodecane}$ at (a) 318 K and (b) 328 K

6 | Thermodynamic Modelling of Mixtures at High Pressure
using Aspen Plus®

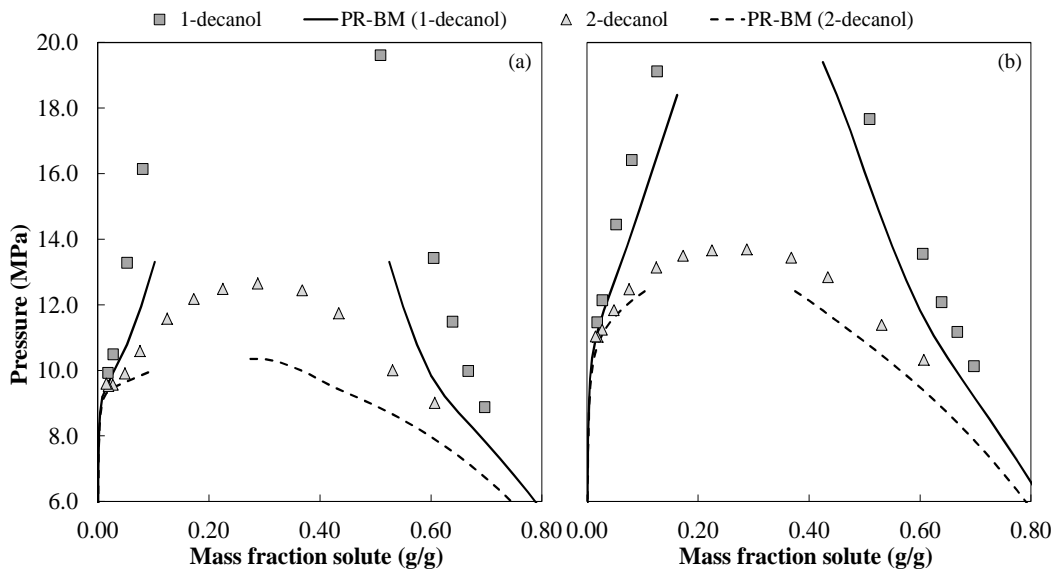


Figure 6-12 VLE prediction with PR-BM (including interaction parameters) for CO_2 +1-decanol and CO_2 +2-decanol at (a) 318 K and (b) 328 K

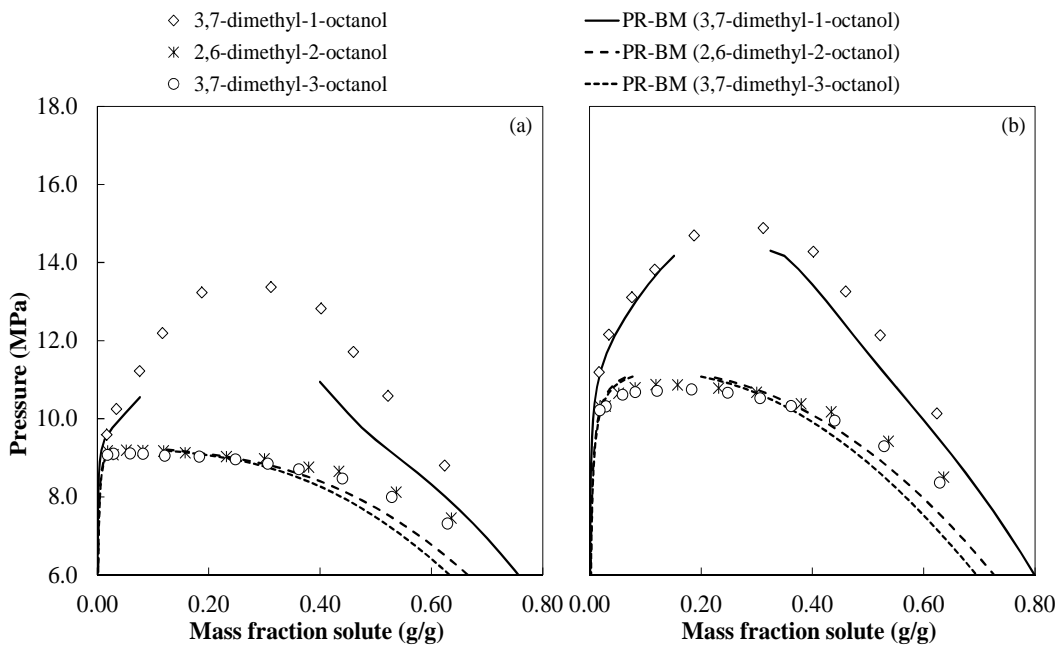


Figure 6-13 VLE prediction with PR-BM (including interaction parameters) for CO_2 +3,7-dimethyl-1-octanol, CO_2 +2,6-dimethyl-2-octanol and CO_2 +3,7-dimethyl-3-octanol at (a) 318 K and (b) 328 K

6 | Thermodynamic Modelling of Mixtures at High Pressure using Aspen Plus®

6.3.3.2 RKS-BM

In Figure 6-14 to Figure 6-16 the VLE data as predicted by the RKS-BM model with the inclusion of the regressed binary interaction parameters (given in Table 6-12) are shown for all the binary systems investigated at temperatures lower than the temperature range used in the regression case to determine the binary interaction parameters. Similar trends are observed for the RKS-BM model and the PR-BM model, but the RKS-BM model exceeds the PR-BM model in the accuracy of the predicted data. VLE trends and values are predicted well for the $\text{CO}_2 + n$ -alkane and $\text{CO}_2 + \text{non}$ -primary alcohol systems. For the $\text{CO}_2 + I$ -alcohol and $\text{CO}_2 + \text{primary}$ branched alcohol systems, very accurate dew point curves were generated – an important characteristic to consider for SFF processes where the low solute concentration region is important. Like for the PR-BM model, the accuracy of the data diminishes as the temperature decreases.

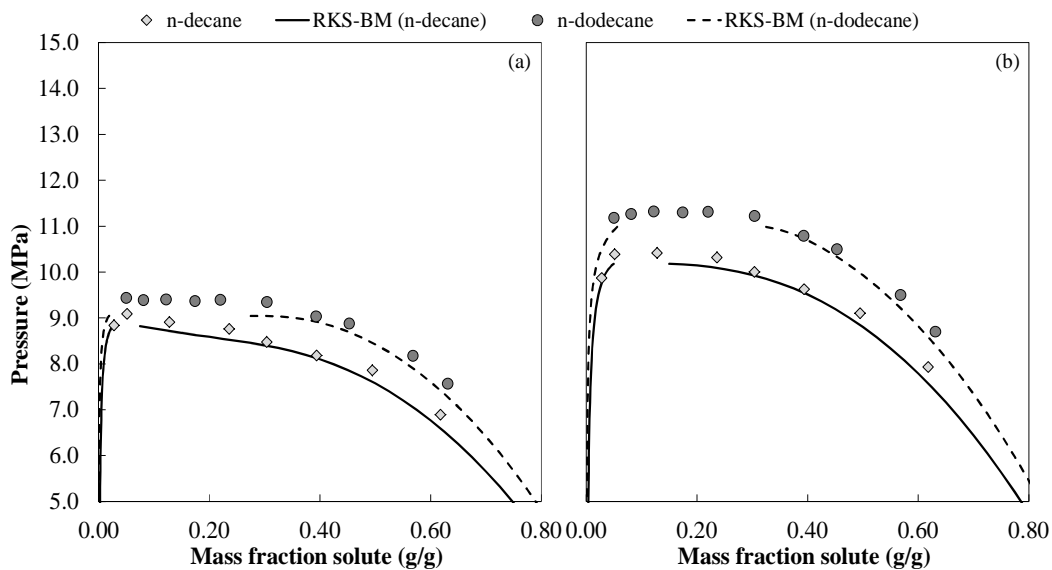


Figure 6-14 VLE prediction with RKS-BM (including interaction parameters) for $\text{CO}_2 + n$ -decane and $\text{CO}_2 + n$ -dodecane at (a) 318 K and (b) 328 K

6 | Thermodynamic Modelling of Mixtures at High Pressure
using Aspen Plus®

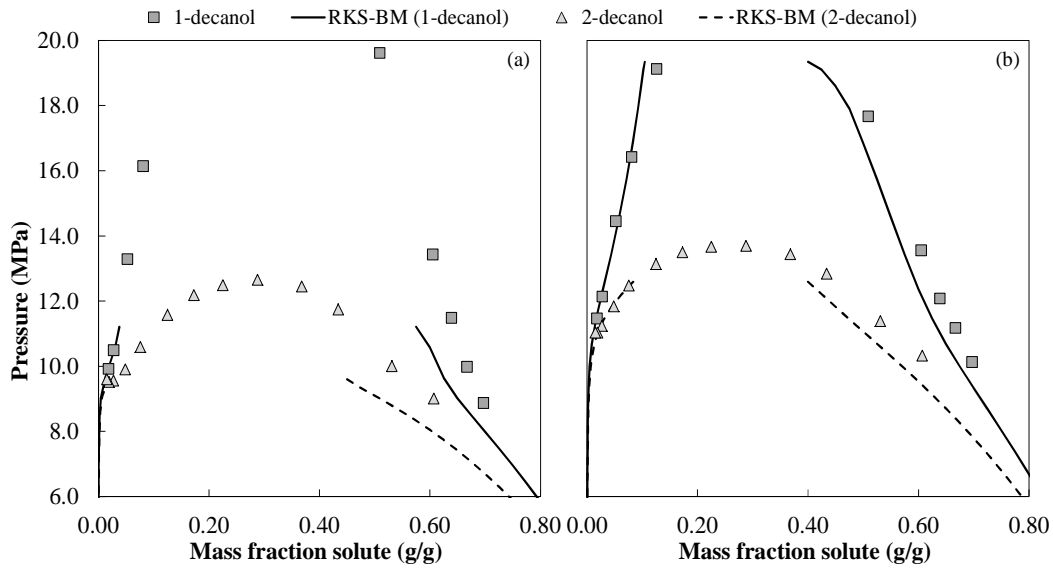


Figure 6-15 VLE prediction with RKS-BM (including interaction parameters) for CO_2 +1-decanol and CO_2 +2-decanol at (a) 318 K and (b) 328 K

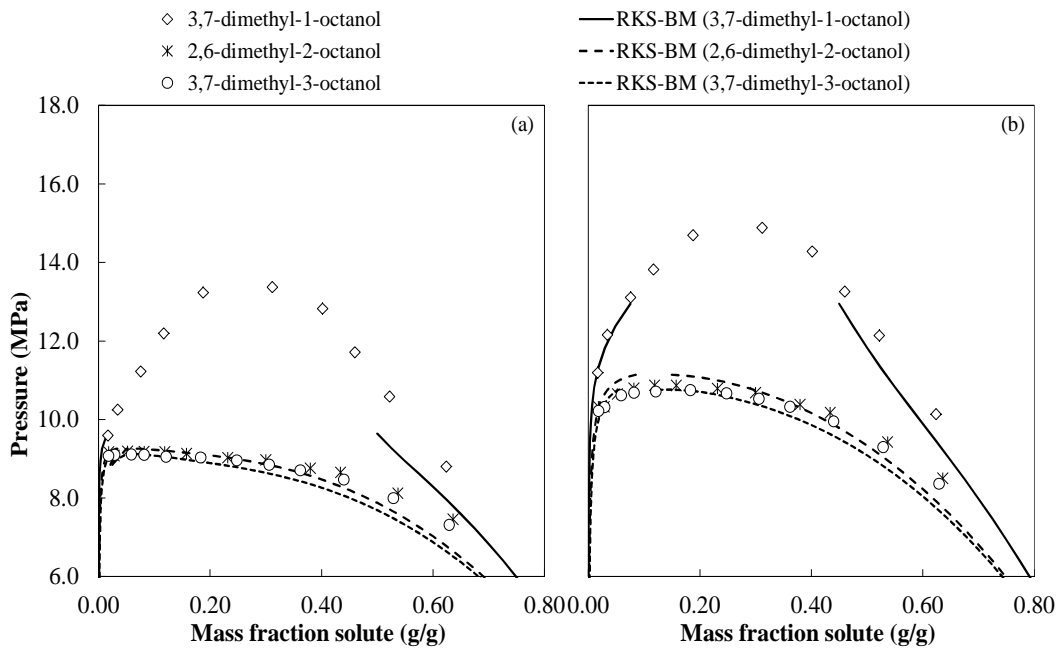


Figure 6-16 VLE prediction with RKS-BM (including interaction parameters) for CO_2 +3,7-dimethyl-1-octanol, CO_2 +2,6-dimethyl-2-octanol and CO_2 +3,7-dimethyl-3-octanol at (a) 318 K and (b) 328 K

6 | Thermodynamic Modelling of Mixtures at High Pressure using Aspen Plus®

6.3.3.3 RK-ASPEN

Figure 6-17 to Figure 6-19 contain the VLE data as predicted by the RK-ASPEN model with the inclusion of the polar parameter (Table 6-9) and binary interaction parameters (Table 6-13) for each binary mixture considered at 318 K and 328 K.

At the low temperature range investigated, the RK-ASPEN model predicts accurate phase transition trends and values for the mixtures containing *n*-alkanes and non-primary branched alcohols. For mixtures containing primary linear and branched alcohols the RK-ASPEN model predicts the correct trends, but struggles to predict accurate phase transition pressure values. Even with the inclusion of an additional regressed parameter, the pure component polar parameter, the RK-ASPEN model produces VLE results that are similar in accuracy to that of the PR-BM and RKS-BM models.

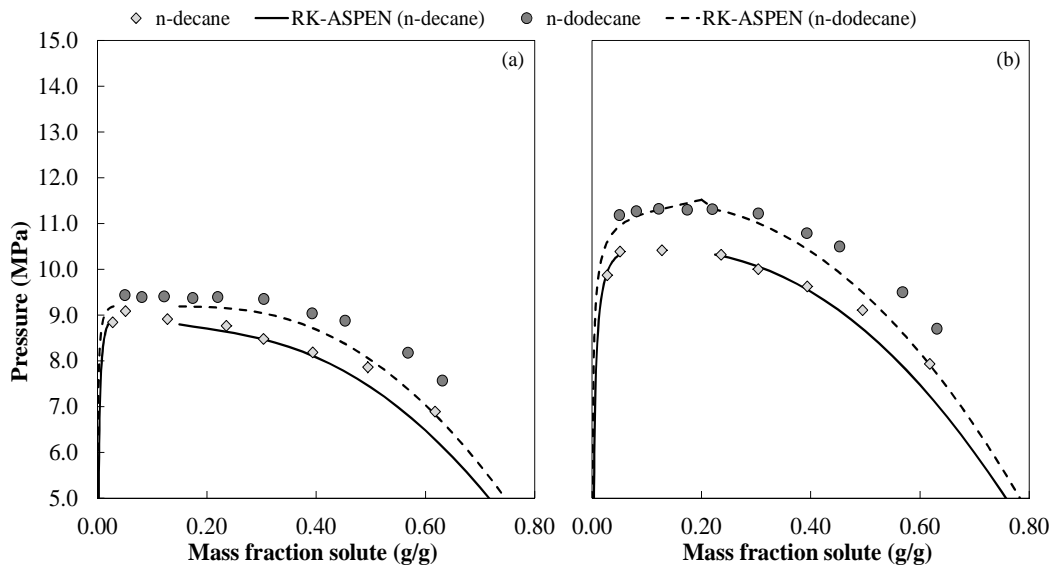


Figure 6-17 VLE prediction with RK-ASPEN (including interaction parameters) for CO_2 +*n*-decane and CO_2 +*n*-dodecane at (a) 318 K and (b) 328 K

6 | Thermodynamic Modelling of Mixtures at High Pressure
using Aspen Plus®

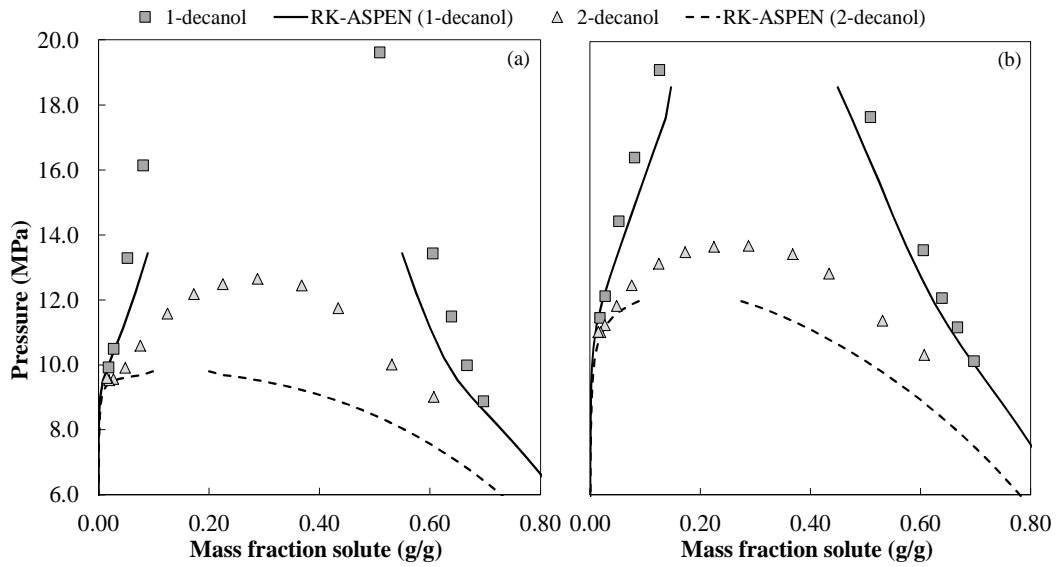


Figure 6-18 VLE prediction with RK-ASPEN (including interaction parameters) for CO_2 +1-decanol and CO_2 +2-decanol at (a) 318 K and (b) 328 K

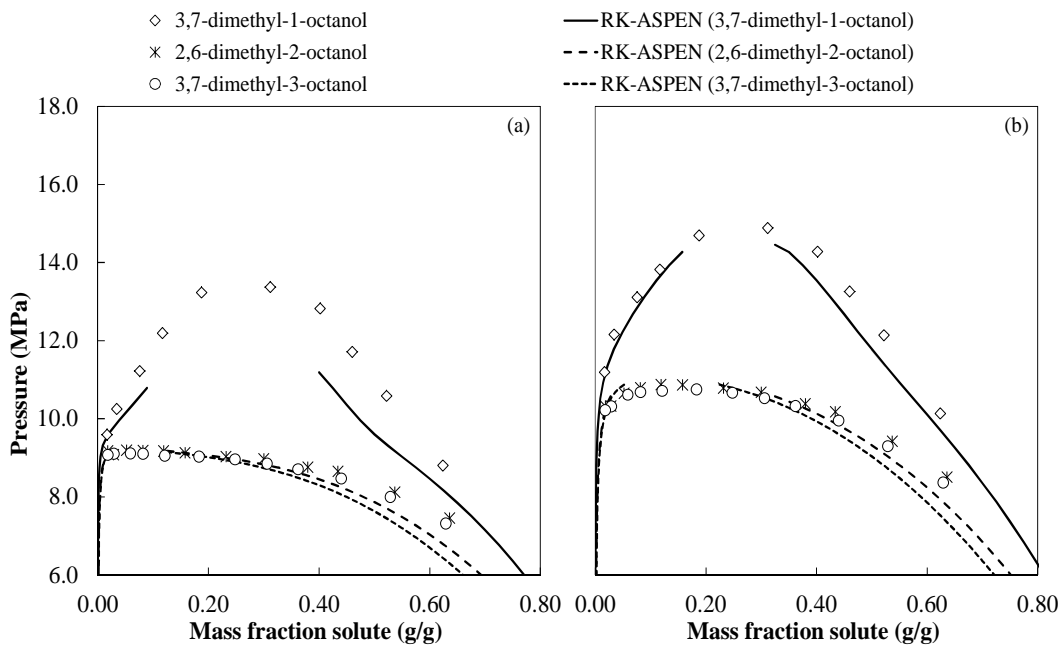


Figure 6-19 VLE prediction with RK-ASPEN (including interaction parameters) for CO_2 +3,7-dimethyl-1-octanol, CO_2 +2,6-dimethyl-2-octanol and CO_2 +3,7-dimethyl-3-octanol at (a) 318 K and (b) 328 K

6 | Thermodynamic Modelling of Mixtures at High Pressure using Aspen Plus®

6.3.3.4 SR-POLAR

Like the RK-ASPEN model the SR-POLAR model was used with three regressed parameters, a pure component polar parameter (see Table 6-10) and two binary interaction parameters (see Table 6-14). The VLE predictions of the SR-POLAR model for binary mixtures at temperatures below 338 K are shown in Figure 6-20 to Figure 6-22.

As expected, the SR-POLAR model performs similar to the RK-ASPEN model, except for the $\text{CO}_2 + 1$ -decanol system. The SR-POLAR model was not able to predict any data for this system at temperatures of 318 K and 328 K, with the inclusion of the regressed parameters. The regression results indicated that the SR-POLAR could not represent the $\text{CO}_2 + 1$ -decanol system very accurately, even at the temperatures used in the regression case. The SR-POLAR model was developed to be able to represent polar compounds well, and thus these results are surprising. It is however, speculated that with the inclusion of additional pure component polar parameters and/or binary interaction parameters, the $\text{CO}_2 + 1$ -decanol system can be represented very well with the SR-POLAR model.

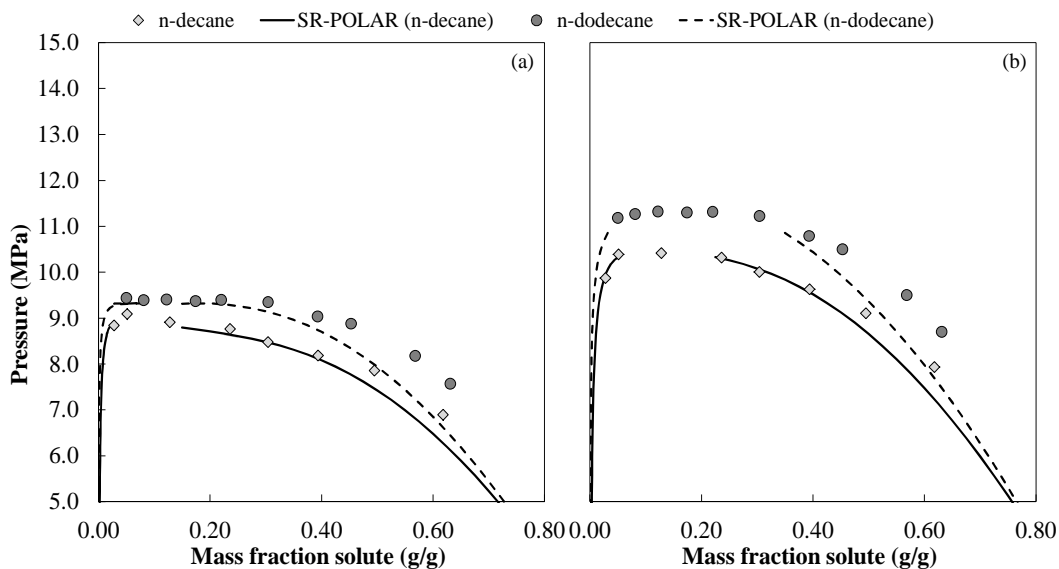


Figure 6-20 VLE prediction with SR-POLAR (including interaction parameters) for $\text{CO}_2 + n$ -decane and $\text{CO}_2 + n$ -dodecane at (a) 318 K and (b) 328 K

6 | Thermodynamic Modelling of Mixtures at High Pressure
using Aspen Plus®

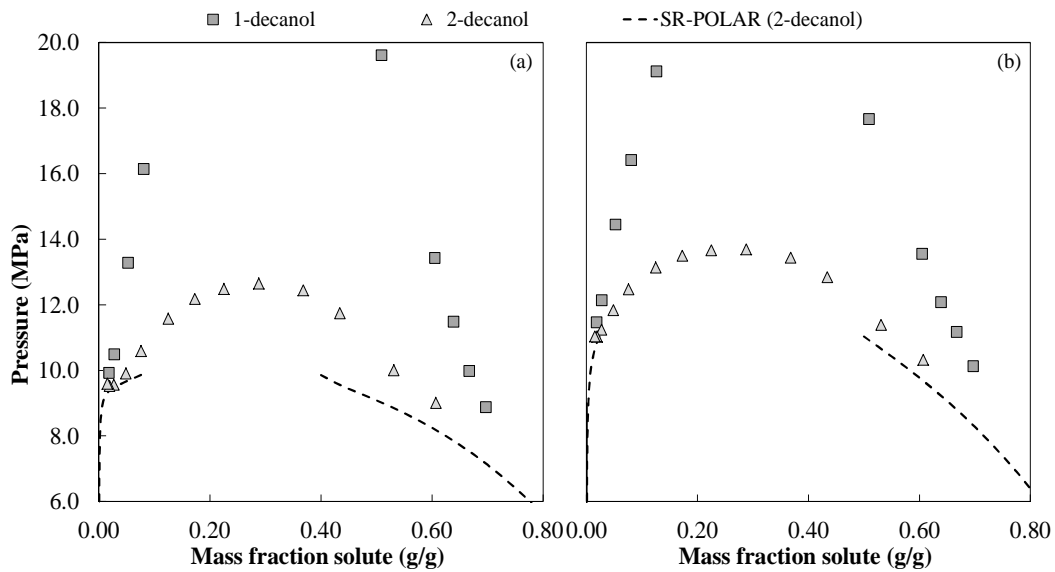


Figure 6-21 VLE prediction with SR-POLAR (including interaction parameters) for CO_2 +1-decanol and CO_2 +2-decanol at (a) 318 K and (b) 328 K

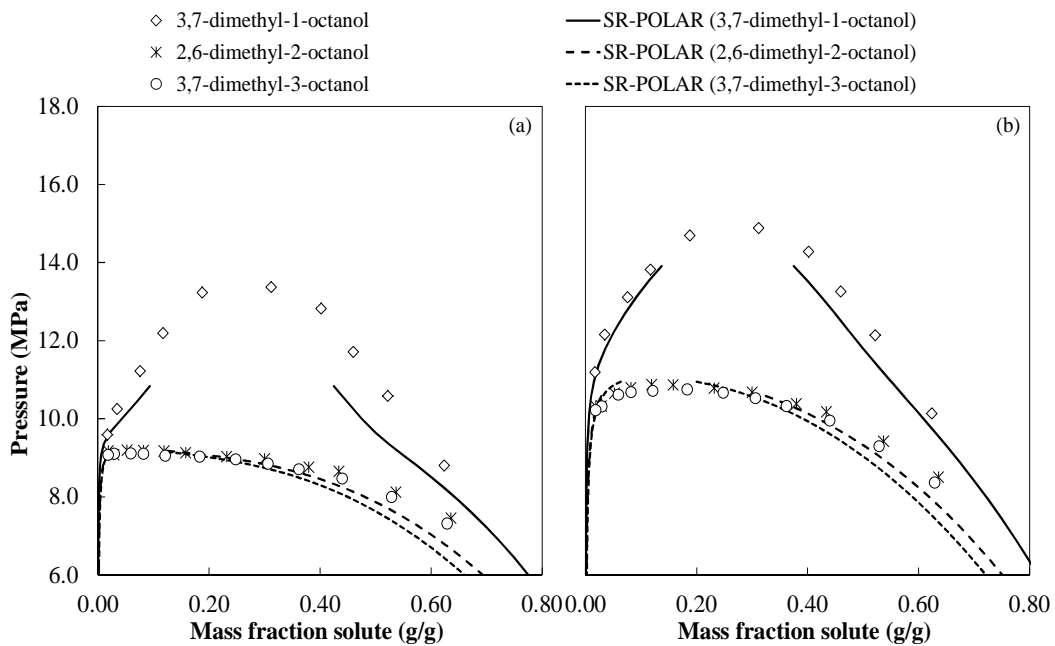


Figure 6-22 VLE prediction with SR-POLAR (including interaction parameters) for CO_2 +3,7-dimethyl-1-octanol, CO_2 +2,6-dimethyl-2-octanol and CO_2 +3,7-dimethyl-3-octanol at (a) 318 K and (b) 328 K

6 | Thermodynamic Modelling of Mixtures at High Pressure using Aspen Plus®

6.3.4 Thermodynamic Model Comparison and Selection

The %AAD values presented in Table 6-11 to Table 6-14 for the regression cases were averaged for all the binary mixtures, for each thermodynamic model investigated. By comparing these values (see Table 6-15) the accuracy of each thermodynamic model in the parameter fitting process is evaluated for all of the compounds investigated.

The RK-ASPEN property method generally performed better than the other property methods, especially in the prediction of the vapour phase compositions. Since the dew point region is the region of importance for SFF processes, it is required that this region be represented well, and thus the RK-ASPEN model looks promising.

Table 6-15 Comparison between the average %AAD of the PR-BM, RKS-BM, RK-ASPEN and SR-POLAR property methods for all the binary mixtures investigated in the respective regression cases

Property Method	%AAD _T	%AAD _P	%AAD _x	%AAD _y
PR-BM	1.49	0.96	0.30	11.96
RKS-BM	1.10	0.81	0.23	12.49
RK-ASPEN	1.03	0.68	0.23	9.34
SR-POLAR	1.72	0.99	0.19	13.97

The four thermodynamic models investigated were also evaluated according to their predictive ability for VLE at lower temperatures, when the regressed parameters are included. None of the models were able to represent or predict VLE data in the mixture critical region. As mentioned previously in section 6.3.1.1, this is a common problem encountered in the thermodynamic modelling of mixtures at high pressures.

From the qualitative analysis in section 6.3.4, the SR-POLAR model was eliminated from consideration since it cannot accurately represent or predict VLE data for the CO₂ + 1-decanol system when only three regressed parameters are included in the model. The RKS-BM model showed the best ability to predict data at temperatures of 318 K and 328 K. The prediction of accurate data outside of the temperature range considered in the regression case is an indicator of a robust thermodynamic model. The RKS-BM model can thus be considered a promising model for the

6 | Thermodynamic Modelling of Mixtures at High Pressure using Aspen Plus®

prediction of high pressure VLE data of mixtures of detergent range alkanes and alcohols in supercritical CO₂.

6.4 Predicting Multi-component Phase Behaviour

In the previous section it was shown that both the RKS-BM and RK-ASPEN models fitted and predicted data well for the type of mixtures investigated in this work, within the temperature range considered. The ability of these two models to predict multi-component VLE data will now be investigated. The experimental bubble and dew point data measured and reported in Chapter 5 for the two multi-component mixtures, CO₂ + (20 % *n*-dodecane + 70 % *I*-decanol + 10 % 3,7-dimethyl-*I*-octanol) and CO₂ + (25 % *n*-decane + 25 % *I*-decanol + 25 % 3,7-dimethyl-*I*-octanol + 25 % 2,6-dimethyl-2-octanol), will be used to evaluate the accuracy of the multi-component data predicted by the RKS-BM and RK-ASPEN models. Since only phase transition pressures were measured for the multi-component mixtures, the ability of the thermodynamic models to predict bubble and dew point data, and not co-existing phase compositions, will be evaluated. It is important that the thermodynamic model employed in a process model be able to predict accurate VLE data, not only for binary mixtures, but for mixtures containing a number of compounds, as well.

Multi-component VLE data was generated with the built-in flash algorithm (FLASH2) in Aspen Plus®. The feed mixture to the flash drum was set equal to the feed used in the experimental high pressure VLE measurements. For a set temperature and feed composition the bubble/dew point pressure was determined.

6.4.1 RKS-BM

Table 6-16 and Table 6-17 contain the experimental and predicted data for the two mixtures considered. The data shown in these tables were predicted with the RKS-BM method, firstly without the use of binary interaction parameters, and secondly with the inclusion of the regressed binary solute-solvent interaction parameters given in Table 6-12.

6 | Thermodynamic Modelling of Mixtures at High Pressure using Aspen Plus®

*Table 6-16 Phase transition pressures of the CO₂ + (20 % *n*-dodecane + 70 % *l*-decanol + 10 % 3,7-dimethyl-*l*-octanol) system as predicted by the RKS-BM model*

Mass fraction solute (g/g)	Phase transition pressure (MPa)											
	Experimental				RKS-BM without any parameters				RKS-BM with solvent-solute parameters			
	Temperature (K)											
	318	328	338	348	318	328	338	348	318	328	338	348
0.640	8.51	9.76	11.01	12.26	5.28	6.20	7.18	8.20	8.39	9.89	11.39	12.84
0.565	9.78	11.26	12.75	14.23	6.03	7.12	8.28	9.48	9.69	11.62	13.41	15.08
0.462	13.09	13.86	15.16	16.33	6.97	8.28	9.67	11.11	-	14.57	16.28	17.95
0.385	14.91	15.29	16.40	17.53	7.61	9.08	10.64	12.24	-	15.76	17.46	19.13
0.302	15.77	15.99	17.07	18.19	8.23	9.88	11.61	13.35	-	-	-	-
0.230	16.44	16.45	17.43	18.50	8.72	10.52	12.37	14.18	-	-	-	-
0.173	15.95	16.10	17.14	18.13	9.07	10.97	12.88	14.69	-	-	-	-
0.117	14.56	15.17	16.16	17.53	9.37	11.33	-	-	-	-	-	-
0.080	12.72	14.05	15.38	16.71	9.53	11.45	13.25	14.81	-	14.61	16.39	17.97
0.052	10.90	12.55	14.20	15.85	-	11.44	13.05	14.40	-	13.07	14.82	16.29
0.0275	9.78	11.64	13.18	14.42	-	11.19	12.49	13.48	-	11.82	13.29	14.45
0.0182	9.47	11.09	12.40	13.39	9.52	10.94	12.01	12.75	-	11.29	12.53	13.44
%AAD					37.1	26.5	23.4	20.9	1.1	3.0	4.4	5.1

There seem to be a significant improvement in the accuracy of the data predicted with the RKS-BM model when binary interaction parameters are included. However, the %AAD values reported in Table 6-16 must be carefully analysed, since it is a reflection of the accuracy of the phase transition pressure data points predicted, and not the overall fit of the model to the system. As can be seen from the data in Table 6-16, the RKS-BM model with the inclusion of binary solute-solvent interaction parameters was not able to produce any phase transition pressure data over a large composition range. However, the data points that could be generated for the CO₂ + (20 % *n*-dodecane + 70 % *l*-decanol + 10 % 3,7-dimethyl-*l*-octanol) mixture, was very accurate as expressed by the low %AAD values in the right hand column of Table 6-16. Although the data predicted by the RKS-BM model are very accurate for this mixture, the model does not represent the phase behaviour of the system very well, with and without the use of binary solute-solvent interaction parameters.

In Table 6-17 the VLE predictions of the RKS-BM model for the CO₂ + (25 % *n*-decane + 25 % *l*-decanol + 25 % 3,7-dimethyl-*l*-octanol + 25 % 2,6-dimethyl-2-octanol) mixture are shown for

6 | Thermodynamic Modelling of Mixtures at High Pressure using Aspen Plus®

two cases, one without the use of any additional parameters, and two with the inclusion of binary solute-solvent interaction parameters.

Similar trends to those discussed for the Mixture 1 (reported in Table 6-16) were observed for Mixture 2 as well. However, it should be noted that the phase transition pressures predicted for Mixture 2 with the RKS-BM model without the use of regressed parameters, are close to the experimentally measured values (as expressed in the %AAD values). The predictive RKS-BM model is thus able to predict phase transition pressures within 11 % of the true value over the temperature range 318 – 348 K for the CO₂ + (25 % *n*-decane + 25 % *l*-decanol + 25 % 3,7-dimethyl-*l*-octanol + 25 % 2,6-dimethyl-2-octanol) mixture.

*Table 6-17 Phase transition pressures of the CO₂ + (25 % *n*-decane + 25 % *l*-decanol + 25 % 3,7-dimethyl-*l*-octanol + 25 % 2,6-dimethyl-2-octanol) system as predicted by the RKS-BM model*

Mass fraction solute (g/g)	Phase transition pressure (MPa)											
	Experimental				RKS-BM without any parameters				RKS-BM with binary solvent- solute parameters			
	Temperature (K)											
	318	328	338	348	318	328	338	348	318	328	338	348
0.637	7.26	8.21	9.17	10.12	5.80	6.78	7.81	8.87	7.27	8.49	9.75	11.01
0.559	8.11	9.34	10.58	11.81	6.58	7.74	8.97	10.22	8.12	9.61	11.15	12.67
0.467	8.70	10.22	11.74	13.26	7.37	8.73	10.17	11.64	8.86	10.73	12.62	14.40
0.388	9.13	10.84	12.56	14.27	7.94	9.47	11.08	12.71	-	11.62	13.71	15.63
0.291	9.48	11.33	13.19	15.04	8.52	10.24	12.05	13.81	-	-	14.46	16.41
0.226	9.95	11.73	13.51	15.29	8.84	10.69	12.58	14.39	-	-	-	-
0.177	10.27	12.03	13.79	15.55	9.06	10.98	12.89	14.68	-	-	-	-
0.115	10.28	12.04	13.80	15.56	9.30	11.26	13.10	14.76	-	-	-	-
0.076	9.92	11.84	13.51	14.93	-	-	13.03	14.49	-	-	-	-
0.050	9.81	11.61	13.11	14.31	-	11.26	12.77	14.00	-	11.70	13.35	14.71
0.0283	9.53	11.12	12.48	13.59	9.48	11.01	12.22	13.11	9.53	11.18	12.52	13.53
0.0189	9.47	10.89	12.08	13.04	9.42	10.75	11.73	12.36	9.40	10.83	11.92	12.67
%AAD					11.1	9.2	7.8	7.3	0.6	2.9	5.2	6.2

6 | Thermodynamic Modelling of Mixtures at High Pressure using Aspen Plus®

6.4.2 RK-ASPEN

In Table 6-18 and Table 6-19 the phase transition pressures as predicted by the RK-ASPEN model for Mixture 1 and 2, are reported. The RK-ASPEN model was able to predict very accurate phase transition pressures for both mixtures, with the inclusion of polar and binary solute-solvent interaction parameters. The composition range in which the RK-ASPEN model could predict phase transition pressure data was considerably larger than that of the RKS-BM model, with the majority of exclusions occurring near the mixture critical point. From the data presented in Table 6-18 and Table 6-19 it is clear that the RK-ASPEN model with the inclusion of regressed parameters, can predict phase transition pressures to within 6 % of the real value for the two mixtures considered in the temperature range 318 – 348 K.

Table 6-18 Phase transition pressures of the CO₂ + (20 % n-dodecane + 70 % 1-decanol + 10 % 3,7-dimethyl-1-octanol) system as predicted by the RK-ASPEN model

Mass fraction solute (g/g)	Phase transition pressure (MPa)											
	Experimental				RK-ASPEN without any parameters				RK-ASPEN with polar and binary solvent-solute parameters			
	Temperature (K)											
	318	328	338	348	318	328	338	348	318	328	338	348
0.640	8.51	9.76	11.01	12.26	5.28	6.20	7.18	8.20	8.32	9.79	11.26	12.68
0.565	9.78	11.26	12.75	14.23	6.03	7.12	8.28	9.48	9.36	11.24	13.01	14.65
0.462	13.09	13.86	15.16	16.33	6.97	8.28	9.67	11.11	-	13.73	15.54	17.25
0.385	14.91	15.29	16.40	17.53	7.61	9.08	10.64	12.24	-	-	17.26	18.90
0.302	15.77	15.99	17.07	18.19	8.23	9.88	11.61	13.35	-	-	18.29	20.02
0.230	16.44	16.45	17.43	18.50	8.72	10.52	12.37	14.18	-	-	-	-
0.173	15.95	16.10	17.14	18.13	9.07	10.97	12.88	14.69	-	-	17.85	19.52
0.117	14.56	15.17	16.16	17.53	9.37	11.33	-	-	-	14.75	16.64	18.34
0.080	12.72	14.05	15.38	16.71	9.53	11.45	13.25	14.81	11.55	13.66	15.55	17.18
0.052	10.90	12.55	14.20	15.85	-	11.44	13.05	14.40	10.71	12.76	14.53	16.01
0.0275	9.78	11.64	13.18	14.42	-	11.19	12.49	13.48	10.03	11.84	13.33	14.49
0.0182	9.47	11.09	12.40	13.39	9.52	10.94	12.01	12.75	9.77	11.39	12.66	13.59
%AAD					37.1	26.5	23.4	20.9	3.9	1.6	3.0	4.4

6 | Thermodynamic Modelling of Mixtures at High Pressure using Aspen Plus®

Table 6-19 Phase transition pressures of the CO₂ + (25 % n-decane + 25 % 1-decanol + 2 % 3,7-dimethyl-1-octanol + 25 % 2,6-dimethyl-2-octanol) system as predicted by the RK-ASPEN model

Mass fraction solute (g/g)	Phase transition pressure (MPa)											
	Experimental				RK-ASPEN without any parameters				RK-ASPEN with polar and binary solvent-solute parameters			
	Temperature (K)											
	318	328	338	348	318	328	338	348	318	328	338	348
0.637	7.26	8.21	9.17	10.12	5.16	6.05	6.98	7.96	7.23	8.44	9.69	10.94
0.559	8.11	9.34	10.58	11.81	5.93	6.98	8.09	9.24	8.06	9.53	11.05	12.55
0.467	8.70	10.22	11.74	13.26	6.76	8.00	9.31	10.65	8.80	10.62	12.47	14.24
0.388	9.13	10.84	12.56	14.27	7.41	8.81	10.28	11.78	9.27	11.47	13.55	15.46
0.291	9.48	11.33	13.19	15.04	8.13	9.72	11.38	13.03	-	12.39	14.56	16.53
0.226	9.95	11.73	13.51	15.29	8.57	10.28	12.04	13.75	-	-	-	16.62
0.177	10.27	12.03	13.79	15.55	8.88	10.67	12.47	14.18	-	-	14.82	16.73
0.115	10.28	12.04	13.80	15.56	9.22	11.07	12.86	-	-	12.37	14.39	16.16
0.076	9.92	11.84	13.51	14.93	9.39	-	12.89	14.33	9.85	11.99	13.85	15.43
0.050	9.81	11.61	13.11	14.31	-	11.21	12.70	13.91	9.68	11.64	13.29	14.64
0.0283	9.53	11.12	12.48	13.59	9.48	11.00	12.20	13.08	9.52	11.18	12.51	13.52
0.0189	9.47	10.89	12.08	13.04	9.43	10.76	11.73	12.36	9.41	10.85	11.95	12.71
%AAD					14.1	13.1	11.7	11.7	0.8	2.9	4.7	5.7

6.4.3 Thermodynamic Model Comparison and Selection

Both the RKS-BM and RK-ASPEN models show a reduced %AAD when regressed parameters are included in the model, but the RK-ASPEN model is applicable over a larger composition range – thus making it the superior model to consider for predicting phase transition pressures of multi-component mixtures.

The data in Table 6-16 to Table 6-19, and Figure 6-23 to Figure 6-26, indicate that Mixture 1, CO₂ + (20 % n-dodecane + 70 % 1-decanol + 10 % 3,7-dimethyl-1-octanol), was the more complex mixture to simulate. Both models struggled to predict phase transition pressure values that approach those observed experimentally, when no regressed parameters were employed. %AAD values for the RKS-BM and RK-ASPEN models were in the range 20 – 40 for Mixture 1, compared to less than 15 for Mixture 2. Mixture 1 displays low temperature phase behaviour that approach that of a temperature inversion – a characteristic not easily represented by simple thermodynamic models.

6 | Thermodynamic Modelling of Mixtures at High Pressure
using Aspen Plus®

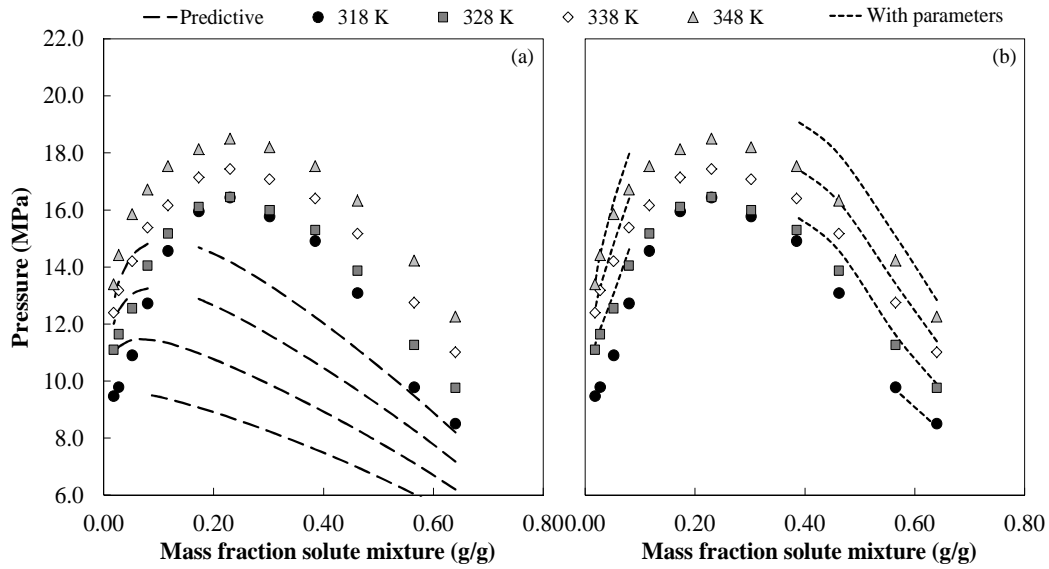


Figure 6-23 VLE predictions at 318 - 348 K for CO_2 + (20 % *n*-dodecane + 70 % 1-decanol + 10 % 3,7-dimethyl-1-octanol) with the RKS-BM model with (a) no parameters included, and (b) binary solute-solvent interaction parameters included

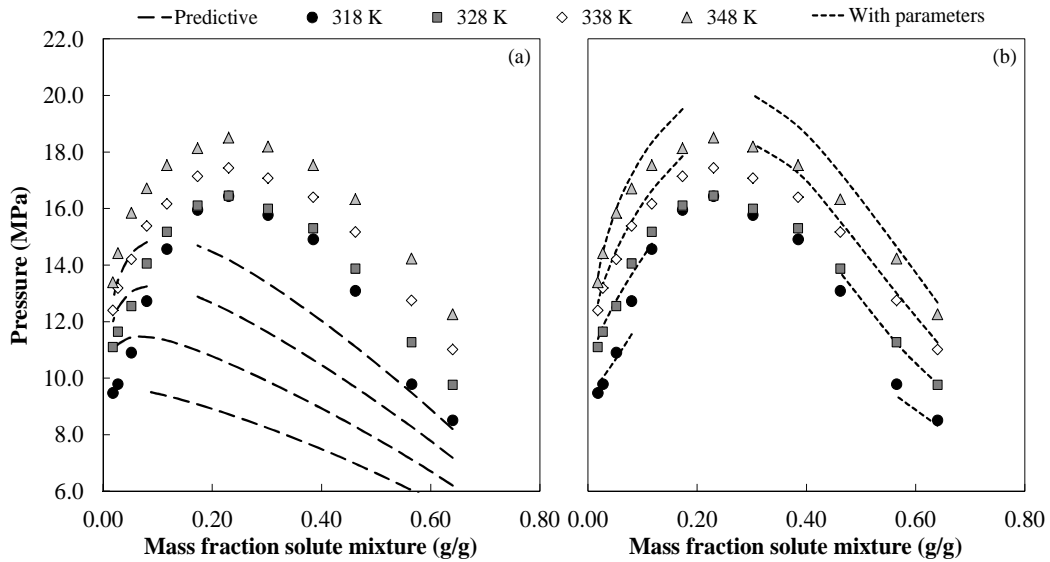


Figure 6-24 VLE predictions at 318 - 348 K for CO_2 + (20 % *n*-dodecane + 70 % 1-decanol + 10 % 3,7-dimethyl-1-octanol) with the RK-ASPEN model with (a) no parameters included, and (b) binary solute-solvent interaction parameters included

6 | Thermodynamic Modelling of Mixtures at High Pressure
using Aspen Plus®

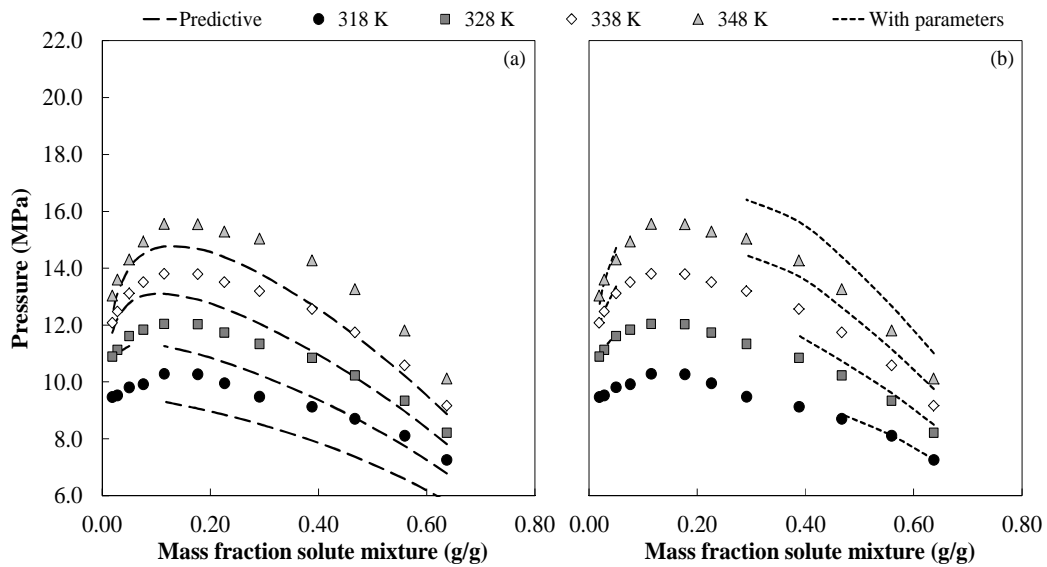


Figure 6-25 VLE predictions at 318 - 348 K for CO_2 + (25 % *n*-decane + 25 % 1-decanol + 25 % 3,7-dimethyl-1-octanol + 25 % 2,6-dimethyl-2-octanol) with the RKS-BM model with (a) no parameters included, and (b) binary solute-solvent interaction parameters included

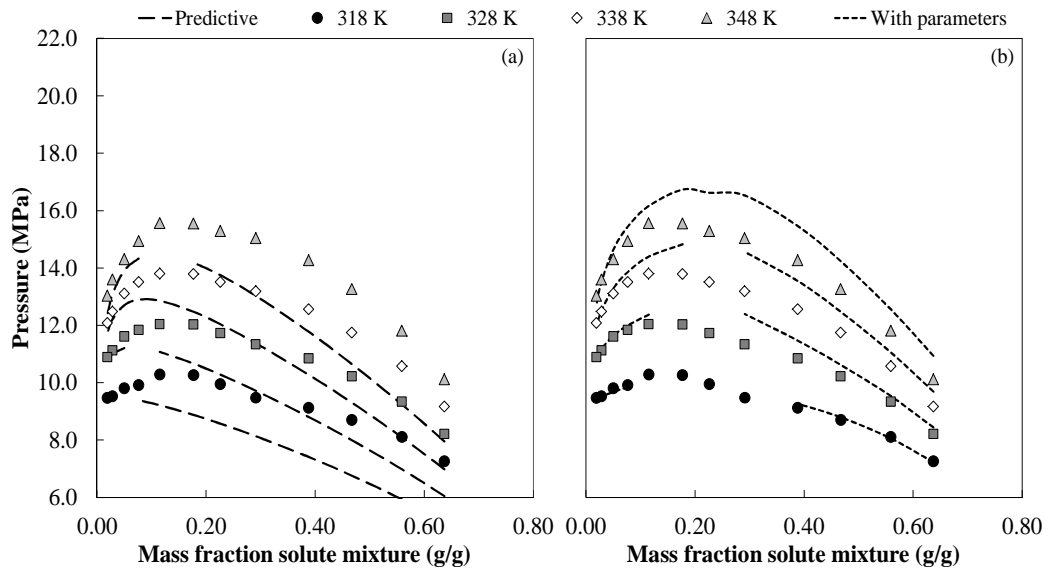


Figure 6-26 VLE predictions at 318 - 348 K for CO_2 + (25 % *n*-decane + 25 % 1-decanol + 25 % 3,7-dimethyl-1-octanol + 25 % 2,6-dimethyl-2-octanol) with the RK-ASPEN model with (a) no parameters included, and (b) polar and binary solute-solvent interaction parameters included

6 | Thermodynamic Modelling of Mixtures at High Pressure using Aspen Plus®

The RK-ASPEN model with the inclusion of regressed parameters was able to predict data over a larger composition range for both mixtures, compared to the RKS-BM model with the inclusion of binary interaction parameters. This trend allowed the RK-ASPEN model predictions to encompass a large portion of the dew point curve, which is the region of importance for SFF processes. Taking this important aspect into account, it is thus suggested that the RK-ASPEN model be incorporated into the SFF process model for the most accurate representation of the thermodynamic properties of the type of mixtures considered.

It is important to note that the accuracy of the predicted phase compositions could not be established since VLE data was not available for the mixtures under consideration. The generation of multi-component VLE data requires significantly more complex equipment and more resources, and do not fall within the scope of this project. Agreement between the experimentally measured and predicted phase transition pressures of Mixture 1 and Mixture 2 by the RK-ASPEN model was deemed sufficient to support the selection thereof for employment in an SFF process model.

6.5 Binary Solute-Solute Interaction Parameters

6.5.1 Rationale for Further Investigation

Previous investigations conducted and reported in this chapter, revealed the RK-ASPEN model as a potential model for the use in a SFF process model aimed at predicting the separation of detergent range alkanes and alcohols with supercritical CO₂. The RK-ASPEN model showed promise according to the criteria mentioned in the introduction of this chapter, in the following ways:

- Acceptable trends were predicted for phase behaviour of binary mixtures of CO₂ + *n*-decane and CO₂ + *l*-decanol within the temperature range 308 – 348 K. However, improvement in the accuracy of the values predicted for the phase transition pressures is required.
- Binary data for all systems was represented well during regression of binary solute-solvent interaction parameters, with the inclusion of the polar parameter, at temperatures of 338 K and 348 K.

6 | Thermodynamic Modelling of Mixtures at High Pressure using Aspen Plus®

- Binary data for CO₂ + *n*-alkanes and CO₂ + non-primary branched alcohols were predicted well at temperatures of 318 K and 328 K, with the inclusion of all regressed parameters. Predictions of binary VLE data for CO₂ + linear alcohols and CO₂ + primary branched alcohols at 318 K and 328 K, was less accurate.
- Phase transition pressures of multi-component mixtures consisting of CO₂ and different ratios of alkanes and alcohol isomers can be predicted within 6 % of the experimentally observed values for the two mixtures investigated, within the temperature range 318 – 348 K.

There exists a possibility that multi-component VLE prediction can be improved with the RK-ASPEN model when solute-solute interaction parameters are included. Since measured VLE data are not available for the two multi-component mixtures considered, this idea cannot be tested by comparing predicted data to experimental data. It can however, be tested once incorporated into the SFF process model where model predictions of the stream compositions can be compared to experimental pilot plant data.

As a first approach to determine the effect of the inclusion of solute-solute interaction parameters on the accuracy of the RK-ASPEN model, only three types of solute-solute interactions were considered. Since the number of possible interactions that can occur in a multi-component mixture can become very large, the aim is to provide representative values, instead of exact values, for interaction parameters between certain types of compounds. The representative solute-solute interaction parameters should at least be able to provide improved phase behaviour predictions for multi-component mixtures that employ similar compounds as those used in the determination of the solute-solute interaction parameters. The three ternary mixtures reported on in Chapter 5 were used to determine the solute-solute interaction parameters. Mixture A was used to determine the interaction parameter between a linear alkane and primary linear alcohol (represented by the 22.2 % *n*-dodecane + 77.8 % *1*-decanol mixture), Mixture B was used to determine the interaction parameter between a primary linear alcohol and a branched alcohol (represented by the 87.5 % *1*-decanol + 12.5 % 3,7-dimethyl-*1*-octanol mixture), and Mixture C was used to determine the interaction parameter between a linear alkane and a branched alcohol (represented by the 66.7 % *n*-dodecane + 33.3 % 3,7-dimethyl-*1*-octanol mixture).

6.5.2 Factors that Require Special Attention

During the regression of the binary solute-solute interactions the following challenge was encountered:

- The data regression function in Aspen Plus® can only be employed when the input data are VLE data, not bubble and dew point data. Since it is significantly more complex to convert ternary bubble and dew point data to VLE data, it was decided to do the regression manually, without the aid of the built-in regression function.

6.5.3 Determining Binary Solute-Solute Interaction Parameters

A flash algorithm was employed to predict the phase transition pressures of the ternary mixtures investigated. The regressed values for the pure component polar parameter and binary solute-solvent parameters were incorporated into the RK-ASPEN model, after which the solute-solute interaction parameters were determined. Ideally the values of the interaction parameters, $k_{a,ij}$ and $k_{b,ij}$, should be determined simultaneously, but due to the large amount of possible combinations that would have to be tested, the optimization approach was simplified by only considering $k_{a,ij}$. The advantage of having a single interaction parameter is in its applicability to similar systems, i.e. allowing the solute-solute interaction parameter to be representative of the type of interaction, and not representative of the specific system. The $k_{a,ij}$ solute-solute interaction parameter was set at a certain value and the %AAD of the predicted phase transition pressure data from the experimental data was determined for temperatures of 338 K and 348 K. This procedure was repeated for a number of different values of the $k_{a,ij}$ solute-solute interaction parameter. The optimum value of $k_{a,ij}$ was determined from the minimum total %AAD at 338 K and 348 K for each ternary mixture. The relationship between the total %AAD of the experimental data and the predicted data, and the values of the solute-solute interaction parameters are depicted in Figure 6-27.

6 | Thermodynamic Modelling of Mixtures at High Pressure using Aspen Plus®

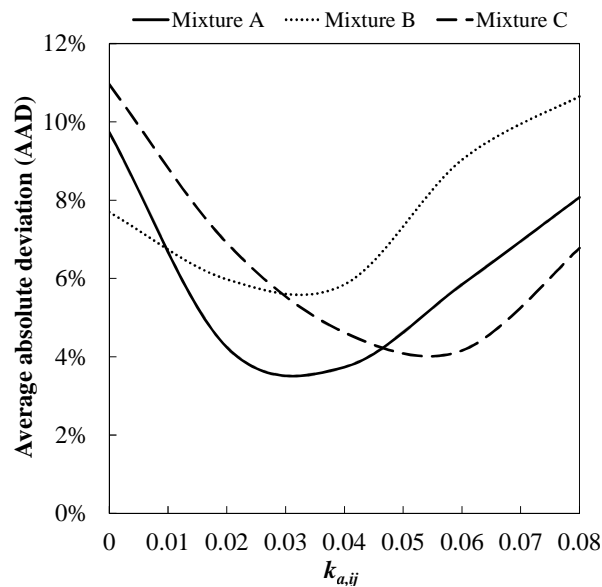


Figure 6-27 Optimization of $k_{a,ij}$ values for the solute-solute interaction parameters in Mixture A, Mixture B and Mixture C

It is unlikely that this conservative method of determining the solute-solute interaction parameters will lead to values of the interaction parameters that represent the true energy and volume effects of the solutes. It only allows values of solute-solute interaction parameters to be generated that leads to the closest fit of the model to the phase transition pressures measured for the ternary systems. The observed best-fit values could possibly be local minima points, with the global minimum being an improved representation of the true energy and volume effects. If solute-solute interactions are significant in the multi-component mixtures investigated, an improvement in the predicted phase transition pressures should be observed with the inclusion of solute-solute interaction parameters, even if the value is not located at the global minimum of the optimization surface. The effect of the inclusion of the determined binary solute-solute interaction parameters on the predicted phase compositions will be tested in the next chapter with the aid of experimental pilot plant data.

6 | Thermodynamic Modelling of Mixtures at High Pressure using Aspen Plus®

Table 6-20 Optimum values of the solute-solute interaction parameters determined from Figure 6-27 for Mixture A, Mixture B and Mixture C

Mixture CO ₂ + ...	Solute-solute Interaction	$k_{a,ij}$
22.2 % <i>n</i> -dodecane + 77.8 % <i>I</i> -decanol	<i>n</i> -alkane + <i>I</i> -alcohol	0.03
87.5 % <i>I</i> -decanol + 12.5 % 3,7-dimethyl- <i>I</i> -octanol	<i>I</i> -alcohol + branched alcohol	0.03
66.7 % <i>n</i> -dodecane + 33.3 % 3,7-dimethyl- <i>I</i> -octanol	<i>n</i> -alkane + branched alcohol	0.055

A comparison between the phase transition pressures predicted with and without the inclusion of a single binary solute-solute interaction parameter (Table 6-21 to Table 6-23), shows that the inclusion of solute-solute interaction in the RK-ASPEN model increases its accuracy. The %AAD values between the predicted and experimental phase transition pressures at 338 K and 348 K, decreased from ± 6 % with no solute-solute interaction parameters to ± 2 % with the inclusion of solute-solute interaction parameters for the ternary mixtures investigated.

The parameters used in the calculation of the phase transition pressures for Mixture A, B and C can be found in Table 6-9 (polar parameters), Table 6-13 (solute-solvent interaction parameters) and Table 6-20 (solute-solute interaction parameters).

6 | Thermodynamic Modelling of Mixtures at High Pressure using Aspen Plus®

Table 6-21 VLE data for the CO₂ + (22.2 % n-dodecane + 77.8 % 1-decanol) system as predicted by the RK-ASPEN model

Mass fraction solute (g/g)	Phase transition pressure (MPa)					
	Experimental		RK-ASPEN with polar parameters and solvent-solute parameters		RK-ASPEN with polar parameters, solvent-solute parameters and solute-solute parameters	
	Temperature (K)					
	338	348	338	348	338	348
0.654	10.77	11.98	10.98	12.34	10.51	11.82
0.551	13.02	14.35	13.42	15.07	12.65	14.29
0.448	14.88	16.31	16.02	17.68	14.83	16.61
0.375	16.57	17.71	17.64	19.21	16.28	18.01
0.312	17.09	18.16	18.44	20.06	-	18.86
0.239	17.57	18.58	18.31	20.17	-	19.22
0.174	17.02	18.01	18.03	19.65	17.19	18.88
0.121	16.49	17.57	16.86	18.53	16.31	18.01
0.078	15.23	16.58	15.53	17.15	15.22	16.83
0.051	14.35	15.77	14.54	16.01	14.35	15.80
0.0276	13.02	14.26	13.37	14.53	13.26	14.40
0.0177	12.22	13.22	12.64	13.57	12.56	13.46
%AAD			4.1	5.7	1.4	2.0

6 | Thermodynamic Modelling of Mixtures at High Pressure using Aspen Plus®

Table 6-22 VLE data for the CO₂ + (87.5 % 1-decanol + 12.5 % 3,7-dimethyl-1-octanol) system as predicted by the RK-ASPEN model

Mass fraction solute (g/g)	Phase transition pressure (MPa)					
	Experimental		RK-ASPEN with polar parameters and solvent-solute parameters		RK-ASPEN with polar parameters, solvent-solute parameters and solute-solute parameters	
	Temperature (K)					
	338	348	338	348	338	348
0.650	11.76	13.01	12.45	13.92	11.98	13.43
0.563	14.64	15.70	15.82	17.37	14.84	16.50
0.467	18.30	18.78	18.80	20.14	17.44	18.99
0.383	20.15	20.61	-	21.86	19.17	20.59
0.303	20.65	20.96	-	22.26	-	21.26
0.237	20.47	20.97	-	22.05	-	21.03
0.181	19.62	20.20	19.55	21.03	18.64	20.24
0.118	18.30	19.09	17.57	19.19	17.02	18.69
0.082	16.97	18.08	16.20	17.81	15.84	17.46
0.049	15.11	16.64	14.74	16.19	14.53	15.97
0.0272	13.54	14.75	13.51	14.67	13.38	14.53
0.0179	12.60	13.60	12.78	13.72	12.68	13.60
%AAD			3.3	4.4	3.6	1.9

6 | Thermodynamic Modelling of Mixtures at High Pressure using Aspen Plus®

Table 6-23 VLE data for the CO₂ + (66.7 % n-dodecane + 33.3 % 3,7-dimethyl-1-octanol) system as predicted by the RK-ASPEN model

Mass fraction solute (g/g)	Phase transition pressure (MPa)					
	Experimental		RK-ASPEN with polar parameters and solvent-solute parameters		RK-ASPEN with polar parameters, solvent-solute parameters and solute-solute parameters	
	Temperature (K)					
	338	348	338	348	338	348
0.640	9.35	10.36	9.13	10.29	8.52	9.60
0.563	10.30	11.51	10.50	11.90	9.77	11.05
0.462	11.47	12.93	12.03	13.71	11.12	12.66
0.377	12.12	13.77	13.09	14.95	12.02	13.73
0.298	12.55	14.31	13.82	15.77	12.64	14.46
0.233	12.85	14.69	14.15	-	12.97	14.84
0.184	12.88	14.75	-	-	13.06	-
0.118	12.74	14.53	13.86	15.62	13.06	14.73
0.080	12.62	14.18	13.44	15.01	12.83	14.30
0.054	12.43	13.82	12.99	14.35	12.51	13.76
0.0288	11.76	12.77	12.20	13.17	11.82	12.66
0.0171	11.18	11.82	11.48	12.10	11.11	11.59
%AAD			5.8	5.2	2.2	1.9

The improvement in the prediction of the phase transition curve of the ternary mixtures with the inclusion of the binary solute-solute interaction parameters (shown in Table 6-20) is evident from the plots shown in Figure 6-28.

6 | Thermodynamic Modelling of Mixtures at High Pressure
using Aspen Plus®

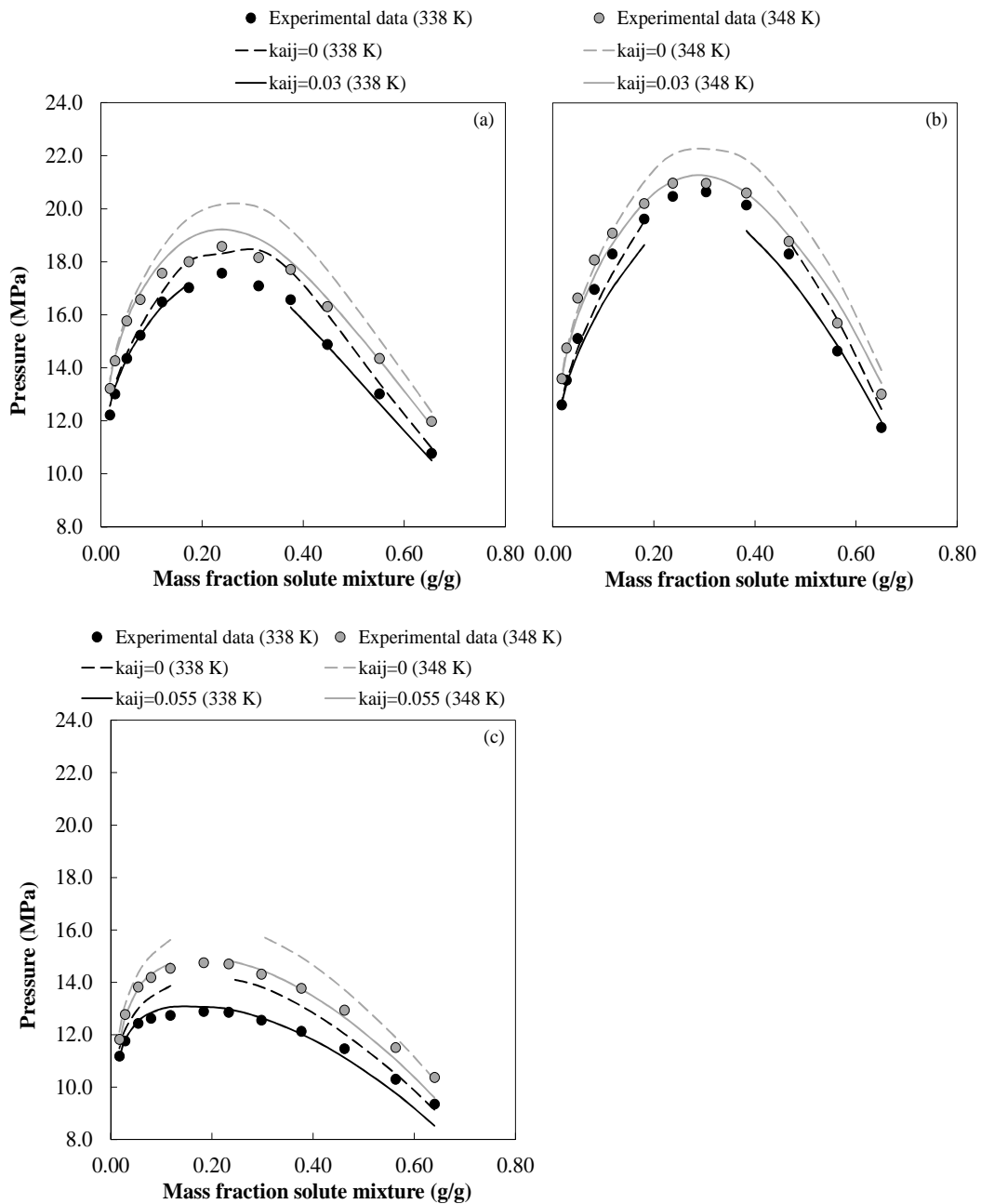


Figure 6-28 Comparison between the phase transition pressures at 338 K and 348 K as predicted with the RK-ASPEN model, with and without the inclusion of solute-solute interaction parameters for (a) Mixture A, (b) Mixture B and (c) Mixture C

6 | Thermodynamic Modelling of Mixtures at High Pressure using Aspen Plus®

It is clear from the work depicted in Figure 6-28 that the RK-ASPEN model fit the ternary phase transition pressure data for Mixture A, B and C better with the inclusion of a solute-solute interaction parameter.

6.5.4 Predicting Multi-component Phase Behaviour

The predictive ability of the RK-ASPEN model with solute-solute interaction parameters are tested for the two multi-component mixtures within the temperature range 318 – 348 K. The experimental and predicted phase transition pressures are given in Table 6-24 and Table 6-25.

Table 6-24 Phase transition pressures of the CO₂ + (20 % n-dodecane + 70 % 1-decanol + 10 % 3,7-dimethyl-1-octanol) system as predicted by the RK-ASPEN model

Mass fraction solute (g/g)	Phase transition pressure (MPa)											
	Experimental				RK-ASPEN with polar parameters and binary solvent-solute parameters				RK-ASPEN with polar parameters, solvent-solute parameters and solute-solute parameters			
	Temperature (K)											
	318	328	338	348	318	328	338	348	318	328	338	348
0.640	8.51	9.76	11.01	12.26	8.32	9.79	11.26	12.68	7.84	9.19	10.57	11.92
0.565	9.78	11.26	12.75	14.23	9.36	11.24	13.01	14.65	8.69	10.36	12.04	13.63
0.462	13.09	13.86	15.16	16.33	-	13.73	15.54	17.25	9.89	12.02	13.99	15.81
0.385	14.91	15.29	16.40	17.53	-	-	17.26	18.90	-	13.43	15.39	17.23
0.302	15.77	15.99	17.07	18.19	-	-	18.29	20.02	-	-	-	18.30
0.230	16.44	16.45	17.43	18.50	-	-	-	-	-	-	-	-
0.173	15.95	16.10	17.14	18.13	-	-	17.85	19.52	-	-	16.57	18.35
0.117	14.56	15.17	16.16	17.53	-	14.75	16.64	18.34	-	13.86	15.81	17.54
0.080	12.72	14.05	15.38	16.71	11.55	13.66	15.55	17.18	10.98	13.12	15.00	16.64
0.052	10.90	12.55	14.20	15.85	10.71	12.76	14.53	16.01	10.40	12.44	14.18	15.64
0.0275	9.78	11.64	13.18	14.42	10.03	11.84	13.33	14.49	9.90	11.68	13.13	14.26
0.0182	9.47	11.09	12.40	13.39	9.77	11.39	12.66	13.59	9.69	11.27	12.50	13.40
%AAD					3.9	1.6	3.0	4.4	9.3	6.4	3.3	1.5

6 | Thermodynamic Modelling of Mixtures at High Pressure using Aspen Plus®

Table 6-25 Phase transition pressures of the CO₂ + (25 % n-decane + 25 % 1-decanol + 25 % 3,7-dimethyl-1-octanol + 25 % 2,6-dimethyl-2-octanol) system as predicted by the RK-ASPEN model

Mass fraction solute (g/g)	Phase transition pressure (MPa)											
	Experimental				RK-ASPEN with polar parameters and binary solvent-solute parameters				RK-ASPEN with polar parameters, solvent-solute parameters and solute-solute parameters			
	Temperature (K)											
	318	328	338	348	318	328	338	348	318	328	338	348
0.637	7.26	8.21	9.17	10.12	7.23	8.44	9.69	10.94	6.70	7.81	8.95	10.10
0.559	8.11	9.34	10.58	11.81	8.06	9.53	11.05	12.55	7.48	8.80	10.16	11.53
0.467	8.70	10.22	11.74	13.26	8.80	10.62	12.47	14.24	8.19	9.75	11.38	12.99
0.388	9.13	10.84	12.56	14.27	9.27	11.47	13.55	15.46	8.62	10.39	12.24	14.03
0.291	9.48	11.33	13.19	15.04	-	12.39	14.56	16.53	8.98	10.99	13.06	14.99
0.226	9.95	11.73	13.51	15.29	-	-	-	16.62	9.12	11.28	13.44	15.38
0.177	10.27	12.03	13.79	15.55	-	-	14.82	16.73	9.20	-	-	-
0.115	10.28	12.04	13.80	15.56	-	12.37	14.39	16.16	-	11.51	13.50	15.24
0.076	9.92	11.84	13.51	14.93	9.85	11.99	13.85	15.43	9.33	11.42	13.23	14.7458
0.050	9.81	11.61	13.11	14.31	9.68	11.64	13.29	14.64	9.36	11.25	12.83	14.10
0.0283	9.53	11.12	12.48	13.59	9.52	11.18	12.51	13.52	9.35	10.93	12.18	13.10
0.0189	9.47	10.89	12.08	13.04	9.41	10.85	11.95	12.71	9.29	10.64	11.65	12.31
%AAD					0.8	2.9	4.7	5.7	5.9	3.8	2.3	1.9

The %AAD values reported in Table 6-24 and Table 6-25 indicate that the inclusion of solute-solute interaction parameters in the RK-ASPEN model does not significantly improve the accuracy of the predicted phase transition pressures of Mixture 1 and Mixture 2 within the temperature range 318 – 348 K. The accuracy of the RK-ASPEN model predictions decreases at lower temperatures due to the exclusion of the lower temperature range in the optimization procedure for the solute-solute interaction parameters. In Figure 6-29 and Figure 6-30 the RK-ASPEN model predictions for three cases are shown: firstly, as an entirely predictive model; secondly, with the inclusion of polar and binary solute-solvent interaction parameters; and thirdly, with the inclusion of polar, binary solute-solvent and binary solute-solute interaction parameters.

6 | Thermodynamic Modelling of Mixtures at High Pressure
using Aspen Plus®

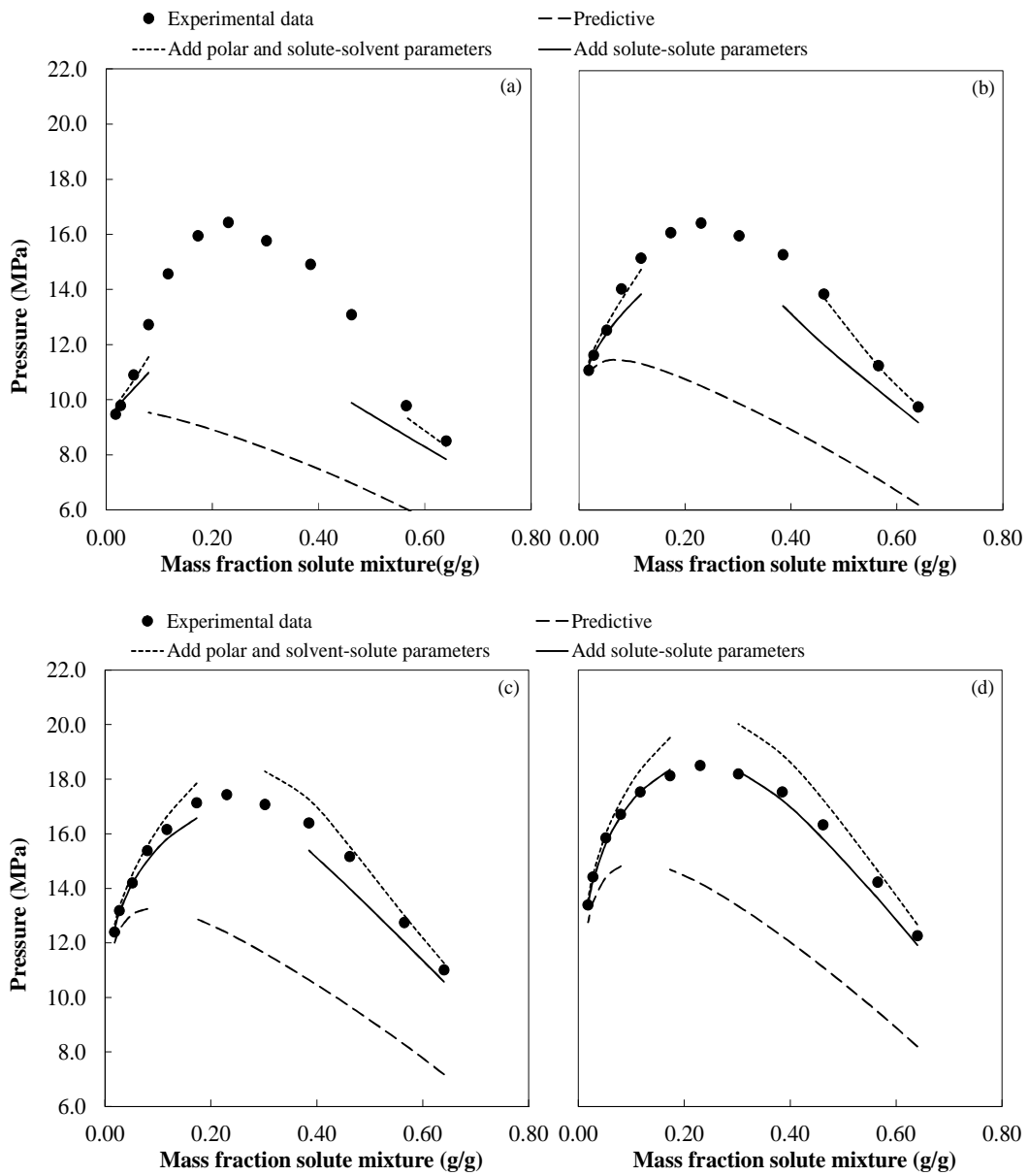


Figure 6-29 Comparison between the effects caused by the inclusion of different parameters in the RK-ASPEN model for the $\text{CO}_2 + (20\% \text{ n-dodecane} + 70\% \text{ 1-decanol} + 10\% \text{ 3,7-dimethyl-1-octanol})$ system at (a) 318 K, (b) 328 K, (c) 338 K and (d) 348 K

6 | Thermodynamic Modelling of Mixtures at High Pressure using Aspen Plus®

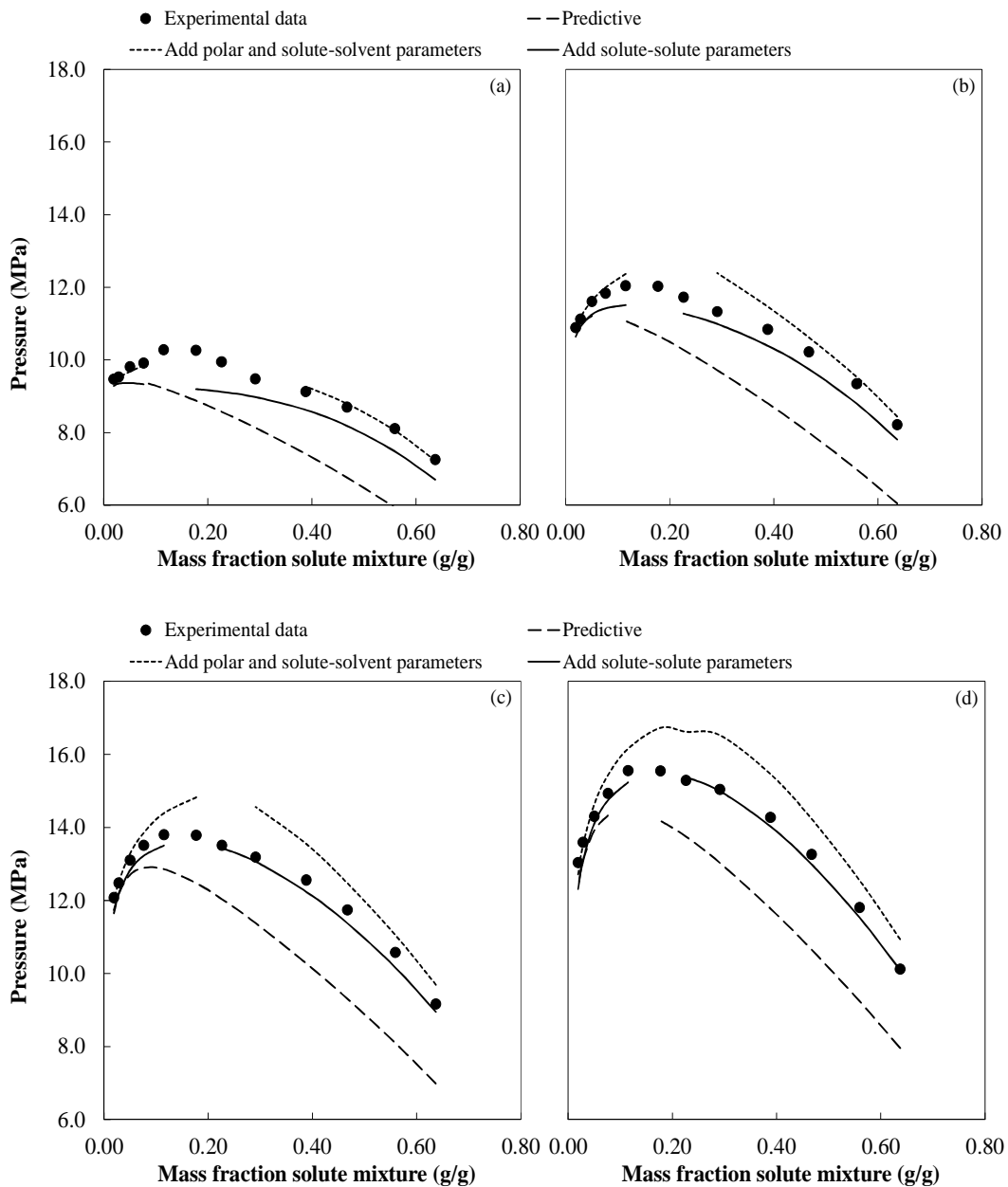


Figure 6-30 Comparison between the effects caused by the inclusion of different parameters in the RK-ASPEN model for the $\text{CO}_2 + (25\% \text{ n-decane} + 25\% \text{ 1-decanol} + 25\% \text{ 3,7-dimethyl-1-octanol} + 25\% \text{ 2,6-dimethyl-2-octanol})$ system at (a) 318 K, (b) 328 K, (c) 338 K and (d) 348 K

From Figure 6-29 and Figure 6-30 it is clear that the RK-ASPEN model without any parameters cannot predict accurate data for mixtures of detergent range alkanes and alcohols with supercritical CO_2 in the temperature range 318 – 348 K. Although the dew point pressures approaches the

6 | Thermodynamic Modelling of Mixtures at High Pressure using Aspen Plus®

experimentally measured values, bubble point pressures are poorly predicted for Mixture 1 and Mixture 2.

As a first attempt to modify the RK-ASPEN model to better represent the specific type of phase behaviour encountered in this investigation, pure component polar parameters and binary solute-solvent interaction parameters were determined and incorporated into the RK-ASPEN model. The phase transition pressure predictions for Mixture 1 and Mixture 2 with the inclusion of the pure component polar parameters and binary solute-solvent interaction parameters are also shown in Figure 6-29 and Figure 6-30. It is clear that the inclusion of these parameters lead to significant improvements in the predicted phase transition pressures. The RK-ASPEN model with the inclusion of polar and binary solute-solvent interaction parameters, predict phase transition curves that have a similar shape to those determined from experimental bubble and dew point data, and only deviate significantly from the experimental data in the mixture critical region. This characteristic is a result of the data fitting process used to determine the binary solute-solvent interaction parameters.

The effect of the inclusion of binary solute-solute parameters can also be seen from the trends plotted in Figure 6-29 and Figure 6-30. Very accurate data are predicted with the inclusion of the binary solute-solute interaction parameters, especially at the higher temperatures where these parameters were determined. The binary solute-solvent interaction parameters were much more sensitive to extrapolation to lower temperatures, compared to the binary solute-solute interaction parameters. At 318 K and 328 K the RK-ASPEN model without the binary solute-solute interaction parameters provided slightly better phase transition predictions. The true effect of the inclusion of the solute-solute interaction parameters in the RK-ASPEN model will be eminent in the prediction of the phase compositions (addressed in the next chapter).

6.6 Outcomes of this Chapter

The aim of this chapter is to establish an accurate thermodynamic model, aimed at the prediction of phase equilibrium data for mixtures of detergent range alkanes and alcohol isomers in supercritical CO₂ – Objective 6 in Chapter 1. The temperature range considered includes 318 K to 348 K. A number of evaluations were performed to determine which thermodynamic model in the Aspen Plus® software package, are best suited to the specific systems and temperature range

6 | Thermodynamic Modelling of Mixtures at High Pressure using Aspen Plus®

investigated. A number of thermodynamic models showed potential, but after their predictive abilities were tested on different levels, the RK-ASPEN model emerged as the best model to represent multi-component mixtures of detergent range alkanes and alcohol isomers within the temperature range considered. The RK-ASPEN model was modified to better represent the systems investigated, by including pure component polar parameters, binary solute-solvent interaction parameters and binary solute-solute interaction parameters. Although data fitting was used to determine these parameters, the robustness of the RK-ASPEN model still allows accurate extrapolation to other temperatures when the regressed polar and binary solute-solvent interaction parameters are included.

The key observations made in this chapter are:

- Cubic EoS with different combinations of mixing rules and alpha functions differ in their accuracy when predicting phase equilibrium data for binary mixtures of CO₂ and detergent range alkanes and alcohols. It is important to select the thermodynamic model that is able to best represent the type of systems investigated. The PR-BM, RKS-BM, RK-ASPEN and SR-POLAR models were the main models investigated in this investigation, since they have the option of additional parameters that can be included to aid in the representation of the phase behaviour of the specific systems considered in this work.
- The PR-BM, RKS-BM, RK-ASPEN and SR-POLAR models can accurately represent the phase transition pressures of binary mixtures of CO₂ + *n*-alkanes and CO₂ + alcohol isomers, when binary solute-solvent interaction parameters are employed.
- The binary interaction parameters determined at 338 K and 348 K can be employed to generate data of acceptable accuracy at 318 K and 328 K. The RKS-BM model showed exceptional robustness in the prediction of VLE data with binary interaction parameters determined outside of the temperature range investigated.
- The RK-ASPEN model has shown good predictive ability for the phase transition pressures of multi-component mixtures within the temperature range 318 – 348 K. This may be attributed to the inclusion of two types of regressed parameters, the pure component polar parameter and the binary solute-solvent interaction parameter.

6 | Thermodynamic Modelling of Mixtures at High Pressure using Aspen Plus®

- The inclusion of solute-solute interaction parameters increases the accuracy of the phase transition pressures predicted by the RK-ASPEN model for multi-component mixtures. However, an improvement in the predictive ability is only observed at the temperatures where the binary solute-solute interactions were determined. The binary solute-solute interactions are thus more sensitive to temperature extrapolation.
- The effect of the inclusion of the solute-solute interaction parameters in the RK-ASPEN model on the phase composition predictions of multi-component mixtures could not be tested since VLE data was not available for such mixtures. This effect is investigated in the following chapter.

In this chapter the RK-ASPEN model was selected and developed further in a number of ways to improve its ability to predict accurate phase transition pressures for multi-component mixtures of supercritical CO₂ and detergent range alkanes and alcohol isomers. It is recommended that the RK-ASPEN model with the inclusion of polar parameters and binary solute-solvent interaction parameters be employed in the proposed SFF process model reported on in the next chapter. The true effect of the inclusion of binary solute-solute interaction parameters on the accuracy of the phase composition predictions with the RK-ASPEN model, will also be determined.

6.7 Significant Contributions

The major contribution of the work presented in this chapter is the development (through selection and improvement) of a thermodynamic model from the Aspen Plus® database that can accurately predict phase transition pressures between 318 K and 348 K for multi-component mixtures of supercritical CO₂ and detergent range alkanes and alcohol isomers.

Some of the significant findings presented in this chapter were published in a peer-reviewed journal:

- M. Zamudio, C.E. Schwarz, J.H. Knoetze, Experimental measurement and modelling with Aspen Plus® of the phase behaviour of supercritical CO₂ + (*n*-dodecane + 1-decanol + 3,7-dimethyl-1-octanol), *The Journal of Supercritical Fluids*. 84 (2013) 132 - 145.

6.8 Nomenclature

Symbol/ Acronym	Description
AAD	Average absolute deviation
<i>a</i>	Energy parameter
<i>a</i>	Parameter used in pure component energy parameter
BWR-LS	Benedict-Webb-Rubin-Lee-Starling
BWRS	Benedict-Webb-Rubin-Starling
<i>b</i>	Co-volume parameter
<i>C</i>	Constants used vapour pressure correlations
<i>c</i>	Parameter used in alpha function
ς	Additional volume parameter in SR-POLAR property method
<i>d</i>	Parameter used in alpha function
EoS	Equation of State
<i>g</i>	Parameter used in volume calculation in SR-POLAR property method
<i>K</i>	Number of data points
<i>k</i>	Interaction parameter
LK-PLOCK	Lee-Kesler-Plöcker
LLE	Liquid-liquid equilibrium
<i>l</i>	Interaction parameters
<i>m</i>	Parameter used in alpha function
η	Polar parameter for the RK-ASPEN property method
<i>P</i>	Pressure
PC-SAFT	Perturbed Chain Statistical Association Fluid Theory
PR-BM	Peng-Robinson-Boston-Mathias
PRMHV2	Peng-Robinson with modified Huron-Vidal mixing rules
PRWS	Peng-Robinson with Wong-Sandler mixing rules
PSRK	Redlich-Kwong-Soave with Holderbaum-Gmehling mixing rules
<i>p</i>	Polar parameter for the SR-POLAR property method
<i>R</i>	Universal gas constant
RK-ASPEN	Redlich-Kwong-Soave with Mathias mixing rules
RKS-BM	Redlich-Kwong-Soave-Boston-Mathias

6 | Thermodynamic Modelling of Mixtures at High Pressure using Aspen Plus®

Symbol/ Acronym	Description
RKSMHV2	Redlich-Kwong-Soave with modified Huron-Vidal mixing rules
RKSWS	Redlich-Kwong-Soave with Wong-Sandler mixing rules
SAFT	Statistical Association Fluid Theory
SR-POLAR	Redlich-Kwong-Soave with Schwarzenuber-Renon mixing rules
<i>T</i>	Temperature
<i>V</i>	Volume
ω	Acentric factor
<i>x</i>	Liquid phase composition
<i>y</i>	Vapour phase composition
Z	Predicted value of a property
ZM	Measured value of a property

Sub/Superscripts	Description
<i>a</i>	Applicable to energy parameter
<i>b</i>	Applicable to volume parameter
<i>c</i>	Critical
<i>i</i>	Pure component <i>i</i>
<i>j</i>	Pure component <i>j</i>
<i>l</i>	Liquid
<i>m</i>	Molal
<i>n</i>	Counter
<i>P</i>	Pressure
<i>r</i>	Reduced
<i>T</i>	Temperature
<i>x</i>	Liquid phase
<i>y</i>	Vapour phase
*	Indicates vapour pressure

6.9 References

- [1] C.E. Schwarz, M.L. Hahn, A.J. de Villiers, J.H. Knoetze, Phase behaviour of high molecular mass methyl esters in supercritical ethane, *Fluid Phase Equilibria*. 311 (2011) 36 – 44.
- [2] E.C. Voutsas, G.D. Pappa, K. Magoulas, D.P. Tassios, Vapour liquid equilibrium modelling of alkane systems with Equations of State: “Simplicity versus complexity,” *Fluid Phase Equilibria*. 240 (2006) 127 – 139.
- [3] D.Y. Peng, D.B. Robinson, A new two-constant equation of state, *Industrial and Engineering Chemistry Fundamentals*. 15 (1976) 59 – 64.
- [4] G. Soave, Equilibrium constants from a modified Redlich-Kwong equation of state, *Chemical Engineering Science*. 27 (1972) 1197 – 1203.
- [5] J. F. Boston, P. M. Mathias, Phase equilibria in a third-generation process simulator, in: 2nd International Conference on Phase Equilibria and Fluid Properties in the Chemical Process Industries, Berlin, 1960.
- [6] Aspen Plus, AspenTech, 2000.
- [7] O. Redlich, N.S. Kwong, On the thermodynamics of solutions. V: An equation of state. Fugacities of gaseous solutions, *Chemical Reviews*. 44 (1949) 233.
- [8] P.M. Mathias, A versatile phase equilibrium equation of state, *Industrial & Engineering Chemistry Process Design and Development*. 22 (1983) 385 – 391.
- [9] J. Schwartzentruber, H. Renon, Extension of UNIFAC to high pressures and temperatures by the use of a cubic equation of state, *Industrial and Engineering Chemistry Research*. 28 (1989) 1055 – 1059.
- [10] B. E. Poling, J. M. Prausnitz, J. P. O’Connell, *The properties of gases and liquids*, 5th ed., McGraw-Hill Companies, Inc., United States of America, 2001.
- [11] AIChE, DIPPR Project 801, in: Design Institute for Physical Property Research, Knovel, 2012.

6 | Thermodynamic Modelling of Mixtures at High Pressure
using Aspen Plus®

- [12] C.L. Yaws, Yaws' thermophysical properties of chemicals and hydrocarbons (Electronic Edition), Knovel, 2010.
- [13] NIST Chemistry WebBook, (n.d.).
- [14] M. Castier, L. A. Galicia-Luna, S. I. Sandler, Modelling the high-pressure behaviour of binary mixtures of carbon dioxide+alkanols using an excess free energy mixing rule, *Brazilian Journal of Chemical Engineering*. 21 (2004) 659 – 666.
- [15] C.E. Schwarz, A.J. de Villiers, C.B. McClune, G.J.K. Bonthuys, A.J. Burger, J.H. Knoetze, High pressure phase equilibrium measurements of long chain alcohols in supercritical ethane, *The Journal of Supercritical Fluids*. 55 (2010) 554 – 565.

7. ESTABLISHING A SUPERCRITICAL FLUID FRACTIONATION MODEL

7.1 PROCESS SIMULATION SETUP	235
7.2 SFF PILOT PLANT DATA	237
7.2.1 Chemicals Used	237
7.2.2 Experimental Setup	237
7.2.2.1 Feed	237
7.2.2.2 Fractionation/Extraction	238
7.2.2.3 Separation.....	239
7.2.2.4 Solvent regeneration.....	240
7.2.2.5 Utilities	240
7.2.3 Factors that Require Special Attention.....	240
7.2.4 Accuracy of Measurements	242
7.2.4.1 Sensors.....	242
7.2.4.2 Fluctuations in the system.....	242
7.2.4.3 Sampling and GC Analysis	243
7.2.5 Discussion on the Pilot Plant Separation Performance Data.....	244
7.2.5.1 Effect of the Fractionation Temperature.....	247
7.2.5.2 Effect of the Fractionation Pressure.....	250
7.2.5.3 Effect of the Solvent-to-Feed Ratio	252
7.3 VALIDATION OF PROCESS SIMULATION MODEL	255
7.3.1 Factors that Require Special Attention.....	255
7.3.2 Generating Data with the Process Model	257

7 | Establishing a Supercritical Fluid Fractionation Model

7.3.2.1	<i>The Effect of Solute-Solute Interaction Parameters.....</i>	257
7.3.2.2	<i>Effect of the Number of Stages.....</i>	259
7.3.2.3	<i>Comparison between Simulated and Experimental Data.....</i>	262
7.5	PREDICTING THE SEPARATION PERFORMANCE AT OTHER CONDITIONS	267
7.5.1	Investigating Other Fractionation Conditions	267
7.5.1.1	<i>Temperature.....</i>	267
7.5.1.2	<i>Pressure</i>	270
7.5.1.3	<i>Solvent-to-feed Ratio.....</i>	273
7.5.2	Investigating Other Feed Mixtures	276
7.5.2.1	<i>Temperature.....</i>	277
7.5.2.2	<i>Pressure</i>	279
7.5.2.3	<i>Solvent-to-feed Ratio.....</i>	282
7.5.3	The Operating Window for the Proposed SFF Process.....	284
7.6	SEPARATION PERFORMANCE COMPARISON TO AZEOTROPIC DISTILLATION	285
7.7	OUTCOMES OF THIS CHAPTER	287
7.8	SIGNIFICANT CONTRIBUTIONS.....	289
7.9	NOMENCLATURE.....	290
7.10	REFERENCES.....	290

7 | Establishing a Supercritical Fluid Fractionation Model

In Objective 7, as discussed in Chapter 1, the aim of this chapter is stated as follows: to establish a working SFF process model in Aspen Plus[®] that can accurately predict the separation performance of process aimed at the removal of alkanes from a mixture of alcohol isomers (within the detergent range) utilizing supercritical CO₂ as the solvent. The process model will be established in Aspen Plus[®] and will contain the thermodynamic model developed in Chapter 6. Verification of the developed process model will be done by comparing the predicted separation performance data with experimental SFF pilot plant data.

This chapter thus reports on a methodology used to set up an accurate SFF model in Aspen Plus[®]. At the end of the chapter the verified model is used to predict the separation performance of an SFF process utilizing model mixtures of components typically encountered in the detergent and surfactant industries. The process model's ability to generate important process data, like yield and selectivity, was used to reach Objective 8, where the feasibility of a separation process with two different feed mixtures was determined.

7.1 Process Simulation Setup

The flowsheet function in Aspen Plus[®] was used to build a model consisting of the typical main units required in an SFF process – a fractionation column, a pressure reduction valve and a separator, with connecting material streams (see Figure 7-1).

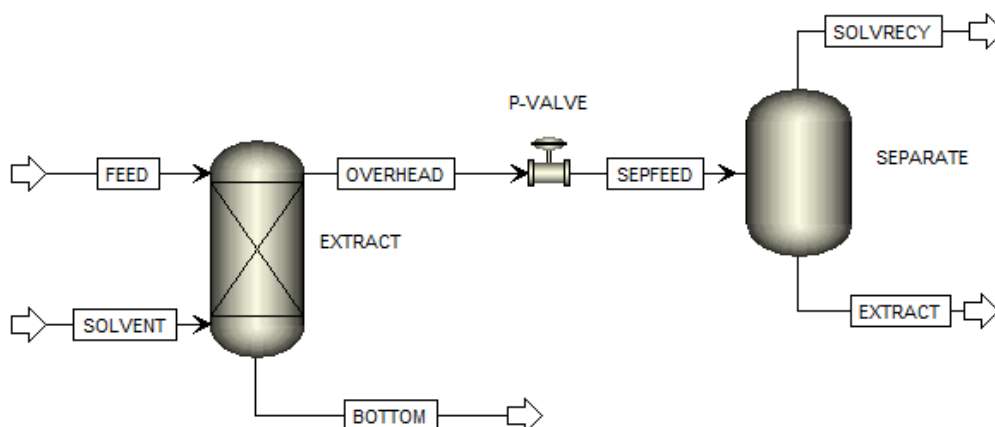


Figure 7-1 Process flow sheet used in the SFF process simulation

7 | Establishing a Supercritical Fluid Fractionation Model

The fractionation column was represented by the liquid-liquid extraction column model (“EXTRACT”). The “EXTRACT” model operates like a module of flash drums, but employs a streamlined algorithm to solve the mathematical equations. The feed stream, consisting of a heavy liquid phase containing detergent range alkanes and alcohols, enters at the top of the column and flows counter-currently to the light supercritical CO₂ stream that enters at the bottom of the column. Each stage of the “EXTRACT” column acts as an equilibrium stage. The “EXTRACT” model that was selected for the fractionation column did not allow for design calculations, and thus the number of stages had to be specified. More details on the determination of the number of stages are presented in section 7.3.2.2.

The overheads product stream contains the loaded solvent which is sent to the separator to release the extracted compounds. The pressure reduction valve allows the separator to operate at a lower pressure than that attained in the fractionation column. A lower operating pressure should lead to reduced solubility of the compounds in the supercritical solvent and precipitation of the extract product in the separator vessel.

The separator was modelled as a two-outlet flash drum (“FLASH2”). The operating temperature of the separator is typically 10 K higher than the operating temperature of the fractionation column, to allow the solubility of the extracted compounds to decrease. The operating pressure in the separator is equal to the vapour pressure of the solvent at the ambient temperature – typically 5.0 MPa for CO₂ at the ambient conditions encountered for the duration of this project. By allowing the separator to operate at the solvent vapour pressure a liquid pump, instead of a compressor, can be used to pressurize the solvent before it enters the fractionation column again. The solvent that exits the separator is generally recycled back to the fractionation column where it can be utilized again. The solvent recycle loop consists of a number of units – a condenser, compressor, heat exchanger, etc., and must be designed to operate effectively [1]. The solvent recycle loop was excluded from the process model due to difficulties encountered in the convergence of the simulation, but can be included manually by allowing the solvent stream to the fractionation column to attain the same composition as that of the solvent recycle stream that exits the separator vessel.

The thermodynamic model employed in all the units of the process model, is the RK-ASPEN model with the parameters developed in Chapter 6.

7.2 SFF Pilot Plant Data

SFF pilot plant data is required to verify the process model built in Aspen Plus[®]. In this section details regarding the experimental equipment and procedure to generate the verification data, is provided.

7.2.1 Chemicals Used

A feed mixture containing 25 mass% each of *n*-decane, 1-decanol, 3,7-dimethyl-1-octanol and 2,6-dimethyl-2-octanol (referred to as Mixture 2 in Chapter 5 and 6) was used in the SFF experimental runs. CO₂ was selected as the solvent and was obtained from Afrox at a purity of 99.9%. The suppliers, catalogue numbers, CAS numbers and respective purities of the compounds used in the feed mixture, are given in Table 7-1.

Table 7-1 Chemicals used for SFF pilot plant performance measurements

Solute	Supplier	CAS number	Catalogue no.	Purity (mass%)
1-Decanol	SAFC	112-30-1	W23,650-0-K	≥ 98
3,7-Dimethyl-1-octanol	SAFC	106-21-8	W23,910-0-K	≥ 98
2,6-Dimethyl-2-octanol	SAFC	18479-57-7	W51,650-3	95
<i>n</i> -Decane	Sigma	124-18-5	457116	≥ 99

7.2.2 Experimental Setup

A schematic of the experimental pilot plant setup is given in Figure 7-1.

7.2.2.1 Feed

The feed vessel (E-101) is an 8 litre open top stainless steel vessel with a copper coil on the inside, through which heating fluid is circulated. The feed mixture flows downwards to the feed pump (P-101) inlet. The feed pump is a variable stroke length diaphragm pump with a maximum rating of 2 litre/hour at 26.0 MPa. The discharge side of the pump is connected to two possible outlets. If V-9 is open (and V-10 closed), the feed is pumped to the top of the column, and if V-10 is open (and V-9 closed) the feed enters the column in the middle. There are two valves located at the

7 | Establishing a Supercritical Fluid Fractionation Model

bottom of the feed lines, V-15 and V-11, which can be used to drain the feed lines and feed vessel after an experimental run.

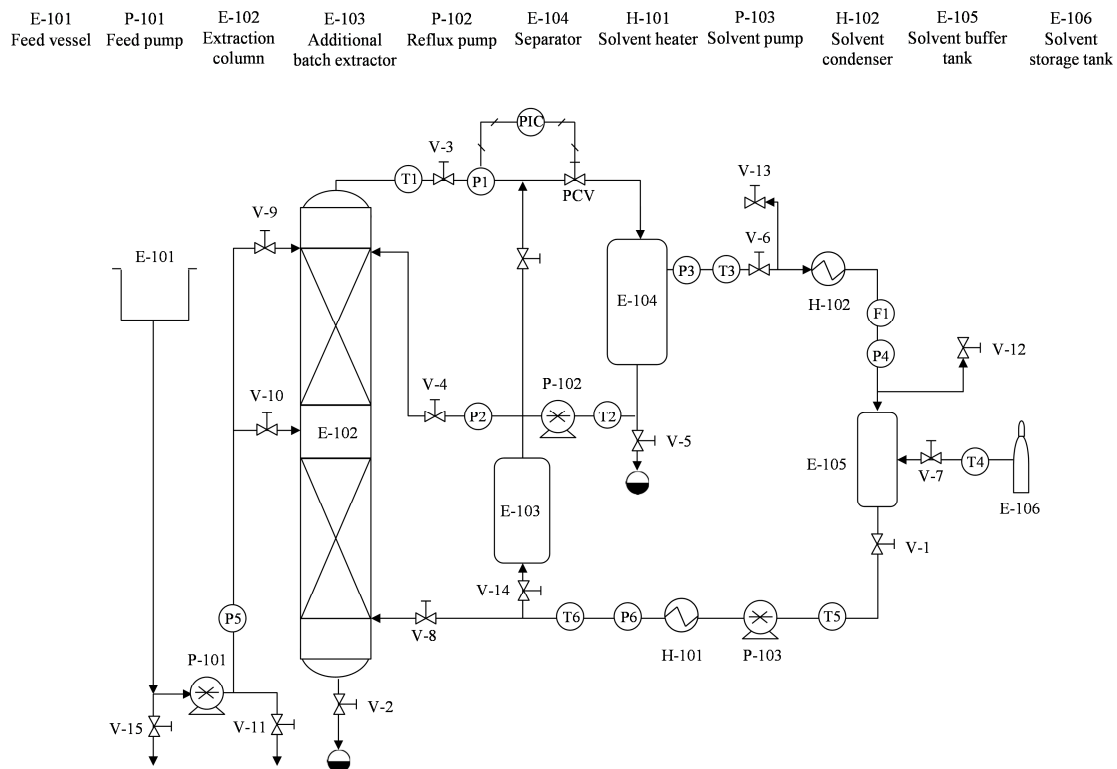


Figure 7-2 Process flow diagram of the SFF pilot plant setup

7.2.2.2 Fractionation/Extraction

In the fractionation column (E-102) the solvent flows counter current to the feed mixture and selectively dissolves certain compounds. The column is 0.028 m in diameter and consists of two 2.16 m high sections of Sulzer DX packing. Sulzer DX packing is a gauze type structured packing woven from stainless steel wire. The specifications of Sulzer DX structured packing are given in Table 7-2.

The column has a maximum operating pressure of 30.0 MPa and maximum operating temperature of 420 K. The column is jacketed and heated with circulating fluid. The solute feed mixture enters the column, either at the top or in the middle. The feed line protrudes to the centre of the column, providing a single drip point. Crause [2] showed that this is sufficient for a column of this diameter, to wet the entire packing section. At the bottom of the column there is a sight glass to

7 | Establishing a Supercritical Fluid Fractionation Model

allow one to observe the liquid level of the bottoms product that accumulates here. The bottoms product can be removed through V-2.

Table 7-2 Geometrics of Sulzer DX packing

Geometric information	Value
Crimp height (mm)	3
Channel base (mm)	6.5
Channel side (mm)	4.4
Surface area (not including column wall area of 140 m ² /m ³) (m ² /m ³)	900
Void fraction (%)	77
Channel angle with horizontal (°)	60

The pilot plant setup can also be operated in batch mode, usually for the extraction of compounds from solid feed matrices. The batch extractor vessel (E-103) is then used, instead of the fractionation column. No details are provided for operation in this mode since it will not be implemented during this investigation.

7.2.2.3 Separation

When the solvent, loaded with extracted compounds, exits the fractionation column it expands over a pressure control valve (PCV), and flows into the separator vessel (E-104). The separator is operated at the solvent vapour pressure in the solvent storage tank (E-106) (which varies slightly with ambient temperature). The separator is equipped with Goodloe knitted packing at the top, which acts as a demister device to aid in the coagulation and droplet formation of the extracted compounds. The separator vessel is also equipped with a sight glass to allow the manual monitoring of the extract product liquid level. The extract product can be withdrawn through V-5. The separator vessel is kept at a temperature slightly higher than the operating temperature of the column with a jacket that holds circulating heating fluid.

If reflux is employed, a fraction of the extracted product is pumped back to the top of the column. The reflux pump (P-102) is a double diaphragm pump with an adjustable stroke length. The maximum capacity of the pump is 8 litres/hour and the maximum discharge pressure is 30.0 MPa. Reflux was not utilized during this investigation.

7.2.2.4 Solvent regeneration

The solvent that exits the separator is condensed in a heat exchanger (H-102) and flows through a mass flow meter (F1) into the solvent buffer vessel (E-105). The solvent condenser consists of two sections, one cooled by cooling water, and the other with chilled propylene glycol water. The solvent condenser and buffer vessel operates at the solvent vapour pressure. The buffer vessel feeds the solvent pump (P-103) and is cooled down to ensure that the solvent provides enough head to the pump. Additional solvent is fed to the buffer vessel from the solvent storage tank (E-106). The solvent pump is a variable stroke length diaphragm pump with a maximum rating of 29 litres/hour at 26.0 MPa. On the discharge side of the solvent pump, the solvent is heated with a heat exchanger (H-101) to reach the column operating temperature. The solvent enters the fractionation column at the bottom, flows upward, exits at the top, unloads extracted solutes in the separator, and then goes through the entire regeneration cycle again.

Most of the solvent is recycled during an experimental run, but there are some losses to the atmosphere when the extract and bottoms products are withdrawn periodically. By keeping the feed line from the solvent storage tank to the solvent buffer tank open during operation, the lost solvent is replaced in the system.

7.2.2.5 Utilities

Two heaters provided the heating fluid to heat up the vessels and pipelines. The heating fluid circulates through copper trace heating lines, as well as through the heating jackets of the fractionation column and separator vessel. One heater was mainly used to heat up the column, while the other heater was usually set to a slightly higher temperature and used to heat up the feed vessel, solvent inlet to the column and the separator vessel.

An industrial water chiller was used to supply chilled water (with propylene glycol) to the solvent condenser and buffer vessel. It was also used to trace the line that feeds the solvent pump. This was done to prevent vapourisation in the line, which can lead to cavitation in the pump.

7.2.3 Factors that Require Special Attention

Operating procedures for the SFF pilot plant is provided in Appendix E. A few important factors, identified during the operation of the SFF pilot plant, are discussed below:

7 | Establishing a Supercritical Fluid Fractionation Model

- To ensure that the solute feed flow rate and solvent flow rate are constant during the experimental run, the respective pumps must be set at a certain stroke length. The stroke length setting of the feed pump was easy to maintain, but the stroke length setting of the solvent pump kept adjusting itself due to the vibration of the solvent feed pump. A temporary solution to this problem was a wire locking mechanism to maintain the stroke length adjustment knob in one position for the duration of the experimental run. An alternative solution to the problem would be to mount the solvent pump on a material that absorbs the vibration more efficiently than the rubber pads currently in use.
- The solvent feed pump is fed by the solvent in the solvent buffer vessel located at a certain height to provide sufficient head to the pump. The buffer vessel, solvent feed line and solvent pump intake are cooled by trace cooling lines. The cooling lines contain chilled water at approximately 4 °C, to keep the CO₂ in the liquid phase as it is being pumped. However, during operation the solvent pump heats up and the liquid CO₂ that enters the solvent feed pump partially vapourises causing cavitation. To avoid cavitation, the CO₂ at the pump inlet must be cooled to temperatures lower than 4°C. The water chiller was thus replaced with a refrigeration unit that can run at temperatures below 0°C.
- The pilot plant setup was originally designed to fractionate paraffin waxes with a very low solubility in the supercritical solvent at the separator conditions. The compounds fractionated in this project, is still partially soluble in the supercritical solvent at the separator conditions and thus the solvent that exits the separator still contains a very low concentration of solutes. These solutes stay in the solvent stream as it moves through the condenser. If the solute has a melting temperature above 0°C, it will solidify in the condenser and cause blockages. Because the solutes are present in such minute concentrations in the solvent stream the blockages are caused by the slow build-up of solutes over time. The solutes that do not precipitate in the condenser are recycled back to the fractionation column where it can cause deviations in the equilibrium conditions. A possible solution to the problem would be to operate the separator at much lower pressures to further decrease the solubility of the compounds in the supercritical solvent. Currently the separator operates at approximately 5.0 MPa for CO₂. Major adjustments to the current setup would be necessary to allow the

separator to operate at atmospheric pressure, since a compressor will be required to compress the solvent to 5.0 MPa before it can enter the solvent regeneration cycle again.

7.2.4 Accuracy of Measurements

7.2.4.1 Sensors

Five temperatures and four pressures were constantly monitored. The sensors are numbered as indicated in Figure 7-2. The accuracies of the temperature and pressure measurements are as follows [3]:

- T1, T5 and T6 are measured with an accuracy of 0.4 K.
- T3 and T5 are measured with an accuracy of 0.5 K.
- P1 is measured with an accuracy of 0.1 MPa.
- P3, P4 and P6 are measured with an accuracy of 0.2 MPa.

The solvent mass flow rate was monitored with a mass flow meter located in the solvent line. This mass flow meter measures the solvent flow rate with an accuracy of 3% [3].

7.2.4.2 Fluctuations in the system

During operation some of the parameters may fluctuate. It is important to know the magnitude of what is considered an insignificant fluctuation. Fluctuations of the following magnitudes did not influence the results of a single run significantly:

- During an experimental run the temperature may fluctuate within 1 K from the intended value.
- Pressure fluctuations of 0.1 MPa were found to be acceptable. These pressure fluctuations were short in duration, and usually occurred after product sampling.
- Fluctuations of up to 1% of the solvent flow rate did not influence the process performance.

At times when fluctuations were observed in the system with values greater than those mentioned above, a significant difference in the amount of extract and bottoms product collected in the 20 minute interval that followed the fluctuation, were observed. The values determined in the abovementioned list were thus determined from failed experimental runs, where the system fluctuated in such a manner that steady amounts of extract and bottoms products could not be collected in subsequent intervals.

7.2.4.3 Sampling and GC Analysis

The mass flow rates of the feed, extracted product and bottoms product were measured manually. The bottoms and extracted products were collected in Erlenmeyer flasks and weighed in 20 min intervals. The combined mass flow rate of the extracted and bottoms products were assumed to be mass flow rate of the feed mixture to the column, i.e. no accumulation or loss of the feed mixture occurs at any point in the process. Samples of the feed mixture, extract product and bottoms product were collected and analysed with gas chromatography.

The analyses were performed on a Varian 3400 gas chromatograph equipped with a 60 m long Phenomenex Zebron ZB-5 column with an inside diameter of 0.32 mm, 0.25 μm packing and a FID detector. Results from duplicate diluted samples showed an error of less than 1 % in the mass of solute.

Samples were diluted with methanol, and *1*-octanol was used as the internal standard. In Table 7-3 the temperature program and retention times of the components are shown.

The measured mass flow rates and mass fraction solutes as determined from the GC analysis were used to do a mass balance on the feed, extract product and bottoms product streams. The error in the mass flow rate of each solute was typically 4 %, with the maximum error in one experimental run being 9 %.

7 | Establishing a Supercritical Fluid Fractionation Model

Table 7-3 GC program used for sample analysis

Parameter	Value
Initial temperature (°C)	50
Holding time at initial temperature (min)	10
Temperature rate (°C/min)	10
Final temperature (°C)	250
Injector temperature (°C)	220
Detector temperature (°C)	250
Column flow (psi)	10
Split ratio	70:1
Injection volume (μ l)	0.1
Retention time (min):	
methanol	6.6
<i>n</i> -decane	18.3
1-octanol	20.0
2,6-dimethyl-2-octanol	20.5
3,7-dimethyl-1-octanol	22.5
1-decanol	24.0

7.2.5 Discussion on the Pilot Plant Separation Performance Data

Six experimental runs were conducted on the SFF pilot plant setup. The feed mixture, consisting of 25 mass % each *n*-decane, 1-decanol, 3,7-dimethyl-1-octanol and 2,6-dimethyl-2-octanol (Mixture 2), was fractionated into two streams using supercritical CO₂. Different fractionation temperatures and pressures, and solvent-to-feed ratios were investigated and the resultant product stream compositions are shown in Table 7-4.

7 | Establishing a Supercritical Fluid Fractionation Model

Table 7-4 Experimental results for the SFF pilot plant runs

	Run 1	Run 2	Run 3	Run 4	Run 5	Run 6
Solvent	CO ₂	CO ₂	CO ₂	CO ₂	CO ₂	CO ₂
T1 (K)	315.9	316.7	315.4	344.5	344.1	344.5
T3 (K)	328.9	326.9	329.3	343.2	344.5	345.4
T4 (K)	287.4	287.3	283.7	286.9	285.5	286.9
T5 (K)	277.1	276.2	276.6	276.8	275.7	276.4
T6 (K)	313.1	314.4	312.4	343.7	343.2	343.9
P1 (MPa)	9.00	9.30	9.00	13.00	13.60	13.10
P3 (MPa)	5.00	5.00	4.60	5.00	5.00	5.10
P4 (MPa)	4.90	4.90	4.50	4.90	4.80	5.00
P6 (MPa)	8.90	9.20	8.90	12.80	13.20	12.80
Solvent flow rate (kg/h)	15.2	14.9	14.3	15.0	14.4	14.6
Feed flow rate (kg/h)	0.839	0.839	0.482	0.808	0.772	0.499
Solvent/Feed Ratio	18.1	17.8	29.7	18.6	18.7	29.3
Extract flow rate (kg/h)	0.434	0.565	0.319	0.435	0.536	0.356
Bottoms flow rate (kg/h)	0.404	0.274	0.163	0.372	0.236	0.142
Extract / Feed Ratio	0.52	0.67	0.66	0.54	0.69	0.71
% <i>I</i>-decanol in feed	27.1	27.1	26.9	28.5	26.1	27.2
% <i>I</i>-decanol in overheads	14.6	16.0	14.5	16.6	15.2	17.2
% <i>I</i>-decanol in bottoms	43.3	51.7	52.7	44.6	51.5	56.0
% <i>n</i>-decane in feed	28.5	28.0	26.4	26.9	27.8	27.7
% <i>n</i>-decane in overheads	47.4	39.7	37.6	42.0	38.8	34.8
% <i>n</i>-decane in bottoms	4.6	3.0	3.5	7.0	5.3	5.8
% 3,7-dimethyl-<i>I</i>-octanol in feed	23.4	23.6	23.7	23.2	22.9	22.9
% 3,7-dimethyl-<i>I</i>-octanol in overheads	15.5	17.3	17.2	16.8	17.4	19.2
% 3,7-dimethyl-<i>I</i>-octanol in bottoms	33.1	37.2	40.0	31.2	38.4	32.7
% 2,6-dimethyl-2-octanol in feed	21.0	21.3	23.0	21.3	23.2	22.3
% 2,6-dimethyl-2-octanol in overheads	22.5	27.0	30.7	24.7	28.6	28.8
% 2,6-dimethyl-2-octanol in bottoms	19.0	8.1	3.8	17.2	4.8	5.6
Selectivity for : <i>I</i>-decanol	0.34	0.31	0.27	0.37	0.30	0.31
<i>n</i>-decane	10.29	13.38	10.83	6.00	7.36	6.01
3,7-dimethyl-<i>I</i>-octanol	0.47	0.47	0.43	0.54	0.45	0.59
2,6-dimethyl-2-octanol	1.18	3.34	8.07	1.44	5.98	5.17
Selectivity Ratio	0.19	0.31	0.81	0.39	0.91	1.01
Recovery (%)	64.2	41.3	44.3	58.7	40.1	37.1

7 | Establishing a Supercritical Fluid Fractionation Model

The separation performance of the SFF process will be evaluated according to five parameters (defined in Chapter 3): the extract-to-feed ratio, the solvent-to-feed ratio, the component selectivity, the selectivity ratio and the recovery. The important equations are repeated below for ease of reference, but a detailed definition of each parameter can be found in section 3.3.3 of Chapter 3.

$$\frac{E}{F} = \frac{\dot{m}_{extract}}{\dot{m}_{feed}} \quad \text{Eq. 3-3}$$

$$\frac{S}{F} = \frac{\dot{m}_{solvent}}{\dot{m}_{feed}} \quad \text{Eq. 3-4}$$

$$S_i = \frac{Y_{i,extract}}{X_{i,bottoms}} \quad \text{Eq. 3-5}$$

$$SR = \frac{\sum S_{i,desired}}{\sum S_{i,undesired}} \quad \text{Eq. 3-6}$$

$$\% R_{product\ stream} = \frac{(\sum \dot{m}_{i,desired})_{product\ stream}}{(\sum \dot{m}_{i,desired})_{feed}} \times 100 \quad \text{Eq. 3-7}$$

As discussed in Chapter 2, the aim of the separation process is to remove the alkanes from the alcohol isomer mixture, i.e. to remove the *n*-decane from the mixture of C₁₀-alcohol isomers. Since this process is intended to be implemented as a downstream refining process in the alcohol production line, the mixture of alcohols generated from this process is regarded as the main product. The alkanes removed from the feed mixture are a by-product that can be further processed or used in other applications.

From the binary phase equilibrium data provided in Chapter 5, *n*-decane is more soluble in supercritical CO₂ than the alcohol isomers present in the mixture considered. Consequently the majority of the *n*-decane is expected to report to the overheads stream and be removed from the process in the extract product stream, while the majority of the alcohol isomers should report to the bottoms stream. The bottoms product stream thus contain the components considered as the main products, and will from hereon be referred to as the main product stream. Based on the definition of the main product stream, *n*-decane is considered the undesired component and the alcohol isomers are considered the desired components.

7 | Establishing a Supercritical Fluid Fractionation Model

From the definitions given in Equations 3-3 to 3-7, it can be reasoned that the optimum operating conditions will lead to the combination of the lowest selectivity ratio and the highest recovery. The lowest *SR* value for the bottoms product stream can be achieved from a low selectivity of the desired components (C_{10} -alcohol isomers) and high selectivity of the undesired components (*n*-decane). Therefore, the best separation performance will be achieved when the solvent can be manipulated to remove as much of the *n*-decane from the feed mixture, without removing too much of the alcohol isomers.

The results in Table 7-4 indicate that the best separation performance of the SFF process aimed at removing the maximum amount of *n*-decane from a mixture of C_{10} -alcohol isomers occurs at Run 1 for the low temperature runs and Run 4 for the high temperature runs. This indicates that at the specific operating temperature, a lower fractionation pressure and lower solvent-to-feed ratio will lead to better separation.

7.2.5.1 Effect of the Fractionation Temperature

Run 1 was conducted at a lower temperature compared to Run 4, and both resulted in approximately the same extract-to-feed ratio. The effect of temperature can thus be isolated by comparing these two runs.

The selectivity ratio of Run 1 is lower than the selectivity ratio of Run 4, and the recovery is higher in Run 1 compared to Run 4, thus indicating that the process performed better at the operating conditions selected for Run 1. From Figure 7-3 it is clear that the largest difference in selectivity occurred for *n*-decane, with all the other components having only slightly higher values of selectivity at the high temperature. At the low operating temperature of 315.9 K, *n*-decane is more soluble compared to the other components in the supercritical CO_2 . As the temperature increases to 344.5 K, the solubility of the C_{10} -alcohols relative to that of *n*-decane increases, allowing a larger fraction of C_{10} -alcohols to report to the overheads product.

7 | Establishing a Supercritical Fluid Fractionation Model

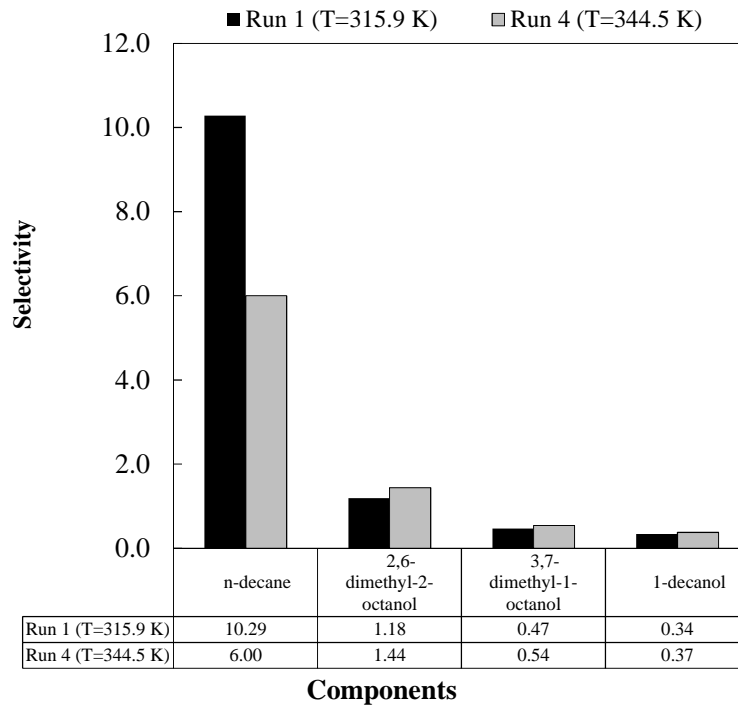


Figure 7-3 Comparison between the selectivity of the components in Run 1 and Run 4

It is important to note that the amount of *n*-decane that exit in the overheads stream stays approximately the same for Run 1 and Run 4, but the fraction of *n*-decane in the overheads stream, and consequently extract product stream, decreases as the temperature is increased. This statement is illustrated at the hand of the calculations that follow:

Mass flow rate of *n*-decane in the feed stream:

$$\text{Run 1: } m_{\text{feed}} \times (x_{n\text{-decane}})_{\text{feed}} = 0.839 \times \left(\frac{28.5}{100}\right) = 0.239 \text{ kg/h}$$

$$\text{Run 4: } m_{\text{feed}} \times (x_{n\text{-decane}})_{\text{feed}} = 0.808 \times \left(\frac{26.9}{100}\right) = 0.217 \text{ kg/h}$$

Mass flow rate of *n*-decane in the extract product stream:

$$\text{Run 1: } m_{\text{extract}} \times (x_{n\text{-decane}})_{\text{overheads}} = 0.434 \times \left(\frac{47.4}{100}\right) = 0.206 \text{ kg/h}$$

7 | Establishing a Supercritical Fluid Fractionation Model

$$\text{Run 4: } m_{\text{extract}} \times (x_{n\text{-decane}})_{\text{overheads}} = 0.435 \times \left(\frac{42.0}{100}\right) = 0.183 \text{ kg/h}$$

Percentage of the total amount of *n*-decane available in the feed stream, that exits in the extract stream:

$$\text{Run 1: } \frac{(\dot{m}_{n\text{-decane}})_{\text{extract}}}{(\dot{m}_{n\text{-decane}})_{\text{feed}}} \times 100 = \frac{0.206}{0.239} \times 100 = 86.2 \%$$

$$\text{Run 4: } \frac{(\dot{m}_{n\text{-decane}})_{\text{extract}}}{(\dot{m}_{n\text{-decane}})_{\text{feed}}} \times 100 = \frac{0.183}{0.217} \times 100 = 84.3 \%$$

Taking into account the maximum error of 9 % in the mass flow rate of the components in the product stream, the two runs produce extract streams that contain similar amounts of *n*-decane.

The same calculations were performed for all the other components and a comparison between Run 1 and Run 4 is provided in Table 7-5. From the results it is clear that an increase in operating temperature causes more of the alcohols, especially the branched alcohol isomers, to become soluble in the supercritical CO₂, and consequently report to the extract product.

Table 7-5 Comparison between the mass % of total available solute that reports to the extract product stream during Run 1 and Run 4

	$(\dot{m}_i)_{\text{feed}}$		$(\dot{m}_i)_{\text{extract}}$		% of total mass reporting to extract product	
	Run 1	Run 4	Run 1	Run 4	Run 1	Run 4
<i>n</i>-decane	0.239	0.217	0.206	0.183	86.2	84.3
2,6-dimethyl-2-octanol	0.176	0.172	0.098	0.107	55.6	62.2
3,7-dimethyl-1-octanol	0.196	0.187	0.067	0.073	34.2	39.0
1-decanol	0.227	0.230	0.063	0.072	27.8	31.3

For the type of compounds investigated in this project, a lower operating temperature leads to better separation of the alkanes from the alcohol isomers. This is in agreement with the results produced by Schwarz et al. [4] for the separation of *n*-tetradecane and 1-dodecanol. However, in that

study it was shown that operation at low temperatures, especially with CO₂ as the supercritical solvent, leads to difficulties in the controllability of the process due to the small operating window.

7.2.5.2 Effect of the Fractionation Pressure

The operating pressure cannot be varied in large increments independently of the operating temperature, due to shifts in the phase behaviour of the components involved [4]. The extract-to-feed ratios are indicative of the extent to which the operating pressure can be varied. The fractionation pressure can be varied between values that will lead to extract-to-feed ratios that fall within the theoretical limits of 0 and 1. Figure 7-4 shows a comparison between the selectivity of Runs 1 and 2, and Runs 4 and 5, both with similar solvent-to-feed ratios and slight variations in the operating pressure.

Similar trends are observed for the high and low temperature runs, with the solubility of *n*-decane and 2,6-dimethyl-2-octanol increasing more, relative to that of 1-decanol and 3,7-dimethyl-1-octanol, when the operating pressure is increased. This means that at the higher operating pressures, the fraction of light components (*n*-decane and 2,6-dimethyl-2-octanol) in the extract stream, increase. It should however be noted that the extract-to-feed ratio also increases at higher operating pressures – the result of an overall increase in the amount of material that is extracted by the supercritical solvent. Similar calculations to those discussed in section 7.2.5.1 were conducted and the results are given in Table 7-6 and Table 7-7.

7 | Establishing a Supercritical Fluid Fractionation Model

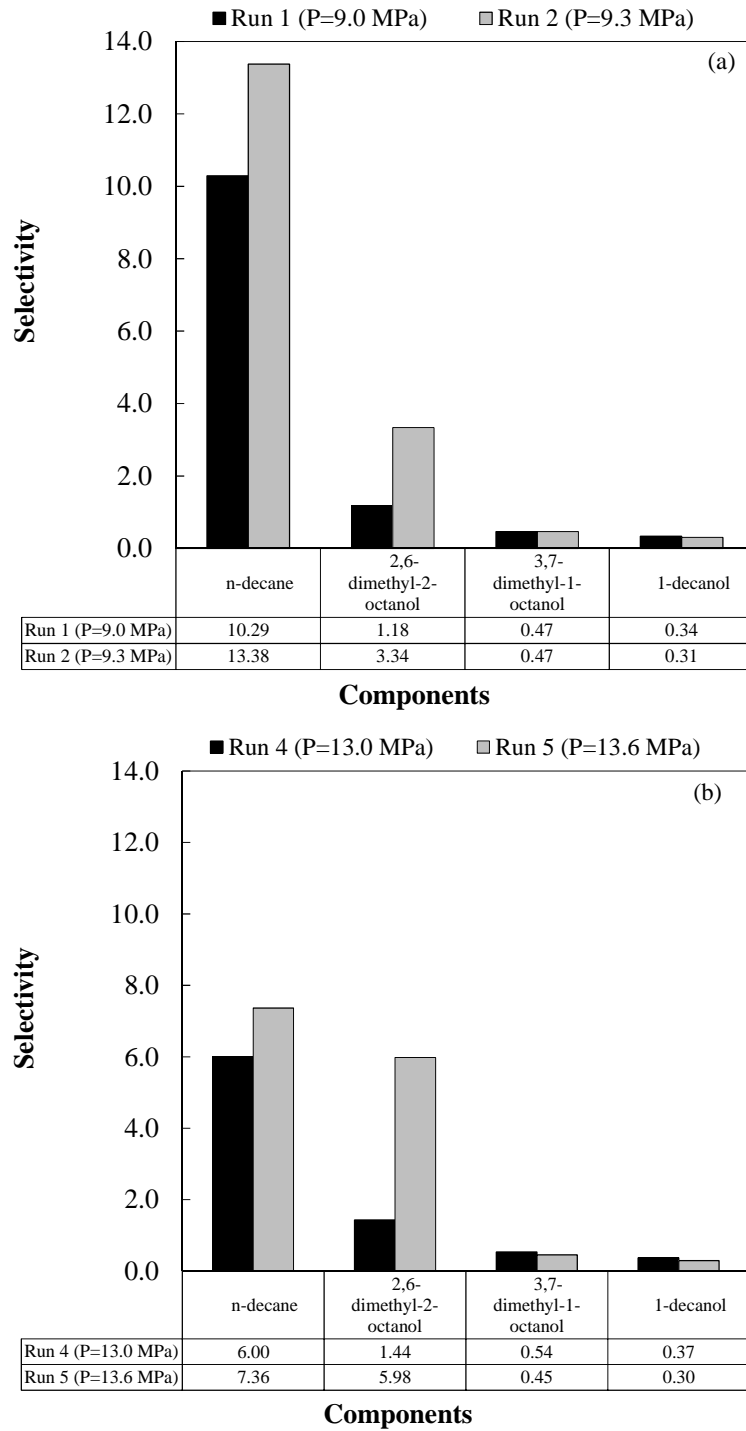


Figure 7-4 Comparison between the selectivity of the components in (a) Run 1 and Run 2, and (b) Run 4 and Run 5

7 | Establishing a Supercritical Fluid Fractionation Model

Table 7-6 Comparison between the mass % of total available solute that reports to the extract product stream during Run 1 and Run 2

	$(\dot{m}_i)_{feed}$		$(\dot{m}_i)_{extract}$		% of total mass reporting to extract product	
	Run 1	Run 2	Run 1	Run 2	Run 1	Run 2
<i>n</i>-decane	0.239	0.235	0.206	0.224	86.2	95.3
2,6-dimethyl-2-octanol	0.176	0.179	0.098	0.153	55.6	85.5
3,7-dimethyl-1-octanol	0.196	0.198	0.067	0.098	34.2	49.5
1-decanol	0.227	0.227	0.063	0.090	27.8	39.6

Table 7-7 Comparison between the mass % of total available solute that reports to the extract product stream during Run 4 and Run 5

	$(\dot{m}_i)_{feed}$		$(\dot{m}_i)_{extract}$		% of total mass reporting to extract product	
	Run 4	Run 5	Run 4	Run 5	Run 4	Run 5
<i>n</i>-decane	0.217	0.215	0.183	0.208	84.3	96.7
2,6-dimethyl-2-octanol	0.172	0.179	0.107	0.153	62.2	85.5
3,7-dimethyl-1-octanol	0.187	0.177	0.073	0.093	39.0	52.5
1-decanol	0.230	0.201	0.072	0.081	31.3	40.3

It is clear from the calculations provided that the percentage of available solute in the feed stream that report to the extract stream, increases with an increase in operating pressure, for all the solutes present. However, all the solutes do not respond in the same manner to an increase in operating pressure. From Figure 7-4 it is clear that the increase in operating pressure causes an increase in the selectivity of the light components, which in turn results in an increased percentage of the available light components in feed, to report to the extract product. The increased amount of heavy components reporting to the extract stream due to an increase in operating pressure can be attributed to the overall increase in amount of solutes loaded in the solvent at higher extract-to-feed ratios.

7.5.2.3 Effect of the Solvent-to-Feed Ratio

Runs 1 and 3 were conducted at approximately the same operating temperature and pressure, with Run 3 having a higher solvent-to-feed ratio. Similarly Runs 4 and 6 were conducted at the same operating temperature and pressure, but with Run 6 having a higher solvent-to-feed ratio. The

7 | Establishing a Supercritical Fluid Fractionation Model

solvent-to-feed ratio was adjusted by changing the feed flow rate rather than the solvent flow rate, to minimise the influence of hydrodynamic effects.

From the results presented in Table 7-4 it can be seen that an increased solvent-to-feed ratio leads to an increased extract-to-feed ratio. The question now arises as to whether the increase in the extract-to-feed ratio is due to an increased amount of light components or due to an increased amount of heavy components, or both.

Figure 7-5 indicates that the selectivity of *n*-decane is not influenced significantly by the solvent-to-feed ratio. However, the selectivity of 2,6-dimethyl-2-octanol significantly increases with an increase in the solvent-to-feed ratio. The selectivity of the heavier components, 1-decanol and 3,7-dimethyl-1-octanol, seem to slightly decrease with an increase in solvent-to-feed ratio.

The amount of each solute that is extracted by the solvent in Run 1, Run 3, Run 4 and Run 6, was calculated and is presented in Table 7-8 and Table 7-9

Table 7-8 Comparison between the mass % of total available solute that reports to the extract product stream during Run 1 and Run 3

	$(\dot{m}_i)_{feed}$		$(\dot{m}_i)_{extract}$		% of total mass reporting to extract product	
	Run 1	Run 3	Run 1	Run 3	Run 1	Run 3
<i>n</i>-decane	0.239	0.127	0.206	0.120	86.2	94.5
2,6-dimethyl-2-octanol	0.176	0.111	0.098	0.098	55.6	88.3
3,7-dimethyl-1-octanol	0.196	0.114	0.067	0.055	34.2	86.0
1-decanol	0.227	0.130	0.063	0.046	27.8	35.4

Table 7-9 Comparison between the mass % of total available solute that reports to the extract product stream during Run 4 and Run 6

	$(\dot{m}_i)_{feed}$		$(\dot{m}_i)_{extract}$		% of total mass reporting to extract product	
	Run 4	Run 6	Run 4	Run 6	Run 4	Run 6
<i>n</i>-decane	0.217	0.138	0.183	0.124	84.3	89.9
2,6-dimethyl-2-octanol	0.172	0.111	0.107	0.103	62.2	92.8
3,7-dimethyl-1-octanol	0.187	0.114	0.073	0.068	39.0	59.6
1-decanol	0.230	0.136	0.072	0.061	31.3	44.9

7 | Establishing a Supercritical Fluid Fractionation Model

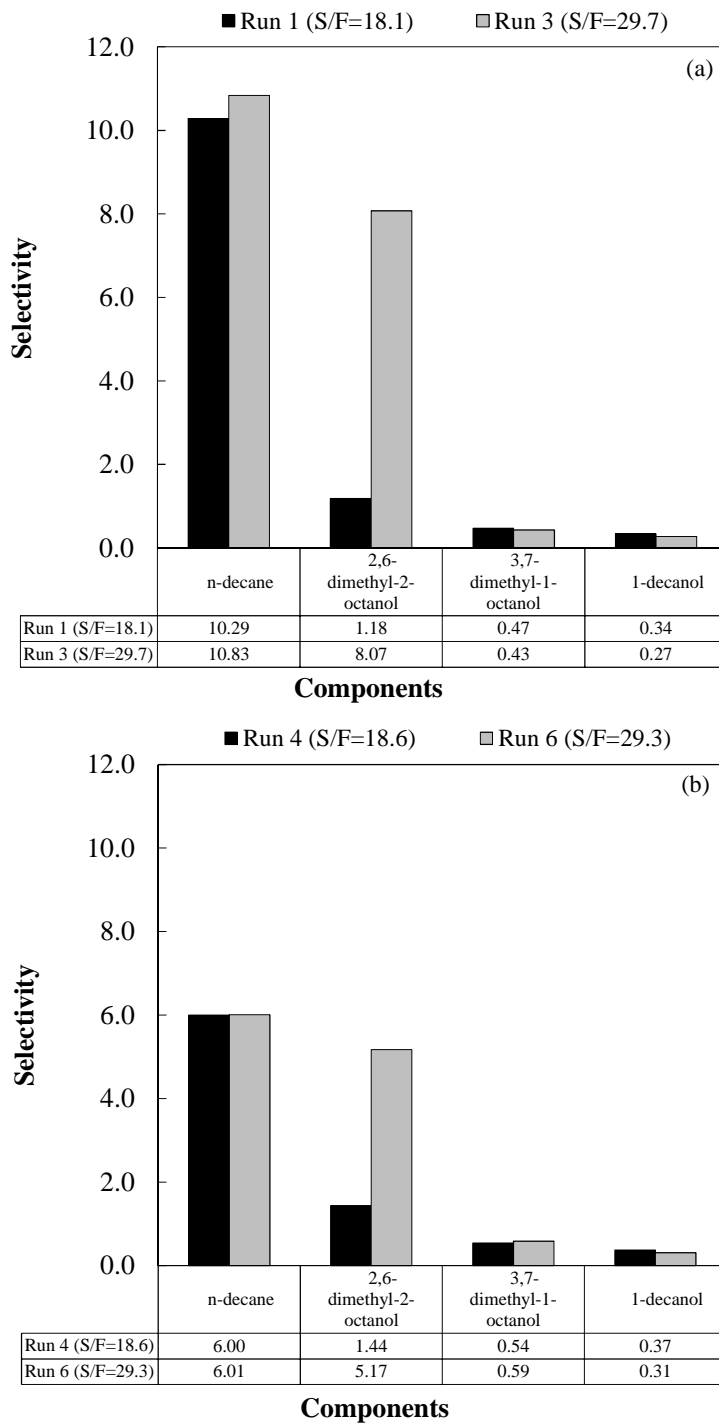


Figure 7-5 Comparison between the selectivity of components in (a) Run 1 and Run 3, and (b) Run 4 and Run 6

As the solvent-to-feed ratio increases, more solvent is available for the same amount of feed mixture. At the selected operating conditions the solvent thus preferentially extracts the lightest

component, but because more solvent is now available, the less soluble compounds can thus also be extracted from the feed mixture. This is the main reason why a higher extract-to-feed ratio is observed when the solvent-to-feed ratio increases. The values in Table 7-8 and Table 7-9 indicate that a larger fraction of each compound available in the feed mixture reports to the extract product. It is necessary to distinguish between the overall increase in material that report to the extract product (higher extract-to-feed ratio), and an increase in the selectivity of a component, as the main cause for the higher percentage component extraction observed at higher solvent-to-feed ratios. It is clear from the similar selectivity values for *n*-decane in Run 1 and 3, and Run 4 and 6, that the main cause of the increase in the fraction of *n*-decane reporting to the extract product at higher solvent-to-feed ratios is the overall increase in total material reporting to the extract product stream.

For 2,6-dimethyl-2-octanol, a very large increase in the selectivity is observed when the solvent-to-feed ratio increases. It can be reasoned that since *n*-decane, the lightest component, is already present at its maximum load at the selected conditions, the excess solvent available is used to extract 2,6-dimethyl-2-octanol, the second lightest compound.

The results indicate that a higher solvent-to-feed ratio will lead to a higher selectivity ratio and a lower recovery. A lower solvent-to-feed ratio does therefore not only lead to better separation performance, but also carries many benefits, especially considering the size and capacity of pumping, heating and cooling equipment used in the solvent cycle.

7.3 Validation of Process Simulation Model

7.3.1 Factors that Require Special Attention

The following important factors were encountered during the SFF process simulation runs:

- The solvent recycle stream that is employed on the real SFF pilot plant, allows for the introduction of variable amounts of fresh CO₂ (see Figure 7-2) to ensure that the solvent feed stream to the fractionation column stay at a constant flow rate. The stream mixing models available in Aspen Plus[®] did not allow for a CO₂ make-up stream with variable flow rate to be added. The solvent recycle loop was thus implemented manually during the simulations. The solvent feed stream composition (labelled as “SOLVENT” in Figure 7-1) was specified to be exactly the same as the composition of

7 | Establishing a Supercritical Fluid Fractionation Model

the top product that exits the separator vessel (labelled as “SOLVRECY” in Figure 7-1). The amount of fresh CO₂ that was added to the solvent feed stream was calculated by allowing the total solvent feed to the fractionation column to remain at the specified flow rate. A change in the composition of the solvent feed stream leads to a change in the composition of the overheads and bottoms products during the simulation. Consequently, the composition of the solvent feed stream (“SOLVENT”) needed to be adjusted until the composition of the top product of the separator (“SOLVRECY”) and the solvent feed stream attained constant values in consecutive runs. This was an indication that the simulation had converged.

- It was anticipated that total separation would occur in the separator, i.e. no solutes would exit in the top product stream of the separator. During the experimental pilot plant runs this assumption was placed under doubt, since blockages occurred in the line that carried the separator top product. This was an indication that small amounts of solutes did exit the separator top product stream. During the process simulations it was confirmed that the conditions in the separator did not allow for 100% separation of the solutes from the solvent. This meant that the method employed to calculate the feed flow rate during the experimental pilot plant runs did not take into account the amount of solutes that circulated in the solvent recycle loop. The simulations indicated that the flow rate of the solutes that enters the solvent recycle loop depends on the operating conditions in the column, but is generally equal to approximately 10 % of the value of the extract product flow rate. The feed flow rates were thus adjusted during the process simulations to accommodate the solutes present in the solvent recycle loop.
- To achieve convergence during a simulation run, good starting values were required for certain parameters. All the simulations were thus started with the fractionation column having 2 stages – the simplest separation case. Thereafter the values stored in the Aspen Plus[®] simulator were used as input values for the next run. This meant that if it was required that 20 stages be simulated in the fractionation column, the simulation had to be conducted utilizing 2 stages, and conducted again with 3 stages, until 20 stages have been reached.

7.3.2 Generating Data with the Process Model

The process model discussed in section 7.1 was used to generate data at the same operating conditions as those used in the pilot plant runs. The RK-ASPEN model with polar parameters and binary solute-solvent interaction parameters were employed in all process units. Two effects were investigated before the model verification could commence: the first being the effect of the inclusion of the binary solute-solute interaction parameters on the predicted component distribution in the product streams, and the second being the effect of the number of stages selected for the fractionation column in the process model.

7.3.2.1 The Effect of Solute-Solute Interaction Parameters

The process model was used to simulate the separation performance at conditions similar to those used in Run 4. The resultant stream compositions with and without the use of solute-solute binary interaction parameters in the RK-ASPEN model are presented in Figure 7-6. The input parameters of the RK-ASPEN model are repeated for ease of reference in Table 7-10, but more detail on each parameter can be found in Chapter 6.

Table 7-10 Input parameters used in the RK-ASPEN model during the process simulations for the CO₂ + (25 % *n*-decane + 25 % 1-decanol + 25 % 3,7-dimethyl-1-octanol + 25 % 2,6-dimethyl-2-octanol) system

	Polar parameter	Binary solute-solvent interaction parameter with CO ₂		Binary solute-solute interaction parameter			
		$k_{a,ij}$	$k_{b,ij}$	<i>n</i> -C ₁₀	<i>l</i> -C ₁₀	3,7- <i>l</i>	2,6-2
<i>n</i>-decane	0.0253	0.0957	0.0286	-	0.03	0.055	0.055
1-decanol	-0.4196	0.0850	-0.0305	0.03	-	0.03	0.03
3,7-dimethyl-1-octanol	0.0924	0.0774	-0.0140	0.055	0.03	-	0
2,6-dimethyl-2-octanol	0.0214	0.0655	-0.0034	0.055	0.03	0	-

7 | Establishing a Supercritical Fluid Fractionation Model

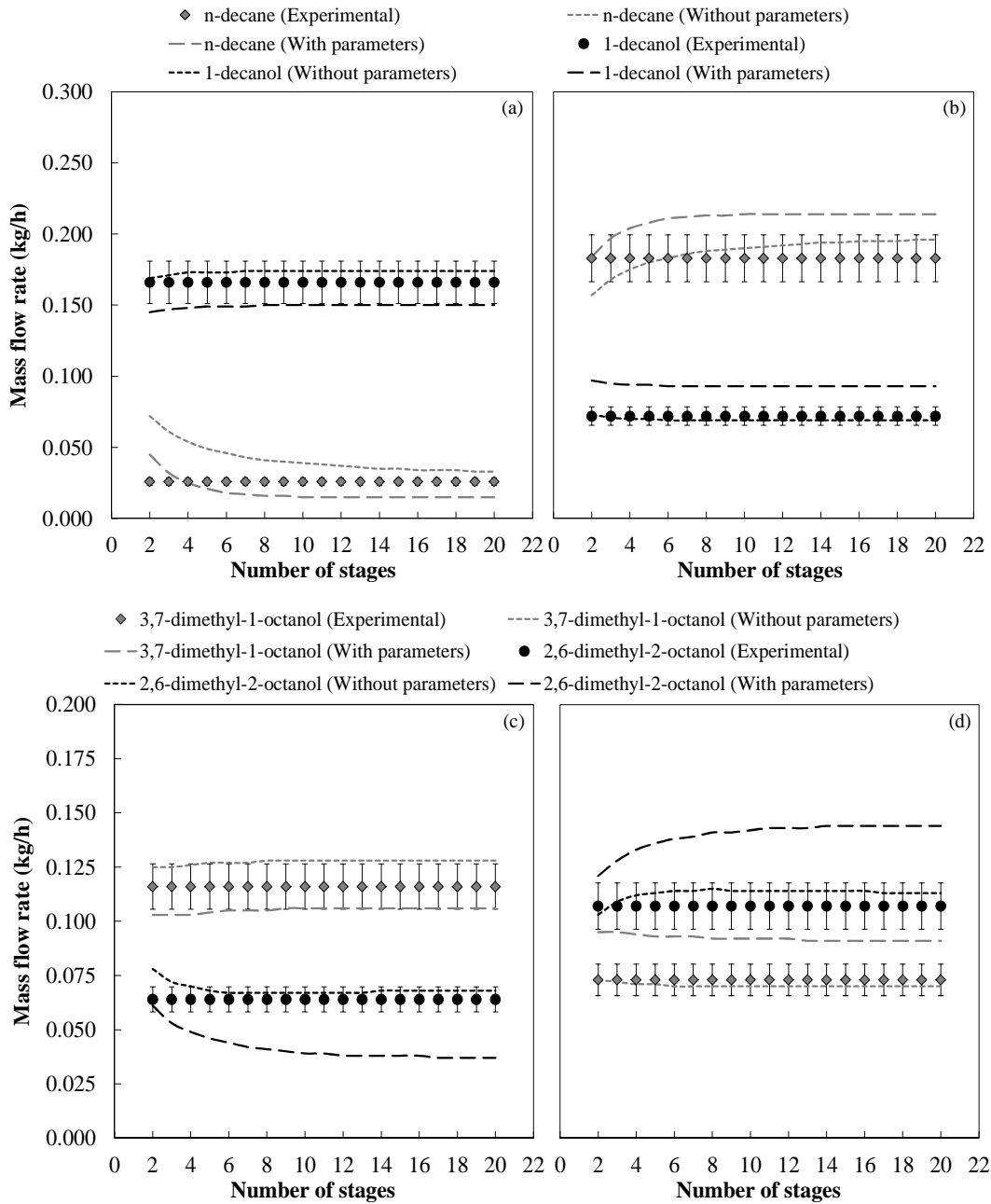


Figure 7-6 Mass flow rates of Run 4 calculated with RK-ASPEN with and without the use of solute-solute interaction parameters for (a) n-decane and 1-decanol in the extract product, (b) n-decane and 1-decanol in the bottoms product, (c) 3,7-dimethyl-1-octanol and 2,6-dimethyl-2-octanol in the extract product, and (d) 3,7-dimethyl-1-octanol and 2,6-dimethyl-2-octanol in the bottoms product

The maximum error calculated for the experimental mass flow rates of each component (9 %) is included in Figure 7-6. It is clear that the RK-ASPEN model with no solute-solute interaction

parameters included give better predictions of the product stream compositions and flow rates. It is possible that the values determined in Chapter 6 for the solute-solute interaction parameters, are not the optimum values for this system. Although the inclusion of solute-solute interaction parameters increase the accuracy of the phase transition pressure predictions for multi-component mixtures (see Chapter 6), no improvement in the component distribution prediction is observed. The RK-ASPEN model without the inclusion of the solute-solute interaction parameters will thus be used from hereon as the thermodynamic model for the SFF process simulations.

7.3.2.2 Effect of the Number of Stages

Crause [5] attempted to determine the number of stages in the same pilot plant used in this investigation, and found seven stages, but with the possibility of pinching. Typical values for the HETP encountered for supercritical systems are believed to be between 0.2 and 1.2 m [6] – which translates to the number of stages for this specific fractionation column to be between 4 and 22.

Since only limited experimental data and highly unreliable estimation methods are available to determine the HETP of high pressure columns, the data generated for Run 4 was used to estimate the number of stages present in the pilot plant column. From Figure 7-6 it is clear that the number of stages selected in the fractionation column will influence the predicted component mass flow rates in the two product streams. The predicted mass flow rate of *n*-decane is influenced most by the number of stages. The data presented in Figure 7-6 indicates that 20 stages or more is required in the fractionation column, since all the components reach their experimental mass flow rate values only if 20 stages or more is employed. Supporting material in the form of component selectivity, selectivity ratio, extract-to-feed ratio and recovery was generated for Run 4, to aid in determining the number of stages present in the fractionation column.

Figure 7-7 clearly show that the selectivity is predicted very accurately for the alcohol isomers, but the values predicted for *n*-decane only approach the experimental values at 20 stages. The alcohol isomers however attain experimental values for all the parameters investigated between 6 – 10 stages, after which the values of the respective parameters do not vary significantly with an increase in the number of stages. The trends predicted for the component mass flow rates thus propagate to the component selectivity.

7 | Establishing a Supercritical Fluid Fractionation Model

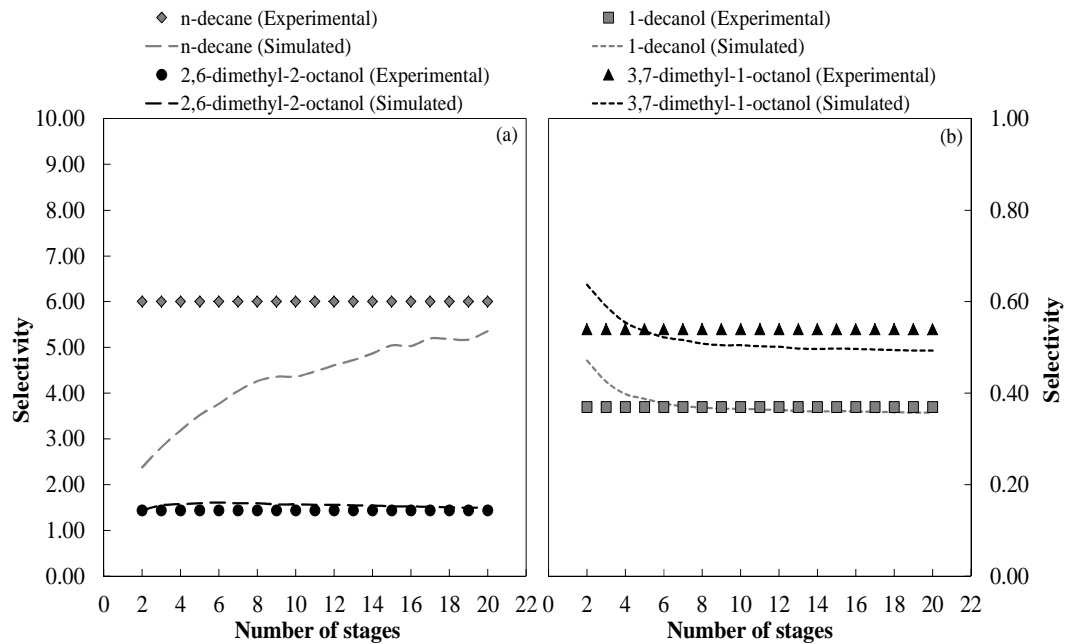


Figure 7-7 Comparison between the experimental and predicted component selectivity of (a) *n*-decane and 2,6-dimethyl-2-octanol, and (b) 1-decanol and 3,7-dimethyl-1-octanol, for Run 4

In Figure 7-8 the recovery of the alcohol isomers in the bottoms product stream is predicted well irrespective of the number of stages selected, but an improved prediction is observed at values of 16 stages and more. The trends depicted in Figure 7-6 to Figure 7-8 thus indicate that it is likely that 20 stages or more were present in the fractionation column used to generate the experimental data for Run 4. Due to the restraints imposed by literature [6], it was decided to assign 20 theoretical stages to Run 4. The HETP value when 20 stages are assumed is 0.216 m for the fractionation column employed in this experimental work. Low HETP values, like this one, are typically encountered for small diameter columns containing structured packing with a large packing surface area per volume [7].

7 | Establishing a Supercritical Fluid Fractionation Model

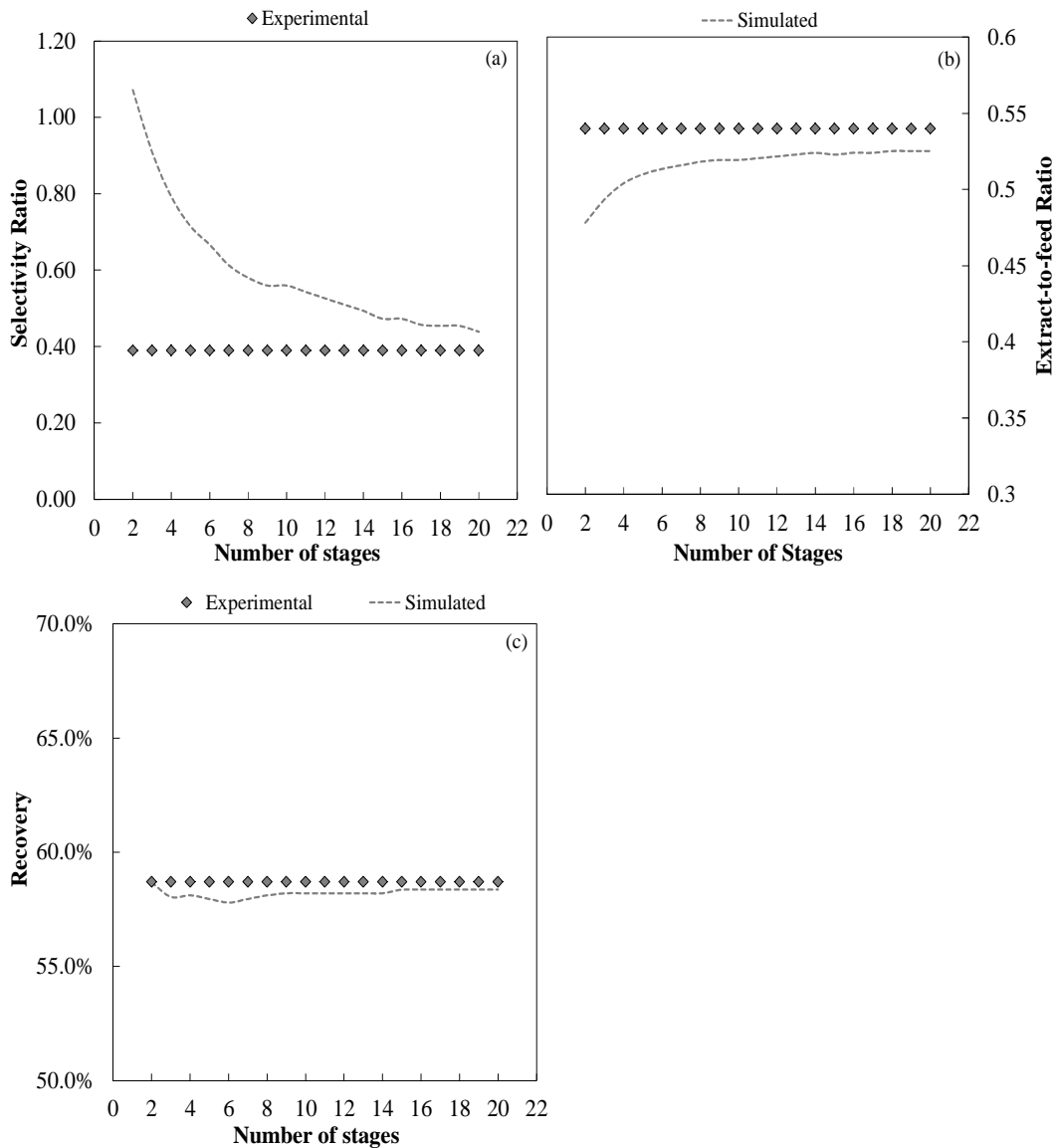


Figure 7-8 Comparison between the experimental and simulated (a) selectivity ratio, (b) extract-to-feed ratio, and (c) recovery, for Run 4

The HETP value is dependent on a number of parameters including the operating pressure, operating temperature, mixture composition and extract-to-feed ratio [8]. In an investigation by de Haan [8] for a supercritical CO_2 + hydrocarbon system, a 0.035 m diameter column with Sulzer BX packing was used to develop a mass transfer model. It was shown that the HETP value decreases with an increase in operating pressure (from 15.0 to 17.5 to 20.0 MPa), as well as with an increase in operating temperature (from 323 to 353 K). As the operating pressure increases the viscosity of the

supercritical phase increases while the diffusivity of the liquid phase decreases, but at the same time the distribution coefficient increases, which means that smaller amounts of solvent is required to achieve the same extract-to-feed ratio. The effect of solvent-to-feed ratio on the HETP was not reported in that study.

It is anticipated that similar HETP values will hold for conditions where small changes in pressure and temperature occurred (e.g. Run 1 and Run 2). According to the study by de Haan [8] an increase of 30 K in the operating temperature (e.g. Run 1 and Run 4) led to a 50 % decrease in the HETP of a similar system to the one used in this study. Changes in the flow rates of the feed or solvent directly influences the hydrodynamic behaviour in the column, and significant differences in the HETP values are expected to occur for runs where the solvent-to-feed ratios differed significantly (e.g. Run 1 and Run 3). In the experimental runs where the solvent-to-feed ratio was adjusted, the feed flow rate was adjusted. At low feed flow rates the solvent must flow over a larger length of column to come into contact with the same amount of feed and therefore the HETP is increased and the number of stages decreased.

It is expected that the HETP values, and consequently the number of stages, will differ at the experimental conditions investigated. Based on the HETP values reported by de Haan [8] for similar systems and the trends discussed in this section, the following number of theoretical stages was assumed for each experimental run: Run 1 = 10, Run 2 = 10, Run 3 = 3, Run 4 = 20, Run 5 = 20, and Run 6 = 7.

7.3.2.3 Comparison between Simulated and Experimental Data

In Table 7-11 a comparison between the experimental and simulated results are given for all the experimental runs. The input parameters to the simulation were kept at the values measured in the experimental work, except for the feed flow rate, which was adjusted according to the discussion in section 7.3.2.1. The RK-ASPEN thermodynamic model was employed with the parameters shown in Table 7-10, but without the solute-solute interaction parameters.

7 | Establishing a Supercritical Fluid Fractionation Model

Table 7-11 Comparison between the results generated on the pilot plant and results generated with the process model

	Run 1		Run 2		Run 3	
	Measured	Simulated	Measured	Simulated	Measured	Simulated
Fractionation Conditions						
Number of Stages	Unknown	10	Unknown	10	Unknown	3
Temperature (K)	315.9	315.9	316.7	316.7	315.4	315.4
Pressure (MPa)	9.0	9.0	9.3	9.3	9.0	9.0
Feed Flow rate (kg/h)	0.839	0.881	0.839	0.896	0.482	0.514
Solvent flow rate (kg/h)	15.2	15.2	14.9	14.9	14.3	14.3
Separation Conditions						
Temperature (K)	328.9		326.9		329.3	
Pressure (MPa)	5.0		5.0		4.6	
Bottoms						
Flow rate (kg/h)	0.404	0.729	0.274	0.668	0.319	0.338
Composition (mass%)						
<i>n</i> -decane	4.6	23.9	3.0	20.5	3.5	16.9
<i>l</i> -decanol	43.3	30.3	51.7	32.2	52.7	34.3
3,7-dimethyl- <i>l</i> -octanol	33.1	25.4	37.2	26.8	40.0	28.1
2,6-dimethyl-2-octanol	19.0	20.4	8.1	20.5	3.8	20.7
Extract						
Flow rate (kg/h)	0.434	0.152	0.565	0.228	0.163	0.175
Composition (mass%)						
<i>n</i> -decane	47.4	50.7	39.7	50.0	37.6	44.6
<i>l</i> -decanol	14.6	11.8	16.0	12.3	14.5	13.1
3,7-dimethyl- <i>l</i> -octanol	15.5	13.8	17.3	14.0	17.2	15.4
2,6-dimethyl-2-octanol	22.5	23.7	27.0	23.7	30.7	27.4
Selectivity						
<i>n</i> -decane	10.29	2.12	13.38	2.44	10.83	2.64
<i>l</i> -decanol	0.34	0.39	0.31	0.38	0.27	0.38
3,7-dimethyl- <i>l</i> -octanol	0.47	0.54	0.47	0.52	0.43	0.55
2,6-dimethyl-2-octanol	1.18	1.16	3.34	1.15	8.07	1.32
Selectivity ratio	0.19	0.99	0.31	0.85	0.81	0.85
Recovery (%)	64.2	87.4	41.3	81.7	44.3	73.2

7 | Establishing a Supercritical Fluid Fractionation Model

Table 7-11 (continued) Comparison between the results generated on the pilot plant and results generated with the process model

	Run 4		Run 5		Run 6	
	Measured	Simulated	Measured	Simulated	Measured	Simulated
Fractionation Conditions						
Number of Stages	Unknown	20	Unknown	20	Unknown	7
Temperature (K)	344.5	344.5	344.1	344.1	344.5	344.5
Pressure (MPa)	13.0	13.0	13.6	13.6	13.1	13.1
Feed Flow rate (kg/h)	0.808	0.851	0.772	0.826	0.499	0.534
Solvent flow rate (kg/h)	15.0	15.0	14.4	14.4	14.6	14.6
Separation Conditions						
Temperature (K)	343.2		344.5		345.4	
Pressure (MPa)	5.0		5.0		5.1	
Bottoms						
Flow rate (kg/h)	0.372	0.403	0.236	0.240	0.142	0.122
Composition (mass%)						
<i>n</i> -decane	7.0	8.2	5.3	5.0	5.8	5.7
<i>l</i> -decanol	44.6	43.2	51.5	51.3	56.0	56.6
3,7-dimethyl- <i>l</i> -octanol	31.2	31.8	38.4	37.5	32.7	32.8
2,6-dimethyl-2-octanol	17.2	16.9	4.8	5.8	5.6	5.7
Extract						
Flow rate (kg/h)	0.479	0.447	0.590	0.585	0.392	0.411
Composition (mass%)						
<i>n</i> -decane	42.0	43.8	38.8	37.3	34.8	34.3
<i>l</i> -decanol	16.6	15.4	15.2	15.7	17.2	18.5
3,7-dimethyl- <i>l</i> -octanol	16.8	15.7	17.4	16.9	19.2	20.0
2,6-dimethyl-2-octanol	24.7	25.3	28.6	30.3	28.8	27.3
Selectivity						
<i>n</i> -decane	6.00	5.35	7.32	7.45	6.00	5.98
<i>l</i> -decanol	0.37	0.36	0.30	0.31	0.31	0.33
3,7-dimethyl- <i>l</i> -octanol	0.54	0.49	0.45	0.45	0.59	0.61
2,6-dimethyl-2-octanol	1.44	1.50	5.96	5.19	5.14	4.75
Selectivity ratio	0.39	0.44	0.92	0.80	1.01	0.95
Recovery (%)	58.7	58.4	40.1	37.2	37.1	28.9

In Table 7-12 the errors between the simulated and experimental mass flow rate of each component in each product stream are given as an absolute value and as a percentage of the experimentally measured value. The results in Table 7-11 and Table 7-12 indicate that the model was

7 | Establishing a Supercritical Fluid Fractionation Model

not able to produce accurate predictions for Run 1, 2 and 3. Very large errors occurred in the data predicted for the mass flow rates of the respective components, especially for the light components, *n*-decane and 2,6-dimethyl-2-octanol in the bottoms product stream.

The main cause of the large deviation between the experimental and simulated data for Run 1, 2 and 3, can then be attributed to the shortcomings of the thermodynamic model. Although the RK-ASPEN predicted accurate phase transition pressures for the CO₂ + (25 % *n*-decane + 25 % 1-decanol + 25 % 3,7-dimethyl-1-octanol + 25 % 2,6-dimethyl-2-octanol) system at low temperatures (see Chapter 6, section 6.5.4), it is clear from the process simulations of Run 1, 2 and 3, that inaccurate phase compositions are predicted at low temperatures. It is thus recommended that the SFF process model not be used to make predictions at low temperatures. Schwarz et al. [4] also showed that an SFF process employing CO₂ as the solvent, have a very small operating window, and consequently poor controllability, at low fractionation temperatures. Operating such an SFF process at low fractionation temperatures will not be practical, and no attempt was made to increase the accuracy of the thermodynamic model at low temperatures, since this region was not investigated any further.

Table 7-12 Evaluation of the accuracy of the process model for Run 1, Run 2 and Run 3

	Run 1		Run 2		Run 3	
	Error (kg/h)	% Error	Error (kg/h)	% Error	Error (kg/h)	% Error
Bottoms						
Flow rate (kg/h)						
<i>n</i> -decane	0.206	1107.0	0.129	1566.7	0.051	899.1
1-decanol	0.063	36.2	0.073	51.8	0.030	35.0
3,7-dimethyl-1-octanol	0.051	38.3	0.077	75.6	0.030	45.7
2,6-dimethyl-2-octanol	0.072	94.1	0.115	517.3	0.064	1030.1
Extract						
Flow rate (kg/h)						
<i>n</i> -decane	0.129	62.6	0.110	49.2	0.042	35.0
1-decanol	0.045	71.6	0.062	69.0	0.023	50.3
3,7-dimethyl-1-octanol	0.046	68.8	0.066	67.3	0.028	50.8
2,6-dimethyl-2-octanol	0.062	63.1	0.099	64.6	0.050	51.0

7 | Establishing a Supercritical Fluid Fractionation Model

Table 7-12 (continued) Evaluation of the accuracy of the process model for Run 4, Run 5 and Run 6

	Run 4		Run 5		Run 6	
	Error (kg/h)	% Error	Error (kg/h)	% Error	Error (kg/h)	% Error
Bottoms						
Flow rate (kg/h)						
<i>n</i> -decane	0.007	26.7	0.001	4.1	0.001	15.0
<i>l</i> -decanol	0.008	4.9	0.001	1.2	0.011	13.2
3,7-dimethyl- <i>l</i> -octanol	0.012	10.3	0.001	0.7	0.006	13.9
2,6-dimethyl-2-octanol	0.004	6.3	0.003	23.6	0.001	12.0
Extract						
Flow rate (kg/h)						
<i>n</i> -decane	0.013	7.3	0.010	4.8	0.017	13.8
<i>l</i> -decanol	0.003	4.4	0.011	12.9	0.015	24.1
3,7-dimethyl- <i>l</i> -octanol	0.003	4.2	0.006	6.2	0.014	20.0
2,6-dimethyl-2-octanol	0.006	5.2	0.024	15.5	0.009	9.2

At the three high temperature runs, Run 4, 5 and 6, very accurate results were produced by the process model. The combined error of the component distribution and the product stream flow rates is observed when evaluating the error of the mass flow rates of the components. For the experimental pilot plant data the maximum error for the component mass flow rates was calculated to be 9 % of the value of the mass flow rate. For the majority of the component mass flow rates, the error fall within or marginally outside the experimental error. The largest percentage error was observed for *n*-decane in the bottoms product stream of Run 4. It should be noted that although the percentage error of 26.7 % is large, the predicted value differed with only 0.007 kg/h from the experimental value. The largest error in predicted mass flow rate, valued at 0.024 kg/h, occurred for the flow rate prediction of 2,6-dimethyl-2-octanol in the extract product stream of Run 5. Taking the possible experimental error into account it can be said that the error in the predicted mass flow rates of the components is 10 – 36 %.

From Table 7-11 it is clear that the extract-to-feed ratio, component selectivity, selectivity ratio and recovery, for the three high temperature runs are predicted very accurately. It is important that accurate component mass flow rates can be produced by the process model, but equal status should be given to the accurate prediction of the parameters used to determine the separation performance of the model. During the stages where the feasibility of a process is being determined, parameters like the selectivity ratio and recovery, play a large role. For the three high temperature runs the maximum

error in the selectivity ratio was 0.08 and the maximum error in the predicted recovery of alcohols in the bottoms stream, 8 %.

It can thus be concluded that the SFF process model developed in Aspen Plus[®] can predict accurate component mass flow rates as well as separation performance parameters at temperatures near 344 K. Since the model has been verified for use at temperatures near 344 K, it can be used to predict the separation performance at other conditions that marginally extend beyond those used in the verification cases, to determine whether optimum operating conditions exist, and how the separation performance is influenced by the choice of operating parameters.

7.5 Predicting the Separation Performance at Other Conditions

7.5.1 Investigating Other Fractionation Conditions

Of the three experimental high pressure runs, the process performed best at the conditions of Run 4. The process model was used to simulate the SFF process at the conditions of Run 4, but varying the temperature, pressure and solvent-to-feed ratio, one at a time. The operating parameters were varied over a range that leads to an extract-to-feed ratio of between 0.3 and 0.7. As a result, the influence of each operating parameter on the separation performance of the process could be evaluated separately over a larger range than that covered experimentally. Although the mass flow rates and product stream compositions are investigated, the extract-to-feed ratio, selectivity ratio and alcohol recovery will be the main parameters to consider when establishing the optimum operating conditions for feed conditions similar to that of Run 4.

As discussed in section 7.3.2.2, the HETP, and consequently the number of stages, is influenced by the operating conditions in the fractionation column. The number of stages was changed as the fractionation temperature, pressure and solvent-to-feed ratio was adjusted, according to the trends discussed in 7.3.2.2.

7.5.1.1 Temperature

At 13.0 MPa and the feed conditions of Run 4, the fractionation temperature was varied between 338 K and 354 K. The effect on the component mass flow rates and distributions in the

7 | Establishing a Supercritical Fluid Fractionation Model

product streams are shown in Figure 7-9. The input parameters for the data points plotted in Figure 7-9, are given in Table 7-13.

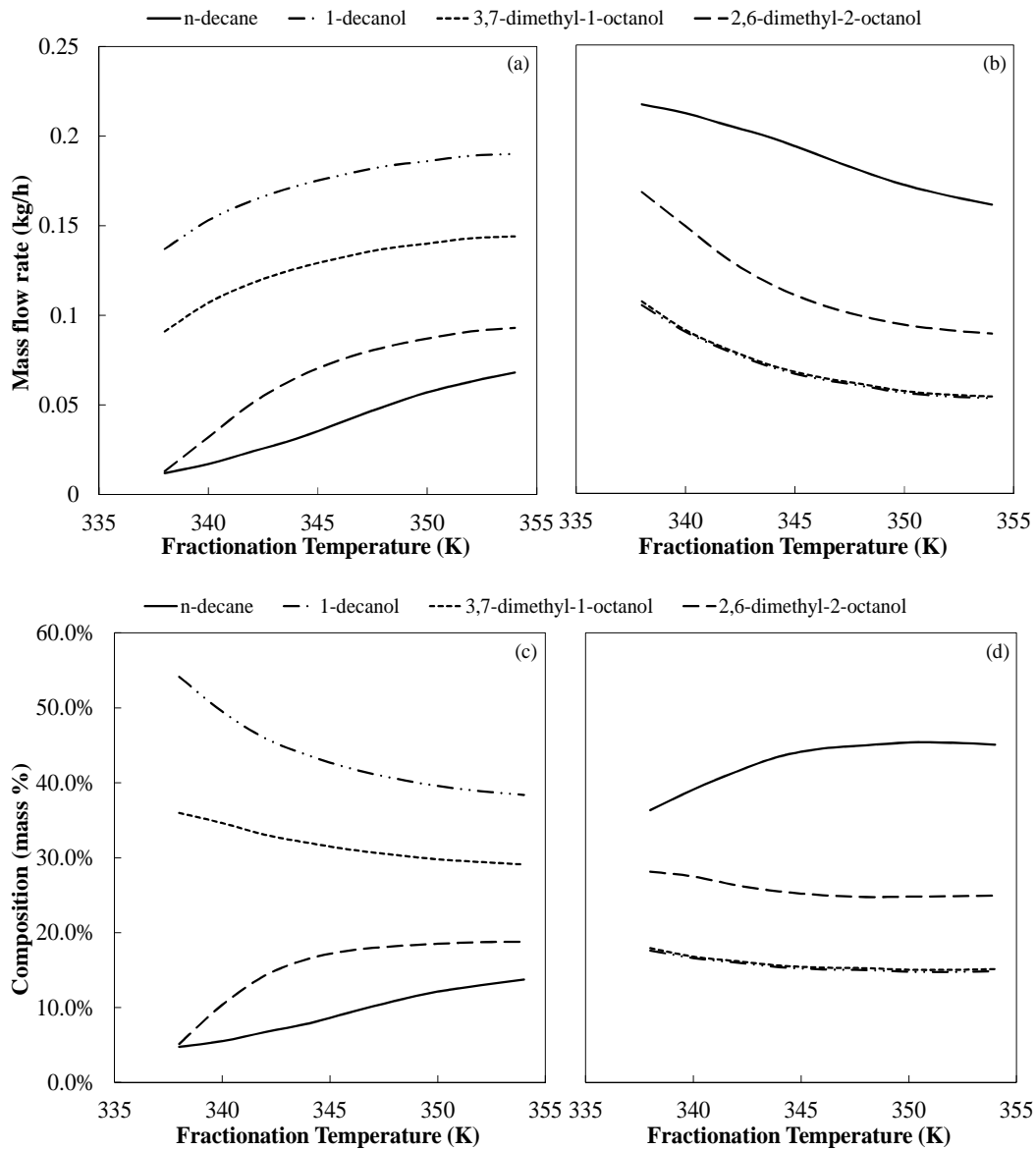


Figure 7-9 Simulated results for the influence of temperature on (a) the component mass flow rates in the bottoms product, (b) the component mass flow rates in the extract product, (c) the component distribution in the bottoms product, and (d) the component distribution in the extract product, for Mixture 2 at feed conditions similar to that used in Run 4

7 | Establishing a Supercritical Fluid Fractionation Model

Table 7-13 Input parameters used to investigate the influence of temperature on the separation performance

Pressure (MPa)	13.0	13.0	13.0	13.0	13.0	13.0	13.0	13.0	13.0
Temperature (K)	338	340	342	344	346	348	350	352	354
Solvent-to-feed ratio (kg/kg)	17.6	17.6	17.6	17.6	17.6	17.6	17.6	17.6	17.6
Number of stages	15	17	19	20	20	20	20	20	20

As the fractionation temperature increases, the amount of material that exits in the bottoms stream increases, which lead to reduced values of the extract-to-feed ratio (also see Figure 7-10). Since the bottoms product stream is the main product stream, an increased yield is beneficial. However, when evaluating the bottom stream composition at higher temperatures, it is evident that the fraction of *n*-decane in the bottoms product stream increases. Although higher yields occur at increased fractionation temperatures, the quality of the product is poor, since it contains more than 10 % of the undesired component, *n*-decane. At fractionation temperatures below 340 K, the fraction of *n*-decane in the bottoms product stream is very low, typically around 4 %. However, if operation should occur at these low temperatures, almost all of the 2,6-dimethyl-2-octanol will be lost in the extract product. It is thus evident that the optimum operating conditions for this scenario do not necessarily occur at the conditions that lead to the lowest fraction of *n*-decane in the bottoms product.

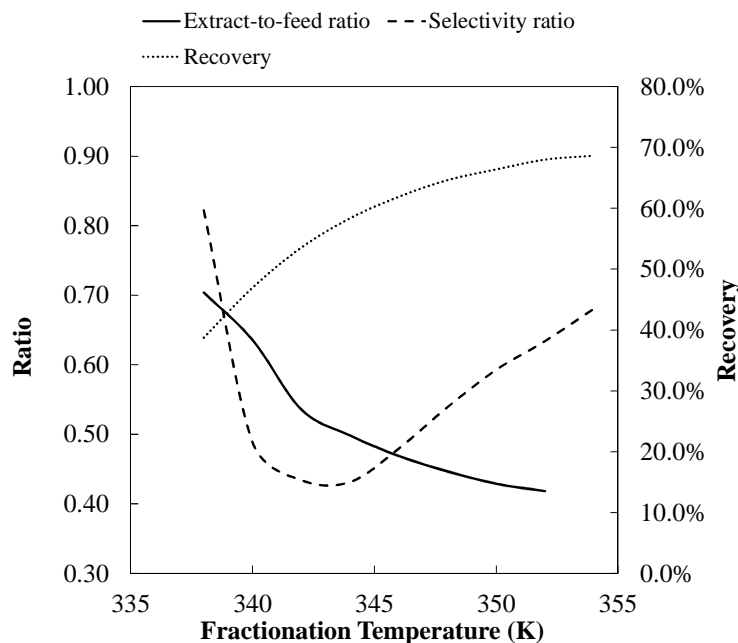


Figure 7-10 Effect of temperature on the extract-to-feed ratio, selectivity ratio and recovery of Mixture 2, for feed conditions similar to that used in Run 4

7 | Establishing a Supercritical Fluid Fractionation Model

The best separation performance will occur at conditions where the lowest selectivity ratio and the highest recovery are simultaneously attained. A low selectivity ratio is the result of the combination of the highest selectivity for *n*-decane and the lowest selectivity for the alcohol isomers. The CO₂ will thus give preference to the extraction of *n*-decane and not the alcohol isomers. The highest alcohol recovery occurs when the largest fraction of the available alcohol isomers in the feed stream, report to the bottoms product. The aim of the separation process is thus to assure the maximum amount of alcohol isomers and the minimum amount of *n*-decane report to the bottoms product stream. Since both types of compounds respond in a similar manner to an increase in temperature, the lowest selectivity ratio and highest alcohol recovery will not occur at the same time. As can be seen from Figure 7-10, these two parameters have the same trend but require opposing optimization approaches. The best operating temperature at the conditions of Run 4 can be any temperature above 344 K, depending on whether selectivity or recovery is the heavier weighted parameter.

Operating at conditions that lead to the lowest selectivity ratio (T = 344 K, P = 13.0 MPa, S/F = 17.6) will lead to a bottoms product stream containing 7.9 mass % *n*-decane and 58 % of the alcohol recovered. Operating at conditions that lead to the highest alcohol recovery in the range investigated (T = 354 K, P = 13.0 MPa, S/F = 17.6), will lead to a bottoms product containing 13.7 mass % *n*-decane with 69 % of the alcohols recovered.

7.5.1.2 Pressure

In Figure 7-11 the component mass flow rates and distribution in the product streams are plotted as a function of the fractionation pressure between 12.2 MPa and 13.6 MPa, at 344 K. The input parameters used to generate the plots are given in Table 7-14.

Table 7-14 Input parameters used to investigate the influence of pressure on the separation performance

Pressure (MPa)	12.2	12.4	12.6	12.8	13.0	13.2	13.4	13.6	13.8
Temperature (K)	344	344	344	344	344	344	344	344	344
Solvent-to-feed ratio (kg/kg)	17.6	17.6	17.6	17.6	17.6	17.6	17.6	17.6	17.6
Number of stages	13	15	17	19	20	20	20	20	20

7 | Establishing a Supercritical Fluid Fractionation Model

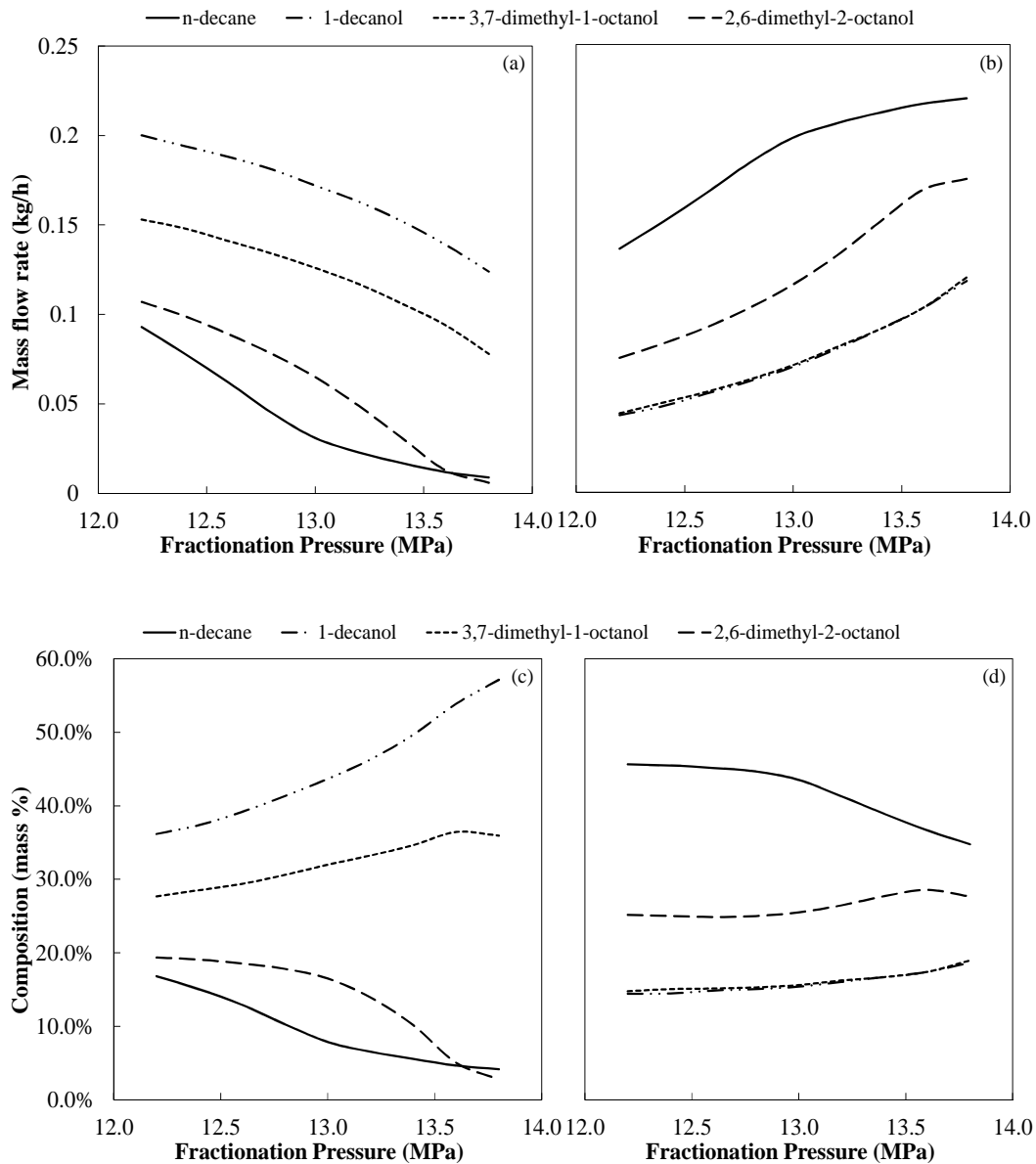


Figure 7-11 Simulated results for the influence of pressure on (a) the component mass flow rates in the bottoms product, (b) the component mass flow rates in the extract product, (c) the component distribution in the bottoms product, and (d) the component distribution in the extract product, for Mixture 2 at feed conditions similar to that used in Run 4

As the fractionation pressure increases, the extract-to-feed ratio increases (see Figure 7-12) and the bottoms product yield decreases. At low pressures, however, large amounts of unwanted *n*-decane occur in the bottoms product. In Figure 7-12 the opposing trends of the selectivity ratio and alcohol recovery as functions of fractionation pressure, is shown. Like for the selection of the optimum

7 | Establishing a Supercritical Fluid Fractionation Model

operating temperature, a compromise on either the selectivity ratio or alcohol recovery or both, is required to determine the fractionation pressure where a reasonable amount of alcohol product at an acceptable quality can be produced. At 344 K, any operating pressure below 13.2 MPa will produce acceptable results with regard to the selectivity ratio and/or the alcohol recovery (see Figure 7-12).

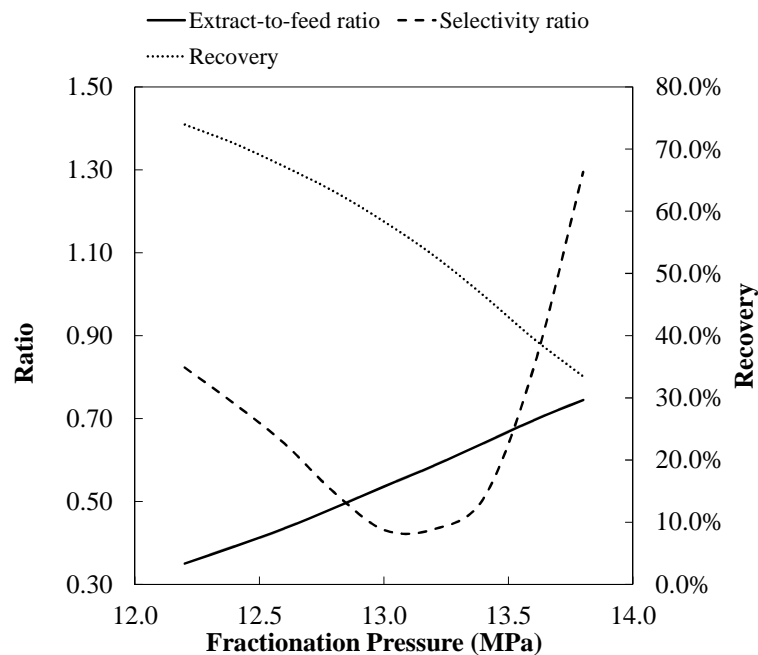


Figure 7-12 Effect of pressure on the extract-to-feed ratio, selectivity ratio and recovery of Mixture 2, for feed conditions similar to that used in Run 4

The change in trend observed for the selectivity ratio at 13.2 MPa, can be attributed to the change in the component distribution in the bottoms product stream at 13.2 MPa. The relationship between *n*-decane and the fractionation pressure at 344 K changes at 13.2 MPa, possibly due to fact that *n*-decane has now become completely soluble in supercritical CO₂. At this point, the CO₂ targets the second lightest component as can be seen from the drastic change in slope of the 2,6-dimethyl-2-octanol fraction in the bottoms product at pressures around 13.2 MPa (see Figure 7-11). At 13.6 MPa 2,6-dimethyl-2-octanol becomes completely soluble in CO₂ at 344 K. Thereafter the CO₂ targets the third lightest component, 3,7-dimethyl-1-octanol, and its fraction in the bottoms product stream start to decrease more with increasing pressure (see Figure 7-11). As the pressure in the fractionation column is increased the density of the solvent increases and along with it its ability to

7 | Establishing a Supercritical Fluid Fractionation Model

carry more solutes. Therefore, an increase in fractionation pressure will lead to an increase in the solubility of all the compounds, but with different trends, depending on whether the pressure exceeds the phase transition pressure of that component in CO₂.

It is thus recommended that for the conditions of Run 4, the fractionation pressure must be kept below 13.2 MPa to ensure the minimum loss of 2,6-dimethyl-2-octanol to the extract product stream. Operating at conditions that leads to the lowest selectivity ratio (T = 344 K, P = 13.2 MPa, S/F = 17.6) will lead to a bottoms product stream containing 6.5 mass % *n*-decane and 53 % of the alcohol recovered. Operating at conditions that leads to the highest alcohol recovery in the range investigated (T = 344 K, P = 12.2 MPa, S/F = 17.6), will lead to a bottoms product containing 16.8 mass % *n*-decane with 74 % of the alcohols recovered.

7.5.1.3 Solvent-to-feed Ratio

In Table 7-15 the input parameters are given for the data points used to generate the plots in Figure 7-13 that show the influence of the solvent-to-feed ratio on the mass flow rates and distribution of the components in the product streams.

Table 7-15 Input parameters used to investigate the influence of solvent-to-feed ratio on the separation performance

Pressure (MPa)	13.0	13.0	13.0	13.0	13.0	13.0	13.0	13.0	13.0
Temperature (K)	344	344	344	344	344	344	344	344	344
Solvent-to-feed ratio (kg/kg)	33.3	27.3	23.1	20.0	17.6	15.8	14.3	13.0	12.0
Number of stages	7	10	13	16	20	20	20	20	20

7 | Establishing a Supercritical Fluid Fractionation Model

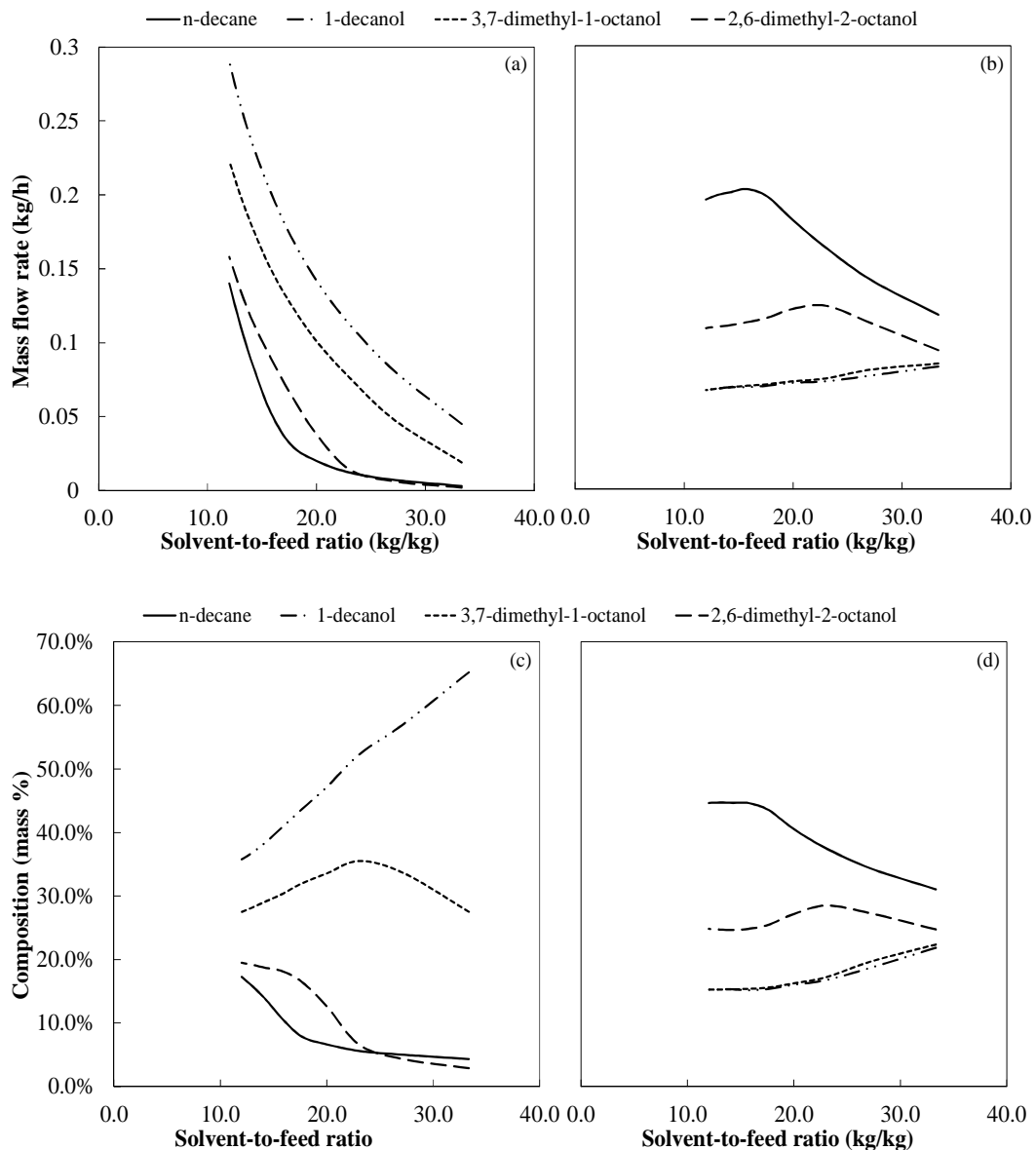


Figure 7-13 Simulated results for the influence of solvent-to-feed ratio on (a) the component mass flow rates in the bottoms product, (b) the component mass flow rates in the extract product, (c) the component distribution in the bottoms product, and (d) the component distribution in the extract product, for Mixture 2 at feed conditions similar to that used in Run 4

The decrease in both the bottoms and extract product mass flow rates with an increase in solvent-to-feed ratio was caused by the reduced amount of material fed to the fractionation column. Although the mass flow rates of the components decrease in the product streams, the extract-to-feed ratio increases with an increase in solvent-to-feed ratio. This trend is in agreement with that observed

7 | Establishing a Supercritical Fluid Fractionation Model

by Schwarz et al. [9]. The solvent-to-feed ratio was adjusted by varying the feed flow rate to the column, and thus lower feed flow rates were required to allow higher solvent-to-feed ratios to be attained. The effect of the solvent-to-feed ratio on the separation performance is more pronounced in the distribution of the components in the product streams. Fractionation at a high solvent-to-feed ratio, typically higher than 20 in this case, will lead to a bottoms product depleted in the undesired component, *n*-decane.

Figure 7-14 shows that even though high solvent-to-feed ratios lead to less *n*-decane in the bottoms product stream, it also leads to higher selectivity ratios which means that a large portion of the alcohols are lost in the extract product. The lowest selectivity ratio occurs at a solvent-to feed ratio of approximately 20, while the optimum alcohol recovery occurs at lower solvent-to-feed ratios. Operating conditions at solvent-to-feed ratios of less than 20 are thus recommended, with the exact value depending on whether the selectivity ratio or alcohol recovery is more highly regarded.

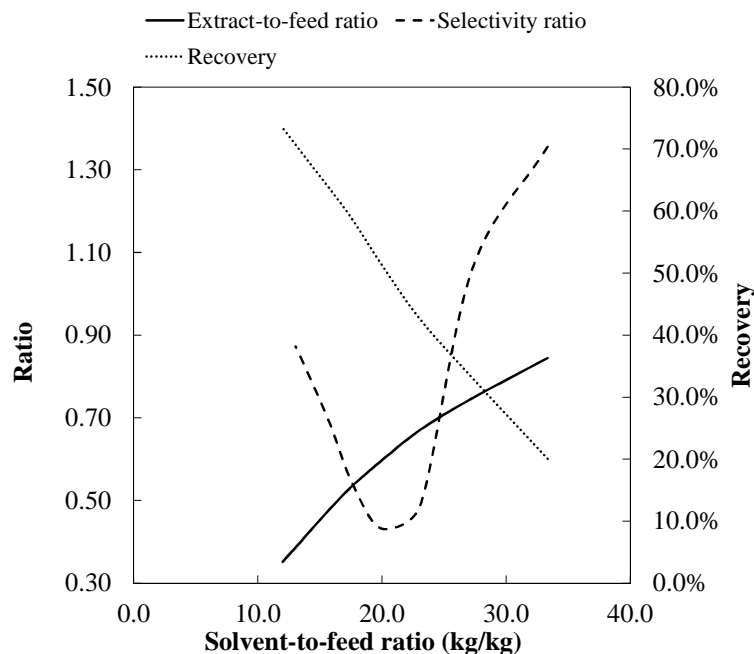


Figure 7-14 Effect of solvent-to-feed ratio on the extract-to-feed ratio, selectivity ratio and recovery of Mixture 2, for feed conditions similar to that used in Run 4

Operating at conditions that lead to the lowest selectivity ratio ($T = 344$ K, $P = 13.0$ MPa, $S/F = 20$) will lead to a bottoms product stream containing 6.6 mass % *n*-decane and 51 % of the

alcohols recovered. Operating at conditions that leads to the highest alcohol recovery in the range investigated ($T = 344$ K, $P = 13.0$ MPa, $S/F = 12$), will lead to a bottoms product containing 17.3 mass % *n*-decane with 73 % of the alcohols recovered.

7.5.2 Investigating Other Feed Mixtures

The SFF process model developed in Aspen Plus[®] can also be used to predict the separation performance of a SFF process with a different feed mixture, consisting of similar components. A prerequisite for the accurate prediction of the separation performance is the accurate representation of the VLE data by the thermodynamic model implemented in the SFF process model. In Chapter 6 it was shown that the RK-ASPEN model with the use of polar parameters and solute-solvent interaction parameters can accurately predict the phase transition pressures of Mixture 1, consisting of $\text{CO}_2 + (20\% \text{ } n\text{-dodecane} + 70\% \text{ } 1\text{-decanol} + 10\% \text{ } 3,7\text{-dimethyl-}1\text{-octanol})$, at temperatures between 318 K and 348 K. It was also shown that the RK-ASPEN model struggles to predict accurate VLE data at low temperatures, and thus it is recommended that the process model developed in Aspen Plus[®] only be used at temperatures higher than 328 K. Care must be taken when extrapolating to temperatures much higher than 348 K, since the thermodynamic model has not been tested in that region.

A similar method of investigation as that conducted for Mixture 2 in section 7.5.1 was applied to investigate the operating region of the SFF process when Mixture 1 is used as the feed mixture. The composition of Mixture 1 differs significantly from Mixture 2, and thus it is expected that different optimum operating conditions will occur. The separation task for Mixture 1, is to remove the *n*-dodecane from the mixture of primary alcohols, *1*-decanol and *3,7*-dimethyl-*1*-octanol. The simulation results with Mixture 1 as the feed mixture will thus reveal whether SFF can successfully separate mixtures of close-boiling detergent range alkanes and alcohols, like *n*-dodecane and *3,7*-dimethyl-*1*-octanol.

Similar feed and solvent flow rates and separation conditions to those used in Run 4 were specified for all the investigations, with the main difference being the composition of the feed mixture. The operating pressure, temperature and solvent-to-feed ratio were varied between values that lead to an extract-to-feed ratio of between 0.3 and 0.7. The extract-to-feed ratio can theoretically be varied between 0 and 1, but it would be unpractical to operate too close to the end points.

7 | Establishing a Supercritical Fluid Fractionation Model

7.5.2.1 Temperature

In Table 7-16 the input parameters for the generation of the plots in Figure 7-15 and Figure 7-16. Mixture 1, CO₂ + (20 % *n*-dodecane + 70 % *l*-decanol + 10 % 3,7-dimethyl-*l*-octanol), requires lower fractionation temperatures at 13.0 MPa compared to that of Mixture 2 (Table 7-13).

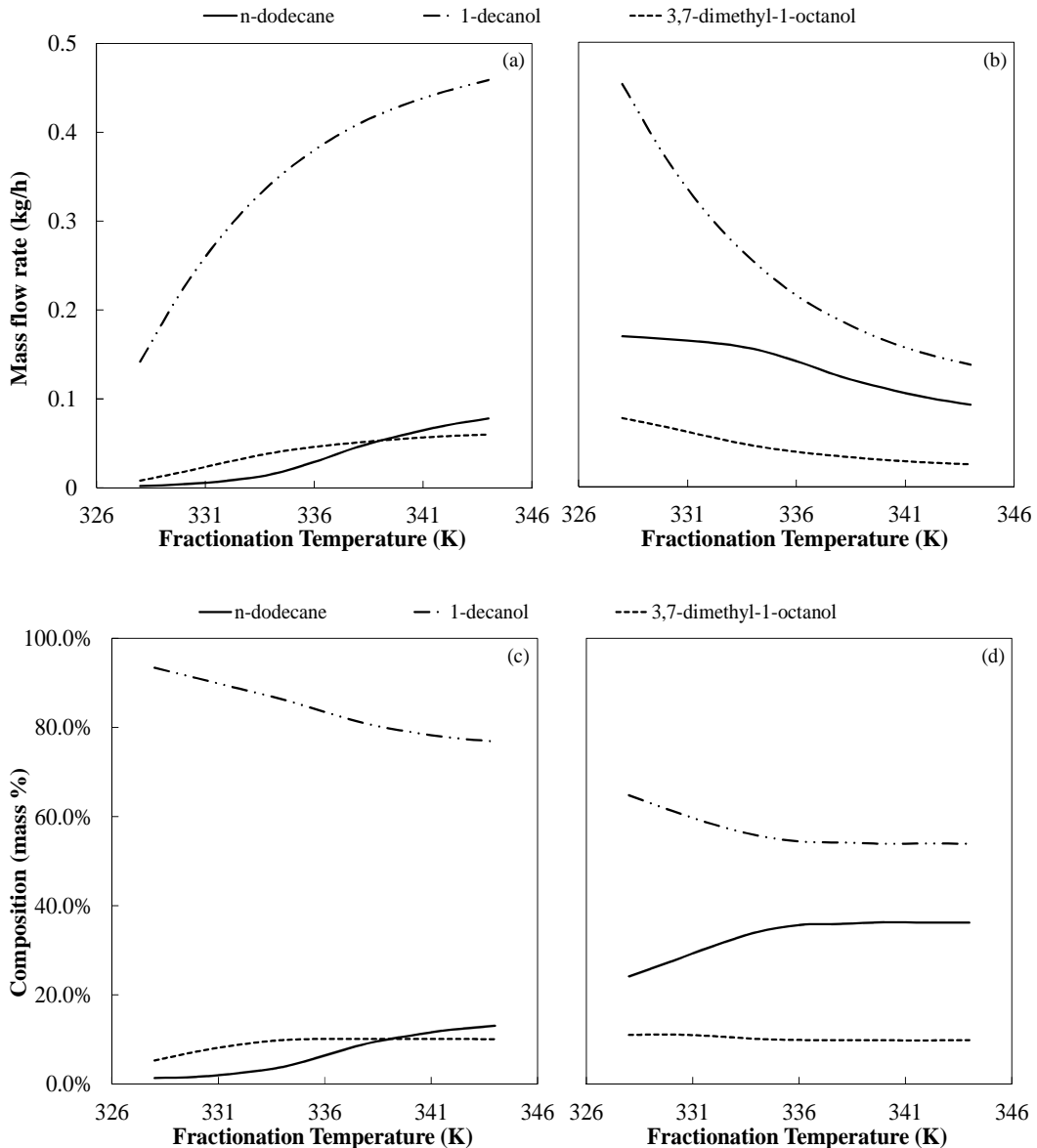


Figure 7-15 Simulated results for the influence of temperature on (a) the component mass flow rates in the bottoms product, (b) the component mass flow rates in the extract product, (c) the component distribution in the bottoms product, and (d) the component distribution in the extract product, for Mixture 1 at feed conditions similar to that used in Run 4

7 | Establishing a Supercritical Fluid Fractionation Model

Table 7-16 Input parameters used to investigate the influence of temperature on the separation performance for Mixture 1

Pressure (MPa)	13.0	13.0	13.0	13.0	13.0	13.0	13.0	13.0	13.0
Temperature (K)	328	330	332	334	336	338	340	342	344
Solvent-to-feed ratio (kg/kg)	17.6	17.6	17.6	17.6	17.6	17.6	17.6	17.6	17.6
Number of stages	8	8	9	11	13	15	17	19	20

From Figure 7-15 it is evident that the *n*-dodecane can be almost completely removed from the alcohol isomer mixture at temperatures below 330 K. However, it is also clear that the mass flow rate of *l*-decanol in the bottoms product stream is very low at low temperatures, indicating that a large portion of *l*-decanol exits in the extract product. The fractionation temperature seem to have a very insignificant effect on the distribution of 3,7-dimethyl-*l*-octanol, since it appears in similar fractions (approximately 10 %) in both the extract and bottoms product stream. The separation performance of the SFF process for the CO₂ + (20 % *n*-dodecane + 70 % *l*-decanol + 10 % 3,7-dimethyl-*l*-octanol) mixture is illustrated in Figure 7-16.

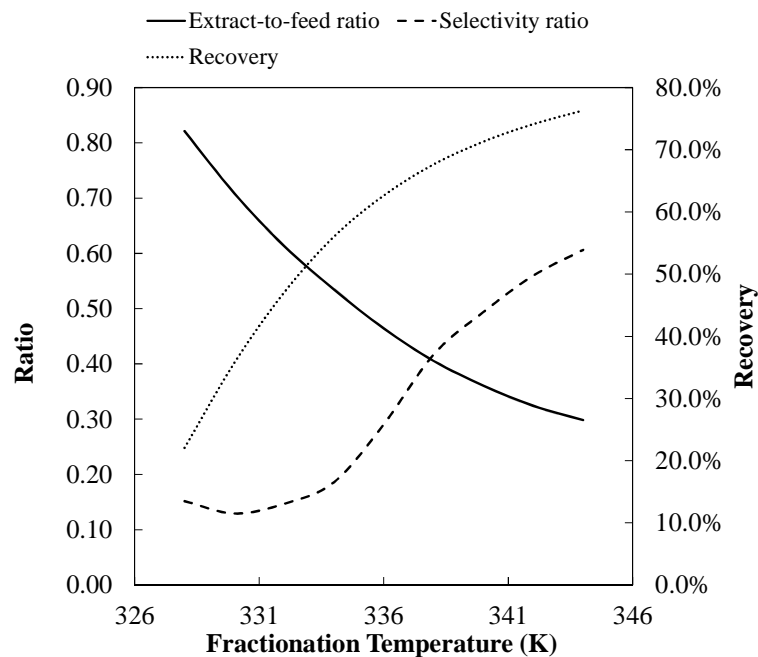


Figure 7-16 Effect of temperature on the extract-to-feed ratio, selectivity ratio and recovery of Mixture 1, for feed conditions similar to that used in Run 4

7 | Establishing a Supercritical Fluid Fractionation Model

The trends observed for the component mass flow rates and distributions in the product streams are evident in the trends of the separation performance parameters. The lowest value of the selectivity ratio occurs near 330 K, but this is also the temperature where the alcohol recovery is lowest. The optimum fractionation temperature of the SFF process for Mixture 1 would thus occur at temperatures higher than 330 K at 13.0 MPa, depending on the required purity and alcohol recovery. If a pure product is required, operation at 330 K will lead to a bottoms stream containing only 1.6 mass % *n*-dodecane, but an alcohol recovery of only 36 %. Operation close to the lower limit of the extract-to-feed ratio (equal to 0.3 for operation at 346 K), will lead to an alcohol recovery of 76 %, but at the cost of a high mass fraction of *n*-dodecane in the bottoms stream (13.0 mass %).

It is interesting to note that the minimum selectivity ratio occurs at an extract-to-feed ratio of approximately 0.5 for Mixture 2 (see Figure 7-10). At extract-to-feed ratios higher and lower than 0.5, the selectivity ratio increases. For Mixture 1 the minimum selectivity ratio occurs closer to the high end of the extract-to-feed ratio. This behaviour can be attributed to the absence of an alcohol isomer with similar phase behaviour than that of the alkane in the mixture. If an alcohol isomer has similar solubility characteristics as that of the alkane, the selectivity ratio is much more sensitive to changes in the phase compositions and a distinct minimum point is observed within the operating limits of the process. The minimum selectivity ratio will then exist at the point where the lowest amount of alkane in combination with the highest amount of alcohol isomer, occurs. However, when the alkanes present in a mixture have phase behaviour that differ significantly from that of the alcohol isomers, the selectivity ratio varies according to the solubility trends of the components, which is usually similar for alkanes and alcohols at higher temperatures. In such a case the selectivity ratio will reach its minimum near the conditions that lead to the minimum amount of the alkane in the bottoms product stream.

7.5.2.2 Pressure

In Figure 7-17 and Figure 7-18 the effect of fractionation pressure on the product streams and separation performance of an SFF process for the separation of the CO₂ + (20 % *n*-dodecane + 70 % 1-decanol + 10 % 3,7-dimethyl-1-octanol) mixture is shown. The input parameters used to generate the plots are shown in Table 7-17.

7 | Establishing a Supercritical Fluid Fractionation Model

Table 7-17 Input parameters used to investigate the influence of pressure on the separation performance for Mixture 1

Pressure (MPa)	12.2	12.4	12.6	12.8	13.0	13.2	13.4	13.6	13.8
Temperature (K)	344	344	344	344	344	344	344	344	344
Solvent-to-feed ratio (kg/kg)	17.6	17.6	17.6	17.6	17.6	17.6	17.6	17.6	17.6
Number of stages	13	15	17	19	20	20	20	20	20

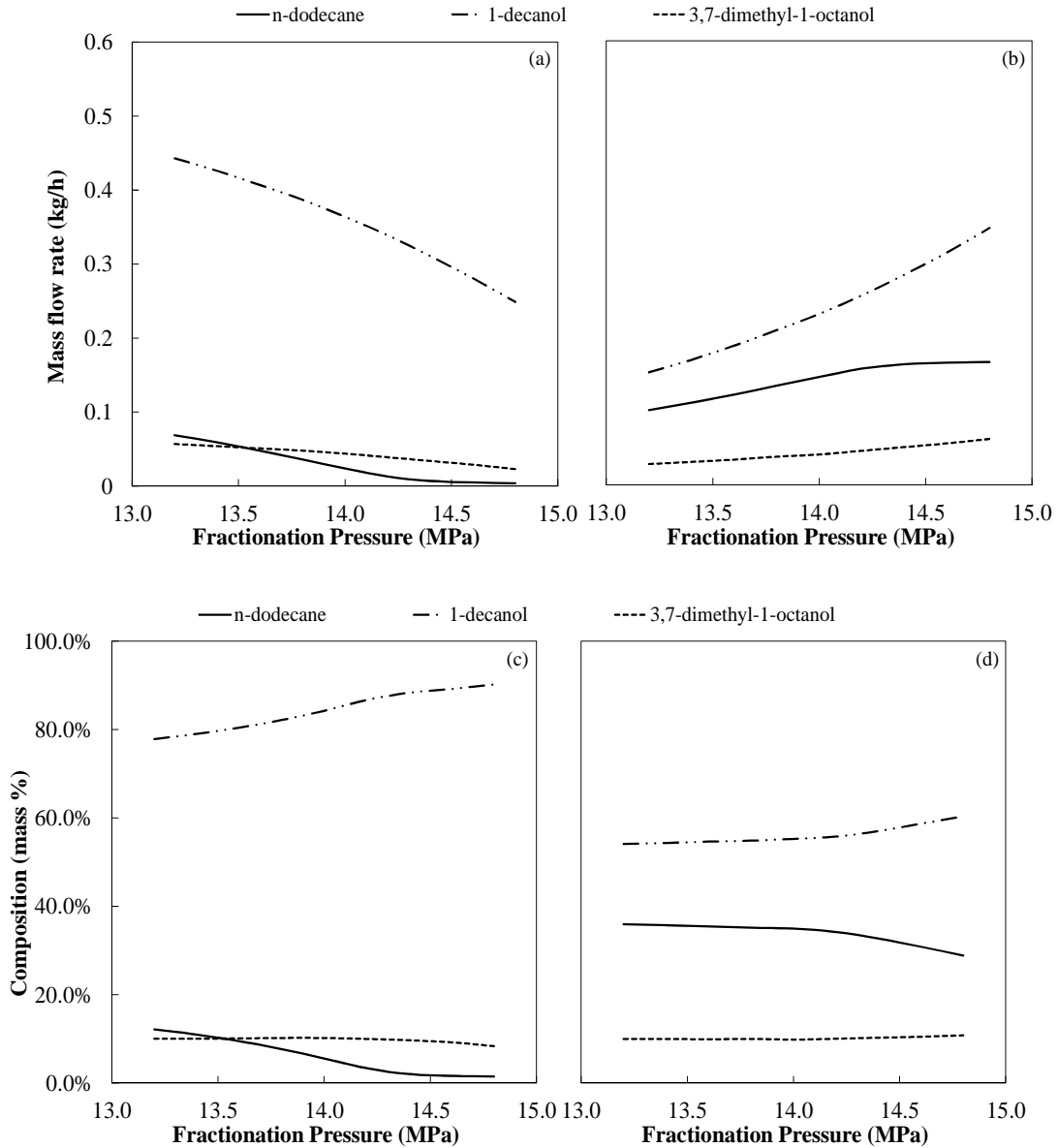


Figure 7-17 Simulated results for the influence of pressure on (a) the component mass flow rates in the bottoms product, (b) the component mass flow rates in the extract product, (c) the component distribution in the bottoms product, and (d) the component distribution in the extract product, for Mixture 1 at feed conditions similar to that used in Run 4

7 | Establishing a Supercritical Fluid Fractionation Model

From Table 7-17 it is clear that the SFF of Mixture 1 requires fractionation pressures much lower than that required for Mixture 2 (see Table 7-14) to generate similar extract-to-feed ratios at 344 K. The plots in Figure 7-17 show a decreased fraction of *n*-dodecane in the bottoms stream as the fractionation pressure is increased. This is similar to the trend observed for Mixture 2 in section 7.5.1.2. However, for Mixture 2 a compromise had to be made on the minimum amount of *n*-dodecane and maximum amount of 2,6-dimethyl-2-octanol in the bottoms product. Since Mixture 1 does not contain an alcohol isomer with similar phase behaviour to that of *n*-dodecane, the fractionation pressures at which the minimum amount of *n*-dodecane occur in the bottoms stream will typically coincide with the minimum selectivity ratio for the process. From Figure 7-18 it is clear that the lowest selectivity ratio occur at pressures higher than 14.6 MPa at 344 K.

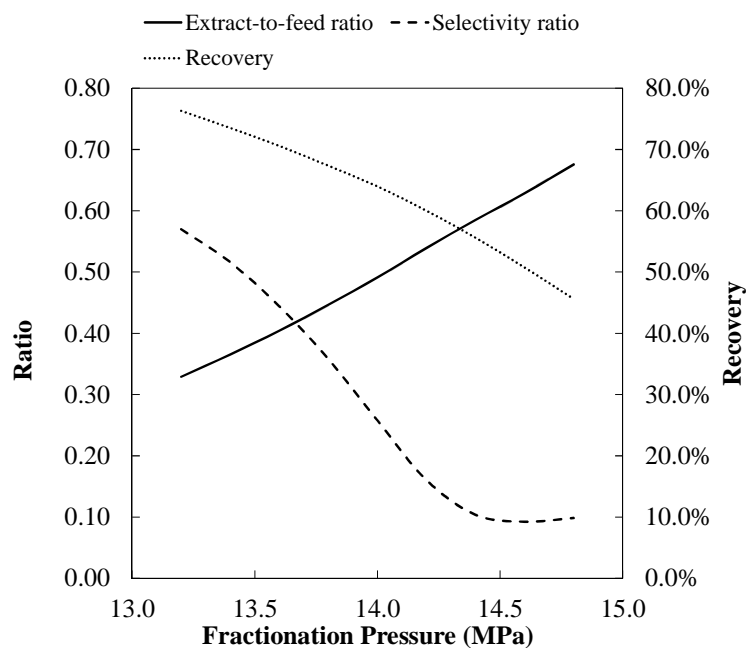


Figure 7-18 Effect of pressure on the extract-to-feed ratio, selectivity ratio and recovery of Mixture 1, for feed conditions similar to that used in Run 4

The optimum fractionation pressure will occur at pressures below 14.6 MPa at 344 K. Within the extract-to-feed ratio range of 0.3 to 0.7 at 344 K, a bottoms product stream with between 1.4 mass % and 12.1 mass % *n*-dodecane can be generated. The alcohol recovery will be between 40 % and 76 %.

7.5.2.3 Solvent-to-feed Ratio

It is clear from Figure 7-19 that a very different relationship exist between the solvent-to-feed ratio and component mass flow rates and distributions, compared to that observed for the fractionation temperature and pressure. The solvent-to-feed ratio was investigated by keeping the solvent flow rate constant and varying the feed flow rate. The conditions used to generate the plots in Figure 7-19 and Figure 7-20 are given in Table 7-18.

Table 7-18 Input parameters used to investigate the influence of solvent-to-feed ratio on the separation performance for Mixture 1

Pressure (MPa)	13.0	13.0	13.0	13.0	13.0	13.0	13.0
Temperature (K)	344	344	344	344	344	344	344
Solvent-to-feed ratio (kg/kg)	42.9	33.3	27.3	23.1	20.0	17.6	15.8
Number of stages	6	7	10	13	16	20	20

Similar to the trend observed for Mixture 2, a higher solvent-to-feed ratio will lead to bottoms product stream depleted in *n*-dodecane. The fraction of 3,7-dimethyl-1-octanol in both the bottoms and extract product stream are not significantly influenced by the fractionation temperature, fractionation pressure or solvent-to-feed ratio. It is interesting to note that the component mass flow rates in the extract stream stay at approximately the same values for all the solvent-to-feed ratios investigated. This is the combined effect of the reduced feed flow rate and increased extract-to-feed ratio, with increasing solvent-to-feed ratios.

7 | Establishing a Supercritical Fluid Fractionation Model

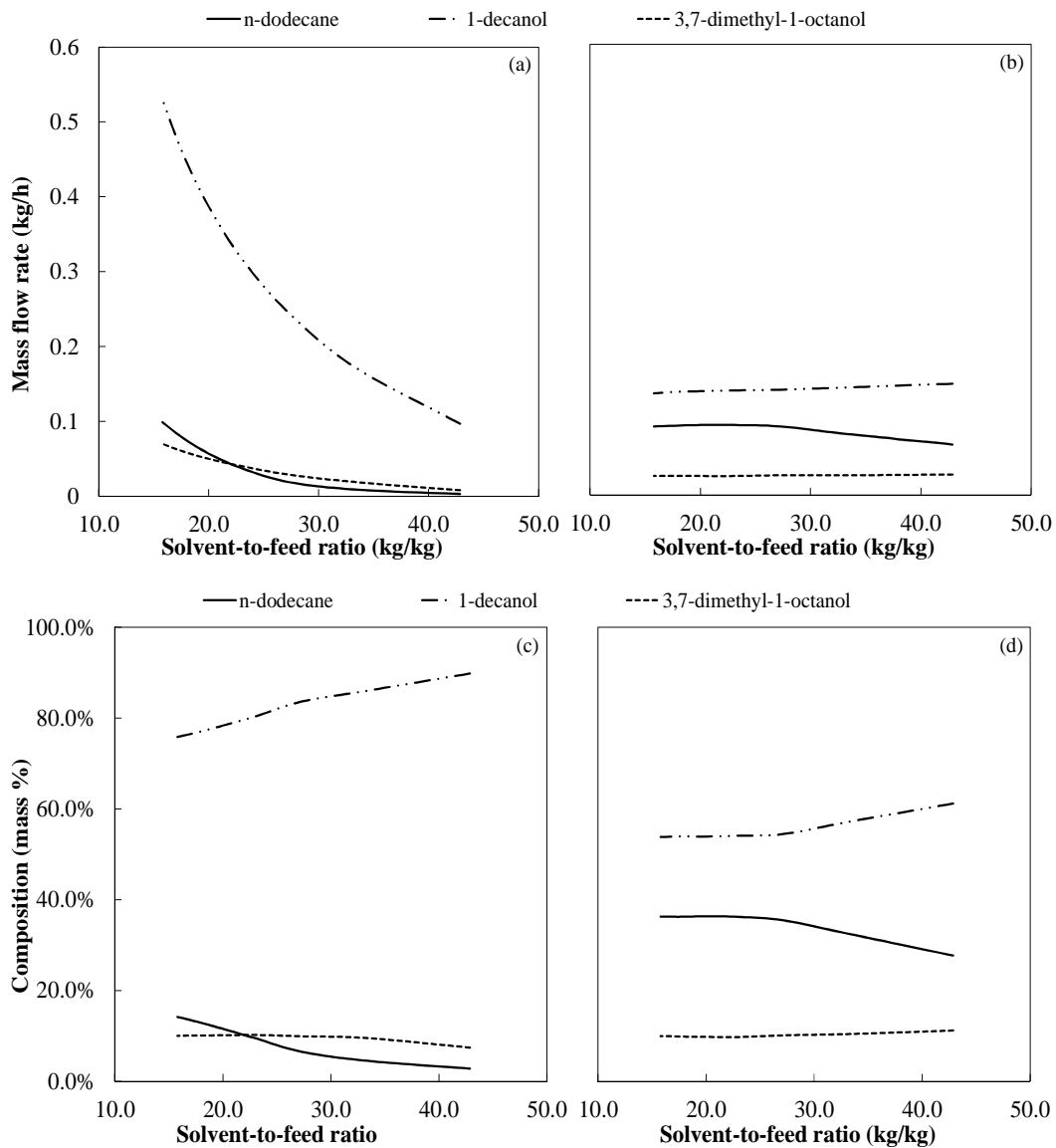


Figure 7-19 Simulated results for the influence of solvent-to-feed ratio on (a) the component mass flow rates in the bottoms product, (b) the component mass flow rates in the extract product, (c) the component distribution in the bottoms product, and (d) the component distribution in the extract product, for Mixture 1 at feed conditions similar to that used in Run 4

7 | Establishing a Supercritical Fluid Fractionation Model

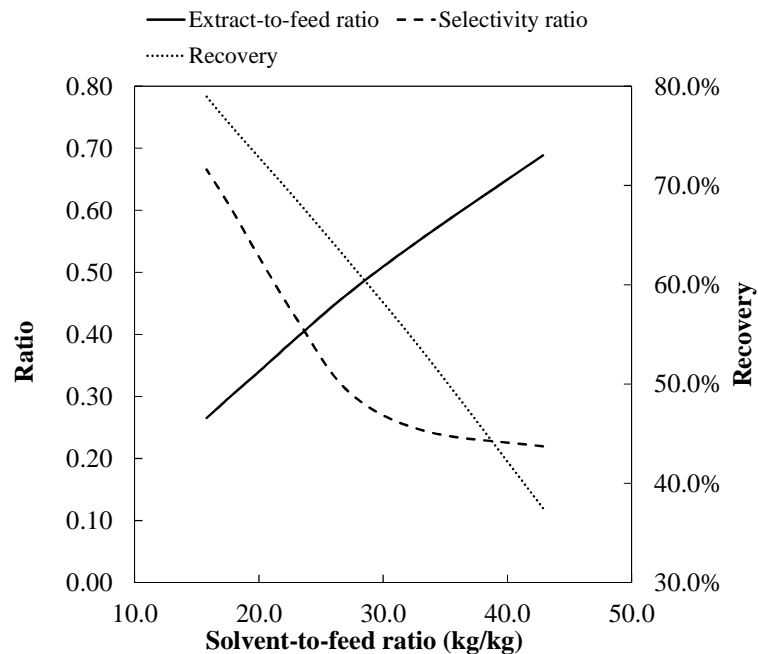


Figure 7-20 Effect of solvent-to-feed ratio on the extract-to-feed ratio, selectivity ratio and recovery of Mixture 1, for feed conditions similar to that used in Run 4

For the removal of *n*-dodecane from Mixture 1, the optimum solvent-to-feed ratio will be less than 30, depending on the required alcohol recovery. An increase in solvent-to-feed ratio beyond 30 does not lead to a significant decrease in the selectivity ratio, but it still causes a reduced alcohol recovery. Lower solvent-to-feed ratios are preferred since it leads to reduced utility and material costs, as well as process units with a reduced capacity. It is thus recommended that the solvent-to-feed ratio be selected based on the hydrodynamic effects in the fractionation column, and the operating temperature and pressure be optimized to generate a bottoms stream that adhere to the product specifications [4].

7.5.3 The Operating Window for the Proposed SFF Process

In the previous sections the SFF process model developed in Aspen Plus[®] was used to investigate the effect of the fractionation temperature, fractionation pressure and solvent-to-feed ratio on the separation performance. This analysis gave some insight into the size of the operating window and the controllability of the process. The limits of the range investigated for each operating parameter was set by the operating limits assumed for the extract-to-feed ratio. An SFF process, such as the one proposed in this project, will typically be operated with an extract-to-feed ratio of between

0.3 and 0.7. For both multi-component mixtures investigated, a fractionation temperature range of 16 K and a fractionation pressure range of 16 MPa lead to operation within the selected limits of the extract-to-feed ratio. An operating window of this size will allow for good controllability of the process [4]. The proposed solvent-to-feed ratio range was slightly larger for Mixture 1, CO₂ + (20 % *n*-dodecane + 70 % *l*-decanol + 10 % 3,7-dimethyl-*l*-octanol), compared to Mixture 2, CO₂ + (25 % *n*-decane + 25 % *l*-decanol + 25 % 3,7-dimethyl-*l*-octanol + 25 % 2,6-dimethyl-2-octanol).

The composition of the feed mixture will have an effect on the limits of operating parameters. Mixture 1 requires operation between 328 K and 344 K at 13.0 MPa and S/F = 17.6, while Mixture 2, requires operation between 338 K and 354 K at 13.0 MPa and S/F = 17.6 for operation within the selected extract-to-feed ratio limits of 0.3 to 0.7. At a certain set of operating conditions a change in the feed composition will influence the limits of the operating window, while it is anticipated that a change in the solvent type and solvent flow rate will lead to a change in the size of the operating window.

Although it is recommended that a separate analysis be conducted for every feed mixture investigated, some of the characteristics observed for the two mixtures investigated in this study can be generalized for the SFF of mixtures of detergent range alkanes and alcohol isomers. When an alcohol and an alkane with similar phase behaviour exist in a mixture a distinct minimum selectivity ratio will occur at a point within the extract-to-feed ratio limits of the process. When the alkanes and alcohols present in a mixture do not have similar or overlapping phase transition pressures, the minimum selectivity ratio will typically cover a small range of extract-to-feed ratios at the high end limit of the extract-to-feed ratio range. Operating the SFF process at conditions that lead to the minimum selectivity ratio, will produce to the most pure alcohol product. In this investigation it was shown that mixtures of close-boiling alkanes and alcohol isomers can be separated with SFF to such an extent that an alcohol product with less than 5 mass % alkanes can be produced. When evaluating an SFF process the presence of components with overlapping phase transition pressures are the main concern, not the presence of components with overlapping boiling points or low relative volatilities.

7.6 Separation Performance Comparison to Azeotropic Distillation

In Table 7-19 the separation performance results of the SFF process investigated for Mixture 1 and Mixture 2 are compared to that reported by Crause [10] for azeotropic distillation of a mixture of C₁₀ – C₁₅ alkanes and C₁₁ – C₁₆ alcohols. In the azeotropic distillation process investigated by Crause

7 | Establishing a Supercritical Fluid Fractionation Model

[10] a bottoms product containing 5.3 mass % alkanes was produced. The operating conditions of the SFF process that lead to approximately the same mass fraction of alkanes in the bottoms product for Mixture 1 and Mixture 2 were selected, and the separation performance compared to the azeotropic distillation process in Table 7-19.

Table 7-19 Comparison between the separation performance of SFF and azeotropic distillation for the separation of detergent range alkanes and alcohols

	This work		Crause [10]
	Mixture 1	Mixture 2	
Operating Conditions			
Temperature (K)	336	340	473
Pressure (MPa)	13.0	13.0	0.0016 – 0.0031
Solvent-to-feed / Entrainer-to-feed ratio	17.6	17.6	1.8
Number of Stages	13	17	35
Feed (mass %)			
Alkanes (linear + branched + other)	20	25	45.6
Branched alcohols	10	50	15.1
Linear alcohols	70	25	30.8
Other alcohols	0	0	8.5
Bottoms Product (mass %)			
Alkanes (linear + branched + other)	6.4	5.5	5.3
Branched alcohols	10.1	45.0	26.0
Linear alcohols	83.5	49.5	53.8
Other alcohols	0	0	14.9
Top Product (mass %)			
Alkanes (linear + branched + other)	35.7	39.1	99.5
Branched alcohols	9.9	44.3	0.5
Linear alcohols	54.4	16.6	0
Other alcohols	0	0	0
Separation Performance			
Extract-to-feed ratio	0.56	0.64	0.49
Selectivity ratio	0.29	0.49	0.12
Alcohol recovery (%)	63.0	47.0	99.6

From the results in Table 7-19 it is clear that the SFF process can produce a bottoms product with similar purity of approximately 95 mass % alcohols, compared to the azeotropic distillation

process. The selectivity ratios for the two processes are of similar magnitude, with the azeotropic distillation process having a slightly lower selectivity ratio. The major difference in the separation performance of the two processes is the recovery of the alcohol product which is almost double for azeotropic distillation. It should, however, be noted that the operating conditions of the SFF process was not optimized for the production of a 95 % pure alcohol product, and thus the possibility exist that other combinations of operating parameters can lead to a bottoms product with similar purity, but with slightly better values for the separation performance parameters. However, it is not expected that the alcohol recovery of the azeotropic distillation process can be matched. To improve the selectivity ratio and especially the alcohol recovery of the SFF process, it is recommended that the extract product stream be routed to a second fractionation column where the remaining alcohols can be separated from the alkane product.

A comparison between the separation performance of the azeotropic distillation process and the SFF process, indicate that the azeotropic distillation process is superior. However, there are a few considerations, other than separation performance, that may promote the SFF process: a much less expensive and harmful solvent is required; smaller columns with fewer stages can be used; much lower operating temperatures are required; less additional process units are required to remove the solvent from the products; and products with a higher purity can be produced.

7.7 Outcomes of this Chapter

In Chapter 7 the methodology employed to develop an SFF process model for the separation of mixtures of detergent range alkanes and alcohols in Aspen Plus[®] is reported – thus addressing Objective 7, as mentioned in Chapter 1. The model was built using process units available in Aspen Plus[®] and implementing the thermodynamic model developed in Chapter 6. Verification of the model was done by comparing the simulated results to results generated on an SFF pilot plant. Once the model was verified, different operating conditions were investigated for two multi-component mixtures. To address Objective 8, it was shown that an SFF process can produce an alcohol product stream that contains less than 5 % alkanes, even if close-boiling alkanes and alcohols occur in the mixture.

7 | Establishing a Supercritical Fluid Fractionation Model

The key observations made in this chapter include:

- From experimental pilot plant data it was found that an SFF process can be used to successfully separate detergent range alkanes and alcohol isomers, even if the alkanes and alcohols have similar boiling points.
- Operating the SFF process at low temperatures with supercritical CO₂ as the solvent will lead to good separation performance, but poor controllability. The thermodynamic model developed in Chapter 6 cannot accurately predict phase compositions at low temperatures. Based on the two observations made, the low temperature region (below 328 K) was not investigated for the proposed process.
- The SFF process model developed in this work can be used to predict the component mass flow rates (kg/h) of the two product streams with an error of 10 – 36 %.
- At a specific fractionation pressure and solvent-to-feed ratio, the selectivity ratio will decrease with decreasing fractionation temperature up to a minimum point after which it will increase again. However, the alcohol recovery decreases continuously with a decrease in the fractionation temperature.
- At a specific fractionation temperature and solvent-to-feed ratio, the selectivity ratio will decrease with increasing fractionation pressure up to a minimum point after which it will increase again. However, the alcohol recovery decreases continuously with an increase in the fractionation pressure.
- At a specific fractionation temperature and pressure, the selectivity ratio will decrease with an increase in solvent-to-feed ratio up to a minimum point after which it will increase again. However, the alcohol recovery decreases continuously with an increase in the fractionation solvent-to-feed ratio.
- When an alcohol and an alkane with similar phase behaviour exist in a mixture, a distinct minimum selectivity ratio will occur at a point within the extract-to-feed ratio limits of the process. When the alkanes and alcohols present in a mixture do not have similar or overlapping phase transition pressures, the minimum selectivity ratio will typically cover a small range of extract-to-feed ratios at the high end limit of the extract-to-feed ratio range.

7 | Establishing a Supercritical Fluid Fractionation Model

- The presence of components with overlapping phase transition pressures are the main concern when evaluating the feasibility of an SFF process, not the presence of components with overlapping boiling points or low relative volatilities.
- The most pure alcohol product will be produced at conditions that lead to the lowest selectivity ratio. This usually occurs in combination with a low alcohol recovery. Recommended optimum operating conditions will be those that lead to a bottoms product containing 90 – 95 % alcohols of which 60 – 70 % can be recovered.
- An operating window size of 16 K and 16 MPa near 344 K and 13.0 MPa exists for the proposed process. Within this operating window extract-to-feed ratios of 0.3 to 0.7 occur. Operating the SFF process at these conditions will lead to good controllability.
- The separation performance of the SFF process compares well to that of azeotropic distillation, but cannot produce similar alcohol recoveries at the required alcohol product purity specifications. The SFF process does hold other advantages with regard to running and capital costs that could make it the superior process to consider for the separation of detergent range alkanes and alcohols, and thus it is recommended that an economic analysis be conducted for both processes.

7.8 Significant Contributions

The main contribution of the work presented in this chapter is in the form of a process model that is able to predict the separation performance of an SFF process for mixtures of detergent range alkanes and alcohols within certain accuracy limits. Results generated with this model was used in combination with experimental data for the CO₂ + (25 % *n*-decane + 25 % *l*-decanol + 25 % 3,7-dimethyl-*l*-octanol + 25 % 2,6-dimethyl-2-octanol) system to prove that is feasible to use an SFF process to separate an alkane from a mixture of alcohol isomers. Simulation results for the CO₂ + (20 % *n*-dodecane + 70 % *l*-decanol + 10 % 3,7-dimethyl-*l*-octanol) mixture, indicated that SFF can be successfully employed to separate an alkane from a mixture of alcohol isomers, where the alkane and one of the alcohol isomers had boiling points located close to one another.

Some of the results discussed in this chapter were compiled and presented separately at two international conferences as a poster and an oral respectively:

- M. Zamudio, C.E. Schwarz, J.H. Knoetze, The effect of branched alcohol isomers on the separation of alkanes and alcohols with supercritical CO₂, The 13th European Meeting on Supercritical Fluids, The Hague, Netherlands (2011).
- M. Zamudio, C.E. Schwarz, J.H. Knoetze, Using Aspen Plus[®] to determine the viability of a supercritical fractionation process for the separation of detergent range alkane and alcohol isomers, The 6th International Symposium on High Pressure Processes Technology, Belgrade, Serbia (2013).

7.9 Nomenclature

Symbol/ Acronym	Description
AAD	Average Absolute Deviation
E	Extract
F	Feed
<i>m</i>	Mass flow rate
R	Recovery
S	Selectivity
SFF	Supercritical Fluid Fractionation
SR	Selectivity Ratio
X	Mass fraction in the heavy phase
Y	Mass fraction in the light phase
Sub/Superscripts	Description
<i>desired</i>	Refers to the components desired in a stream
<i>product stream</i>	Refers to one of the product streams
<i>undesired</i>	Refers to the components not desired in a stream

7.10 References

- [1] G. Brunner, Counter-current separations, The Journal of Supercritical Fluids. 47 (2009) 574 – 582.

- [2] J.C. Crause, Supercritical fluid extraction of paraffin wax, PhD Dissertation, Stellenbosch University, 2001.
- [3] G.J.K. Bonthuys, C.E. Schwarz, A.J. Burger, J.H. Knoetze, Separation of alkanes and alcohols with supercritical fluids. Part I: Phase equilibria and viability study, *The Journal of Supercritical Fluids*. 57 (2011) 101 – 111.
- [4] C.E. Schwarz, G.J.K. Bonthuys, R.F. van Schalkwyk, D.L. Laubscher, A.J. Burger, J.H. Knoetze, Separation of alkanes and alcohols with supercritical fluids. Part II. Influence of process parameters and size of operating window, *The Journal of Supercritical Fluids*. 58 (2011) 352 – 359.
- [5] J.C. Crause, I. Nieuwoudt, Fractionation of paraffin wax mixtures, *Industrial & Engineering Chemistry Research*. 39 (2000) 4871 – 4876.
- [6] W. Pietzonka, Ch.Trepp, Multistage high pressure mixer-settler system, in: *Process Technology*, Elsevier Science B.V., The Netherlands, 1996: pp. 609 – 614.
- [7] J.D. Seader, E.J. Henley, *Separation Process Principles*, 2nd ed., John Wiley & Sons, Inc., New Jersey, 2006.
- [8] A. B. de Haan, J. de Graauw, Mass transfer in supercritical extraction columns with structured packings for hydrocarbon processing, *Industrial & Engineering Chemistry Research*. 30 (1991) 2463 – 2470.
- [9] C.E. Schwarz, I. Nieuwoudt, J.H. Knoetze, Concentration of Wax-like Alcohol Ethoxylates with Supercritical Propane, *Chemical Engineering Technology*. 30 (2007) 737 – 741.
- [10] J.C. Crause, Production of detergent range alcohols, US 7652173 B2, 2010.

8. CONCLUSIONS AND RECOMMENDATIONS

8.1 REVIEWING THE OBJECTIVES OF THIS STUDY	294
8.2 THE SEPARATION OF DETERGENT RANGE ALKANE-ALCOHOL MIXTURES	295
8.2.1 Objective 1: The Current Separation Process.....	296
8.2.2 Objective 2: The Proposed Separation Process	296
8.3 REQUIREMENTS FOR ESTABLISHING A PROCESS MODEL	297
8.3.1 Objective 2: Confirmed Process Modelling Strategies in Aspen Plus®	297
8.3.2 Objective 3: Confirmed Thermodynamic Modelling Strategies in Aspen Plus® ..	297
8.3.3 The Proposed Strategy.....	298
8.4 OBJECTIVE 4: THE PHASE BEHAVIOUR OF BINARY MIXTURES	299
8.5 OBJECTIVE 5: THE PHASE BEHAVIOUR OF MULTI-COMPONENT MIXTURES	300
8.6 OBJECTIVE 6: THERMODYNAMIC MODEL DEVELOPMENT	301
8.7 OBJECTIVE 7: SFF PROCESS MODEL DEVELOPMENT	302
8.8 OBJECTIVE 8: THE FEASIBILITY OF THE PROPOSED SFF PROCESS	303
8.9 NOVEL CONTRIBUTIONS OF THIS WORK	303
8.10 RECOMMENDATIONS FOR FUTURE WORK	305
8.10.1 Investigating Co-solvency Effects.....	305
8.10.2 Improving the Thermodynamic Model	305
8.10.3 Investigating Variations in the SFF Process Configuration	306

8.11 NOMENCLATURE.....	306
8.12 REFERENCES.....	306

The main aim of this study was to develop a working process model in Aspen Plus® for a supercritical fluid fractionation (SFF) process aimed at the separation of detergent range alkanes and alcohol isomers. Once such a process model was established, the secondary aim was to use it to predict the feasibility and separation performance of the process for different feed mixtures (of detergent range alkanes and alcohol isomers) and different operating conditions, within the accuracy limits of the model. This significantly reduced the amount of experimental work required to determine the feasibility of an SFF process for the separation of a specific feed mixture.

This chapter gives an overview of the objectives that were formulated for this study and the methods employed to achieve those objectives. The significant observations that were made during the development of the SFF process model are also presented. Recommendations for future work that can lead to an improved process model are given at end.

8.1 Reviewing the Objectives of this Study

In order to achieve the main aim of this project, the following objectives were formulated:

1. Conduct a literature review to determine the source, production and application of alkane-alcohol mixtures that occur in the detergent and surfactant industries, and the current separation technologies employed to separate such mixtures.
2. Report on the use of SFF for the purpose of separating detergent range alkane-alcohol mixtures, as well as on the modelling of SFF processes, as published in the literature.
3. Conduct a literature review to determine the expected phase behaviour of the mixtures to be used in this study, and report on previous attempts to model the phase behaviour of such mixtures.

4. Investigate the phase behaviour of isomers of detergent range alkanes and alcohols in supercritical solvents by experimentally measuring and comparing bubble and dew point data. These results will also be used to investigate solute-solvent interactions for the different compounds.
5. Investigate the effect of solute-solute interactions in mixtures by experimentally measuring the bubble and dew point data of ternary and multi-component mixtures and comparing it to the phase behaviour of that reported for the binary mixtures.
6. Develop a thermodynamic model in Aspen Plus[®] that can accurately predict the phase behaviour of the multi-component mixtures used in this investigation. The accuracy of the model will be verified by comparing it to experimentally measured bubble and dew point data.
7. Develop a process model in Aspen Plus[®] that can accurately predict the process performance of an SFF process intended for the separation of detergent range alkanes and alcohol isomers. The accuracy of the model will be verified by comparing it to experimentally measured pilot plant data.
8. Determine the feasibility of an SFF process for the separation of detergent range alkanes from mixtures of detergent range alcohol isomers, by evaluating the predicted separation performance for different feed mixtures.

In the sections that follow the results of the studies conducted to reach each objective, are reported.

8.2 The Separation of Detergent Range Alkane-Alcohol Mixtures

In Chapter 2 it was reported that alkane-alcohol mixtures commonly occur in the detergent, surfactant and phthalate industries. They are usually encountered in the product streams of alcohol manufacturing processes, like the Oxo process. To obtain a more pure alcohol product, it is required that the alkanes be removed from the alcohol isomer mixtures. Conventional separation processes, like distillation, cannot be considered in this case since the co-existing detergent range alkanes and alcohol isomers often have overlapping boiling points and/or low relative volatilities. The process currently employed in industry for the separation of detergent range alkanes and alcohol isomers, is

azeotropic distillation. The azeotropic distillation process performs well, but some concerns regarding the operating conditions prompted an investigation into an alternative separation process. In this work supercritical fluid fractionation (SFF) is considered as a potential process for the separation of mixtures of detergent range alkanes and alcohol isomers.

8.2.1 Objective 1: The Current Separation Process

The azeotropic distillation process that is proposed by Crause [1] for the separation of detergent range alkanes and alcohol isomers, are to be operated at 0.016 – 0.031 MPa and 473 K with diethylene glycol (DEG) as the entrainer in an entrainer-to-feed ratio of 1:1.8. The process requires 35 stages and can produce an alcohol isomer stream containing only 5 mass % alkanes while recovering 99.6 % of the alcohols in the feed mixture.

The major concern regarding the azeotropic distillation process is the use of harmful entrainers like DEG. DEG is toxic to humans and thus it not only poses a health risk to plant operators, but also limits the use of the alkane or alcohol product generated by this process to products not intended for human consumption. Other inconveniences regarding the azeotropic distillation process are: high operating temperatures which can lead to degradation of compounds; and additional processing equipment and materials (like water) to separate the entrainer from the top product.

8.2.2 Objective 2: The Proposed Separation Process

The problematic aspects of the azeotropic distillation process can be addressed by replacing it with an SFF process. Chapter 3 was concerned with the research of the feasibility of the SFF process for the separation of detergent range alkanes and alcohols.

Previous studies were found in the literature where SFF was successfully employed to separate alkanes according to chain length [2] and to separate a primary linear alcohol from a linear alkane [3,4]. From the results produced by these studies it was concluded that SFF does have the potential to separate a mixture of alkanes and alcohol isomers, if the phase behaviour of the compounds required to be separated differ significantly in the solvent. It was thus important to investigate the phase behaviour of typical compounds encountered in the product streams of the alcohol manufacturing process, and thus Objective 4 was formulated.

The grossly contracted version of the proposed SFF process consists of a fractionation column and a separator, of which the operating conditions and separation performance are to be determined

from an investigation using the developed process model. The benefits of using an SFF process instead of an azeotropic distillation process are: less harmful solvents, like CO₂, are considered; mild operating temperatures well below 373 K will in all likelihood bring about sufficient separation; a single processing unit and no additional material streams are required to remove the solvent from the top product.

8.3 Requirements for Establishing a Process Model

Since other studies in the literature reported successful results with SFF for similar compounds, it was decided to pursue the investigation of this process for the separation of typical mixtures of detergent range alkanes and alcohols. The aim was to obtain information about the operating window size and separation performance of the process without conducting an excessive amount of pilot plant experiments. It was decided to develop a process model in Aspen Plus[®] that will enable the accurate prediction of the required process performance data.

8.3.1 Objective 2: Confirmed Process Modelling Strategies in Aspen Plus[®]

An equilibrium stage modelling approach was taken in the development of the SFF process model. Since the scope of this study includes the evaluation of the feasibility of the proposed SFF process, and not the detailed design of the process, a more simplistic approach is justified.

Two other studies were found in the literature that reported successful SFF process modelling results with the use of Aspen Plus[®] [5,6]. Both these studies used a module of flash drums to simulate the equilibrium stages of the fractionation column. A similar approach was followed in this work with the use of the Aspen Plus[®] built-in liquid-liquid extraction column (*Extract*) model, which is similar to a module of flash drums, but employs a different solution algorithm.

8.3.2 Objective 3: Confirmed Thermodynamic Modelling Strategies in Aspen Plus[®]

An accurate thermodynamic model needs to be employed in the SFF process model to ensure that accurate phase compositions and other thermodynamic properties are predicted. From data published in the literature it was concluded that simple and robust models, like cubic equations of state (EoS) can predict sufficiently accurate data for mixtures at high pressures and therefore the use of a complex model, like SAFT, are not required [7,8]. The use of simple models with less

parameters are often preferred for industrial applications [9], and thus it was decided to focus on the use of cubic EoS to model the phase behaviour of the systems investigated in this work.

Aspen Plus[®] has a variety of built-in cubic EoS available for use in the SFF process model. Different mixing rules and alpha functions can be employed in the cubic EoS to improve their accuracy for the specific type of system under consideration. It is recommended that binary interaction parameters be employed to increase the ability of cubic EoS to represent the type of systems considered in this work [10]. An investigation into the most appropriate model for the systems used in this study was conducted, which aided in the fulfilment of Objective 6.

8.3.3 The Proposed Strategy

The methodology depicted in Figure 8-1 was employed in this investigation to develop a working SFF process model in Aspen Plus[®]. The methodology was developed based on the reported process and thermodynamic modelling approaches for similar systems to the ones being investigated in this study.

Pure component and binary interaction parameters can be obtained by experimentally measuring data, or by using published data or correlations to predict the data required for the calculation of these parameters. In this work the data required to determine the pure component parameters were obtained from published databases and predicted from correlations. The data required for the calculation of the binary interaction parameters were experimentally measured.

In this study two verification steps were employed which allowed detection of the shortcomings of both the thermodynamic model and the process model.

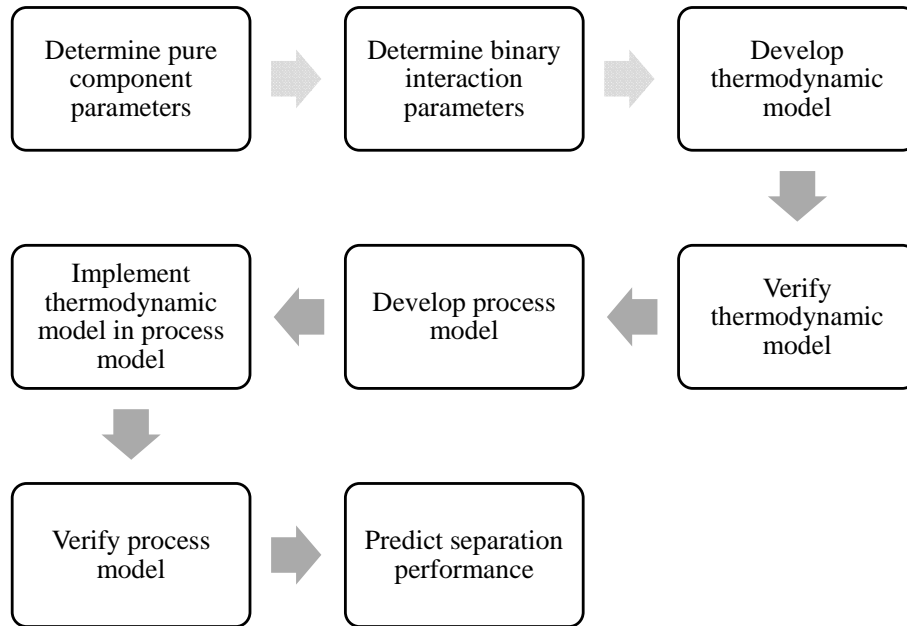


Figure 8-1 Proposed methodology for the development of an equilibrium stage separation process model in a commercial simulation software program

8.4 Objective 4: The Phase Behaviour of Binary Mixtures

The process model developed in this work is applicable to isomeric mixtures of detergent range alkanes and alcohols. Very little information on the phase behaviour of isomers of linear detergent range alkanes and alcohols in supercritical solvents are available in the literature [11,12], and thus an experimental study was conducted to determine if and how the phase behaviour of alkane and alcohol isomers differ in supercritical solvents.

C₁₀-alkanes and C₁₀-alcohols were selected as model compounds to investigate the separation of detergent range alkanes and alcohols. Bubble and dew point data were experimentally measured for nine compounds in both supercritical CO₂ and ethane with a static synthetic method utilizing a high pressure view cell. Measurements were conducted in the temperature range 308 – 348 K and at compositions of 0.01 – 0.7 mass fraction solute. The solutes investigated were as follows: *n*-decane, 2-methylnonane, 3-methylnonane, 4-methylnonane, 1-decanol, 2-decanol, 3,7-dimethyl-1-octanol, 2,6-dimethyl-2-octanol, and 3,7-dimethyl-3-octanol.

The phase transition pressures of the C₁₀-alkane isomers did not differ significantly from one another in the temperature, pressure and composition range studied. Since neither of the solvents could distinguish between the methyl-branched isomers of *n*-decane, separation of these compounds with supercritical fluid fractionation is in all likelihood not possible.

Significant differences were observed for the phase behaviour of some of the branched C₁₀-alcohol isomers in both supercritical CO₂ and ethane. The measured phase transition data of the C₁₀-alcohol isomers indicated that movement of the hydroxyl group away from the primary carbon atom towards the centre of the hydrocarbon backbone leads to a decrease in the phase transition pressure of the compound. The addition of side branches and accompanying shortening of the hydrocarbon backbone also leads to a decrease in the phase transition pressure. Both these phenomena can be ascribed to the shielding of the polar hydroxyl group by the hydrocarbon backbone and/or side branches, and the accompanying decrease in interaction between solute molecules. The order in which the phase transition pressures of the C₁₀-alcohol isomers increased was as follows: 3,7-dimethyl-3-octanol, 2,6-dimethyl-2-octanol, 2-decanol, 3,7-dimethyl-1-octanol and 1-decanol. Similar trends were displayed in supercritical CO₂ and ethane. The use of supercritical ethane led to significantly lower phase transition pressures being observed for all the compounds investigated, but apart from this no other advantages for the use of ethane instead of CO₂, e.g. improved selectivity, occurred. CO₂ was thus selected as the solvent to be used for further investigation, since it is non-toxic, non-flammable, inert, readily available and less expensive, compared to ethane.

8.5 Objective 5: The Phase Behaviour of Multi-component Mixtures

Ternary and multi-component mixtures consisting of the compounds used to study the binary phase behaviour of detergent range alkane and alcohol isomers in supercritical fluids were constructed and the phase transition pressures measured. The same experimental method, equipment and range reported for the investigation of the phase behaviour of the binary mixtures, was applied for the investigation into the phase behaviour of the multi-component mixtures.

The phase behaviour of the multi-component mixtures in supercritical CO₂ revealed that solute-solute interactions are present and that the phase behaviour in the majority of the composition range of the multi-component mixtures cannot be anticipated by studying the phase behaviour of the comprising binary mixtures. In the low solute mixture concentration region, where the solute-solute interactions are minimal, the phase transition pressures can be approximated by the ratios of the

solutes in the mixture and their respective binary phase transition pressures in the solvent. However, for certain mixtures of alkanes and alcohols complex effects, like co-solvency, can occur.

8.6 Objective 6: Thermodynamic Model Development

To use the proposed SFF process model to predict the separation performance of a process, a thermodynamic model that can accurately predict the phase behaviour of multi-component mixtures of detergent range alkanes and alcohol isomers in supercritical CO₂, is required. The RK-ASPEN thermodynamic model was selected for use in the process model due to its ability to accurately predict multi-component VLE data for mixtures of CO₂ and different compositions of alkanes and alcohols, within the temperature range 318 K – 348 K with the inclusion of regressed pure component polar and binary solute-solvent interaction parameters.

The predictive ability of the RK-ASPEN model was evaluated by comparing the phase transition pressures predicted by the model to experimentally measured phase transition pressures for two mixtures: CO₂ + (20 % *n*-dodecane + 70 % *l*-decanol + 10 % 3,7-dimethyl-*l*-octanol); and CO₂ + (25 % *n*-decane + 25 % *l*-decanol + 25 % 3,7-dimethyl-*l*-octanol + 25 % 2,6-dimethyl-2-octanol). Generally the phase transition pressures were predicted more accurately at the high temperatures (338 – 348 K). For Mixture 1 the percentage average absolute deviation (%AAD) in the predicted phase transition data decreased from 20.9 % to 4.4 % at 348 K when the regressed polar parameters and binary solute-solvent parameters were included in the RK-ASPEN model. For Mixture 2 the %AAD decreased from 11.7 % to 5.7 % at 348 K. Further improvements were observed when the regressed solute-solute interaction parameters were included in the RK-ASPEN model when the %AAD reduced to 1.5 % and 1.9 % at 348 K for Mixture 1 and 2 respectively. Although an improvement in the phase transition pressure predictions of multi-component mixtures were observed, verification of the predicted phase compositions was not possible since only experimental phase transition pressures were measured. The accuracy of the phase composition predictions were later evaluated with experimental pilot plant data, and it was found that the RK-ASPEN model without the use of solute-solute interaction parameters predict more accurate phase compositions, and was thus selected for use in the process model.

8.7 Objective 7: SFF Process Model Development

The main process units required to simulate the performance of an SFF process, the fractionation column and separator, was simulated in Aspen Plus[®]. The RK-ASPEN model with the inclusion of regressed polar parameters and binary solute-solvent interaction parameters was implemented in all the process units. Five parameters were defined for the evaluation of the separation performance of the process: the extract-to-feed ratio, the solvent-to-feed ratio, the component selectivity, the selectivity ratio and the alcohol recovery. By comparing these parameters at different operating conditions the operating region that leads to the optimum performance of the process can be located.

Mixture 2, CO₂ + (25 % *n*-decane + 25 % *l*-decanol + 25 % 3,7-dimethyl-*l*-octanol + 25 % 2,6-dimethyl-2-octanol), was used to conduct six pilot plant experimental runs at different experimental operating conditions. Three of the runs were conducted at temperatures near 316 K and the other three at temperatures near 344 K. The results (with a maximum experimental error of 9 % in the component mass flow rates) revealed that separation of the alkane from the mixture of alcohols is possible. Runs that were conducted at low temperatures showed slightly better separation performance than those conducted at higher temperatures. Apart from confirming the feasibility of the proposed separation process, the pilot plant experiments also yielded some information on the location of possible optimum operating points.

The process model was used to simulate the process performance at similar operating conditions to those used on the pilot plant. Studies into the hydrodynamic effects inside an SFF column [13,14] was used to estimate the number of stages present in the column at each set of operating conditions. It was found that the proposed process model cannot accurately predict the component distribution and mass flow rates in the product streams at the low operating temperature. Poor prediction of the separation performance parameters was also observed for the low temperature runs. However, the three high temperature runs could be simulated very well with errors between 10 % and 36 % for the predicted component mass flow rates in the product streams. The selectivity ratio and alcohol recovery were predicted very well and similar trends to those observed in the experimental results were generated for these parameters with the process model. The fact that the process model was able to predict accurate data for the three high temperature runs, but not for the three low temperature runs, is in all likelihood an indication of the inadequacies in the predictive ability of the thermodynamic model at low temperatures.

Once the accuracy of the process model was verified, it was used to predict the size of the operating window that leads to an extract-to-feed ratio of 0.3 to 0.7 for Mixture 1 and 2 at temperatures near 344 K. It was found that the size and location of the operating window of the fractionation temperature and pressure will depend on the composition of the feed mixture and the selected solvent-to-feed ratio. The composition of the feed mixture will also have a large influence on the selectivity ratio of the process. When an alcohol and an alkane with similar phase behaviour exist in a mixture, a distinct minimum selectivity ratio will occur at a point within the extract-to-feed ratio limits of the process. When the alkanes and alcohols present in a mixture do not have similar or overlapping phase transition pressures, the minimum selectivity ratio will typically cover a small range of extract-to-feed ratios at the high end limit of the extract-to-feed ratio range. The presence of components with overlapping phase transition pressures are thus the main concern when evaluating the feasibility of an SFF process, not the presence of components with overlapping boiling points or low relative volatilities.

8.8 Objective 8: The Feasibility of the Proposed SFF Process

Experimental and simulated results showed that an SFF process is a feasible separation process to consider for the separation of detergent range alkanes from mixtures of detergent range alcohol isomers.

A comparison between the separation performance of the azeotropic distillation process currently employed, and the SFF process proposed in this work for the separation of detergent range alkanes and alcohols, showed that an alcohol product of similar purity can be produced, but the alcohol recovery achieved in the azeotropic distillation process cannot be matched by the SFF process in its current configuration. SFF can however be used to produce a more pure alcohol product compared to that produced by azeotropic distillation.

8.9 Novel Contributions of this Work

A working process model was developed in Aspen Plus[®] that can be used to predict the separation performance of an SFF process aimed at the separation of detergent range alkanes from a mixture of alcohol isomers. This model, along with a minimal amount of experimental data, was used

in a novel application to prove that it is possible to separate detergent range alkanes from mixtures of alcohol isomers, even when these compounds have similar boiling points, using an SFF process.

During the development of the model several significant observations were made that were accepted by the scientific community and published in peer-reviewed journals:

- M. Zamudio, C.E. Schwarz, J.H. Knoetze, Phase equilibria of branched isomers of C₁₀-alcohols and C₁₀-alkanes in supercritical ethane, *The Journal of Supercritical Fluids*. 58 (2011) 330 – 342.
- M. Zamudio, C.E. Schwarz, J.H. Knoetze, Phase equilibria of branched isomers of C₁₀-alcohols and C₁₀-alkanes in supercritical carbon dioxide, *The Journal of Supercritical Fluids*. 59 (2011) 14 – 26.
- M. Zamudio, C.E. Schwarz, J.H. Knoetze, Experimental measurement and modelling with Aspen Plus[®] of the phase behaviour of supercritical CO₂ + (*n*-dodecane + *I*-decanol + 3,7 dimethyl *I*-octanol), *The Journal of Supercritical Fluids*. 84 (2013) 132 – 145.

Parts of the work reported in this manuscript were also presented at international conferences:

- M. Zamudio, C.E. Schwarz, J.H. Knoetze, The effect of branched alcohol isomers on the separation of alkanes and alcohols with supercritical CO₂, 13th European Meeting on Supercritical Fluids, 2011, The Hague, Netherlands (Poster presentation).
- M. Zamudio, C.E. Schwarz, J.H. Knoetze, Using Aspen Plus[®] to determine the viability of a supercritical fluid fractionation process for the separation of detergent range alkane and alcohol isomers, 6th International Symposium on High Pressure Process Technology, 2013, Belgrade, Serbia (Oral presentation).

8.10 Recommendations for Future Work

8.10.1 Investigating Co-solvency Effects

In one ternary mixture investigated in this work co-solvency effects were observed. These effects have been reported for certain mixtures of alkanes and alcohols in a number of supercritical solvents. Co-solvency effects lead to lower phase transition pressures being observed for a ternary mixture compared to the phase transition pressures of the comprising binary mixtures. The occurrence of such behaviour will in all likelihood have a unique effect on the separation performance of an SFF process.

It is recommended that the phase behaviour of mixtures that show co-solvency effects be experimentally measured to allow the range in which such effects occur to be determined. The effect of the type of co-solvent and relative amounts thereof on the phase behaviour and ultimately the separation performance should be investigated to determine how the effect of the co-solvent can be adequately utilized. It would also be interesting to know how such a mixture responds to variations in the operating conditions of an SFF process.

8.10.2 Improving the Thermodynamic Model

The RK-ASPEN model can be further improved by improving its predictive ability for phase compositions at low temperatures. This can either be done by investigating the effect of the use of new temperature dependant interaction parameters and/or determining solute-solute interaction parameters from multi-component VLE data instead of bubble and dew point data. More complex experimental equipment than that utilized in this project will be required to analyse the compositions of co-existing phases in multi-component mixtures. If the applicability of the thermodynamic model can be extended to include the low temperature region, more information on the separation performance of an SFF process at low temperatures can be generated.

Further potential for research on the topic of the high pressure separation of alkane-alcohol mixtures lie in the investigation of the applicability of other thermodynamic models e.g. models based on association theory. Also, the impact of other mixing rules on the accuracy of the thermodynamic models can be investigated. This investigation focussed on one combination of a thermodynamic model and a set of mixing rules, but numerous other combinations can be tested. Since thermodynamic models and mixing rules are constantly developed and improved, improved model

predictions can be expected to occur for high pressure mixtures of alkanes and alcohols with the use of new, improved or adapted thermodynamic models and/or mixing rules.

8.10.3 Investigating Variations in the SFF Process Configuration

The process configuration investigated in this study lead to the production of an alcohol product of similar purity to that produced by an azeotropic distillation process. However, the alcohol recovery of the SFF process was very poor compared to that achieved in the azeotropic distillation process. Since a change in the operating conditions will not improve the alcohol recovery at the same purity, it is thus recommended that alternative configurations of the process setup be investigated. Possible alterations to the process configuration include the addition of a fractionation column to further process the extract product and recover the alcohols present therein.

8.11 Nomenclature

Symbol/ Acronym	Description
AAD	Average Absolute Deviation
DEG	Diethylene glycol
EoS	Equation of State
SFF	Supercritical Fluid Fractionation

8.12 References

- [1] J.C. Crause, Production of detergent range alcohols, US 7652173 B2, 2010.
- [2] J.C. Crause, Supercritical fluid extraction of paraffin wax, PhD Dissertation, Stellenbosch University, 2001.
- [3] G.J.K. Bonthuys, C.E. Schwarz, A.J. Burger, J.H. Knoetze, Separation of alkanes and alcohols with supercritical fluids. Part I: Phase equilibria and viability study, *The Journal of Supercritical Fluids*. 57 (2011) 101 – 111.

- [4] C.E. Schwarz, G.J.K. Bonthuys, R.F. van Schalkwyk, D.L. Laubscher, A.J. Burger, J.H. Knoetze, Separation of alkanes and alcohols with supercritical fluids. Part II. Influence of process parameters and size of operating window, *The Journal of Supercritical Fluids*. 58 (2011) 352 – 359.
- [5] F. Benvenuti, F. Gironi, L. Lamberti, Supercritical deterpenation of lemon essential oil, experimental data and simulation of the semicontinuous extraction process, *The Journal of Supercritical Fluids*. 20 (2001) 29 – 44.
- [6] Z.A Manan, C.S. Lim, A.N. Mustapa, Development of a new process for palm oil refining based on supercritical fluid extraction technology, *Industrial & Engineering Chemistry Research*. 48 (2009) 5420 – 5426.
- [7] C.E. Schwarz, M.L. Hahn, A.J. de Villiers, J.H. Knoetze, Phase behaviour of high molecular mass methyl esters in supercritical ethane, *Fluid Phase Equilibria*. 311 (2011) 36 – 44.
- [8] E.C. Voutsas, G.D. Pappa, K. Magoulas, D.P. Tassios, Vapour liquid equilibrium modelling of alkane systems with Equations of State: “Simplicity versus complexity,” *Fluid Phase Equilibria*. 240 (2006) 127 – 139.
- [9] C. Tsonopoulos, J. L. Heidman, High pressure vapour-liquid equilibria with cubic equations of state, *Fluid Phase Equilibria*. 29 (1986) 391 – 414.
- [10] Aspen Plus, AspenTech, 2000.
- [11] F.C.v.N. Fourie, C.E. Schwarz, J.H. Knoetze, Phase equilibria of alcohols in supercritical fluids: Part I. The effect of the position of the hydroxyl group for linear C₈ alcohols in supercritical carbon dioxide, *The Journal of Supercritical Fluids*. 47 (2008) 161 – 167.
- [12] C.E. Schwarz, F.C.v.N. Fourie, J.H. Knoetze, Phase equilibria of alcohols in supercritical fluids Part II. The effect of side branching on C₈ alcohols in supercritical carbon dioxide, *The Journal of Supercritical Fluids*. 51 (2009) 128 – 135.
- [13] W. Pietzonka, Ch.Trepp, Multistage high pressure mixer-settler system, in: *Process Technology*, Elsevier Science B.V., The Netherlands, 1996: pp. 609 – 614.
- [14] A. B. de Haan, J. de Graauw, Mass transfer in supercritical extraction columns with structured packings for hydrocarbon processing, *Industrial & Engineering Chemistry Research*. 30 (1991) 2463 – 2470.

BIBLIOGRAPHY

Aspen Plus[®], AspenTech, 2000.

Bahrmann, H., Bach, H., Oxo Synthesis, Ullmann's Encyclopaedia of Industrial Chemistry. (2012).

Benvenuti, F., Gironi, F., Lamberti, L., Supercritical deterpenation of lemon essential oil, experimental data and simulation of the semi-continuous extraction process, The Journal of Supercritical Fluids. 20 (2001) 29 – 44.

Bolz, A., Deiters, U. K., Peters, C. J., de Loos, T.W., Nomenclature for phase diagrams with particular reference to vapour-liquid and liquid-liquid equilibria, Pure & Applied Chemistry. 70 (1998) 2233 – 2257.

Bonthuys, G.J.K., Schwarz, C.E., Burger, A.J., Knoetze, J.H., Separation of alkanes and alcohols with supercritical fluids. Part I: Phase equilibria and viability study, The Journal of Supercritical Fluids. 57 (2011) 101 – 111.

Boston, J. F., Mathias, P. M., Phase equilibria in a third-generation process simulator, at: 2nd International Conference on Phase Equilibria and Fluid Properties in the Chemical Process Industries. Berlin, 1960.

Brunner, G., Supercritical fluids: technology and application to food processing, Journal of Food Engineering. 67 (2005) 21 – 33.

Brunner, G., Counter-current separations, The Journal of Supercritical Fluids. 47 (2009) 574–582.

Bufkin, B. A., Robinson, R. L., Estrera, S. S., Luks, K. D., Solubility of ethane in *n*-decane at pressures to 8.2 MPa and temperatures from 278 to 411 K, Journal of Chemical & Engineering Data. 31 (1986) 421 – 423.

Castier, M., Galicia-Luna, L. A., Sandler, S. I., Modelling the high-pressure behaviour of binary mixtures of carbon dioxide+alkanols using an excess free energy mixing rule, Brazilian Journal of Chemical Engineering. 21 (2004) 659 – 666.

Chang, C. J., Chiu, K-L., Day, C-Y., A new apparatus for the determination of P - x - y diagrams and Henry's constants in high pressure alcohols with critical carbon dioxide, *The Journal of Supercritical Fluids*. 12 (1998) 223 – 237.

Chen, S. J., Randelman, R. E., Seldomridge, R. L., Radosz, M., Mass spectrometer composition probe for batch cell studies of supercritical fluid phase equilibria, *Journal of Chemical & Engineering Data*. 38 (1993) 211 – 216.

Chester, T. L., Haynes, B. S., Estimation of pressure-temperature critical loci of CO₂ binary mixtures with methyl-tert-butyl ether, ethyl acetate, methyl-ethyl ketone, dioxane and decane, *The Journal of Supercritical Fluids*. 11 (1997) 15 – 20.

Choi, E-J., Yeo, S-D., Critical properties for carbon dioxide + n -alkane mixtures using a variable-volume view cell, *Journal of Chemical & Engineering Data*. 43 (1998) 714 – 716.

Chou, G. F., Forbert, R. R., Prausnitz, J. M., High-pressure vapour-liquid equilibria for carbon dioxide/ n -decane, carbon dioxide/tetralin, and carbon dioxide/ n -decane/tetralin at 71.1 and 104.4 °C, *Journal of Chemical & Engineering Data*. 35 (1990) 26 – 29.

Chrisochoou, A. A., Schaber, K., Stephan, K., Phase equilibria with supercritical carbon dioxide for the enzymatic production of an enantiopure pyrethroid component. Part 1. Binary systems, *Journal of Chemical & Engineering Data*. 42 (1997) 551 – 557.

Chylinski, K., Gregorowicz, J., Solubilities of l -propanol and $l,2$ -propanediol in supercritical carbon dioxide. New analytical procedure and measurements, *Fluid Phase Equilibria*. 143 (1998) 163 – 172.

Clifford, T., *Fundamentals of Supercritical Fluids*, Oxford University Press, Inc., New York, 1999.

Constantinou, L., Gani, R., New group contribution method for estimating properties of pure compounds, *AIChE Journal*. 40 (1994) 1697 – 1710.

Crause, J.C., *Supercritical Fluid Extraction of Paraffin Wax*, PhD Dissertation, Stellenbosch University, 2001.

Crause, J.C., Production of detergent range alcohols, US 7652173 B2, 2010.

Crause, J. C., Nieuwoudt, I., Fractionation of paraffin wax mixtures, *Industrial & Engineering Chemistry Research*. 39 (2000) 4871 – 4876.

De Haan, A. B., de Graauw, J., Mass transfer in supercritical extraction columns with structured packings for hydrocarbon processing, *Industrial & Engineering Chemistry Research*. 30 (1991) 2463 – 2470.

De Loos, T. W., Understanding phase diagrams, in: *Supercritical Fluids: Fundamentals for Application*, Kluwer Academic Publishers, The Netherlands, 1994.

Diaz, M.S., Brignole, E.A., Modelling and optimization of supercritical fluid processes, *The Journal of Supercritical Fluids*. 47 (2009) 611 – 618.

DIPPR Project 801, in: Design Institute for Physical Property Research, Knovel, 2012.

Dixon, D.J., Johnston, K.P., Supercritical Fluids, *Encyclopaedia of Separation Technology*. (1997).

Eckert, C.A., Knutson, B.L., Debenedetti, P.G., Supercritical fluids as solvents for chemical and materials processing, *Nature*. 383 (1996) 313 – 318.

European Council for Plasticisers and Intermediates (ECP), Plasticisers, Plasticisers and Flexible PVC Information Centre. (2010).

Eustaquio-Rincon, R., Trejo, A., Solubility of *n*-octadecane in supercritical carbon dioxide at 310, 313, 333, and 353 K, in the range 10 - 20 MPa, *Fluid Phase Equilibria*. 185 (2001) 231 – 239.

Falbe, J., Lipps, W., Mayer, D., Alcohols, Aliphatic, *Ullmann's Encyclopaedia of Industrial Chemistry*. (2012).

Feng, L-C., Cheng, K-W., Tang, M., Chen, Y-P., Vapour-liquid equilibria of carbon dioxide with ethyl benzoate, diethyl succinate and isoamyl acetate binary mixtures at elevated pressures, *The Journal of Supercritical Fluids*. 21 (2001) 111 – 121.

Fonseca, M. S., Dohrn, R., Peper, S., High-pressure fluid-phase equilibria: Experimental methods and systems investigated (2005 - 2008), *Fluid Phase Equilibria*. 300 (2011) 1 – 69.

Fourie, F.C.v.N., Schwarz, C.E., Knoetze, J.H., Phase equilibria of alcohols in supercritical fluids: Part I. The effect of the position of the hydroxyl group for linear C₈ alcohols in supercritical carbon dioxide, *The Journal of Supercritical Fluids*. 47 (2008) 161 – 167.

Fu, D., Liang, L., Li, X-S., Yan, S., Liao, T., Investigation of vapour-liquid equilibria for supercritical carbon dioxide and hydrocarbon mixtures by perturbed-chain statistical associating fluid theory, *Industrial & Engineering Chemistry Research*. 45 (2006) 4364 – 4370.

Fusco, S.J., Maggart, R.C., Overberger, W.F., Linear Oxo phthalate plasticizers, in: *Plasticizer and Plasticizer Processes*, n.d.

Gamse, T., Marr, R., Phase equilibrium properties of the 1-phenylethanol-carbon dioxide and 2-octanol-carbon dioxide binary systems at 303.15 K, 313.15 K and 323.15 K, *Journal of Chemical & Engineering Data*. 46 (2001) 117 – 119.

Gardeler, H., Fischer, K., Gmehling, J., Experimental determination of vapour-liquid equilibrium data for asymmetric systems, *Industrial & Engineering Chemistry Research*. 41 (2002) 1051 – 1056.

Gardeler, H., Gmehling, J., Experimental determination of phase equilibria and comprehensive examination of the predictive capabilities of group contribution equations of state with a view to the synthesis of supercritical extraction processes, in: *Supercritical Fluids as Solvents and Reaction Media*, Elsevier B.V., Amsterdam, 2004.

Ghaziaskar, H. S., Eskandari, H., Daneshfar, A., Solubility of 2-ethyl-1-hexanol, 2-ethylhexanoic acid, and their mixtures in supercritical carbon dioxide, *Journal of Chemical & Engineering Data*. 48 (2003) 236 – 240.

Greager, I.P., Crause, J.C., Production of detergent range alcohols, US2009/0203804A1, 2009.

Gregorowicz, J., de Loos, T. W., de Swaan Arons, J., The system propane and eicosane: *P*, *T*, and *x* measurements in the temperature range 288-358 K, *Journal of Chemical & Engineering Data*. 37 (1992) 356 – 358.

Gui, X., Tang, Z., Fei, W., Solubility of CO₂ in alcohols, glycols, ethers, and ketones at high pressures from (288.15 to 318.15) K, *Journal of Chemical & Engineering Data*. 56 (2011) 2420 – 2429.

Han, B., Peng, D-Y., Fu, C-T., Vilcsak, G., An apparatus for phase equilibrium studies of carbon dioxide + heavy hydrocarbon systems, *Canadian Journal Chemical Engineering* 70 (1992) 1164 – 1171.

Hölscher, I. F., Spee, M., Schneider, G. M., Fluid-phase equilibria of binary and ternary mixtures of CO₂ with hexadecane, *1*-dodecanol, *1*-hexadecanol and 2-ethoxy-ethanol at 333.2 and 393.2 K and at pressures up to 33 MPa, *Fluid Phase Equilibria*. 49 (1989) 103 – 113.

Hu, B., The universality of critical phenomena in chemical reactions in a binary liquid mixture, PhD Dissertation, The University of Alabama, 2009.

Hwu, W-H., Cheng, J-S., Cheng, K-W., Chen, Y-P., Vapour-liquid equilibrium of carbon dioxide with ethyl caproate, ethyl caprylate and ethyl caprate at elevated pressures, *The Journal of Supercritical Fluids*. 28 (2004) 1 – 9.

Inomata, H., Arai, K., Saito, S., Measurement of vapour-liquid equilibria at elevated temperatures and pressures using a flow type apparatus, *Fluid Phase Equilibria*. 29 (1986) 225 – 232.

Iwai, Y., Hosotani, N., Morotomi, T., Koga, Y., Arai, Y., High-pressure vapour-liquid equilibria for carbon dioxide + linalool, *Journal of Chemical & Engineering Data*. 39 (1994) 900 – 902.

Jaubert, J-N., Mutelet, F., VLE predictions with the Peng-Robinson equation of state and temperature dependant k_{ij} calculated through a group contribution method, *Fluid Phase Equilibria*. 224 (2004) 285 – 304.

Jennings, D. W., Schucker, R. C., Comparison of high-pressure vapour–liquid equilibria of mixtures of CO₂ or propane with nonane and C₉ alkylbenzenes, *Journal of Chemical & Engineering Data*. 41 (1996) 831 – 838.

Jiménez-Gallegos, R., Galicia-Luna, L. A., Elizalde-Solis, O., Experimental vapour–liquid equilibria for the carbon dioxide + octane and carbon dioxide + decane systems, *Journal of Chemical & Engineering Data*. 51 (2006) 1624 – 1628.

Joback, K. G., A unified approach to physical property estimation using multivariate statistical techniques, S. M. Thesis, Massachusetts Institute of Technology, 1984.

Joback, K. G., Reid, R. C., Estimation of pure-component properties from group-contributions, *Chemical Engineering Communications*. 57 (1987) 233 – 243.

Kaneko, T., Derbyshire, F., Makino, E., Gray, D., Tamura, M., Li, K., Coal liquefaction, *Ullmann’s Encyclopaedia of Industrial Chemistry*. (2012).

Kontogeorgis, G. M., Folas, G. K., Thermodynamic models for industrial applications: from classical and advanced mixing rules to association theories, 1st ed., John Wiley & Sons Ltd, United Kingdom, 2010.

Kordikowski, A., Schneider, G.M., Fluid phase equilibria of binary and ternary mixtures of supercritical carbon dioxide with low-volatility organic substances up to 100 MPa and 393 K: cosolvency effects and miscibility windows, *Fluid Phase Equilibria*. 90 (1993) 149 – 162.

Kramer, A., Thodos, G., Solubility of *l*-hexadecanol and palmitic acid in supercritical carbon dioxide, *Journal of Chemical & Engineering Data*. 33 (1988) 230 – 234.

Kukarni, A. A., Zarah, B. Y., Luks, K. D., Kohn, J. P., Phase-equilibrium behaviour of system carbon dioxide-*n*-decane at low temperatures, *Journal of Chemical & Engineering Data*. 19 (1974) 92 – 94.

Lam, D. H., Jangkamolkulchai, A., Luks, K. D., Liquid-liquid-vapour phase equilibrium behaviour of certain binary ethane + *n*-alkanol mixtures, *Fluid Phase Equilibria*. 59 (1990a) 263 – 277.

Lam, D. H., Jangkamolkulchai, A., Luks, K. D., Liquid-liquid-vapour phase equilibrium behaviour of certain binary carbon dioxide + *n*-alkanol mixtures, *Fluid Phase Equilibria*. 60 (1990b) 131 – 141.

Lang, Q., Wai, C.M., Supercritical fluid extraction in herbal and natural product studies — a practical review, *Talanta*. 53 (2001) 771 – 782.

Lee, L-S., Huang, J-F., Zhu, O-X., Solubilities of solid benzoic acid, phenanthrene, and 2,3-dimethylhexane in supercritical carbon dioxide, *Journal of Chemical & Engineering Data*. 46 (2001) 1156 – 1159.

Lee, M-J., Chen, J-T., Vapour-liquid equilibrium for carbon dioxide/alcohol systems, *Fluid Phase Equilibria*. 92 (1994) 215 – 231.

Levelt Sengers, J.M.H., Critical behaviour of fluids: concepts and applications, in: *Supercritical Fluids: Fundamentals for Application*, Kluwer Academic Publishers, The Netherlands, 1994.

Lim, C.S., Manan, Z.A., Sarmidi, M.R., Simulation modelling of the phase behaviour of palm oil-supercritical carbon dioxide, *Journal of the American Oil Chemists' Society*. 80 (2003) 1147 – 1156.

Liong, K.K., Wells, P.A., Foster, N.R., Diffusion in supercritical fluids, *The Journal of Supercritical Fluids*. 4 (1991) 91 – 108.

Longman Group Ltd, de Bussy, J.H., Natural organic materials and related synthetic products, Materials and Technology. V (1972).

Llovell, F., Vega, L. F., Phase equilibria, critical behaviour and derivative properties of selected *n*-alkane/*n*-alkane and *n*-alkane/*l*-alkanol mixtures by the crossover soft-SAFT equation of state, The Journal of Supercritical Fluids. 41 (2007) 204 – 216.

Luks, K. D., The occurrence and measurement of multiphase equilibria behaviour, Fluid Phase Equilibria. 29 (1986) 209 – 224.

Lundeen, A.J., Alcohols, Chemical and Process Technology Encyclopaedia. (1974).

Manan, Z.A., Lim, C.S., Mustapa, A.N., Development of a new process for palm oil refining based on supercritical fluid extraction technology, Industrial & Engineering Chemistry Research. 48 (2009) 5420 – 5426.

Marerro-Morejon, J., Pardillo-Fontdevila, E., Estimation of pure compound properties using group-interaction contributions, AIChE Journal. 45 (1999) 615 – 621.

Mathias, P. M., A versatile phase equilibrium equation of state, Industrial & Engineering Chemistry Process Design and Development. 22 (1983) 385–391.

McHugh, M.A., Krukonis, V.J., Supercritical Fluid Extraction: Principles and Practice, 2nd ed., Butterworth-Heinemann, Massachusettes, 1994.

Mills, H.A., Alcohols, Fatty (via Hydrogenation), Chemical and Process Technology Encyclopaedia. (1974).

Mutelet, F., Vitu, S., Privat, R., Jaubert, J-N., Solubility of CO₂ in branched alkanes in order to extend the PPR78 model (predictive 1978, Peng-Robinson EOS with temperature-dependent k_{ij} calculated through a group contribution method) to such systems, Fluid Phase Equilibria. 238 (2005) 157 – 168.

Nagarajan, N., Robinson, R. L., Equilibrium phase compositions, phase densities, and interfacial tensions for carbon dioxide + hydrocarbon systems. 2. Carbon dioxide + *n*-decane, Journal of Chemical & Engineering Data. 31 (1986) 168 – 171.

Nieuwoudt, I., Vapour-liquid equilibria and densities for the system butane + hexacontane, Journal of Chemical & Engineering Data. 41 (1996) 1024 – 1027.

Nieuwoudt, I., du Rand, M., Measurement of phase equilibria of supercritical carbon dioxide and paraffins, *The Journal of Supercritical Fluids*. 22 (2002) 185 – 199.

NIST Chemistry WebBook, (n.d.)

Patton, C. L., Luks, K. D., Multiphase equilibria of the binary mixture xenon + *l*-decanol, *Fluid Phase Equilibria*. 98 (1994) 201 – 211.

Peng, D-Y., Robinson, D. B., A new two-constant equation of state, *Industrial and Engineering Chemistry Fundamentals*. 15 (1976) 59 – 64.

Peper, S., Dohrn, R., Sampling from fluid mixtures under high pressure: review, case study and evaluation, *The Journal of Supercritical Fluids*. 66 (2012) 2 – 15.

Pereda, S, Bottini, S. B., Brignole, E. A., *Fundamentals of Supercritical Fluid Technology*, (n.d.).

Peters, C. J., Multiphase equilibria in near-critical solvents, in: *Supercritical Fluids: Fundamentals for Application*, Kluwer Academic Publishers, The Netherlands, 1994.

Peters, C. J., de Roo, J. L., de Swaan Arons, J., Measurement and calculations of phase equilibria in binary mixtures of propane + tetratriacontane, *Fluid Phase Equilibria*. 72 (1992) 251 – 266.

Peters, C. J., de Roo, J. L., de Swaan Arons, J., Phase equilibria in binary mixtures of propane and hexacontane, *Fluid Phase Equilibria*. 85 (1993) 301 – 312.

Peters, C. J., Florusse, L. J., Hahre, S., de Swaan Arons, J., Fluid multiphase equilibria and critical phenomena in binary and ternary mixtures of carbon dioxide, certain *n*-alkanols and tetradecane, *Fluid Phase Equilibria*. 110 (1995) 157 – 173.

Peters, C. J., Gauter, K., Occurrence of holes in ternary fluid multiphase systems of near-critical carbon dioxide and certain solutes, *Chemical Reviews*. 99 (1999) 419 – 431.

Peters, C. J., Lichtenthaler, R. N., de Swaan Arons, J., Three phase equilibria in binary mixtures of ethane and higher *n*-alkanes, *Fluid Phase Equilibria*. 29 (1986) 495 – 504.

Pietzonka, W., Trepp, Ch., Multistage high pressure mixer-settler system, in: *Process Technology*, Elsevier Science B.V., The Netherlands, 1996: pp. 609 – 614.

Pöhler, H., Scheidgen, A. L., Schneider, G. M., Fluid phase equilibria of binary and ternary mixtures of supercritical carbon dioxide with a *l*-alkanol and an *n*-alkane up to 100 MPa and 393 K - cosolvency effect and miscibility windows (Part II), *Fluid Phase Equilibria*. 115 (1996) 165 – 177.

Poling, B. E., Prausnitz, J. M., O'Connell, J. P., The properties of gases and liquids, 5th ed., McGraw-Hill Companies, Inc., United States of America, 2001.

Polishuk, I., Wisniak, J., Seguro, H., Simultaneous prediction of the critical and sub-critical phase behaviour in mixtures using equations of state II. Carbon dioxide-heavy *n*-alkanes, *Chemical Engineering Science*. 58 (2003) 2529 – 2550.

Raal, J. D., Mulbauer, A. L., Phase Equilibria: Measurement and Computation, Taylor & Francis, Washington D.C, 1998.

Reamer, H. H., Sage, B. H., Phase equilibria in hydrocarbon systems. Volumetric and phase behaviour of the ethane-*n*-decane system, *Journal of Chemical & Engineering Data*. 7 (1962) 161 – 168.

Reamer, H. H., Sage, B. H., Phase equilibria in hydrocarbon systems. Volumetric and phase behaviour of the *n*-decane-CO₂ System., *Journal of Chemical & Engineering Data*. 8 (1963) 508 – 513.

Redlich, O., Kwong, N. S., On the thermodynamics of solutions. V: An equation of state. Fugacities of gaseous solutions, *Chemical Reviews*. 44 (1949) 233.

Seader, J.D., Henley, E.J., Separation Process Principles, 2nd ed., John Wiley & Sons, Inc., New Jersey, 2006.

Scheidgen, A. L., Schneider, G. M., Fluid phase equilibria of (carbon dioxide + a *l*-alkanol + an alkane) up to 100 MPa and T=393 K: cosolvency effect, miscibility windows, and holes in the critical surface, *Journal of Chemical Thermodynamics*. 32 (2000) 1183 – 1201.

Scheidgen, A. L., Schneider, G. M., New phase phenomena in ternary systems at high pressures - cosolvency and miscibility windows up to 100 MPa, *Physical Chemistry Chemical Physics*. 4 (2002) 963 – 967.

Schwartzentruber, J., Renon, H., Extension of UNIFAC to high pressures and temperatures by the use of a cubic equation of state, *Industrial and Engineering Chemistry Research*. 28 (1989) 1055–1059.

Schwarz, C.E., Phase equilibrium of alkanes and supercritical fluids, Masters Thesis, Stellenbosch University, 2001.

Schwarz, C.E., The processing of wax and wax additives with supercritical fluids, PhD Dissertation, University of Stellenbosch, 2005.

Schwarz, C. E., Bonthuys, G. J. K., Knoetze, J. H., Burger, A. J., The influence of functional end groups on the high-pressure phase equilibria of long chain molecules in supercritical propane, *The Journal of Supercritical Fluids*. 46 (2008) 233 – 237.

Schwarz, C.E., Bonthuys, G.J.K., van Schalkwyk, R.F., Laubscher, D.L., Burger, A.J., Knoetze, J.H., Separation of alkanes and alcohols with supercritical fluids. Part II. Influence of process parameters and size of operating window, *The Journal of Supercritical Fluids*. 58 (2011a) 352 – 359.

Schwarz, C.E., de Villiers, A.J., McClune, C.B., Bonthuys, G.J.K., Burger, A.J., Knoetze, J.H., High pressure phase equilibrium measurements of long chain alcohols in supercritical ethane, *The Journal of Supercritical Fluids*. 55 (2010) 554 – 565.

Schwarz, C. E., Fourie, F. C. v. N., Knoetze, J.H., Phase equilibria of alcohols in supercritical fluids Part II. The effect of side branching on C₈ alcohols in supercritical carbon dioxide, *The Journal of Supercritical Fluids*. 51 (2009) 128 – 135.

Schwarz, C. E., Hahn, M. L., de Villiers, A. J., Knoetze, J. H., Phase behaviour of high molecular mass methyl esters in supercritical ethane, *Fluid Phase Equilibria*. 311 (2011b) 36 – 44.

Schwarz, C. E., Nieuwoudt, I., Phase equilibrium of propane and alkanes: Part I. Experimental procedures, dotriacontane equilibrium and EOS modelling, *The Journal of Supercritical Fluids*. 27 (2003) 133–144.

Schwarz, C. E., Nieuwoudt, I., Knoetze, J. H., Concentration of wax-like alcohol ethoxylates with supercritical propane, *Chemical Engineering Technology*. 30 (2007) 737 – 741.

Schwarz, C.E., Nieuwoudt, I., Knoetze, J.H., Phase equilibria of long chain *n*-alkanes in supercritical ethane: Review, measurements and prediction, *The Journal of Supercritical Fluids*. 46 (2008) 226 – 232.

Sebastian, H. M., Simnick, J. J., Lin, H-M., Chao, K-C., Vapour-liquid equilibrium in binary mixtures of carbon dioxide + *n*-decane and carbon dioxide + *n*-hexadecane, *Journal of Chemical & Engineering Data*. 25 (1980) 138 – 140.

Shaver, R. D., Robinson, R. L., Gasem, K. A. M., An automated apparatus for equilibrium phase compositions, densities, and interfacial tensions: data for carbon dioxide + decane, *Fluid Phase Equilibria*. 179 (2001) 43 – 66.

Singh, H., Lucien, F. P., Foster, N. R., Critical properties for binary mixtures of ethane containing low concentrations of *n*-alkane, *Journal of Chemical & Engineering Data*. 45 (2000) 131 – 135.

Soave, G., Equilibrium constants from a modified Redlich-Kwong equation of state, *Chemical Engineering Science*. 27 (1972) 1197 – 1203.

Spee, M., Schneider, G. M., Fluid phase equilibrium studies on binary and ternary mixtures of carbon dioxide with hexadecane, *1*-dodecanol, *1,8*-octanediol and dotriacontane at 393.2 K and at pressures up to 100 MPa, *Fluid Phase Equilibria*. 65 (1991) 263 – 274.

Stamatakis, S., Tassios, D., Performance of cubic EoS at high pressures, *Oil & Gas Science and Technology*. 53 (1998) 367 – 377.

Taylor, R., Krishna, R., Kooijman, H., Real-world modelling of distillation, *CEP*. (2003) 28 – 39.

Tsonopoulos, C., Heidman, J. L., High pressure vapour-liquid equilibria with cubic equations of state, *Fluid Phase Equilibria*. 29 (1986) 391 – 414.

Tsuji, T., Tanaka, S., Hiaki, T., Saito, R., Measurements of bubble point pressure for CO₂ + decane and CO₂ + lubricating oil, *Fluid Phase Equilibria*. 219 (2004) 87 – 92.

Valderrama, J. O., The state of the cubic equations of state, *Industrial & Engineering Chemistry Research*. 42 (2003) 1603 – 1618.

Van Konynenburg, P.H., Scott, R.L., Critical lines and phase equilibria in binary van der Waals Mixtures, *Philosophical Transactions of the Royal Society of London. A* 298 (1980) 495 – 540.

Vitu, S., Privat, R., Jaubert, J-N., Mutelet, F., Predicting the phase equilibria of CO₂ + hydrocarbon systems with the PPR78 model (PR EOS and k_{ij} calculated through a group contribution method), *The Journal of Supercritical Fluids*. 45 (2008) 1 – 26.

Voutsas, E. C., Pappa, G. D., Magoulas, K., Tassios, D. P., Vapour liquid equilibrium modelling of alkane systems with equations of state: “Simplicity versus complexity,” *Fluid Phase Equilibria*. 240 (2006) 127 – 139.

Wei, Y. S., Sadus, R. J., Phase behaviour of ternary mixtures: a theoretical investigation of the critical properties of mixtures with equal size components, *Physical Chemistry Chemical Physics*. (1999) 4329 – 4336.

Weir, H. M., *The OXO Process For Alcohol Manufacture From Olefins*, 1945.

Weng, W. L., Lee, M.J., Vapour-liquid equilibrium of the octane/carbon dioxide, octane/ethane, and octane/ethylene systems, *Journal of Chemical & Engineering Data*. 37 (1992a) 213 – 215.

Weng, W. L., Lee, M. J., Phase equilibrium measurements for the binary mixtures of *l*-octanol plus CO₂, C₂H₆ and C₂H₄, *Fluid Phase Equilibria*. 73 (1992b) 117 – 127.

Weng, W-L., Chen, J-T., Lee, M-J., High-pressure vapour-liquid equilibria for mixtures containing a supercritical fluid, *Industrial & Engineering Chemistry Research*. 33 (1994) 1955 – 1961.

Wilcock, R. J., Battino, R., Danforth, W. F., Wilhelm, E., Solubilities of gases in liquids II. The solubilities of He, Ne, Ar, Kr, O₂, N₂, CO, CO₂, CH₄, CF₄, and SF₆ in *n*-octane, *l*-octanol, *n*-decane, and *l*-decanol, *The Journal of Chemical Thermodynamics*. 10 (1978) 817 – 822.

Wilson, G. M., Jasperson, L. V., Critical constants T_c , P_c , estimation based on zero first and second order methods, in: *New Orleans, LA*, 1996.

Yaws, C.L., *Yaws’ thermophysical properties of chemicals and hydrocarbons (Electronic Edition)*, Knovel, 2010.

APPENDICES

A. CALIBRATION DATA	I
B. RAW EXPERIMENTAL DATA	XXXIX
C. INPUT DATA FOR THE REGRESSION OF BINARY INTERACTION PARAMETERS	CXLIII
D. OPERATING PROCEDURE: HIGH PRESSURE PHASE EQUILIBRIUM CELL	CLV
E. OPERATING PROCEDURE: SUPERCRITICAL FLUID FRACTIONATION PILOT PLANT	CLXV

A. CALIBRATION DATA

A.1 PRESSURE SENSOR CALIBRATION.....	I
A.2 VOLUME-DENSITY CALIBRATION.....	XII
A.3 TEMPERATURE SENSOR CALIBRATION.....	XXXIII
A.4 NOMENCLATURE.....	XXXVIII
A.5 REFERENCES.....	XXXVIII

A.1 Pressure Sensor Calibration

Pressure sensor calibrations were done biannually for both pressure sensors on the small and large equilibrium cell. Superscripts in the tables containing the raw experimental data (Appendix B) indicate what pressure calibration data set was used to adjust the experimental data.

The pressure sensor was calibrated with the aid of a dead weight tester. A set pressure was applied to the cell, determined by the number of weights that is loaded onto the dead weight tester. The value displayed on the pressure indicator was recorded along with the actual pressure exerted by the dead weigh tester and the operating temperature. The difference in the exerted and displayed pressures was calculated at each of the five different operating temperatures. During the processing of the experimental data the pressure difference to be added to the measured pressure value for each data point was calculated from the calibration data with an interpolation program written in MS Excel.

All the pressure calibration data sets are given in the tables to follow.

Table 1 Pressure sensor calibration data set 1 (small equilibrium cell)

Dead Weight Pressure (bar)	$T_{set}=39^{\circ}\text{C}$			$T_{set}=51^{\circ}\text{C}$			$T_{set}=62^{\circ}\text{C}$			$T_{set}=73^{\circ}\text{C}$			$T_{set}=84^{\circ}\text{C}$		
	P_{meas}	T_{meas}	ΔP	P_{meas}	T_{meas}	ΔP	P_{meas}	T_{meas}	ΔP	P_{meas}	T_{meas}	ΔP	P_{meas}	T_{meas}	ΔP
50	50.8	33.4	-0.8	51.4	43.6	-1.4	51.8	53.8	-1.8	52.4	63.7	-2.4	52.9	73.6	-2.9
65	66.1	33.4	-1.1	66.6	43.6	-1.6	67.1	53.8	-2.1	67.6	63.7	-2.6	67.7	73.6	-2.7
80	81.3	33.4	-1.3	81.8	43.6	-1.8	82.4	53.8	-2.4	82.5	63.7	-2.5	82.9	73.6	-2.9
95	96.4	33.4	-1.4	96.9	43.6	-1.9	97.5	53.8	-2.5	97.6	63.7	-2.6	98.1	73.6	-3.1
110	111.6	33.4	-1.6	111.8	43.6	-1.8	112.3	53.8	-2.3	112.8	63.7	-2.8	113.2	73.6	-3.2
125	126.5	33.4	-1.5	127.0	43.6	-2.0	127.5	53.8	-2.5	128.1	63.7	-3.1	128.1	73.6	-3.1
140	141.7	33.4	-1.7	141.7	43.6	-1.7	142.3	53.8	-2.3	142.8	63.7	-2.8	143.3	73.6	-3.3
155	156.5	33.4	-1.5	157.0	43.6	-2.0	157.5	53.8	-2.5	158.0	63.7	-3.0	158.6	73.6	-3.6
170	171.7	33.4	-1.7	172.2	43.6	-2.2	172.8	53.8	-2.8	173.2	63.7	-3.2	173.3	73.6	-3.3
185	187.0	33.4	-2.0	187.0	43.6	-2.0	187.5	53.9	-2.5	188.0	63.8	-3.0	188.1	73.6	-3.1
200	201.7	33.4	-1.7	202.2	43.6	-2.2	202.3	53.8	-2.3	202.7	63.8	-2.7	203.3	73.6	-3.3
215	216.9	33.4	-1.9	216.9	43.6	-1.9	217.5	53.9	-2.5	218.0	63.8	-3.0	218.0	73.6	-3.0
230	231.7	33.4	-1.7	232.2	43.6	-2.2	232.2	53.9	-2.2	232.7	63.8	-2.7	233.2	73.6	-3.2
245	246.4	33.4	-1.4	246.9	43.6	-1.9	247.4	53.9	-2.4	247.5	63.8	-2.5	248.0	73.7	-3.0
260	261.5	33.4	-1.5	261.6	43.6	-1.6	262.2	53.9	-2.2	262.7	63.8	-2.7	263.2	73.7	-3.2
275	276.3	33.4	-1.3	276.3	43.6	-1.3	276.9	53.9	-1.9	277.4	63.8	-2.4	277.9	73.7	-2.9
290	291.1	33.4	-1.1	291.1	43.6	-1.1	291.6	53.9	-1.6	292.1	63.8	-2.1	292.6	73.7	-2.6

Table 2 Pressure sensor calibration data set 2 (large equilibrium cell)

Dead Weight Pressure (bar)	$T_{set}=36^{\circ}\text{C}$			$T_{set}=46^{\circ}\text{C}$			$T_{set}=56^{\circ}\text{C}$			$T_{set}=67^{\circ}\text{C}$			$T_{set}=77^{\circ}\text{C}$		
	P_{meas}	T_{meas}	ΔP	P_{meas}	T_{meas}	ΔP	P_{meas}	T_{meas}	ΔP	P_{meas}	T_{meas}	ΔP	P_{meas}	T_{meas}	ΔP
50	46.5	35.3	3.5	47.0	45.0	3.0	47.9	54.6	2.1	48.4	65.1	1.6	49.1	74.6	0.9
65	60.5	35.3	4.5	61.2	45.0	3.8	62.0	54.6	3.0	62.4	65.1	2.6	63.1	74.6	1.9
80	75.5	35.3	4.5	76.0	45.0	4.0	77.0	54.6	3.0	77.4	65.1	2.6	78.1	74.6	1.9
95	90.8	35.3	4.2	91.4	45.0	3.6	92.3	54.6	2.7	92.9	65.1	2.1	93.6	74.7	1.4
110	106.4	35.3	3.6	107.1	45.0	2.9	108.0	54.6	2.0	108.7	65.1	1.3	109.4	74.6	0.6
125	122.2	35.3	2.8	122.9	45.0	2.1	123.8	54.6	1.2	124.6	65.1	0.4	125.3	74.6	-0.3
140	138.1	35.3	1.9	138.9	45.0	1.1	139.8	54.6	0.2	140.5	65.1	-0.5	141.3	74.6	-1.3
155	154.1	35.3	0.9	154.9	45.0	0.1	155.9	54.6	-0.9	156.6	65.1	-1.6	157.3	74.7	-2.3
170	170.2	35.3	-10.2	171.0	45.0	-1.0	171.9	54.6	-1.9	172.6	65.1	-2.6	173.3	74.7	-3.3
185	186.3	35.3	-1.3	187.1	45.0	-2.1	188.0	54.6	-3.0	188.8	65.1	-3.8	189.4	74.7	-4.4
200	202.4	35.3	-2.4	203.2	45.0	-3.2	204.2	54.6	-4.2	204.9	65.1	-4.9	205.6	74.7	-5.6
215	218.5	35.3	-3.5	219.4	45.0	-4.4	220.4	54.6	-5.4	221.1	65.1	-6.1	221.7	74.7	-6.7
230	234.7	35.3	-4.7	235.5	45.0	-5.5	236.5	54.6	-6.5	237.3	65.1	-7.3	237.8	74.7	-7.8
245	250.8	35.3	-5.8	251.7	45.0	-6.7	252.6	54.6	-7.6	253.4	65.1	-8.4	254.0	74.7	-9.0
260	267.0	35.3	-7.0	267.8	45.0	-7.8	268.8	54.6	-8.8	269.5	65.1	-9.5	270.1	74.7	-10.1
275	283.0	35.3	-8.0	283.9	45.0	-8.9	284.9	54.6	-9.9	285.6	65.1	-10.6	286.1	74.7	-11.1
290	299.1	35.3	-9.1	299.9	45.0	-9.9	300.9	54.6	-10.9	301.7	65.1	-11.7	302.2	74.7	-12.2

Table 3 Pressure sensor calibration data set 3 (small cell)

Dead Weight Pressure (bar)	$T_{set}=40^{\circ}\text{C}$			$T_{set}=51^{\circ}\text{C}$			$T_{set}=62^{\circ}\text{C}$			$T_{set}=73^{\circ}\text{C}$			$T_{set}=85^{\circ}\text{C}$		
	P_{meas}	T_{meas}	ΔP	P_{meas}	T_{meas}	ΔP	P_{meas}	T_{meas}	ΔP	P_{meas}	T_{meas}	ΔP	P_{meas}	T_{meas}	ΔP
50	51.3	34.6	-1.3	51.8	44.0	-1.8	52.4	53.6	-2.4	52.9	63.2	-2.9	53.0	73.5	-3.0
65	66.6	34.6	-1.6	67.1	44.0	-2.1	67.6	53.6	-2.6	67.6	63.2	-2.6	68.2	73.5	-3.2
80	81.9	34.6	-1.9	82.4	44.0	-2.4	82.4	53.6	-2.4	82.9	63.2	-2.9	83.5	73.6	-3.5
95	97.1	34.6	-2.1	97.2	44.0	-2.2	97.6	53.6	-2.6	98.1	63.2	-3.1	98.7	73.6	-3.7
110	111.8	34.6	-1.8	112.3	44.0	-2.3	112.8	53.6	-2.8	113.0	63.2	-3.0	113.4	73.6	-3.4
125	127.0	34.6	-2.0	127.6	44.0	-2.6	128.1	53.6	-3.1	128.1	63.2	-3.1	128.6	73.6	-3.6
140	142.2	34.6	-2.2	142.3	44.0	-2.3	142.8	53.6	-2.8	143.3	63.2	-3.3	143.4	73.6	-3.4
155	157.1	34.6	-2.1	157.5	44.0	-2.5	158.0	53.6	-3.0	158.6	63.2	-3.6	158.6	73.6	-3.6
170	172.3	34.6	-2.3	172.8	44.0	-2.8	172.9	53.6	-2.9	173.3	63.2	-3.3	173.8	73.6	-3.8
185	187.4	34.6	-2.4	187.5	44.0	-2.5	188.0	53.6	-3.0	188.2	63.3	-3.2	188.6	73.6	-3.6
200	202.2	34.7	-2.2	202.6	44.0	-2.6	202.8	53.6	-2.8	203.3	63.3	-3.3	203.8	73.6	-3.8
215	217.0	34.7	-2.0	217.5	44.0	-2.5	218.0	53.6	-3.0	218.0	63.3	-3.0	218.5	73.6	-3.5
230	232.2	34.6	-2.2	232.3	44.0	-2.3	232.7	53.6	-2.7	233.3	63.3	-3.3	233.8	73.6	-3.8
245	246.9	34.7	-1.9	247.4	44.0	-2.4	247.8	53.6	-2.8	248.0	63.3	-3.0	248.5	73.7	-3.5
260	261.6	34.6	-1.6	262.1	44.0	-2.1	262.7	53.6	-2.7	263.2	63.3	-3.2	263.2	73.7	-3.2
275	279.8	34.7	-4.8	276.9	44.0	-1.9	277.4	53.6	-2.4	277.9	63.3	-2.9	277.9	73.7	-2.9
290	291.1	34.7	-1.1	291.6	44.1	-1.6	292.1	53.7	-2.1	292.7	63.3	-2.7	292.7	73.7	-2.7

Table 4 Pressure sensor calibration data set 4 (large cell)

Dead Weight Pressure (bar)	$T_{set}=36^{\circ}\text{C}$			$T_{set}=46^{\circ}\text{C}$			$T_{set}=56^{\circ}\text{C}$			$T_{set}=67^{\circ}\text{C}$			$T_{set}=77^{\circ}\text{C}$		
	P_{meas}	T_{meas}	ΔP	P_{meas}	T_{meas}	ΔP	P_{meas}	T_{meas}	ΔP	P_{meas}	T_{meas}	ΔP	P_{meas}	T_{meas}	ΔP
50	46.4	35.3	3.6	47.0	45.0	3.0	47.6	54.7	2.4	48.2	65.3	1.8	48.9	75.0	1.1
65	60.6	35.3	4.4	61.2	45.0	3.8	61.8	54.7	3.2	62.5	65.3	2.5	63.1	75.0	1.9
80	75.5	35.3	4.5	76.1	45.0	3.9	76.7	54.7	3.3	77.4	65.3	2.6	78.0	74.9	2.0
95	90.8	35.3	4.2	91.4	45.0	3.6	92.0	54.7	3.0	92.8	65.3	2.2	93.4	74.9	1.6
110	106.4	35.3	3.6	107.0	45.0	3.0	107.7	54.7	2.3	108.4	65.3	1.6	109.1	74.9	0.9
125	122.2	35.3	2.8	122.9	45.0	2.1	123.6	54.7	1.4	124.3	65.3	0.7	124.9	74.9	0.1
140	138.2	35.3	1.8	138.9	45.0	1.1	139.6	54.7	0.4	140.3	65.3	-0.3	141.0	74.9	-1.0
155	154.3	35.3	0.7	154.9	45.0	0.1	155.6	54.7	-0.6	156.3	65.3	-1.3	157.0	74.9	-2.0
170	170.3	35.3	-0.3	171.0	45.0	-1.0	171.7	54.7	-1.7	172.4	65.3	-2.4	173.0	74.9	-3.0
185	186.4	35.3	-1.4	187.1	45.0	-2.1	187.8	54.7	-2.8	188.5	65.3	-3.5	189.1	74.9	-4.1
200	202.6	35.3	-2.6	203.3	45.0	-3.3	203.9	54.7	-3.9	204.6	65.3	-4.6	205.3	74.9	-5.3
215	218.7	35.3	-3.7	219.4	45.0	-4.4	220.1	54.7	-5.1	220.8	65.3	-5.8	221.4	74.9	-6.4
230	234.8	35.3	-4.8	235.5	45.0	-5.5	236.2	54.7	-6.2	236.9	65.3	-6.9	237.5	74.9	-7.5
245	250.9	35.3	-5.9	251.6	45.0	-6.6	252.2	54.7	-7.2	253.0	65.3	-8.0	253.6	74.9	-8.6
260	267.0	35.3	-7.0	267.7	45.0	-7.7	268.3	54.7	-8.3	269.0	65.3	-9.0	269.7	74.8	-9.7
275	283.0	35.3	-8.0	283.6	45.0	-8.6	284.4	54.7	-9.4	285.0	65.3	-10.0	285.7	74.8	-10.7
290	299.0	35.3	-9.0	299.5	45.0	-9.5	300.0	54.7	-10.0	300.9	65.3	-10.9	301.6	74.9	-11.6

Table 5 Pressure sensor calibration data set 5 (small cell)

Dead Weight Pressure (bar)	$T_{set}=30^{\circ}\text{C}$			$T_{set}=45^{\circ}\text{C}$			$T_{set}=60^{\circ}\text{C}$			$T_{set}=75^{\circ}\text{C}$			$T_{set}=90^{\circ}\text{C}$		
	P_{meas}	T_{meas}	ΔP	P_{meas}	T_{meas}	ΔP	P_{meas}	T_{meas}	ΔP	P_{meas}	T_{meas}	ΔP	P_{meas}	T_{meas}	ΔP
50	51.9	28.5	-1.9	52.4	41.0	-2.4	53.0	54.3	-3.0	53.4	67.5	-3.4	54.0	81.4	-4.0
65	67.0	28.0	-2.0	67.6	41.1	-2.6	68.2	54.4	-3.2	68.7	67.5	-3.7	69.3	81.4	-4.3
80	82.3	28.6	-2.3	82.4	41.1	-2.4	83.3	54.4	-3.3	83.8	67.5	-3.8	84.5	81.4	-4.5
95	97.3	28.6	-2.3	97.6	41.1	-2.6	98.6	54.4	-3.6	99.1	67.5	-4.1	99.7	81.4	-4.7
110	112.3	28.7	-2.3	112.8	41.1	-2.8	113.4	54.5	-3.4	113.9	67.5	-3.9	114.5	81.4	-4.5
125	127.6	28.7	-2.6	128.1	41.1	-3.1	128.6	54.3	-3.6	129.1	67.6	-4.1	129.7	81.4	-4.7
140	142.3	28.7	-2.3	143.3	41.2	-3.3	143.4	54.4	-3.4	143.9	67.6	-3.9	144.9	81.4	-4.9
155	157.5	28.7	-2.5	158.1	41.2	-3.1	158.6	54.5	-3.6	159.1	67.6	-4.1	159.7	81.4	-4.7
170	172.8	28.8	-2.8	173.3	41.2	-3.3	173.8	54.5	-3.8	174.3	67.6	-4.3	174.9	81.4	-4.9
185	188.0	28.8	-3.0	188.0	41.2	-3.0	188.5	54.5	-3.5	189.1	67.7	-4.1	190.0	81.4	-5.0
200	202.8	28.9	-2.8	203.3	41.2	-3.3	203.8	54.5	-3.8	204.3	67.7	-4.3	204.8	81.4	-4.8
215	217.5	28.9	-2.5	218.0	41.2	-3.0	218.6	54.5	-3.6	219.1	67.7	-4.1	219.6	81.4	-4.6
230	232.7	29.9	-2.7	233.2	41.3	-3.2	233.8	54.5	-3.8	234.3	67.7	-4.3	234.8	81.4	-4.8
245	247.4	29.0	-2.4	248.4	41.3	-3.4	248.9	54.5	-3.9	249.0	67.7	-4.0	249.5	81.4	-4.5
260	262.7	29.0	-2.7	263.2	41.3	-3.2	263.7	54.5	-3.7	263.7	67.7	-3.7	264.3	81.4	-4.3
275	277.4	29.0	-2.4	277.9	41.3	-2.9	278.5	54.6	-3.5	279.0	67.7	-4.0	279.5	81.4	-4.5
290	292.7	29.0	-2.7	293.2	41.3	-3.2	293.2	54.6	-3.2	293.7	67.7	-3.7	294.2	81.4	-4.2

Table 6 Pressure sensor calibration data set 6 (large cell)

Dead Weight Pressure (bar)	$T_{set}=36^{\circ}\text{C}$			$T_{set}=47^{\circ}\text{C}$			$T_{set}=58^{\circ}\text{C}$			$T_{set}=69^{\circ}\text{C}$			$T_{set}=79^{\circ}\text{C}$		
	P_{meas}	T_{meas}	ΔP	P_{meas}	T_{meas}	ΔP	P_{meas}	T_{meas}	ΔP	P_{meas}	T_{meas}	ΔP	P_{meas}	T_{meas}	ΔP
50	45.6	34.9	4.4	46.6	44.8	3.4	47.3	54.9	2.7	47.5	64.9	2.5	48.3	74.2	1.7
65	59.2	34.9	5.8	60.2	44.8	4.8	61.0	54.9	4.0	61.2	64.9	3.8	62.0	74.2	3.0
80	73.7	34.9	6.3	74.7	44.8	5.3	75.4	54.9	4.6	75.7	64.9	4.3	76.4	74.2	3.6
95	88.9	34.9	6.1	89.9	44.8	5.1	90.5	54.9	4.5	90.9	64.9	4.1	91.6	74.2	3.4
110	104.7	34.9	5.3	105.6	44.8	4.4	106.3	54.9	3.7	106.6	64.9	3.4	107.4	74.2	2.6
125	120.9	34.9	4.1	121.8	44.8	3.2	122.5	54.9	2.5	122.9	64.9	2.1	123.5	74.2	1.5
140	137.4	34.9	2.6	138.3	44.8	1.7	139.0	54.9	1.0	139.4	64.9	0.6	140.0	74.2	0.0
155	154.0	34.9	1.0	154.9	44.8	0.1	155.5	54.9	-0.5	156.0	64.9	-1.0	156.5	74.2	-1.5
170	170.6	34.9	-0.6	171.5	44.8	-1.5	172.2	54.9	-2.2	172.6	64.9	-2.6	173.2	74.2	-3.2
185	187.3	34.9	-2.3	188.2	44.8	-3.2	188.9	54.9	-3.9	189.3	64.9	-4.3	189.9	74.2	-4.9
200	204.1	34.9	-4.1	204.9	44.8	-4.9	205.6	54.9	-5.6	206.1	64.9	-6.1	206.6	74.2	-6.6
215	220.9	34.9	-5.9	221.7	44.8	-6.7	222.3	54.9	-7.3	222.8	64.9	-7.8	223.3	74.2	-8.3
230	237.5	34.9	-7.5	238.4	44.8	-8.4	239.1	54.9	-9.1	239.5	64.9	-9.5	240.1	74.2	-10.1
245	254.4	34.9	-9.4	255.2	44.8	-10.2	255.9	54.9	-10.9	256.2	65.0	-11.2	256.8	74.2	-11.8
260	271.1	34.8	-11.1	271.9	44.8	-11.9	272.6	54.9	-12.6	273.1	65.0	-13.1	273.6	74.2	-13.6
275	287.8	34.8	-12.8	288.7	44.8	-13.7	289.3	54.9	-14.3	289.8	65.0	-14.8	290.3	74.2	-15.3
290	304.5	34.8	-14.5	305.4	44.8	-15.4	306.1	54.9	-16.1	306.5	65.0	-16.5	307.0	74.2	-17.0

Table 7 Pressure sensor calibration data set 7 (small cell)

Dead Weight Pressure (bar)	$T_{set}=35^{\circ}\text{C}$			$T_{set}=50^{\circ}\text{C}$			$T_{set}=65^{\circ}\text{C}$			$T_{set}=80^{\circ}\text{C}$			$T_{set}=95^{\circ}\text{C}$		
	P_{meas}	T_{meas}	ΔP	P_{meas}	T_{meas}	ΔP	P_{meas}	T_{meas}	ΔP	P_{meas}	T_{meas}	ΔP	P_{meas}	T_{meas}	ΔP
50	52.4	32.0	-2.4	53.0	45.3	-3.0	53.5	58.7	-3.5	54.0	71.9	-4.0	54.5	85.3	-4.5
65	67.6	32.0	-2.6	68.0	45.3	-3.0	68.7	58.6	-3.7	69.2	71.8	-4.2	69.7	85.3	-4.7
80	82.4	32.0	-2.4	82.9	45.3	-2.9	83.5	58.5	-3.5	84.5	71.8	-4.5	84.6	85.3	-4.6
95	97.6	32.0	-2.6	98.1	45.3	-3.1	98.8	58.5	-3.8	99.4	71.7	-4.4	99.7	85.2	-4.7
110	112.8	32.0	-2.8	113.4	45.3	-3.4	113.9	58.5	-3.9	114.4	71.7	-4.4	114.9	85.2	-4.9
125	128.1	32.1	-3.1	128.6	45.4	-3.6	129.1	58.6	-4.1	129.6	71.7	-4.6	130.1	85.1	-5.1
140	143.1	32.1	-3.1	143.3	45.4	-3.3	143.8	58.5	-3.8	144.5	71.6	-4.5	145.0	85.1	-5.0
155	158.1	32.1	-3.1	158.6	45.4	-3.6	159.1	58.6	-4.1	159.6	71.6	-4.6	160.1	85.1	-5.1
170	173.3	32.1	-3.3	173.7	45.4	-3.7	174.4	58.4	-4.4	174.9	71.6	-4.9	175.4	85.1	-5.4
185	188.1	32.1	-3.1	188.6	45.4	-3.6	189.1	58.4	-4.1	189.6	71.6	-4.6	190.1	85.1	-5.1
200	203.3	32.1	-3.3	203.8	45.4	-3.8	204.3	58.4	-4.3	204.9	71.5	-4.9	205.0	85.1	-5.0
215	218.0	32.1	-3.0	218.5	45.4	-3.5	219.1	58.4	-4.1	219.6	71.5	-4.6	220.1	85.1	-5.1
230	233.2	32.2	-3.2	233.8	45.4	-3.8	234.3	58.4	-4.3	234.5	71.5	-4.5	234.8	85.1	-4.8
245	248.0	32.2	-3.0	248.5	45.4	-3.5	249.0	58.4	-4.0	249.5	71.5	-4.5	250.1	85.1	-5.1
260	263.2	32.2	-3.2	263.7	45.4	-3.7	263.8	58.4	-3.8	264.3	71.5	-4.3	264.8	85.1	-4.8
275	277.9	32.2	-2.9	278.5	45.4	-3.5	279.0	58.4	-4.0	279.5	71.5	-4.5	280.0	85.1	-5.0
290	293.2	32.2	-3.2	293.2	45.4	-3.2	293.7	58.4	-3.7	294.2	71.5	-4.2	294.7	85.1	-4.7

Table 8 Pressure sensor calibration data set 8 (large cell)

Dead Weight Pressure (bar)	$T_{set}=34^{\circ}\text{C}$			$T_{set}=47^{\circ}\text{C}$			$T_{set}=62^{\circ}\text{C}$			$T_{set}=75^{\circ}\text{C}$			$T_{set}=89^{\circ}\text{C}$		
	P_{meas}	T_{meas}	ΔP	P_{meas}	T_{meas}	ΔP	P_{meas}	T_{meas}	ΔP	P_{meas}	T_{meas}	ΔP	P_{meas}	T_{meas}	ΔP
50	43.3	32.2	6.7	43.8	44.7	6.2	44.1	58.8	5.9	45.3	71.3	4.7	46.4	84.8	3.6
65	57.3	32.2	7.7	57.5	44.7	7.5	57.7	58.8	7.3	58.9	71.3	6.1	60.0	84.8	5.0
80	71.9	32.3	8.1	72.0	44.7	8.0	72.2	58.9	7.8	73.4	71.3	6.6	74.4	84.8	5.6
95	87.0	32.3	8.0	87.1	44.7	7.9	87.3	58.9	7.7	88.5	71.3	6.5	89.5	84.8	5.5
110	102.4	32.3	7.6	102.6	44.7	7.4	102.3	58.9	7.7	103.9	71.3	6.1	104.9	84.8	5.1
125	118.0	32.3	7.0	118.2	44.7	6.8	118.4	58.9	6.6	119.6	71.3	5.4	120.6	84.8	4.4
140	133.9	32.3	6.1	134.0	44.7	6.0	134.3	58.9	5.7	135.5	71.3	4.5	136.6	84.8	3.4
155	149.8	32.3	5.2	150.0	44.7	5.0	150.5	58.9	4.5	151.7	71.3	3.3	152.7	84.8	2.3
170	165.9	32.3	4.1	166.1	44.7	3.9	166.7	58.9	3.3	167.8	71.3	2.2	168.0	84.8	2.0
185	182.1	32.3	2.9	182.3	44.7	2.7	183.0	58.9	2.0	184.1	71.3	0.9	185.1	84.8	-0.1
200	198.2	32.3	1.8	198.5	44.7	1.5	199.3	58.9	0.7	200.4	71.4	-0.4	201.4	84.8	-1.4
215	214.3	32.3	0.7	214.8	44.7	0.2	215.7	58.9	-0.7	216.8	71.4	-1.8	217.8	84.8	-2.8
230	230.5	32.3	-0.5	231.2	44.7	-1.2	232.0	58.9	-2.0	233.1	71.4	-3.1	234.1	84.8	-4.1
245	246.7	32.3	-1.7	247.5	44.7	-2.5	248.4	58.9	-3.4	249.4	71.4	-4.4	250.5	84.8	-5.5
260	263.0	32.3	-3.0	263.9	44.7	-3.9	264.7	58.9	-4.7	265.8	71.4	-5.8	266.9	84.8	-6.9
275	279.2	32.3	-4.2	280.3	44.7	-5.3	281.1	59.0	-6.1	282.1	71.4	-7.1	283.1	84.8	-8.1
290	295.5	32.3	-5.5	296.5	44.7	-6.5	297.3	59.0	-7.3	298.5	71.4	-8.5	299.6	84.8	-9.6

Table 9 Pressure sensor calibration data set 9 (small cell)

Dead Weight Pressure (bar)	$T_{set}=35^{\circ}\text{C}$			$T_{set}=50^{\circ}\text{C}$			$T_{set}=65^{\circ}\text{C}$			$T_{set}=80^{\circ}\text{C}$			$T_{set}=95^{\circ}\text{C}$		
	P_{meas}	T_{meas}	ΔP	P_{meas}	T_{meas}	ΔP	P_{meas}	T_{meas}	ΔP	P_{meas}	T_{meas}	ΔP	P_{meas}	T_{meas}	ΔP
50	52.4	32.1	-2.4	53.0	44.6	-3.0	53.5	58.8	-3.5	54.3	72.1	-4.3	55.1	85.0	-5.1
65	67.6	32.1	-2.6	68.2	44.7	-3.2	68.9	58.8	-3.9	69.7	72.1	-4.7	70.2	85.0	-5.2
80	82.5	32.1	-2.5	83.4	44.7	-3.4	84.0	58.9	-4.0	84.5	72.2	-4.5	85.0	85.1	-5.0
95	97.7	32.1	-2.7	98.8	44.7	-3.8	99.3	58.9	-4.3	99.7	72.2	-4.7	100.5	85.1	-5.5
110	112.9	32.2	-2.9	113.5	44.8	-3.5	114.5	58.9	-4.5	114.8	72.2	-4.8	115.6	85.2	-5.6
125	128.1	32.2	-3.1	128.7	44.8	-3.7	129.2	58.9	-4.2	129.8	72.2	-4.8	130.3	85.2	-5.3
140	143.2	32.2	-3.2	143.8	44.8	-3.8	144.4	58.9	-4.4	145.0	72.2	-5.0	145.5	85.3	-5.5
155	158.1	32.2	-3.1	158.6	44.8	-3.6	159.3	59.0	-4.3	160.2	72.3	-5.2	160.3	85.3	-5.3
170	173.3	32.2	-3.3	173.9	44.9	-3.9	174.4	59.0	-4.4	174.9	72.3	-4.9	175.5	85.3	-5.5
185	188.0	32.2	-3.0	188.7	44.9	-3.7	189.6	59.0	-4.6	190.2	72.3	-5.2	190.6	85.3	-5.6
200	203.3	32.2	-3.3	203.8	44.9	-3.8	204.6	59.0	-4.6	204.9	72.3	-4.9	205.4	85.3	-5.4
215	218.0	32.2	-3.0	219.1	44.9	-4.1	219.6	59.0	-4.6	220.1	72.3	-5.1	220.6	85.3	-5.6
230	233.3	32.2	-3.3	233.8	44.9	-3.8	234.3	59.0	-4.3	234.8	72.3	-4.8	235.4	85.3	-5.4
245	248.4	32.2	-3.4	249.1	44.9	-4.1	249.5	59.0	-4.5	250.1	72.3	-5.1	250.6	85.3	-5.6
260	263.3	32.3	-3.3	263.8	45.0	-3.8	264.3	59.1	-4.3	264.8	72.3	-4.8	265.3	85.3	-5.3
275	277.9	32.3	-2.9	278.5	45.0	-3.5	279.4	59.2	-4.4	279.6	72.3	-4.6	280.0	85.3	-5.0
290	293.2	32.3	-3.2	293.6	45.0	-3.6	294.2	59.2	-4.2	294.7	72.3	-4.7	294.7	85.4	-4.7

Table 10 Pressure sensor calibration data set 10 (large cell)

Dead Weight Pressure (bar)	$T_{set}=32^{\circ}\text{C}$			$T_{set}=43^{\circ}\text{C}$			$T_{set}=54^{\circ}\text{C}$			$T_{set}=66^{\circ}\text{C}$			$T_{set}=78^{\circ}\text{C}$		
	P_{meas}	T_{meas}	ΔP	P_{meas}	T_{meas}	ΔP	P_{meas}	T_{meas}	ΔP	P_{meas}	T_{meas}	ΔP	P_{meas}	T_{meas}	ΔP
50	42.7	31.8	7.3	44.4	42.0	5.6	44.7	52.7	5.3	45.6	64.3	4.4	46.0	75.7	4.0
65	55.8	31.8	9.2	57.7	42.0	7.3	58.0	52.7	7.0	58.8	64.3	6.2	59.3	75.7	5.7
80	69.9	31.9	10.1	71.8	42.1	8.2	72.2	52.7	7.8	73.0	64.3	7.0	73.4	75.7	6.6
95	84.6	31.9	10.4	86.5	42.1	8.5	87.0	52.7	8.0	87.7	64.3	7.3	88.2	75.7	6.8
110	99.8	31.9	10.2	101.7	42.1	8.3	102.1	52.7	7.9	102.9	64.3	7.1	103.4	75.8	6.6
125	115.4	31.9	9.6	117.2	42.1	7.8	117.6	52.7	7.4	118.4	64.3	6.6	118.9	75.8	6.1
140	131.3	32.0	8.7	132.8	42.1	7.2	133.2	52.7	6.8	134.1	64.3	5.9	134.7	75.8	5.3
155	147.3	32.0	7.7	148.7	42.1	6.3	149.1	52.7	5.9	150.0	64.3	5.0	150.6	75.8	4.4
170	163.4	32.0	6.6	164.6	42.1	5.4	165.2	52.7	4.8	166.1	64.3	3.9	166.7	75.8	3.3
185	179.6	32.0	5.4	180.7	42.1	4.3	181.2	52.7	3.8	182.1	64.3	2.9	182.8	75.8	2.2
200	195.7	32.0	4.3	196.8	42.1	3.2	197.4	52.7	2.6	198.3	64.3	1.7	199.0	75.8	1.0
215	211.9	32.0	3.1	213.0	42.1	2.0	213.6	52.7	1.4	214.5	64.3	0.5	215.2	75.8	-0.2
230	228.1	32.0	1.9	229.2	42.2	0.8	229.8	52.7	0.2	230.7	64.3	-0.7	231.3	75.8	-1.3
245	244.3	32.0	0.7	245.4	42.2	-0.4	246.0	52.7	-1.0	247.0	64.3	-2.0	247.6	75.8	-2.6
260	260.5	32.0	-0.5	261.6	42.2	-1.6	262.2	52.8	-2.2	263.1	64.3	-3.1	263.8	75.8	-3.8
275	276.7	32.0	-1.7	277.8	42.2	-2.8	278.4	52.8	-3.4	279.3	64.3	-4.3	280.0	75.8	-5.0
290	292.9	32.0	-2.9	293.9	42.2	-3.9	294.6	52.8	-4.6	295.5	64.3	-5.5	296.2	75.8	-6.2

A.2 Volume-Density Calibration

Volume calibrations were done on the equilibrium cells to determine the relationship between the piston position and the volume of the cell. This data was then used to determine the density of the mixture in the cell. This indirect way of measuring the density of a binary supercritical mixture is not very accurate, but it gives a good estimation of the density range of the mixture at different operating temperatures, pressures and compositions.

The piston has a Teflon seal at the one end which contracts and expands depending on the operating temperature and pressure. This causes small differences in the measured piston length, which translates to significant differences in the calculated density values. Consecutive piston length measurements revealed an accuracy of 0.2 mm in the measurements.

To determine the relationship of the piston length to the cell volume, the cell is filled with a known amount of CO₂ and allowed a few minutes to reach the first operating temperature. The piston length, operating temperature and operating pressure is recorded. The pressure is increased a small amount by adding nitrogen to the low pressure chamber to push the piston into the cell. The same parameters are recorded at ten different pressures. This procedure is repeated at different operating temperatures. The recorded pressure is adapted according to the pressure calibration data to determine the actual pressure value. The density of CO₂ at each of the recorded operating temperature and pressure combinations are determined from the data tables published by the National Institute of Standards and Technology (NIST) [1]. With the density data and the known amount of CO₂ in the cell, the volume of the cell that corresponds to the piston length can then be determined for each data point. A straight line correlation exists between the volume of the cell and the piston position.

After small alterations to the equilibrium cells are made (e.g. repairs, maintenance or replacement of any component), new volume calibrations are required. The specific volume calibration correlation that was used to calculate the density of the mixture is indicated as a superscript in the raw data (Appendix B).

Table 11 Volume calibration data set 1 (small cell)

Mass Solvent: 11.97 g						
T (°C)	T (K)	P (barg)	Corrected P ⁽¹⁾ (barA)	Piston Position (mm)	Calculated density (kg/m ³)	Volume (cm ³)
36.0	309.2	75.0	74.1	93.7	250.8	47.7
36.0	309.2	77.8	76.9	81.1	286.3	41.8
35.9	309.1	79.7	78.7	68.8	321.6	37.2
36.1	309.3	82.4	81.4	52.8	401.0	29.8
36.2	309.4	84.0	82.9	40.1	471.5	25.4
36.3	309.5	86.0	84.9	32.7	545.1	22.0
36.3	309.5	88.2	87.1	29.0	592.6	20.2
36.3	309.5	94.5	93.3	24.7	656.6	18.2
36.3	309.5	102.3	101.2	21.7	698.6	17.1
36.3	309.5	110.2	109.2	20.4	726.7	16.5
44.5	317.7	81.9	80.5	93.6	247.2	48.4
44.7	317.9	84.0	82.6	87.1	262.6	45.6
44.9	318.1	88.2	86.7	74.5	299.2	40.0
45.0	318.2	91.3	89.8	63.6	334.2	35.8
45.0	318.2	94.4	92.8	55.5	377.0	31.8
45.1	318.3	97.1	95.5	47.8	419.3	28.5
45.2	318.4	99.7	98.1	41.3	460.9	26.0
45.2	318.4	103.9	102.4	35.1	524.8	22.8
45.3	318.5	112.4	110.9	28.3	603.1	19.8
45.3	318.5	128.1	126.4	23.2	678.0	17.7
54.6	327.8	90.3	88.6	93.7	248.9	48.1
54.8	328.0	93.7	92.0	85.6	268.6	44.6
55.0	328.2	98.1	96.4	75.9	297.2	40.3
55.2	328.4	101.9	100.1	67.9	323.7	37.0
55.3	328.5	106.0	104.1	60.1	356.1	33.6
55.4	328.6	110.8	108.8	52.1	397.4	30.1
55.5	328.7	115.4	113.4	45.7	438.8	27.3
55.5	328.7	122.8	120.7	38.1	501.5	23.9
55.6	328.8	131.7	129.5	31.6	559.7	21.4
55.7	328.9	150.7	148.7	25.5	642.1	18.6

Table 11 (continued) Volume calibration data set 1 (small cell)

T (°C)	T (K)	P (barg)	Corrected P⁽¹⁾ (barA)	Piston Position (mm)	Calculated density (kg/m³)	Volume (cm³)
64.5	337.7	98.1	95.9	93.8	247.7	48.3
64.7	337.9	103.9	101.6	83.5	275.1	43.5
65.1	338.3	108.7	106.3	75.7	298.3	40.1
65.2	338.4	116.5	114.0	63.2	342.8	34.9
65.3	338.5	121.2	118.7	56.8	371.6	32.2
65.4	338.6	128.1	125.6	49.7	415.0	28.8
65.5	338.7	134.4	131.9	43.6	453.5	26.4
65.5	338.7	144.3	141.9	37.1	509.9	23.5
65.5	338.7	158.6	156.0	30.8	582.4	20.6
65.6	338.8	175.4	173.0	26.6	627.0	19.1
74.9	348.1	106.5	103.7	93.8	247.8	48.3
75.1	348.3	110.7	107.9	87.0	264.2	45.3
75.3	348.5	116.5	113.7	78.5	288.1	41.5
75.4	348.6	123.3	120.6	70.0	318.9	37.5
75.6	348.8	132.3	129.7	60.0	361.2	33.1
75.6	348.8	138.1	135.4	54.1	389.0	30.8
75.6	348.8	147.4	144.6	46.9	433.4	27.6
75.7	348.9	158.6	156.0	40.3	483.6	24.8
75.7	348.9	179.0	176.3	32.0	558.0	21.5
75.7	348.9	198.0	195.3	27.8	610.4	19.6

Table 12 Volume calibration data set 2 (large cell)

Mass Solvent: 18.11 g						
T (°C)	T (K)	P (barg)	Corrected P ⁽²⁾ (barA)	Piston Position (mm)	Calculated density (kg/m ³)	Volume (cm ³)
35.2	308.4	68.9	72.6	117.0	242.4	74.7
35.3	308.5	70.7	74.4	109.4	261.5	69.3
35.4	308.6	72.1	75.8	103.2	279.2	64.9
35.4	308.6	73.9	77.6	94.4	310.8	58.3
35.5	308.7	75.6	79.3	84.6	352.6	51.4
35.6	308.8	76.7	80.4	76.0	391.2	46.3
35.6	308.8	77.9	81.6	67.9	461.4	39.2
35.6	308.8	79.1	82.8	59.7	525.5	34.5
35.7	308.9	84.6	88.1	51.0	627.8	28.8
35.7	308.9	93.4	96.8	47.4	688.8	26.3
45.2	318.4	78.1	81.1	117.1	247.9	73.1
45.3	318.5	82.0	84.9	105.4	278.4	65.1
45.3	318.5	84.8	87.7	97.1	306.1	59.2
45.4	318.6	89.3	92.1	84.2	359.7	50.3
45.4	318.6	92.0	94.7	76.8	399.7	45.3
45.5	318.7	95.3	97.9	68.8	450.6	40.2
45.5	318.7	100.1	102.5	60.6	519.4	34.9
45.5	318.7	110.8	112.8	52.2	613.0	29.5
45.5	318.7	123.2	124.6	48.3	669.8	27.0
45.5	318.7	136.2	136.8	46.0	707.8	25.6
55.0	328.2	86.6	89.0	117.1	249.7	72.5
55.0	328.2	89.8	92.1	109.8	268.4	67.5
55.2	328.4	99.0	101.0	90.7	331.4	54.6
55.2	328.4	105.2	107.0	79.7	383.9	47.2
55.2	328.4	111.2	112.8	70.7	438.5	41.3
55.2	328.4	116.6	117.9	64.5	484.2	37.4
55.2	328.4	122.3	123.3	59.8	526.3	34.4
55.2	328.4	130.0	130.6	55.4	572.0	31.7
55.3	328.5	144.7	144.4	50.4	631.9	28.7
55.3	328.5	161.3	160.0	47.5	678.6	26.7

Table 12 (continued) Volume calibration data set 2 (large cell)

T (°C)	T (K)	P (barg)	Corrected P⁽²⁾ (barA)	Piston Position (mm)	Calculated density (kg/m³)	Volume (cm³)
64.8	338.0	94.9	96.5	117.0	249.6	72.5
64.9	338.1	101.7	103.0	104.9	281.7	64.3
64.9	338.1	107.6	108.7	95.3	313.3	57.8
65.0	338.2	116.2	116.9	83.6	362.9	49.9
65.0	338.2	122.1	122.5	76.6	399.2	45.4
65.0	338.2	130.4	130.3	68.7	449.3	40.3
65.0	338.2	137.6	137.1	63.3	489.8	37.0
65.0	338.2	148.2	147.1	58.0	540.9	33.5
65.1	338.3	169.6	167.0	51.8	614.2	29.5
65.1	338.3	189.4	185.5	48.6	662.0	27.4
75.4	348.6	103.6	104.2	117.0	248.5	72.9
75.5	348.7	112.0	112.2	104.7	281.1	64.4
75.6	348.8	118.2	118.1	96.7	306.7	59.0
75.6	348.8	124.2	123.8	89.7	333.1	54.4
75.6	348.8	131.6	130.8	82.3	366.9	49.4
75.7	348.9	141.8	140.4	73.6	413.0	43.9
75.7	348.9	159.0	156.5	63.6	486.1	37.3
75.7	348.9	173.5	170.1	58.0	537.9	33.7
75.7	348.9	192.4	187.7	53.5	591.5	30.6
75.7	348.9	220.1	213.4	49.3	649.6	27.9

Table 13 Volume calibration data set 3 (small cell)

Mass Solvent: 9.18 g						
T (°C)	T (K)	P (barg)	Corrected P ⁽³⁾ (barA)	Piston Position (mm)	Calculated density (kg/m ³)	Volume (cm ³)
34.2	307.4	58.7	58.3	93.4	152.5	60.2
34.3	307.5	60.8	60.3	86.2	161.8	56.7
34.4	307.6	62.4	61.9	81.0	169.8	54.1
34.5	307.7	65.6	65.0	73.3	187.1	49.1
34.5	307.7	67.7	67.1	66.5	200.7	45.7
34.6	307.8	71.4	70.7	56.0	228.5	40.2
34.7	307.9	73.5	72.8	49.9	248.7	36.9
34.7	307.9	76.1	75.3	41.6	281.7	32.6
34.9	308.1	79.3	78.4	31.4	347.7	26.4
35.2	308.4	82.4	81.5	17.7	498.9	18.4
45.3	318.5	64.0	62.9	93.5	152.1	60.4
45.4	318.6	66.8	65.6	85.3	162.7	56.4
45.4	318.6	69.7	68.5	78.8	175.3	52.4
45.5	318.7	74.0	72.7	69.4	195.2	47.0
45.6	318.8	77.6	76.3	60.6	214.6	42.8
45.7	318.9	81.9	80.5	52.7	240.9	38.1
45.8	319.0	87.1	85.7	42.8	281.5	32.6
45.9	319.1	92.9	91.6	32.7	344.6	26.6
46.1	319.3	100.2	98.9	20.4	450.5	20.4
46.1	319.3	105.0	103.7	15.0	519.2	17.7
54.7	327.9	68.1	66.5	93.5	151.1	60.8
54.8	328.0	71.9	70.3	85.0	164.5	55.8
54.8	328.0	75.6	74.1	77.3	179.0	51.3
54.9	328.1	80.3	78.8	68.1	198.5	46.2
55.0	328.2	84.0	82.5	61.2	215.4	42.6
55.0	328.2	88.7	87.1	53.3	239.0	38.4
55.2	328.4	96.1	94.4	42.1	282.3	32.5
55.3	328.5	102.9	101.2	33.3	332.1	27.6
55.4	328.6	110.2	108.4	25.2	394.4	23.3
55.5	328.7	119.2	117.3	17.8	474.4	19.4

Table 13 (continued) Volume calibration data set 3 (small cell)

T (°C)	T (K)	P (barg)	Corrected P⁽³⁾ (barA)	Piston Position (mm)	Calculated density (kg/m³)	Volume (cm³)
64.4	337.6	72.4	70.6	93.5	151.7	60.5
64.5	337.7	74.6	72.8	88.6	158.5	57.9
64.5	337.7	77.7	75.8	82.8	168.3	54.6
64.6	337.8	80.3	78.4	77.9	176.9	51.9
64.7	337.9	86.1	84.1	67.9	197.4	46.5
64.8	338.0	92.4	90.3	58.7	222.0	41.4
64.8	338.0	97.6	95.4	51.4	244.5	37.5
65.0	338.2	108.1	106.0	39.4	297.5	30.9
65.3	338.5	121.2	119.1	27.7	374.5	24.5
65.4	338.6	132.8	130.6	20.0	447.1	20.5
74.7	347.9	76.7	74.3	93.5	150.5	61.0
74.8	348.0	83.4	80.9	81.2	169.5	54.2
74.9	348.1	89.4	86.8	72.0	187.7	48.9
75.0	348.2	96.0	93.3	62.6	209.2	43.9
75.0	348.2	100.6	97.9	57.0	225.6	40.7
75.0	348.2	105.5	102.9	52.6	244.6	37.5
75.2	348.4	113.9	111.5	43.3	279.2	32.9
75.2	348.4	119.2	116.7	38.3	302.1	30.4
75.3	348.5	129.2	126.6	30.7	348.2	26.4
75.6	348.8	150.7	148.2	19.6	450.5	20.4

Table 14 Volume calibration data set 4 (large cell)

Mass Solvent: 15.48 g						
T (°C)	T (K)	P (barg)	Corrected P ⁽⁴⁾ (barA)	Piston Position (mm)	Calculated density (kg/m ³)	Volume (cm ³)
35.6	308.8	62.3	67.7	117.5	200.2	77.3
35.6	308.8	65.7	71.1	105.4	225.7	68.6
35.7	308.9	68.8	74.2	93.5	255.1	60.7
35.8	309.0	71.8	77.2	82.2	295.2	52.4
35.8	309.0	73.8	79.3	73.0	341.2	45.4
35.9	309.1	75.4	80.9	64.2	394.6	39.2
36.0	309.2	77.7	83.3	54.4	513.1	30.2
36.1	309.3	82.1	88.2	43.5	616.8	25.1
36.1	309.3	97.1	102.3	38.2	706.5	21.9
36.1	309.3	112.2	116.5	36.0	748.9	20.7
45.3	318.5	69.1	73.9	117.4	202.2	76.6
45.4	318.6	72.1	76.9	109.1	218.9	70.7
45.4	318.6	74.3	79.2	103.1	233.5	66.3
45.4	318.6	78.3	83.1	92.6	262.2	59.0
45.5	318.7	81.2	86.0	85.3	286.9	54.0
45.6	318.8	87.3	91.9	71.2	353.4	43.8
45.7	318.9	90.6	95.2	63.0	400.8	38.6
45.7	318.9	96.3	100.7	53.6	489.0	31.7
45.8	319.0	107.7	111.6	43.7	599.8	25.8
45.8	319.0	128.5	131.2	38.7	688.8	22.5
55.0	328.2	75.7	80.0	117.3	203.6	76.0
55.0	328.2	80.9	85.1	105.6	228.4	67.8
55.1	328.3	87.5	91.6	92.7	264.8	58.5
55.2	328.4	92.7	96.6	83.1	297.6	52.0
55.2	328.4	98.7	102.4	73.4	343.0	45.1
55.3	328.5	103.3	106.8	66.4	380.9	40.6
55.4	328.6	109.6	112.7	58.8	434.6	35.6
55.4	328.6	115.7	118.5	53.1	486.1	31.8
55.4	328.6	131.4	133.3	45.0	583.6	26.5
55.4	328.6	148.8	149.6	40.9	648.4	23.9

Table 14 (continued) Volume calibration data set 4 (large cell)

T (°C)	T (K)	P (barg)	Corrected P⁽⁴⁾ (barA)	Piston Position (mm)	Calculated density (kg/m³)	Volume (cm³)
65.7	338.9	83.1	86.5	117.3	204.4	75.7
65.7	338.9	90.2	93.4	104.4	232.7	66.5
65.8	339.0	96.1	99.1	94.7	258.3	59.9
65.9	339.1	106.8	109.4	80.1	311.5	49.7
65.9	339.1	110.7	113.1	75.0	333.0	46.5
65.9	339.1	118.8	120.8	66.5	380.4	40.7
66.1	339.3	130.6	131.9	57.3	447.9	34.6
66.1	339.3	144.2	144.6	49.8	517.8	29.9
66.2	339.4	170.6	169.3	43.0	611.9	25.3
66.1	339.3	201.1	197.7	39.2	680.2	22.8
75.3	348.5	89.5	92.2	117.4	204.8	75.6
75.4	348.6	97.1	99.5	105.4	230.5	67.1
75.5	348.7	108.2	110.1	90.4	272.1	56.9
75.6	348.8	119.7	121.1	77.8	320.5	48.3
75.6	348.8	129.3	130.1	69.0	363.5	42.6
75.7	348.9	139.7	139.8	61.9	410.1	37.7
75.8	349.0	159.3	158.2	52.3	492.3	31.4
75.8	349.0	184.5	181.7	45.3	574.0	27.0
75.8	349.0	211.9	207.1	41.3	636.4	24.3
75.8	349.0	255.0	247.3	37.8	703.9	22.0

Table 15 Volume calibration data set 5 (small cell)

Mass Solvent: 13.71 g						
T (°C)	T (K)	P (barg)	Corrected P ⁽³⁾ (barA)	Piston Position (mm)	Calculated density (kg/m ³)	Volume (cm ³)
35.2	308.4	77.6	76.8	93.5	299.1	45.8
35.5	308.7	79.2	78.3	82.9	324.2	42.3
35.5	308.7	80.1	79.2	78.1	349.3	39.2
35.6	308.8	81.3	80.4	66.8	391.2	35.0
35.8	309.0	83.0	82.0	57.3	464.9	29.5
36.1	309.3	85.4	84.4	45.4	545.9	25.1
36.5	309.7	92.9	91.8	34.2	641.8	21.4
36.8	310.0	116.0	115.0	26.9	738.1	18.6
36.6	309.8	133.4	132.2	24.1	776.7	17.7
36.6	309.8	163.8	162.5	21.8	820.1	16.7
45.9	319.1	88.7	87.4	93.6	296.7	46.2
46.1	319.3	91.3	90.0	86.8	322.3	42.5
46.2	319.4	93.4	92.1	79.0	346.4	39.6
46.4	319.6	96.0	94.7	70.6	378.5	36.2
46.6	319.8	100.3	99.0	59.2	439.3	31.2
46.6	319.8	104.4	103.0	50.1	497.5	27.6
46.9	320.1	113.3	111.8	39.8	581.0	23.6
47.2	320.4	131.8	130.1	31.7	669.7	20.5
47.3	320.5	158.6	156.9	26.9	737.2	18.6
47.2	320.4	188.6	186.9	23.9	784.6	17.5
54.7	327.9	101.3	99.6	84.8	324.5	42.3
55.0	328.2	107.0	105.2	73.0	369.8	37.1
55.1	328.3	111.8	110.0	64.8	413.5	33.2
55.3	328.5	116.5	114.6	56.7	453.6	30.2
55.7	328.9	127.0	124.9	45.5	530.0	25.9
55.9	329.1	142.3	140.4	36.7	610.0	22.5
56.1	329.3	165.4	163.3	30.6	680.0	20.2
56.1	329.3	189.1	187.1	27.4	727.9	18.8
56.1	329.3	217.0	215.0	24.5	767.9	17.9
54.7	327.9	101.3	99.6	84.8	324.5	42.3

Table 15 (continued) Volume calibration data set 5 (small cell)

T (°C)	T (K)	P (barg)	Corrected P⁽³⁾ (barA)	Piston Position (mm)	Calculated density (kg/m³)	Volume (cm³)
63.9	337.1	107.3	105.2	93.6	298.9	45.9
64.3	337.5	114.4	112.4	81.6	339.6	40.4
64.7	337.9	121.2	119.1	70.6	379.6	36.1
64.8	338.0	127.0	124.8	63.2	416.1	32.9
65.1	338.3	138.1	135.8	52.9	481.4	28.5
65.6	338.8	155.9	153.3	42.0	561.6	24.4
65.5	338.7	168.1	165.6	37.1	606.5	22.6
65.8	339.0	195.9	193.5	31.4	674.0	20.3
65.9	339.1	229.6	227.2	27.1	729.1	18.8
65.8	339.0	251.1	249.0	25.3	756.8	18.1
73.5	346.7	116.5	114.1	93.5	297.6	46.1
73.5	346.7	122.3	119.8	85.5	324.8	42.2
74.3	347.5	131.8	129.2	73.9	367.0	37.4
74.7	347.9	143.3	140.9	62.6	422.7	32.4
74.9	348.1	154.4	151.9	53.6	472.6	29.0
75.2	348.4	169.6	166.9	45.4	530.5	25.8
75.5	348.7	191.7	189.1	38.0	596.5	23.0
75.2	348.4	214.3	211.7	32.9	649.3	21.1
75.6	348.8	255.3	252.9	28.5	712.4	19.2
75.5	348.7	282.7	280.9	26.1	745.7	18.4

Table 16 Volume calibration data set 6 (large cell)

Mass Solvent: 14.15 g						
T (°C)	T (K)	P (barg)	Corrected P ⁽⁶⁾ (barA)	Piston Position (mm)	Calculated density (kg/m ³)	Volume (cm ³)
34.4	307.6	56.4	62.9	118.1	175.16	80.8
34.5	307.7	59.7	66.5	106.3	196.65	72.0
34.6	307.8	62.8	69.7	95.7	219.89	64.4
34.6	307.8	65.1	72.1	87.4	242.08	58.5
34.6	307.8	67.6	74.7	77.7	273.98	51.7
34.7	307.9	69.9	77.1	67.0	316.96	44.6
34.8	308.0	72.3	79.6	55.3	412.54	34.3
34.9	308.1	75.1	82.4	43.0	563.81	25.1
34.9	308.1	83.1	90.3	36.7	666.38	21.2
34.8	308.0	95.6	102.4	34.2	723.89	19.6
44.9	318.1	64.5	70.4	111.0	185.39	76.3
45.0	318.2	68.3	74.4	101.1	205.90	68.7
45.1	318.3	73.9	80.2	87.6	241.93	58.5
45.1	318.3	77.8	84.0	78.3	271.92	52.0
45.2	318.4	81.6	87.8	69.8	308.33	45.9
45.4	318.6	87.0	93.1	58.5	374.44	37.8
45.3	318.5	91.4	97.4	50.8	447.74	31.6
45.5	318.7	98.8	104.5	43.5	543.54	26.0
45.5	318.7	107.1	112.3	39.5	609.80	23.2
45.6	318.8	124.5	128.4	35.6	682.00	20.8
54.5	327.7	67.5	72.8	116.4	174.48	81.1
54.6	327.8	73.0	78.5	103.3	197.96	71.5
54.6	327.8	80.0	85.6	89.4	232.45	60.9
54.7	327.9	86.3	91.8	78.0	268.15	52.8
54.8	328.0	93.3	98.7	67.5	316.44	44.7
54.9	328.1	99.8	104.8	59.2	367.34	38.5
55.0	328.2	109.0	113.5	49.4	448.05	31.6
55.0	328.2	117.8	121.6	43.7	516.86	27.4
55.0	328.2	127.7	130.7	39.4	575.16	24.6
55.0	328.2	140.5	142.4	36.9	627.74	22.5

Table 16 (continued) Volume calibration data set 6 (large cell)

T (°C)	T (K)	P (barg)	Corrected P⁽⁶⁾ (barA)	Piston Position (mm)	Calculated density (kg/m³)	Volume (cm³)
65.2	338.4	78.8	84.0	107.6	196.00	72.2
65.2	338.4	85.0	90.2	97.0	220.48	64.2
65.2	338.4	92.9	97.9	84.9	254.82	55.5
65.3	338.5	105.1	109.6	72.1	316.18	44.8
65.4	338.6	112.3	116.2	62.8	355.37	39.8
65.5	338.7	122.5	125.6	54.5	414.53	34.1
65.5	338.7	131.6	133.9	49.4	466.04	30.4
65.6	338.8	144.6	145.7	44.2	528.22	26.8
65.6	338.8	158.6	158.3	40.7	547.79	25.8
65.5	338.7	165.3	164.4	38.8	548.78	25.8
74.6	347.8	79.1	83.7	118.3	178.34	79.3
74.7	347.9	85.3	89.8	107.3	197.85	71.5
74.8	348.0	92.2	96.6	96.5	221.34	63.9
74.8	348.0	98.2	102.3	88.5	242.78	58.3
74.9	348.1	107.5	111.1	78.4	278.56	50.8
75.0	348.2	118.2	121.1	68.8	323.42	43.8
75.0	348.2	130.7	132.5	59.5	379.01	37.3
75.0	348.2	139.5	140.5	54.5	418.52	33.8
75.0	348.2	154.9	154.5	47.8	463.33	30.5
75.1	348.3	174.1	171.8	42.7	548.30	25.8

Table 17 Volume calibration data set 7 (small cell)

Mass Solvent: 11.86 g						
T (°C)	T (K)	P (barg)	Corrected P ⁽⁵⁾ (barA)	Piston Position (mm)	Calculated density (kg/m ³)	Volume (cm ³)
41.7	314.9	153.3	151.1	20.9	769.11	15.4
41.6	314.8	142.3	140.0	21.5	749.71	15.8
41.6	314.8	131.1	128.9	23.0	724.82	16.4
41.6	314.8	121.8	119.8	24.1	698.66	17.0
41.4	314.6	111.3	109.5	27.2	657.11	18.0
41.5	314.7	106.8	105.1	28.0	633.75	18.7
41.5	314.7	102.9	101.2	30.6	604.54	19.6
41.5	314.7	97.1	95.5	36.7	536.63	22.1
41.5	314.7	99.2	97.6	34.8	566.85	20.9
41.5	314.7	95.5	93.9	37.8	507.73	23.4
41.5	314.7	94.0	92.4	43.5	475.80	24.9
41.5	314.7	93.3	91.7	44.8	459.61	25.8
50.2	323.4	142.3	139.9	26.6	669.29	17.7
50.0	323.2	132.3	129.9	28.6	635.08	18.7
50.0	323.2	127.6	125.2	30.0	613.35	19.3
50.0	323.2	120.7	118.4	33.3	573.36	20.7
50.0	323.2	116.6	114.4	35.9	542.97	21.8
50.0	323.2	111.3	109.1	41.5	492.08	24.1
50.0	323.2	109.2	107.0	44.1	468.45	25.3
50.0	323.2	106.4	104.2	49.1	434.74	27.3
50.0	323.2	104.5	102.3	52.9	411.31	28.8
50.0	323.2	102.8	100.6	56.0	390.66	30.4
50.0	323.2	100.8	98.6	61.3	367.32	32.3
50.0	323.2	98.2	96.0	67.2	339.17	35.0
50.0	323.2	96.1	94.1	72.3	320.35	37.0
58.9	332.1	198.1	195.1	23.0	722.43	16.4
58.7	331.9	185.8	182.9	24.4	702.06	16.9
58.9	332.1	185.4	182.5	24.7	699.87	16.9
58.8	332.0	173.8	170.7	25.9	675.43	17.6
58.8	332.0	166.5	163.5	27.1	657.41	18.0

Table 17 (continued) Volume calibration data set 7 (small cell)

T (°C)	T (K)	P (barg)	Corrected P⁽⁵⁾ (barA)	Piston Position (mm)	Calculated density (kg/m³)	Volume (cm³)
58.8	332.0	158.6	155.7	28.7	634.81	18.7
58.8	332.0	150.8	148.0	30.5	608.28	19.5
58.8	332.0	141.8	139.1	33.7	570.30	20.8
58.8	332.0	134.3	131.5	37.4	529.33	22.4
58.8	332.0	131.3	128.5	39.6	510.50	23.2
58.8	332.0	129.1	126.2	40.0	494.99	24.0
58.8	332.0	126.5	123.6	43.4	476.37	24.9
58.8	332.0	123.4	120.6	46.3	453.61	26.1
58.8	332.0	121.3	118.5	48.3	437.04	27.1
58.8	332.0	118.2	115.5	52.3	412.87	28.7

Table 18 Volume calibration data set 8 (large cell)

Mass Solvent: 14.47 g						
T (°C)	T (K)	P (barg)	Corrected P ⁽⁸⁾ (barA)	Piston Position (mm)	Calculated density (kg/m ³)	Volume (cm ³)
34.4	307.6	55.4	63.9	108.1	180.83	80.0
34.5	307.7	59.2	67.9	94.0	206.42	70.1
34.6	307.8	61.4	70.2	86.8	224.12	64.6
34.6	307.8	63.6	72.4	78.4	245.24	59.0
34.7	307.9	66.9	75.8	65.4	290.13	49.9
34.7	307.9	69.0	78.0	54.6	342.50	42.2
34.8	308.0	70.2	79.2	46.0	387.91	37.3
34.9	308.1	71.7	80.8	37.6	489.57	29.6
34.9	308.1	72.9	82.0	31.9	550.72	26.3
34.9	308.1	79.5	88.5	26.5	652.89	22.2
49.0	322.2	62.5	71.1	107.9	178.76	80.9
49.0	322.2	65.7	74.4	99.6	193.77	74.7
49.0	322.2	70.8	79.7	86.8	221.21	65.4
49.1	322.3	75.4	84.3	76.5	248.96	58.1
49.1	322.3	78.9	87.8	69.0	274.10	52.8
49.1	322.3	83.1	92.0	60.4	309.97	46.7
49.2	322.4	87.0	95.8	53.3	347.72	41.6
49.2	322.4	90.3	99.1	47.2	386.64	37.4
49.2	322.4	94.9	103.6	40.9	444.48	32.6
49.3	322.5	108.9	117.1	30.7	576.91	25.1
63.1	336.3	69.9	78.2	108.0	178.84	80.9
63.1	336.3	73.2	81.6	101.0	191.31	75.6
63.1	336.3	77.9	86.3	91.6	209.81	69.0
63.2	336.4	81.5	89.8	85.3	224.36	64.5
63.2	336.4	87.8	96.1	75.2	253.64	57.0
63.3	336.5	94.6	102.8	65.3	288.48	50.2
63.3	336.5	97.3	105.5	61.6	304.01	47.6
63.3	336.5	104.3	112.3	53.8	346.36	41.8
63.3	336.5	112.3	119.9	46.2	397.78	36.4
63.4	336.6	122.4	129.4	39.2	460.85	31.4

Table 18 (continued) Volume calibration data set 8 (large cell)

T (°C)	T (K)	P (barg)	Corrected P⁽⁸⁾ (barA)	Piston Position (mm)	Calculated density (kg/m³)	Volume (cm³)
77.4	350.6	77.0	84.1	107.9	175.45	82.5
77.5	350.7	89.5	96.5	87.8	215.00	67.3
77.5	350.7	97.5	104.3	77.2	242.98	59.6
77.5	350.7	104.4	111.0	69.8	269.02	53.8
77.5	350.7	111.0	117.3	63.1	295.19	49.0
77.6	350.8	120.3	126.2	55.3	334.11	43.3
77.6	350.8	127.0	132.5	50.6	363.17	39.8
77.6	350.8	134.9	140.0	45.8	398.20	36.3
77.6	350.8	148.2	152.3	39.5	453.78	31.9
77.6	350.8	164.3	167.6	34.4	514.72	28.1

Table 19 Volume calibration data set 9 (small cell)

Mass Solvent: 10.02 g						
T (°C)	T (K)	P (barg)	Corrected P ⁽⁷⁾ (barA)	Piston Position (mm)	Calculated density (kg/m ³)	Volume (cm ³)
32.4	306.1	68.2	66.6	97.3	204.10	49.1
32.5	306.2	70.3	68.7	90.1	220.60	45.4
32.5	306.2	71.9	70.3	82.3	235.91	42.5
32.8	306.5	76.1	74.6	61.9	293.22	34.2
32.9	306.6	78.2	76.7	49.8	352.99	28.4
32.8	306.5	78.2	76.7	42.6	359.46	27.9
33.0	306.7	79.2	77.7	33.7	411.74	24.3
33.3	307.0	83.5	82.0	24.5	610.95	16.4
44.9	318.7	77.1	75.2	97.4	208.46	48.1
44.9	318.7	78.6	76.7	92.4	217.12	46.1
45.0	318.8	80.8	78.9	87.4	230.35	43.5
45.1	318.9	83.0	81.1	80.7	244.81	40.9
45.3	319.1	87.1	85.1	70.6	274.92	36.4
45.5	319.3	93.9	91.9	54.9	344.62	29.1
45.7	319.5	98.7	96.6	43.8	407.97	24.6
45.7	319.5	102.9	100.7	36.1	471.55	21.2
57.6	331.5	85.5	83.0	97.3	226.42	44.3
57.8	331.7	91.8	89.2	84.7	236.55	42.4
57.9	331.8	96.5	93.9	75.7	261.09	38.4
58.0	331.9	101.3	98.5	67.6	287.84	34.8
58.1	332.0	104.9	102.1	61.8	310.67	32.3
58.4	332.3	111.3	108.4	53.2	353.55	28.3
58.6	332.5	118.6	115.6	44.1	407.77	24.6
58.9	332.8	129.1	126.0	35.2	483.08	20.7
70.9	344.9	98.7	95.3	90.4	223.85	44.8
71.1	345.1	103.4	100.0	82.6	241.82	41.4
71.3	345.3	112.3	108.9	70.3	279.38	35.9
71.5	345.5	120.3	116.8	60.7	315.93	31.7
71.7	345.7	131.2	127.6	50.1	370.06	27.1
71.8	345.8	143.9	140.4	40.8	436.10	23.0
72.3	346.3	164.3	160.6	31.7	523.30	19.1
72.3	346.3	189.1	185.5	25.7	603.72	16.6

Table 19 (continued) Volume calibration data set 9 (small cell)

T (°C)	T (K)	P (barg)	Corrected P⁽⁷⁾ (barA)	Piston Position (mm)	Calculated density (kg/m³)	Volume (cm³)
84.5	358.4	107.6	103.8	90.7	223.08	44.9
84.6	358.5	112.3	108.5	84.5	238.19	42.1
84.7	358.6	119.1	115.2	76.2	260.83	38.4
84.8	358.7	127.6	123.5	67.2	290.51	34.5
84.9	358.8	135.4	131.3	60.2	319.72	31.3
85.2	359.1	149.1	145.1	50.2	372.52	26.9
85.4	359.3	167.5	163.3	40.0	441.33	22.7
85.5	359.4	200.6	196.6	29.7	546.27	18.3

Table 20 Volume calibration data set 10 (large cell)

Mass Solvent: 14.16 g						
T (°C)	T (K)	P (barg)	Corrected P ⁽¹⁰⁾ (barA)	Piston Position (mm)	Calculated density (kg/m ³)	Volume (cm ³)
53.7	326.9	68.7	77.2	105.3	194.47	72.8
53.8	327.0	71.6	80.3	99.0	208.41	67.9
53.8	327.0	74.3	83.1	92.6	222.24	63.7
53.8	327.0	79.3	88.1	83.0	249.86	56.7
53.9	327.1	84.6	93.5	72.9	284.93	49.7
53.9	327.1	88.9	97.8	64.6	317.68	44.6
53.9	327.1	93.7	102.6	57.4	359.81	39.4
53.9	327.1	98.4	107.2	51.3	404.76	35.0
53.9	327.1	104.1	112.9	46.4	461.63	30.7
53.9	327.1	110.1	118.7	42.5	513.26	27.6
54.0	327.2	117.4	125.7	39.7	559.99	25.3
54.0	327.2	130.1	137.9	36.0	621.29	22.8
63.3	336.5	76.4	84.5	101.9	202.08	70.1
63.4	336.6	79.1	87.3	96.4	213.17	66.4
63.4	336.6	83.9	92.2	88.4	234.45	60.4
63.4	336.6	87.4	95.7	82.4	250.92	56.4
63.4	336.6	92.8	101.1	74.9	278.63	50.8
63.4	336.6	98.4	106.6	67.5	309.94	45.7
63.4	336.6	105.3	113.4	59.0	352.81	40.1
63.4	336.6	112.5	120.4	52.1	400.25	35.4
63.4	336.6	123.5	130.9	45.6	470.41	30.1
63.5	336.7	135.0	141.9	41.4	532.76	26.6
63.5	336.7	145.0	151.3	38.6	574.07	24.7
63.5	336.7	152.7	158.6	36.8	601.24	23.6

Table 20 (continued) Volume calibration data set 10 (large cell)

T (°C)	T (K)	P (barg)	Corrected P ⁽¹⁰⁾ (barA)	Piston Position (mm)	Calculated density (kg/m ³)	Volume (cm ³)
72.9	346.1	82.1	89.9	102.3	201.64	70.2
73.0	346.2	86.0	93.9	95.7	215.65	65.7
73.0	346.2	90.4	98.3	89.5	232.17	61.0
73.0	346.2	94.6	102.4	83.5	248.45	57.0
73.0	346.2	99.8	107.6	77.0	270.38	52.4
73.1	346.3	104.6	112.3	71.8	291.04	48.7
73.1	346.3	110.5	118.0	66.5	318.04	44.5
73.1	346.3	119.2	126.4	58.4	360.27	39.3
73.1	346.3	129.6	136.3	52.4	411.59	34.4
73.1	346.3	136.7	143.0	48.7	445.46	31.8
73.1	346.3	146.3	152.1	44.8	488.22	29.0
73.1	346.3	155.1	160.3	41.9	522.54	27.1

The correlations for the volume-piston position relationship were determined by plotting the calibration data and fitting a straight line to it. The correlations for the volume calibration data sets given in Table 11 to Table 20 are given by Equations A.1 to A.10. Volume is calculated in cm³, and piston length in mm.

$$Volume_{(1)} = (0.4317 \times Piston) + 7.6180 \quad \text{Eq. A-1}$$

$$Volume_{(2)} = (0.6696 \times Piston) - 5.4812 \quad \text{Eq. A-2}$$

$$Volume_{(3)} = (0.5479 \times Piston) + 9.3174 \quad \text{Eq. A-3}$$

$$Volume_{(4)} = (0.6852 \times Piston) - 4.5348 \quad \text{Eq. A-4}$$

$$Volume_{(5)} = (0.4066 \times Piston) + 7.5116 \quad \text{Eq. A-5}$$

$$Volume_{(6)} = (0.7210 \times Piston) - 4.7324 \quad \text{Eq. A-6}$$

$$Volume_{(7)} = (0.4206 \times Piston) + 6.7045 \quad \text{Eq. A-7}$$

$$Volume_{(8)} = (0.7182 \times Piston) + 3.2984 \quad \text{Eq. A-8}$$

$$Volume_{(9)} = (0.4244 \times Piston) + 6.3702 \quad \text{Eq. A-9}$$

$$Volume_{(10)} = (0.7152 \times Piston) - 2.6391 \quad \text{Eq. A-10}$$

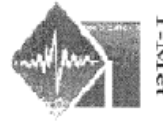
A.3 Temperature Sensor Calibration

The temperature sensors of both equilibrium cells were calibrated by Testing Metrology Technology CC (T-Met), a South African National Accreditation System (SANAS) accredited calibration laboratory. The calibration certificates are included, and show that within the experimental temperature range one sensor was 100% accurate while the other one showed a maximum deviation of 0.2 K at low temperatures. No temperature adjustments were made to the temperature values that were measured during the VLE and solubility experiments.



Lab no 155/355

Testing Metrology Technology cc t/a T-Met
PO Box 3822, Durbanville, 7550.
Unit G1, Centurion Business Park, Milnerton.
Tel 021 551 4595 Fax 021 551 4827
Vat No : 4360219325.
Registration no: CK2004/122069/23cc



Testing Metrology Technology

Certificate of Calibration

SANAS accredited laboratory no 155/355

The South African National Accreditation Service (SANAS) is a member of the International Laboratory Accreditation Cooperation (ILAC) Mutual Recognition Agreement (MRA). This arrangement allows for the mutual recognition of technical test and calibration data by the member accreditation bodies worldwide. For more information on the arrangement please consult www.ilac.org

Manufacturer : Testo AG, Germany
Description : Digital Thermometer and Probe
Model No : 720
Asset No : TM26541
Serial No : 90583200137
Calibrated for : University of Stellenbosch- Department of Process Engineering
: Stellenbosch
Temperature : 23 °C ± 3 °C
Relative humidity : 45 % RH ± 2 %RH
Date of calibration : 12 April 2010
Issue Date : 13 April 2010
Calibrated by : JF van Ewyk

This certificate is issued without alteration, and in accordance with the conditions of accreditation granted by the SANAS. It is a correct record of the measurements made at the time of calibration. Copyright of this certificate is owned jointly by T Met and may not be reproduced other than in full, except with the prior written approval of T-Met. The values given in this certificate were correct at the time of calibration. Subsequently the accuracy will depend on factors such as care exercised in handling the instrument and frequency of use. Recalibration should be performed after a period, which has been chosen to ensure that, under normal circumstances, the instruments accuracy remains within the desired limits. The reported expanded uncertainty is based on a standard uncertainty multiplied by a coverage factor $k = 2$ providing a level of confidence of approximately 95%, the uncertainty of measurement has been estimated in accordance with the principles defined in the GUM, Guide to Uncertainty of Measurement, ISO, Geneva, 1993

Technical Signatory
ZW de Witt
Certificate no TM26541

Page 1 of 2

Certificate of Calibration

1. Standards and equipment

Ref	Make	Model	Description	Serial no
74	Fluke	741B	Process Calibrator	8572023
50	Fluke	5500A	Calibrator	7270009
18	Fluke	7103	Stirred Liquid Bath	A5B833
57	Hart Scientific	5699	SPRT Probe	0085
228	Guildline	9540	Resistance Thermometer	228
35	Hart Scientific	1620 (2626-H)	Thermo hygrometer @ Probe	A53650

2. Procedure

- 2.1.1 The UUT (Unit under Test) was submitted for calibration in terms of the International Temperature Scale of 1990 (ITS-90)
- 2.1.2 Calibration Procedure no TM P3 008 was used.
- 2.1.3 The UUT test probe was immersed to an approximate depth of 100 mm into a temperature calibrator.
- 2.1.4 The temperature was stabilised and then set to rise at a slow constant rate to the nominal set point.
- 2.1.5 Readings were performed when the reading coincided with the nominal value of the temperature calibrator and or Reference Probe and recorded simultaneously

3. Results

3.1 Temperature Response

Range (°C)	Nominal Input (°C)	Applied Temperature (°C)	Tolerance (± 0.5 °C)		UUT Reading (°C)	Difference (°C)	Measurement uncertainty
			Low	Hi			
-50 To 275	-10	-10.0	-10.5	-9.5	-10.2	-0.2	± 1 °C
	0	0.0	-0.5	0.5	0.1	0.1	± 1 °C
	20	20.0	19.5	20.5	19.9	-0.1	± 1 °C
	40	40.0	39.5	40.5	39.9	-0.1	± 1 °C
	60	60.0	59.5	60.5	60.0	0.0	± 1 °C
	80	80.0	79.5	80.5	79.9	-0.1	± 1 °C

4. Comments

- 4.1 **Bold** - highlights result values, where applicable, indicate limitation imposed

Technical Signatory
 ZW de Witt
 Certificate no TM26541

Page 2 of 2



Lab no 155/355

Testing Metrology Technology cc t/a T-Met
PO Box 3822, Durbanville, 7550.
Unit G1, Centurion Business Park, Milnerton.
Tel 021 551 4595 Fax 021 551 4827
Vat No : 4360219325.
Registration no: CK2004/122069/23cc



Certificate of Calibration

SANAS accredited laboratory no 155/355

The South African National Accreditation Service (SANAS) is a member of the International Laboratory Accreditation Cooperation (ILAC) Mutual Recognition Agreement (MRA). This arrangement allows for the mutual recognition of technical test and calibration data by the member accreditation bodies worldwide. For more information on the arrangement please consult www.ilac.org

Manufacturer : Testo AG, Germany
Description : Digital Thermometer and Probe
Model No : 720
Asset No : TM26542
Serial No : 01253903/607
Calibrated for : University of Stellenbosch- Department of Process Engineering
: Stellenbosch
Temperature : 23 °C ± 3 °C
Relative humidity : 45 % RH ± 2 %RH
Date of calibration : 12 April 2010
Issue Date : 13 April 2010
Calibrated by : JF van Ewyk

This certificate is issued without alteration, and in accordance with the conditions of accreditation granted by the SANAS. It is a correct record of the measurements made at the time of calibration. Copyright of this certificate is owned jointly by T Met and may not be reproduced other than in full, except with the prior written approval of T-Met. The values given in this certificate were correct at the time of calibration. Subsequently the accuracy will depend on factors such as care exercised in handling the instrument and frequency of use. Recalibration should be performed after a period, which has been chosen to ensure that, under normal circumstances, the instruments accuracy remains within the desired limits. The reported expanded uncertainty is based on a standard uncertainty multiplied by a coverage factor $k = 2$ providing a level of confidence of approximately 95%, the uncertainty of measurement has been estimated in accordance with the principles defined in the GUM, Guide to Uncertainty of Measurement, ISO, Geneva, 1993

Technical/Signatory
ZW de Witt
Certificate no TM26542

Page 1 of 2

Certificate of Calibration

1. Standards and equipment

Ref	Make	Model	Description	Serial no
74	Fluke	741B	Process Calibrator	8572023
50	Fluke	5500A	Calibrator	7270009
18	Fluke	7103	Stirred Liquid Bath	A5B833
57	Hart Scientific	5699	SPRT Probe	0085
228	Guildline	9540	Resistance Thermometer	228
35	Hart Scientific	1620 (2626-H)	Thermo hygrometer @ Probe	A53650

2. Procedure

- 2.1.1 The UUT (Unit under Test) was submitted for calibration in terms of the International Temperature Scale of 1990 (ITS-90)
- 2.1.2 Calibration Procedure no TM P3 008 was used.
- 2.1.3 The UUT test probe was immersed to an approximate depth of 100 mm into a temperature calibrator.
- 2.1.4 The temperature was stabilised and then set to rise at a slow constant rate to the nominal set point.
- 2.1.5 Readings were performed when the reading coincided with the nominal value of the temperature calibrator and or Reference Probe and recorded simultaneously

3. Results

3.1 Temperature Response

Range (°C)	Nominal Input (°C)	Applied Temperature (°C)	Tolerance (± 0.5 °C)		UUT Reading (°C)	Difference (°C)	Measurement uncertainty
			Low	Hi			
-50 To 275	-10	-10.0	-10.5	-9.5	-10.0	0.0	± 1 °C
	0	0.0	-0.5	0.5	0.0	0.0	± 1 °C
	20	20.0	19.5	20.5	20.0	0.0	± 1 °C
	40	40.0	39.5	40.5	40.0	0.0	± 1 °C
	60	60.0	59.5	60.5	60.0	0.0	± 1 °C
	80	80.0	79.5	80.5	80.0	0.0	± 1 °C

4. Comments

- 4.1 **Bold** - highlights result values, where applicable, indicate limitation imposed

Technical Signatory
 ZW de Wit
 Certificate no TM26542

Page 2 of 2

A.4 Nomenclature

Symbol/ Acronym	Description
-----------------	-------------

<i>P</i>	Pressure
----------	----------

<i>T</i>	Temperature
----------	-------------

Sub/Superscripts	Description
------------------	-------------

set	Refers to the set value
-----	-------------------------

meas	Refers to the measured value
------	------------------------------

A.5 References

[1] NIST Chemistry WebBook, (n.d.).

B. RAW EXPERIMENTAL DATA

B.1 BINARY VLE DATAXXXIX

B.2 TERNARY AND MULTI-COMPONENT DATA CXV

B.1 Binary VLE data

Binary VLE data was measured for the following components with both CO₂ and ethane as respective solvents:

- *1*-decanol
- *2*-decanol
- *3,7*-dimethyl-*1*-octanol
- *2,6*-dimethyl-*2*-octanol
- *3,7*-dimethyl-*3*-octanol
- *n*-decane
- *2*-methylnonane
- *3*-methylnonane
- *4*-methylnonane
- *n*-dodecane¹

¹ Only CO₂ was used as the solvent.

Table 1 Experimental data for the CO₂+1-decanol system

Solute			I-Decanol							
Solvent			Carbon Dioxide							
Solute Molar Mass (g/mol)			158.28							
Solvent Molar Mass (g/mol)			44.01							
Solute mass (g)	Solvent mass (g)	Total mass (g)	Mass fraction (g/g)	Molar fraction (mol/mol)	Pressure (barg)	Piston position (mm)	Corrected pressure (barA)	Temperature (°C)	Converted Temperature (K)	Density (kg/m ³)
15.63	6.79	22.42	0.697	0.39029	70.1	49.3	75.6 ⁽²⁾	35.5	308.7	789.1 ⁽²⁾
					84.9	49.6	89.7 ⁽²⁾	45.1	318.3	783.4 ⁽²⁾
					99.6	50.1	103.0 ⁽²⁾	55.0	328.2	774.1 ⁽²⁾
					113.4	50.8	115.4 ⁽²⁾	65.5	338.7	761.3 ⁽²⁾
					125.0	51.2	125.7 ⁽²⁾	75.3	348.5	754.3 ⁽²⁾
14.50	7.24	21.74	0.667	0.35769	84.4	45.0	89.7 ⁽²⁾	35.3	308.5	881.3 ⁽²⁾
					93.8	45.6	98.3 ⁽²⁾	45.1	318.3	867.1 ⁽²⁾
					109.1	46.0	112.0 ⁽²⁾	54.8	328.0	858.0 ⁽²⁾
					123.3	46.7	124.7 ⁽²⁾	65.6	338.8	842.4 ⁽²⁾
					136.4	47.1	136.4 ⁽²⁾	75.3	348.5	833.7 ⁽²⁾

Table 1 (continued) Experimental data for the CO₂+1-decanol system.

Solute mass (g)	Solvent mass (g)	Total mass (g)	Mass fraction (g/g)	Molar fraction (mol/mol)	Pressure (barg)	Piston position (mm)	Corrected pressure (barA)	Temperature (°C)	Converted Temperature (K)	Density (kg/m ³)
14.82	8.37	23.19	0.639	0.32993	109.7	48.2	114.1 ⁽²⁾	35.7	308.9	810.8 ⁽²⁾
					109.0	49.0	112.8 ⁽²⁾	45.3	318.5	794.9 ⁽²⁾
					118.9	49.6	121.3 ⁽²⁾	55.0	328.2	783.4 ⁽²⁾
					132.5	50.3	133.4 ⁽²⁾	65.6	338.8	770.4 ⁽²⁾
13.56	8.86	22.42	0.605	0.29858	144.9	50.8	144.4 ⁽²⁾	75.3	348.5	761.3 ⁽²⁾
					146.1	46.8	148.5 ⁽²⁾	35.4	308.6	840.2 ⁽²⁾
					131.1	47.6	133.7 ⁽²⁾	45.1	318.3	823.1 ⁽²⁾
					134.8	48.2	136.3 ⁽²⁾	54.9	328.1	810.8 ⁽²⁾
10.74	10.35	21.09	0.509	0.22392	145.4	48.8	145.5 ⁽²⁾	65.4	338.6	798.8 ⁽²⁾
					157.0	49.7	155.7 ⁽²⁾	75.2	348.4	781.5 ⁽²⁾
					258.8	46.4	253.4 ⁽²⁾	35.5	308.7	849.0 ⁽²⁾
					195.0	47.3	193.3 ⁽²⁾	45.2	318.4	829.5 ⁽²⁾
10.74	10.35	21.09	0.509	0.22392	180.4	48.1	178.9 ⁽²⁾	54.9	328.1	812.8 ⁽²⁾
					180.8	49.0	178.6 ⁽²⁾	65.5	338.7	794.9 ⁽²⁾
					187.7	49.7	184.4 ⁽²⁾	75.1	348.3	781.5 ⁽²⁾

Table 1 (continued) Experimental data for the CO₂+1-decanol system.

Solute mass (g)	Solvent mass (g)	Total mass (g)	Mass fraction (g/g)	Molar fraction (mol/mol)	Pressure (barg)	Piston position (mm)	Corrected pressure (barA)	Temperature (°C)	Converted Temperature (K)	Density (kg/m ³)
8.37	12.64	21.01	0.398	0.15546	269.5	45.2	263.0 ⁽²⁾	40.2	313.4	876.5 ⁽²⁾
					235.6	45.7	231.1 ⁽²⁾	45.1	318.3	864.8 ⁽²⁾
					209.5	47.0	205.9 ⁽²⁾	54.8	328.0	835.9 ⁽²⁾
					205.5	48.2	201.5 ⁽²⁾	65.4	338.6	810.8 ⁽²⁾
					210.1	49.2	205.2 ⁽²⁾	75.2	348.4	791.0 ⁽²⁾
6.23	14.34	20.57	0.303	0.10772	282.7	40.5	275.3 ⁽²⁾	40.2	313.4	1004.0 ⁽²⁾
					245.6	41.2	240.4 ⁽²⁾	45.0	318.2	982.7 ⁽²⁾
					216.5	42.7	212.4 ⁽²⁾	54.8	328.0	940.0 ⁽²⁾
					211.8	44.2	207.4 ⁽²⁾	65.5	338.7	900.8 ⁽²⁾
					216.2	45.6	210.9 ⁽²⁾	75.1	348.3	867.1 ⁽²⁾
4.90	15.37	20.27	0.242	0.08141	277.5	45.8	270.4 ⁽²⁾	40.6	313.8	862.5 ⁽²⁾
					242.2	46.9	237.2 ⁽²⁾	45.4	318.6	838.0 ⁽²⁾
					215.5	48.4	211.4 ⁽²⁾	55.0	328.2	806.8 ⁽²⁾
					211.1	50.1	206.7 ⁽²⁾	65.7	338.9	774.1 ⁽²⁾
					215.8	51.6	210.5 ⁽²⁾	75.4	348.6	747.3 ⁽²⁾

Table 1 (continued) Experimental data for the CO₂+1-decanol system.

Solute mass (g)	Solvent mass (g)	Total mass (g)	Mass fraction (g/g)	Molar fraction (mol/mol)	Pressure (barg)	Piston position (mm)	Corrected pressure (barA)	Temperature (°C)	Converted Temperature (K)	Density (kg/m ³)
3.73	16.77	20.50	0.182	0.05818	260.6	44.2	254.7 ⁽²⁾	40.3	313.5	900.8 ⁽²⁾
					225.0	45.8	221.0 ⁽²⁾	47.0	320.2	862.5 ⁽²⁾
					209.5	47.4	205.9 ⁽²⁾	55.1	328.3	827.3 ⁽²⁾
					207.7	49.5	203.6 ⁽²⁾	65.7	338.9	785.3 ⁽²⁾
2.62	18.20	20.82	0.126	0.03847	213.3	51.2	208.2 ⁽²⁾	75.4	348.6	754.3 ⁽²⁾
					226.9	41.8	223.4 ⁽²⁾	40.3	313.5	965.1 ⁽²⁾
					206.4	43.0	203.9 ⁽²⁾	45.3	318.5	931.9 ⁽²⁾
					194.6	45.3	192.1 ⁽²⁾	55.1	328.3	874.1 ⁽²⁾
1.72	19.59	21.31	0.0808	0.02386	197.6	47.6	194.2 ⁽²⁾	65.7	338.9	823.1 ⁽²⁾
					205.1	50.0	200.5 ⁽²⁾	75.4	348.6	775.9 ⁽²⁾
					171.9	43.3	172.6 ⁽²⁾	35.3	308.5	923.9 ⁽²⁾
					160.2	46.0	160.9 ⁽²⁾	45.1	318.3	858.0 ⁽²⁾
1.72	19.59	21.31	0.0808	0.02386	165.3	48.8	164.8 ⁽²⁾	54.8	328.0	798.8 ⁽²⁾
					176.7	51.8	174.8 ⁽²⁾	65.5	338.7	743.9 ⁽²⁾
					188.6	54.6	185.3 ⁽²⁾	75.2	348.4	699.0 ⁽²⁾

Table 1 (continued) Experimental data for the CO₂+1-decanol system.

Solute mass (g)	Solvent mass (g)	Total mass (g)	Mass fraction (g/g)	Molar fraction (mol/mol)	Pressure (barg)	Piston position (mm)	Corrected pressure (barA)	Temperature (°C)	Converted Temperature (K)	Density (kg/m ³)
1.17	21.27	22.44	0.0521	0.01505	120.3	48.0	124.2 ⁽²⁾	35.6	308.8	814.9 ⁽²⁾
					129.3	51.1	132.0 ⁽²⁾	45.3	318.5	756.0 ⁽²⁾
					141.3	55.0	142.4 ⁽²⁾	55.0	328.2	693.0 ⁽²⁾
					158.5	58.6	157.7 ⁽²⁾	65.6	338.8	643.6 ⁽²⁾
					171.2	62.2	169.0 ⁽²⁾	75.2	348.4	600.7 ⁽²⁾
0.63	22.33	22.96	0.0275	0.00781	82.1	59.9	87.5 ⁽²⁾	35.5	308.7	627.4 ⁽²⁾
					102.3	65.0	106.4 ⁽²⁾	45.2	318.4	571.1 ⁽²⁾
					120.9	69.7	123.2 ⁽²⁾	54.9	328.1	527.4 ⁽²⁾
					140.9	73.4	141.3 ⁽²⁾	65.7	338.9	497.5 ⁽²⁾
					153.7	78.5	152.6 ⁽²⁾	75.4	348.6	461.4 ⁽²⁾
0.44	23.82	24.26	0.0180	0.00508	76.1	67.0	81.6 ⁽²⁾	35.6	308.8	551.7 ⁽²⁾
					97.2	71.2	101.5 ⁽²⁾	45.3	318.5	514.9 ⁽²⁾
					115.5	75.7	118.1 ⁽²⁾	54.9	328.1	480.6 ⁽²⁾
					131.9	81.8	132.9 ⁽²⁾	65.5	338.7	440.8 ⁽²⁾
					142.8	87.4	142.4 ⁽²⁾	75.0	348.2	409.6 ⁽²⁾

Table 2 Experimental data for the CO₂+2-decanol system

Solute			2-Decanol							
Solvent			Carbon Dioxide							
Solute Molar Mass (g/mol)			158.28							
Solvent Molar Mass (g/mol)			44.01							
Solute mass (g)	Solvent mass (g)	Total mass (g)	Mass fraction (g/g)	Molar fraction (mol/mol)	Pressure (barg)	Piston position (mm)	Corrected pressure (barA)	Temperature (°C)	Converted Temperature (K)	Density (kg/m ³)
11.04	7.14	18.18	0.607	0.30066	75.6	35.9	75.3 ⁽¹⁾	34.0	307.2	786.1 ⁽¹⁾
					93.5	36.6	92.5 ⁽¹⁾	46.0	319.2	776.0 ⁽¹⁾
					106.0	37.4	104.6 ⁽¹⁾	55.2	328.4	764.7 ⁽¹⁾
					119.1	38.2	117.2 ⁽¹⁾	65.0	338.2	753.7 ⁽¹⁾
					130.9	38.6	128.9 ⁽¹⁾	74.8	348.0	748.4 ⁽¹⁾
9.40	8.29	17.69	0.531	0.23963	85.0	33.4	84.7 ⁽¹⁾	33.9	307.1	802.2 ⁽¹⁾
					100.2	34.2	99.3 ⁽¹⁾	44.8	318.0	789.8 ⁽¹⁾
					116.0	35.0	114.6 ⁽¹⁾	54.8	328.0	777.8 ⁽¹⁾
					130.0	35.5	127.9 ⁽¹⁾	64.4	337.6	770.5 ⁽¹⁾
					142.3	36.0	140.0 ⁽¹⁾	74.5	347.7	763.3 ⁽¹⁾

Table 2 (continued) Experimental data for the CO₂+2-decanol system.

Solute mass (g)	Solvent mass (g)	Total mass (g)	Mass fraction (g/g)	Molar fraction (mol/mol)	Pressure (barg)	Piston position (mm)	Corrected pressure (barA)	Temperature (°C)	Converted Temperature (K)	Density (kg/m ³)
7.58	9.89	17.47	0.434	0.17565	109.7	32.3	109.1 ⁽¹⁾	34.9	308.1	809.8 ⁽¹⁾
					117.0	33.1	116.0 ⁽¹⁾	45.9	319.1	797.0 ⁽¹⁾
					130.7	34.2	129.1 ⁽¹⁾	55.5	328.7	780.1 ⁽¹⁾
					144.4	35.0	142.5 ⁽¹⁾	64.9	338.1	768.3 ⁽¹⁾
7.90	13.58	21.48	0.368	0.13925	159.0	36.2	156.4 ⁽¹⁾	75.3	348.5	751.1 ⁽¹⁾
					114.6	44.0	118.8 ⁽²⁾	35.4	308.6	895.1 ⁽²⁾
					119.8	45.0	123.0 ⁽²⁾	45.2	318.4	870.8 ⁽²⁾
					133.0	46.1	134.6 ⁽²⁾	54.9	328.1	845.5 ⁽²⁾
6.30	15.60	21.90	0.288	0.10100	150.0	47.0	149.8 ⁽²⁾	65.5	338.7	825.9 ⁽²⁾
					165.3	48.0	163.5 ⁽²⁾	75.3	348.5	805.2 ⁽²⁾
					116.4	48.2	120.5 ⁽²⁾	35.9	309.1	816.9 ⁽²⁾
					122.2	49.5	125.3 ⁽²⁾	45.2	318.4	791.2 ⁽²⁾
6.30	15.60	21.90	0.288	0.10100	135.7	50.8	137.1 ⁽²⁾	55.0	328.2	767.0 ⁽²⁾
					153.1	52.4	152.7 ⁽²⁾	65.5	338.7	739.3 ⁽²⁾
					168.1	53.4	166.1 ⁽²⁾	75.0	348.2	722.9 ⁽²⁾

Table 2 (continued) Experimental data for the CO₂+2-decanol system.

Solute mass (g)	Solvent mass (g)	Total mass (g)	Mass fraction (g/g)	Molar fraction (mol/mol)	Pressure (barg)	Piston position (mm)	Corrected pressure (barA)	Temperature (°C)	Converted Temperature (K)	Density (kg/m ³)
4.86	16.78	21.64	0.225	0.07456	112.6	48.3	116.9 ⁽²⁾	35.6	308.8	805.1 ⁽²⁾
					120.3	49.9	123.5 ⁽²⁾	45.2	318.4	774.3 ⁽²⁾
					135.8	51.5	137.2 ⁽²⁾	55.0	328.2	745.7 ⁽²⁾
					153.7	53.1	153.3 ⁽²⁾	65.7	338.9	719.1 ⁽²⁾
					169.8	54.8	167.7 ⁽²⁾	75.4	348.6	692.9 ⁽²⁾
3.59	17.22	20.81	0.173	0.05481	106.8	44.1	111.4 ⁽²⁾	35.4	308.6	864.7 ⁽²⁾
					117.2	46.0	120.6 ⁽²⁾	45.0	318.2	821.3 ⁽²⁾
					133.5	47.7	135.1 ⁽²⁾	54.8	328.0	786.0 ⁽²⁾
					152.1	50.1	151.8 ⁽²⁾	65.5	338.7	741.0 ⁽²⁾
					168.1	52.0	166.1 ⁽²⁾	75.2	348.4	708.8 ⁽²⁾
2.60	18.10	20.70	0.125	0.03834	97.0	45.0	101.9 ⁽²⁾	35.6	308.8	838.9 ⁽²⁾
					112.4	47.5	116.0 ⁽²⁾	45.4	318.6	785.6 ⁽²⁾
					130.6	49.4	132.3 ⁽²⁾	55.1	328.3	749.4 ⁽²⁾
					149.3	51.9	149.2 ⁽²⁾	65.7	338.9	706.5 ⁽²⁾
					165.3	54.3	163.5 ⁽²⁾	75.4	348.6	669.7 ⁽²⁾

Table.2 (continued) Experimental data for the CO₂+2-decanol system.

Solute mass (g)	Solvent mass (g)	Total mass (g)	Mass fraction (g/g)	Molar fraction (mol/mol)	Pressure (barg)	Piston position (mm)	Corrected pressure (barA)	Temperature (°C)	Converted Temperature (K)	Density (kg/m ³)
1.67	20.34	22.01	0.0758	0.02231	81.4	53.1	86.8 ⁽²⁾	35.7	308.9	731.3 ⁽²⁾
					102.5	56.0	106.6 ⁽²⁾	45.2	318.4	686.9 ⁽²⁾
					122.6	58.7	124.8 ⁽²⁾	54.9	328.1	650.2 ⁽²⁾
					142.1	62.2	142.5 ⁽²⁾	65.6	338.8	608.1 ⁽²⁾
1.33	26.09	27.42	0.0485	0.01399	157.5	65.7	156.2 ⁽²⁾	75.3	348.5	571.1 ⁽²⁾
					72.3	67.7	77.8 ⁽²⁾	35.3	308.5	687.6 ⁽²⁾
					95.4	71.8	99.8 ⁽²⁾	45.2	318.4	643.3 ⁽²⁾
					116.3	75.5	118.9 ⁽²⁾	54.9	328.1	608.0 ⁽²⁾
0.61	21.77	22.38	0.0271	0.00768	134.6	81.4	135.4 ⁽²⁾	65.6	338.8	559.0 ⁽²⁾
					150.1	85.7	149.2 ⁽²⁾	75.4	348.6	528.0 ⁽²⁾
					72.2	66.6	77.7 ⁽²⁾	35.4	308.6	571.7 ⁽²⁾
					91.0	73.6	95.6 ⁽²⁾	45.1	318.3	510.5 ⁽²⁾
0.61	21.77	22.38	0.0271	0.00768	110.0	77.1	112.9 ⁽²⁾	55.0	328.2	484.6 ⁽²⁾
					126.8	81.8	128.0 ⁽²⁾	65.6	338.8	453.6 ⁽²⁾
					139.5	86.4	139.3 ⁽²⁾	75.4	348.6	427.0 ⁽²⁾

Table 2 (continued) Experimental data for the CO₂+2-decanol system.

Solute mass (g)	Solvent mass (g)	Total mass (g)	Mass fraction (g/g)	Molar fraction (mol/mol)	Pressure (barg)	Piston position (mm)	Corrected pressure (barA)	Temperature (°C)	Converted Temperature (K)	Density (kg/m ³)
0.46	23.43	23.89	0.0193	0.00545	74.0	70.9	79.5 ⁽²⁾	35.8	309.0	568.6 ⁽²⁾
					91.2	77.0	95.8 ⁽²⁾	45.3	318.5	518.2 ⁽²⁾
					107.4	81.6	110.4 ⁽²⁾	55.0	328.2	485.7 ⁽²⁾
					122.8	87.8	124.3 ⁽²⁾	65.7	338.9	447.9 ⁽²⁾
					133.1	93.8	133.3 ⁽²⁾	75.4	348.6	416.5 ⁽²⁾
0.31	19.70	20.01	0.0153	0.00429	75.7	64.2	81.2 ⁽⁴⁾	36.0	309.2	605.8 ⁽⁴⁾
					92.4	69.2	96.9 ⁽⁴⁾	45.7	318.9	557.4 ⁽⁴⁾
					108.1	72.0	111.3 ⁽⁴⁾	55.6	328.8	533.5 ⁽⁴⁾
					121.2	76.8	123.1 ⁽⁴⁾	65.5	338.7	497.0 ⁽⁴⁾
					130.4	82.6	131.1 ⁽⁴⁾	75.4	348.6	459.1 ⁽⁴⁾

Table 3 Experimental data for the CO₂+3,7-dimethyl-1-octanol system

Solute			3,7-Dimethyl-1-octanol							
Solvent			Carbon Dioxide							
Solute Molar Mass (g/mol)			158.28							
Solvent Molar Mass (g/mol)			44.01							
Solute mass (g)	Solvent mass (g)	Total mass (g)	Mass fraction (g/g)	Molar fraction (mol/mol)	Pressure (barg)	Piston position (mm)	Corrected pressure (barA)	Temperature (°C)	Converted Temperature (K)	Density (kg/m ³)
10.98	6.61	17.59	0.624	0.31591	73.5	34.6	73.3 ⁽¹⁾	34.3	307.5	779.4 ⁽¹⁾
					88.1	34.7	87.2 ⁽¹⁾	44.0	317.2	777.9 ⁽¹⁾
					101.8	35.6	100.4 ⁽¹⁾	53.8	327.0	764.8 ⁽¹⁾
					115.5	36.2	113.7 ⁽¹⁾	63.6	336.8	756.3 ⁽¹⁾
					128.1	36.9	126.0 ⁽¹⁾	73.9	347.1	746.6 ⁽¹⁾
9.45	8.65	18.10	0.522	0.23305	88.1	34.9	87.7 ⁽¹⁾	33.9	307.1	797.7 ⁽¹⁾
					107.1	35.7	106.2 ⁽¹⁾	44.7	317.9	785.7 ⁽¹⁾
					123.9	36.8	122.4 ⁽¹⁾	55.0	328.2	769.8 ⁽¹⁾
					139.9	37.8	138.0 ⁽¹⁾	64.9	338.1	755.9 ⁽¹⁾
					154.4	38.9	151.9 ⁽¹⁾	75.3	348.5	741.2 ⁽¹⁾

Table 3 (continued) Experimental data for the CO₂+3,7-dimethyl-1-octanol system.

Solute mass (g)	Solvent mass (g)	Total mass (g)	Mass fraction (g/g)	Molar fraction (mol/mol)	Pressure (barg)	Piston position (mm)	Corrected pressure (barA)	Temperature (°C)	Converted Temperature (K)	Density (kg/m ³)
6.35	7.46	13.81	0.460	0.19142	103.9	20.9	102.9 ⁽³⁾	35.5	308.7	862.7 ⁽⁵⁾
					118.6	21.8	117.1 ⁽³⁾	45.2	318.4	843.4 ⁽⁵⁾
					134.9	22.4	132.9 ⁽³⁾	54.9	328.1	831.0 ⁽⁵⁾
					151.7	23.2	149.2 ⁽³⁾	65.5	338.7	815.1 ⁽⁵⁾
5.69	8.47	14.16	0.402	0.15747	166.5	23.9	163.8 ⁽³⁾	75.2	348.4	801.6 ⁽⁵⁾
					116.5	21.0	115.6 ⁽³⁾	35.6	308.8	882.4 ⁽⁵⁾
					129.1	21.9	127.5 ⁽³⁾	45.1	318.3	862.8 ⁽⁵⁾
					143.9	22.7	142.0 ⁽³⁾	54.6	327.8	846.0 ⁽⁵⁾
4.34	9.57	13.91	0.312	0.11207	160.0	23.6	157.4 ⁽³⁾	64.6	337.8	827.9 ⁽⁵⁾
					173.8	24.5	171.0 ⁽³⁾	74.0	347.2	810.6 ⁽⁵⁾
					122.0	20.8	126.1 ⁽³⁾	35.8	309.0	871.3 ⁽⁵⁾
					134.9	22.0	137.6 ⁽³⁾	45.2	318.4	845.5 ⁽⁵⁾
4.34	9.57	13.91	0.312	0.11207	150.1	23.1	150.9 ⁽³⁾	54.8	328.0	823.1 ⁽⁵⁾
					166.6	24.2	165.5 ⁽³⁾	65.0	338.2	801.9 ⁽⁵⁾
					181.6	25.4	178.9 ⁽³⁾	74.4	347.6	780.0 ⁽⁵⁾

Table 3 (continued) Experimental data for the CO₂+3,7-dimethyl-1-octanol system.

Solute mass (g)	Solvent mass (g)	Total mass (g)	Mass fraction (g/g)	Molar fraction (mol/mol)	Pressure (barg)	Piston position (mm)	Corrected pressure (barA)	Temperature (°C)	Converted Temperature (K)	Density (kg/m ³)
3.80	16.40	20.20	0.188	0.06051	115.3	45.3	119.4 ⁽²⁾	35.6	308.8	812.2 ⁽²⁾
					129.5	46.9	132.2 ⁽²⁾	45.3	318.5	778.6 ⁽²⁾
					146.1	48.2	146.8 ⁽²⁾	55.0	328.2	753.3 ⁽²⁾
					164.3	50.0	163.2 ⁽²⁾	65.7	338.9	720.9 ⁽²⁾
					179.8	51.6	177.1 ⁽²⁾	75.4	348.6	694.3 ⁽²⁾
2.60	19.54	22.14	0.117	0.03561	101.1	48.6	105.9 ⁽²⁾	35.7	308.9	817.4 ⁽²⁾
					119.2	50.6	122.5 ⁽²⁾	45.3	318.5	778.8 ⁽²⁾
					139.5	52.9	140.6 ⁽²⁾	55.0	328.2	738.8 ⁽²⁾
					157.0	55.1	156.3 ⁽²⁾	65.7	338.9	704.1 ⁽²⁾
					172.4	57.7	170.2 ⁽²⁾	75.4	348.6	667.2 ⁽²⁾
1.69	20.50	22.19	0.0760	0.02236	86.9	49.7	92.2 ⁽²⁾	35.3	308.5	797.5 ⁽²⁾
					108.6	52.3	112.4 ⁽²⁾	45.0	318.2	750.5 ⁽²⁾
					130.9	55.0	132.6 ⁽²⁾	55.7	328.9	707.3 ⁽²⁾
					148.8	58.0	148.7 ⁽²⁾	65.4	338.6	664.7 ⁽²⁾
					164.5	61.0	162.7 ⁽²⁾	75.1	348.3	626.9 ⁽²⁾

Table 3 (continued) Experimental data for the CO₂+3,7-dimethyl-1-octanol system.

Solute mass (g)	Solvent mass (g)	Total mass (g)	Mass fraction (g/g)	Molar fraction (mol/mol)	Pressure (barg)	Piston position (mm)	Corrected pressure (barA)	Temperature (°C)	Converted Temperature (K)	Density (kg/m ³)
0.43	12.04	12.47	0.0344	0.00980	82.3	25.4	81.4 ⁽³⁾	35.3	308.5	698.9 ⁽⁵⁾
					104.4	28.3	103.1 ⁽³⁾	45.1	318.3	655.6 ⁽⁵⁾
					122.8	31.7	120.8 ⁽³⁾	54.5	327.7	611.2 ⁽⁵⁾
					140.0	35.5	137.7 ⁽³⁾	64.9	338.1	568.2 ⁽⁵⁾
0.50	29.32	29.82	0.0168	0.00473	152.7	39.5	150.2 ⁽³⁾	74.5	347.7	529.0 ⁽⁵⁾
					73.2	87.0	78.7 ⁽²⁾	35.6	308.8	564.7 ⁽²⁾
					92.2	93.1	96.7 ⁽²⁾	45.3	318.5	524.1 ⁽²⁾
					109.1	99.4	112.0 ⁽²⁾	55.0	328.2	487.9 ⁽²⁾
0.50	29.32	29.82	0.0168	0.00473	125.2	105.3	126.5 ⁽²⁾	65.7	338.9	458.3 ⁽²⁾
					136.3	111.7	136.3 ⁽²⁾	75.1	348.3	430.0 ⁽²⁾

Table 4 Experimental data for the CO₂+3,7-dimethyl-1-octanol system used to prove reproducibility

Solute		3,7-Dimethyl-1-octanol								
Solvent		Carbon Dioxide								
Solute Molar Mass (g/mol)		158.28								
Solvent Molar Mass (g/mol)		44.01								
Solute mass (g)	Solvent mass (g)	Total mass (g)	Mass fraction (g/g)	Molar fraction (mol/mol)	Pressure (barg)	Piston position (mm)	Corrected pressure (barA)	Temperature (°C)	Converted Temperature (K)	Density (kg/m ³)
0.65	19.62	20.27	0.0323	0.00918	75.2	53.0	80.7 ⁽²⁾	35.4	308.6	415.2 ⁽²⁾
					98.0	56.5	102.3 ⁽²⁾	45.3	318.5	385.1 ⁽²⁾
					118.6	59.5	121.0 ⁽²⁾	55.0	328.2	362.6 ⁽²⁾
					136.6	63.8	137.3 ⁽²⁾	65.6	338.8	334.6 ⁽²⁾
					149.7	67.5	148.9 ⁽²⁾	75.3	348.5	313.7 ⁽²⁾

Table 5 Experimental data for the CO₂+2,6-dimethyl-2-octanol system

Solute			2,6-Dimethyl-2-octanol							
Solvent			Carbon Dioxide							
Solute Molar Mass (g/mol)			158.28							
Solvent Molar Mass (g/mol)			44.01							
Solute mass (g)	Solvent mass (g)	Total mass (g)	Mass fraction (g/g)	Molar fraction (mol/mol)	Pressure (barg)	Piston position (mm)	Corrected pressure (barA)	Temperature (°C)	Converted Temperature (K)	Density (kg/m ³)
13.86	7.95	21.81	0.636	0.32654	59.1	46.0	64.5 ⁽²⁾	35.5	308.7	860.8 ⁽²⁾
					70.3	46.5	75.2 ⁽²⁾	45.3	318.5	849.6 ⁽²⁾
					81.6	47.1	85.5 ⁽²⁾	55.0	328.2	836.5 ⁽²⁾
					93.4	48.0	96.4 ⁽²⁾	65.6	338.8	817.6 ⁽²⁾
					104.1	48.7	106.0 ⁽²⁾	75.4	348.6	803.5 ⁽²⁾
11.62	10.00	21.62	0.537	0.24420	63.2	45.5	68.7 ⁽²⁾	35.5	308.7	864.7 ⁽²⁾
					77.0	45.8	81.9 ⁽²⁾	45.3	318.5	857.8 ⁽²⁾
					91.0	46.7	94.7 ⁽²⁾	55.0	328.2	837.7 ⁽²⁾
					106.2	47.5	108.6 ⁽²⁾	65.7	338.9	820.7 ⁽²⁾
					119.8	48.3	120.8 ⁽²⁾	75.4	348.6	804.3 ⁽²⁾

Table 5 (continued) Experimental data for the CO₂+2,6-dimethyl-2-octanol system.

Solute mass (g)	Solvent mass (g)	Total mass (g)	Mass fraction (g/g)	Molar fraction (mol/mol)	Pressure (barg)	Piston position (mm)	Corrected pressure (barA)	Temperature (°C)	Converted Temperature (K)	Density (kg/m ³)
9.61	12.52	22.13	0.434	0.17595	67.0	46.3	72.5 ⁽²⁾	35.6	308.8	866.6 ⁽²⁾
					82.2	47.0	87.0 ⁽²⁾	45.3	318.5	851.0 ⁽²⁾
					98.7	47.9	102.1 ⁽²⁾	55.0	328.2	831.7 ⁽²⁾
					116.5	49.2	118.3 ⁽²⁾	65.6	338.8	805.4 ⁽²⁾
8.06	13.16	21.22	0.380	0.14556	132.5	49.9	132.7 ⁽²⁾	75.3	348.5	791.9 ⁽²⁾
					67.1	52.0	72.6 ⁽²⁾	35.6	308.8	722.9 ⁽²⁾
					83.3	52.5	88.1 ⁽²⁾	45.2	318.4	714.7 ⁽²⁾
					100.4	53.4	103.7 ⁽²⁾	54.9	328.1	700.5 ⁽²⁾
6.35	14.79	21.14	0.300	0.10660	119.8	54.4	121.4 ⁽²⁾	65.5	338.7	685.3 ⁽²⁾
					136.8	55.6	136.8 ⁽²⁾	75.3	348.5	668.0 ⁽²⁾
					68.5	45.0	74.0 ⁽²⁾	35.6	308.8	856.8 ⁽²⁾
					84.8	46.1	89.6 ⁽²⁾	45.1	318.3	832.0 ⁽²⁾
6.35	14.79	21.14	0.300	0.10660	103.6	47.7	106.8 ⁽²⁾	54.8	328.0	798.3 ⁽²⁾
					124.3	49.0	125.7 ⁽²⁾	65.5	338.7	772.9 ⁽²⁾
					141.3	50.3	141.0 ⁽²⁾	75.1	348.3	749.0 ⁽²⁾

Table 5 (continued) Experimental data for the CO₂+2,6-dimethyl-2-octanol system.

Solute mass (g)	Solvent mass (g)	Total mass (g)	Mass fraction (g/g)	Molar fraction (mol/mol)	Pressure (barg)	Piston position (mm)	Corrected pressure (barA)	Temperature (°C)	Converted Temperature (K)	Density (kg/m ³)
4.70	15.51	20.21	0.232	0.07766	68.5	43.8	74.0 ⁽²⁾	35.5	308.7	846.7 ⁽²⁾
					85.4	45.6	90.1 ⁽²⁾	45.1	318.3	806.0 ⁽²⁾
					105.0	47.1	108.1 ⁽²⁾	54.9	328.1	774.9 ⁽²⁾
					126.4	49.0	127.7 ⁽²⁾	65.6	338.8	738.9 ⁽²⁾
3.13	16.70	19.83	0.158	0.04952	143.6	51.0	143.2 ⁽²⁾	75.3	348.5	704.3 ⁽²⁾
					69.6	45.5	75.1 ⁽²⁾	35.6	308.8	793.0 ⁽²⁾
					86.6	47.9	91.3 ⁽²⁾	45.2	318.4	745.1 ⁽²⁾
					106.2	50.3	109.3 ⁽²⁾	54.8	328.0	702.7 ⁽²⁾
2.63	19.43	22.06	0.119	0.03623	126.9	52.9	128.1 ⁽²⁾	65.6	338.8	661.8 ⁽²⁾
					143.5	55.0	143.1 ⁽²⁾	75.2	348.4	632.1 ⁽²⁾
					69.9	50.5	75.4 ⁽²⁾	35.4	308.6	777.9 ⁽²⁾
					87.2	54.6	91.9 ⁽²⁾	45.2	318.4	709.2 ⁽²⁾
2.63	19.43	22.06	0.119	0.03623	106.5	58.2	109.5 ⁽²⁾	54.9	328.1	658.2 ⁽²⁾
					126.5	61.3	127.8 ⁽²⁾	65.5	338.7	619.8 ⁽²⁾
					142.6	64.3	142.2 ⁽²⁾	75.2	348.4	586.6 ⁽²⁾

Table 5 (continued) Experimental data for the CO₂+2,6-dimethyl-2-octanol system.

Solute mass (g)	Solvent mass (g)	Total mass (g)	Mass fraction (g/g)	Molar fraction (mol/mol)	Pressure (barg)	Piston position (mm)	Corrected pressure (barA)	Temperature (°C)	Converted Temperature (K)	Density (kg/m ³)
1.66	18.65	20.31	0.0818	0.02418	70.7	56.0	76.2 ⁽²⁾	35.5	308.7	634.0 ⁽²⁾
					87.6	61.1	92.3 ⁽²⁾	45.2	318.4	572.9 ⁽²⁾
					105.6	64.5	108.7 ⁽²⁾	54.9	328.1	538.3 ⁽²⁾
					125.0	67.5	126.3 ⁽²⁾	65.6	338.8	511.1 ⁽²⁾
0.95	17.25	18.20	0.0523	0.01511	140.1	70.7	139.9 ⁽²⁾	75.4	348.6	484.9 ⁽²⁾
					72.2	47.4	77.7 ⁽²⁾	35.8	309.0	692.7 ⁽²⁾
					87.7	55.1	92.4 ⁽²⁾	45.2	318.4	579.0 ⁽²⁾
					105.2	59.0	108.3 ⁽²⁾	55.0	328.2	534.6 ⁽²⁾
0.59	20.24	20.83	0.0285	0.00808	121.8	62.6	123.3 ⁽²⁾	65.6	338.8	499.2 ⁽²⁾
					134.0	66.2	134.2 ⁽²⁾	75.0	348.2	468.2 ⁽²⁾
					71.8	57.4	77.3 ⁽²⁾	35.4	308.6	631.7 ⁽²⁾
					86.7	70.7	91.4 ⁽²⁾	45.1	318.3	497.4 ⁽²⁾
0.59	20.24	20.83	0.0285	0.00808	102.2	74.5	105.4 ⁽²⁾	54.9	328.1	468.9 ⁽²⁾
					116.3	80.0	118.1 ⁽²⁾	65.5	338.7	432.9 ⁽²⁾
					125.8	85.7	126.5 ⁽²⁾	75.3	348.5	401.1 ⁽²⁾

Table 5 (continued) Experimental data for the CO₂+2,6-dimethyl-2-octanol system.

Solute mass (g)	Solvent mass (g)	Total mass (g)	Mass fraction (g/g)	Molar fraction (mol/mol)	Pressure (barg)	Piston position (mm)	Corrected pressure (barA)	Temperature (°C)	Converted Temperature (K)	Density (kg/m ³)
0.39	20.68	21.07	0.0183	0.00515	73.7	64.2	79.2 ⁽²⁾	35.6	308.8	561.2 ⁽²⁾
					87.0	81.4	91.7 ⁽²⁾	45.3	318.5	429.4 ⁽²⁾
					100.0	86.8	103.3 ⁽²⁾	54.8	328.0	399.9 ⁽²⁾
					111.0	94.1	113.1 ⁽²⁾	65.5	338.7	365.9 ⁽²⁾
					117.5	102.5	118.6 ⁽²⁾	75.2	348.4	333.3 ⁽²⁾

Table 6 Experimental data for the CO₂+3,7-dimethyl-3-octanol system

Solute			3,7-Dimethyl-3-octanol							
Solvent			Carbon Dioxide							
Solute Molar Mass (g/mol)			158.28							
Solvent Molar Mass (g/mol)			44.01							
Solute mass (g)	Solvent mass (g)	Total mass (g)	Mass fraction (g/g)	Molar fraction (mol/mol)	Pressure (barg)	Piston position (mm)	Corrected pressure (barA)	Temperature (°C)	Converted Temperature (K)	Density (kg/m ³)
13.41	7.92	21.33	0.629	0.32015	57.9	47.8	63.2 ⁽²⁾	35.6	308.8	803.7 ⁽²⁾
					69.0	48.5	73.9 ⁽²⁾	45.4	318.6	789.7 ⁽²⁾
					80.1	49.0	84.0 ⁽²⁾	55.1	328.3	780.1 ⁽²⁾
					92.5	49.7	95.6 ⁽²⁾	65.8	339.0	766.9 ⁽²⁾
					102.9	50.3	104.8 ⁽²⁾	75.5	348.7	756.0 ⁽²⁾
11.28	10.04	21.32	0.529	0.23798	62.4	45.6	67.9 ⁽²⁾	35.6	308.8	798.4 ⁽⁴⁾
					75.5	46.1	80.5 ⁽²⁾	45.2	318.4	788.2 ⁽⁴⁾
					89.4	47.1	93.1 ⁽²⁾	55.0	328.2	768.8 ⁽⁴⁾
					104.7	47.8	107.2 ⁽²⁾	65.6	338.8	755.7 ⁽⁴⁾
					118.2	48.5	119.3 ⁽²⁾	75.3	348.5	743.1 ⁽⁴⁾

Table.6 (continued) Experimental data for the CO₂+3,7-dimethyl-3-octanol system.

Solute mass (g)	Solvent mass (g)	Total mass (g)	Mass fraction (g/g)	Molar fraction (mol/mol)	Pressure (barg)	Piston position (mm)	Corrected pressure (barA)	Temperature (°C)	Converted Temperature (K)	Density (kg/m ³)
9.34	11.86	21.20	0.440	0.17957	65.6	44.4	71.1 ⁽²⁾	35.7	308.9	823.7 ⁽⁴⁾
					80.4	44.9	85.3 ⁽²⁾	45.3	318.5	813.0 ⁽⁴⁾
					96.2	46.0	99.7 ⁽²⁾	54.9	328.1	790.3 ⁽⁴⁾
					113.7	47.0	115.7 ⁽²⁾	65.6	338.8	770.7 ⁽⁴⁾
7.62	13.46	21.08	0.362	0.13602	128.9	47.8	129.4 ⁽²⁾	75.2	348.4	755.7 ⁽⁴⁾
					67.0	45.4	72.5 ⁽²⁾	35.7	308.9	802.5 ⁽⁴⁾
					82.7	46.2	87.5 ⁽²⁾	45.3	318.5	786.3 ⁽⁴⁾
					100.0	47.2	103.3 ⁽²⁾	55.0	328.2	766.9 ⁽⁴⁾
6.14	13.90	20.04	0.306	0.10937	119.2	48.6	120.9 ⁽²⁾	65.6	338.8	741.3 ⁽⁴⁾
					136.1	49.7	136.1 ⁽²⁾	75.2	348.4	722.4 ⁽⁴⁾
					68.2	51.7	73.7 ⁽²⁾	35.9	309.1	690.3 ⁽⁴⁾
					84.4	52.5	89.1 ⁽²⁾	45.4	318.6	678.3 ⁽⁴⁾
6.14	13.90	20.04	0.306	0.10937	102.6	53.5	105.8 ⁽²⁾	55.2	328.4	663.8 ⁽⁴⁾
					122.8	55.0	124.2 ⁽²⁾	65.9	339.1	643.2 ⁽⁴⁾
					140.1	56.2	139.9 ⁽²⁾	75.6	348.8	627.7 ⁽⁴⁾

Table 6 (continued) Experimental data for the CO₂+3,7-dimethyl-3-octanol system.

Solute mass (g)	Solvent mass (g)	Total mass (g)	Mass fraction (g/g)	Molar fraction (mol/mol)	Pressure (barg)	Piston position (mm)	Corrected pressure (barA)	Temperature (°C)	Converted Temperature (K)	Density (kg/m ³)
4.71	14.24	18.95	0.248	0.08419	68.9	43.4	74.4 ⁽²⁾	35.8	309.0	846.1 ⁽⁴⁾
					85.4	44.8	90.1 ⁽²⁾	45.5	318.7	815.1 ⁽⁴⁾
					104.2	46.2	107.3 ⁽²⁾	55.1	328.3	786.3 ⁽⁴⁾
					124.4	48.0	125.8 ⁽²⁾	65.7	338.9	752.1 ⁽⁴⁾
3.77	16.79	20.56	0.183	0.05880	141.5	49.5	141.2 ⁽²⁾	75.4	348.6	725.7 ⁽⁴⁾
					68.7	45.7	74.2 ⁽²⁾	35.5	308.7	796.3 ⁽⁴⁾
					85.8	47.9	90.5 ⁽²⁾	45.2	318.4	753.9 ⁽⁴⁾
					104.7	50.4	107.8 ⁽²⁾	54.8	328.0	710.8 ⁽⁴⁾
2.45	17.85	20.30	0.121	0.03682	125.0	52.9	126.4 ⁽²⁾	65.4	338.6	672.4 ⁽⁴⁾
					142.0	55.1	141.7 ⁽²⁾	75.1	348.3	641.9 ⁽⁴⁾
					69.2	48.3	74.7 ⁽²⁾	35.6	308.8	746.6 ⁽⁴⁾
					86.2	51.3	90.9 ⁽²⁾	45.2	318.4	696.5 ⁽⁴⁾
2.45	17.85	20.30	0.121	0.03682	104.9	55.1	108.0 ⁽²⁾	54.9	328.1	641.9 ⁽⁴⁾
					124.5	58.2	125.9 ⁽²⁾	65.6	338.8	603.3 ⁽⁴⁾
					140.6	60.8	140.3 ⁽²⁾	75.4	348.6	574.4 ⁽⁴⁾

Table 6 (continued) Experimental data for the CO₂+3,7-dimethyl-3-octanol system.

Solute mass (g)	Solvent mass (g)	Total mass (g)	Mass fraction (g/g)	Molar fraction (mol/mol)	Pressure (barg)	Piston position (mm)	Corrected pressure (barA)	Temperature (°C)	Converted Temperature (K)	Density (kg/m ³)
1.67	18.69	20.36	0.0819	0.02420	70.3	48.9	75.8 ⁽²⁾	35.6	308.8	736.0 ⁽⁴⁾
					86.9	54.0	91.6 ⁽²⁾	45.2	318.4	656.8 ⁽⁴⁾
					104.6	58.8	107.7 ⁽²⁾	54.9	328.1	596.4 ⁽⁴⁾
					123.1	62.0	124.6 ⁽²⁾	65.5	338.7	561.9 ⁽⁴⁾
1.18	18.75	19.93	0.0590	0.01714	138.3	65.3	138.2 ⁽²⁾	75.4	348.6	530.3 ⁽⁴⁾
					70.1	48.7	75.6 ⁽²⁾	35.3	308.5	739.5 ⁽⁴⁾
					87.0	56.5	91.7 ⁽²⁾	45.0	318.2	623.9 ⁽⁴⁾
					103.8	61.3	107.0 ⁽²⁾	54.6	327.8	569.1 ⁽⁴⁾
0.64	21.37	22.01	0.0290	0.00825	121.5	65.1	123.1 ⁽²⁾	65.3	338.5	532.1 ⁽⁴⁾
					134.8	68.9	134.9 ⁽²⁾	75.0	348.2	499.7 ⁽⁴⁾
					72.6	67.7	78.1 ⁽²⁾	35.5	308.7	509.5 ⁽⁴⁾
					87.1	82.9	91.8 ⁽²⁾	45.2	318.4	408.0 ⁽⁴⁾
0.64	21.37	22.01	0.0290	0.00825	102.2	87.3	105.4 ⁽²⁾	55.0	328.2	385.7 ⁽⁴⁾
					115.7	92.0	117.6 ⁽²⁾	65.6	338.8	364.5 ⁽⁴⁾
					125.0	95.6	125.7 ⁽²⁾	75.3	348.5	349.7 ⁽⁴⁾

Table 6 (continued) Experimental data for the CO₂+3,7-dimethyl-3-octanol system.

Solute mass (g)	Solvent mass (g)	Total mass (g)	Mass fraction (g/g)	Molar fraction (mol/mol)	Pressure (barg)	Piston position (mm)	Corrected pressure (barA)	Temperature (°C)	Converted Temperature (K)	Density (kg/m ³)
0.40	21.58	21.98	0.0181	0.00511	72.4	63.8	77.9 ⁽²⁾	35.3	308.5	544.2 ⁽⁴⁾
					85.6	85.5	90.4 ⁽²⁾	45.0	318.2	394.5 ⁽⁴⁾
					98.8	90.8	102.2 ⁽²⁾	54.7	327.9	369.7 ⁽⁴⁾
					109.9	98.2	112.1 ⁽²⁾	65.4	338.6	339.8 ⁽⁴⁾
					116.8	106.4	118.0 ⁽²⁾	75.0	348.2	311.9 ⁽⁴⁾

Table 7 Experimental data for the CO₂+ n-decane system

Solute			<i>n</i> -Decane							
Solvent			Carbon Dioxide							
Solute Molar Mass (g/mol)			158.28							
Solvent Molar Mass (g/mol)			44.01							
Solute mass (g)	Solvent mass (g)	Total mass (g)	Mass fraction (g/g)	Molar fraction (mol/mol)	Pressure (barg)	Piston position (mm)	Corrected pressure (barA)	Temperature (°C)	Converted Temperature (K)	Density (kg/m ³)
13.61	8.42	22.03	0.618	0.33328	54.1	51.4	59.1 ⁽²⁾	35.5	308.7	735.2 ⁽²⁾
					64.5	52.2	69.3 ⁽²⁾	45.3	318.5	721.8 ⁽²⁾
					75.6	53.0	79.6 ⁽²⁾	55.1	328.3	708.9 ⁽²⁾
					87.7	54.0	90.9 ⁽²⁾	65.7	338.9	693.4 ⁽²⁾
					98.6	54.8	100.7 ⁽²⁾	75.5	348.7	681.5 ⁽²⁾
8.49	8.67	17.16	0.495	0.23247	67.1	37.3	66.5 ⁽³⁾	35.0	308.2	897.0 ⁽¹⁾
					79.4	38.3	78.1 ⁽³⁾	44.7	317.9	881.0 ⁽¹⁾
					91.8	39.6	90.2 ⁽³⁾	54.3	327.5	861.0 ⁽¹⁾
					106.0	39.7	103.9 ⁽³⁾	65.0	338.2	859.5 ⁽¹⁾
					118.6	40.0	116.1 ⁽³⁾	75.0	348.2	855.0 ⁽¹⁾

Table 7 (continued) Experimental data for the CO₂+n-decane system.

Solute mass (g)	Solvent mass (g)	Total mass (g)	Mass fraction (g/g)	Molar fraction (mol/mol)	Pressure (barg)	Piston position (mm)	Corrected pressure (barA)	Temperature (°C)	Converted Temperature (K)	Density (kg/m ³)
8.38	12.91	21.29	0.394	0.16717	63.1	47.9	68.6 ⁽²⁾	35.6	308.8	799.9 ⁽²⁾
					77.3	49.0	82.2 ⁽²⁾	45.2	318.4	778.4 ⁽²⁾
					92.6	50.3	96.3 ⁽²⁾	55.0	328.2	754.4 ⁽²⁾
					109.7	51.7	111.9 ⁽²⁾	65.6	338.8	730.1 ⁽²⁾
6.31	14.44	20.75	0.304	0.11913	125.0	53.2	125.7 ⁽²⁾	75.3	348.5	705.8 ⁽²⁾
					65.4	51.2	70.9 ⁽²⁾	35.7	308.9	738.6 ⁽²⁾
					80.4	52.5	85.3 ⁽²⁾	45.3	318.5	716.9 ⁽²⁾
					96.6	54.0	100.1 ⁽²⁾	55.0	328.2	693.4 ⁽²⁾
3.87	12.51	16.38	0.236	0.08733	114.5	55.7	116.5 ⁽²⁾	65.4	338.6	668.6 ⁽²⁾
					130.9	57.4	131.2 ⁽²⁾	75.4	348.6	645.5 ⁽²⁾
					72.4	34.6	71.7 ⁽³⁾	34.4	307.6	943.4 ⁽¹⁾
					87.1	36.0	85.8 ⁽³⁾	44.1	317.3	918.8 ⁽¹⁾
3.87	12.51	16.38	0.236	0.08733	104.0	37.8	102.3 ⁽³⁾	54.2	327.4	888.9 ⁽¹⁾
					122.3	40.0	120.1 ⁽³⁾	65.4	338.6	855.0 ⁽¹⁾
					136.5	42.0	134.0 ⁽³⁾	74.9	348.1	826.3 ⁽¹⁾

Table 7 (continued) Experimental data for the CO₂+n-decane system.

Solute mass (g)	Solvent mass (g)	Total mass (g)	Mass fraction (g/g)	Molar fraction (mol/mol)	Pressure (barg)	Piston position (mm)	Corrected pressure (barA)	Temperature (°C)	Converted Temperature (K)	Density (kg/m ³)
2.03	13.78	15.81	0.128	0.04360	74.5	34.0	73.7 ⁽³⁾	34.9	308.1	954.4 ⁽¹⁾
					89.7	36.6	88.4 ⁽³⁾	44.5	317.7	908.6 ⁽¹⁾
					105.4	40.1	103.7 ⁽³⁾	54.0	327.2	853.5 ⁽¹⁾
					120.7	43.6	118.6 ⁽³⁾	64.2	337.4	804.7 ⁽¹⁾
0.88	16.21	17.09	0.0513	0.01647	134.9	45.5	132.4 ⁽³⁾	74.0	347.2	780.5 ⁽¹⁾
					77.1	43.7	76.3 ⁽³⁾	34.9	308.1	803.4 ⁽¹⁾
					92.4	55.8	91.1 ⁽³⁾	45.2	318.4	671.0 ⁽¹⁾
					105.5	60.4	103.8 ⁽³⁾	54.8	328.0	631.5 ⁽¹⁾
0.57	19.85	20.42	0.0278	0.00876	117.6	62.7	115.5 ⁽³⁾	64.9	338.1	613.4 ⁽¹⁾
					127.0	65.6	124.4 ⁽³⁾	74.6	347.8	592.0 ⁽¹⁾
					71.5	57.1	77.0 ⁽²⁾	35.4	308.6	649.5 ⁽²⁾
					83.3	78.5	88.1 ⁽²⁾	45.0	318.2	451.8 ⁽²⁾
0.57	19.85	20.42	0.0278	0.00876	94.8	87.1	98.4 ⁽²⁾	54.7	327.9	402.6 ⁽²⁾
					105.7	94.9	108.1 ⁽²⁾	65.5	338.7	366.4 ⁽²⁾
					111.5	103.6	113.0 ⁽²⁾	75.3	348.5	333.0 ⁽²⁾

Table 8 Experimental data for the CO₂+2-methylnonane system

Solute			2-Methylnonane							
Solvent			Carbon Dioxide							
Solute Molar Mass (g/mol)			142.29							
Solvent Molar Mass (g/mol)			44.01							
Solute mass (g)	Solvent mass (g)	Total mass (g)	Mass fraction (g/g)	Molar fraction (mol/mol)	Pressure (barg)	Piston position (mm)	Corrected pressure (barA)	Temperature (°C)	Converted Temperature (K)	Density (kg/m ³)
9.72	5.41	15.13	0.642	0.35713	57.8	31.6	57.3 ⁽³⁾	36.0	309.2	575.0 ⁽³⁾
					66.6	32.4	65.4 ⁽³⁾	45.3	318.5	565.7 ⁽³⁾
					75.0	33.3	73.5 ⁽³⁾	54.0	327.2	555.6 ⁽³⁾
					85.5	34.0	83.5 ⁽³⁾	64.7	337.9	548.0 ⁽³⁾
					94.5	34.7	91.9 ⁽³⁾	74.3	347.5	540.6 ⁽³⁾
8.19	7.13	15.32	0.534	0.26203	63.9	30.9	63.3 ⁽³⁾	35.4	308.6	583.4 ⁽³⁾
					74.4	31.5	73.2 ⁽³⁾	44.2	317.4	576.2 ⁽³⁾
					87.7	32.2	86.1 ⁽³⁾	55.3	328.5	568.0 ⁽³⁾
					98.7	31.9	96.5 ⁽³⁾	64.3	337.5	571.5 ⁽³⁾
					109.8	32.0	107.3 ⁽³⁾	74.5	347.7	570.3 ⁽³⁾

Table 8 (continued) Experimental data for the CO₂+2-methylnonane system.

Solute mass (g)	Solvent mass (g)	Total mass (g)	Mass fraction (g/g)	Molar fraction (mol/mol)	Pressure (barg)	Piston position (mm)	Corrected pressure (barA)	Temperature (°C)	Converted Temperature (K)	Density (kg/m ³)
6.71	8.06	14.77	0.454	0.20474	67.5	28.5	66.8 ⁽³⁾	35.4	308.6	614.2 ⁽³⁾
					79.1	28.7	77.8 ⁽³⁾	44.4	317.6	611.5 ⁽³⁾
					93.0	29.4	91.4 ⁽³⁾	54.9	328.1	602.3 ⁽³⁾
					107.0	29.0	104.9 ⁽³⁾	65.2	338.4	607.5 ⁽³⁾
5.48	9.68	15.16	0.361	0.14893	119.1	29.6	116.6 ⁽³⁾	74.5	347.7	599.7 ⁽³⁾
					68.7	30.2	68.1 ⁽³⁾	34.6	307.8	592.1 ⁽³⁾
					82.9	31.8	81.5 ⁽³⁾	44.8	318.0	572.7 ⁽³⁾
					98.2	32.8	96.5 ⁽³⁾	55.0	328.2	561.2 ⁽³⁾
4.45	8.94	13.39	0.332	0.13330	112.3	33.8	110.2 ⁽³⁾	64.5	337.7	550.1 ⁽³⁾
					126.5	34.7	123.9 ⁽³⁾	74.5	347.7	540.6 ⁽³⁾
					70.7	24.6	70.0 ⁽³⁾	35.4	308.6	671.8 ⁽³⁾
					84.5	24.7	83.1 ⁽³⁾	45.0	318.2	670.2 ⁽³⁾
4.45	8.94	13.39	0.332	0.13330	99.7	25.1	98.0 ⁽³⁾	54.9	328.1	663.8 ⁽³⁾
					114.4	25.6	112.3 ⁽³⁾	64.7	337.9	656.0 ⁽³⁾
					128.6	25.7	126.0 ⁽³⁾	74.6	347.8	654.5 ⁽³⁾

Table 8 (continued) Experimental data for the CO₂+2-methylnonane system.

Solute mass (g)	Solvent mass (g)	Total mass (g)	Mass fraction (g/g)	Molar fraction (mol/mol)	Pressure (barg)	Piston position (mm)	Corrected pressure (barA)	Temperature (°C)	Converted Temperature (K)	Density (kg/m ³)
3.21	9.57	12.78	0.251	0.09402	73.3	22.6	72.5 ⁽³⁾	35.8	309.0	917.0 ⁽⁵⁾
					87.6	24.2	86.2 ⁽³⁾	45.5	318.7	882.7 ⁽⁵⁾
					102.8	25.9	101.1 ⁽³⁾	54.9	328.1	848.8 ⁽⁵⁾
					119.7	28.3	117.6 ⁽³⁾	65.5	338.7	805.3 ⁽⁵⁾
2.36	11.09	13.45	0.176	0.06185	133.4	30.6	130.9 ⁽³⁾	75.0	348.2	767.5 ⁽⁵⁾
					74.5	25.8	73.7 ⁽³⁾	35.4	308.6	850.8 ⁽⁵⁾
					90.3	28.8	89.0 ⁽³⁾	45.8	319.0	796.8 ⁽⁵⁾
					106.0	31.7	104.2 ⁽³⁾	55.2	328.4	750.7 ⁽⁵⁾
0.85	10.55	11.40	0.0748	0.02441	121.3	35.1	119.2 ⁽³⁾	65.1	338.3	703.1 ⁽⁵⁾
					133.9	38.0	131.4 ⁽³⁾	74.0	347.2	667.0 ⁽⁵⁾
					77.7	20.9	76.8 ⁽³⁾	35.7	308.9	956.6 ⁽⁵⁾
					92.3	27.6	91.0 ⁽³⁾	45.4	318.6	817.5 ⁽⁵⁾
0.85	10.55	11.40	0.0748	0.02441	106.0	34.6	104.2 ⁽³⁾	55.1	328.3	709.7 ⁽⁵⁾
					122.3	37.4	120.1 ⁽³⁾	65.8	339.0	674.1 ⁽⁵⁾
					132.3	42.1	129.7 ⁽³⁾	75.5	348.7	621.8 ⁽⁵⁾

Table 8 (continued) Experimental data for the CO₂+2-methylnonane system.

Solute mass (g)	Solvent mass (g)	Total mass (g)	Mass fraction (g/g)	Molar fraction (mol/mol)	Pressure (barg)	Piston position (mm)	Corrected pressure (barA)	Temperature (°C)	Converted Temperature (K)	Density (kg/m ³)
0.38	10.62	11.00	0.0343	0.01088	79.3	25.4	78.4 ⁽³⁾	35.5	308.7	858.5 ⁽⁵⁾
					91.8	40.9	90.5 ⁽³⁾	45.3	318.5	634.4 ⁽⁵⁾
					103.4	46.9	101.7 ⁽³⁾	54.9	328.1	576.2 ⁽⁵⁾
					112.8	53.5	110.7 ⁽³⁾	65.7	338.9	523.3 ⁽⁵⁾
					117.1	62.7	114.7 ⁽³⁾	75.4	348.6	464.0 ⁽⁵⁾

Table 9 Experimental data for the CO₂+3-methylnonane system

Solute			3-Methylnonane							
Solvent			Carbon Dioxide							
Solute Molar Mass (g/mol)			142.29							
Solvent Molar Mass (g/mol)			44.01							
Solute mass (g)	Solvent mass (g)	Total mass (g)	Mass fraction (g/g)	Molar fraction (mol/mol)	Pressure (barg)	Piston position (mm)	Corrected pressure (barA)	Temperature (°C)	Converted Temperature (K)	Density (kg/m ³)
9.71	4.91	14.62	0.664	0.37959	54.5	29.2	54.1 ⁽³⁾	35.4	308.6	823.5 ⁽⁵⁾
					63.5	29.5	62.4 ⁽³⁾	44.9	318.1	818.3 ⁽⁵⁾
					71.8	30.2	70.2 ⁽³⁾	54.5	327.7	806.6 ⁽⁵⁾
					81.3	31.0	79.3 ⁽³⁾	65.1	338.3	793.5 ⁽⁵⁾
					89.7	31.8	87.1 ⁽³⁾	74.5	347.7	780.9 ⁽⁵⁾
8.30	7.66	15.96	0.520	0.25108	66.0	32.7	65.4 ⁽³⁾	35.6	308.8	767.2 ⁽⁵⁾
					77.6	34.6	76.3 ⁽³⁾	45.3	318.5	739.7 ⁽⁵⁾
					89.7	35.4	88.1 ⁽³⁾	55.0	328.2	728.7 ⁽⁵⁾
					102.9	36.7	100.7 ⁽³⁾	65.6	338.8	711.5 ⁽⁵⁾
					114.5	37.8	112.0 ⁽³⁾	75.4	348.6	697.6 ⁽⁵⁾

Table 9 (continued) Experimental data for the CO₂+3-methylnonane system.

Solute mass (g)	Solvent mass (g)	Total mass (g)	Mass fraction (g/g)	Molar fraction (mol/mol)	Pressure (barg)	Piston position (mm)	Corrected pressure (barA)	Temperature (°C)	Converted Temperature (K)	Density (kg/m ³)
6.72	8.21	14.93	0.450	0.20192	68.7	29.0	68.0 ⁽³⁾	35.5	308.7	827.0 ⁽⁵⁾
					81.3	30.6	79.9 ⁽³⁾	45.3	318.5	800.0 ⁽⁵⁾
					94.4	32.1	92.7 ⁽³⁾	54.8	328.0	776.3 ⁽⁵⁾
					109.2	33.4	107.1 ⁽³⁾	65.5	338.7	756.8 ⁽⁵⁾
4.08	9.21	13.29	0.307	0.12047	122.4	34.2	119.9 ⁽³⁾	75.1	348.3	745.3 ⁽⁵⁾
					72.4	24.0	71.6 ⁽³⁾	35.6	308.8	924.3 ⁽⁵⁾
					86.7	25.5	85.3 ⁽³⁾	45.2	318.4	892.8 ⁽⁵⁾
					101.9	26.9	100.2 ⁽³⁾	54.8	328.0	865.2 ⁽⁵⁾
3.02	9.88	12.90	0.234	0.08640	118.2	28.8	116.1 ⁽³⁾	65.3	338.5	830.5 ⁽⁵⁾
					132.9	30.4	130.4 ⁽³⁾	75.1	348.3	803.3 ⁽⁵⁾
					74.3	22.7	73.5 ⁽³⁾	35.7	308.9	953.5 ⁽⁵⁾
					89.2	24.6	87.9 ⁽³⁾	45.4	318.6	911.4 ⁽⁵⁾
3.02	9.88	12.90	0.234	0.08640	104.6	26.2	102.9 ⁽³⁾	54.9	328.1	878.8 ⁽⁵⁾
					121.5	29.0	119.3 ⁽³⁾	65.7	338.9	827.0 ⁽⁵⁾
					135.9	31.4	133.4 ⁽³⁾	75.2	348.4	787.2 ⁽⁵⁾

Table 9 (continued) Experimental data for the CO₂+3-methylnonane system.

Solute mass (g)	Solvent mass (g)	Total mass (g)	Mass fraction (g/g)	Molar fraction (mol/mol)	Pressure (barg)	Piston position (mm)	Corrected pressure (barA)	Temperature (°C)	Converted Temperature (K)	Density (kg/m ³)
1.71	10.12	11.83	0.144	0.04964	76.5	19.8	75.6 ⁽³⁾	35.8	309.0	1025.7 ⁽⁵⁾
					91.5	22.5	90.2 ⁽³⁾	45.4	318.6	958.1 ⁽⁵⁾
					106.7	26.4	104.9 ⁽³⁾	55.0	328.2	874.9 ⁽⁵⁾
					122.6	30.0	120.5 ⁽³⁾	65.2	338.4	809.9 ⁽⁵⁾
0.93	9.43	10.36	0.0902	0.02975	136.5	33.1	134.0 ⁽³⁾	75.4	348.6	761.2 ⁽⁵⁾
					77.6	16.4	77.3 ⁽³⁾	35.6	308.8	1125.7 ⁽⁵⁾
					92.7	21.1	91.4 ⁽³⁾	45.1	318.3	992.0 ⁽⁵⁾
					107.2	26.4	105.4 ⁽³⁾	54.9	328.1	874.9 ⁽⁵⁾
0.48	8.90	9.38	0.0514	0.01649	122.9	29.5	120.7 ⁽³⁾	65.6	338.8	818.3 ⁽⁵⁾
					134.4	32.9	131.9 ⁽³⁾	75.2	348.4	764.2 ⁽⁵⁾
					82.4	16.7	81.3 ⁽³⁾	37.6	310.8	1116.1 ⁽⁵⁾
					93.5	22.7	92.2 ⁽³⁾	45.4	318.6	953.5 ⁽⁵⁾
0.48	8.90	9.38	0.0514	0.01649	106.2	27.7	104.4 ⁽³⁾	55.0	328.2	850.2 ⁽⁵⁾
					118.7	30.9	116.6 ⁽³⁾	65.2	338.4	795.1 ⁽⁵⁾
					128.2	34.3	125.6 ⁽³⁾	74.9	348.1	743.9 ⁽⁵⁾

Table 10 Experimental data for the CO₂+4-methylnonane system

Solute			4-Methylnonane							
Solvent			Carbon Dioxide							
Solute Molar Mass (g/mol)			142.29							
Solvent Molar Mass (g/mol)			44.01							
Solute mass (g)	Solvent mass (g)	Total mass (g)	Mass fraction (g/g)	Molar fraction (mol/mol)	Pressure (barg)	Piston position (mm)	Corrected pressure (barA)	Temperature (°C)	Converted Temperature (K)	Density (kg/m ³)
9.41	6.04	15.45	0.609	0.32510	59.7	32.0	59.2 ⁽³⁾	35.6	308.8	724.1 ⁽⁵⁾
					69.7	32.7	68.5 ⁽³⁾	45.2	318.4	714.2 ⁽⁵⁾
					80.1	33.8	78.6 ⁽³⁾	54.7	327.9	699.1 ⁽⁵⁾
					91.4	34.3	89.3 ⁽³⁾	65.1	338.3	692.5 ⁽⁵⁾
					101.3	35.3	98.7 ⁽³⁾	74.6	347.8	679.6 ⁽⁵⁾
7.81	7.05	14.86	0.526	0.25520	64.8	29.9	64.2 ⁽³⁾	35.8	309.0	755.5 ⁽⁵⁾
					76.0	30.6	74.7 ⁽³⁾	45.4	318.6	744.7 ⁽⁵⁾
					87.7	31.4	86.2 ⁽³⁾	54.9	328.1	732.8 ⁽⁵⁾
					100.2	33.0	98.0 ⁽³⁾	65.4	338.6	710.0 ⁽⁵⁾
					111.8	34.2	109.4 ⁽³⁾	74.9	348.1	693.8 ⁽⁵⁾

Table 10 (continued) Experimental data for the CO₂+4-methylnonane system.

Solute mass (g)	Solvent mass (g)	Total mass (g)	Mass fraction (g/g)	Molar fraction (mol/mol)	Pressure (barg)	Piston position (mm)	Corrected pressure (barA)	Temperature (°C)	Converted Temperature (K)	Density (kg/m ³)
6.78	7.67	14.45	0.469	0.21472	67.1	27.4	66.4 ⁽³⁾	35.8	309.0	796.7 ⁽⁵⁾
					79.2	28.4	77.8 ⁽³⁾	45.4	318.6	779.7 ⁽⁵⁾
					91.8	29.7	90.2 ⁽³⁾	55.0	328.2	758.6 ⁽⁵⁾
					105.5	31.4	103.3 ⁽³⁾	65.5	338.7	732.8 ⁽⁵⁾
5.24	8.75	13.99	0.375	0.15631	118.1	32.4	115.6 ⁽³⁾	75.1	348.3	718.4 ⁽⁵⁾
					70.3	25.6	69.9 ⁽³⁾	35.8	309.0	829.2 ⁽⁵⁾
					83.5	26.9	82.1 ⁽³⁾	45.2	318.4	805.5 ⁽⁵⁾
					97.6	28.2	95.9 ⁽³⁾	54.9	328.1	783.0 ⁽⁵⁾
4.21	9.22	13.43	0.313	0.12367	112.9	30.0	110.8 ⁽³⁾	65.3	338.5	753.9 ⁽⁵⁾
					126.5	31.4	123.9 ⁽³⁾	74.9	348.1	732.8 ⁽⁵⁾
					71.8	24.3	71.0 ⁽³⁾	35.7	308.9	854.4 ⁽⁵⁾
					85.8	25.4	84.4 ⁽³⁾	45.5	318.7	833.0 ⁽⁵⁾
4.21	9.22	13.43	0.313	0.12367	100.2	26.8	98.5 ⁽³⁾	55.2	328.4	807.2 ⁽⁵⁾
					116.7	28.9	114.6 ⁽³⁾	65.7	338.9	771.4 ⁽⁵⁾
					130.8	30.5	128.2 ⁽³⁾	75.4	348.6	746.2 ⁽⁵⁾

Table 10 (continued) Experimental data for the CO₂+4-methylnonane system.

Solute mass (g)	Solvent mass (g)	Total mass (g)	Mass fraction (g/g)	Molar fraction (mol/mol)	Pressure (barg)	Piston position (mm)	Corrected pressure (barA)	Temperature (°C)	Converted Temperature (K)	Density (kg/m ³)
2.88	9.77	12.65	0.228	0.08360	73.5	21.0	72.7 ⁽³⁾	35.6	308.8	925.8 ⁽⁵⁾
					88.2	22.4	86.9 ⁽³⁾	45.2	318.4	894.1 ⁽⁵⁾
					103.8	25.0	102.1 ⁽³⁾	54.9	328.1	840.7 ⁽⁵⁾
					120.7	27.4	118.5 ⁽³⁾	65.6	338.8	796.7 ⁽⁵⁾
1.92	8.71	10.63	0.180	0.06377	134.5	30.1	132.0 ⁽³⁾	75.2	348.4	752.4 ⁽⁵⁾
					77.8	15.6	76.8 ⁽³⁾	37.7	310.9	1072.6 ⁽⁵⁾
					89.8	17.1	88.5 ⁽³⁾	45.3	318.5	1027.3 ⁽⁵⁾
					105.0	20.0	103.3 ⁽³⁾	54.8	328.0	949.9 ⁽⁵⁾
1.45	9.69	11.14	0.130	0.04433	121.2	22.9	119.1 ⁽³⁾	65.3	338.5	883.3 ⁽⁵⁾
					134.3	25.3	131.8 ⁽³⁾	74.8	348.0	834.9 ⁽⁵⁾
					75.5	18.2	74.7 ⁽³⁾	35.6	308.8	996.5 ⁽⁵⁾
					90.4	21.0	89.1 ⁽³⁾	45.0	318.2	925.8 ⁽⁵⁾
1.45	9.69	11.14	0.130	0.04433	105.3	25.4	103.6 ⁽³⁾	54.8	328.0	833.0 ⁽⁵⁾
					121.0	29.3	118.9 ⁽³⁾	65.4	338.6	765.0 ⁽⁵⁾
					133.8	32.4	131.3 ⁽³⁾	74.8	348.0	718.4 ⁽⁵⁾

Table 10 (continued) Experimental data for the CO₂+4-methylnonane system.

Solute mass (g)	Solvent mass (g)	Total mass (g)	Mass fraction (g/g)	Molar fraction (mol/mol)	Pressure (barg)	Piston position (mm)	Corrected pressure (barA)	Temperature (°C)	Converted Temperature (K)	Density (kg/m ³)
0.93	9.61	10.54	0.0882	0.02904	77.1	17.8	76.2 ⁽³⁾	35.8	309.0	1007.5 ⁽⁵⁾
					91.7	22.7	90.4 ⁽³⁾	45.2	318.4	887.6 ⁽⁵⁾
					106.0	28.5	104.2 ⁽³⁾	54.8	328.0	778.0 ⁽⁵⁾
					120.7	32.3	118.6 ⁽³⁾	65.4	338.6	719.8 ⁽⁵⁾
					132.3	35.7	129.7 ⁽³⁾	75.0	348.2	674.6 ⁽⁵⁾
0.45	9.73	10.18	0.0441	0.01406	78.7	19.7	77.8 ⁽³⁾	35.6	308.8	957.4 ⁽⁵⁾
					91.8	31.9	90.5 ⁽³⁾	45.1	318.3	725.5 ⁽⁵⁾
					104.4	37.2	102.7 ⁽³⁾	54.9	328.1	656.4 ⁽⁵⁾
					118.6	39.7	116.5 ⁽³⁾	65.4	338.6	628.2 ⁽⁵⁾
					125.5	45.8	122.9 ⁽³⁾	75.0	348.2	568.6 ⁽⁵⁾

Table 11 Experimental data for the ethane+1-decanol system

Solute			I-Decanol							
Solvent			Ethane							
Solute Molar Mass (g/mol)			158.28							
Solvent Molar Mass (g/mol)			30.07							
Solute mass (g)	Solvent mass (g)	Total mass (g)	Mass fraction (g/g)	Molar fraction (mol/mol)	Pressure (barg)	Piston position (mm)	Corrected pressure (barA)	Temperature (°C)	Converted Temperature (K)	Density (kg/m ³)
9.54	5.01	14.55	0.656	0.26559	51.5	41.5	56.4 ⁽⁴⁾	35.6	308.8	608.8 ⁽⁴⁾
					76.7	42.2	81.3 ⁽⁴⁾	50.1	323.3	596.9 ⁽⁴⁾
					100.2	43.0	103.1 ⁽⁴⁾	65.6	338.8	583.7 ⁽⁴⁾
					118.4	43.9	119.8 ⁽⁴⁾	80.1	353.3	569.6 ⁽⁴⁾
8.35	6.36	14.71	0.568	0.19969	71.9	43.6	77.3 ⁽⁴⁾	35.8	309.0	574.3 ⁽⁴⁾
					97.6	44.5	101.6 ⁽⁴⁾	50.1	323.3	560.6 ⁽⁴⁾
					121.0	45.4	122.9 ⁽⁴⁾	65.6	338.8	547.6 ⁽⁴⁾
					137.7	46.4	137.9 ⁽⁴⁾	79.9	353.1	533.8 ⁽⁴⁾
6.62	8.35	14.97	0.442	0.13083	87.7	49.0	92.9 ⁽⁴⁾	35.6	308.8	501.1 ⁽⁴⁾
					113.2	50.2	116.5 ⁽⁴⁾	50.0	323.2	487.3 ⁽⁴⁾
					135.0	51.6	136.0 ⁽⁴⁾	65.4	338.6	472.1 ⁽⁴⁾
					150.7	53.0	150.1 ⁽⁴⁾	79.9	353.1	457.9 ⁽⁴⁾

Table 11 (continued) Experimental data for the ethane+1-decanol system.

Solute mass (g)	Solvent mass (g)	Total mass (g)	Mass fraction (g/g)	Molar fraction (mol/mol)	Pressure (barg)	Piston position (mm)	Corrected pressure (barA)	Temperature (°C)	Converted Temperature (K)	Density (kg/m ³)
5.37	8.77	14.14	0.380	0.10424	90.9	51.0	96.1 ⁽⁴⁾	35.7	308.9	478.5 ⁽⁴⁾
					115.9	52.2	119.0 ⁽⁴⁾	50.1	323.3	465.9 ⁽⁴⁾
					137.6	54.0	138.5 ⁽⁴⁾	65.5	338.7	448.2 ⁽⁴⁾
					152.9	55.3	152.2 ⁽⁴⁾	80.1	353.3	436.2 ⁽⁴⁾
2.76	6.76	9.52	0.290	0.07190	97.6	31.8	96.5 ⁽³⁾	35.8	309.0	711.6 ⁽⁵⁾
					120.7	33.6	118.9 ⁽³⁾	50.0	323.2	687.0 ⁽⁵⁾
					140.7	35.6	138.4 ⁽³⁾	65.5	338.7	661.6 ⁽⁵⁾
2.92	9.99	12.91	0.226	0.05265	154.4	38.0	151.9 ⁽³⁾	80.3	353.5	633.5 ⁽⁵⁾
					90.2	48.9	95.4 ⁽⁴⁾	35.6	308.8	502.3 ⁽⁴⁾
					114.6	50.3	117.8 ⁽⁴⁾	49.8	323.0	486.2 ⁽⁴⁾
2.42	10.58	13.00	0.186	0.04164	135.6	52.0	136.6 ⁽⁴⁾	65.2	338.4	468.0 ⁽⁴⁾
					150.7	54.3	150.1 ⁽⁴⁾	79.9	353.1	445.4 ⁽⁴⁾
					87.7	55.5	92.9 ⁽⁴⁾	35.6	308.8	434.5 ⁽⁴⁾
2.42	10.58	13.00	0.186	0.04164	111.9	57.4	115.3 ⁽⁴⁾	49.9	323.1	418.2 ⁽⁴⁾
					132.0	59.8	133.2 ⁽⁴⁾	65.1	338.3	399.3 ⁽⁴⁾
					146.5	62.4	146.2 ⁽⁴⁾	79.8	353.0	380.7 ⁽⁴⁾

Table 11 (continued) Experimental data for the ethane+1-decanol system.

Solute mass (g)	Solvent mass (g)	Total mass (g)	Mass fraction (g/g)	Molar fraction (mol/mol)	Pressure (barg)	Piston position (mm)	Corrected pressure (barA)	Temperature (°C)	Converted Temperature (K)	Density (kg/m ³)
1.11	8.00	9.11	0.122	0.02566	90.3	37.7	89.2 ⁽³⁾	36.0	309.2	636.9 ⁽⁵⁾
					112.5	40.4	110.9 ⁽³⁾	50.5	323.7	607.7 ⁽⁵⁾
					130.3	44.0	128.0 ⁽³⁾	66.1	339.3	572.7 ⁽⁵⁾
					141.8	48.4	139.4 ⁽³⁾	80.3	353.5	535.0 ⁽⁵⁾
0.92	10.56	11.48	0.0798	0.01621	74.4	53.3	79.9 ⁽⁴⁾	35.6	308.8	454.9 ⁽⁴⁾
					98.0	55.7	102.0 ⁽⁴⁾	50.2	323.4	432.7 ⁽⁴⁾
					116.3	59.0	118.4 ⁽⁴⁾	65.6	338.8	405.4 ⁽⁴⁾
0.54	10.14	10.68	0.0507	0.01005	128.4	63.0	129.3 ⁽⁴⁾	80.1	353.3	376.7 ⁽⁴⁾
					65.6	52.1	71.0 ⁽⁴⁾	35.7	308.9	466.9 ⁽⁴⁾
					87.5	55.2	91.9 ⁽⁴⁾	50.2	323.4	437.1 ⁽⁴⁾
					105.0	59.4	107.7 ⁽⁴⁾	65.7	338.9	402.4 ⁽⁴⁾
0.25	8.70	8.95	0.0284	0.00552	115.0	65.7	116.6 ⁽⁴⁾	80.1	353.3	359.4 ⁽⁴⁾
					53.5	48.4	58.5 ⁽⁴⁾	35.6	308.8	508.3 ⁽⁴⁾
					74.3	52.0	78.9 ⁽⁴⁾	50.2	323.4	468.0 ⁽⁴⁾
					91.2	57.6	94.4 ⁽⁴⁾	65.7	338.9	416.6 ⁽⁴⁾
					102.2	63.8	104.4 ⁽⁴⁾	80.1	353.3	371.4 ⁽⁴⁾

Table 11 (continued) Experimental data for the ethane+1-decanol system.

Solute mass (g)	Solvent mass (g)	Total mass (g)	Mass fraction (g/g)	Molar fraction (mol/mol)	Pressure (barg)	Piston position (mm)	Corrected pressure (barA)	Temperature (°C)	Converted Temperature (K)	Density (kg/m ³)
0.14	7.47	7.61	0.0182	0.00350	50.6	45.2	55.4 ⁽⁴⁾	35.7	308.9	550.4 ⁽⁴⁾
					70.5	49.0	75.0 ⁽⁴⁾	50.3	323.5	501.1 ⁽⁴⁾
					85.9	54.7	89.3 ⁽⁴⁾	65.7	338.9	441.7 ⁽⁴⁾
					94.7	62.5	97.2 ⁽⁴⁾	80.3	353.5	380.0 ⁽⁴⁾

Table 12 Experimental data for the ethane+2-decanol system

Solute			2-Decanol							
Solvent			Ethane							
Solute Molar Mass (g/mol)			158.28							
Solvent Molar Mass (g/mol)			30.07							
Solute mass (g)	Solvent mass (g)	Total mass (g)	Mass fraction (g/g)	Molar fraction (mol/mol)	Pressure (barg)	Piston position (mm)	Corrected pressure (barA)	Temperature (°C)	Converted Temperature (K)	Density (kg/m ³)
9.52	5.16	14.68	0.648	0.25953	43.3	42.0	47.9 ⁽⁴⁾	35.6	308.8	605.7 ⁽⁴⁾
					58.7	42.7	63.0 ⁽⁴⁾	50.1	323.3	594.0 ⁽⁴⁾
					78.1	43.5	81.7 ⁽⁴⁾	65.6	338.8	581.1 ⁽⁴⁾
					95.1	44.7	97.6 ⁽⁴⁾	80.3	353.5	562.8 ⁽⁴⁾
8.32	6.93	15.25	0.546	0.18578	49.7	46.0	54.5 ⁽⁴⁾	35.8	309.0	544.2 ⁽⁴⁾
					73.0	46.9	77.6 ⁽⁴⁾	50.2	323.4	532.0 ⁽⁴⁾
					95.2	48.1	98.3 ⁽⁴⁾	65.7	338.9	516.6 ⁽⁴⁾
					112.7	49.3	114.4 ⁽⁴⁾	80.4	353.6	502.1 ⁽⁴⁾
6.86	7.81	14.67	0.468	0.14308	56.2	48.2	61.3 ⁽⁴⁾	35.7	308.9	515.4 ⁽⁴⁾
					81.0	49.4	85.5 ⁽⁴⁾	50.3	323.5	500.9 ⁽⁴⁾
					102.7	50.9	105.5 ⁽⁴⁾	65.8	339.0	484.0 ⁽⁴⁾
					119.5	52.6	120.9 ⁽⁴⁾	80.4	353.6	466.1 ⁽⁴⁾

Table 12 (continued) Experimental data for the ethane+2-decanol system.

Solute mass (g)	Solvent mass (g)	Total mass (g)	Mass fraction (g/g)	Molar fraction (mol/mol)	Pressure (barg)	Piston position (mm)	Corrected pressure (barA)	Temperature (°C)	Converted Temperature (K)	Density (kg/m ³)
4.86	7.80	12.66	0.384	0.10591	59.8	45.1	65.1 ⁽⁴⁾	36.0	309.2	556.9 ⁽⁴⁾
					83.8	46.3	88.2 ⁽⁴⁾	50.3	323.5	540.1 ⁽⁴⁾
					105.3	48.0	108.0 ⁽⁴⁾	65.7	338.9	517.9 ⁽⁴⁾
					121.7	49.8	123.0 ⁽⁴⁾	80.2	353.4	496.3 ⁽⁴⁾
3.69	8.54	12.23	0.302	0.07590	60.8	47.6	66.1 ⁽⁴⁾	36.1	309.3	522.9 ⁽⁴⁾
					85.4	49.0	89.8 ⁽⁴⁾	50.8	324.0	505.7 ⁽⁴⁾
					105.5	50.9	108.2 ⁽⁴⁾	65.4	338.6	484.0 ⁽⁴⁾
					121.8	53.2	123.1 ⁽⁴⁾	80.3	353.5	460.1 ⁽⁴⁾
2.81	9.51	12.32	0.228	0.05317	59.7	50.6	65.0 ⁽⁴⁾	35.8	309.0	487.3 ⁽⁴⁾
					83.7	52.4	88.1 ⁽⁴⁾	50.4	323.6	468.1 ⁽⁴⁾
					104.6	55.1	107.3 ⁽⁴⁾	65.9	339.1	442.0 ⁽⁴⁾
					119.9	57.9	121.3 ⁽⁴⁾	80.3	353.5	417.9 ⁽⁴⁾
1.97	9.48	11.45	0.172	0.03791	57.0	48.3	62.2 ⁽⁴⁾	35.6	308.8	514.2 ⁽⁴⁾
					80.7	50.4	85.2 ⁽⁴⁾	50.0	323.2	489.5 ⁽⁴⁾
					101.5	53.3	104.4 ⁽⁴⁾	65.4	338.6	459.1 ⁽⁴⁾
					116.5	56.4	118.0 ⁽⁴⁾	79.8	353.0	430.5 ⁽⁴⁾

Table 12 (continued) Experimental data for the ethane+2-decanol system.

Solute mass (g)	Solvent mass (g)	Total mass (g)	Mass fraction (g/g)	Molar fraction (mol/mol)	Pressure (barg)	Piston position (mm)	Corrected pressure (barA)	Temperature (°C)	Converted Temperature (K)	Density (kg/m ³)
1.20	8.92	10.12	0.119	0.02494	54.7	48.3	59.7 ⁽⁴⁾	35.7	308.9	514.2 ⁽⁴⁾
					77.6	50.8	82.2 ⁽⁴⁾	50.2	323.4	485.1 ⁽⁴⁾
					97.4	54.0	100.4 ⁽⁴⁾	65.8	339.0	452.3 ⁽⁴⁾
					111.7	57.7	113.5 ⁽⁴⁾	80.3	353.5	419.5 ⁽⁴⁾
0.78	8.73	9.51	0.0822	0.01673	51.5	49.2	56.4 ⁽⁴⁾	35.7	308.9	503.3 ⁽⁴⁾
					73.4	51.8	78.0 ⁽⁴⁾	50.2	323.4	474.3 ⁽⁴⁾
					92.3	55.7	95.5 ⁽⁴⁾	65.7	338.9	436.6 ⁽⁴⁾
					105.6	60.6	107.7 ⁽⁴⁾	80.3	353.5	397.0 ⁽⁴⁾
0.48	8.82	9.30	0.0519	0.01029	48.8	53.0	53.5 ⁽⁴⁾	35.7	308.9	462.1 ⁽⁴⁾
					69.3	56.4	73.8 ⁽⁴⁾	50.2	323.4	430.5 ⁽⁴⁾
					87.0	61.3	90.3 ⁽⁴⁾	65.7	338.9	391.9 ⁽⁴⁾
					98.7	67.8	101.1 ⁽⁴⁾	80.3	353.5	350.3 ⁽⁴⁾
0.28	9.02	9.30	0.0298	0.00579	47.3	58.7	51.9 ⁽⁴⁾	35.7	308.9	411.5 ⁽⁴⁾
					65.4	63.4	69.9 ⁽⁴⁾	50.2	323.4	377.4 ⁽⁴⁾
					81.2	70.6	86.6 ⁽⁴⁾	65.7	338.9	335.0 ⁽⁴⁾
					90.8	79.8	94.5 ⁽⁴⁾	80.3	353.5	292.8 ⁽⁴⁾

Table 12 (continued) Experimental data for the ethane+2-decanol system.

Solute mass (g)	Solvent mass (g)	Total mass (g)	Mass fraction (g/g)	Molar fraction (mol/mol)	Pressure (barg)	Piston position (mm)	Corrected pressure (barA)	Temperature (°C)	Converted Temperature (K)	Density (kg/m ³)
0.10	8.42	8.52	0.0120	0.00231	48.2	62.6	52.9 ⁽⁴⁾	35.9	309.1	382.8 ⁽⁴⁾
					63.3	65.2	67.8 ⁽⁴⁾	50.5	323.7	365.8 ⁽⁴⁾
					75.6	72.3	79.2 ⁽⁴⁾	65.2	338.4	326.3 ⁽⁴⁾
					82.8	83.3	85.7 ⁽⁴⁾	80.0	353.2	279.5 ⁽⁴⁾

Table 13 Experimental data for the ethane+3,7-dimethyl-1-octanol system

Solute			3,7-Dimethyl-1-octanol							
Solvent			Ethane							
Solute Molar Mass (g/mol)			158.28							
Solvent Molar Mass (g/mol)			30.07							
Solute mass (g)	Solvent mass (g)	Total mass (g)	Mass fraction (g/g)	Molar fraction (mol/mol)	Pressure (barg)	Piston position (mm)	Corrected pressure (barA)	Temperature (°C)	Converted Temperature (K)	Density (kg/m ³)
9.58	5.31	14.89	0.644	0.25536	45.5	44.8	50.1 ⁽⁴⁾	35.8	309.0	569.5 ⁽⁴⁾
					64.6	45.3	69.1 ⁽⁴⁾	50.4	323.6	562.2 ⁽⁴⁾
					87.3	46.1	90.6 ⁽⁴⁾	66.0	339.2	550.8 ⁽⁴⁾
					105.9	47.0	107.9 ⁽⁴⁾	80.5	353.7	538.5 ⁽⁴⁾
8.32	6.82	15.14	0.550	0.18822	53.1	46.8	58.0 ⁽⁴⁾	35.9	309.1	541.2 ⁽⁴⁾
					79.1	47.7	83.6 ⁽⁴⁾	50.4	323.6	529.3 ⁽⁴⁾
					103.5	48.8	106.2 ⁽⁴⁾	66.0	339.2	515.5 ⁽⁴⁾
					122.0	49.9	123.2 ⁽⁴⁾	80.4	353.6	502.4 ⁽⁴⁾
6.16	7.40	13.56	0.454	0.13652	59.8	46.1	65.1 ⁽⁴⁾	35.5	308.7	550.8 ⁽⁴⁾
					87.3	47.2	91.7 ⁽⁴⁾	50.2	323.4	535.8 ⁽⁴⁾
					111.9	48.5	114.3 ⁽⁴⁾	65.8	339.0	519.2 ⁽⁴⁾
					129.8	50.0	129.6 ⁽⁴⁾	80.4	353.6	501.3 ⁽⁴⁾

Table 13 (continued) Experimental data for the ethane+3,7-dimethyl-1-octanol system.

Solute mass (g)	Solvent mass (g)	Total mass (g)	Mass fraction (g/g)	Molar fraction (mol/mol)	Pressure (barg)	Piston position (mm)	Corrected pressure (barA)	Temperature (°C)	Converted Temperature (K)	Density (kg/m ³)
5.41	8.92	14.33	0.378	0.10339	63.9	51.6	69.3 ⁽⁴⁾	35.8	309.0	483.4 ⁽⁴⁾
					90.3	52.9	94.6 ⁽⁴⁾	50.3	323.5	469.8 ⁽⁴⁾
					114.0	54.7	116.2 ⁽⁴⁾	65.9	339.1	452.3 ⁽⁴⁾
					131.6	56.5	132.2 ⁽⁴⁾	80.5	353.7	435.9 ⁽⁴⁾
4.16	9.95	14.11	0.295	0.07358	63.7	57.7	69.1 ⁽⁴⁾	35.7	308.9	425.7 ⁽⁴⁾
					90.2	59.4	94.5 ⁽⁴⁾	50.3	323.5	412.0 ⁽⁴⁾
					113.6	61.5	113.3 ⁽⁴⁾	66.1	339.3	396.2 ⁽⁴⁾
					130.9	63.9	131.6 ⁽⁴⁾	80.6	353.8	379.6 ⁽⁴⁾
2.73	9.46	12.19	0.224	0.05191	63.2	50.4	68.6 ⁽⁴⁾	35.6	308.8	496.7 ⁽⁴⁾
					90.0	52.1	94.3 ⁽⁴⁾	50.4	323.6	478.1 ⁽⁴⁾
					113.0	54.2	115.3 ⁽⁴⁾	65.9	339.1	457.0 ⁽⁴⁾
					129.8	56.5	130.6 ⁽⁴⁾	80.4	353.6	435.9 ⁽⁴⁾
1.81	8.46	10.27	0.176	0.03901	61.2	46.0	66.6 ⁽⁴⁾	35.5	308.7	552.2 ⁽⁴⁾
					87.3	47.8	91.7 ⁽⁴⁾	50.2	323.4	528.0 ⁽⁴⁾
					109.7	50.3	112.2 ⁽⁴⁾	65.9	339.1	497.8 ⁽⁴⁾
					125.8	52.8	126.8 ⁽⁴⁾	80.6	353.8	470.9 ⁽⁴⁾

Table 13 (continued) Experimental data for the ethane+3,7-dimethyl-1-octanol system.

Solute mass (g)	Solvent mass (g)	Total mass (g)	Mass fraction (g/g)	Molar fraction (mol/mol)	Pressure (barg)	Piston position (mm)	Corrected pressure (barA)	Temperature (°C)	Converted Temperature (K)	Density (kg/m ³)
1.15	8.81	9.96	0.115	0.02419	58.2	47.1	63.4 ⁽⁴⁾	35.7	308.9	537.2 ⁽⁴⁾
					83.0	49.2	87.5 ⁽⁴⁾	50.1	323.3	510.7 ⁽⁴⁾
					104.2	52.1	106.9 ⁽⁴⁾	65.8	339.0	478.1 ⁽⁴⁾
					119.0	55.7	119.6 ⁽⁴⁾	80.5	353.7	443.0 ⁽⁴⁾
0.77	9.52	10.29	0.0745	0.01507	53.8	51.5	58.8 ⁽⁴⁾	35.5	308.7	484.5 ⁽⁴⁾
					76.6	54.5	81.2 ⁽⁴⁾	50.1	323.3	454.1 ⁽⁴⁾
					95.6	59.0	98.7 ⁽⁴⁾	65.7	338.9	415.1 ⁽⁴⁾
					108.0	65.0	109.9 ⁽⁴⁾	80.5	353.7	372.5 ⁽⁴⁾
0.57	10.90	11.47	0.0499	0.00988	50.0	60.5	54.8 ⁽⁴⁾	35.5	308.7	403.6 ⁽⁴⁾
					71.4	64.8	75.9 ⁽⁴⁾	50.2	323.4	373.7 ⁽⁴⁾
					88.9	70.8	92.2 ⁽⁴⁾	65.5	338.7	338.8 ⁽⁴⁾
					98.3	81.5	100.7 ⁽⁴⁾	80.3	353.5	290.4 ⁽⁴⁾
0.25	9.21	9.46	0.0267	0.00518	48.6	40.0	53.3 ⁽⁴⁾	35.9	309.1	651.4 ⁽⁴⁾
					68.5	42.5	73.0 ⁽⁴⁾	50.2	323.4	606.0 ⁽⁴⁾
					82.6	49.1	86.0 ⁽⁴⁾	65.7	338.9	511.9 ⁽⁴⁾
					94.4	53.8	97.0 ⁽⁴⁾	80.3	353.5	460.9 ⁽⁴⁾

Table 13 (continued) Experimental data for the ethane+3,7-dimethyl-1-octanol system.

Solute mass (g)	Solvent mass (g)	Total mass (g)	Mass fraction (g/g)	Molar fraction (mol/mol)	Pressure (barg)	Piston position (mm)	Corrected pressure (barA)	Temperature (°C)	Converted Temperature (K)	Density (kg/m ³)
0.22	10.78	11.00	0.0202	0.00389	47.2	69.3	51.8 ⁽⁴⁾	35.8	309.0	346.9 ⁽⁴⁾
					64.8	73.9	69.3 ⁽⁴⁾	50.1	323.3	323.2 ⁽⁴⁾
					79.9	81.7	83.4 ⁽⁴⁾	65.4	338.6	289.6 ⁽⁴⁾
					89.0	93.1	91.7 ⁽⁴⁾	80.0	353.2	251.4 ⁽⁴⁾

Table 14 Experimental data for the ethane+2,6-dimethyl-2-octanol system

Solute			2,6-Dimethyl-2-octanol							
Solvent			Ethane							
Solute Molar Mass (g/mol)			158.28							
Solvent Molar Mass (g/mol)			30.07							
Solute mass (g)	Solvent mass (g)	Total mass (g)	Mass fraction (g/g)	Molar fraction (mol/mol)	Pressure (barg)	Piston position (mm)	Corrected pressure (barA)	Temperature (°C)	Converted Temperature (K)	Density (kg/m ³)
9.65	5.39	15.04	0.642	0.25372	44.1	45.8	48.7 ⁽⁴⁾	36.0	309.2	560.2 ⁽⁴⁾
					56.7	46.6	60.9 ⁽⁴⁾	50.8	324.0	549.0 ⁽⁴⁾
					71.9	47.7	75.4 ⁽⁴⁾	66.5	339.7	534.3 ⁽⁴⁾
					85.2	48.7	88.0 ⁽⁴⁾	80.3	353.5	521.6 ⁽⁴⁾
7.46	6.64	14.10	0.529	0.17594	47.2	45.8	51.8 ⁽⁴⁾	36.0	309.2	560.2 ⁽⁴⁾
					62.4	46.7	66.8 ⁽⁴⁾	50.8	324.0	547.7 ⁽⁴⁾
					79.8	48.1	83.3 ⁽⁴⁾	65.5	338.7	529.2 ⁽⁴⁾
6.20	7.72	13.92	0.445	0.13229	96.0	49.6	98.5 ⁽⁴⁾	80.2	353.4	510.7 ⁽⁴⁾
					47.4	48.7	52.0 ⁽⁴⁾	36.0	309.2	521.6 ⁽⁴⁾
					64.6	50.0	69.1 ⁽⁴⁾	50.7	323.9	506.0 ⁽⁴⁾
					83.4	51.7	86.8 ⁽⁴⁾	65.3	338.5	486.9 ⁽⁴⁾
					100.5	53.6	102.8 ⁽⁴⁾	80.3	353.5	467.2 ⁽⁴⁾

Table 14 (continued) Experimental data for the ethane+2,6-dimethyl-2-octanol system.

Solute mass (g)	Solvent mass (g)	Total mass (g)	Mass fraction (g/g)	Molar fraction (mol/mol)	Pressure (barg)	Piston position (mm)	Corrected pressure (barA)	Temperature (°C)	Converted Temperature (K)	Density (kg/m ³)
5.01	7.94	12.95	0.387	0.10700	48.7	47.3	53.4 ⁽⁴⁾	36.2	309.4	539.6 ⁽⁴⁾
					66.2	48.8	70.7 ⁽⁴⁾	50.8	324.0	520.4 ⁽⁴⁾
					85.2	50.3	88.6 ⁽⁴⁾	65.5	338.7	502.5 ⁽⁴⁾
					101.3	52.2	103.5 ⁽⁴⁾	80.1	353.3	481.6 ⁽⁴⁾
3.93	9.26	13.19	0.298	0.07458	47.9	53.0	52.5 ⁽⁴⁾	35.9	309.1	473.3 ⁽⁴⁾
					67.4	55.5	71.9 ⁽⁴⁾	50.7	323.9	449.1 ⁽⁴⁾
					86.7	58.2	90.1 ⁽⁴⁾	65.4	338.6	425.6 ⁽⁴⁾
					102.8	61.8	105.0 ⁽⁴⁾	80.2	353.4	397.8 ⁽⁴⁾
2.76	8.89	11.65	0.237	0.05570	48.4	53.1	53.1 ⁽⁴⁾	36.0	309.2	472.3 ⁽⁴⁾
					68.0	56.1	72.5 ⁽⁴⁾	50.8	324.0	443.6 ⁽⁴⁾
					86.6	58.9	89.9 ⁽⁴⁾	65.5	338.7	419.9 ⁽⁴⁾
					102.4	62.2	104.6 ⁽⁴⁾	80.2	353.4	394.9 ⁽⁴⁾
1.73	8.23	9.96	0.174	0.03847	47.7	46.5	52.3 ⁽⁴⁾	35.9	309.1	550.4 ⁽⁴⁾
					67.1	49.4	71.6 ⁽⁴⁾	50.7	323.9	513.1 ⁽⁴⁾
					85.8	52.5	89.2 ⁽⁴⁾	65.4	338.6	478.4 ⁽⁴⁾
					101.0	56.1	103.3 ⁽⁴⁾	80.2	353.4	443.6 ⁽⁴⁾

Table 14 (continued) Experimental data for the ethane+2,6-dimethyl-2-octanol system.

Solute mass (g)	Solvent mass (g)	Total mass (g)	Mass fraction (g/g)	Molar fraction (mol/mol)	Pressure (barg)	Piston position (mm)	Corrected pressure (barA)	Temperature (°C)	Converted Temperature (K)	Density (kg/m ³)
1.13	8.14	9.27	0.122	0.02570	48.5	47.3	53.2 ⁽⁴⁾	36.0	309.2	539.6 ⁽⁴⁾
					66.7	50.7	71.2 ⁽⁴⁾	50.7	323.9	498.0 ⁽⁴⁾
					84.4	54.4	87.8 ⁽⁴⁾	65.4	338.6	459.4 ⁽⁴⁾
					98.3	59.3	100.7 ⁽⁴⁾	80.2	353.4	416.7 ⁽⁴⁾
0.73	8.35	9.08	0.0800	0.01625	49.0	50.2	53.7 ⁽⁴⁾	36.4	309.6	503.7 ⁽⁴⁾
					65.5	55.9	70.0 ⁽⁴⁾	50.8	324.0	445.4 ⁽⁴⁾
					81.6	61.0	85.1 ⁽⁴⁾	65.7	338.9	403.6 ⁽⁴⁾
0.39	6.97	7.36	0.0535	0.01063	93.1	67.6	95.7 ⁽⁴⁾	80.5	353.7	360.0 ⁽⁴⁾
					48.7	45.3	53.4 ⁽⁴⁾	35.9	309.1	567.5 ⁽⁴⁾
					64.2	50.8	68.7 ⁽⁴⁾	50.5	323.7	496.8 ⁽⁴⁾
0.25	8.35	8.60	0.0285	0.00555	79.0	57.4	82.5 ⁽⁴⁾	65.7	338.9	432.3 ⁽⁴⁾
					88.2	65.0	90.9 ⁽⁴⁾	80.3	353.5	376.0 ⁽⁴⁾
					49.5	55.0	54.2 ⁽⁴⁾	36.1	309.3	453.7 ⁽⁴⁾
0.25	8.35	8.60	0.0285	0.00555	62.9	67.0	67.4 ⁽⁴⁾	50.7	323.9	363.5 ⁽⁴⁾
					74.3	74.7	77.9 ⁽⁴⁾	65.3	338.5	322.4 ⁽⁴⁾
					81.0	87.3	83.9 ⁽⁴⁾	80.2	353.4	272.1 ⁽⁴⁾

Table 14 (continued) Experimental data for the ethane+2,6-dimethyl-2-octanol system.

Solute mass (g)	Solvent mass (g)	Total mass (g)	Mass fraction (g/g)	Molar fraction (mol/mol)	Pressure (barg)	Piston position (mm)	Corrected pressure (barA)	Temperature (°C)	Converted Temperature (K)	Density (kg/m ³)
0.13	8.34	8.47	0.0150	0.00288	49.6	61.5	54.3 ⁽⁴⁾	36.0	309.2	400.0 ⁽⁴⁾
					62.0	75.2	66.5 ⁽⁴⁾	50.7	323.9	320.1 ⁽⁴⁾
					71.6	86.6	75.1 ⁽⁴⁾	65.6	338.8	274.4 ⁽⁴⁾
					75.2	103.2	78.2 ⁽⁴⁾	80.5	353.7	227.3 ⁽⁴⁾

Table 15 Experimental data for the ethane+3,7-dimethyl-3-octanol system

Solute			3,7-Dimethyl-3-octanol							
Solvent			Ethane							
Solute Molar Mass (g/mol)			158.28							
Solvent Molar Mass (g/mol)			30.07							
Solute mass (g)	Solvent mass (g)	Total mass (g)	Mass fraction (g/g)	Molar fraction (mol/mol)	Pressure (barg)	Piston position (mm)	Corrected pressure (barA)	Temperature (°C)	Converted Temperature (K)	Density (kg/m ³)
9.67	5.19	14.86	0.651	0.26150	43.2	43.0	47.8 ⁽⁴⁾	36.0	309.2	596.4 ⁽⁴⁾
					54.6	43.6	58.6 ⁽⁴⁾	50.8	324.0	586.8 ⁽⁴⁾
					68.1	44.8	71.6 ⁽⁴⁾	66.6	339.8	568.3 ⁽⁴⁾
					81.2	46.1	84.1 ⁽⁴⁾	81.4	354.6	549.6 ⁽⁴⁾
7.72	5.25	12.97	0.595	0.21845	45.5	40.4	50.1 ⁽⁴⁾	36.2	309.4	642.4 ⁽⁴⁾
					57.8	40.9	62.0 ⁽⁴⁾	50.8	324.0	633.0 ⁽⁴⁾
					72.0	42.1	75.6 ⁽⁴⁾	65.5	338.7	611.6 ⁽⁴⁾
					86.7	43.3	89.5 ⁽⁴⁾	80.3	353.5	591.6 ⁽⁴⁾
5.88	6.94	12.82	0.459	0.13862	47.0	43.8	51.6 ⁽⁴⁾	36.0	309.2	583.6 ⁽⁴⁾
					61.9	45.1	66.3 ⁽⁴⁾	50.8	324.0	563.9 ⁽⁴⁾
					79.3	46.9	82.8 ⁽⁴⁾	65.6	338.8	538.7 ⁽⁴⁾
					95.7	48.5	98.2 ⁽⁴⁾	80.4	353.6	518.1 ⁽⁴⁾

Table 15 (continued) Experimental data for the ethane+3,7-dimethyl-3-octanol system.

Solute mass (g)	Solvent mass (g)	Total mass (g)	Mass fraction (g/g)	Molar fraction (mol/mol)	Pressure (barg)	Piston position (mm)	Corrected pressure (barA)	Temperature (°C)	Converted Temperature (K)	Density (kg/m ³)
5.08	7.97	13.05	0.389	0.10809	47.9	47.6	52.5 ⁽⁴⁾	36.1	309.3	529.5 ⁽⁴⁾
					63.4	49.0	67.8 ⁽⁴⁾	51.0	324.2	512.0 ⁽⁴⁾
					81.7	51.0	85.2 ⁽⁴⁾	65.7	338.9	488.9 ⁽⁴⁾
					98.4	53.5	100.8 ⁽⁴⁾	80.5	353.7	462.9 ⁽⁴⁾
3.35	7.75	11.10	0.302	0.07588	48.0	43.9	52.6 ⁽⁴⁾	36.0	309.2	582.0 ⁽⁴⁾
					64.7	45.9	69.2 ⁽⁴⁾	50.8	324.0	552.4 ⁽⁴⁾
					83.4	48.4	86.8 ⁽⁴⁾	65.6	338.8	519.4 ⁽⁴⁾
					100.0	50.9	102.3 ⁽⁴⁾	80.5	353.7	490.0 ⁽⁴⁾
2.37	7.85	10.22	0.232	0.05418	47.5	45.7	52.1 ⁽⁴⁾	36.0	309.2	555.2 ⁽⁴⁾
					64.4	48.7	68.9 ⁽⁴⁾	50.8	324.0	515.7 ⁽⁴⁾
					83.1	51.3	86.5 ⁽⁴⁾	65.6	338.8	485.6 ⁽⁴⁾
					99.0	54.3	101.4 ⁽⁴⁾	80.4	353.6	455.1 ⁽⁴⁾
1.71	6.70	8.41	0.203	0.04625	47.7	38.8	52.3 ⁽⁴⁾	36.0	309.2	674.3 ⁽⁴⁾
					64.8	41.5	69.3 ⁽⁴⁾	50.8	324.0	622.1 ⁽⁴⁾
					82.9	44.0	86.3 ⁽⁴⁾	65.6	338.8	580.5 ⁽⁴⁾
					98.6	46.7	101.0 ⁽⁴⁾	80.4	353.6	541.4 ⁽⁴⁾

Table 15 (continued) Experimental data for the ethane+3,7-dimethyl-3-octanol system.

Solute mass (g)	Solvent mass (g)	Total mass (g)	Mass fraction (g/g)	Molar fraction (mol/mol)	Pressure (barg)	Piston position (mm)	Corrected pressure (barA)	Temperature (°C)	Converted Temperature (K)	Density (kg/m ³)
1.13	7.98	9.11	0.124	0.02626	47.8	46.2	52.4 ⁽⁴⁾	35.9	309.1	548.2 ⁽⁴⁾
					63.7	51.5	68.2 ⁽⁴⁾	50.7	323.9	483.5 ⁽⁴⁾
					80.7	55.2	84.2 ⁽⁴⁾	65.5	338.7	446.7 ⁽⁴⁾
					95.0	59.7	97.5 ⁽⁴⁾	80.4	353.6	408.8 ⁽⁴⁾
0.77	8.81	9.58	0.0808	0.01641	48.1	48.8	52.8 ⁽⁴⁾	35.9	309.1	514.4 ⁽⁴⁾
					63.2	55.0	67.7 ⁽⁴⁾	50.6	323.8	448.5 ⁽⁴⁾
					78.9	59.8	82.5 ⁽⁴⁾	65.4	338.6	408.0 ⁽⁴⁾
					92.4	64.3	95.0 ⁽⁴⁾	80.2	353.4	376.2 ⁽⁴⁾
0.52	9.55	10.07	0.0513	0.01016	48.7	58.5	53.4 ⁽⁴⁾	35.9	309.1	418.2 ⁽⁴⁾
					62.7	70.6	67.2 ⁽⁴⁾	50.7	323.9	339.1 ⁽⁴⁾
					76.5	77.7	80.1 ⁽⁴⁾	65.5	338.7	305.3 ⁽⁴⁾
					86.4	86.9	89.2 ⁽⁴⁾	80.3	353.5	270.3 ⁽⁴⁾
0.27	8.34	8.61	0.0314	0.00613	48.3	53.4	53.0 ⁽⁴⁾	35.8	309.0	463.8 ⁽⁴⁾
					61.2	69.3	65.6 ⁽⁴⁾	50.5	323.7	346.2 ⁽⁴⁾
					72.1	77.7	75.7 ⁽⁴⁾	65.3	338.5	305.3 ⁽⁴⁾
					79.0	89.1	82.0 ⁽⁴⁾	80.1	353.3	263.1 ⁽⁴⁾

Table 15 (continued) Experimental data for the ethane+3,7-dimethyl-3-octanol system.

Solute mass (g)	Solvent mass (g)	Total mass (g)	Mass fraction (g/g)	Molar fraction (mol/mol)	Pressure (barg)	Piston position (mm)	Corrected pressure (barA)	Temperature (°C)	Converted Temperature (K)	Density (kg/m ³)
0.17	8.04	8.21	0.0202	0.00390	48.9	55.0	53.6 ⁽⁴⁾	36.0	309.2	448.5 ⁽⁴⁾
					60.8	72.2	65.2 ⁽⁴⁾	50.6	323.8	330.9 ⁽⁴⁾
					70.5	82.0	74.0 ⁽⁴⁾	65.5	338.7	287.9 ⁽⁴⁾
					75.0	96.7	78.0 ⁽⁴⁾	80.3	353.5	240.9 ⁽⁴⁾

Table 16 Experimental data for the ethane+n-decane system

Solute			<i>n</i> -Decane							
Solvent			Ethane							
Solute Molar Mass (g/mol)			142.29							
Solvent Molar Mass (g/mol)			30.07							
Solute mass (g)	Solvent mass (g)	Total mass (g)	Mass fraction (g/g)	Molar fraction (mol/mol)	Pressure (barg)	Piston position (mm)	Corrected pressure (barA)	Temperature (°C)	Converted Temperature (K)	Density (kg/m ³)
6.45	3.29	9.74	0.662	0.29288	32.9	24.1	32.6 ⁽³⁾	35.6	308.8	645.6 ⁽³⁾
					42.2	24.3	41.1 ⁽³⁾	49.8	323.0	642.5 ⁽³⁾
					52.3	25.1	50.4 ⁽³⁾	64.8	338.0	630.3 ⁽³⁾
					62.2	27.0	60.1 ⁽³⁾	79.9	353.1	603.1 ⁽³⁾
5.47	4.32	9.79	0.559	0.21116	37.7	26.0	37.4 ⁽³⁾	35.1	308.3	617.1 ⁽³⁾
					48.7	26.1	47.6 ⁽³⁾	49.4	322.6	615.7 ⁽³⁾
					60.7	27.3	58.9 ⁽³⁾	64.7	337.9	599.0 ⁽³⁾
					72.7	28.3	70.4 ⁽³⁾	80.0	353.2	585.8 ⁽³⁾
4.48	5.22	9.70	0.462	0.15348	40.8	29.5	40.5 ⁽³⁾	34.7	307.9	570.6 ⁽³⁾
					52.8	30.7	51.7 ⁽³⁾	48.8	322.0	556.3 ⁽³⁾
					66.6	32.5	64.9 ⁽³⁾	64.6	337.8	536.1 ⁽³⁾
					80.3	34.2	77.9 ⁽³⁾	79.8	353.0	518.3 ⁽³⁾

Table 16 (continued) Experimental data for the ethane+n-decane system.

Solute mass (g)	Solvent mass (g)	Total mass (g)	Mass fraction (g/g)	Molar fraction (mol/mol)	Pressure (barg)	Piston position (mm)	Corrected pressure (barA)	Temperature (°C)	Converted Temperature (K)	Density (kg/m ³)
3.73	6.35	10.08	0.370	0.11049	43.7	34.4	43.4 ⁽³⁾	35.1	308.3	516.2 ⁽³⁾
					56.1	34.6	54.9 ⁽³⁾	49.3	322.5	514.2 ⁽³⁾
					70.3	35.9	68.6 ⁽³⁾	64.0	337.2	501.6 ⁽³⁾
					85.1	36.4	82.6 ⁽³⁾	79.9	353.1	496.9 ⁽³⁾
4.41	10.13	14.54	0.303	0.08428	41.5	57.6	46.1 ⁽⁴⁾	35.8	309.0	416.4 ⁽⁴⁾
					53.7	60.7	57.7 ⁽⁴⁾	50.3	323.5	392.5 ⁽⁴⁾
					69.5	65.4	73.0 ⁽⁴⁾	65.8	339.0	361.2 ⁽⁴⁾
					83.5	70.6	86.4 ⁽⁴⁾	80.3	353.5	331.8 ⁽⁴⁾
2.02	7.02	9.04	0.224	0.05739	47.7	32.8	47.4 ⁽³⁾	35.3	308.5	532.8 ⁽³⁾
					61.2	33.8	59.9 ⁽³⁾	49.2	322.4	522.3 ⁽³⁾
					75.5	35.4	73.7 ⁽³⁾	63.5	336.7	506.4 ⁽³⁾
					88.7	39.2	86.1 ⁽³⁾	78.3	351.5	472.2 ⁽³⁾
1.60	7.30	8.90	0.180	0.04423	48.7	38.2	48.4 ⁽³⁾	35.7	308.9	480.7 ⁽³⁾
					62.4	40.1	61.1 ⁽³⁾	49.6	322.8	464.7 ⁽³⁾
					77.1	45.6	75.2 ⁽³⁾	64.8	338.0	423.9 ⁽³⁾
					89.2	50.7	86.6 ⁽³⁾	79.8	353.0	392.0 ⁽³⁾

Table 16 (continued) Experimental data for the ethane+n-decane system.

Solute mass (g)	Solvent mass (g)	Total mass (g)	Mass fraction (g/g)	Molar fraction (mol/mol)	Pressure (barg)	Piston position (mm)	Corrected pressure (barA)	Temperature (°C)	Converted Temperature (K)	Density (kg/m ³)
1.20	8.82	10.02	0.120	0.02798	44.6	49.6	49.2 ⁽⁴⁾	35.7	308.9	340.4 ⁽⁴⁾
					57.6	57.4	61.9 ⁽⁴⁾	50.1	323.3	288.1 ⁽⁴⁾
					71.3	68.1	74.8 ⁽⁴⁾	65.7	338.9	238.0 ⁽⁴⁾
					82.2	76.2	85.1 ⁽⁴⁾	80.1	353.3	210.3 ⁽⁴⁾
0.65	7.97	8.62	0.0753	0.01692	44.4	46.9	49.0 ⁽⁴⁾	35.6	308.8	312.4 ⁽⁴⁾
					57.2	57.9	61.4 ⁽⁴⁾	50.1	323.3	245.4 ⁽⁴⁾
					69.4	68.5	72.9 ⁽⁴⁾	65.5	338.7	203.3 ⁽⁴⁾
					78.5	77.2	81.5 ⁽⁴⁾	80.1	353.3	178.3 ⁽⁴⁾
0.39	7.78	8.17	0.0483	0.01061	44.1	45.1	48.7 ⁽⁴⁾	35.3	308.5	310.1 ⁽⁴⁾
					56.0	62.3	60.2 ⁽⁴⁾	49.7	322.9	214.3 ⁽⁴⁾
					66.8	73.9	70.3 ⁽⁴⁾	65.1	338.3	177.4 ⁽⁴⁾
					73.9	84.3	76.9 ⁽⁴⁾	79.8	353.0	153.6 ⁽⁴⁾
0.24	8.36	8.60	0.0278	0.00601	44.7	47.5	49.3 ⁽⁴⁾	35.4	308.6	307.1 ⁽⁴⁾
					54.6	72.4	58.7 ⁽⁴⁾	49.7	322.9	190.8 ⁽⁴⁾
					62.7	86.5	66.2 ⁽⁴⁾	65.3	338.5	157.2 ⁽⁴⁾
					65.4	103.2	68.3 ⁽⁴⁾	79.9	353.1	130.0 ⁽⁴⁾

Table 17 Experimental data for the ethane+n-decane system used as verification data

Solute mass (g)	Solvent mass (g)	Total mass (g)	Mass fraction (g/g)	Molar fraction (mol/mol)	Pressure (barg)	Piston position (mm)	Corrected pressure (barA)	Temperature (°C)	Converted Temperature (K)	Density (kg/m ³)
Operator 1										
0.72	8.67	9.39	0.077	0.01725	46.0	51.4	50.6 ⁽⁴⁾	35.6	308.8	474.1 ⁽⁴⁾
					57.8	69.9	62.1 ⁽⁴⁾	50.0	323.2	335.5 ⁽⁴⁾
					70.0	79.9	73.5 ⁽⁴⁾	65.6	338.8	289.7 ⁽⁴⁾
					78.0	90.6	81.0 ⁽⁴⁾	80.4	353.6	252.8 ⁽⁴⁾
Operator 2										
0.72	8.67	9.39	0.077	0.01725	45.9	51.3	50.5 ⁽⁴⁾	35.6	308.8	475.1 ⁽⁴⁾
					57.8	69.7	62.1 ⁽⁴⁾	50.0	323.2	336.5 ⁽⁴⁾
					70.0	80.1	73.5 ⁽⁴⁾	65.6	338.8	288.9 ⁽⁴⁾
					77.7	90.1	80.7 ⁽⁴⁾	80.0	353.2	254.3 ⁽⁴⁾

Table 18 Experimental data for the ethane+2-methylnonane system

Solute			2-Methylnonane							
Solvent			Ethane							
Solute Molar Mass (g/mol)			142.29							
Solvent Molar Mass (g/mol)			30.07							
Solute mass (g)	Solvent mass (g)	Total mass (g)	Mass fraction (g/g)	Molar fraction (mol/mol)	Pressure (barg)	Piston position (mm)	Corrected pressure (barA)	Temperature (°C)	Converted Temperature (K)	Density (kg/m ³)
6.44	3.35	9.79	0.658	0.28900	32.4	24.1	32.1 ⁽³⁾	35.0	308.2	434.8 ⁽³⁾
					40.8	24.5	39.7 ⁽³⁾	48.8	322.0	430.6 ⁽³⁾
					50.9	25.4	49.0 ⁽³⁾	63.9	337.1	421.5 ⁽³⁾
					62.4	26.2	60.3 ⁽³⁾	80.2	353.4	413.7 ⁽³⁾
5.45	4.84	10.29	0.529	0.19209	37.9	29.8	37.6 ⁽³⁾	34.4	307.6	381.8 ⁽³⁾
					48.8	30.2	47.7 ⁽³⁾	48.7	321.9	378.6 ⁽³⁾
					63.4	30.9	61.6 ⁽³⁾	67.0	340.2	373.1 ⁽³⁾
					73.5	32.3	71.2 ⁽³⁾	79.8	353.0	362.5 ⁽³⁾
4.41	5.19	9.60	0.459	0.15220	40.2	27.4	39.9 ⁽³⁾	34.6	307.8	402.5 ⁽³⁾
					52.3	28.0	51.2 ⁽³⁾	49.3	322.5	397.1 ⁽³⁾
					65.0	29.3	63.3 ⁽³⁾	64.1	337.3	386.0 ⁽³⁾
					78.0	31.0	75.6 ⁽³⁾	78.9	352.1	372.3 ⁽³⁾

Table 18 (continued) Experimental data for the ethane+2-methylnonane system.

Solute mass (g)	Solvent mass (g)	Total mass (g)	Mass fraction (g/g)	Molar fraction (mol/mol)	Pressure (barg)	Piston position (mm)	Corrected pressure (barA)	Temperature (°C)	Converted Temperature (K)	Density (kg/m ³)
3.42	6.01	9.43	0.363	0.10748	45.3	29.2	45.0 ⁽³⁾	36.5	309.7	386.8 ⁽³⁾
					57.1	30.3	55.9 ⁽³⁾	49.5	322.7	377.8 ⁽³⁾
					71.3	31.9	69.5 ⁽³⁾	64.8	338.0	365.4 ⁽³⁾
					85.6	32.9	83.1 ⁽³⁾	80.3	353.5	358.1 ⁽³⁾
2.68	6.65	9.33	0.288	0.07859	46.4	29.7	46.1 ⁽³⁾	35.7	308.9	382.7 ⁽³⁾
					59.2	30.6	58.0 ⁽³⁾	49.3	322.5	375.4 ⁽³⁾
					73.2	32.5	71.5 ⁽³⁾	63.9	337.1	361.0 ⁽³⁾
1.73	6.46	8.19	0.211	0.05350	87.0	35.5	84.5 ⁽³⁾	79.0	352.2	340.4 ⁽³⁾
					47.0	33.0	46.7 ⁽³⁾	34.8	308.0	467.9 ⁽⁵⁾
					62.7	38.7	61.3 ⁽³⁾	50.7	323.9	421.3 ⁽⁵⁾
1.10	6.67	7.77	0.142	0.03378	76.6	46.0	74.7 ⁽³⁾	65.3	338.5	373.6 ⁽⁵⁾
					88.2	54.0	85.6 ⁽³⁾	79.5	352.7	332.3 ⁽⁵⁾
					49.8	33.8	49.5 ⁽³⁾	36.0	309.2	460.8 ⁽⁵⁾
1.10	6.67	7.77	0.142	0.03378	64.0	41.6	62.6 ⁽³⁾	50.3	323.5	400.9 ⁽⁵⁾
					77.3	53.7	75.4 ⁽³⁾	65.6	338.8	333.7 ⁽⁵⁾
					89.2	61.8	86.6 ⁽³⁾	80.1	353.3	300.0 ⁽⁵⁾

Table 18 (continued) Experimental data for the ethane+2-methylnonane system.

Solute mass (g)	Solvent mass (g)	Total mass (g)	Mass fraction (g/g)	Molar fraction (mol/mol)	Pressure (barg)	Piston position (mm)	Corrected pressure (barA)	Temperature (°C)	Converted Temperature (K)	Density (kg/m ³)
0.49	6.14	6.63	0.0741	0.01664	51.1	31.7	50.8 ⁽³⁾	35.3	308.5	480.0 ⁽⁵⁾
					64.2	48.2	62.9 ⁽³⁾	49.6	322.8	361.2 ⁽⁵⁾
					75.9	62.0	74.0 ⁽³⁾	64.9	338.1	299.3 ⁽⁵⁾
					84.0	71.6	81.5 ⁽³⁾	78.4	351.6	267.4 ⁽⁵⁾

Table 19 Experimental data for the ethane+3-methylnonane system

Solute			3-Methylnonane							
Solvent			Ethane							
Solute Molar Mass (g/mol)			142.29							
Solvent Molar Mass (g/mol)			30.07							
Solute mass (g)	Solvent mass (g)	Total mass (g)	Mass fraction (g/g)	Molar fraction (mol/mol)	Pressure (barg)	Piston position (mm)	Corrected pressure (barA)	Temperature (°C)	Converted Temperature (K)	Density (kg/m ³)
6.26	4.25	10.51	0.596	0.23752	37.3	29.7	37.0 ⁽³⁾	35.7	308.9	536.8 ⁽⁵⁾
					47.2	30.9	46.1 ⁽³⁾	49.8	323.0	523.8 ⁽⁵⁾
					59.2	32.6	57.4 ⁽³⁾	65.5	338.7	506.3 ⁽⁵⁾
					69.8	34.1	67.6 ⁽³⁾	79.3	352.5	491.9 ⁽⁵⁾
4.93	4.60	9.53	0.517	0.18452	40.3	28.0	40.0 ⁽³⁾	35.6	308.8	556.4 ⁽⁵⁾
					51.4	29.3	50.3 ⁽³⁾	50.1	323.3	541.3 ⁽⁵⁾
					64.5	31.6	62.7 ⁽³⁾	65.3	338.5	516.4 ⁽⁵⁾
					76.4	33.2	74.0 ⁽³⁾	79.4	352.6	500.4 ⁽⁵⁾
3.80	5.52	9.32	0.408	0.12714	43.9	30.4	43.6 ⁽³⁾	35.5	308.7	529.1 ⁽⁵⁾
					56.4	32.7	55.2 ⁽³⁾	50.0	323.2	505.3 ⁽⁵⁾
					70.8	35.3	69.0 ⁽³⁾	65.5	338.7	480.9 ⁽⁵⁾
					84.3	38.4	81.8 ⁽³⁾	79.9	353.1	454.7 ⁽⁵⁾

Table 19 (continued) Experimental data for the ethane+3-methylnonane system.

Solute mass (g)	Solvent mass (g)	Total mass (g)	Mass fraction (g/g)	Molar fraction (mol/mol)	Pressure (barg)	Piston position (mm)	Corrected pressure (barA)	Temperature (°C)	Converted Temperature (K)	Density (kg/m ³)
2.08	5.55	7.63	0.273	0.07337	47.1	26.0	46.8 ⁽³⁾	35.4	308.6	581.5 ⁽⁵⁾
					60.8	29.1	59.5 ⁽³⁾	49.6	322.8	543.6 ⁽⁵⁾
					76.0	33.8	74.1 ⁽³⁾	64.9	338.1	494.7 ⁽⁵⁾
					88.7	39.4	86.1 ⁽³⁾	79.2	352.4	446.8 ⁽⁵⁾
1.16	6.50	7.66	0.152	0.03640	49.2	33.1	48.9 ⁽³⁾	35.3	308.5	501.4 ⁽⁵⁾
					64.0	39.9	62.6 ⁽³⁾	50.1	323.3	443.0 ⁽⁵⁾
					77.7	50.8	75.8 ⁽³⁾	65.3	338.5	373.3 ⁽⁵⁾
					88.9	59.6	86.3 ⁽³⁾	79.6	352.8	331.2 ⁽⁵⁾
0.70	5.57	6.27	0.111	0.02576	50.5	23.9	50.2 ⁽³⁾	35.6	308.8	610.3 ⁽⁵⁾
					64.4	32.4	63.0 ⁽³⁾	50.1	323.3	508.3 ⁽⁵⁾
					77.4	42.9	75.5 ⁽³⁾	65.4	338.6	421.4 ⁽⁵⁾
					87.2	51.4	84.7 ⁽³⁾	79.8	353.0	370.1 ⁽⁵⁾
0.27	5.76	6.03	0.0444	0.00973	52.4	32.2	52.0 ⁽³⁾	35.9	309.1	510.3 ⁽⁵⁾
					64.4	54.7	63.0 ⁽³⁾	50.1	323.3	353.4 ⁽⁵⁾
					73.9	69.8	72.0 ⁽³⁾	65.5	338.7	293.0 ⁽⁵⁾
					78.2	84.7	75.8 ⁽³⁾	80.0	353.2	250.6 ⁽⁵⁾

Table 20 Experimental data for the ethane+4-methylnonane system

Solute			4-Methylnonane							
Solvent			Ethane							
Solute Molar Mass (g/mol)			142.29							
Solvent Molar Mass (g/mol)			30.07							
Solute mass (g)	Solvent mass (g)	Total mass (g)	Mass fraction (g/g)	Molar fraction (mol/mol)	Pressure (barg)	Piston position (mm)	Corrected pressure (barA)	Temperature (°C)	Converted Temperature (K)	Density (kg/m ³)
6.44	4.54	10.98	0.587	0.23063	36.6	27.8	36.3 ⁽³⁾	35.7	308.9	583.6 ⁽⁵⁾
					46.6	28.8	45.5 ⁽³⁾	49.8	323.0	571.2 ⁽⁵⁾
					58.2	30.6	56.3 ⁽³⁾	65.5	338.7	550.3 ⁽⁵⁾
					69.7	32.2	67.5 ⁽³⁾	79.3	352.5	532.9 ⁽⁵⁾
4.92	5.62	10.54	0.467	0.15619	41.8	32.8	41.5 ⁽³⁾	35.9	309.1	526.7 ⁽⁵⁾
					53.4	34.7	52.2 ⁽³⁾	50.3	323.5	507.8 ⁽⁵⁾
					66.6	37.2	64.9 ⁽³⁾	65.6	338.8	485.0 ⁽⁵⁾
					79.2	40.6	76.8 ⁽³⁾	80.0	353.2	457.1 ⁽⁵⁾
3.58	6.51	10.09	0.355	0.10405	45.1	33.6	44.8 ⁽³⁾	36.0	309.2	518.6 ⁽⁵⁾
					57.7	36.4	56.4 ⁽³⁾	50.0	323.2	492.1 ⁽⁵⁾
					72.4	39.9	70.6 ⁽³⁾	65.5	338.7	462.6 ⁽⁵⁾
					85.6	44.0	83.1 ⁽³⁾	80.2	353.4	432.2 ⁽⁵⁾

Table 20 (continued) Experimental data for the ethane+4-methylnonane system.

Solute mass (g)	Solvent mass (g)	Total mass (g)	Mass fraction (g/g)	Molar fraction (mol/mol)	Pressure (barg)	Piston position (mm)	Corrected pressure (barA)	Temperature (°C)	Converted Temperature (K)	Density (kg/m ³)
2.69	9.01	11.70	0.230	0.05928	47.6	53.3	47.3 ⁽³⁾	35.8	309.0	376.2 ⁽⁵⁾
					61.3	59.5	60.0 ⁽³⁾	49.9	323.1	346.3 ⁽⁵⁾
					76.0	69.2	74.1 ⁽³⁾	65.1	338.3	308.0 ⁽⁵⁾
					88.1	79.9	85.5 ⁽³⁾	79.1	352.3	274.5 ⁽⁵⁾
1.63	7.37	9.00	0.181	0.04463	48.7	40.5	48.4 ⁽³⁾	35.8	309.0	457.9 ⁽⁵⁾
					62.4	47.4	61.1 ⁽³⁾	49.8	323.0	409.9 ⁽⁵⁾
					76.5	57.8	74.6 ⁽³⁾	64.9	338.1	354.0 ⁽⁵⁾
					87.6	69.1	85.0 ⁽³⁾	79.2	352.4	308.4 ⁽⁵⁾
0.99	7.49	8.48	0.116	0.02710	49.7	42.4	49.4 ⁽³⁾	35.6	308.8	443.6 ⁽⁵⁾
					63.5	54.1	62.2 ⁽³⁾	49.8	323.0	372.1 ⁽⁵⁾
					76.0	70.2	74.1 ⁽³⁾	65.1	338.3	304.5 ⁽⁵⁾
					86.0	81.5	83.5 ⁽³⁾	79.2	352.4	270.1 ⁽⁵⁾
0.43	6.11	6.54	0.0653	0.01455	50.3	32.6	50.0 ⁽³⁾	35.4	308.6	528.7 ⁽⁵⁾
					63.4	51.2	62.1 ⁽³⁾	49.9	323.1	387.6 ⁽⁵⁾
					74.5	64.9	72.6 ⁽³⁾	65.3	338.5	323.9 ⁽⁵⁾
					82.9	75.4	80.4 ⁽³⁾	79.8	353.0	287.7 ⁽⁵⁾

Table 20 (continued) Experimental data for the ethane+4-methylnonane system.

Solute mass (g)	Solvent mass (g)	Total mass (g)	Mass fraction (g/g)	Molar fraction (mol/mol)	Pressure (barg)	Piston position (mm)	Corrected pressure (barA)	Temperature (°C)	Converted Temperature (K)	Density (kg/m ³)
0.19	5.11	5.30	0.0362	0.00789	51.9	25.1	51.5 ⁽³⁾	35.5	308.7	619.7 ⁽⁵⁾
					63.3	48.2	62.0 ⁽³⁾	49.8	323.0	405.0 ⁽⁵⁾
					74.0	56.5	72.2 ⁽³⁾	65.3	338.5	360.2 ⁽⁵⁾
					78.5	69.0	76.1 ⁽³⁾	79.5	352.7	308.7 ⁽⁵⁾

Table 21 Experimental data for the CO₂+n-dodecane system

Solute			<i>n</i> -Dodecane							
Solvent			Carbon Dioxide							
Solute Molar Mass (g/mol)			170.33							
Solvent Molar Mass (g/mol)			44.01							
Solute mass (g)	Solvent mass (g)	Total mass (g)	Mass fraction (g/g)	Molar fraction (mol/mol)	Pressure (barg)	Piston position (mm)	Corrected pressure (barA)	Temperature (°C)	Converted Temperature (K)	Density (kg/m ³)
13.61	7.96	21.57	0.631	0.30632	57.7	48.1	64.3 ⁽⁶⁾	34.7	307.9	720.1 ⁽⁶⁾
					68.7	48.5	74.9 ⁽⁶⁾	44.2	317.4	713.3 ⁽⁶⁾
					81.2	49.3	86.8 ⁽⁶⁾	54.8	328.0	699.9 ⁽⁶⁾
					92.7	49.7	97.7 ⁽⁶⁾	64.2	337.4	693.4 ⁽⁶⁾
					105.8	50.6	109.5 ⁽⁶⁾	74.7	347.9	679.2 ⁽⁶⁾
11.94	9.09	21.03	0.568	0.25339	61.9	46.6	68.8 ⁽⁶⁾	34.8	308.0	728.6 ⁽⁶⁾
					74.5	47.4	80.8 ⁽⁶⁾	44.3	317.5	714.3 ⁽⁶⁾
					88.9	48.0	94.4 ⁽⁶⁾	54.7	327.9	704.0 ⁽⁶⁾
					103.1	48.4	107.7 ⁽⁶⁾	64.2	337.4	697.2 ⁽⁶⁾
					118.4	49.2	121.2 ⁽⁶⁾	74.6	347.8	684.2 ⁽⁶⁾

Table 21 (continued) Experimental data for the CO₂+n-dodecane system

Solute mass (g)	Solvent mass (g)	Total mass (g)	Mass fraction (g/g)	Molar fraction (mol/mol)	Pressure (barg)	Piston position (mm)	Corrected pressure (barA)	Temperature (°C)	Converted Temperature (K)	Density (kg/m ³)
9.47	11.45	20.92	0.453	0.17610	66.6	46.2	73.6 ⁽⁶⁾	35.1	308.3	732.2 ⁽⁶⁾
					81.3	46.7	87.4 ⁽⁶⁾	44.5	317.7	723.0 ⁽⁶⁾
					100.0	47.4	105.0 ⁽⁶⁾	55.0	328.2	710.6 ⁽⁶⁾
					119.4	48.5	122.7 ⁽⁶⁾	65.5	338.7	692.0 ⁽⁶⁾
7.97	12.30	20.27	0.393	0.14346	136.0	49.3	137.4 ⁽⁶⁾	74.9	348.1	679.1 ⁽⁶⁾
					66.1	44.8	73.1 ⁽⁶⁾	34.6	307.8	735.4 ⁽⁶⁾
					82.0	45.1	88.3 ⁽⁶⁾	44.2	317.4	729.7 ⁽⁶⁾
					102.7	46.2	107.6 ⁽⁶⁾	54.8	328.0	709.5 ⁽⁶⁾
6.34	14.49	20.83	0.304	0.10162	124.0	47.3	127.0 ⁽⁶⁾	65.4	338.6	690.3 ⁽⁶⁾
					141.9	48.1	142.7 ⁽⁶⁾	74.8	348.0	677.0 ⁽⁶⁾
					69.2	45.1	76.3 ⁽⁶⁾	35.3	308.5	749.9 ⁽⁶⁾
					87.4	46.4	93.5 ⁽⁶⁾	45.5	318.7	725.4 ⁽⁶⁾
6.34	14.49	20.83	0.304	0.10162	108.0	47.5	112.6 ⁽⁶⁾	55.0	328.2	705.9 ⁽⁶⁾
					130.9	48.8	133.2 ⁽⁶⁾	65.6	338.8	684.2 ⁽⁶⁾
					149.4	49.9	149.5 ⁽⁶⁾	75.0	348.2	666.8 ⁽⁶⁾

Table 21 (continued) Experimental data for the CO₂+n-dodecane system

Solute mass (g)	Solvent mass (g)	Total mass (g)	Mass fraction (g/g)	Molar fraction (mol/mol)	Pressure (barg)	Piston position (mm)	Corrected pressure (barA)	Temperature (°C)	Converted Temperature (K)	Density (kg/m ³)
4.80	16.96	21.76	0.220	0.06810	67.5	48.0	74.6 ⁽⁶⁾	34.5	307.7	728.3 ⁽⁶⁾
					86.4	49.8	92.5 ⁽⁶⁾	44.9	318.1	698.0 ⁽⁶⁾
					108.3	51.3	112.9 ⁽⁶⁾	54.4	327.6	674.6 ⁽⁶⁾
					131.6	53.2	133.9 ⁽⁶⁾	65.0	338.2	647.1 ⁽⁶⁾
2.67	12.66	15.33	0.174	0.05173	150.6	54.7	150.6 ⁽⁶⁾	74.8	348.0	626.9 ⁽⁶⁾
					76.1	34.6	74.8 ⁽⁵⁾	34.8	308.0	721.3 ⁽⁷⁾
					93.8	37.5	92.0 ⁽⁵⁾	44.7	317.9	682.2 ⁽⁷⁾
					114.9	39.4	112.5 ⁽⁵⁾	54.3	327.5	658.7 ⁽⁷⁾
1.80	12.96	14.76	0.122	0.03460	136.5	41.8	133.6 ⁽⁵⁾	64.9	338.1	631.3 ⁽⁷⁾
					153.8	43.9	150.4 ⁽⁵⁾	74.7	347.9	609.2 ⁽⁷⁾
					77.2	33.5	75.9 ⁽⁵⁾	35.2	308.4	1110.5 ⁽⁷⁾
					94.6	37.4	92.8 ⁽⁵⁾	44.8	318.0	970.0 ⁽⁷⁾
1.80	12.96	14.76	0.122	0.03460	115.6	39.3	113.2 ⁽⁵⁾	54.5	327.7	913.7 ⁽⁷⁾
					137.0	41.3	134.1 ⁽⁵⁾	65.2	338.4	861.1 ⁽⁷⁾
					153.8	43.4	150.4 ⁽⁵⁾	74.7	347.9	812.0 ⁽⁷⁾

Table 21 (continued) Experimental data for the CO₂+n-dodecane system

Solute mass (g)	Solvent mass (g)	Total mass (g)	Mass fraction (g/g)	Molar fraction (mol/mol)	Pressure (barg)	Piston position (mm)	Corrected pressure (barA)	Temperature (°C)	Converted Temperature (K)	Density (kg/m ³)
1.59	17.90	19.49	0.0815	0.02240	67.8	47.0	74.8 ⁽⁶⁾	34.8	308.0	739.7 ⁽⁶⁾
					87.0	50.9	93.1 ⁽⁶⁾	45.1	318.3	674.6 ⁽⁶⁾
					108.3	52.6	112.9 ⁽⁶⁾	54.7	327.9	649.7 ⁽⁶⁾
					129.7	54.6	132.1 ⁽⁶⁾	65.3	338.5	622.7 ⁽⁶⁾
0.90	17.10	18.00	0.0498	0.01335	147.1	56.3	147.3 ⁽⁶⁾	74.8	348.0	601.4 ⁽⁶⁾
					68.0	46.0	75.1 ⁽⁶⁾	34.6	307.8	758.5 ⁽⁶⁾
					86.9	50.9	93.0 ⁽⁶⁾	45.0	318.2	674.6 ⁽⁶⁾
					107.5	52.0	112.1 ⁽⁶⁾	54.7	327.9	658.3 ⁽⁶⁾
0.47	17.32	17.79	0.0264	0.00696	126.0	54.9	128.8 ⁽⁶⁾	65.2	338.4	618.8 ⁽⁶⁾
					138.9	57.8	140.0 ⁽⁶⁾	74.9	348.1	583.8 ⁽⁶⁾
					67.3	48.7	74.4 ⁽⁶⁾	34.1	307.3	709.9 ⁽⁶⁾
					87.0	53.7	93.1 ⁽⁶⁾	44.8	318.0	634.6 ⁽⁶⁾
0.47	17.32	17.79	0.0264	0.00696	107.0	55.0	111.7 ⁽⁶⁾	54.5	327.7	617.5 ⁽⁶⁾
					125.6	57.6	128.4 ⁽⁶⁾	65.2	338.4	586.1 ⁽⁶⁾
					135.6	52.3	137.0 ⁽⁶⁾	74.8	348.0	654.0 ⁽⁶⁾

B.2 Ternary and Multi-component Data

In this section experimental solubility data of CO₂ with the following ternary and multi-component mixtures are presented:

- *n*-decane + *l*-decanol + 3,7-dimethyl-*l*-octanol + 2,6-dimethyl-2-octanol
- *n*-dodecane + *l*-decanol + 3,7-dimethyl-*l*-octanol
- *n*-dodecane + *l*-decanol
- *l*-decanol + 3,7-dimethyl-*l*-octanol
- *n*-dodecane + 3,7-dimethyl-*l*-octanol

In Table 27 the experimental data used to compare the influence of the purity of 3,7-dimethyl-*l*-octanol (305774) to 3,7-dimethyl-*l*-octanol (W23,910-0-K) on the binary phase behaviour with supercritical CO₂, is given.

Table 22 Experimental data for the CO_2 +(*n*-decane+1-decanol+3,7-dimethyl-1-octanol+2,6-dimethyl-2-octanol) system

Solute		25% <i>n</i> -decane + 25% 1-decanol + 25% 3,7-dimethyl-1-octanol + 25% 2,6-dimethyl-2-octanol								
Solvent		Carbon Dioxide								
Solute Molar Mass (g/mol)		154.28								
Solvent Molar Mass (g/mol)		44.01								
Solute mass (g)	Solvent mass (g)	Total mass (g)	Mass fraction (g/g)	Molar fraction (mol/mol)	Pressure (barg)	Piston position (mm)	Corrected pressure (barA)	Temperature (°C)	Converted Temperature (K)	Density (kg/m ³)
10.33	5.88	16.21	0.637	0.33381	66.0	35.6	64.3 ⁽⁹⁾	35.8	309.5	759.4 ⁽⁹⁾
					76.5	36.7	74.2 ⁽⁹⁾	45.8	319.5	738.6 ⁽⁹⁾
					85.6	36.9	82.7 ⁽⁹⁾	54.8	328.6	735.7 ⁽⁹⁾
					96.1	37.0	92.7 ⁽⁹⁾	65.4	339.3	734.3 ⁽⁹⁾
					106.5	37.8	102.6 ⁽⁹⁾	75.5	349.4	723.2 ⁽⁹⁾
8.22	6.49	14.71	0.559	0.26551	71.3	30.0	69.6 ⁽⁹⁾	34.9	308.6	848.5 ⁽⁹⁾
					84.8	30.5	82.3 ⁽⁹⁾	45.5	319.2	839.2 ⁽⁹⁾
					96.0	30.7	93.0 ⁽⁹⁾	54.0	327.8	835.5 ⁽⁹⁾
					111.8	32.0	108.2 ⁽⁹⁾	65.5	339.4	812.4 ⁽⁹⁾
					122.8	32.2	118.9 ⁽⁹⁾	75.1	349.0	809.0 ⁽⁹⁾

Table 22 (continued) Experimental data for the CO_2 +(n-decane+1-decanol+3,7-dimethyl-1-octanol+2,6-dimethyl-2-octanol) system

Solute mass (g)	Solvent mass (g)	Total mass (g)	Mass fraction (g/g)	Molar fraction (mol/mol)	Pressure (barg)	Piston position (mm)	Corrected pressure (barA)	Temperature (°C)	Converted Temperature (K)	Density (kg/m^3)
6.66	7.60	14.26	0.467	0.19987	74.5	28.3	72.8 ⁽⁹⁾	35.1	308.8	881.8 ⁽⁹⁾
					91.3	28.8	88.7 ⁽⁹⁾	45.5	319.2	871.8 ⁽⁹⁾
					106.0	29.5	102.9 ⁽⁹⁾	54.5	328.3	858.1 ⁽⁹⁾
					122.9	30.2	119.4 ⁽⁹⁾	65.0	338.9	844.8 ⁽⁹⁾
					137.6	31.0	133.6 ⁽⁹⁾	75.1	349.0	830.1 ⁽⁹⁾
5.20	8.19	13.39	0.388	0.15338	78.0	25.8	76.2 ⁽⁹⁾	35.9	309.6	935.9 ⁽⁹⁾
					96.0	25.9	93.3 ⁽⁹⁾	45.0	318.7	933.6 ⁽⁹⁾
					111.8	25.3	108.6 ⁽⁹⁾	54.6	328.4	947.5 ⁽⁹⁾
					132.9	27.0	129.4 ⁽⁹⁾	65.8	339.7	909.1 ⁽⁹⁾
					149.2	28.3	145.0 ⁽⁹⁾	75.8	349.7	881.8 ⁽⁹⁾
6.02	14.65	20.67	0.291	0.10500	67.4	34.8	77.6 ⁽¹⁰⁾	35.4	309.1	728.5 ⁽¹⁰⁾
					86.5	36.1	95.9 ⁽¹⁰⁾	45.0	318.7	699.3 ⁽¹⁰⁾
					108.6	37.2	117.1 ⁽¹⁰⁾	55.7	329.5	676.3 ⁽¹⁰⁾
					127.7	38.4	134.8 ⁽¹⁰⁾	65.2	339.1	652.9 ⁽¹⁰⁾
					144.9	39.6	150.7 ⁽¹⁰⁾	74.9	348.8	631.1 ⁽¹⁰⁾

Table 22 (continued) Experimental data for the $CO_2+(n\text{-decane}+1\text{-decanol}+3,7\text{-dimethyl-1-octanol}+2,6\text{-dimethyl-2-octanol})$ system

Solute mass (g)	Solvent mass (g)	Total mass (g)	Mass fraction (g/g)	Molar fraction (mol/mol)	Pressure (barg)	Piston position (mm)	Corrected pressure (barA)	Temperature (°C)	Converted Temperature (K)	Density (kg/m ³)
4.43	15.22	19.65	0.226	0.07672	73.4	33.2	83.8 ⁽¹⁰⁾	35.7	309.4	768.0 ⁽¹⁰⁾
					91.9	34.5	101.2 ⁽¹⁰⁾	45.4	319.1	735.6 ⁽¹⁰⁾
					112.9	36.0	121.2 ⁽¹⁰⁾	56.0	329.8	701.4 ⁽¹⁰⁾
					131.4	37.4	138.4 ⁽¹⁰⁾	65.5	339.4	672.3 ⁽¹⁰⁾
					148.0	38.9	153.5 ⁽¹⁰⁾	75.0	348.9	643.6 ⁽¹⁰⁾
3.23	15.06	18.29	0.177	0.05766	75.2	30.7	85.7 ⁽¹⁰⁾	35.4	308.6	839.0 ⁽¹⁰⁾
					93.5	32.3	102.8 ⁽¹⁰⁾	45.1	318.3	792.1 ⁽¹⁰⁾
					114.3	34.0	122.6 ⁽¹⁰⁾	55.7	328.9	747.7 ⁽¹⁰⁾
					132.7	35.6	139.5 ⁽¹⁰⁾	65.3	338.5	710.2 ⁽¹⁰⁾
					149.3	37.1	154.8 ⁽¹⁰⁾	75.0	348.2	678.3 ⁽¹⁰⁾
2.19	16.94	19.13	0.115	0.03559	75.8	29.7	86.3 ⁽¹⁰⁾	35.9	309.1	871.3 ⁽¹⁰⁾
					94.4	31.5	103.7 ⁽¹⁰⁾	45.4	318.6	814.9 ⁽¹⁰⁾
					115.3	33.5	123.6 ⁽¹⁰⁾	55.9	329.1	760.2 ⁽¹⁰⁾
					133.1	35.2	140.0 ⁽¹⁰⁾	65.5	338.7	719.2 ⁽¹⁰⁾
					148.9	37.3	154.4 ⁽¹⁰⁾	74.9	348.1	674.3 ⁽¹⁰⁾

Table 22 (continued) Experimental data for the $CO_2+(n\text{-decane}+1\text{-decanol}+3,7\text{-dimethyl-1-octanol}+2,6\text{-dimethyl-2-octanol})$ system

Solute mass (g)	Solvent mass (g)	Total mass (g)	Mass fraction (g/g)	Molar fraction (mol/mol)	Pressure (barg)	Piston position (mm)	Corrected pressure (barA)	Temperature (°C)	Converted Temperature (K)	Density (kg/m ³)
1.53	18.60	20.13	0.0762	0.02299	68.3	38.0	78.6 ⁽¹⁰⁾	35.4	308.6	660.5 ⁽¹⁰⁾
					90.6	40.0	99.9 ⁽¹⁰⁾	45.0	318.2	624.1 ⁽¹⁰⁾
					110.8	43.3	119.2 ⁽¹⁰⁾	55.6	328.8	572.1 ⁽¹⁰⁾
					128.7	45.8	135.8 ⁽¹⁰⁾	65.1	338.3	538.2 ⁽¹⁰⁾
					143.3	49.1	149.2 ⁽¹⁰⁾	74.8	348.0	499.1 ⁽¹⁰⁾
1.00	19.08	20.08	0.0500	0.01480	68.7	41.2	78.9 ⁽¹⁰⁾	35.9	309.1	604.2 ⁽¹⁰⁾
					91.2	42.7	100.5 ⁽¹⁰⁾	45.4	318.6	580.9 ⁽¹⁰⁾
					108.6	47.4	117.1 ⁽¹⁰⁾	55.8	329.0	518.5 ⁽¹⁰⁾
					123.8	51.6	131.1 ⁽¹⁰⁾	65.3	338.5	473.0 ⁽¹⁰⁾
					137.2	55.1	143.4 ⁽¹⁰⁾	74.8	348.0	440.8 ⁽¹⁰⁾
0.51	17.59	18.10	0.0283	0.00825	68.8	44.4	79.1 ⁽¹⁰⁾	35.8	309.0	556.7 ⁽¹⁰⁾
					85.9	49.0	95.2 ⁽¹⁰⁾	45.1	318.3	500.2 ⁽¹⁰⁾
					104.0	53.7	112.6 ⁽¹⁰⁾	55.8	329.0	453.2 ⁽¹⁰⁾
					118.5	57.8	126.0 ⁽¹⁰⁾	65.4	338.6	418.8 ⁽¹⁰⁾
					129.2	62.5	135.8 ⁽¹⁰⁾	75.0	348.2	385.4 ⁽¹⁰⁾

Table 22 (continued) Experimental data for the $CO_2+(n\text{-decane}+1\text{-decanol}+3,7\text{-dimethyl-1-octanol}+2,6\text{-dimethyl-2-octanol})$ system

Solute mass (g)	Solvent mass (g)	Total mass (g)	Mass fraction (g/g)	Molar fraction (mol/mol)	Pressure (barg)	Piston position (mm)	Corrected pressure (barA)	Temperature (°C)	Converted Temperature (K)	Density (kg/m ³)
					70.4	57.5	80.7 ⁽¹⁰⁾	36.1	309.3	421.2 ⁽¹⁰⁾
					85.6	63.9	94.9 ⁽¹⁰⁾	45.4	318.6	376.4 ⁽¹⁰⁾
0.39	20.48	20.87	0.0189	0.00545	101.8	68.7	110.5 ⁽¹⁰⁾	55.8	329.0	348.6 ⁽¹⁰⁾
					113.8	74.1	121.5 ⁽¹⁰⁾	65.4	338.6	321.9 ⁽¹⁰⁾
					123.3	78.9	130.2 ⁽¹⁰⁾	74.8	348.0	301.3 ⁽¹⁰⁾

Table 23 Experimental data for the CO₂+(*n*-dodecane+1-decanol+3,7-dimethyl-1-octanol) system

Solute			20% <i>n</i> -dodecane + 70% 1-decanol + 10% 3,7-dimethyl-1-octanol							
Solvent			Carbon Dioxide							
Solute Molar Mass (g/mol)			160.69							
Solvent Molar Mass (g/mol)			44.01							
Solute mass (g)	Solvent mass (g)	Total mass (g)	Mass fraction (g/g)	Molar fraction (mol/mol)	Pressure (barg)	Piston position (mm)	Corrected pressure (barA)	Temperature (°C)	Converted Temperature (K)	Density (kg/m ³)
10.89	6.13	17.02	0.640	0.32733	73.5	36.5	72.2 ⁽⁵⁾	35.2	308.4	788.6 ⁽⁷⁾
					87.1	36.3	85.4 ⁽⁵⁾	44.9	318.1	794.0 ⁽⁷⁾
					100.3	36.7	97.7 ⁽⁵⁾	54.5	327.7	783.4 ⁽⁷⁾
					114.4	37.5	111.6 ⁽⁵⁾	65.2	338.4	763.2 ⁽⁷⁾
					124.9	38.3	121.5 ⁽⁵⁾	74.9	348.1	743.9 ⁽⁷⁾
9.37	7.22	16.59	0.565	0.26215	85.0	34.0	83.6 ⁽⁵⁾	35.4	308.6	838.5 ⁽⁷⁾
					99.4	34.8	97.5 ⁽⁵⁾	45.0	318.2	814.8 ⁽⁷⁾
					115.5	35.5	113.1 ⁽⁵⁾	54.6	327.8	795.0 ⁽⁷⁾
					131.3	36.2	128.3 ⁽⁵⁾	65.0	338.2	776.3 ⁽⁷⁾
					144.4	37.0	141.0 ⁽⁵⁾	74.5	347.7	755.9 ⁽⁷⁾

Table 23 (continued) Experimental data for the CO₂+(*n*-dodecane+1-decanol+3,7-dimethyl-1-octanol) system

Solute mass (g)	Solvent mass (g)	Total mass (g)	Mass fraction (g/g)	Molar fraction (mol/mol)	Pressure (barg)	Piston position (mm)	Corrected pressure (barA)	Temperature (°C)	Converted Temperature (K)	Density (kg/m ³)
7.22	8.40	15.62	0.462	0.19064	136.5	29.5	134.7 ⁽⁵⁾	35.2	308.4	944.8 ⁽⁷⁾
					132.8	30.7	130.5 ⁽⁵⁾	44.8	318.0	897.9 ⁽⁷⁾
					141.2	31.5	138.8 ⁽⁵⁾	54.5	327.7	869.1 ⁽⁷⁾
					154.4	32.6	151.5 ⁽⁵⁾	65.0	338.2	832.3 ⁽⁷⁾
					166.5	33.5	163.0 ⁽⁵⁾	74.4	347.6	804.5 ⁽⁷⁾
5.70	9.12	14.82	0.385	0.14623	160.2	26.7	158.3 ⁽⁵⁾	35.5	308.7	1021.1 ⁽⁷⁾
					150.8	27.9	148.5 ⁽⁵⁾	45.1	318.3	963.6 ⁽⁷⁾
					156.0	29.2	153.7 ⁽⁵⁾	54.8	328.0	908.3 ⁽⁷⁾
					167.1	30.1	164.0 ⁽⁵⁾	65.3	338.5	873.6 ⁽⁷⁾
4.50	10.40	14.90	0.302	0.10591	179.1	31.2	175.5 ⁽⁵⁾	74.9	348.1	834.6 ⁽⁷⁾
					174.4	26.2	172.3 ⁽⁵⁾	35.0	308.2	1052.3 ⁽⁷⁾
					159.6	27.5	157.4 ⁽⁵⁾	44.6	317.8	987.0 ⁽⁷⁾
					163.4	28.9	160.7 ⁽⁵⁾	55.1	328.3	925.1 ⁽⁷⁾
					173.3	29.6	170.1 ⁽⁵⁾	64.7	337.9	897.0 ⁽⁷⁾
					186.0	30.6	182.4 ⁽⁵⁾	75.3	348.5	859.7 ⁽⁷⁾

Table 23 (continued) Experimental data for the CO₂+(*n*-dodecane+1-decanol+3,7-dimethyl-1-octanol) system

Solute mass (g)	Solvent mass (g)	Total mass (g)	Mass fraction (g/g)	Molar fraction (mol/mol)	Pressure (barg)	Piston position (mm)	Corrected pressure (barA)	Temperature (°C)	Converted Temperature (K)	Density (kg/m ³)
3.42	11.67	15.09	0.227	0.07425	183.0	26.4	181.0 ⁽⁵⁾	35.4	308.6	1055.0 ⁽⁷⁾
					165.9	26.5	163.5 ⁽⁵⁾	45.4	318.6	1049.7 ⁽⁷⁾
					168.1	26.5	165.4 ⁽⁵⁾	55.1	328.3	1049.7 ⁽⁷⁾
					178.1	26.3	174.9 ⁽⁵⁾	65.7	338.9	1060.3 ⁽⁷⁾
					189.1	24.3	185.5 ⁽⁵⁾	75.3	348.5	1179.9 ⁽⁷⁾
3.61	17.22	20.83	0.173	0.05427	177.6	41.2	177.3 ⁽⁶⁾	34.4	307.6	866.6 ⁽⁶⁾
					158.7	43.0	159.5 ⁽⁶⁾	44.0	317.2	840.2 ⁽⁶⁾
					162.0	45.0	161.8 ⁽⁶⁾	54.7	327.9	812.6 ⁽⁶⁾
					171.9	46.4	170.4 ⁽⁶⁾	64.5	337.7	794.3 ⁽⁶⁾
					185.0	48.2	181.6 ⁽⁶⁾	75.1	348.3	772.0 ⁽⁶⁾
2.26	17.04	19.30	0.117	0.03506	141.0	39.7	144.2 ⁽⁶⁾	35.1	308.3	712.5 ⁽⁶⁾
					141.7	41.2	144.1 ⁽⁶⁾	44.8	318.0	681.6 ⁽⁶⁾
					151.2	43.2	152.1 ⁽⁶⁾	55.4	328.6	644.4 ⁽⁶⁾
					164.1	45.0	163.3 ⁽⁶⁾	65.0	338.2	614.2 ⁽⁶⁾
					178.5	47.1	175.8 ⁽⁶⁾	75.6	348.8	582.4 ⁽⁶⁾

Table 23 (continued) Experimental data for the CO₂+(*n*-dodecane+1-decanol+3,7-dimethyl-1-octanol) system

Solute mass (g)	Solvent mass (g)	Total mass (g)	Mass fraction (g/g)	Molar fraction (mol/mol)	Pressure (barg)	Piston position (mm)	Corrected pressure (barA)	Temperature (°C)	Converted Temperature (K)	Density (kg/m ³)
1.44	16.52	17.96	0.0803	0.02335	108.8	38.8	114.8 ⁽⁶⁾	34.7	307.9	732.4 ⁽⁶⁾
					122.0	40.8	126.2 ⁽⁶⁾	45.1	318.3	689.6 ⁽⁶⁾
					137.6	42.5	139.7 ⁽⁶⁾	54.6	327.8	657.0 ⁽⁶⁾
					154.8	44.6	154.9 ⁽⁶⁾	65.1	338.3	620.7 ⁽⁶⁾
					169.0	46.6	167.2 ⁽⁶⁾	74.9	348.1	589.7 ⁽⁶⁾
0.91	16.44	17.35	0.0522	0.01487	84.6	39.9	91.7 ⁽⁶⁾	35.1	308.3	708.2 ⁽⁶⁾
					103.4	41.8	108.9 ⁽⁶⁾	44.6	317.8	670.0 ⁽⁶⁾
					123.9	44.0	127.3 ⁽⁶⁾	55.0	328.2	630.6 ⁽⁶⁾
					142.9	46.2	144.1 ⁽⁶⁾	65.5	338.7	595.6 ⁽⁶⁾
					157.9	48.0	157.3 ⁽⁶⁾	75.1	348.3	569.8 ⁽⁶⁾
0.47	16.58	17.05	0.0275	0.00768	69.1	44.0	76.2 ⁽⁶⁾	34.8	308.0	630.6 ⁽⁶⁾
					90.4	46.0	96.5 ⁽⁶⁾	44.3	317.5	598.7 ⁽⁶⁾
					112.3	47.8	116.6 ⁽⁶⁾	54.8	328.0	572.5 ⁽⁶⁾
					130.0	50.6	132.4 ⁽⁶⁾	65.4	338.6	536.1 ⁽⁶⁾
					143.7	53.2	144.4 ⁽⁶⁾	75.0	348.2	506.2 ⁽⁶⁾

Table 23 (continued) Experimental data for the CO₂+(*n*-dodecane+1-decanol+3,7-dimethyl-1-octanol) system

Solute mass (g)	Solvent mass (g)	Total mass (g)	Mass fraction (g/g)	Molar fraction (mol/mol)	Pressure (barg)	Piston position (mm)	Corrected pressure (barA)	Temperature (°C)	Converted Temperature (K)	Density (kg/m ³)
0.31	16.98	17.29	0.0182	0.00505	68.9	49.8	76.0 ⁽⁶⁾	35.1	308.3	546.0 ⁽⁶⁾
					87.9	50.8	93.8 ⁽⁶⁾	44.5	317.7	533.7 ⁽⁶⁾
					107.5	53.3	111.3 ⁽⁶⁾	55.1	328.3	505.2 ⁽⁶⁾
					123.3	56.0	125.2 ⁽⁶⁾	65.7	338.9	477.6 ⁽⁶⁾
					134.2	59.4	133.9 ⁽⁶⁾	75.0	348.2	446.8 ⁽⁶⁾

Table 24 Experimental data for the CO₂+(*n*-dodecane+1-decanol) system

Solute		22.2% <i>n</i> -dodecane + 77.8% 1-decanol								
Solvent		Carbon Dioxide								
Solute Molar Mass (g/mol)		160.80								
Solvent Molar Mass (g/mol)		44.01								
Solute mass (g)	Solvent mass (g)	Total mass (g)	Mass fraction (g/g)	Molar fraction (mol/mol)	Pressure (barg)	Piston position (mm)	Corrected pressure (barA)	Temperature (°C)	Converted Temperature (K)	Density (kg/m ³)
10.87	5.74	16.61	0.654	0.34134	71.9	35.5	70.6 ⁽⁵⁾	34.9	308.1	767.6 ⁽⁷⁾
					86.1	35.4	84.4 ⁽⁵⁾	45.2	318.4	769.1 ⁽⁷⁾
					99.1	35.9	96.5 ⁽⁵⁾	54.7	327.9	761.7 ⁽⁷⁾
					111.8	36.5	109.0 ⁽⁵⁾	65.1	338.3	753.0 ⁽⁷⁾
					121.3	37.5	118.0 ⁽⁵⁾	74.5	347.7	738.9 ⁽⁷⁾
8.76	7.13	15.89	0.551	0.25173	92.4	31.4	91.0 ⁽⁵⁾	34.5	307.7	834.1 ⁽⁷⁾
					103.4	31.9	101.5 ⁽⁵⁾	44.8	318.0	825.4 ⁽⁷⁾
					118.1	32.4	115.7 ⁽⁵⁾	54.2	327.4	816.8 ⁽⁷⁾
					133.9	33.0	131.0 ⁽⁵⁾	64.5	337.7	806.8 ⁽⁷⁾
					146.5	33.4	143.1 ⁽⁵⁾	74.8	348.0	800.3 ⁽⁷⁾

Table 24 (continued) Experimental data for the CO₂+(n-dodecane+1-decanol) system

Solute mass (g)	Solvent mass (g)	Total mass (g)	Mass fraction (g/g)	Molar fraction (mol/mol)	Pressure (barg)	Piston position (mm)	Corrected pressure (barA)	Temperature (°C)	Converted Temperature (K)	Density (kg/m ³)
7.19	8.85	16.04	0.448	0.18182	144.0	29.6	142.2 ⁽⁵⁾	34.5	307.7	867.1 ⁽⁷⁾
					137.6	30.2	135.3 ⁽⁵⁾	45.2	318.4	855.8 ⁽⁷⁾
					142.8	30.7	140.4 ⁽⁵⁾	54.7	327.9	846.6 ⁽⁷⁾
					154.4	30.6	151.5 ⁽⁵⁾	65.2	338.4	848.4 ⁽⁷⁾
					167.0	31.2	163.5 ⁽⁵⁾	75.7	348.9	837.6 ⁽⁷⁾
6.03	10.03	16.06	0.375	0.14127	169.1	29.7	167.1 ⁽⁵⁾	35.4	308.6	865.2 ⁽⁷⁾
					155.4	30.0	153.1 ⁽⁵⁾	45.0	318.2	859.5 ⁽⁷⁾
					159.7	30.8	157.0 ⁽⁵⁾	55.6	328.8	844.8 ⁽⁷⁾
					168.6	30.7	165.5 ⁽⁵⁾	65.2	338.4	846.6 ⁽⁷⁾
					181.7	31.7	178.1 ⁽⁵⁾	75.7	348.9	828.9 ⁽⁷⁾
4.79	10.55	15.34	0.312	0.11057	181.2	26.5	179.2 ⁽⁵⁾	35.8	309.0	930.4 ⁽⁷⁾
					162.8	26.3	160.5 ⁽⁵⁾	45.7	318.9	934.8 ⁽⁷⁾
					165.4	27.4	162.7 ⁽⁵⁾	55.9	329.1	911.1 ⁽⁷⁾
					174.4	28.4	171.2 ⁽⁵⁾	65.6	338.8	890.5 ⁽⁷⁾
					186.5	29.2	182.8 ⁽⁵⁾	76.3	349.5	874.8 ⁽⁷⁾

Table 24 (continued) Experimental data for the CO₂+(n-dodecane+1-decanol) system

Solute mass (g)	Solvent mass (g)	Total mass (g)	Mass fraction (g/g)	Molar fraction (mol/mol)	Pressure (barg)	Piston position (mm)	Corrected pressure (barA)	Temperature (°C)	Converted Temperature (K)	Density (kg/m ³)
3.58	11.37	14.95	0.239	0.07927	195.9	23.5	193.9 ⁽⁵⁾	34.7	307.9	1001.2 ⁽⁷⁾
					170.0	24.5	167.6 ⁽⁵⁾	45.2	318.4	976.4 ⁽⁷⁾
					170.2	26.8	167.4 ⁽⁵⁾	54.8	328.0	923.9 ⁽⁷⁾
					178.6	28.5	175.5 ⁽⁵⁾	65.2	338.4	888.5 ⁽⁷⁾
					190.1	30.2	186.5 ⁽⁵⁾	75.7	348.9	855.8 ⁽⁷⁾
3.54	16.75	20.29	0.174	0.05467	184.1	40.2	183.1 ⁽⁶⁾	34.9	308.1	684.9 ⁽⁶⁾
					160.9	41.8	161.4 ⁽⁶⁾	44.5	317.7	653.8 ⁽⁶⁾
					161.9	43.4	161.7 ⁽⁶⁾	55.0	328.2	625.4 ⁽⁶⁾
					170.9	44.6	169.5 ⁽⁶⁾	64.7	337.9	605.6 ⁽⁶⁾
					183.9	45.8	180.6 ⁽⁶⁾	75.5	348.7	587.1 ⁽⁶⁾
2.31	16.75	19.06	0.121	0.03644	156.0	38.8	157.8 ⁽⁶⁾	35.0	308.2	714.6 ⁽⁶⁾
					146.8	40.4	148.7 ⁽⁶⁾	44.7	317.9	680.8 ⁽⁶⁾
					154.0	42.2	154.6 ⁽⁶⁾	55.2	328.4	646.4 ⁽⁶⁾
					165.4	43.7	164.5 ⁽⁶⁾	64.9	338.1	620.3 ⁽⁶⁾
					179.1	45.4	176.3 ⁽⁶⁾	75.5	348.7	593.2 ⁽⁶⁾

Table 24 (continued) Experimental data for the CO₂+(n-dodecane+1-decanol) system

Solute mass (g)	Solvent mass (g)	Total mass (g)	Mass fraction (g/g)	Molar fraction (mol/mol)	Pressure (barg)	Piston position (mm)	Corrected pressure (barA)	Temperature (°C)	Converted Temperature (K)	Density (kg/m ³)
1.38	16.47	17.85	0.0775	0.02248	105.8	38.7	112.0 ⁽⁶⁾	34.8	308.0	716.8 ⁽⁶⁾
					120.6	40.0	124.9 ⁽⁶⁾	44.6	317.8	689.0 ⁽⁶⁾
					136.3	42.0	138.5 ⁽⁶⁾	55.2	328.4	650.1 ⁽⁶⁾
					152.3	43.6	152.7 ⁽⁶⁾	64.9	338.1	622.0 ⁽⁶⁾
					168.5	45.2	166.8 ⁽⁶⁾	75.5	348.7	596.2 ⁽⁶⁾
0.78	14.42	15.20	0.0512	0.01456	83.6	35.1	90.8 ⁽⁶⁾	34.8	308.0	807.3 ⁽⁶⁾
					103.8	35.9	109.3 ⁽⁶⁾	44.4	317.6	785.3 ⁽⁶⁾
					124.4	37.7	127.7 ⁽⁶⁾	55.0	328.2	739.9 ⁽⁶⁾
					142.2	38.4	143.5 ⁽⁶⁾	64.7	337.9	723.6 ⁽⁶⁾
					158.9	39.9	158.2 ⁽⁶⁾	75.3	348.5	691.0 ⁽⁶⁾
0.53	18.57	19.10	0.0276	0.00770	70.2	48.6	77.4 ⁽⁶⁾	34.9	308.1	548.0 ⁽⁶⁾
					91.6	50.5	97.7 ⁽⁶⁾	44.5	317.7	524.3 ⁽⁶⁾
					110.3	54.6	114.7 ⁽⁶⁾	55.1	328.3	479.6 ⁽⁶⁾
					127.4	56.0	130.1 ⁽⁶⁾	64.5	337.7	466.0 ⁽⁶⁾
					141.8	59.6	142.6 ⁽⁶⁾	74.9	348.1	434.3 ⁽⁶⁾

Table 24 (continued) Experimental data for the CO₂+(n-dodecane+1-decanol) system

Solute mass (g)	Solvent mass (g)	Total mass (g)	Mass fraction (g/g)	Molar fraction (mol/mol)	Pressure (barg)	Piston position (mm)	Corrected pressure (barA)	Temperature (°C)	Converted Temperature (K)	Density (kg/m ³)
0.37	20.67	21.04	0.0177	0.00490	68.5	61.6	75.6 ⁽⁶⁾	34.8	308.0	418.6 ⁽⁶⁾
					87.4	64.7	93.3 ⁽⁶⁾	44.5	317.7	396.2 ⁽⁶⁾
					105.8	69.8	109.6 ⁽⁶⁾	55.2	328.4	364.3 ⁽⁶⁾
					120.7	73.3	122.6 ⁽⁶⁾	64.8	338.0	345.2 ⁽⁶⁾
					132.8	78.3	132.5 ⁽⁶⁾	75.4	348.6	321.1 ⁽⁶⁾

Table 25 Experimental data for the CO₂+(1-decanol+3,7-dimethyl-1-octanol) system

Solute			87.5% 1-decanol + 12.5% 3,7-dimethyl-1-octanol							
Solvent			Carbon Dioxide							
Solute Molar Mass (g/mol)			158.28							
Solvent Molar Mass (g/mol)			44.01							
Solute mass (g)	Solvent mass (g)	Total mass (g)	Mass fraction (g/g)	Molar fraction (mol/mol)	Pressure (barg)	Piston position (mm)	Corrected pressure (barA)	Temperature (°C)	Converted Temperature (K)	Density (kg/m ³)
10.32	5.55	15.87	0.650	0.34085	79.2	30.6	77.9 ⁽⁵⁾	34.7	307.9	810.8 ⁽⁷⁾
					95.9	30.9	94.0 ⁽⁵⁾	45.1	318.3	805.6 ⁽⁷⁾
					108.1	31.6	105.6 ⁽⁵⁾	54.6	327.8	793.8 ⁽⁷⁾
					121.8	31.6	118.9 ⁽⁵⁾	65.0	338.2	793.8 ⁽⁷⁾
					132.7	31.9	129.3 ⁽⁵⁾	75.5	348.7	788.8 ⁽⁷⁾
8.69	6.74	15.43	0.563	0.26389	146.5	27.7	144.7 ⁽⁵⁾	34.9	308.1	864.7 ⁽⁷⁾
					135.5	28.1	133.2 ⁽⁵⁾	45.5	318.7	856.8 ⁽⁷⁾
					139.7	28.4	137.2 ⁽⁵⁾	55.2	328.4	851.0 ⁽⁷⁾
					150.2	28.6	147.3 ⁽⁵⁾	65.9	339.1	847.2 ⁽⁷⁾
					161.2	28.7	157.7 ⁽⁵⁾	75.6	348.8	845.3 ⁽⁷⁾

Table 25 (continued) Experimental data for the CO₂+(1-decanol+3,7-dimethyl-1-octanol) system

Solute mass (g)	Solvent mass (g)	Total mass (g)	Mass fraction (g/g)	Molar fraction (mol/mol)	Pressure (barg)	Piston position (mm)	Corrected pressure (barA)	Temperature (°C)	Converted Temperature (K)	Density (kg/m ³)
7.13	8.15	15.28	0.467	0.19571	252.2	26.2	250.3 ⁽⁵⁾	34.8	308.0	895.5 ⁽⁷⁾
					198.0	27.4	195.7 ⁽⁵⁾	44.2	317.4	870.7 ⁽⁷⁾
					183.3	28.4	180.7 ⁽⁵⁾	54.6	327.8	851.0 ⁽⁷⁾
					184.9	29.0	181.9 ⁽⁵⁾	65.0	338.2	839.7 ⁽⁷⁾
					191.7	29.3	188.1 ⁽⁵⁾	74.5	347.7	834.1 ⁽⁷⁾
5.76	9.29	15.05	0.383	0.14710	254.3	25.6	252.1 ⁽⁵⁾	39.8	313.0	908.4 ⁽⁷⁾
					226.8	26.7	224.5 ⁽⁵⁾	44.6	317.8	885.0 ⁽⁷⁾
					205.4	28.0	202.6 ⁽⁵⁾	55.0	328.2	858.8 ⁽⁷⁾
					204.3	29.3	201.1 ⁽⁵⁾	65.5	338.7	834.1 ⁽⁷⁾
					209.7	30.2	206.2 ⁽⁵⁾	76.0	349.2	817.8 ⁽⁷⁾
4.44	10.22	14.66	0.303	0.10781	261.1	24.2	259.0 ⁽⁵⁾	39.2	312.4	940.1 ⁽⁷⁾
					227.5	25.2	225.2 ⁽⁵⁾	44.2	317.4	917.2 ⁽⁷⁾
					208.5	26.3	205.7 ⁽⁵⁾	55.3	328.5	893.4 ⁽⁷⁾
					208.0	27.2	204.9 ⁽⁵⁾	65.1	338.3	874.7 ⁽⁷⁾
					213.3	27.8	209.8 ⁽⁵⁾	75.3	348.5	862.7 ⁽⁷⁾

Table 25 (continued) Experimental data for the CO₂+(1-decanol+3,7-dimethyl-1-octanol) system

Solute mass (g)	Solvent mass (g)	Total mass (g)	Mass fraction (g/g)	Molar fraction (mol/mol)	Pressure (barg)	Piston position (mm)	Corrected pressure (barA)	Temperature (°C)	Converted Temperature (K)	Density (kg/m ³)
3.46	11.14	14.60	0.237	0.07942	254.3	23.0	252.1 ⁽⁵⁾	39.4	312.6	969.1 ⁽⁷⁾
					224.4	24.5	222.2 ⁽⁵⁾	44.9	318.1	933.1 ⁽⁷⁾
					207.0	26.4	204.2 ⁽⁵⁾	54.8	328.0	891.2 ⁽⁷⁾
					207.5	27.7	204.3 ⁽⁵⁾	65.4	338.6	864.7 ⁽⁷⁾
					213.3	29.0	209.9 ⁽⁵⁾	74.8	348.0	839.7 ⁽⁷⁾
3.40	15.38	18.78	0.181	0.05793	235.2	36.6	228.5 ⁽⁶⁾	40.2	313.4	732.9 ⁽⁶⁾
					216.0	38.2	210.9 ⁽⁶⁾	44.7	317.9	695.9 ⁽⁶⁾
					199.4	39.6	195.4 ⁽⁶⁾	55.2	328.4	666.4 ⁽⁶⁾
					200.3	41.1	195.8 ⁽⁶⁾	64.8	338.0	637.4 ⁽⁶⁾
					208.0	42.6	202.3 ⁽⁶⁾	75.4	348.6	610.9 ⁽⁶⁾
2.26	16.91	19.17	0.118	0.03576	215.8	37.2	211.4 ⁽⁶⁾	34.9	308.1	718.6 ⁽⁶⁾
					181.8	38.8	180.3 ⁽⁶⁾	44.4	317.6	682.9 ⁽⁶⁾
					178.5	40.4	176.7 ⁽⁶⁾	55.0	328.2	650.6 ⁽⁶⁾
					184.6	42.0	181.8 ⁽⁶⁾	64.6	337.8	621.2 ⁽⁶⁾
					195.7	43.6	191.2 ⁽⁶⁾	75.0	348.2	594.4 ⁽⁶⁾

Table 25 (continued) Experimental data for the CO₂+(1-decanol+3,7-dimethyl-1-octanol) system

Solute mass (g)	Solvent mass (g)	Total mass (g)	Mass fraction (g/g)	Molar fraction (mol/mol)	Pressure (barg)	Piston position (mm)	Corrected pressure (barA)	Temperature (°C)	Converted Temperature (K)	Density (kg/m ³)
1.46	16.28	17.74	0.0821	0.02428	155.0	35.9	156.9 ⁽⁶⁾	35.2	308.4	750.4 ⁽⁶⁾
					150.2	36.5	151.8 ⁽⁶⁾	44.6	317.8	735.4 ⁽⁶⁾
					158.7	37.0	158.9 ⁽⁶⁾	55.2	328.4	723.3 ⁽⁶⁾
					170.7	38.8	169.3 ⁽⁶⁾	64.8	338.0	682.9 ⁽⁶⁾
					184.6	40.7	181.2 ⁽⁶⁾	75.3	348.5	644.9 ⁽⁶⁾
0.84	16.28	17.12	0.0490	0.01414	98.6	37.8	105.2 ⁽⁶⁾	35.1	308.3	704.8 ⁽⁶⁾
					115.4	39.5	120.1 ⁽⁶⁾	44.6	317.8	668.4 ⁽⁶⁾
					134.6	41.3	137.0 ⁽⁶⁾	55.1	328.3	633.8 ⁽⁶⁾
					151.3	43.0	151.8 ⁽⁶⁾	64.6	337.8	604.2 ⁽⁶⁾
					167.6	44.5	166.0 ⁽⁶⁾	75.3	348.5	580.3 ⁽⁶⁾
0.52	18.76	19.28	0.0272	0.00771	71.5	48.2	78.7 ⁽⁶⁾	34.6	307.8	528.7 ⁽⁶⁾
					96.5	50.5	102.3 ⁽⁶⁾	45.3	318.5	501.1 ⁽⁶⁾
					116.6	53.0	120.5 ⁽⁶⁾	55.2	328.4	474.1 ⁽⁶⁾
					133.1	55.3	135.3 ⁽⁶⁾	64.8	338.0	451.7 ⁽⁶⁾
					147.8	58.5	148.1 ⁽⁶⁾	75.4	348.6	423.9 ⁽⁶⁾

Table 25 (continued) Experimental data for the CO_2 +(1-decanol+3,7-dimethyl-1-octanol) system

Solute mass (g)	Solvent mass (g)	Total mass (g)	Mass fraction (g/g)	Molar fraction (mol/mol)	Pressure (barg)	Piston position (mm)	Corrected pressure (barA)	Temperature (°C)	Converted Temperature (K)	Density (kg/m ³)
0.40	21.67	22.07	0.0179	0.00505	70.6	60.6	77.7 ⁽⁶⁾	35.3	308.5	407.4 ⁽⁶⁾
					90.4	63.6	96.5 ⁽⁶⁾	44.9	318.1	386.0 ⁽⁶⁾
					109.2	68.3	113.7 ⁽⁶⁾	55.4	328.6	356.6 ⁽⁶⁾
					123.0	72.7	126.1 ⁽⁶⁾	64.9	338.1	332.9 ⁽⁶⁾
					134.9	77.9	136.4 ⁽⁶⁾	75.4	348.6	308.6 ⁽⁶⁾

Table 26 Experimental data for the CO₂+(*n*-dodecane+3,7-dimethyl-1-octanol) system

Solute		66.7% <i>n</i> -dodecane + 33.3% 3,7-dimethyl-1-octanol								
Solvent		Carbon Dioxide								
Solute Molar Mass (g/mol)		166.32								
Solvent Molar Mass (g/mol)		44.01								
Solute mass (g)	Solvent mass (g)	Total mass (g)	Mass fraction (g/g)	Molar fraction (mol/mol)	Pressure (barg)	Piston position (mm)	Corrected pressure (barA)	Temperature (°C)	Converted Temperature (K)	Density (kg/m ³)
10.28	5.77	16.05	0.640	0.32037	64.9	37.4	63.3 ⁽⁷⁾	34.7	308.4	715.3 ⁽⁹⁾
					77.0	39.0	75.0 ⁽⁷⁾	46.0	319.7	694.5 ⁽⁹⁾
					86.1	39.7	83.7 ⁽⁷⁾	54.7	328.5	685.8 ⁽⁹⁾
					98.6	40.6	95.5 ⁽⁷⁾	65.7	339.6	674.8 ⁽⁹⁾
					108.7	41.7	105.2 ⁽⁷⁾	75.9	349.8	662.0 ⁽⁹⁾
8.21	6.37	14.58	0.563	0.25431	69.2	32.7	67.5 ⁽⁷⁾	35.2	308.9	784.4 ⁽⁹⁾
					80.3	33.3	78.4 ⁽⁷⁾	43.8	317.5	774.9 ⁽⁹⁾
					93.9	33.7	91.4 ⁽⁷⁾	54.6	328.4	768.6 ⁽⁹⁾
					106.0	34.0	102.9 ⁽⁷⁾	63.9	337.8	764.0 ⁽⁹⁾
					118.1	34.6	114.6 ⁽⁷⁾	73.9	347.8	755.0 ⁽⁹⁾

Table 26 (continued) Experimental data for the CO₂+(n-dodecane+3,7-dimethyl-1-octanol) system

Solute mass (g)	Solvent mass (g)	Total mass (g)	Mass fraction (g/g)	Molar fraction (mol/mol)	Pressure (barg)	Piston position (mm)	Corrected pressure (barA)	Temperature (°C)	Converted Temperature (K)	Density (kg/m ³)
6.32	7.36	13.68	0.462	0.18515	72.3	29.0	70.7 ⁽⁷⁾	34.5	308.2	849.0 ⁽⁹⁾
					87.7	30.0	85.8 ⁽⁷⁾	44.7	318.4	830.6 ⁽⁹⁾
					102.8	30.0	100.2 ⁽⁷⁾	54.2	328.0	830.6 ⁽⁹⁾
					118.6	30.2	115.8 ⁽⁷⁾	64.7	338.6	827.0 ⁽⁹⁾
					133.3	30.8	129.6 ⁽⁷⁾	74.5	348.4	816.3 ⁽⁹⁾
5.31	8.77	14.08	0.377	0.13818	75.5	30.4	73.9 ⁽⁷⁾	35.5	309.2	823.4 ⁽⁹⁾
					91.4	31.0	89.4 ⁽⁷⁾	45.2	318.9	812.9 ⁽⁹⁾
					108.1	31.1	105.4 ⁽⁷⁾	54.4	328.2	811.1 ⁽⁹⁾
					123.9	31.8	120.7 ⁽⁷⁾	63.5	337.4	799.2 ⁽⁹⁾
					142.9	32.7	139.3 ⁽⁷⁾	75.3	349.2	784.4 ⁽⁹⁾
4.15	9.75	13.90	0.298	0.10116	76.9	29.3	75.3 ⁽⁷⁾	35.6	309.3	843.4 ⁽⁹⁾
					94.1	29.8	92.0 ⁽⁷⁾	45.5	319.2	834.2 ⁽⁹⁾
					112.4	30.0	109.6 ⁽⁷⁾	55.2	329.0	830.6 ⁽⁹⁾
					132.3	30.5	129.0 ⁽⁷⁾	65.8	339.7	821.6 ⁽⁹⁾
					149.7	31.4	146.0 ⁽⁷⁾	75.9	349.8	806.0 ⁽⁹⁾

Table 26 (continued) Experimental data for the CO₂+(*n*-dodecane+3,7-dimethyl-1-octanol) system

Solute mass (g)	Solvent mass (g)	Total mass (g)	Mass fraction (g/g)	Molar fraction (mol/mol)	Pressure (barg)	Piston position (mm)	Corrected pressure (barA)	Temperature (°C)	Converted Temperature (K)	Density (kg/m ³)
3.13	10.28	13.41	0.233	0.07457	78.3	27.2	76.7 ⁽⁷⁾	36.0	309.7	884.5 ⁽⁹⁾
					95.9	27.9	93.8 ⁽⁷⁾	45.9	319.6	870.3 ⁽⁹⁾
					113.9	28.1	111.1 ⁽⁷⁾	54.7	328.5	866.4 ⁽⁹⁾
					135.0	28.9	131.7 ⁽⁷⁾	65.5	339.4	850.9 ⁽⁹⁾
					151.8	29.7	148.1 ⁽⁷⁾	74.9	348.8	836.0 ⁽⁹⁾
3.56	15.78	19.34	0.184	0.05632	65.1	33.0	74.0 ⁽⁸⁾	35.4	308.6	842.0 ⁽⁸⁾
					82.0	34.6	90.9 ⁽⁸⁾	45.1	318.3	794.0 ⁽⁸⁾
					104.2	36.2	112.7 ⁽⁸⁾	55.6	328.8	751.1 ⁽⁸⁾
					124.0	37.7	130.7 ⁽⁸⁾	65.3	338.5	714.9 ⁽⁸⁾
					141.5	39.2	146.3 ⁽⁸⁾	74.8	348.0	682.1 ⁽⁸⁾
2.34	17.50	19.84	0.118	0.03418	65.8	36.0	74.7 ⁽⁸⁾	35.6	308.8	756.2 ⁽⁸⁾
					81.9	38.1	90.8 ⁽⁸⁾	45.0	318.2	705.9 ⁽⁸⁾
					101.2	41.4	109.8 ⁽⁸⁾	54.6	327.8	639.0 ⁽⁸⁾
					122.5	43.4	129.3 ⁽⁸⁾	65.4	338.6	604.3 ⁽⁸⁾
					139.3	45.5	144.3 ⁽⁸⁾	74.8	348.0	571.7 ⁽⁸⁾

Table 26 (continued) Experimental data for the CO₂+(n-dodecane+3,7-dimethyl-1-octanol) system

Solute mass (g)	Solvent mass (g)	Total mass (g)	Mass fraction (g/g)	Molar fraction (mol/mol)	Pressure (barg)	Piston position (mm)	Corrected pressure (barA)	Temperature (°C)	Converted Temperature (K)	Density (kg/m ³)
1.45	16.73	18.18	0.0797	0.02240	66.0	34.0	74.9 ⁽⁸⁾	35.5	308.7	811.3 ⁽⁸⁾
					82.1	38.2	91.0 ⁽⁸⁾	44.9	318.1	703.6 ⁽⁸⁾
					102.4	40.5	111.0 ⁽⁸⁾	55.5	328.7	655.9 ⁽⁸⁾
					120.2	42.7	127.1 ⁽⁸⁾	65.1	338.3	616.0 ⁽⁸⁾
					136.2	45.0	141.4 ⁽⁸⁾	74.8	348.0	579.1 ⁽⁸⁾
0.91	15.82	16.73	0.0544	0.01499	68.4	35.5	77.4 ⁽⁸⁾	36.2	309.4	769.3 ⁽⁸⁾
					83.0	39.5	91.9 ⁽⁸⁾	45.3	318.5	675.8 ⁽⁸⁾
					102.3	41.6	110.9 ⁽⁸⁾	55.9	329.1	635.3 ⁽⁸⁾
					119.0	43.3	126.0 ⁽⁸⁾	65.4	338.6	605.9 ⁽⁸⁾
					132.4	46.2	137.8 ⁽⁸⁾	74.9	348.1	561.6 ⁽⁸⁾
0.43	14.57	15.00	0.0288	0.00779	68.5	33.4	77.5 ⁽⁸⁾	35.7	308.9	829.5 ⁽⁸⁾
					81.4	43.4	90.3 ⁽⁸⁾	45.2	318.4	604.3 ⁽⁸⁾
					99.1	43.6	107.8 ⁽⁸⁾	55.6	328.8	601.0 ⁽⁸⁾
					110.4	49.0	117.9 ⁽⁸⁾	65.3	338.5	524.5 ⁽⁸⁾
					121.5	51.2	127.5 ⁽⁸⁾	74.8	348.0	498.7 ⁽⁸⁾

Table 26 (continued) Experimental data for the CO₂+(n-dodecane+3,7-dimethyl-1-octanol) system

Solute mass (g)	Solvent mass (g)	Total mass (g)	Mass fraction (g/g)	Molar fraction (mol/mol)	Pressure (barg)	Piston position (mm)	Corrected pressure (barA)	Temperature (°C)	Converted Temperature (K)	Density (kg/m ³)
0.29	16.36	16.65	0.0171	0.00459	69.6	45.8	78.6 ⁽⁸⁾	35.9	309.1	567.3 ⁽⁸⁾
					81.8	52.2	90.7 ⁽⁸⁾	45.4	318.6	487.8 ⁽⁸⁾
					95.6	57.2	104.3 ⁽⁸⁾	55.7	328.9	439.6 ⁽⁸⁾
					104.3	64.6	112.1 ⁽⁸⁾	65.3	338.5	383.6 ⁽⁸⁾
					111.5	68.0	118.0 ⁽⁸⁾	74.7	347.9	362.3 ⁽⁸⁾

Table 27 Experimental data for the CO₂+3,7-dimethyl-1-octanol system to check for purity

Solute			3,7-Dimethyl-1-octanol							
Solvent			Carbon Dioxide							
Solute Molar Mass (g/mol)			158.28							
Solvent Molar Mass (g/mol)			44.01							
Solute mass (g)	Solvent mass (g)	Total mass (g)	Mass fraction (g/g)	Molar fraction (mol/mol)	Pressure (barg)	Piston position (mm)	Corrected pressure (barA)	Temperature (°C)	Converted Temperature (K)	Density (kg/m ³)
6.78	14.72	21.50	0.315	0.11351	113.8	32.5	121.9 ⁽⁸⁾	35.5	308.7	671.3 ⁽⁸⁾
					126.9	33.6	134.2 ⁽⁸⁾	45.8	319.0	657.2 ⁽⁸⁾
					142.7	34.3	148.9 ⁽⁸⁾	55.4	328.6	648.4 ⁽⁸⁾
					159.0	35.1	163.3 ⁽⁸⁾	65.0	338.2	638.8 ⁽⁸⁾
					174.0	36.0	176.6 ⁽⁸⁾	74.5	347.7	628.2 ⁽⁸⁾

C. INPUT DATA FOR THE REGRESSION OF BINARY INTERACTION PARAMETERS

C.1 BINARY VLE DATACXLIII

C.2 NOMENCLATURE..... CLIII

C.1 Binary VLE Data

The data used in the regression cases for the binary interaction parameters in Chapter 6 was determined from the experimentally measured data given in Appendix B. Since Aspen Plus[®] can only do regression on VLE data the measured bubble and dew point data were converted to P - x - y VLE data for all the binary systems investigated at 338 K and 348 K, and are given in Table 1 to Table 7.

C|Input Data for the Regression of Binary Interaction
Parameters

Table 1 VLE data for the CO₂+n-decane system

Temperature = 338 K		
<i>x</i>	<i>y</i>	Pressure (MPa)
0.437125	0.030673	10.8
0.405112	0.034360	11.0
0.371087	0.037712	11.2
0.330526	0.044249	11.4
0.291640	0.060172	11.6
0.259292	0.090006	11.8

Temperature = 348 K		
<i>x</i>	<i>y</i>	Pressure (MPa)
0.512047	0.029667	11.4
0.494616	0.032516	11.6
0.475508	0.034528	11.8
0.455395	0.037712	12.0
0.432935	0.041902	12.2
0.408297	0.048439	12.4
0.381814	0.057658	12.6
0.350304	0.069390	12.8
0.313597	0.082967	13.0
0.281752	0.099895	13.2
0.243537	0.122858	13.4

C|Input Data for the Regression of Binary Interaction
Parameters

Table 2 VLE data for the CO₂+1-decanol system

Temperature = 338 K		
x	y	Pressure (MPa)
0.634398	0.019773	13.6
0.630278	0.022245	13.8
0.626571	0.024717	14.0
0.622039	0.027600	14.2
0.617920	0.02966	14.4
0.613388	0.032544	14.6
0.608033	0.035427	14.8
0.60309	0.037487	15.0
0.597322	0.040783	15.2
0.591555	0.042842	15.4
0.586612	0.045726	15.6
0.582492	0.048610	15.8
0.575901	0.051493	16.0
0.57137	0.054377	16.2
0.566014	0.056849	16.4
0.561071	0.060144	16.6
0.555304	0.062616	16.8
0.549537	0.065911	17.0
0.544593	0.068795	17.2
0.538826	0.072091	17.4
0.533059	0.075798	17.6
0.52688	0.079918	17.8
0.521112	0.083625	18.0
0.513697	0.086921	18.2
0.507518	0.09104	18.4
0.498867	0.09516	18.6
0.491864	0.099691	18.8
0.483625	0.103811	19.0
0.475386	0.108342	19.2
0.463028	0.112873	19.4
0.455201	0.119053	19.6
0.443666	0.12482	19.8
0.432956	0.132235	20.0

C|Input Data for the Regression of Binary Interaction
Parameters

Table 2 (continued) VLE data for the CO₂+1-decanol system

Temperature = 338 K		
x	y	Pressure (MPa)
0.422657	0.140886	20.2
0.409063	0.153244	20.4
0.395469	0.169722	20.6
0.378991	0.185788	20.8
0.351802	0.209681	13.4
0.300721	0.263646	13.2
Temperature = 348 K		
x	y	Pressure (MPa)
0.627394	0.020185	14.8
0.621215	0.021833	15.0
0.614624	0.023893	15.2
0.608445	0.026365	15.4
0.601854	0.030072	15.6
0.596087	0.033368	15.8
0.589495	0.037487	16.0
0.583316	0.041195	16.2
0.576725	0.044902	16.4
0.570546	0.049022	16.6
0.564367	0.052317	16.8
0.557775	0.055201	17.0
0.551596	0.058496	17.2
0.545005	0.06138	17.4
0.538002	0.064676	17.6
0.530999	0.067971	17.8
0.524408	0.070855	18.0
0.516581	0.074562	18.2
0.508754	0.07827	18.4
0.500515	0.083213	18.6
0.491864	0.087745	18.8
0.481977	0.092688	19.0
0.472915	0.098043	19.2
0.462616	0.103811	19.4
0.452729	0.10999	19.6

C|Input Data for the Regression of Binary Interaction
Parameters

Table 2 (continued) VLE data for the CO₂+1-decanol system

Temperature = 348 K		
<i>x</i>	<i>y</i>	Pressure (MPa)
0.44243	0.116581	19.8
0.432132	0.124408	20.0
0.41895	0.134295	20.2
0.406591	0.146241	20.4
0.391349	0.161895	20.6

C|Input Data for the Regression of Binary Interaction
Parameters

Table 3 VLE data for the CO₂+3,7-dimethyl-1-octanol system

Temperature = 338 K		
x	y	Pressure (MPa)
0.563028	0.020185	12.8
0.554016	0.021988	13.0
0.544645	0.02415	13.2
0.535633	0.027394	13.4
0.525541	0.030639	13.6
0.516169	0.035324	13.8
0.505355	0.041452	14.0
0.494542	0.049022	14.2
0.483368	0.057312	14.4
0.470752	0.067044	14.6
0.459578	0.076777	14.8
0.448043	0.086509	15.0
0.43759	0.099125	15.2
0.426777	0.113903	15.4
0.412719	0.129042	15.6
0.395417	0.143821	15.8
0.375232	0.163646	16.0
0.352523	0.196807	16.2
Temperature = 348 K		
x	y	Pressure (MPa)
0.582492	0.018744	13.8
0.574202	0.020546	14.0
0.565911	0.022348	14.2
0.557981	0.02415	14.4
0.549691	0.025953	14.6
0.541401	0.029197	14.8
0.53275	0.032801	15.0
0.523378	0.037848	15.2
0.514006	0.043254	15.4
0.503913	0.050103	15.6
0.492739	0.057673	15.8
0.480844	0.065603	16.0
0.467508	0.074253	16.2

C|Input Data for the Regression of Binary Interaction
Parameters

Table 3 (continued) VLE data for the CO₂+3,7-dimethyl-1-octanol system

Temperature = 348 K		
x	y	Pressure (MPa)
0.455613	0.081823	16.4
0.431823	0.099485	16.8
0.418486	0.11138	17.0
0.400824	0.127961	17.2
0.382801	0.148867	17.4

C|Input Data for the Regression of Binary Interaction
Parameters

Table 4 VLE data for the CO₂+2,6-dimethyl-2-octanol system

Temperature = 338 K		
x	y	Pressure (MPa)
0.467443	0.023008	11.4
0.445746	0.029561	11.6
0.419971	0.037716	11.8
0.38109	0.046453	12.0
0.341336	0.059122	12.2
0.297649	0.081693	12.4

Temperature = 348 K		
x	y	Pressure (MPa)
0.539559	0.0198	12.0
0.523253	0.021693	12.2
0.507092	0.022858	12.4
0.49166	0.025478	12.6
0.473024	0.028536	12.8
0.455553	0.033049	13.0
0.435607	0.038727	13.2
0.414351	0.046007	13.4
0.383195	0.054305	13.6
0.352912	0.064788	13.8
0.320882	0.080657	14.0
0.274438	0.107009	14.2

C|Input Data for the Regression of Binary Interaction
Parameters

Table 5 VLE data for the CO₂+2-decanol system

Temperature = 338 K		
x	y	Pressure (MPa)
0.556101	0.021337	12.4
0.542651	0.025233	12.6
0.528529	0.03007	12.8
0.515348	0.034638	13.0
0.501898	0.040147	13.2
0.488582	0.045791	13.4
0.474863	0.052511	13.6
0.460606	0.059634	13.8
0.446349	0.068371	14.0
0.430614	0.080334	14.2
0.412188	0.095794	14.4
0.388788	0.11354	14.6
0.355975	0.136933	14.8
0.298286	0.181303	15.0
Temperature = 348 K		
x	y	Pressure (MPa)
0.591129	0.017742	13.2
0.578495	0.020833	13.4
0.565726	0.022984	13.6
0.552823	0.025807	13.8
0.540591	0.02957	14.0
0.527823	0.033602	14.2
0.515457	0.037903	14.4
0.503495	0.042473	14.6
0.491129	0.047715	14.8
0.47957	0.053629	15.0
0.467339	0.060081	15.2
0.454301	0.067876	15.4
0.440591	0.078091	15.6
0.426344	0.089785	15.8
0.410215	0.103226	16.0
0.389247	0.11828	16.2
0.359543	0.138441	16.4
0.308065	0.172312	16.6

C|Input Data for the Regression of Binary Interaction
Parameters

Table 6 VLE data for the CO₂+3,7-dimethyl-3-octanol system

Temperature = 338 K		
x	y	Pressure (MPa)
0.464774	0.020119	11.2
0.44372	0.025594	11.4
0.414159	0.033088	11.6
0.3833	0.043032	11.8
0.34898	0.053121	12.0
0.307308	0.071427	12.2

Temperature = 348 K		
x	y	Pressure (MPa)
0.519736	0.02019	12.0
0.501998	0.022497	12.2
0.48426	0.025093	12.4
0.467244	0.027256	12.6
0.449506	0.03115	12.8
0.429028	0.037639	13.0
0.405089	0.044705	13.2
0.380861	0.051339	13.4
0.354471	0.057829	13.6
0.31986	0.077153	13.8
0.269242	0.112917	14.0

C|Input Data for the Regression of Binary Interaction Parameters

Table 7 VLE data for the CO₂+n-dodecane system

Temperature = 338 K		
<i>x</i>	<i>y</i>	Pressure (MPa)
0.354325	0.05587	12.8
0.322606	0.072091	13.0
0.253759	0.105252	13.2
Temperature = 348 K		
<i>x</i>	<i>y</i>	Pressure (MPa)
0.40551	0.05551	14.2
0.379918	0.063079	14.4
0.356488	0.070649	14.6
0.329815	0.082544	14.8
0.29449	0.098043	15.0

C.2 Nomenclature

Symbol/ Acronym	Description
<i>x</i>	Mass fraction in the vapour phase
<i>y</i>	Mass fraction in the liquid phase

D. OPERATING PROCEDURE: HIGH PRESSURE PHASE EQUILIBRIUM CELL

D.1 LOADING PROCEDURE.....	CLV
D.2 OPERATING PROCEDURE.....	CLVIII
D.3 UNLOADING AND CLEANING PROCEDURE.....	CLIX
D.4 SAFETY PRECAUTIONS.....	CLX
D.4.1 Chemicals	CLX
D.4.2 Temperature.....	CLXII
D.4.3 Pressure.....	CLXIII

D.1 Loading Procedure

To start the loading procedure the low pressure chamber connected to the piston need to be removed from the equilibrium cell. The equilibrium cell can now be swivelled into a vertical position with the entrance of the cell facing upwards. The inlet/outlet valve of the cell must be closed while the cell is in this position.

1. Weigh the correct amount of solute in a small glass beaker. The amount of solute required is determined from the desired concentration and the expected density of the mixture. For the high solute concentration data points a larger amount of material is usually required in the equilibrium cell, and for the low concentration data points less material is required. For the systems used in this investigation the following rules of thumb (Table 1) were followed when determining the amount of solute required:

D | Operating Procedure: High Pressure Phase Equilibrium Cell

Table 1 Total amount of material loaded into equilibrium cells

Solute	Total amount of solute + solvent loaded (g)			
	Small Cell		Large Cell	
	CO ₂	Ethane	CO ₂	Ethane
C₁₀-alkanes	9 - 16	5 - 11	20 - 22	7 - 13
C₁₀-alcohols	12 - 18	6 - 11	21	7 - 15

2. The correctly weighed mass of solute can now be transferred to the cell with a pipette (liquids) or ladle (solids). The magnetic stirrer must also be put into the cell at this point. The equilibrium cell can now be closed by connecting the low pressure chamber with the piston rod tightly inserted into the cell entrance. The Teflon seal on the piston tip must be secured by tightening the nut at the other end of the piston rod. The contents of the cell are now sealed off from the environment.

3. The cell can now be swivelled back into the horizontal position. The four-way connection must be fastened onto the inlet/outlet valve, with all the valves on the four-way connection in the closed position. At this point all the residual air must be removed from the cell. Switch on the vacuum pump and allow it run for a few minutes to heat up. The valve on the vacuum line of the four-way connection can now be opened. Open the inlet/outlet valve of the cell VERY SLOWLY. At this point it is beneficial to have the camera and light source in front of the sight glass and the monitor switched on, to see how the solute in the cell reacts while vacuum is being drawn. It is important to ensure that the solute is not removed through the inlet/outlet valve (in the case of liquids) or does not expand into the inlet/outlet valve (in the case of solids) during the evacuation of air. Keep an eye on the pressure indicator to see when the pressure has dropped to at least 0.01 MPa. The inlet/outlet valve, as well as the valve on the vacuum line of the four-way connection can now be closed, and the vacuum pump switched off.

4. The next step involves the flushing of the equilibrium cell to remove any residual air or other compounds in the cell. A gas sample cylinder filled with the solvent that is to be used in the run, must now be connected to the designated port on the four-way connection. *Ensure that all the valves on the four-way connection, as well as the inlet/outlet valve of the cell are closed. Quickly open and close the bottom valve of the gas sample cylinder to allow a small amount of solvent to fill the lines of the four-way connection. SLOWLY open the inlet/outlet valve of the

D | Operating Procedure: High Pressure Phase Equilibrium Cell

equilibrium cell to allow this small amount of solvent to move into the cell. With the inlet/outlet valve in the open position, open the top valve of the four-way connection to flush all the solvent in the cell out to the atmosphere. Close the top valve of the four-way connection, as well as the inlet/outlet valve of the cell. Repeat this flushing procedure (starting from the *) six times. During the final flush make sure that the pressure in the cell is at a value slightly above atmospheric pressure to allow the minimum amount of solvent to be left behind while still ensuring that no air move back into the cell.

5. Make sure that all the valves on the four-way connection and gas sample cylinder, as well as the inlet/ outlet valve is securely closed, and remove the gas sample cylinder. The amount of solvent as calculated in step 1 must now be present in the gas sample cylinder. The weight of the “empty” gas sample cylinder varies with the type of solvent used as well as the amount loaded into it to start off with. To know the anticipated weight of the empty gas sample cylinder requires some prior experience. A small gas sample cylinder was used to convey the ethane (weight= ± 496 g) and a larger gas sample cylinder was used to convey the CO₂ (weight= ± 604 g). If there is too much solvent in the gas sample cylinder some of the solvent can be let out through one of the valves, and if there is not enough solvent in the gas sample cylinder, more solvent can be loaded at the gas canister.
6. When the gas sample cylinder contains the exact amount of solvent required, it can be connected to the designated port on the four-way connection. Switch on the vacuum pump and open the valve on the vacuum line of the four-way connection to allow vacuum to be drawn over the lines of the four-way connection. While this is happening, use the hairdryer to heat up the gas sample cylinder for 60 – 90 seconds. Switch of the vacuum pump and closed the valve on the vacuum line of the four-way connection. Now slowly open the inlet/outlet valve of the cell to the full open position. Open the bottom valve of the gas sample cylinder VERY SLOWLY to allow the heated solvent the flow from the gas sample cylinder into the equilibrium cell. Keep an eye on the monitor to see when the solvent stops flowing into the cell. When this happens use the hairdryer to heat up the bottom part of the gas sample cylinder for 15 seconds to force more solvent to move from it. Then close the bottom valve of the gas sample cylinder and continue to heat up all the lines as well as the body of the four-way connection, heating each part for 15 seconds to force the remaining solvent in the lines into the cell. Close the inlet/outlet valve when finished.

D | Operating Procedure: High Pressure Phase Equilibrium Cell

7. The lines of the four-way connection will still contain a small amount of solvent. To release the solvent into the atmosphere, open the top valve of the four-way connection. Remove the gas sample cylinder and weigh it to determine the exact amount of solvent transferred into the cell. Also, remove the four-way connection from the cell.
8. Calculate the total amount of material in the cell, and make sure that it is not too much or too little. The results from previous runs will guide this decision. If the incorrect amount of solvent was loaded, the loading procedure must be repeated.
9. Switch on the heating bath and set it to the desired temperature (usually a value slightly above the required temperature of the cell contents). Place the magnetic stirrer plate beneath the equilibrium cell and switch it on. Switch the magnetic stirrer on. Insulation material can now be put around the cell to minimize the heat loss from the heating jacket.
10. The nitrogen line can be connected to the low pressure chamber and the pressure increased until the cell contents exist as a single phase. As the pressure is increased by allowing more nitrogen into the low pressure chamber, the piston will move further into the cell. The pressure indicator must be monitored closely during this process to ensure that the pressure in the cell does not exceed the safety limit of 27.5 MPa. Once the cell contents are in a single phase, sufficient time must be allowed for the system to attain thermal equilibrium.

D.2 Operating Procedure

1. After the cell contents have reached the desired temperature, the pressure can be reduced in small increments by allowing the nitrogen to escape from the low pressure chamber through a release valve on the nitrogen line. As the pressure is incrementally lowered the monitor must be watched closely to look for any indication of the appearance of a second phase. The second phase will appear as either small bubbles on the roof of the equilibrium cell, or a small droplet on the bottom of the sight glass, or the sudden appearance of a cloudy mist.
2. At the point where the second phase appears the temperature and pressure must be recorded. The piston length must also be measured with a vernier calliper and recorded to allow the density to be calculated at a later stage.

D | Operating Procedure: High Pressure Phase Equilibrium Cell

3. Step 1 to 3 can be repeated up to three times to ensure that the phase transition pressure observed is accurate. Each time the nitrogen pressure is increased to force the contents of the cell back into the single phase region.
4. After the first data point has been logged, the temperature setting on the heating bath can be adjusted to the next operating temperature. The pressure can also be increased until the mixture is in the single phase.
5. Steps 1 to 4 must be repeated for all the operating temperatures investigated.

D.3 Unloading and Cleaning Procedure

1. After the last data point for the specific experimental run has been logged, all the nitrogen must be released from the low pressure chamber to allow the piston to move to its maximum position. The heating bath temperature must be adjusted to approximately 293 K and the cooling water be turned on. The insulation material can be removed and the cell left to cool down.

**[For solutes with melting points above 25°C a different procedure must be followed.]
2. Once the equilibrium cell has cooled down sufficiently, the cooling water as well as the heating bath can be switched off. The magnetic stirrer plate can also be switched off and removed from beneath the cell. Remove the camera and light source and switch of the monitor. Disconnect the nitrogen line from the low pressure chamber and swivel the cell 180° until it is in the horizontal upside down position (i.e. with the inlet/outlet valve facing downwards).
3. Use an Erlenmeyer flask and hold it beneath the inlet/outlet valve. SLOWLY open the inlet/outlet valve to allow the solute to flow from the cell into the Erlenmeyer flask. The solvent will escape with the solute and dissipate into the air. Once all the solute and solvent has been removed from the cell, it can be swivelled back 90° into the vertical upright position, and the low pressure chamber with the piston rod can be loosened (by loosening the nut on the on the back of the piston rod to relieve the Teflon seal) and removed from the equilibrium cell.
4. Swivel the equilibrium cell back slightly more than 90° to allow it to sit at an angle with the entrance facing slightly downwards. Put a beaker beneath the cell entrance and use a plastic squeeze bottle filled with xylene to rinse the cell. The xylene will dissolve any solute still left clinging to the cell walls. Use another squeeze bottle filled with methanol to rinse out all the

D | Operating Procedure: High Pressure Phase Equilibrium Cell

residual xylene from the cell. This procedure can be repeated several times to ensure than all the solutes are removed from the cell. The same procedure must be followed to clean the piston head and magnetic stirrer bar, as these parts were also in contact with the mixture.

5. Use pressurized air to blow over the inner cell walls and evaporate any methanol left behind. Finally, a paper towel can be used to wipe out the cell.

D.4 Safety Precautions

D.4.1 Chemicals

It is important that the operator is aware of the possible dangers of exposure to the alkanes and alcohols used. The Material Safety Data Sheets (MSDS) of all the alkanes and alcohols used were obtained from the supplier. During phase equilibrium experiments very small amounts of alkanes and alcohols are handled and thus the risk of inhalation of large amounts of vapour or ingestion of chemicals is minimal. There were no major concerns regarding the dangers posed by the alkanes or alcohols to the operator or the environment. The use of full personal protective equipment (PPE), i.e. a lab coat, safety goggles, closed shoes and surgical gloves, is mandatory for the operator working with the chemicals, but no additional safety precautions were necessary.

Ethane is a highly flammable substance and thus no open flames, smoking or sparks were allowed near the experimental setup. Also, the room containing the experimental equipment was well ventilated to prevent the build-up of chemicals.

CO₂ and nitrogen were also used during the phase equilibrium experiments. Both these gasses can cause weakness, dizziness and loss of consciousness when inhaled in large amounts, as it lowers the concentration of oxygen in the body. If any loss of containment is suspected in the room where the gas canisters with CO₂ and nitrogen are held, the room should be evacuated immediately.

During the cleaning procedure xylene and methanol were used. These solvents are also highly flammable and no open flames, smoking or sparks are allowed near the experimental equipment during the cleaning procedure. It is also important that the room is well ventilated to eliminate the inhalation of the vapours.

D | Operating Procedure: High Pressure Phase Equilibrium Cell

Table 2 shows the main issues addressed in the MSDSs' of the chemicals handled in this investigation.

Table 2 Hazards of and precautions for handling the chemicals used in this investigation

Chemical Compound	Main Hazards	Main Precautions
1-Decanol	Toxic by inhalation. Irritating to eyes, respiratory system and skin. Toxic to aquatic organisms.	Avoid breathing dust / fume / gas / mist / vapours / spray. Avoid release to environment. If in eyes, rinse with water. If ingested, call poison centre or doctor / physician. Dispose material and container as hazardous waste.
2-Decanol	Irritating to eyes. Toxic to aquatic organisms.	Avoid release to environment. If in eyes, rinse with water.
3,7-Dimethyl-1-octanol	Irritating to eyes, respiratory system and skin.	Avoid breathing dust / fume / gas / mist / vapours / spray. If in eyes, rinse with water. Wear protective clothing.
2,6-Dimethyl-2-octanol	Irritating to eyes. Harmful to aquatic organisms.	If in eyes, rinse with water. Avoid release to environment.
3,7-Dimethyl-3-octanol	Irritating to eyes, respiratory system and skin.	Avoid breathing dust / fume / gas / mist / vapours / spray. If in eyes, rinse with water. Wear suitable protective clothing.
n-Decane	Flammable. Harmful/fatal: cause lung damage if swallowed or enters airways.	If swallowed, call poison centre or doctor / physician. Do not induce vomiting.
2-Methylnonane	Flammable.	-
3-Methylnonane	Flammable.	-
4-Methylnonane	Flammable.	-

D | Operating Procedure: High Pressure Phase Equilibrium Cell

Table 2 (continued) Hazards of and precautions for handling the chemicals used in this investigation

Chemical Compound	Main Hazards	Main Precautions
Ethane	Extremely flammable. Contains gas under pressure.	Keep away from heat / sparks / open flames / hot surfaces. No smoking. Keep container in well-ventilated place. Take precautionary measures against static discharges.
CO₂	Contains gas under pressure – can explode if heated.	Protect from sunlight. Keep container in well-ventilated place.
Nitrogen	Contains gas under pressure – can explode if heated.	Protect from sunlight. Keep container in well-ventilated place.
Xylene	Flammable. Irritating to skin. Harmful by inhalation and when in contact with skin.	Wear gloves and protective clothing.
Methanol	Extremely flammable. Toxic by inhalation, when in contact with skin and if swallowed. Causes irreversible damage to organs if inhaled, contacts skin or swallowed.	Keep away from heat / sparks / open flames / hot surfaces. Avoid breathing dust / fume / gas / mist / vapours / spray. Wear gloves and protective clothing. If ingested, call poison centre or doctor / physician.

D.4.2 Temperature

No excessively high temperatures were used during the experimental runs. The highest temperature used was 353 K. Although this is not very high, care should still be taken when working with the equipment. Loading, unloading and cleaning all happen at room temperature. Should it be required that the equipment be handled at any time during the experimental run while it is still hot, thermal gloves should be worn to prevent skin burns.

D|Operating Procedure: High Pressure Phase Equilibrium Cell

D.4.3 Pressure

Very high pressures are reached during the phase equilibrium experiments. The phase equilibrium cells were designed to withstand a pressure of 50.0 MPa, but with the large safety margins for this type of setup, the highest operating pressure is 27.5 MPa. The main danger of working at the high pressures is the rupture of the cell or the leaking of the contents of the cell through a seal. To prevent the seals from leaking, they are inspected often to evaluate the creep.

E. OPERATING PROCEDURE: SUPERCRITICAL FLUID FRACTIONATION PILOT PLANT

E.1 PUMP CALIBRATION	CLXV
E.2 INTRODUCTION OF NEW FEED AND SOLVENT	CLXVII
E.2.1 Introduction of a new Solvent.....	CLXVII
E.2.2 Introduction of a New Feed Mixture.....	CLXVIII
E.3 LOADING PROCEDURE	CLXVIII
E.4 OPERATING PROCEDURE	CLXX
E.5 UNLOADING PROCEDURE	CLXX
E.6 SAFETY PRECAUTIONS.....	CLXXI
E.6.1 Chemicals.....	CLXXI
E.6.2 Temperature	CLXXII
E.6.3 Pressure	CLXXIII

E.1 Pump Calibration

The three pumps on the supercritical fluid fractionation pilot plant, the feed pump, the solvent pump and the reflux pump, were calibrated to determine their output flow rates at different settings. The calibration was conducted at a positive pressure of 5.0 MPa and 338 K. *1*-Decanol was used to calibrate the feed and reflux pumps, while CO₂ was used for the solvent pump.

E|Operating Procedure: Supercritical Fluid Fractionation Pilot Plant

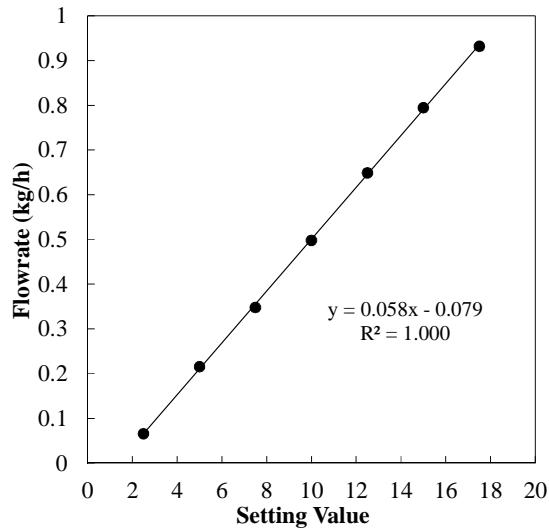


Figure 1 Feed pump calibration data

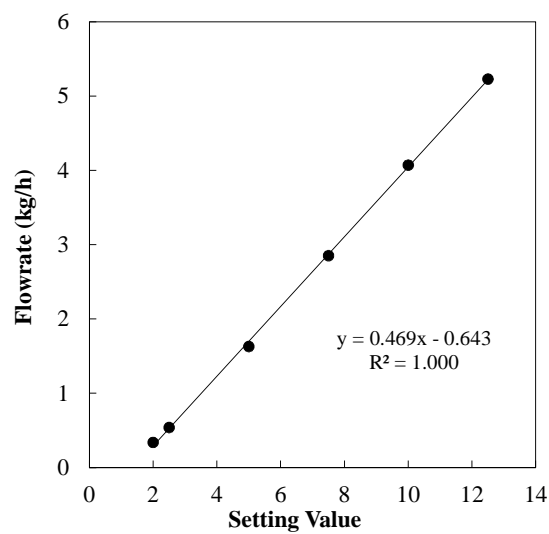


Figure 2 Reflux pump calibration data

E|Operating Procedure: Supercritical Fluid Fractionation Pilot Plant

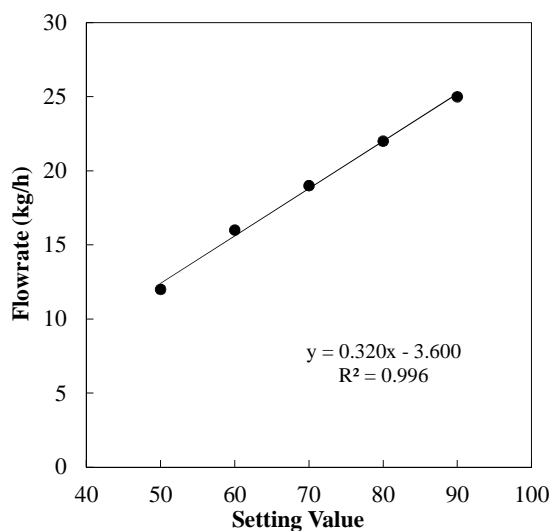


Figure 3 Solvent pump calibration data

E.2 Introduction of New Feed and Solvent

The introduction of a new solvent and/or feed usually occurs when the plant is not in operation. The replacement of a solvent cylinder¹ or addition of make-up feed² can occur while the plant is in operation.

E.2.1 Introduction of a new Solvent

1. Ensure that the following valves are fully closed: V2, V4, V5, V7, V9, V10, V11-V15.
2. Ensure that the following valves are fully open: V1, V3, V6, V8.
3. Open V12 and V13 to vent the entire system. Pressure on P1, P3, P4 and P6 should all read 0 MPa.

¹ To replace a solvent cylinder while the plant is in operation, close V7, and replace the solvent cylinder. Once this is done, open V7, and carry on with normal operation.

² To add make-up feed during an experimental run, no adjustments need to be made, it can just be added to the feed tank. This is however not recommended, since the new feed may differ slightly in composition.

E | Operating Procedure: Supercritical Fluid Fractionation Pilot Plant

4. Once all the solvent has been removed from the system, connect the new solvent to the solvent feed line, and slowly open V7.
5. Allow the new solvent to fill the entire system.

E.2.2 Introduction of a New Feed Mixture

1. Drain all the feed mixture still in the feed tank and lines by opening the feed drain valve at the bottom of the feed line, near the feed pump inlet.
2. Fill the feed tank with the new feed mixture, only during loading of the next run.

E.3 Loading Procedure

1. Switch on the main power. Switch on the top and bottom heaters approximately 2 - 3 hours prior to an experimental run.
2. For the temperatures used in this study, the following settings were made to the respective heaters:

Table 1 Heater settings for specific operating temperatures

Operating temperature (K)	Top heater (K)	Bottom heater (K)
± 313 K	317	348
± 343 K	347	361

3. Switch on the cooling water in the lab, and make sure that the valves on the cooling water lines are fully open to the plant. The valves on the sections of the cooling lines that feed both the heaters must be closed. Switch on the chiller 30 min prior to the start of the experiment.
4. Before the experiment commences, ensure that the following valves are fully closed: V2, V4, V5, V7, V9, V10, V11-V15.

E | Operating Procedure: Supercritical Fluid Fractionation Pilot Plant

5. Ensure that the following valves are fully open: V1, V3, V6, V8.
6. Open the solvent gas cylinder.
7. Slowly open V7. The solvent vapour pressure can now be viewed on P4. Allow the entire system to reach the solvent vapour pressure (leave for ± 5 min).
8. Fill the feed tank with the pre-mixed feed mixture and allow it to heat up. Ensure that there is enough feed mixture to last through the entire experiment. Once the feed mixture is in the feed tank, mix it thoroughly, and take a sample.
9. On the control panel set the control valve opening to 20%. Switch on the solvent pump, and set it to the minimum capacity (approximately 50%). Allow the solvent to circulate through the system for ± 30 min.
10. Make sure V9 and V10 are fully closed. Adjust the feed pump stroke length to the appropriate value. Switch on the feed pump and PAY ATTENTION to the pressure on P5. If it reaches a pressure slightly higher (± 1.0 MPa) than the column pressure (P1), switch off the feed pump.
11. Open V9 or V10, depending on the feed position required. Switch the feed pump back on. Allow the feed mixture to fully wet the column internals by letting it flow for ± 30 min.
12. While the solvent and feed is pumping, start to record values of T1, T3, T4, T5, T6, P1, P3, P4, P6 and the mass flow rate of the solvent.
13. The solvent pump stroke can be adjusted to allow the mass flow rate of the solvent to attain the desired value.
14. The control valve opening can be adjusted on the control panel to get the desired column pressure.
15. Once these values stabilize, the experimental run can proceed. The system takes approximately 1 hour after the solvent has been introduced to the system, to stabilize.

E.4 Operating Procedure

1. Empty the bottoms (V2) and the overheads (V4) to remove the products that collected during the stabilization period.
2. Log the values of T1, T3, T4, T5, T6, P1, P3, P4, P6 and the mass flow rate of the solvent in intervals of 20 - 30min.
3. After each data log, empty the bottoms and overheads products and weigh the amount of product collected from each sample point. Add the values of the bottoms and overheads product collected in 1 hour to calculate the feed rate of the mixture in kg/h.
4. After the removal of the bottoms and overheads products, the pressure in the column will drop approximately 0.5 – 1 MPa. Increase the solvent pump capacity to the maximum value (100%) for a short time (± 2 min) to get the column back to the original operating pressure. Then reduce the capacity of the solvent pump to the prior set value.
5. The solvent-to-feed ratio and overheads-to-feed ratio can thus be calculated hourly. Once these values are the same for two consecutive hours, the system is assumed to be at steady-state. The system takes approximately 3 – 4 hours to reach steady-state.
6. When the system operates at steady-state, allow it to run for another 20 – 30 min after the last removal of the bottoms and overheads products. Sampling can now commence, by emptying the bottoms and overheads products into a sample container.
7. All the bottoms and overheads product that was removed during the experimental run can be added together to make up the feed for the following run. Take a sample of the combined feed after completion of the experimental run, to see if and how it should be adjusted to the same initial composition for the next run.

E.5 Unloading Procedure

1. Once the experimental run has been conducted and the required samples collected, the solute feed pump can be switch off, and V9 or V10 closed (depending on the one used during the run).

E | Operating Procedure: Supercritical Fluid Fractionation Pilot Plant

2. Drain the rest of the feed mixture still left in the feed tank and feed line by opening the draining valve and collecting the rest of the feed in a vessel.
3. Switch off both heaters.
4. Set the control valve opening to 30%, and monitor P3 and P4 closely. If the pressure values increase to values above 7.0 MPa, the release valves V12 and V13 can be opened to relieve some of the pressure.
5. Allow the solvent to cycle for another 30 min to 1 hour.
6. Drain both the bottoms and overheads products.
7. Switch off the solvent pump.
8. Close V3.
9. Switch off the chiller and close the cooling water feed line. Switch of the cooling water in the lab (make sure it is not used by anyone else).
10. Switch off the main power.

E.6 Safety Precautions

E.6.1 Chemicals

The same safety precautions as that mentioned in section C.4 are applicable when operating the supercritical fluid extraction plant. The only difference is that much larger quantities of solute and solvent are handled. Closer attention should be given to the main precautions listed in Table 2 in Appendix C when handling larger quantities of chemicals.

The main concern regarding operation of the supercritical fluid fractionation pilot plant is the solvents, CO₂ and ethane. Large amounts of solvent are present in the system during its operation. Important safety precautions include the following:

E | Operating Procedure: Supercritical Fluid Fractionation Pilot Plant

- Large fans in the lab should be switched on during the pilot plant operation. With the air intake at the top and air outlet at the bottom of the lab, air will circulate and prevent solvent build-up in the atmosphere surrounding the pilot plant.
- Apart from the fans, lab doors should be kept open at all times to ensure good ventilation.
- No experiments may commence when the operator is alone. People that are able to assist in case of an emergency must be in close proximity.
- When ethane is used additional safety measures must be followed:
 - If any other experimental setups are in operation in close proximity to the pilot plant, the compatibility with ethane should be investigated prior to the experimental run.
 - No welding, grinding or use of electrical equipment is allowed in the vicinity of the pilot plant during an experimental run, as well as at least 2 hours after the run is completed.
 - No cars may be parked in the vicinity of the pilot plant.
 - The use of a red/green flag is recommended to alert surrounding personnel of the situation around the pilot plant. If the red flag is on show, no electrical equipment, cars or sources of sparks are allowed close to the pilot plant. If the green flag is on show, it indicates that the surrounding area is declared safe.
 - A fire extinguisher must be located near the pilot plant.

E.6.2 Temperature

The maximum temperature used on the supercritical fluid extraction plant is 358 K. Although this is not extremely high, care should still be taken when working close to hot surfaces. Gloves should be worn when required.

E|Operating Procedure: Supercritical Fluid Fractionation Pilot Plant

E.6.3 Pressure

The extraction column was designed to hold a pressure of 30.0 MPa. Auxiliary units all have different operating pressure limits. Wherever possible, operate well beneath the operating limits of the equipment.

The operator may not leave the unit unattended. Manual pressure monitoring will aid in the detection of a problem before it damages equipment.

Relief valves were incorporated in the design of the extraction unit, and will aid in the prevention of runaway pressure build-up.